

2

AD-A152 119

Proceedings of the 33rd International Wire and Cable Symposium

November 13 thru 15 1984

Sponsored by the
US Army
Communications-Electronics Command
Fort Monmouth, New Jersey

DTIC
ELECTE
MAR 12 1985
S E D



This document has been approved
for public release and sale its
distribution is unlimited.

DTIC FILE COPY

85 02 25 009

PROCEEDINGS OF 33rd INTERNATIONAL WIRE AND CABLE SYMPOSIUM

Sponsored by
US Army Communications-Electronics Command
(CECOM)
Fort Monmouth, New Jersey

RENO, NEVADA
NOVEMBER 13, 14 and 15, 1984

Accession For	
NTIS GRA&I	<input checked="" type="checkbox"/>
DTIC TAB	<input type="checkbox"/>
Unannounced	<input type="checkbox"/>
Justification	
By	
Distribution/	
Availability Codes	
Dist	Avail and/or Special
A-1	

APPROVED FOR PUBLIC RELEASE: DISTRIBUTION UNLIMITED



Document will be sold according to DTIC
price schedule per Mr. Larry Goldberg,
Army Electronics R & D Comd/DELS-D-L-S

33RD INTERNATIONAL WIRE AND CABLE SYMPOSIUM

SYMPOSIUM COMMITTEE

Elmer F. Godwin, Director, GEF Associates (201) 741-8864
Susan Burgher, Assistant, US Army CECOM (201) 544-2770
William Chervenak, Corning Glass Works
Robert Depp, Defense Electronics Supply Center
Andrew Dunin, DuPont Canada Inc.
Joseph McCann, US Army CECOM
Kazuo Nomura, Sumitomo Electric, USA
Eugene Riley, Anaconda-Ericsson, Inc.
John Thompson, Nokia, Inc.
James Tyler, Essex Group
George Webster, Bell Laboratories
Austin Wetherell, Underwriters Laboratories

ADVISORY

Michael A. DeLucia, David W. Taylor Naval Ship R&D Center
Marta Farago, Northern Telecom Canada Ltd.
Irving Kolodny, General Cable Company
Joe Neigh, AMP, Inc.
Frank Short, R. T. Vanderbilt Company, Inc.

TECHNICAL SESSIONS

Tuesday, 13 November 1984

9:30 a.m.	SESSION I	Panel Discussion-TELCO Systems Standardization and Procurement Practices—The Impact of Divestiture
2:00 p.m.	SESSION II	Fire, Smoke, and Toxicity Technology
2:00 p.m.	SESSION III	Connectors, Splices, Enclosures I
2:00 p.m.	SESSION IV	Fiber Optic Cable Design

Wednesday, 14 November 1984

9:00 a.m.	SESSION V	Cable Design and Testing I
9:00 a.m.	SESSION VI	Connectors, Splices, Enclosures II
2:30 p.m.	SESSION VII	Cable Design and Testing II
2:30 p.m.	SESSION VIII	Fiber Optic Cable Design and Single-Mode Fiber System

Thursday, 15 November 1984

9:00 a.m.	SESSION IX	Cable Materials and Processing
9:00 a.m.	SESSION X	Undercarpet, Interoffice Cable
2:00 p.m.	SESSION XI	Fiber Optic Applications and Installations
2:00 p.m.	SESSION XII	Fiber Optic Materials and Testing

PAPERS

Responsibility for contents rests upon the authors and not the symposium committee or its members. After the symposium, all the publication rights of each paper are reserved by their authors, and requests for republication of a paper should be addressed to the appropriate author. Abstracting is permitted, and it would be appreciated if the symposium is credited when abstracts or papers are republished. Requests for individual copies of papers should be addressed to the authors.



Message from the Director

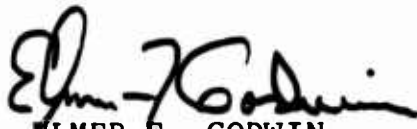
On behalf of the US Army Communications-Electronics Command (CECOM) and the symposium committee, welcome to the 33rd International Wire and Cable Symposium (IWCS). The conflict in meeting dates with the Wire Association caused a slight drop in attendance last year, however, the number of foreign attendees (226) from 26 countries increased significantly over the previous year.

The response this year to the call for papers was greater than ever, with many excellent abstracts (133) submitted for consideration. As a result, the committee expects this year's excellent technical program of 63 papers and a tutorial session on "Telco Systems Standardization and Procurement Practices - The Impact of Divestiture" to provide the interest and enthusiasm for the most successful symposium to date. In addition, it is hoped that the move to the MGM Grand Hotel, Reno, with its excellent facilities will provide all the attendees with the comfort and conveniences essential for an enjoyable and productive meeting.

Committee members William Chervenak of Corning Glass Works, Andrew Dunin of DuPont Canada and James Tyler of the Essex Group, are retiring from the committee. Each member contributed significantly to the success of the symposium. On behalf of the committee, I extend to each, a very special thanks for their sincere dedication, cooperation, and support of the symposium objectives and activities. I wish to express my appreciation to all committee members for their dedicated efforts and cooperation and to the individual governmental and industrial organizations that provide technical assistance and/or contributions.

To ensure success in years to come, the committee solicits the continued support of all members of the wire and cable industry. Therefore, comments and suggestions are solicited and warranted from all attendees of the symposium.

The symposium (34th) will return to the Cherry Hill Hyatt Hotel, Cherry Hill, New Jersey in 1985. If this year's symposium in the MGM Grand Hotel, Reno, is successful, as expected, it is anticipated that the 35th symposium (1986) will return to the MGM Grand Hotel in Reno, Nevada.


ELMER F. GODWIN
Director, IWCS

PROCEEDINGS INTERNATIONAL WIRE & CABLE SYMPOSIUM BOUND—AVAILABLE AT FORT MONMOUTH

27th International Wire & Cable Symposium Proceedings—1978—\$8.00
28th International Wire & Cable Symposium Proceedings—1979—\$8.00
29th International Wire & Cable Symposium Proceedings—Not Available
30th International Wire & Cable Symposium Proceedings—1981—\$8.00
31st International Wire & Cable Symposium Proceedings—1982—\$8.00
32nd International Wire & Cable Symposium Proceedings—1983—\$10.00
*33rd International Wire & Cable Symposium Proceedings—1984—\$15.00

*Extra copies: 1-3 \$15.00; next 4-10 \$10.00; next 11 & above \$8.00 each

Make check or bank draft payable in US dollars to the INTERNATIONAL WIRE & CABLE SYMPOSIUM and forward request to:

International Wire & Cable Symposium
US Army Communications-Electronics Command
ATTN: AMSEL-COM-D-4
Fort Monmouth, NJ 07703-5202
USA

PHOTOCOPIES—AVAILABLE AT DEPARTMENT OF COMMERCE

Photocopies are available for complete sets of papers for 1964 and 1966 thru 1982. Information on prices and shipping charges should be requested from the:

US Department of Commerce
National Technical Information Service
Springfield, Virginia 22151
USA

Include Title, Year and "AD" Number

13th Annual Wire & Cable Symposium (1964)	—AD 787164
15th Annual Wire & Cable Symposium (1966)	—AD A006601
16th International Wire & Cable Symposium (1967)	—AD 787165
17th International Wire & Cable Symposium (1968)	—AD 787166
18th International Wire & Cable Symposium (1969)	—AD 787167
19th International Wire & Cable Symposium Proceedings 1970	—AD 714985
20th International Wire & Cable Symposium Proceedings 1971	—AD 733399
21st International Wire & Cable Symposium Proceedings 1972	—AD 752908
22nd International Wire & Cable Symposium Proceedings 1973	—AD 772914
23rd International Wire & Cable Symposium Proceedings 1974	—AD A003251
24th International Wire & Cable Symposium Proceedings 1975	—AD A017787
25th International Wire & Cable Symposium Proceedings 1976	—AD A032801
26th International Wire & Cable Symposium Proceedings 1977	—AD A047609
27th International Wire & Cable Symposium Proceedings 1978	—AD A062322
28th International Wire & Cable Symposium Proceedings 1979	—AD A081428
29th International Wire & Cable Symposium Proceedings 1980	—AD A096308
30th International Wire & Cable Symposium Proceedings 1981	—AD A110859
31st International Wire & Cable Symposium Proceedings 1982	—AD A125662
32nd International Wire & Cable Symposium Proceedings 1983	—AD A136749
Kwic Index of Technical Papers, International Wire & Cable Symposium (1952-1975)	—AD A027558

**Highlights of the 32nd
International Wire and Cable Symposium
November 15, 16, 17, 1983
Hyatt Cherry Hill, Cherry Hill, NJ**



Panel Members—Tutorial Session:
(left to right) Mr. C. E. Gabrielson, Principle Engineer, Ericsson Communication; Dr. R. Jones, Dir. of Engineering, Siecor FiberLan; Dr. D. Hanson, Section Manager, Fiber Optics Products, Hewlett Packard and Mr. H. Dorris, District Manager, Systems Standards AT&T Information Systems.



Committee member Dr. W. Chervenak (center), Corning Glass Works, presenting the awards for Outstanding Technical Paper to (right) Mr. R. H. Whitely, Raychem Ltd. and for Best Presentation to (left) Mr. T. Nishikawa; accepting for Mr. A. Yoshizawa, The Furukawa Electric Co.



Committee member Mr. E. Riley (right), Anaconda-Ericsson, Inc. presenting Retirement Certificate to committee member Mr. J. Brazee (left).



Banquet Guest Speaker—Mr. Vico E. Henriques, President of The Computer and Business Equipment Manufacturers Association (CBEMA)



Advisory member Mr. J. Neigh (right) AMP, Inc., presenting to IWCS Director, Mr. E. Godwin, an award for ten years of service to the symposium.



32nd Annual
INTERNATIONAL
WIRE and CABLE
SYMPOSIUM
1983



AWARDS

Outstanding Technical Paper

- | | |
|---|------|
| H. Lubars and J. A. Olszewski, General Cable Corp.—"Analysis of Structural Return Loss in CATV Coaxial Cable" | 1968 |
| J. P. McGann, R. Sabia and B. Wargotz, Bell Laboratories—"Characterization of Filler and Insulation in Waterproof Cable" | 1969 |
| D. E. Setzer and A. S. Windeler, Bell Laboratories—"A Low Capacitance Cable for the T2 Digital Transmission Line" | 1970 |
| R. Lyenger, R. McClean and T. McManus, Bell Northern Research—"An Advanced Multi-Unit Coaxial Cable for Toll PCM Systems" | 1971 |
| J. B. Howard, Bell Laboratories—"Stabilization Problems with Low Density Polyethylene Insulations" | 1972 |
| Dr. H. Margin, Kabelmetal—"High Power Radio Frequency Coaxial Cables, Their Design and Rating" | 1973 |
| D. Doty, AMP Inc.—"Mass Wire Insulation Displacing Termination of Flat Cable" | 1974 |
| T. S. Choo, Dow Chemical U.S.A.—"Corrosion Studies on Shielding Materials for Underground Telephone Cables" | 1975 |
| N. J. Cogelia, Bell Telephone Laboratories and G. K. Lavoie and J. F. Glahn, US Department of Interior—"Rodent Biting Pressure and Chemical Action and Their Effects on Wire and Cable Sheath" | 1976 |
| Thomas K. McManus, Northern Telecom Canada Ltd. and R. Beveridge, Saskatchewan Telecommunications, Canada—"A New Generation of Filled Core Cable" | 1977 |
| Fumio Suzuki, Shizuyoshi Sato, Akinori Mori and Yoichi Suzuki, Sumitomo Electric Industries, Ltd., Japan—"Microcoaxial Cables Insulated with Highly Expanded Polyethylene By Chemical Blowing Method" | 1978 |
| S. Masaki, Y. Yamazaki and T. Ideguchi, Nippon Telegraph and Telephone Public Corporation, Japan—"New Aluminum Sheath Cable Used for Electromagnetic Shielding" | 1979 |
| P. Kish and Y. LeBorgne, Northern Telecom Canada Limited, Montreal, Canada—"General Crosstalk Model For Paired Communication Cables" | 1980 |
| C. J. Arroyo, N. J. Cogelia, Bell Laboratories, and R. J. Darsey, Western Electric—"Thermal Behavior of Experimental Plenum Cable Sheaths Determined in a Radiant Heat Chamber" | 1981 |
| R. H. Whiteley, Raychem Ltd.—"A Comprehensive Small Scale Smoke Test" | 1982 |
| V. A. Fentress, Raychem Corp. and D. V. Nelson, Stanford University—"Fracture Mechanics Evaluation of the Static Fatigue Life of Optical Fibers in Bending" | 1983 |

Best Presentation

- | | |
|--|--|
| N. Dean, B.I.C.C.—"The Development of Fully Filled Cables for Distribution Network" | |
| J. D. Kirk, Alberta Government Telephones—"Progress and Pitfalls of Rural Buried Cable" | |
| Dr. O. Leuchs, Kable and Metalwerke—"A New Self-Extinguishing Hydrogen Chloride Binding PVC Jacketing Compound for Cables" | |
| S. Nordblad, Telefonaktiebolaget L. M. Ericsson—"Multi-Paired Cable of Nonlayer Design for Low Capacitance Unbalance Telecommunications Network" | |
| N. Kojima, Nippon Telegraph and Telephone—"New Type Paired Cable for High Speed PCM Transmission" | |
| S. Kaufman, Bell Laboratories—"Reclamation of Water-Logged Buried PIC Telephone Cable" | |
| R. J. Oakley, Northern Electric Co., Ltd.—"A Study Into Paired Cable Crosstalk" | |
| G. H. Webster, Bell Laboratories—"Material Savings by Design in Exchange and Trunk Telephone Cable" | |
| J. E. Wimsey, United States Air Force—"The Bare Base Electrical Systems" | |
| Michael DeLucia, Naval Ship Research and Development Center—"Highly Fire-Retardant Navy Shipboard Cable" | |
| William L. Schmacher, AMP Inc.—"Design Considerations for Single Fiber Connector" | |
| Richard C. Mondello, Bell Labs—"Design and Manufacture of an Experimental Lightguide Cable For Undersea Transmission Systems" | |
| I. Wadehra, IBM Corporation—"Performance of Polyvinyl Chloride Communication Cables in Modified Steiner Tunnel Test" | |
| J. J. Refi, Bell Laboratories—"Mean Power Sum Far-End Crosstalk of PIC Cables as a Function of Average Twist Helix Angle" | |
| G. S. Anderson, Belden Corporation—"Installation of Fiber Optic Cable on 457 Meter Tower" | |
| A. Yoshizawa, The Furukawa Electric Co., Ltd.—"Structure and Characteristics of Cables for Robots" | |
| J. R. Bury, Standard Telecommunication Laboratories, Ltd., Hallow, England—"Development of Flame Retardant, Low Aggressivity Cables" | |

CONTRIBUTORS

- A-C Polyethylene**
 Morristown, NJ
AFA Industries
 Garfield, NJ
Alambres y Cables Venezolanos
C.A. "ALCAVE"
 Caracas, Venezuela
Allied Corporation (Engineered Plastics)
 Morristown, NJ
Alpha Wire Corporation
 Elizabeth, NJ
AMP Incorporated
 Harrisburg, PA
Anaconda Wire & Cable Company
 Greenwich, CT
Anixter Bros., Inc.
 Skokie, IL
Arco Chemical Co.
 Philadelphia, PA
Arvey Corporation—Lamcote Division
 Cedar Grove, NJ
Associated Lead Inc.
 Philadelphia, PA
Astro Wire & Cable Corporation
 Worcester, MA
ATC (PTY) Limited
 Brits. Transvaal., South Africa
Austral Standard Cables PTY Limited
 Australia
Badische Corporation
 Williamsburg, VA
Barcel Wire & Cable Corporation
 Irvine, CA
Bayshore Industrial, Inc.
 La Porte, TX
Beacon Reel Co.
 Beacon Falls, CT
Belden Cooper Industries
 Richmond, IN
Belden Technical Research Center
 Geneva, IL
Belding Corticelli Thread Company
 New York, NY
Bell Canada
 Ontario, Canada
Bell Communications Research
 Basking Ridge, NJ
Bentley-Harris Mfg. Co.
 Lionville, PA
Berkshire Electric Cable Co.
 Leeds, MA
Berk-Tek Inc.
 Reading, PA
BICC Telecommunications Cables Ltd.
 Merseyside, England
Borden Chemical—Thermoplastics Div.
 Leominster, MA
Boston Insulated Wire & Cable Company, Ltd.
 Hamilton, Ont., Canada
BRAND-REX Company
 Willimantic, CT
Breen Color Concentrates, Inc.
 Lambertville, NJ
Burgess Pigment Company
 Sandersville, GA
Camden Wire Co., Inc.
 Camden, NY
Canada Wire and Cable Limited
 Winnipeg, Canada
- Carlew Chemicals Ltd.**
 Montreal, Quebec
R. E. Carroll Inc.
 Trenton, NJ
Cary Chemicals Inc.
 Howell, NJ
CasChem, Inc.
 Bayonne, NJ
Chase & Sons Inc.
 Randolph, MA
Chromatics—Colorant Group
 Danbury, CT
Chromatics, Inc.
 Danbury, CT
Ciba-Geigy Corporation
 Hawthorne, NY
Colorant AB
 Knivsta, Sweden
Colorite Plastics Co.
 Ridgefield, NJ
Communications Technology Corporation
 Los Angeles, CA
Conduccion Corporation
 Leominster, MA
Conoco Chemicals
 Houston, TX
Conoco Chemicals
 Saddle Brook, NJ
Corning Glass Works
Telecommunications Products Division
 Corning, NY
Crellin, Inc.
 Chatham, NY
Dainichi-Nippon Cables, Ltd.
 Japan
Davis-Standard Division
Crompton & Knowles Corporation
 Pawcatuck, CT
Dow Chemical U.S.A.
 Midland, MI
Dow Corning Corporation
 Midland, MI
Eastman Chemical Products, Inc.
 Kingsport, TN
The Electric Wire & Cable Co. of Israel Ltd.
 Haifa, Israel
Electrical Wire Products Bay Associates, Inc.
 Menlo Park, CA
EnviroStrand, Inc.
 Leominster, MA
Essex Group
 Decatur, IL
Ethyl Corporation
 Sayreville, NJ
Excelsior Wire Corp.
 Los Angeles, CA
F&G Telecommunication Cables and Systems
A Member of Philips Kommunikations Industrie AG
 West Germany
Facile Technologies, Inc.
 Paterson, NJ
Formulabs Ind. Inks, Inc.
 Escondido, CA
Freeport Kaolin Co.
 Gordon, GA
Fujikura Ltd.
 Tokyo, Japan
Gary Chemical Corp.
 Leominster, MA

Gavitt Wire and Cable Co., Inc.
 Brookfield, MA
Gem Gravure Company
 Hanover, MA
General Cable Co.—Fiber Optics Div.
 Edison, NJ
Global Plastics Polymers Div.
 Leominster, MA
BF Goodrich Company—Chemical Division
 Cleveland, OH
W.L. Gore & Associates, Inc.
 Lakewood, CO
Great Lakes Chemical Corporation
 West Lafayette, IN
Harbour Industries, Inc.
 Arlington, TX
Hitemp Wires
 Bohemia, NY
Hong Kong Telephone
 Hong Kong
Hudson Wire Co.
 Ossining, NY
Ibaraki Electrical Communications Lab.,
Nippon Telegraph & Telephone Public Corp.
 Japan
International Wire Product Company
 Wyckoff, NJ
ITT Surprenant Division
 Clinton, MA
Joyo Bank Ltd.
 Tokyo, Japan
Judd Wire Div., HVE
 Turners Falls, MA
Jutland Telephone
 Denmark
Kables Tapes Ltd.
 Manitoba, Canada
Kenrich Petrochemicals, Inc.
 Bayonne, NJ
Kingsley Machine Co.
 Hollywood, CA
Lamart Corp.
 Clifton, NJ
Lignes Telegraphiques et Telephoniques
 France
J. J. Lowe Associates, Inc.
 Bedford Hills, NY
Lynn Plastics Corporation
 Lynn, MA
M&T Chemicals Inc.
 Woodbridge, NJ
Maillefer Company
 South Hadley, MA
Manning Paper Company
 Troy, NY
Mitsubishi Petrochemical Co., Ltd.
 Japan
Mobay Chemical Corporation
 Pittsburgh, PA
Monsanto Polymer Products Co.
 St. Louis, MO
The Montgomery Co. Canal Bank
 Windsor Locks, CT
Montrose Products Company
 Auburn, MA
Mossberg Industries Inc.
 Cumberland, RI
Neptco Incorporated
 Pawtucket, RI
Nesor Alloy Corporation
 West Caldwell, NJ

The New Brunswick Telephone Co.
 Canada
New Zealand Post Office
 Wellington, New Zealand
NKF Kabel B.V.
 The Netherlands
NKT Electronik
 Denmark
Nokia Inc.
 Atlanta, GA
Northern Telecom Canada Limited
 Montreal, Canada
Northern Telecom—Optical Systems Division
 Kanata, Ontario, Canada
Occidental Chemical Corporation
 Niagara Falls, NY
OKI Electric Cable Co. Ltd.
 Japan
Omego Wire Inc.
 Camden, NY
The Ore & Chemical Corporation
A Member of the Metallgesellschaft Group
 New York, NY
Pantasote Inc.
 Passaic, NJ
Pennwalt Corporation
 Philadelphia, PA
Penreco
 Butler, PA
A.E. Petsche Company, Inc.
 Arlington, TX
Phalo Corporation
 Shrewsbury, MA
Phillips Cables Ltd.
 Vancouver, B.C., Canada
Phillips Chemical Company
 Pasadena, TX
Prestolite
 Sidney, NE
Prestolite Wire
 Sidney, Nebraska, and Port Huron, MI
Raychem Corporation
 Fuquay-Varina, NC
Raychem Corporation
 Menlo Park, CA
Rea Magnet Wire Company, Inc.
 Ft. Wayne, IN
Reichhold Chemicals, Inc.
 Hackettstown, NJ
Reliance Comm/Tec
 Chicago, IL
Walter Rose GmbH & Co. KG
 West Germany
Santech Inc.
 Ontario, Canada
Shell Chemical Company
 Houston, TX
Showa Electric Wire and Cable Co., Ltd.
 Japan
Siecor Corporation
 Hickory, NC
Siemens AG
 Munich, Germany
Siemens AG, NK E LWL
 Germany
Sieverts Kabelverk AB
Hudikvallsfabriken
 Sweden
Sieverts Kabelverk AB
 Sundbyberg, Sweden
Societe Anonyme de Telecommunications
 France

Solem Industries Inc./J.M. Huber Corp.
 Norcross, GA
Soltex Polymer Corporation
 Houston, TX
Southwest Chemical Services Inc.
 Houston, TX
Southwire Company
 Carrollton, GA
Standard Electrica, S.A.
 Santander, Spain
Sterling Davis Electric
 Wallingford, CT
Symplex Wire and Cable Company
 Portsmouth, NH
SYNCRO Machine Company
 Perth Amboy, NJ
Taconic Plastics, Ltd.
 Petersburg, NY
Tamaqua Cable Products Corp.
 Schuylkill Haven, PA
Teknor Apex Co.
 Pawtucket, RI
TELECOM
 Melbourne, Australia
Teledyne Farris Engineering
 Palisades Park, NJ
Teledyne Thermatics
 Elm City, NC
Tensolite Company
Division Carlisle Corp.
 Buchanan, NY
Thermax Wire Corp.
 Flushing, NY
Thomas & Betts—Insulation
Products Division
 Raritan, NJ
3M
 St. Paul, MN

Times Fiber Communications, Inc.
 Wallingford, CT
Torpedo Wire & Strip, Inc.
 Pittsfield, PA
Trea International Ltd.
 North Kingstown, RI
TRW Inc.
 Philadelphia, PA
UBE Industries
 Japan
Union Carbide Corporation
 Danbury, CT
Union Carbide Corporation
 Long Beach, CA
U.S. Industrial Chemicals Co.
 Cincinnati, OH
USS Chemicals Division
 Pittsburgh, PA
Valtec
 W. Woylston, MA
R. T. Vanderbilt Co. Inc.
 Norwalk, CT
The Watson Machine Co.
 Paterson, NJ
Weber & Scher Mfg. Co., Inc.
 Newark, NJ
Whitmor Wire & Cable Corp.
 No. Hollywood, CA
Wilson Fiberfil International
 Neshanic Station, NJ
Wyre Wynd Inc.
 Jewett City, CT
Wyrough and Loser Inc.
 Trenton, NJ
Zumbach Electronics Corp.
 Mount Kisco, NY

TABLE OF CONTENTS

Exposition Topics include:

TUESDAY, NOVEMBER 13, 1984—9:30 AM - 12:00 PM

Grand Ballroom, Hall of Fame Area

Greeting: Mr. Theodore Pfeiffer, Technical Director, US Army Communications-Electronics Command, Fort Monmouth, N.J.

SESSION I: TELCO SYSTEMS STANDARDIZATION AND PROCUREMENT PRACTICES—THE IMPACT OF DIVESTITURE

Chairperson: James Tyler, Essex Group

Panel Members:

Mr. E. J. Cohen, Engineering Management and Standards Engineer, Rural Electrification Administration, Washington, D.C.

Mr. M. Cain, Assistant Manager Technology and Standards, National Communication System, Washington, D.C.

Mr. F. Andrews, V.P. Technology Systems, Bellcore, Red Bank, New Jersey.

Mr. O. J. Gasella, Executive Director, Exchange Carriers Standards Association, Parsippany, New Jersey.

Mr. R. Cole, District Manager, Procurement Administration, Pacific Bell, San Francisco, California.

TUESDAY, NOVEMBER 13, 1984—2:00-5:00 PM

Bijou Complex

SESSION II: FIRE, SMOKE, and TOXICITY TECHNOLOGY

Chairperson: Austin Wetherell, Underwriters Laboratories

Arlyoxphosphazene Elastomers—New Flame Retardant Insulation Materials—*J. T. Books, D. M. Indyke, and W. O. Muenchinger*, Ethyl Corp., Baton Rouge, Louisiana..... 1

Fire Testing of Riser Cables—*L. J. Przybyla*, Underwriters Laboratories, Northbrook, Illinois, *T. J. Guida*, Underwriters Laboratories, Melville, New York, and *J. L. Williams, S. Kaufman*, AT&T Bell Laboratories, Norcross, Georgia..... 5

New Reduced Smoke, Flame Retardant Wire and Cable Formulations Containing Halogenated Additives—*Dr. J. J. Duffy and C. S. Ilardo*, Occidental Chemical Corporation, Niagara Falls, New York..... 14

Parameters for the Assessment of Fire Hazard from Electrical Wires and Cables—*M. M. Khan and A. Tewarson*, Factory Mutual Research Corporation, Norwood, Massachusetts..... 19

The Acid Index—A Property of Polymer Combustion—*P. C. Warren*, Bell Communications Research, Inc., Murray Hill, New Jersey..... 34

Fire Safety of Wire and Cable Materials, Part III: An Approach to Estimating Cable Fire Hazard—*F. B. Clarke and P. J. DiNenno*, Benjamin/Clarke Associates, Inc., Kensington, Maryland..... 40

TUESDAY, NOVEMBER 13, 1984—2:00-5:00 PM

Capitol Rooms

SESSION III: CONNECTORS, SPLICES, ENCLOSURES

Chairperson: William Chervenak, Corning Glass Works

Fully-Automatic Optical Fiber Splice Machine—*R. Arioka, T. Haibara, and M. Tachikura*, Ibaraki Electrical Communication Laboratory, N.T.T., Tokai, Japan..... 50

A Portable Self-Aligning Fusion Splicer for Single-Mode Fibres—*P. V. Andrews, R. Grigsby, R. J. Hazelden, M. T. McDonough and S. Saha*, BICC Research and Engineering Limited, London, England..... 58

Self-Core-Alignment Arc-Fusion Splicer Based on a Simple Local Monitoring Method—*M. Fujise and Y. Iwamoto*, KDD Research & Development Laboratories, Tokyo, Japan..... 67

Statistical Modeling of Mechanical Splice and Connector Losses for Optical Fibers—*D. E. Vokey and T. Goldring*, Siecor Corporation, Hickory, North Carolina..... 76

Improvement of Fiber Reliability in Splice Enclosures Resulting from the Reduction of Relative Movement Between Cable Core and Sheath—*Y. Ishihata, S. Koshika, S. Hasegawa, E. Hayasaka, Y. Tabata and F. Ohtsuka*, Tohoku Electric Power Co., Inc., Sendai, Japan..... 82

A Technique for the Rapid Confirmation of the Water-Tightness of Joined Plant Closures—*H. J. C. Spencer*, Telspec Ltd., Rochester, England..... 92

TUESDAY, NOVEMBER 13, 1984—2:00-5:00 PM

Adelphi Room

SESSION IV: FIBER OPTIC CABLE DESIGN ;

Chairperson: Robert Depp, Defense Electronics Supply Center

Composite Buffering for High Performance Fiber Cables—*P. R. Bark* and *D. O. Lawrence*, Siecor Corporation, Hickory, North Carolina, and *U. Oestreich* and *E. Mayr*, Siemens AG, Munich, West Germany 98

Development of Strain-Free Optical Fiber Cable—*S. Yonechi*, Sumitomo Electric Industries, Ltd., Yokohama, Japan 102

Evaluation of Shrinkage Forces and Thermal Transitions of Fluorinated Ethylene-Propylene (FEP) Cable Insulations and Buffered Optic Fibers at Low Temperatures—*G. L. Grune* and *L. A. Hilliard*, IBM Corp., Research Triangle Park, North Carolina 108

Improved Composite Fiber-Optic Overhead Ground Wire—*Y. Saito*, *M. Ishikawa*, *S. Kawabata*, and *Y. Kitayama*, Sumitomo Electric Industries, Ltd., Yokohama, Japan 118

Progress in the Development of an E-CTFE Jacketed High Temperature Fiber Optic Cable—*D. R. Maack*, EOTec Corporation, West Haven, Connecticut, *S. P. Dudek*, Allied Chemical Co., Morristown, New Jersey, and *T. Allsworth*, Deutsch, Los Angeles, California 123

Applications and Comparative Performance of Lightwave Cable Sheaths—*K. Cornelison* and *M. Fleck*, Anaconda Wire and Cable Company, Overland Park, Kansas 130

WEDNESDAY, NOVEMBER 14, 1984—9:00 AM-12:00 PM

Adelphi Room

SESSION V: CABLE DESIGN AND TESTING I

Chairperson: Joseph McCann, USA CECOM

Composite Conductors for Cable Electromagnetic Compatibility—*D. Chalk*, Brand Rex Company, Willimantic, Connecticut, and *L. E. McBride*, Texas Instruments Inc., Attleboro, Massachusetts 141

The Adaptation of an Air-Dielectric RF Cable for Use as an Oil-Filled High Voltage Pulse Transmission Line—*W. C. Weiss*, *R. L. Copp*, *L. L. Reginato*, and *J. A. Schmidt*, Lawrence Livermore National Laboratory, Livermore, California 146

Filling Compound Flow Test—*C. K. Eoll*, Siecor Corporation, Hickory, North Carolina . 152

Water Blocking Optical Fiber Cable Filled with Grease Compound—*T. Kaneko*, *S. Yamaguchi*, *H. Tanaka*, *T. Maeda*, *Y. Ijiri*, *K. Mio* and *Y. Hayashi*, Dainichi-Nippon Cables, Ltd., Itami, Japan 160

A Highly Effective Approach to Waterproofing Cable—*H. Hughes*, *R. A. Hunn*, and *J. T. Joubert*, South African Inventions Development Corporation, Pretoria, South Africa 166

WEDNESDAY, NOVEMBER 14, 1984—9:00 AM-12:00 PM

Capitol Rooms

SESSION VI: CONNECTORS, SPLICES, ENCLOSURES II

Chairperson: Kazuo Nomura, Sumitomo Electric

Dynamic Splicing of Protected Optical Fibers—*Th. Touchais*, Raychem Pontoise SA, St. Ouen L'Aumone, France, *J. P. Hulin* and *M. De Vecchis*, Thomson/CSF, Conflans Ste. Honore, France 174

Arc Fusion Splicing Machine with an Application of Local Monitoring Method—*N. Hakamata*, *S. Suzuki*, *Y. Usui*, and *T. Kakii*, Sumitomo Electric Industries, Ltd., Yokohama, Japan 184

Short-Haul Fiber-Optic-Link Connector Loss—*D. H. Rice* and *G. E. Keiser*, GTE Government Systems Corporation, Needham Heights, Massachusetts 190

Field Usable Single Mode Fibre Splicing Applying Local Core Alignment—*C. M. de Blok* and *P. Matthijsse*, PTT, Dr. Neher Laboratories, Leidschendam, Netherlands... 193

A Customer Designed Splice Closure—*G. S. Cobb*, *J. F. Malluck*, *J. R. Massey* and *A. H. Williamson, Jr.*, AT&T Bell Laboratories, Norcross, Georgia 197

WEDNESDAY, NOVEMBER 14, 1984—2:30 PM-5:30 PM

Adelphi Room

SESSION VII: CABLE DESIGN AND TESTING II

Chairperson: James Tyler, Essex Group

Bonded ASP: A Superior Sheath for Buried and Underground Filled Cables—*D. M. Mitchell* and *R. P. Collins*, AT&T Bell Laboratories, Norcross, Georgia, *D. E. West* and *M. D. Kinard*, AT&T Technologies, Inc., Norcross, Georgia 207

Advancement in Pulp Cable Design and Manufacture—*P. P. Kish* and *P. A. McGettigan*, Northern Telecom Canada Limited, Montreal, Quebec 213

Digital Pulse Transmission Characteristics of Inside Wire and Cable— <i>J. C. Hyder</i> and <i>J. T. Loadholt</i> , AT&T Bell Laboratories, Norcross, Georgia	220
Digital Performance of Metallic Twisted Pair Transmission Media— <i>J. W. Kincaid, Jr.</i> and <i>D. Johnson</i> , Belden Technical Research Center, Geneva, Illinois	228
The Inelastica: The Effect of Internal Friction on the Shape and Tension of a Bent Cable— <i>A. L. Hale</i> , AT&T Bell Laboratories, Whippany, New Jersey	237

WEDNESDAY, NOVEMBER 14, 1984—2:30 PM-5:30 PM

Capitol Rooms

SESSION VIII: Fiber Optic Cable Design and Single-Mode Fiber System

Chairperson: George Webster, Bell Laboratories

Development of Radiation Resistant Multi-Fiber Optical Cable Incorporating Graded Index Type Fibers— <i>M. Dazai</i> , <i>H. Yokota</i> , <i>M. Nakasuji</i> , <i>H. Horima</i> and <i>M. Watanabe</i> , Sumitomo Electric Industries, Ltd., Yokohama, Japan	244
--	-----

Environmental Characteristics of Optical Fiber Cable for Use in Nuclear Power Plants— <i>K. Shibuya</i> , <i>S. Ohashi</i> , <i>Y. Kumazawa</i> , <i>F. Nakane</i> and <i>T. Kojima</i> , Showa Electric Wire and Cable Co., Ltd., Kanagawa, Japan	251
--	-----

Fiber Optic Cable for Applications in Thermal Radiation Environments— <i>G. Anderson</i> , <i>J. C. Smith</i> , <i>J. McAlarney</i> , ITT Electro-Optical Products Division, Roanoke, Virginia, <i>S. Share</i> and <i>A. Baba</i> , Harry Diamond Laboratory, Adelphi, Maryland	258
--	-----

Bandwidth and Cut-Off Wavelength of Single-Mode Lightguide-System Considerations— <i>R. W. Tarwater</i> , AT&T Bell Laboratories, Norcross, Georgia, <i>M. J. Maslaney</i> , Tau-Tron, Inc., Norcross, Georgia, <i>D. L. Philen</i> and <i>F. T. Stone</i> , AT&T Bell Laboratories, Norcross, Georgia, and <i>D. G. Duff</i> , AT&T Bell Laboratories, Holmdel, New Jersey	261
---	-----

Deterioration of the Signal Quality in Realistic Single-Mode Fiber Systems— <i>S. Heckmann</i> , Philips Kommunikations Industrie AG, Cologne, West Germany	266
---	-----

Describing Dispersion in Concatenated Single-Mode Fiber Cables— <i>T. C. Olson</i> , <i>F. P. Kapron</i> , and <i>T. W. Geyer</i> , ITT Electro-Optical Products Division, Roanoke, Virginia	276
--	-----

THURSDAY, NOVEMBER 15, 1984—9:00 AM-12:00 PM

Adelphi Room

SESSION IX: CABLE MATERIALS AND PROCESSING

Chairperson: Andrew Dunin, Dupont Canada

Effect of Screw Designs on Quality and Rate of Flexible PVC Compounds— <i>H. T. Kim</i> , BF Goodrich Company, Avon Lake, Ohio	283
--	-----

Ultra-High Speed Extrusion of Highly Expanded Polyethylene Insulation for Communication Cables— <i>Y. Morita</i> , <i>T. Takai</i> , <i>S. Yamaguchi</i> , Dainichi-Nippon Cable, Ltd., and <i>K. Nishida</i> , Mitsubishi Petrochemical Co., Ltd., Mie, Japan	287
--	-----

High Speed Miniature Coaxial Cable Insulated with Highly Expanded Irradiated Polyolefin— <i>F. Suzuki</i> , <i>T. Komura</i> , and <i>A. Mori</i> , Sumitomo Electric Industries, Ltd., Tochigi, Japan	300
--	-----

Computer Prediction of Coaxial Cable Structural Return Loss During Core Extension— <i>L. Visser</i> , Belden, Geneva, Illinois	308
--	-----

Multipulling and Cabling in Line: A New Process— <i>A. Gouronnec</i> , <i>G. Le Noane</i> , <i>P. Grosso</i> , <i>P. Valette</i> , <i>Y. Guegan</i> , and <i>A. Benoist</i> , CNET/Lannion B, LAB/ROC/FCO, Lannion, France	316
--	-----

THURSDAY, NOVEMBER 15, 1984—9:00 AM-12:00 PM

Capitol Room

SESSION X: UNDERCARPET, INTEROFFICE CABLE

Chairperson: William Chervenal, Corning Glass Works

Developments of Undercarpet Data Transmission Cables— <i>T. Yamamoto</i> , <i>N. Hirasaka</i> , <i>H. Yokosuka</i> , and <i>K. Seto</i> , Fujikura Ltd., Tokyo, Japan	324
---	-----

A Hybrid Local Area Network CSMA/CD Method by Using Optical Fiber and Coaxial Cables— <i>Y. Enomoto</i> , <i>J. Kikuchi</i> , <i>T. Takahashi</i> , <i>K. Negishi</i> , <i>T. Kato</i> , and <i>S. Ishikawa</i> , The Furukawa Electric Co. Ltd., Tokyo, Japan	331
--	-----

Plenum, Small-Diameter Optical Fiber Cable— <i>O. Ichikawa</i> , <i>Y. Saito</i> , <i>T. Ono</i> , <i>S. Tanaka</i> , and <i>A. Mori</i> , Sumitomo Electric Industries, Ltd., Yokohama, Japan	338
--	-----

Optical Fiber Under-Carpet Cable System— <i>K. Omae</i> , <i>F. Takahashi</i> , <i>A. Otake</i> , <i>M. Nomura</i> , and <i>T. Mishima</i> , The Furukawa Electric Co., Ltd., Tokyo, Japan	345
--	-----

Optimizing Short Distance Fiber Optic Links:
A Real World Approach—*D. R. Maack* and *J. J. Magera*, EOTec Corporation, West Haven,
Connecticut 351

THURSDAY, NOVEMBER 15, 1984—2:00 PM-5:00 PM

Adelphi Room

SESSION XI: FIBER OPTIC APPLICATIONS AND
INSTALLATIONS

Chairperson: Eugene Riley, Anaconda-Ericsson,
Inc.

Design of Customer Premises Fiber Optic
Cables—*J. T. Loadholt* and *T. M. Williamson*,
AT&T Bell Laboratories, Norcross, Georgia .. 357

The Clarification of Movement of Non-Me-
tallic Self-Supporting Optical Cable
Caused by Wind and the Design of Its In-
stallation at Steel Pylons—*E. Hayasaka*, *Y. Ishihata*, Tohoku Electric Power Co., Inc.,
Sendai, Japan, *H. Horima*, *S. Hisano*,
Sumitomo Electric Industries, Ltd.,
Yokohama, Japan, *T. Shishido* and *T. Omori*,
Kitanihon Electric Wire Co., Ltd., Sendai,
Japan..... 365

Computerised Method of Predicting Cable
Pulling-In Tensions—*J. Macaulay*, British
Telecommunications plc, Wembley, England 372

Digital Transmission System by Optical
Fibers Lashed to the Ground Wire of High
Tension Lines—*C. G. Cortines*, *F. J. Saez de la Maza*, and *F. Gomez Martin*, Standard Elec-
trica, S.A., Santander, Spain 380

Tactical Fiber Optic System Re-
quirements—*V. E. Kalomiris*, U.S. Army
Communications-Electronics Command, Fort
Monmouth, New Jersey 388

Optical Submarine Cable with Stress Free
Fibers Even at Extreme Levels of Cable
Elongation—*H. Damsgaard*, *A. B. Sørensen*,
Ax. Andersen, *N. Enggaard*, *L. Grüner-Nielsen*
and *H. Rosendal*, NKT Elektronik, Glostrup,
Denmark 395

THURSDAY, NOVEMBER 15, 1984—2:00 PM-5:00 PM

Capitol Rooms

SESSION XII: FIBER OPTIC MATERIALS AND
TESTING

Chairperson: John Thompson, Nokia, Inc.

Hydrogen Evolving Tendencies of Cable
Fillers and Optical Fiber Coatings—*W. E. Dennis*, *D. A. Sierawski*, and *D. N. In-
gebrigtsen*, Dow Corning Corporation,
Midland, Michigan 401

Qualification Testing of Fiber Optic
Cables—*R. Ohlhaber*, *P. Angeles*, and *T. Uli-
jasz*, Belden, Technical Research Center,
Geneva, Illinois 409

Prevention of Hydrogen Gas Induced Loss in
Optical Fibers by Proper Lightguide Cable
Design—*D. L. Philen* and *C. H. Gartside, III*,
AT&T Bell Laboratories, Norcross, Georgia .. 415

A Product Assurance Program for Fiber Op-
tics—*R. E. Depp*, *B. P. McNicholl*, and *J. F. Raye*, Defense Electronics Supply Center,
Dayton, Ohio 419

Cable Design to Minimize Hydrogen-Induced
Attenuation Increases in Optical Fiber—*K. Abe*, *R. Lowe* and *E. Thomson*, Northern
Telecom Optical Systems Division, Kanata,
Ontario, Canada 424

ARYLOXPHOSPHAZENE ELASTOMERS -
NEW FLAME RETARDANT INSULATION MATERIALS

J. T. Books, D. M. Indyke and W. O. Muenchinger

Ethyl Corporation
Baton Rouge, Louisiana

Abstract

Aryloxyphosphazene polymers offer a versatile new chemistry which is finding applications in the field of flame retardant, low smoke wire and cable coatings. A wide variety of chemical species may be attached to the $[-P=N-]$ backbone, providing a range of thermal, mechanical, and flammability properties. In particular, mixed phenoxy, p-ethylphenoxy substituents give a nearly halogen-free elastomer with an oxygen index of 28 and glass transition temperature of -18°C . Compounds based on this polymer char in a flaming environment without dripping or flowing and produce combustion products with low toxicity. These materials have excellent solvent resistance and satisfactory electrical insulation values. High strength, commercially viable compounds have now been developed.

History¹

The progression toward the current commercial and developmental polyphosphazene products began over a century ago. Polymers based on the $[-P=N-]$ repeating unit were discovered around the mid 1800's when the cyclic structure, $(\text{NPCl}_2)_3$, or "trimer", was found among the products of a reaction between ammonia and phosphorus pentachloride (PCl_5). In 1897, H. N. Stokes synthesized the first linear phosphazene high polymer, $(\text{NPCl}_2)_n$, or chloropolymer, which he described as "inorganic rubber".² Raw chloropolymer is strong and very elastic but gradually loses its rubbery qualities when exposed to atmospheric moisture.

In the 1960's, several investigators found that the chlorine atoms could be replaced with certain organic groups to give hydrolytically stable polyorganophosphazenes. Soon many different compositions were discovered, all based upon the phosphorus-nitrogen backbone. Subsequent development has shown the utility of these polymers for many applications.

Early in the 1970's, Horizons Research, Inc., under contract to the U.S. Navy, began working on inherently flame-retardant, low toxicity wire and cable compounds based on phosphazene polymers. Some filled poly (aryloxyphosphazene) compositions for wire coverings were disclosed in a 1978 patent assigned to The Firestone Tire & Rubber Co.³ Firestone commercialized the first polyphosphazene product, PNF®, phosphonitrilic fluoroelastomer, in the late 1970's. The Ethyl Corporation obtained an exclusive world wide license for phosphazene polymer technology and patents from Firestone in 1983. Ethyl Corporation is now developing polyphosphazenes for several application areas, including the wire and cable field. Ethyl has announced a plant to produce phosphazene polymers which is scheduled for start-up in early 1985.

Chemistry

Linear phosphazene high polymers are classically made from cyclic trimer. A catalyst or heat induces polymerization of the trimer rings to form chloropolymer chains. The chlorine atoms are subsequently replaced with organic groups. Many organic groups can be used. Mixtures of groups are used to make polymers with elastomeric properties. Obviously many combinations are possible. Both plastic and elastomeric resins with a wide range of thermal, mechanical, and flammability properties have been prepared.

A particular, poly (phenoxy, p-ethylphenoxy phosphazene), which will hereafter be referred to by the generic designation for poly (aryloxyphosphazenes), PZ (as per ASTM D1418), is a composition of significant interest for the development of wire and cable covering compounds. PZ is a peroxide-curable elastomer with a glass transition temperature of -18°C and a limiting oxygen index (LOI) of 28⁴. PZ tailored for wire and cable use can be virtually halogen-free and has low toxicity and corrosivity of combustion off-gases. The combination of high LOI and low toxicity and corrosivity are highly

desirable characteristics for electrical insulation applications that must take into account the current concerns about fire safety of polymeric materials.

Compounds and Properties

The early work by Horizons Research⁴⁻⁶ resulted in two different PZ compounds that were labelled "wire covering" and "cable covering". The reported properties of each are listed below:

	Cable Covering	Wire Covering
Tensile Strength, psi	1,000	760
Elongation at break, %	140	135
LOI, ASTM D2863	47	38
Flame Spread Index, ASTM E162	6	8
NBS Smoke Density, D_{mc} :		
Smoldering	18	20
Flaming	49	75
Dielectric Strength, V/mil	>730	>870
Dielectric Constant at 10^4 Hz	-	4.98
Dissipation Factor at 10^4 Hz	-	0.0233

The initial development work by Ethyl yielded a compound with higher tensile strength. Extrudability on conventional equipment was also demonstrated.

Tensile Strength, psi	1270
Elongation at break, %	105
NBS Smoke Density, D_{mc} :	
Smoldering	65
Dielectric Strength, V/mil	1000
Dielectric Constant at 10^4 Hz	4.7

Although this compound demonstrated outstanding resistance to fire, low smoke generation and excellent processing characteristics, its overall "toughness" was deemed inadequate for most applications.

The Naval Sea Systems Command has prepared a specification (MIL-C-24640) which includes requirements for fire resistant, low halogen jacket materials. Previous PZ compounds fell significantly short of the 1300 psi tensile strength, 160% minimum elongation and 35 ppi tear strength required in this specification. Recently, significant progress has been made toward meeting these requirements. New PZ compounds with tear strengths above 40 ppi, 200% and higher elongations, and tensile strengths up to 1700 psi have been prepared. Electrical properties include:

4.0 dielectric constant at 10^4 Hz, 0.02 dissipation factor at 10^4 Hz, and volume resistivity of 1×10^{14} ohm-cm.

PZ wire and cable coating compounds have significant resistance to attack by many functional fluids. In side by side tests, PZ performed very well compared to other materials:

	PZ	CR*	CSM*	ANM*
% Weight Change after 24 hrs. @ 100°C in:				
ASTM Oil #1	+ 0.8	- 0.5	- 6.3	+ 0.6
ASTM Oil #2	+ 2.4	+19.8	+2.7	+ 7.9
ASTM Oil #3	+11.4	+44.0	+16.1	+20.7
After 24 hours @ 23°C in Isopropyl Alcohol:				
% Weight Gain	3.7			
% Retention Tensile Strength	98			
% Retention Elongation	57			

After 24 hours @ 23°C in Monsanto CoolanolTM 25 Fluid:

% Weight Gain	4.8
% Retention Tensile Strength	87
% Retention Elongation	95

After 24 hours @ 50°C in MIL-H-5606 Hydraulic Fluid:

% Weight Gain	23
% Retention Tensile Strength	74
% Retention Elongation	94

* CR = Polychloroprene
CSM = Chlorosulfonated Polyethylene
ANM = Copolymer (of) ethylene and methyl methacrylate

Fire Retardance and Combustion Toxicity

The phosphorus-nitrogen combination that forms the polymer backbone gives the organophosphazene molecule its inherent flame resistance. Uncompounded PZ has an LOI of 28 and is self-extinguishing under ambient conditions. Compounding techniques can be used to raise the LOI further. Compounds can be designed to char rather than drip or flow when exposed to flame. The residue that is left after combustion could help to preserve circuit integrity.

The toxicity of combustion products of poly (aryloxyphosphazenes) has been studied by Magill, Alarie, and coworkers, as reported in a series of papers from 1978-1980⁷⁻¹⁰. Extensive testing was conducted on foams and cured slabs, including thermo-gravimetric analyses, flame spread, smoke density and LOI measurements, as well as exposure of small animals to combustion gases. These researchers rated the poly (aryloxyphosphazene) compounds on relative toxicity scales. These studies indicated that the combustion products of PZ were less toxic than most other materials studied⁹.

Processing of Poly (Aryloxyphosphazene) Compounds

PZ compounds can be easily processed on conventional equipment. Extrusion onto bare wire has been done without difficulty using a standard single screw extruder with a crosshead die. Processing temperatures of about 100°C are recommended. Limited Instron capillary rheometer tests of PZ compounds at shear rates up to 3000 s⁻¹ indicate melt fracture at 50°C but not at 90°C. The proper choice of a peroxide curing agent provides a combination of sufficient scorch safety, fast cure, and non-irritating vulcanization products. Laboratory compression molding of slab samples is complete in 15-20 minutes at 177°C. PZ compounds have not been tested in continuous vulcanization systems. Conventional steam continuous vulcanization and salt bath curing are expected to yield satisfactory results.

Future Directions

The composition, poly (phenoxy, p-ethylphenoxy phosphazene), can provide a beneficial range of properties in wire and cable applications. Many other poly (organophosphazene) structures are possible. Polymers containing different organic side groups are being evaluated.

Other compounding techniques are being explored. Compositions with combined prop-

erties of 1650 psi tensile strength, 490% elongation and 34 ppi tear strength have been prepared.

Significant progress has recently been made toward preparing phosphazene polymers and compositions which exhibit useful combinations of physical, electrical, and fire safety properties. Additional progress can be expected as we gain experience with this new class of polymers.

Acknowledgement

The authors are indebted to their colleagues at Ethyl Corporation, Dr. F. A. Pettigrew, G. S. Lum, W. B. Mueller, P. Robertson, and J. Arroave for their contributions to this work.

References:

1. H. R. Allcock, "Phosphorus-Nitrogen Compounds", Academic Press, New York 1972
2. H. N. Stokes, Amer. Chem. J., 19, 1782 (1897)
3. J. C. Vicic and K. A. Reynard, U.S. Patent No. 4,120,838
4. J. C. Vicic and K. A. Reynard, "Polyphosphazene Wire Coverings", Naval Ship Engineering Center, Contract N00024-75-C-4402, Horizons, Inc., Cleveland, Ohio, June, 1976
5. J. C. Vicic and K. A. Reynard, "Polyphosphazene Wire Coverings", Naval Ship Systems Command, Contract No. N00024-75-C-4402, Horizons, Inc., Cleveland, Ohio, November, 1975
6. T. C. Peterson, "Polyphosphazene Wire and Cable Insulation", Naval Sea Systems Command, Contract No. N00024-78-C-4644, Horizons Research Inc., Cleveland, Ohio, December, 1979
7. K. Sebata, J. H. Magill, and Y. C. Alarie, Journal of Fire & Flammability, 9, 50 (January, 1978)
8. S. V. Peddada and J. H. Magill, Journal of Fire & Flammability, 11, 63 (January, 1980)
9. P. J. Lieu, J. H. Magill, and Y. C. Alarie, Journal of Fire and Flammability, 11, 167 (July, 1980)

10. P. J. Lieu, J. H. Magill, and Y. C. Alarie, Journal of Combustion Technology, 7, 143 (August, 1980)



J. T. (Jeff) Books earned both a B.S. and M.S. in Chemistry from The Virginia Polytechnic Institute and State University. Prior to joining Ethyl, he was employed by Akzona, working in polymer research. Currently he is a Senior Polymer Applications Chemist in the Materials Research and Applications Section at Ethyl and has spent the past two years working on the development of applications for phosphazene polymers.



W. O. (Bill) Muenchinger is Manager - Polymers in the Commercial Development Section of Ethyl R&D. He received his B.S. degree in Chemical Engineering from The University of Michigan and was employed by Morton International prior to joining Ethyl.



D. M. (David) Indyke is an Applications Engineer in the Materials Research and Applications Section at Ethyl Corporation, Baton Rouge, La. He joined Ethyl after receiving a B.S. degree in Chemical Engineering from Rutgers University in 1979 and has worked in general chemical process and development, polymerization research, and plastic and elastomer applications development.

FIRE TESTING OF RISER CABLES

L. J. Przybyla
Underwriters Laboratories
Northbrook, Illinois

T. J. Guida
Underwriters Laboratories
Melville, New York

J. L. Williams
S. Kaufman
AT&T Bell Laboratories
Norcross, Georgia

ABSTRACT

A vertical riser fire test has been developed to evaluate cables for Classification in accordance with the vertical fire spread requirements of the 1984 National Electrical Code. The test simulates a cable installation in a riser shaft with exposure to a large fire source. A variety of copper conductor cables and optical fiber cables were tested. Some cables exhibited only minor flame propagation and are now Classified by Underwriters Laboratories for use in riser shafts.

INTRODUCTION

Cables should be designed and installed so they do not spread fire through a building. This common-sense notion is expressed in several parts of the 1984 National Electrical Code. Paragraph 800-3(b) of the Code covers communications circuits in vertical runs and states that:

"Communications wires and cables, both metallic conductor and optical fiber types, in a vertical run in a shaft shall be listed as having fire-resistant characteristics capable of preventing the carrying of fire from floor to floor."*

The term "listed" is defined in the Code. Part of the definition is, "Equipment or materials included in a list published by an organization acceptable to the authority having

jurisdiction and concerned with product evaluation...". One such organization is Underwriters Laboratories, which is now Classifying communications cables in accordance with this requirement.

This paper reports on the development of a test for evaluating the flame propagation of cables installed in vertical runs and on the performance of different constructions of communications cables. The cables tested were copper conductor and optical fiber cables, so-called "riser" cables, as well as "station cables" and cables which could also be installed in air handling plenums.

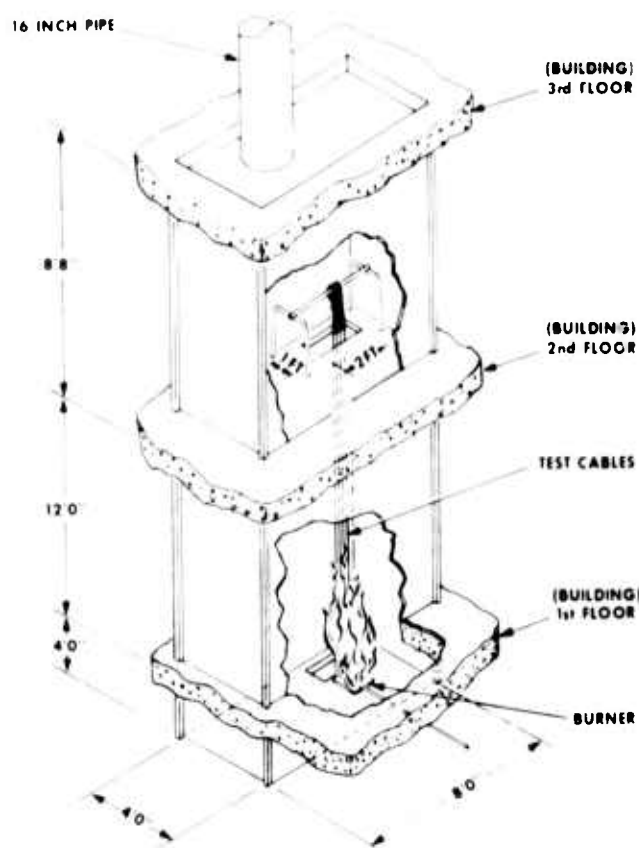
Much of the background research for the development of the test has been previously reported.¹ First, a survey of telephone riser shafts was conducted to determine the typical shaft construction, number of cables and fuel load. A typical shaft was found to be a series of vertically aligned rooms, connected by holes or slots through each floor for passage of cable. Based on the survey results, a fire test facility was built that modeled one story of a typical riser shaft in size and shape. Although holes are more common than slots in shaft rooms, slots were used in the test facility because a slot offers more opportunity for fire propagation because of its larger open area.

A propane burner flame was used to simulate a fire from combustibles which may be present in a shaft room. The size of the flame was chosen to be large enough to rapidly ignite the cables but not cause fire propagation from floor to floor in the absence of cables. Preliminary work demonstrated that a 145 kW propane flame met these criteria. This test flame produced a temperature of approximately 230°C at the upper slot in the ceiling of the test room, which is slightly below the flash ignition temperature of wood.

*Similar requirements are contained in Article 760 - Fire Protective Signaling Systems (Section 760-28(b) (4) and Article 770 - Optical Fiber Cables (Section 770-6).

FIRE TEST FACILITY

The fire tests were conducted inside a test enclosure consisting of two compartments, one for testing and the other for observation and smoke collection (Fig. 1). The test compartment was 4 feet by 8 feet by 12 feet high. Vertically aligned rectangular slots, 1 foot by 2 feet, were located in both the floor and the ceiling near one corner. The observation and collection compartment was located above the test compartment and was 4 feet by 8 feet, but only 8 feet, 8 inches high. A 16 inch diameter exhaust duct was located in the roof. The exhaust was natural convection. The test enclosure was located inside of a laboratory building.



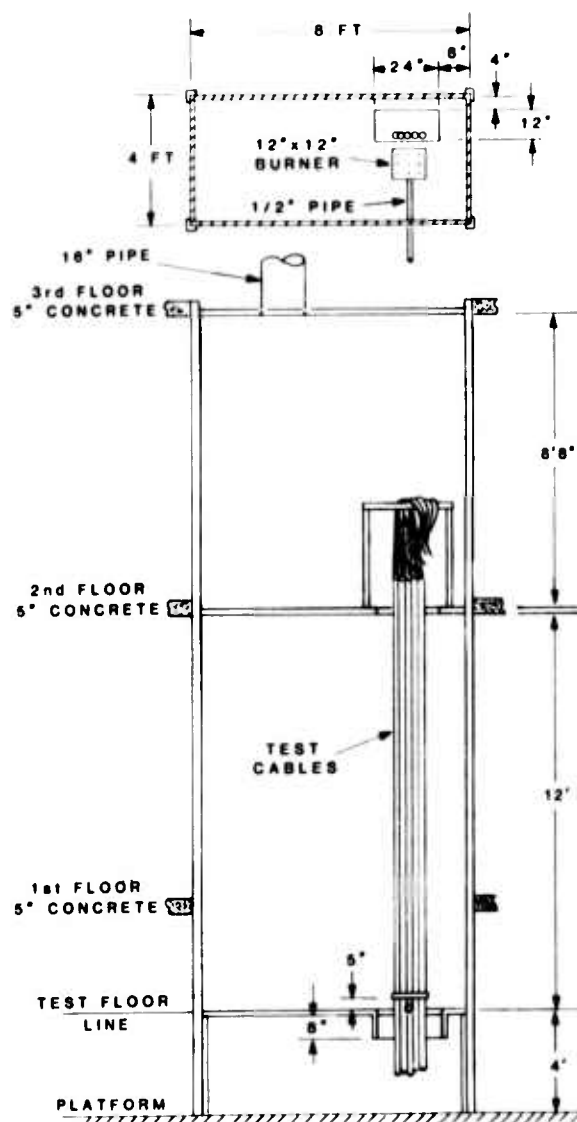
FIRE TEST FACILITY - SIMULATED RISER SHAFT

FIGURE 1

The burner apparatus for the ignition flame consisted of a 1/2 inch diameter steel pipe with a diffusion plate. The plate was 12 inches square and formed from 1/4 inch thick cold rolled steel with nine 1/2 inch diameter holes (Fig. 2). The plate was placed 3-3/4 inches above the end of the pipe.

TEST METHOD

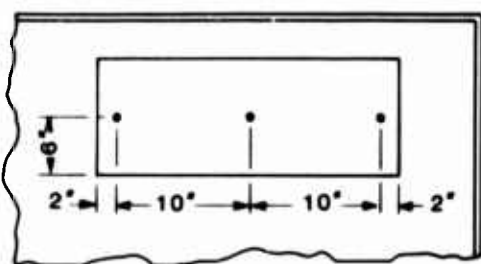
For each test, multiple 16 foot cable pieces were installed through the slots and fastened at the top and bottom as shown in Figure 2. A sufficient number of pieces were used to make a single layer of cables, approximately 1 foot wide (Tables I and II). This sample procedure was selected after developmental tests showed that flame propagation was greater for samples consisting of a single layer than a sample of a few 3 inch diameter bundles of cable pieces.



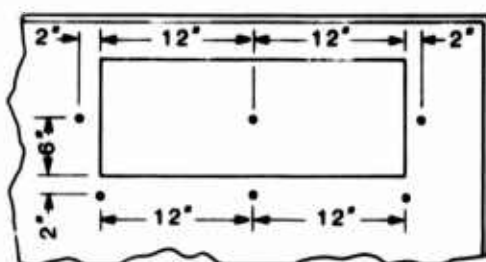
SCHEMATIC OF FIRE TEST FACILITY SHOWING PLACEMENT OF BURNER AND CABLES

FIGURE 2

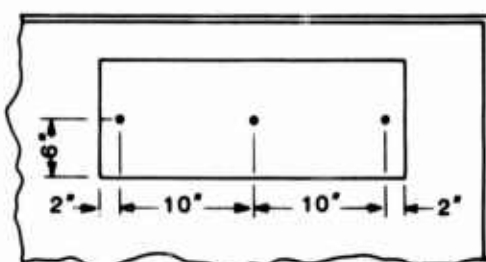
The air velocity through the test chamber, as measured at the bottom slot, varied from 3 to 4 m/s due to the ignition flame, natural convection and test facility design. A temperature of $75 \pm 10^\circ\text{F}$ was established inside the enclosure prior to each test. For supplemental information, thermocouples were used to measure temperatures at different locations within the test enclosure. The locations of these thermocouples are shown in Figure 3.



THERMOCOUPLES 12" ABOVE SLOT



THERMOCOUPLES 2" ABOVE SLOT



THERMOCOUPLES 3" BELOW SLOT

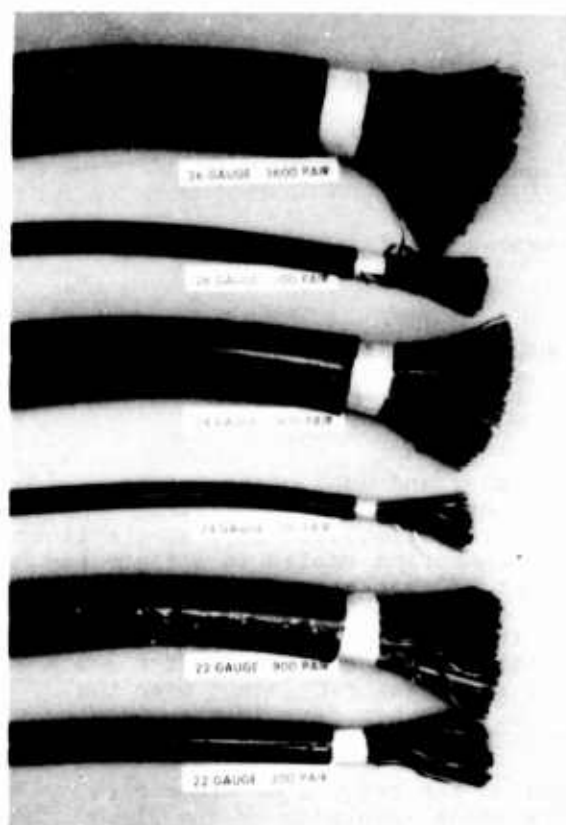
THERMOCOUPLE LOCATIONS - SECOND FLOOR SLOT

FIGURE 3

The flow rate of propane to the burner was established as 211 ± 11 SCFL. The maximum flame height of the burning cables as determined by visual observation was recorded at least every minute. Each test was continued for 30 minutes, unless the sample was consumed before that time, in which case, the test was terminated. After each test, the maximum cable damage height was recorded.

CABLES TESTED

The riser cables tested (Figure 4) had a flame retardant PVC jacket adhesively bonded to a corrugated aluminum shield. The copper wires were insulated with a dual insulation of foamed high density polyethylene with a PVC skin, and the core was covered with composite wrap of polypropylene film and nonwoven polyester. These cables were made with 22, 24 or 26 AWG copper conductors, and pair sizes ranging from 100 to 3600. The smallest and largest cable in each gauge was tested. The development of the materials and construction of these cables are described in the paper by Dillow and Dougherty.²

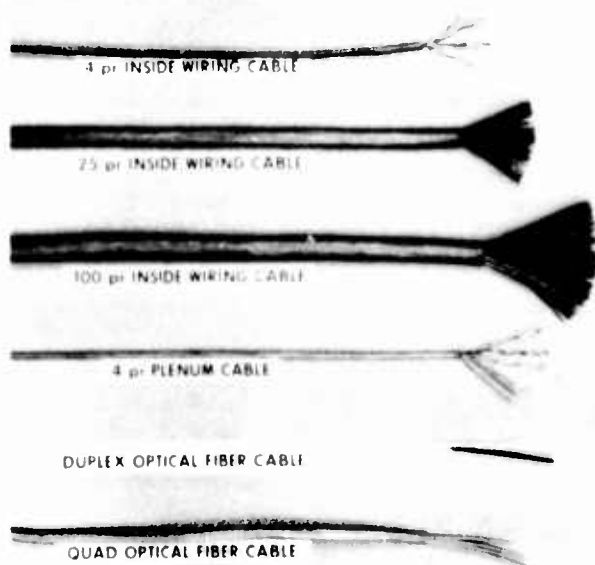


RISER CABLES TESTED

FIGURE 4

The inside wiring cables (Figure 5) had 24 gauge copper conductors insulated with a flame retardant semirigid PVC insulation and jacketed with a flame retardant flexible PVC jacket. The development and fire properties of these cables have been described by Kaufman and Landreth,³ and by Kaufman and Yocum.⁴

The plenum cables (Figure 5) had the same PVC insulated wires as inside wiring cable, a nonwoven aramid thermal wrap and a polyvinylidene fluoride jacket. Some of the characteristics of this cable have been published by Arroyo and Bursh.⁵



BUILDING DISTRIBUTION CABLES TESTED
FIGURE 5

The duplex and quad optical fiber interconnection cables (Figure 5) had two or four, respectively, single fiber interconnection cables in a flame retardant PVC jacket. The single fiber cable had a flame retardant PVC buffer over the coated fiber, an aramid strength member over the buffer and a flame retardant PVC jacket over the aramid. Further details are given by Loadholt and Williamson.⁶

Based on the results of other fire tests and a knowledge of the flame retardant properties of the materials used in the cables, we anticipated the following rank ordering of performance of the copper cables:

Plenum cable was expected to have the least amount of flame propagation since it is UL Classified to a demanding flame spread requirement, viz., no more than 5 feet⁷ in the UL 910 test.^{8,9}

The PVC jackets on the inside wiring cable and riser cable had the same degree of flame retardation. The insulation on the conductors for the inside wiring cable was flame retardant PVC, whereas the insulation on the conductors for the riser cable was about 60 percent of this PVC and 40 percent foamed polyethylene.² Since the insulation of the inside wiring conductors had a higher degree of flame retardation than the insulation of the riser conductors, it was anticipated that the inside wiring cables would exhibit less flame propagation than similarly sized riser cables.

The optical fiber interconnection cables utilized a more flexible (and hence slightly less flame retardant) jacket than inside wiring cable, which would make these cables less flame retardant than they would otherwise be if they utilized the same jacket as inside wiring cable. On the other hand, these optical fiber cables contained no metallic members which could conduct heat and more quickly pyrolyze the jacket in front of the flame and thereby promote flame propagation along the cable.

RESULTS

Figures 6-8 show the flame height versus time curves for the three large riser cables. Since each test was run in triplicate, three curves are shown in each figure. The ignition flame was approximately 4 feet high; at the beginning of each test, it was close to, but not impinging on the cables. Consequently, all of the flame height versus time curves exhibit a short delay before the flame propagated up the first 4 feet of cable. The large riser cables all exhibited low values of peak flame height of 8.5 feet or less.

Figures 9-11 show the results for the three small riser cables. In general, these cables exhibited higher peak flame heights than the larger riser cables. Two cables did not propagate flames through the upper slot (100 pair, 24 gauge; 200 pair, 22 gauge). The 300 pair, 26 gauge cable was tested four times; in three of the tests flames propagated through the upper slot, and in the remaining test, the peak flame height was only 8 feet.

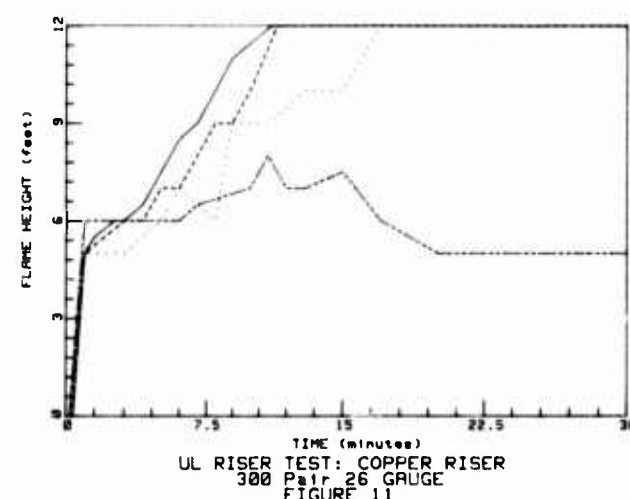
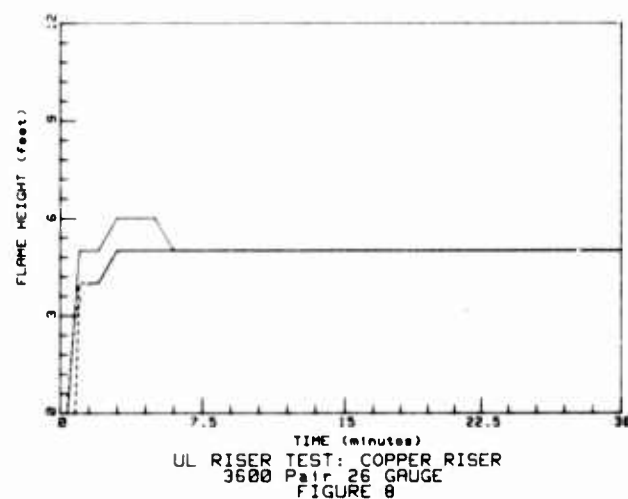
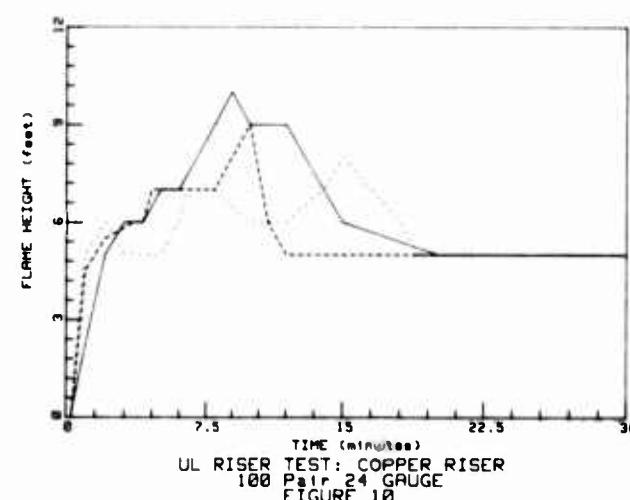
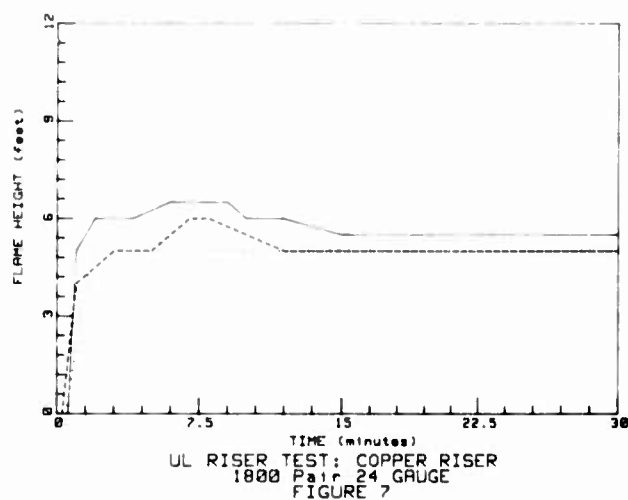
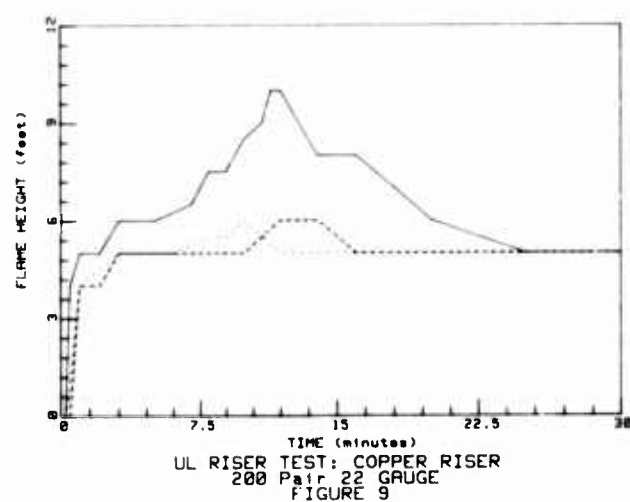
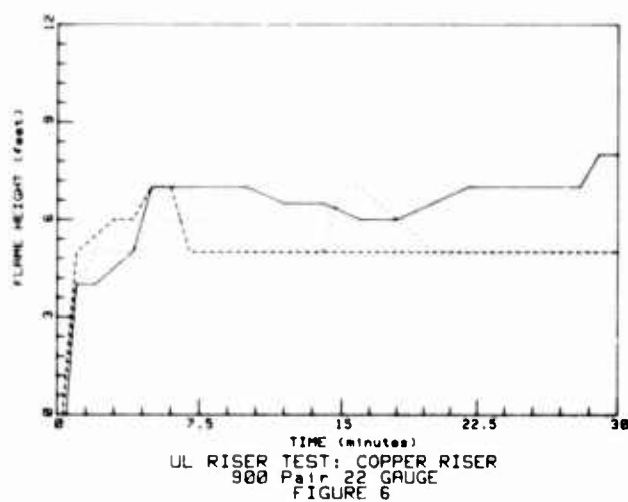
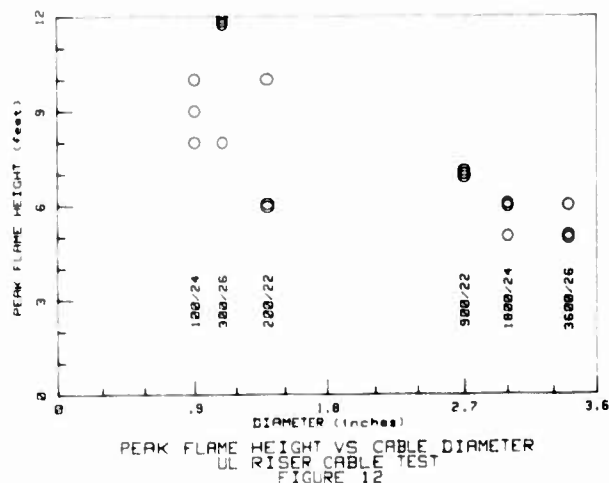
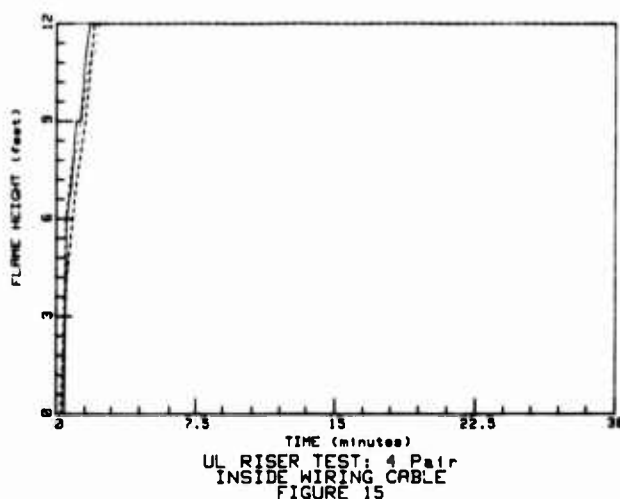
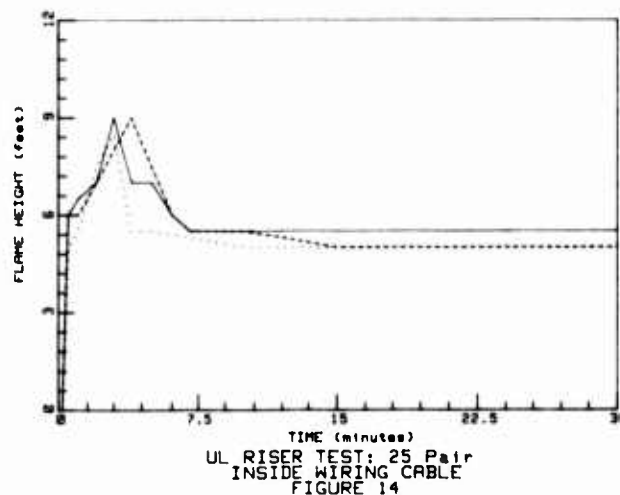
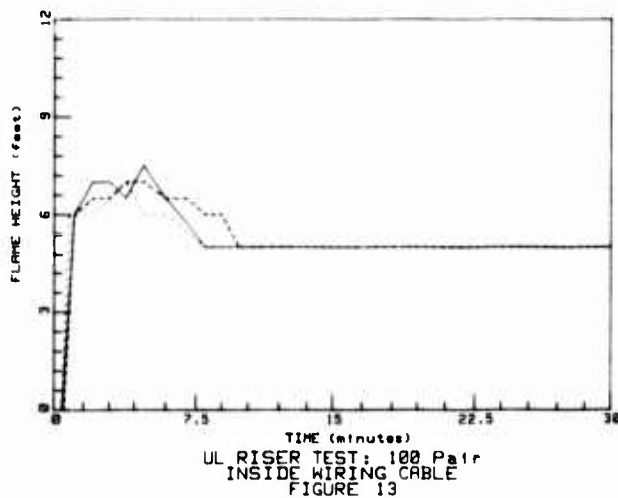


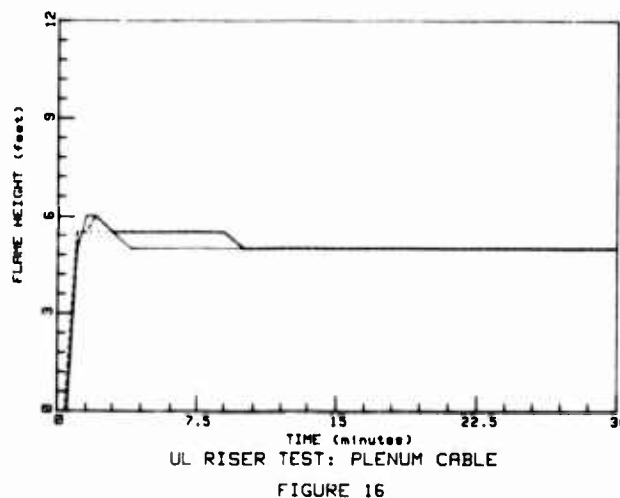
Figure 12 shows the variation of peak flame height with diameter of the riser cables. The smaller cables generally propagated flame higher than the larger cables and also exhibited more scatter in peak flame height. The gauge of the cable also appears to be a factor; the 300 pair, 26 gauge cable propagated flames through the slot in three out of four tests, whereas the smaller diameter 100 pair, 24 gauge cable did not.



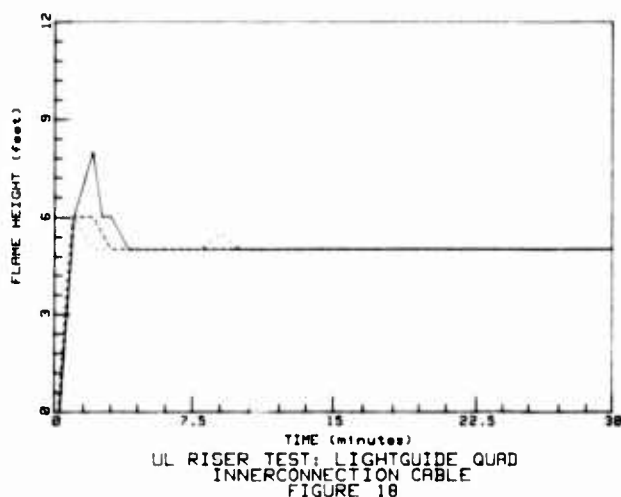
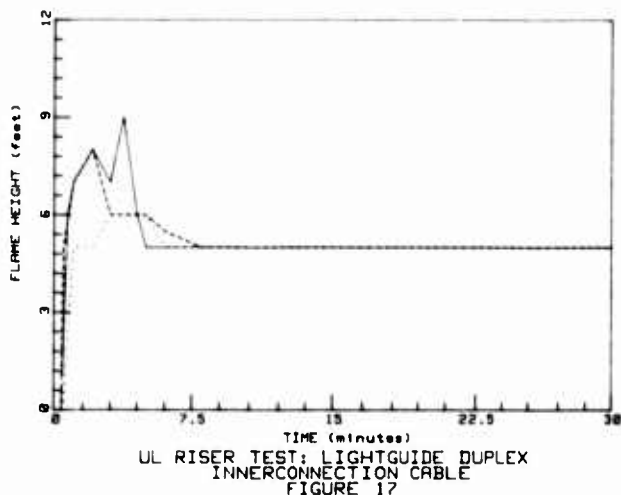
The results for inside wiring cable are shown in Figures 13-15. These figures exhibit two features 1) good reproducibility and 2) a dependence on cable size. The 100 pair cables propagated flame to the 8 foot level and 25 pair cables 8-9 feet, whereas the 4 pair cable propagated flame through the upper slot.



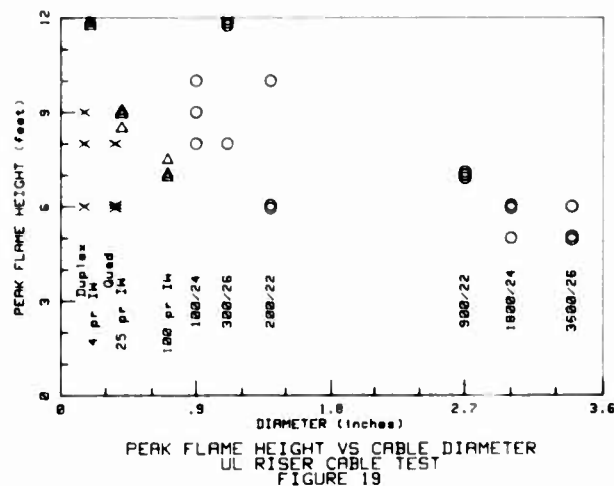
Four pair plenum cable, which had a fluoropolymer jacket, performed well (as expected), Figure 16.



Both of the optical fiber interconnection cables exhibited low peak flame heights, Figures 17-18, notwithstanding the fact that the duplex cable had a smaller diameter than the 4 pair inside wiring cable.



Peak flame height versus diameter for the riser, inside wiring, and interconnection cables is shown in Figure 19. Within each cable design, peak flame height generally increased as cable diameter decreased. The absence of a metallic member appears to be an important factor in the low flame propagation of the optical fiber cables.



DISCUSSION AND CONCLUSIONS

A vertical riser fire test has been developed for the purpose of evaluating the flame propagation of cables for Classification in accordance with the vertical fire spread requirements of the 1984 National Electrical Code. This test simulates a cable installation in a riser shaft and provides an intense fire exposure.

Several aspects of the simulation were arranged in order to increase the severity of the test and thus represent a worst case fire scenario. One of the most important factors in this test procedure is the size of the ignition source. The 145 kW propane flame is considerably larger than ignition sources in other large scale cable tests, ¹⁰ 21 kW in the IEEE-383 vertical rack fire test and 88 kW in the UL 910 horizontal rack fire test for plenum cables. Earlier research¹ has shown that the size of the ignition flame is an important factor in determining whether cables will propagate fire through the upper slot of a riser shaft. The fire source used is slightly smaller than one that could propagate fire even in the absence of cable. Furthermore, using a slot rather than holes for cable penetration, and mounting the cables along the edge of the slot closest to the fire source, results in a very rigorous fire test that separates cables according to their degree of flame retardation. Under the conditions of this test only the most highly flame retardant cables exhibited relatively minor flame propagation.

A variety of copper conductor cables and optical fiber cables were evaluated in this program. Some exhibited only a small amount of flame propagation in this test while others propagated flame through to the upper floor. Two factors which greatly influenced the performance of the cables were the diameter of the cable as well as the degree of flame retardation of the jacket. Other factors influencing performance were the degree of flame retardation of insulation materials and the presence or absence of metallic members in the cable.

The dependence of peak flame height on cable diameter in this test is opposite of the trend observed in the horizontal fire test for plenum cables (UL 910). Kaufman and Yocum³ found that the flame spread of inside wiring cable in the UL 910 test increases as diameter (and number of pairs in the cable) increases. More investigation is needed to understand this phenomenon.

The largest and smallest pair size of 22 and 24 gauge riser cables did not propagate flames through the upper slot and these cables, including all intermediate pair sizes, have been Classified by UL per Section 800-3(b) of the Code. Testing is continuing on the 26 gauge riser cables. Inside wiring cables, 25 pair through 100 pair, have been Classified by UL and testing of smaller inside wiring cables is continuing. Plenum cable was tested in the smallest size only because at the time of testing, the effects of cable size had been discovered. Plenum cable from 4 pair through 25 pair is now dually Classified by UL for both plenum and riser use.

Both the duplex and quad optical fiber interconnection cables have been Classified for riser use per Section 770-6 of the Code.

REFERENCES

1. S. Kaufman, J. L. Williams, E. E. Smith, L. J. Przybyla, "Large Scale Fire Tests of Building Riser Cables," *Journal of Fire Sciences*, Vol. 1-January/February 1983, pp. 54-65.
2. H. M. Dillow, T. S. Dougherty, "New Color Coded Dual Insulated Riser Cables," *Proceedings of the 30th International Wire and Cable Symposium* 1981, pp. 318-323.
3. S. Kaufman, C. A. Landreth, "Development of Improved Flame Resistant Interior Wiring Cables," *Proceedings of the 24th International Wire and Cable Symposium*, 1975, pp. 9-14.
4. S. Kaufman, M. M. Yocum, "The Behaviour of Fire-Resistant Communications Cables in Large-Scale Fire Tests," *Plastics and Rubber: Materials and Applications*, Vol. 4, No. 4, pp. 149-157, November 1979.
5. C. J. Arroyo, T. P. Bursh, "Circuit Transmission Integrity of Plenum Cables in a Developing Fire Scenario," *Proceedings of the 32nd International Wire and Cable Symposium*, 1983, pp. 372-380.
6. J. T. Loadholt, T. M. Williamson, "Design of Fiber Optic Cables for Customer Premises Applications," *Proceedings of the 33rd International Wire and Cable Symposium*, 1984, in press.
7. National Fire Protection Association, 1984 National Electrical Code, Section 800-3(d).
8. Underwriters Laboratories, UL 910 Standard for Test Method for Fire and Smoke Characteristics of Cable Used in Air-Handling Spaces.
9. J. R. Beyreis, J. W. Skjordahl, S. Kaufman, M. M. Yocum, "A Test Method for Measuring and Classifying the Flame Spreading and Smoke Generating Characteristics of Communications Cable," *Proceedings of the Twenty-Fifth International Wire and Cable Symposium*, 1976, pp. 291-295.
10. J. L. Williams, S. Kaufman, "A Comparison of Cable Fire Tests," *Proceedings of the International Conference in Fire Safety*, Volume 9, 1984, pp. 166-181.
11. L. J. Przybyla, T. J. Guida, Underwriters Laboratories Report on Telephone Cable - Classified for Flame Propagation, April 19, 1984

TABLE I

Copper Conductor Cables Tested

Gauge	Number of Pairs	Diameter, Inches	Number of Cables Per Test
<u>Riser</u>			
22	900	2.7	5
22	200	1.4	9
24	1800	3.0	4
24	100	0.9	14
26	3600	3.4	3
26	300	1.1	11
<u>Inside Wiring</u>			
24	4	0.19	80
24	25	0.38	24
24	100	0.71	12
<u>Plenum</u>			
24	4	0.18	80



L. J. Przybyla is an Engineering Group Leader in the Fire Protection Department of Underwriters Laboratories, Inc. He has been involved in a large scale

fire testing and the development of fire test methods for wire and cable. He attended the University of Illinois, Chicago and received a B.S. in Engineering in 1972. He is a registered professional engineer and a member of the Society of Fire Protection Engineers.



Stanley Kaufman is the Supervisor of the Metallurgy and Fire-Resistant Plastics Group at AT&T Bell Laboratories in Norcross, Georgia. He received a B.S. in Physics from the

City College of the City University of the City of New York, and a Ph.D. in Chemistry from Brown University. Before joining Bell Laboratories in 1970, he was a research scientist at the Uniroyal Research Center.

TABLE II

Optical Fiber Cables Tested

Type	Number of Fibers	Dimensions, Inches	Number of Cables Per Test
Duplex	2	0.12 x 0.22 (oval)	80
Quad	4	0.38 (round)	34



T. J. Guida is a Staff Engineer in the Electrical Department of Underwriters Laboratories, Inc. He has been with UL for eleven years working in the wire and cable area.

Previously he worked for both the Okonite and Hatfield Wire and Cable Companies. Mr. Guida graduated from Manhattan College in 1966 with a Bachelor of Chemical Engineering Degree. He is a member of National Electrical Code Panel 7, and ASTM. Mr. Guida is a Registered Professional Engineer in New York State.



J. L. Williams, a graduate of Johns Hopkins University of Baltimore (B.S.), was employed by the Glen L. Martin Company prior to joining AT&T Bell Laboratories in 1962. Since 1980 he

has been involved in the development of fire tests and fire testing of flame-retardant plastics. Prior to joining the Fire-Resistant Plastics Group he was active in the research and development of materials and methods for use in the outside plant.

NEW REDUCED SMOKE, FLAME RETARDANT WIRE AND CABLE FORMULATIONS CONTAINING HALOGENATED ADDITIVES

Dr. James J. Duffy and Mr. Charles S. Ilardo

Occidental Chemical Corporation

ABSTRACT

Halogenated additives in combination with antimony oxide have provided well accepted flame retardant wire and cable formulations. These materials have proven to increase the smoke emission during combustion versus non-flame retardant compositions. Technology is now available which will allow the development of new low smoke wire and cable formulations containing traditional halogen additives.

The selection of a chlorinated additive versus a brominated additive yields an advantage in smoke emission. Further reduction in the level of smoke can be achieved by the addition of small amounts of an iron compound along with a surface treated talc to the formulation.

Formulations have been developed in various polyolefin copolymers giving levels of smoke emission very close to those obtained from non-flame retardant compositions. These starting formulations should serve to allow development of future products based on well known halogen additives.

INTRODUCTION

Millions of pounds of polyolefins and polyolefin copolymers containing halogenated additives have been produced over a number of years to meet the high standards of the wire and cable industry. Formulators are now faced with the additional task of how to provide the same critical performance in combustion properties while providing reduced smoke during combustion.

Progress is continually being made to introduce compositions with reduced smoke generation by formulation modification¹ or by the use of halogen substitutes such as aluminum trihydrate.² Technology has now been developed which will allow the continued use of the traditionally accepted halogenated additives. Formulations based on these additives will provide reduced smoke generation versus current materials while maintaining the critical properties of previous formulations.

This performance is achieved by proper selection of the halogenated additive, an iron containing additive and a surface modified talc. Chlorinated alicyclic additives offer the best choice of halogenated materials. They are superior to brominated additives in their ability to promote char and less smoke in current flame retardant formulations.

The technology developed is concentrated on polyolefins. The formulations should provide a starting point for further work and final formulation development in other laboratories. Test data presented is based on standard small scale laboratory procedures. Typical tests include the Oxygen Index evaluation, Arapahoe Smoke evaluations and the NBS Smoke Chamber. While these may not be the ultimate in procedures versus large scale testing they should serve to stimulate further research and development and serve as the basis of product development.

MATERIALS AND PROCEDURES

Materials

The polymers and other materials used in these evaluations are those generally available from commercial sources. The experimental samples were mixed on a two roll mill to obtain a homogeneous sample. Compounded polymer samples were sheeted and granulated prior to molding. Molding was accomplished by standard techniques. Samples for smoke evaluation were molded into 6 by 6 by 0.075 inch sheets from which specimens were cut.

Testing

Physical Properties. Properties were determined by standard ASTM methods in the laboratory.

Oxygen Index. The test employed is the ASTM D-2863-70. The volume proportion of oxygen and nitrogen flowing through the test apparatus is adjusted until ignition and combustion of the test sample is just possible.

Smoke Generation ASTM E-662-79. Testing was performed in a National Bureau of Standards (NBS) Smoke Chamber according to ASTM E-662-79. The samples are exposed to a source of radiant heat (smoldering combustion) or radiant heat plus propane microburners (flaming combustion). Smoke evolution is continually recorded during the test period. Results are reported as specific optical density D_s or the maximum optical density D_{max} versus time.

Arapahoe testing was performed according to standard procedures for this test. Samples are exposed to a propane flame for thirty seconds and

no flame for an additional thirty seconds. The amount of filterable volatile products produced during this period is collected. Results are reported as material collected and as char yield from the sample remaining after the test.

Typical Formulations

Flame retardant wire and cable formulations have been developed for specific applications over many years. A typical generalized formulation for polyolefin copolymers is shown in Table 1.

TABLE 1

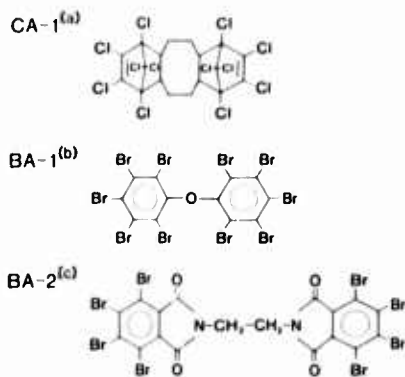
GENERALIZED FLAME RETARDANT POLYOLEFIN FORMULATION
FOR WIRE AND CABLE

COMPONENT	WEIGHT PERCENT	
	Insulation Material	Jacket Material
Polyolefin	50-60	50-60
Filler	5-25	10-40
Halogenated Additive	15-25	5-20
Antimony Oxide	5-10	5-10
Other (Coupling Agents, Crosslinker, etc.)	0.5-5	0.5-5

Halogenated Additives

In the current work the halogenated additives were selected to be representative of materials useful in typical formulations. The structures of the additives used and the designation used below are shown in Figure 1.

Figure 1
Halogenated Additives



- (a) Dechlorane Plus® Occidental Chemical Corporation
(b) Decabromodiphenyl Oxide
(c) Saytech BT-93® Ethyl Corporation

RESULTS

Samples of formulations were prepared as described previously and evaluated in the National Bureau of Standards Smoke Chamber.

Figure 2 shows a typical performance in EVA for flaming combustion. This figure serves to illustrate the difference in smoke generation attainable by selection of the halogenated additive. This is further exemplified by the data contained in Table 2 where flaming combustion results for the different halogenated additives in a number of polymer systems is shown. Data is displayed here in terms of D_s at 4 minutes and D_{max} obtained. The chlorinated additive in the formulation yields less smoke than the brominated additives. This tendency is supported by data developed in evaluations where char yield is measured. The char yield from the chlorinated material is significantly larger than that obtained from the brominated materials. These results are from the Arapahoe Chamber determination.

Figure 2
Smoke Generation Flame Retardant
EVA Compositions ASTM E-662-79
Comparison of Performance of
Brominated Versus Chlorinated Additives

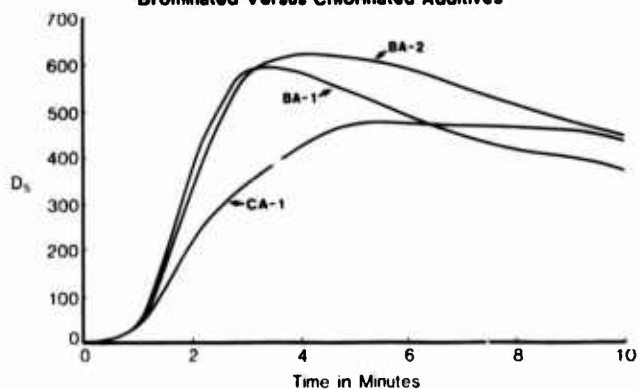


Table 2

SMOKE GENERATION FROM FLAME RETARDANT POLYOLEFIN
COPOLYMER COMPOSITIONS [ASTM E-662-79]

Polymer	Halogenated Additive	Optical Density	
		D_s @ 4 Min.	D_{max}
XLPE	CA-1	525 ± 59	592 ± 53
	BA-1	463 ± 16	481 ± 13
	BA-2	679 ± 50	690 ± 61
EVA	CA-1	430 ± 27	484 ± 40
	BA-1	564 ± 11	601 ± 8
	BA-2	624 ± 111	627 ± 121
EPDM	CA-1	321 ± 21	441 ± 53
	BA-1	643 ± 112	713 ± 66
	BA-2	586 ± 119	641 ± 116

The formulations used in the above evaluations are shown in Tables 3A and 3B.

Table 3A

TYPICAL FLAME RETARDANT CROSSLINKED POLYETHYLENE FORMULATIONS

COMPONENT	WEIGHT PERCENT		
	XLPE/CA-1	XLPE/BA-1	XLPE/BA-2
XLPE	67.5	77.9	77.9
CA-1	25.0		
BA-1		15.0	
BA-2			16.0
Antimony Oxide	5.0	4.0	4.0
Peroxide	1.4	1.4	1.4
Antioxidant	0.7	0.7	0.7

Table 3B

TYPICAL FLAME RETARDANT EPDM FORMULATIONS

COMPONENT	WEIGHT PERCENT		
	EPDM/CA-1	EPDM/BA-1	EPDM/BA-2
EPDM	38.2	38.5	38.5
CA-1	13.9		
BA-1		13.6	
BA-2			13.6
Antimony Oxide	5.1	5.1	5.1
Polyethylene	8.4	8.4	8.4
Zinc Oxide	2.1	2.1	2.1
Stabilizer	2.1	2.1	2.1
Paraffin Wax	2.1	2.1	2.1
Antioxidant	1.0	1.0	1.0
Clay	25.3	25.3	25.3
Coupling Agent	0.6	0.6	0.6
Peroxide	1.2	1.2	1.2

While selection of a chlorinated additive led to low smoke values versus brominated additives further reduction in smoke generation was desired. Various approaches led to the selection of a combination of a low level of an iron containing compound in combination with a talc containing a zinc stearate coating as an effective method of further reducing smoke.

This system once again led to increased values of char formation and smoke reduction. It was especially effective in the formulations containing chlorinated additives. Figure 3 shows the effectiveness of XLPE in the flaming combustion mode. Figure 4 compares the performance in EPDM in flaming and non-flaming modes. Table 4 indicates the effectiveness in other polyolefin systems.

Figure 3
Smoke Generation Flame Retardant
XLPE Compositions ASTM E-662-79
Comparison of Standard and Low Smoke Modified Formulations

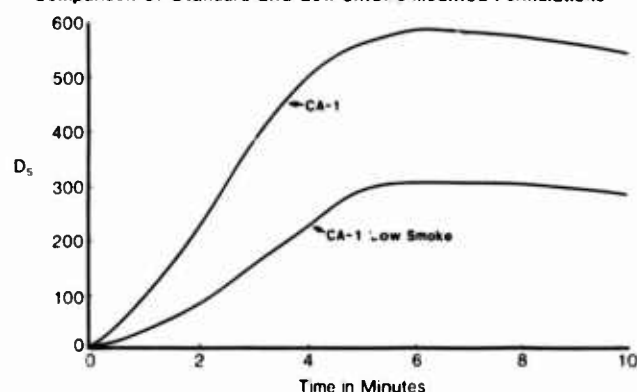


Figure 4
Smoke Generation Flame Retardant
EPDM Compositions ASTM E-662-79
Comparison of Standard and Low Smoke Modified Formulations Flaming/Non-Flaming

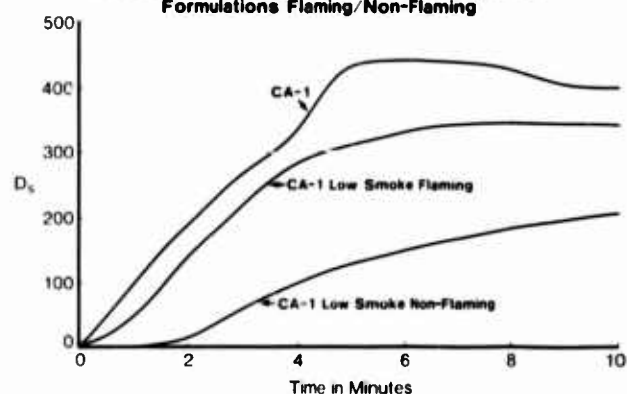


Table 4

SMOKE GENERATION FROM FLAME RETARDANT LOW SMOKE POLYOLEFIN COPOLYMER
COMPOSITIONS [ASTM E-662-79]

Polymer	Halogenated Additive	Optical Density			
		Flaming Mode		Non-Flaming Mode	
		Ds @ 4 Min.	Dmax	Ds @ 4 Min.	Dmax
XLPE	CA-1	230 ± 33	310 ± 23	75	262
	BA-1	594 ± 78	657 ± 86		
	BA-2	501 ± 35	535 ± 32		
EVA	CA-1	216 ± 19	343 ± 26	75	243
	BA-1	679 ± 78	740 ± 94		
	BA-2	507 ± 32	606 ± 54		
EPDM	CA-1	295 ± 45	385 ± 40	100	259
	BA-1	685 ± 88	715 ± 88		
	BA-2	548 ± 92	606 ± 90		
EEA	CA-1	151 ± 15	219 ± 33	130	312

Typical formulations are given in Table 5.

SUMMARY

The historical use of halogenated additives along with antimony oxide in conventional polyolefin systems has led to widely used and accepted insulation and jacketing formulations. The current emphasis on reducing smoke in wire and cable has led some to move in the direction of alternate technologies where properties or experience may be lacking. Proper selection of the total formulation package will allow continued use of accepted additive systems.

Figure 5 summarizes the effectiveness of proper selection of the formulation. Halogenated additives containing cycloaliphatic chlorine offer an advantage over other halogen types. Smoke can be further controlled by use of additional additives significantly reducing smoke for all halogens but especially the chlorine containing materials. In fact, the level of smoke generation which can be achieved approaches the level expected from a non-flame retarded version of the same polymer tested under similar conditions. Figure 6 illustrates this point.

Table 5A

TYPICAL FLAME RETARDANT LOW SMOKE EVA FORMULATIONS

COMPONENT	WEIGHT PERCENT		
	EVA/CA-1	EVA/BA-1	EVA/BA-2
EVA	47.7	47.7	47.7
CA-1	25.0		
BA-1		16.7	
BA-2			16.7
Antimony Oxide	5.0	3.3	3.3
Talc			
[Zinc Stearate Coated]	20.0	30.0	30.0
Iron Compound	0.2	0.2	0.2
Peroxide	1.4	1.4	1.4
Antioxidant	0.7	0.7	0.7

Table 5B

TYPICAL FLAME RETARDANT LOW SMOKE EPDM FORMULATIONS

COMPONENT	WEIGHT PERCENT		
	EPDM/CA-1	EPDM/BA-1	EPDM/BA-2
EPDM	38.2	38.4	38.4
CA-1	13.9		
BA-1		13.6	
BA-2			13.6
Antimony Oxide	5.1	5.1	5.1
Polyethylene	8.4	8.4	8.4
Zinc Oxide	2.1	2.1	2.1
Stabilizer	2.1	2.1	2.1
Paraffin Wax	2.1	2.1	2.1
Antioxidant	1.0	1.0	1.0
Talc			
[Zinc Stearate Coated]	25.3	25.3	25.3
Coupling Agent	0.6	0.6	0.6
Peroxide	1.2	1.2	1.2
Iron Compound	0.05	0.05	0.05

Figure 5
Smoke Generation Flame Retardant
Polyolefin Compositions ASTM E-662-79
Summary of Composition of
Brominated and Chlorinated Additives Low Smoke

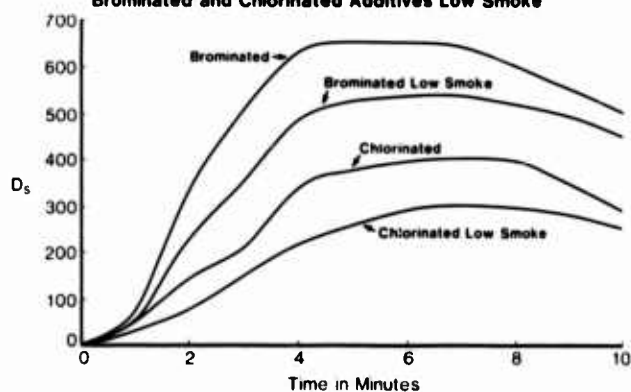
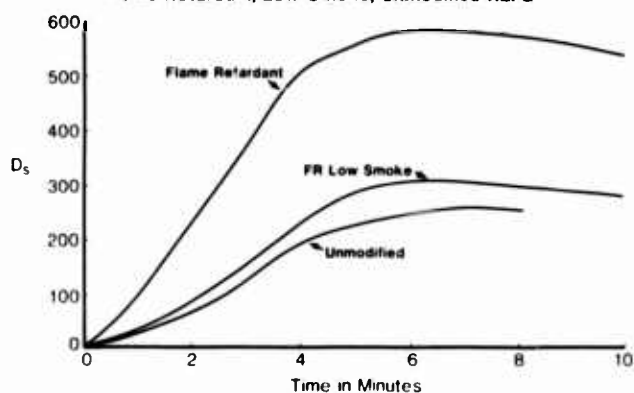


Figure 6
Smoke Generation XLPE Compositions ASTM E-662-79
Comparison of Performance
Flame Retardant, Low Smoke, Unmodified XLPE



CONCLUSIONS

This report has shown that well accepted wire and cable formulations containing halogenated additives do not have to be abandoned in the face of the need to reduce smoke. The selection of the halogenated additive is of prime concern in creating low smoke compositions with conventional polyolefin copolymers. Further with the addition of other readily available and acceptable fillers significant smoke reduction may be achieved.

The formulation data presented is considered as a starting point for further development which will allow the overall safety of wire and cable compositions to be further improved.

- 1) M. J. Keough, "Flame Retardant Acrylene-Alkyl Acrylate Copolymer Composition", U.S.P. 4,243,579, January 6, 1981 (Union Carbide Corporation)
- 2) J. R. Pedersen, et.al., "Low-Smoke, Halogen Free Ship-Off Shore/On Shore Cables with Improved Flame Retardance and Fire Resistance", IWCS, Cherry Hill, November 1983.

James J. Duffy



James J. Duffy is a Senior Scientist at Occidental Chemical Corporation, Grand Island, New York, Research and Development laboratories. He holds a B.S. degree from Canisius College and a Ph.D. in Chemistry from the University of Kentucky. Jim has held various technical and management positions in R&D. His interests include organo halogen and phosphorus chemistry, polymer additives, flame retardancy, and polymer properties.

Charles S. Ilardo



Graduated from SUNY with a B.A. in Chemistry. Two years of graduate work in Chemistry and Education.

Employed by Occidental Chemical Corporation in Research and Development since 1953 as a Plastics Technologist. Emphasis through this time period has been flame retardance as applied to plastics.

Recently formulation research has been in the direction of flame retardance coupled with low smoke.

My educational background was utilized during the 1967-1975 time period as a Chemistry Instructor at Erie Community College.

PARAMETERS FOR THE ASSESSMENT OF FIRE HAZARD FROM ELECTRICAL WIRES AND CABLES

M. M. Khan, and A. Tewarson

Factory Mutual Research Corporation - Norwood, MA

ABSTRACT

This paper describes the concepts and the measurement techniques for evaluation of fire parameters of wires and cables needed for the assessment of fire hazard. The parameters reflect the behavior of wires and cables in terms of ignition, electrical failure, fuel vapor generation, heat generation, toxic product generation, corrosivity of fire products, and light transmission through smoke. In the study, different types of wires and cables, ranging in size from 10 AWG to 2000 MCM, of various insulation/jacket materials, have been examined in the Factory Mutual Combustibility Apparatus, in which materials are examined over a wide range of environmental conditions expected in large-scale fires.

In addition to fire hazard evaluation, this technique can be applied to the development of new and improved fire-resistant polymers.

INTRODUCTION

The fire hazards expected from wire and cable depend on the generic nature of the insulation/jacket materials, on additives and on size and construction¹⁻⁵. Under a given thermal environment, the wires and cables may undergo a series of fire stages such as initiation of degradation of the insulation/jacket materials, ignition, fire growth, maximum burning, fire decay, and extinction. Therefore, the important aspects of fire hazard evaluations include damage, ease of ignition or rate of surface spread of flame, electrical failure, generation of fuel vapors, heat, toxic and corrosive fire products and light obscuration (visibility), all of which need to be quantified. This paper reviews the concepts and measurement techniques for fire parameters needed for the assessment of fire hazard from wires and cables.

FIRE PARAMETERS CONCEPTS

The concepts used for obtaining the fire hazard parameters are presented in the following discussion. These parameters are apparatus independent as long as they are measured properly and accurately.

Damage, Ignition, Flame Spread, and Electrical Failure

When a wire or cable is subjected to heat, the temperature at the surface increases with time as governed by transient heat conduction relationships⁶. These relationships can be modified by using empirical constants,

$$t_i = \frac{(k \Delta T_i)^2}{Pa (\dot{q}_n'')^2} \quad (1)$$

$$\text{or, } E_i = \frac{(k \Delta T_i)^2}{Pa \dot{q}_n''} \quad (2)$$

where t_i = time in sec; E_i = total absorbed energy in kJ/m^2 , and ΔT_i = temperature rise above the normal cable operating temperature (K). The subscript i denotes the processes occurring during the thermal exposure such as damage (d) of polymers in insulation/jacket materials (i.e., initiation of combustible vapors), ignition (ig) or electrical failure (ef). k is the thermal conductivity (kJ/mK), and a is the thermal diffusivity (m^2/s) of the polymeric materials of the sample, respectively. P is an empirical constant derived for the specific cable type and configuration; \dot{q}_n'' (kJ/m^2) is the net heat flux received by the sample. The heat transferred to the cable by a fire can be in the form of radiation, convection, and/or conduction. Part of the heat transferred to the cable is expended in raising the cable temperature above its normal operating temperature and part of it is balanced by compensating reradiation and convective heat losses from the surface. Considering all the probable heat gains and losses, \dot{q}_n'' in Eq (1) or (2) is given as,

$$\dot{q}_n'' = (\dot{q}_e'' + \dot{q}_a'') - (\beta \dot{q}_r'' + \dot{q}_{cl}'') \quad (3)$$

where \dot{q}_e'' = heat supplied by external source in kJ/m^2 (For radiative heat sources, \dot{q}_e'' is multiplied by the surface absorptivity.); \dot{q}_a'' = heat flux in kJ/m^2 supplied by the cable flame and any additional sources; β is surface emissivity; \dot{q}_r'' = surface reradiation loss in kJ/m^2 ; and \dot{q}_{cl}'' = convective heat losses from the surface in kJ/m^2 .

As $(\dot{q}_e'' + \dot{q}_n'')$ equals $(\beta \dot{q}_{rl}'' + \dot{q}_{cl}'')$ in Eq. (3), the critical condition occurs when the heat fluxes received and lost are in equilibrium. From Eqs. (1) and (2), t_i and E_i will approach infinity. The heat flux for this condition is defined as critical heat flux, \dot{q}_{cr}'' , at or below which the process, 1, cannot occur.

When $\dot{q}_n'' \gg \dot{q}_e''$ in Eqs (1) or (2), \dot{q}_e'' can be neglected, in which case the equation represents a process sustained by its own flame or sources other than external. When $\dot{q}_n'' \gg \dot{q}_e''$, the process is then sustained by external sources.

In Eq (2), $\frac{k \Delta T_i}{\dot{q}_n''}$ is related to the thermal

thickness of the cable. Cables can behave as: 1) thermally thick because they are physically thick, e.g. a 2000 MCM cable, or because

$\frac{k \Delta T_i}{\dot{q}_n''} \ll l$ (where l is actual thickness); or 2)

thermally thin, e.g., a single 12 AWG wire, or because $\frac{k \Delta T_i}{\dot{q}_n''} \gg l$.

For high \dot{q}_n'' values or if thermal properties change because of structural and physical

changes in the polymer, $\frac{k \Delta T_i}{\dot{q}_n''}$ may become

extremely small; under this condition the major portion of the heat is carried away in the physical removal of fuel vapors and E_i becomes a constant in Eq (2) or $1/t_i$ becomes a linear function of \dot{q}_n'' rather than $\dot{q}_n'^2$ in Eq (1).

After ignition, the flame propagation depends on the magnitudes of heat flux provided by the flame of the burning material and external heat source such that critical heat flux and ignition energy requirements are satisfied. For self-sustained flame propagation, heat flux from the flame becomes important; the flame will continue to propagate on the surface of the material without the assistance of external heat sources, as long as heat flux from the flames is sufficient to satisfy ignition energy requirements. The magnitude of the heat flux from the flame depends on the size and geometry of the material. For the quantification of damage, ignition and electrical failure, Eqs (1) and (2) are used.

Fuel Generation

The generation rate of fuel vapors per unit sample surface area, \dot{G}_f'' , can be expressed as:

$$\dot{G}_f'' = \dot{q}_n''/L \quad (4)$$

where \dot{G}_f'' is in g/m^2s ; \dot{q}_n'' is the net heat flux received by the sample, defined in Eq (3); L = heat of gasification of the sample (in kJ/g) which is the heat required to generate a unit mass of vapors. Normalizing Eq (4) by \dot{q}_n'' ,

$$\dot{G}_{comb}''/\dot{q}_n'' = 1/L \quad (5)$$

The larger the value of $1/L$, the higher is the generation rate of the fuel vapors, and thus $1/L$ can be defined as the fuel vapor generation parameter (g/kJ) which is the amount of fuel vapor generated per unit of heat received by the sample.

In large fires, \dot{q}_n'' in Eq (3) is predominantly due to flame radiation and in small fires \dot{q}_n'' is predominantly due to flame convection. Thus, in order to simulate large-scale fire conditions for small samples, oxygen concentration in the environment is increased for radiation-scaling⁷ to determine flame heat flux to the surface.

For large \dot{q}_n'' values in Eq (3), in normal air and normalizing by \dot{q}_e'' ,

$$\dot{G}_f''/\dot{q}_e'' = \left[1 + \frac{\dot{q}_a'' - (\beta \dot{q}_{rl}'' + \dot{q}_{cl}'')}{\dot{q}_e''} \right] / L \quad (6)$$

when $\frac{\dot{q}_a'' - (\beta \dot{q}_{rl}'' + \dot{q}_{cl}'')}{\dot{q}_e''} \ll 1.0$,

then, $\dot{G}_f''/\dot{q}_e'' = 1/L$. (7)

Heat Generation

The fire products generated from the sample consist of heat and various chemical compounds such as "smoke", toxic, and corrosive products. The generation rate of heat actually released in flaming fires is defined as the actual heat release rate per unit sample surface area, \dot{Q}_A'' (kW/m²) and can be expressed as:

$$\dot{Q}_A'' = \dot{Q}_C'' + \dot{Q}_R'' \quad (8)$$

where \dot{Q}_C'' = convective heat release rate (kW/m²); and \dot{Q}_R'' = radiative heat release rate (kW/m²).

\dot{Q}_A'' , \dot{Q}_C'' , and \dot{Q}_R'' are functions of the generation rate of the combustible vapors, \dot{G}_f'' ,

$$\dot{Q}_A'' = H_A \dot{G}_f'' \quad (9)$$

$$\dot{Q}_C'' = H_C \dot{G}_f'' \quad (10)$$

$$\dot{Q}_R'' = H_R \dot{Q}_f'' \quad (11)$$

where H_A , H_C , and H_R are the actual, convective, and radiative heat of combustion respectively in kJ/g. From Eqs (4) and (9) to (11),

$$\dot{Q}_A'' = (H_A/L) \dot{q}_n'' \quad (12)$$

$$\dot{Q}_C'' = (H_C/L) \dot{q}_n'' \quad (13)$$

$$\dot{Q}_R'' = (H_R/L) \dot{q}_n'' \quad (14)$$

$$\text{and } H_A/L = H_C/L + H_R/L \quad (15)$$

Normalizing eqs (12) to (14) by \dot{q}_n'' we obtain:

$$\dot{Q}_A''/\dot{q}_n'' = H_A/L \quad (16)$$

$$\dot{Q}_C''/\dot{q}_n'' = H_C/L \quad (17)$$

$$\dot{Q}_R''/\dot{q}_n'' = H_R/L \quad (18)$$

H_A/L , H_C/L , and H_R/L are the amounts of actual, convective, and radiative heat produced per unit amount of heat received by the sample and, thus, can be defined as the heat generation parameter (kJ/kJ) of the sample (actual, convective, or radiative).

The higher the values of the heat generation parameters, the higher are the generation rates of heat expected in fires.

For large \dot{q}_e'' values in Eq (3), for small samples in normal air, and normalizing Eq. (12), by \dot{q}_e'' ,

$$\dot{Q}_A''/\dot{q}_e'' = (H_A/L) \left[1 + \frac{\dot{q}_a'' - (\beta \dot{q}_{rl}'' + \dot{q}_{cl}'')}{\dot{q}_e''} \right] \quad (19)$$

$$\text{when } \frac{\dot{q}_a'' - (\beta \dot{q}_{rl}'' + \dot{q}_{cl}'')}{\dot{q}_e''} < 1.0,$$

$$\text{then, } \dot{Q}_A''/\dot{q}_e'' \approx H_A/L \quad (20)$$

$$\text{Similarly, } \dot{Q}_C''/\dot{q}_e'' \approx H_C/L \quad (21)$$

$$\text{and } \dot{Q}_R''/\dot{q}_e'' \approx H_R/L \quad (22)$$

Toxic Product Generation

The generation rates of toxic compounds are functions of the generation rate of fuel vapors:

$$\dot{G}_j'' = Y_j \dot{G}_f'' \quad (23)$$

where Y_j is the yield of compound, j (g/g); compound j represents a toxic compound such as CO, HCN, HCl, etc. From Eqs (4) and (23),

$$\dot{G}_j'' = Y_j \dot{q}_n''/L \quad (24)$$

Normalizing Eq (24) by \dot{q}_n'' , we have

$$\dot{G}_j''/\dot{q}_n'' = Y_j/L \quad (25)$$

Y_j/L is the amount of toxic compound, j , produced per unit amount of heat received by the sample. Thus, Y_j/L can be defined as the toxic compound generation parameter (g/kJ) of the sample.

For large \dot{q}_e'' values in Eq. (3) for small samples in normal air, and normalizing Eq. (25) by \dot{q}_e'' ,

$$\dot{G}_j''/\dot{q}_e'' = Y_j/L \left[1 + \frac{\dot{q}_a'' - (\beta \dot{q}_{rl}'' + \dot{q}_{cl}'')}{\dot{q}_e''} \right] \quad (26)$$

$$\text{if } \frac{\dot{q}_a'' - (\beta \dot{q}_{rl}'' + \dot{q}_{cl}'')}{\dot{q}_e''} < 1.0$$

$$\dot{G}_j''/\dot{q}_e'' \approx Y_j/L \quad (27)$$

Light Transmission Through "Smoke"

The fraction of light transmitted through "smoke", I/I_0 , can be expressed as:

$$\ln(I_0/I) = \sigma \ell \quad (28)$$

where ℓ is the optical path length (m); σ is the mass attenuation coefficient of "smoke" (m^2/g); and g is the mass concentration of "smoke" (g/m^3). $\ln(I_0/I)$ is defined as the optical density, D . The concentration of "smoke" in Eq. (28) can be expressed as:

$$c = y_{\text{smoke}} \dot{G}_f'' A/\dot{V} \quad (29)$$

where A = sample surface area (m^2); y_{smoke} = yield of "smoke" (g/g); and \dot{V} = volumetric flow rate of fire product-air mixture (m^3/s).

From Eqs (28) and (29):

$$D = \sigma y_{\text{smoke}} \dot{G}_f'' A \ell / \dot{V} \quad (30)$$

Converting D from $\ln(I_0/I)$ to $\log_{10}(I_0/I)$ and rearranging Eq (30),

$$\sigma y_{\text{smoke}} = \frac{D}{2.303} \frac{\dot{V}}{\dot{G}_f'' A \ell} \quad (31)$$

For a closed system, such as the NBS smoke chamber, Eq (31) can be expressed as:

$$\sigma y_{\text{smoke}} = \frac{DL}{W \ell} \quad (32)$$

where D is expressed as $\log_{10} (I_0/I)$, V is the volume of the chamber (m^3); and W is the weight of sample vaporized (g). The specific optical density, D_s , in the NRS smoke chamber is defined as:

$$D_s = DV/A\ell \quad (33)$$

From Eqs (32) and (33),

$$\sigma y_{\text{smoke}} = D_s A/W \quad (34)$$

The mass attenuation coefficient, σ , is a function of the chemical and physical properties of the "smoke"; y_{smoke} is a function of the chemical and physical properties of the combustible. Thus, the value of σy_{smoke} for a material is expected to be similar in different types of experiments, as long as the combustion/pyrolysis chemistry remains invariant.

From Eqs (4) and (30), we have,

$$D = \left[\frac{\sigma y_{\text{smoke}}}{L} \right] \left[\frac{A\ell}{\dot{V}} \right] \dot{q}_n'' \quad (35)$$

Normalizing Eq (35) by \dot{q}_n'' ,

$$D/\dot{q}_n'' = \left[\frac{\sigma y_{\text{smoke}}}{L} \right] \left[\frac{A\ell}{\dot{V}} \right] \quad (36)$$

Since A , ℓ , and \dot{V} are known, from D/\dot{q}_n'' values, $\sigma y_{\text{smoke}}/L$ can be calculated. σ is a characteristic property of the "smoke"; y_{smoke}/L is the amount of "smoke" in grams generated per unit of heat received by the sample. $\sigma y_{\text{smoke}}/L$ thus can be defined as the light obscuration parameter (m^2/kJ) of "smoke."

For large \dot{q}_e'' values in Eq (3), for small sample in normal air, and normalizing Eq. (36) by \dot{q}_e'' ,

$$D/\dot{q}_e'' = \left[\frac{\sigma y_{\text{smoke}}}{L} \right] \left[\frac{A\ell}{\dot{V}} \right] \left[1 + \frac{\dot{q}_a'' - (\beta \dot{q}_{rl}'' + \dot{q}_{cl}'')}{\dot{q}_e''} \right] \quad (37)$$

$$\text{if } \dot{q}_a'' - \frac{(\beta \dot{q}_{rl}'' + \dot{q}_{cl}'')}{\dot{q}_e''} < < 1.0 \quad ,$$

$$\text{then, } D/\dot{q}_e'' = \left[\frac{\sigma y_{\text{smoke}}}{L} \right] \left[\frac{A\ell}{\dot{V}} \right] \quad (38)$$

Corrosive Products

The corrosion parameter, C_r , ($\mu m/kJ$) was obtained for a 100-ml solution of water soluble fire products, by dividing the corrosion of mild steel (4 mils thick) by W , the total weight loss (in g) of the sample in the test and multiplying it by the fuel vapor generation parameter (g/kJ), i.e.,

$$C_r = \frac{\mu m \text{ of metal loss}}{W} \times \frac{\dot{G}_f''}{\dot{q}_n''} \quad (39)$$

where \dot{q}_n'' is the net heat flux received by the sample defined in Eq (3)

For large \dot{q}_e'' values in Eq. (3), for small sample in normal air, and using Eq. (7), we have:

$$C_r = \frac{\mu m \text{ of metal loss}}{W} \times \frac{\dot{G}_f''}{\dot{q}_e''} \quad (40)$$

EXPERIMENTAL APPROACH

General Background

The experimental approach taken in this study is based on work performed during the last 12 years on the combustibility of polymeric materials at Factory Mutual Research Corporation (FMRC). To simulate the fire environment, the following parameters are varied: 1) external heat flux (by exposure of samples to varying heat flux from radiant heaters); 2) flame radiation (by varying oxygen concentration in air), 3) ventilation (by varying inlet air flow rate, temperature and contaminants in the air); and (4) surface area of the fuel.

By using small samples and proper combinations of external heat flux, oxygen concentrations and inlet air flow rate (including temperature and contaminants), the generalized fire behavior of materials is established for variable fire size, flame radiation, and ventilation (defined as the combined simulation of flame and external radiation). Predictions are then made for a particular fire scenario and confirmed by direct measurements using larger-scale fires. For this purpose, the following three apparatuses, shown in Figure 1, are used:

1) Factory Mutual Small-Scale Combustibility Apparatus, for samples ~ 0.1 -m diameter, ~ 0.1 -m high, and ~ 0.02 -m thick. The external heat source is simulated by using four coaxially placed quartz-tungsten radiant heaters (peak at 1.15μ). Flame radiative heat flux is simulated by varying the mass fraction of oxygen in air. Ventilation is provided by introducing air at the bottom of the apparatus with variable

flow rate, temperature, and contamination. Experiments can also be performed under natural air flow. A small pilot flame is provided for ignition.

2) Factory Mutual Intermediate-Scale Combustibility Apparatus⁸ for samples $\sim 0.3 \times 0.3 \times 0.1$ -m high. The external heat source is simulated by using four coaxially placed, high-density radiant heaters. Experiments are performed in natural as well as forced air flow.

3) Factory Mutual Large-Scale Apparatus⁹ for samples $\sim 3 \times 3 \times 3$ -m high. No external heat source is used and experiments are performed under natural air flow.

In all three apparatuses, fire products are captured in the respective sampling ducts, diluted with ambient air, and well mixed before sampling. Measurements are made for total flow rate, gas temperature, concentrations of CO , CO_2 , O_2 , total gaseous hydrocarbons "smoke" (defined as a mixture of soot and low vapor-pressure liquids), HCl , HCN , and NO_x , and optical transmission through fire products. Other measurements include time to ignition (auto or piloted), generation rate of combustible vapors, and water application rate for fire suppression and extinguishment. For toxicity evaluations, animal exposure experiments are performed¹⁰. Heat of gasification and surface reradiation loss are determined from the mass loss as a function of external heat flux in pyrolysis experiments. Standard methods are used for the measurement of elemental composition of the sample and "smoke", heat of complete combustion of the sample and "smoke", corrosion properties of the fire products, and electrical failure.

All measurements are made at intervals of ~ 1 s (or longer) for the entire fire duration. Analog-to-digital data acquisition systems collect data for analysis.

It has been shown that reliable predictions can be made for overventilated, large-scale, horizontal pool fires, based on small-scale apparatus results¹¹. In addition, the fire properties of materials obtained from the small-scale apparatus can be used as input parameters for various fire models for the evaluation of fire hazards and protection from such hazards. All important fire properties can be measured simultaneously in the small-scale apparatus with accuracy and repeatability.

Experimental Procedure

Experiments were conducted in the Factory Mutual Small-Scale Combustibility Apparatus with radiant heaters used as external heat sources. Prior to the experiments, the radiant heat flux at the sample location was precalibrated with a heat flux gage covering a range up to about 70 kW/m^2 .

Wire and cable samples, about 0.06 m in length, were placed vertically as well as horizontally inside the apparatus. A small premixed C_2H_4 -air pilot flame (~ 0.01 m in length) was positioned about 0.01 m above the top surface of the sample to ignite combustible vapors (for piloted ignition). The experiments were conducted at an air flow rate of $0.003 \text{ m}^3/\text{s}$ (an overventilated fire condition) in normal air and under natural air flow in normal air. Using several external radiant heat flux values, simultaneous measurements were made for time to ignition, fuel vapor generation rate, heat release rate, generation rate of toxic and corrosive products, and light obscuration through smoke. Detailed descriptions of the apparatus and experimental procedures are given in References 1-4.

For the quantification of the corrosivity of fire products¹, fire products (fuel vapor) were bubbled through a fixed volume of distilled water (100 ml). A mild steel probe was immersed in the solution and its resistance was measured as a function of time. The resistance of metal changes because of loss of metal due to corrosion. From the measurements, the rate of cumulative corrosion of the metal was determined.

For measurement of time to electrical failure in wire or cable as a function of external heat flux, the techniques developed in Reference 2 for multiconductor cables and in Reference 1 for single-conductor cables were used. Electrical failure in a cable is defined as the electrical shorting between two or more conductors or between conductor to ground. Experiments were conducted in conjunction with the FM Combustibility Apparatus under natural air flow conditions with a pilot flame as igniter. Details are given in References 1-3. These electrical failure measurement techniques use only 24 or 70 Vdc on each conductor; there could be different effects if the cables were tested under higher voltage. In addition, stresses placed on the cables, as well as cable arrangements, could also produce different results. Recently, we have developed a new technique which can be used in conjunction with a mini-computer for both single- and multiconductor cables, up to a maximum of 16 conductors. Currently the technique is limited to a maximum of 300 V on each conductor, although it can be modified for higher voltages. Using this new technique, it is possible to quantify electric faults in wires or cable quite repeatably by measuring the extent of change in the initially applied voltage as a function of time.

RESULTS AND DISCUSSIONS

Damage, Ignition, Flame Spread, and Electrical Failure

As a result of fire exposure, insulation/jacket materials in a cable will reach the decomposition temperature (ΔT_d); at that time the damage process will initiate. With continued fire exposure, the temperature of the insulation/jacket will increase above ΔT_d and, depending upon the presence or absence of an ignition source, and of melting or nonmelting polymers, the cable will reach either its ignition temperature (ΔT_{ig}) or the temperature for electrical failure (ΔT_{ef}). The order in which these processes occurs will be either $\Delta T_d < \Delta T_{ig}$ (piloted ignition) $< \Delta T_{ef}$, or, $\Delta T_d < \Delta T_{ef} < \Delta T_{ig}$ (autoignition).

The damage process is defined in terms of the generation of combustible vapors and quantified in terms of the time at which the generation of combustible vapors from the cable is initiated as a function of heat flux. Insulation/jacket damage implies decrease in insulation resistance, dielectric loss, etc., causing impairment to the normal function of the cable^{2-3,5}.

The energy, E , associated with cable damage, ignition, and electrical failure processes is equal to the time to initiate each process multiplied by the external heat flux. And, the minimum value of heat flux needed to initiate each of the above processes is defined as the critical heat flux (\dot{q}''_c) for that process. Critical heat flux remains approximately the same for various processes, as determined in our studies²⁻³. Table 1 presents the critical heat flux and energy associated with damage for selected wires and cables. The higher the value of critical flux and energy for damage, the higher will be the resistance to damage initiation.

Ignition data (for selected cables) are shown in Figures 2 through 4 for piloted- and autoignition under natural and forced air flow conditions, using a single cable exposed to radiant heat flux. The figures show that $1/E_{ig}$ follows \dot{q}''_c as expected from Eq. (2), where the slope [in cases where $(\beta \dot{q}''_c + \dot{q}''_c)/\dot{q}''_c + \dot{q}''_c$] $\ll 1.0$ is expected to be approximately equal to $P\alpha/(k\Delta T_{ig})^2$ and the intercept is equal to a flux (critical flux) at or below which $1/E_{ig} = 0$ or t_{ig} approaches infinity and the ignition process cannot occur. The same conclusions can be drawn for damage and electrical failure processes.

ΔT_{ig} is higher for autoignition than for piloted ignition. Also, the ignition source is absent in the autoignition case; thus, \dot{q}''_c is smaller for autoignition than for piloted ignition, indicating that t_{ig} will be longer or E_{ig} will be higher for autoignition than for the

piloted ignition, as can be noted in Figures 2 and 3.

\dot{q}''_c is smaller under natural than under forced air flow and increases as air flow rate (i.e., ventilation) is increased. Thus, t_{ig} will be longer or E_{ig} will be higher under forced than under natural air flow, as indicated by our data in Figures 2 and 3 for ignition.

As \dot{q}''_c is varied, t_{ig} or E_{ig} will vary. \dot{q}''_c will vary as a result of changes in: ignition source strength, location of the ignition source from the surface, internal cable temperature, oxygen concentration in air. For example, as oxygen concentration is decreased (air contaminated with fire products), flame heat flux will decrease and t_{ig} or E_{ig} will increase¹².

Cable coatings and wrappings will decrease α [in Eq. (1) or (2)] and thus increase E_d , E_{ig} , and E_{ef} or t_d , t_{ig} , and t_{ef} . This is supported by our study² as shown in Figure 4 for ignition.

As $k\Delta T/\dot{q}''_c$ becomes very small for larger \dot{q}''_c values, E_{ig} will become a constant. This can be noted in Figures 2 to 4.

Table 2 lists the critical flux and energy associated with ignition and electrical failure (at 50 kW/m² or higher external heat flux values) for some selected wire and cable samples. For comparison, ignition energy values for red oak and flexible polyurethane foams are also listed. The higher the value of energy and critical flux, the higher will be the resistance of the cable to fire initiation, flame propagation on the surface, and electrical failure. As can be noted in Table 2, wire and cable samples listed are expected to show higher resistance to ignition and flame propagation on the surface than red oak and flexible polyurethane foams.

Except for some PTFE and ECTFE cables which melt, in general the ignition energy is lower than the electrical failure energy^(1,5,13). Electrical failure energy increases as the size of the cable increases. For some cables, no electrical failure was observed as a result of charring.

The resistance to damage, ignition, electrical failure, and flame propagation on the surface are functions not only of the insulation-jacket material, but also of wire and cable construction and size.

Fire Parameters

Table 3 presents the fire parameters of some selected wire and cable samples together with the fire parameters of some research polymers (at 50 kW/m² or higher external heat flux values) for comparison purposes. In addition to critical heat flux and energy associated with damage, ignition, flame spread and electrical

failure, these fire parameters are also needed for the assessment of fire hazard from the cables. These parameters have been defined in terms of fuel vapor, heat and toxic products generation, corrosivity of fire products, and light obscuration through "smoke". The smaller the values of these parameters, the better the cables are expected to be in terms of reduced contribution of fuel vapors, heat, toxic and corrosive products, and light obscuration in a fire accident.

Table 3 indicates that the fire properties of cables are not only the functions of insulation/jacket materials, but also of cable size and construction. As compared to the fire parameters for research polymers, i.e., polypropylene, polyethylene, and polyvinyl chloride, the cable fire parameters are generally lower, indicating the influence of additives, size, and construction on the cable combustibility.

The fire parameters by themselves, however, cannot be used for the qualification of wires and cables, because different wires and cables provide different magnitudes of heat from their flames in real fires. By multiplying the fire parameters by the flame heat flux received by the surface of wires and cables as well as from other sources, estimations can be made for the generation rate of fuel vapors, heat release rate, generation rate of toxic products, corrosivity of fire products, and light obscuration by smoke.

At FMRC, a technique has been developed (Ref. 7) to estimate the flame heat flux from burning materials representative of large-scale fires. In the technique, high oxygen concentrations are used in the air supplied to the fire and the generation rate of fuel vapors is measured. The measurements are then used to estimate the flame heat flux expected in large-scale fires. This technique has not yet been used for wires and cables.

CONCLUSIONS

1) Pertinent fire parameters for the assessment of fire hazard from electrical wires and cables have been identified and techniques and apparatus for their quantification are described.

2) The fire parameters, including critical flux and energy for damage, ignition, and electrical failure, can be quantified quite accurately by using the Factory Mutual Small-Scale Combustibility Apparatus.

3) In general, cable damage is expected to occur first, followed by ignition, and finally electrical failure (for nonmelting polymers).

4) Fire parameters are useful for general evaluation of wires and cables and for the improvement and development of new polymers for wires and cables.

5) The fire parameters can also be used to assess hazards in large-scale fires provided measurements are made to estimate the heat flux from the flame of burning wires and cables and other heat sources expected in large-scale fires. A technique at FMRC to estimate the flame heat flux is suggested as one of the techniques. The fire hazards expected in large-scale fires are assessed by multiplying the fire parameters by the flame heat flux and other heat fluxes expected in large-scale fires. By setting limits for intended end-use applications and performing large-scale validation tests, wires and cables can be qualified by the FMRC test procedure.

ACKNOWLEDGMENTS

This work was supported by U.S. Department of Transportation, Cambridge, Massachusetts; Florida Power and Light Co., Juno Beach, Florida; and Electric Power Research Institute, Palo Alto, California.

REFERENCES

- 1) Tewarson, A., Khan, M.M., and Steciak, J., "Combustibility of Electrical Wire and Cable for Rail Rapid Transit Systems," Final Report, FMRC J.I. OFON4.RC, U.S. Department of Transportation, Transportation Systems Center, Cambridge, MA, May 1983.
- 2) Khan, M.M., Steciak, J. and Tewarson, A., "Small-Scale Testing of Flame-Retardant Coated Cables," Technical Report, FMRC J.I. OG3R9.RC, prepared by Factory Mutual Research Corporation, Norwood, MA, for Florida Power and Light Co., Juno Beach, FL, February 1983.
- 3) Lee, J.L., "A Study of Damageability of Electrical Cables in Simulated Fire Environments," Final report EPRI NP-1767, Project 1165-1-1, Electric Power Research Institute, Palo Alto, CA, March 1981.
- 4) Tewarson, A., Lee, J.L., and Pion, R.F., "Categorization of Cable Flammability Part I: Laboratory Evaluation of Cable Flammability," Interim Report EPRI NP-1200 Part I Project 1165-1, Electric Power Research Institute, Palo Alto, CA, October 1979.
- 5) Khan, M.M. and Tewarson, A., "Evaluation of Electrical Wire and Cable Behavior in Fires," Conference Proceedings, Nonferrous/Electrical Divisional Meeting, held in Providence, Rhode Island, May 21-23, 1984, Wire Association International Guilford, CT, 06437 USA

6) Carslaw, H.C. and Jaeger, J.S., Conduction of Heat in Solids, 2nd Edition, Oxford University Press, Oxford, UK, 1959.

7) Tewarson, A., Lee, J.L., and Pion, R.F., "The Influence of Oxygen Concentration on Fuel Parameters for Fire Modeling," 18th Symposium (International) on Combustion, The Combustion Institute, 1981.

8) Newman, J.S. and Brown, J.R., "Standard Test Criteria for Evaluation of Underground Fire Detection Systems - Phase II," prepared for U.S. Bureau of Mines by Factory Mutual Research Corporation, Norwood, Massachusetts, FMRC J.I. OG2N4.RC, December 1982.

9) Heskestad, G., "A Fire Products Collector for Calorimetry into the MW Range," Factory Mutual Research Corporation, J.I. OC2E1.RA, June 1981.

10) "Determination of Toxicity of Combustion Products of Habitability Foams Concurrently with Flammability Studies of These Materials," Arthur D. Little Report No. 50426-00, U.S. Navy Contract No. N00167-84-C-0018, June 1984.

11) Tewarson A. and Khan, M.M., "Study of Flammability of Electrical Insulation," Seventh International Conference on Fire Safety, Stanford Research Institute, Menlo Park, California 1982.

12) Steciak, J., Tewarson, A., and Newman, J.S., "Fire Properties of Combustible Materials Commonly Found in Nuclear Fuel Cycle Facilities," Technical Report FMRC J.I. OG3R8.RC, prepared by Factory Mutual Research Corporation, Norwood, MA for Battelle/Pacific-Northwest Laboratories, Richland, WA, February 1983.

13) Tewarson, A. and Khan, M.M., "The Cable Combustibility Test Program at Factory Mutual Research Corporation," Workshop 1 - Progress Toward a Smokeless Cable. APTA 1983 Rapid Transit Conference, June 20-23, 1983, William Penn Hotel, Pittsburgh, Pennsylvania.

AUTHORS BIOGRAPHICAL SKETCHES

M. M. Khan, Factory Mutual Research Corporation, Norwood, MA 02062.

Mohammed M. Khan joined Factory Mutual Research Corporation in 1978 and is an Advanced Research Scientist. He received a Masters degree in Applied Physics from the University of Dhaka, Bangladesh and received another Masters degree from the Mechanical Engineering Department at MIT. Mr. Khan has been involved in experimental research on the combustibility behavior of cables, packaging materials, and other polymeric materials. Prior to joining FMRC, he was with Consumer Testing Laboratories, Inc., Canton, MA.

A. Tewarson, Factory Mutual Research Corporation, Norwood, MA 02062.

Archibald Tewarson joined Factory Mutual Research Corporation in 1968. He is Senior Research Specialist and Manager of the Flammability Section. Dr. Tewarson received his PhD degree in Fuel Science from Pennsylvania State University. His research on the physico-chemical aspects of fires including flammability of materials, smoke, and toxic compounds generated in fires is internationally recognized and has resulted in over 60 publications in this field.

Table 1 - Critical Flux and Energy Associated with Damage for Some Selected Wires and Cables^a

Insulation/Jacket Materials	Wire and Cable Size	Number of Conductor	Critical Flux (kW/m ²)	Energy for Damage (kJ/m ²)
PTFE/PTFE	16 AWG	7	16	9160
Silicone/Asbestos	14 AWG	9	18	1620
EPR/PE/Cl, S	9 AWG	7	19	1420
XPE/Neoprene	16 AWG	2	14	1330
PE/PVC	-	5	18	1000
Butyl/PVC	12 AWG	3	14	950

^a Data taken from Ref. 2-3, 5.
Forced Air Flow; Auto Ignition

Table 2 - Critical Heat Flux and Energy Associated with Ignition and Electrical Failure

Primary Insulation	Jacket Material	No. of Conductors	Wire and Cable Size	Critical Flux (kW/m ²)	Ignition Energy (kJ/m ²)	Energy for Electrical Failure (kJ/m ²)
Flexible Polyurethane Foams	Research Polymers	-	-	14	140	-
Red Oak Research Sample		-	-	11	600	-
Polyethylene	Polyvinylchloride	3	16 AWG	14	1100	3500
		9	12 AWG	14	1200	5200
Cross-linked Polyolefin	None	1	12 AWG	25	2100	3800
		1	12 AWG	25	2600	4000
		1	12 AWG	25	2600	6000
		1	646 MCM	25	3000	NF
		1	12 AWG	25	3900	3400
		1	12 AWG	25	5600	9000
		1	4/0 AWG	25	5600	25,000
		1	313 MCM	25	7100	33,000
		1	444 MCM	25	7700	25,000
Cross-linked Polyolefin	Polyvinylchloride	3	12 AWG	14	900	3200
		1	2/0 AWG	14	900	5000
		7	12 AWG	14	1100	7100
Cross-linked Polyolefin	Neoprene	2	16 AWG	14	1300	7700
Ethylene-Propylene Rubber	PE/Cl ₂ S	1	14 AWG	25	1300	10,000
		1	1000 MCM	25	1600	NF
Ethylene-Propylene Rubber	Polyolefin	1	12 AWG	25	2200	4800
		1	12 AWG	25	2300	4500
		1	12 AWG	25	3500	6300
		1	250 MCM	25	3900	25,000
		1	500 MCM	25	4200	NF
		1	500 MCM	25	4800	NF
		1	1000 MCM	25	5900	NF
		1	1500 MCM	25	7700	NF
	Neoprene	1	646 MCM	25	2500	33,000
Ethylene-Propylene Diene-Rubber	PE/Cl ₂ S	1	14 AWG	25	1500	6200
		1	12 AWG	25	1500	4000
Ethylene-Propylene Diene-Rubber	Polyolefin	1	2000 MCM	25	5000	NF
Silicone	Polyolefin	1	12 AWG	25	6700	13,000
		1	250 MCM	25	7700	20,000
ECTFE	None	1	4/0 AWG	25	12,500	9100
PTFE	None	1	2/0 AWG	25	16,700	20,000
Polyimide	PTFE	1	10 AWG	25	No ignition	NF

NF: No electrical failure at 60 kW/m² heat flux up to 10 minutes

^a: Data taken from Ref. 1-5.

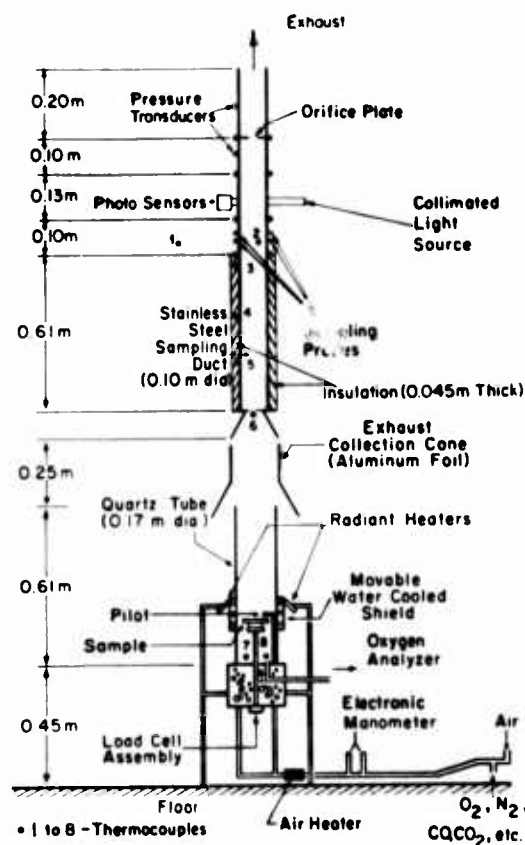
Forced air flow (piloted ignition)

^b: Under natural air flow (piloted ignition)

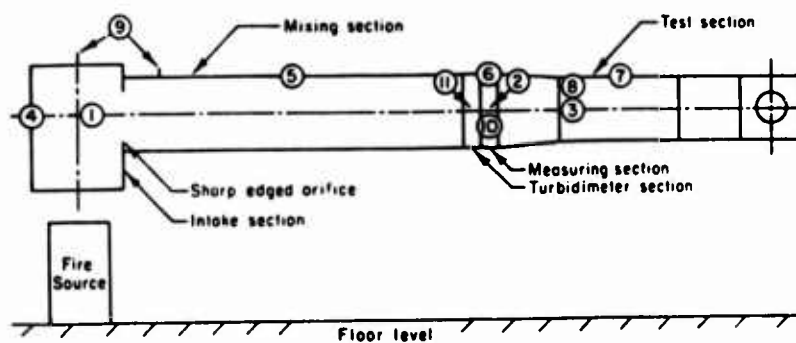
Table 3 - Fire Parameters Of Selected Wire And Cable Samples^a

Primary Insulation	Jacket Materials	Wire And Cable Size	Fuel Vapors (g/kJ)	Generation Parameter Heat ^d Toxic Product, CO (g/kJ)	Corrosion parameter ^b (micrometer of metal loss/kJ)	Light Obscuration Parameter (m ² /kJ)
Polystyrene	Research polymer	-	0.59	16	0.03	0.48
Polypropylene	Research polymer	-	0.49	19	0.02	0.19
Polyethylene	Research polymer	-	0.49	22	0.03	0.22
Polyvinyl chloride	Research polymer	-	0.40	2	0.02	1.2 ^c
Polyethylene	Polyvinyl chloride	12 AWG	0.30	5	0.01	0.18
	Polyvinyl chloride	16 AWG	0.46	8	0.01	0.32
	none	4/0 AWG	0.16	6	0.01	0.05
	none	313 MCM	0.17	6	0.01	0.03
	none	444 MCM	0.30	8	0.04	1.1
	Polyvinyl chloride	12 AWG	0.27	8	0.01	0.13
	Polyvinyl chloride	2/0 AWG	0.21	8	0.01	0.09
	Neoprene	16 AWG	0.38	5	0.02	0.17
	Cross-linked polyolefin	12 AWG	0.44	14	0.02	0.20
Ethylene propylene rubber	Cross-linked polyolefin	500 MCM	0.23	9	0.01	0.05
	Cross-linked polyolefin	1000 MCM	0.22	6	0.01	0.04
	Cross-linked polyolefin	1500 MCM	0.17	4	0.01	0.02
	PE/Cl,S	14 AWG	0.37	7	0.04	0.12
	PE/Cl,S	1000 MCM	0.22	4	0.04	0.08
	Neoprene	646 MCM	0.13	6	0.01	0.03
Silicone	Polyolefin	250 MCM	0.35	6	0.05	0.13
PTFE	none	2/0 AWG	0.25	2	0.03	0.001
ECTFE	none	4/0 AWG	0.18	2	0.01	0.002

^a Data from Refs. 1-2 and 4-5. All samples of wires and cables about 6 cm long; forced air flow, piloted ignition^b products dissolved in 100 ml of distilled water (30 hr exposure);^c Under nonflaming burning conditions^d Based on actual heat of combustion

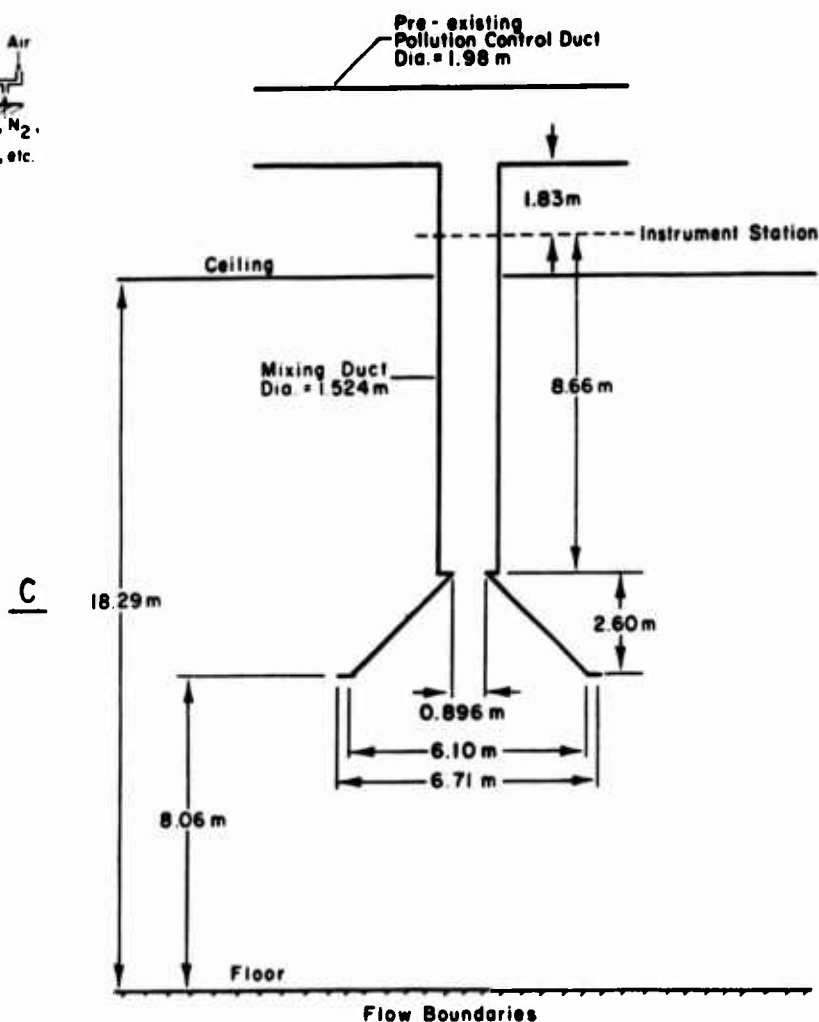


A



LOCATION	INSTRUMENTATION DESCRIPTION
① - ③	Gas temperatures
④ - ⑦	Wall temperatures
⑧	Pilot - static probe
⑨	Differential pressure transducer
⑩	Gas sampling probe
⑪	Smoke turbidimeter

B



C

Figure 1 Factory Mutual Combustibility Apparatuses: A, Small-Scale; B, Intermediate-Scale; C, Large-Scale

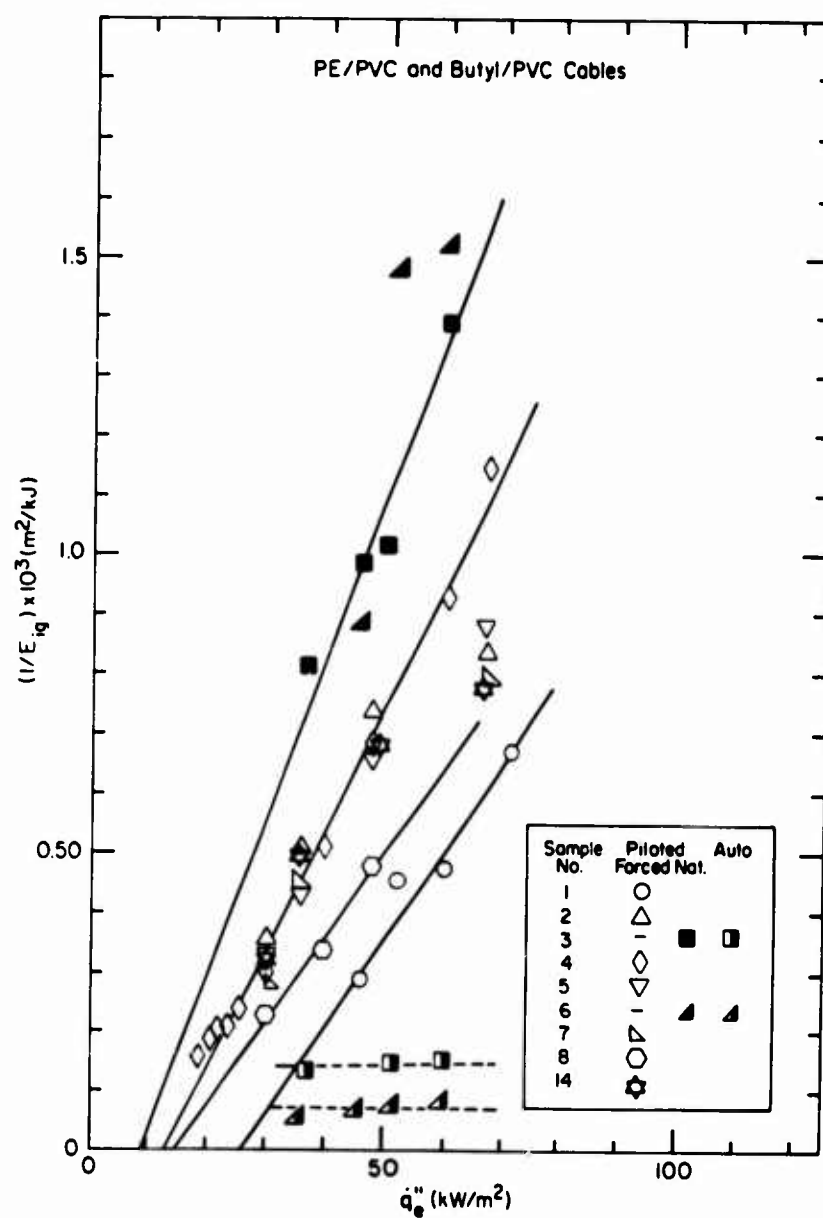


Figure 2. Inverse of ignition energy as a function of external radiant heat flux for piloted and autoignition under forced and natural air flow for PE/PVC and butyl/PVC cables. (sample length~0.06m, no correction for surface absorptivity)

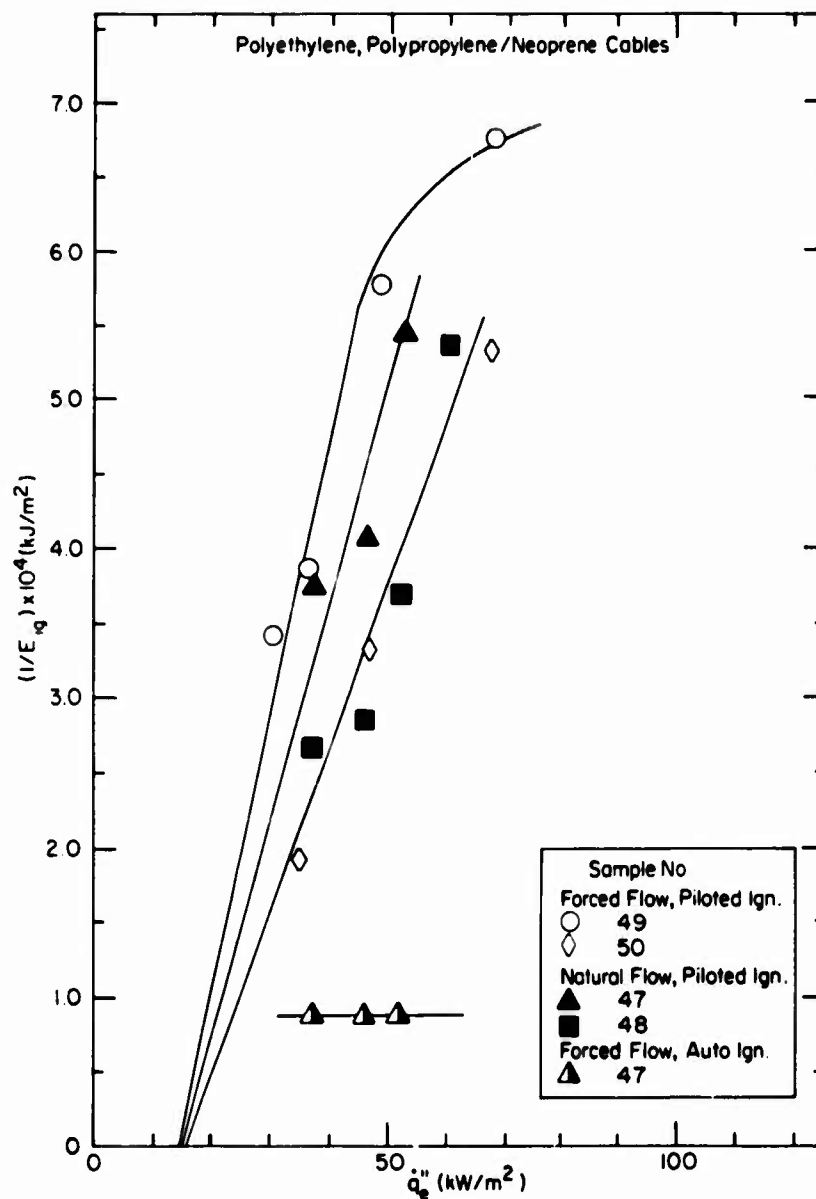


Figure 3. Inverse of ignition energy as a function of external radiant heat flux for piloted and autoignition under natural and forced air flow for polyethylene, polypropylene/neoprene cables (sample length ~ 0.06m, no correction for surface absorptivity)

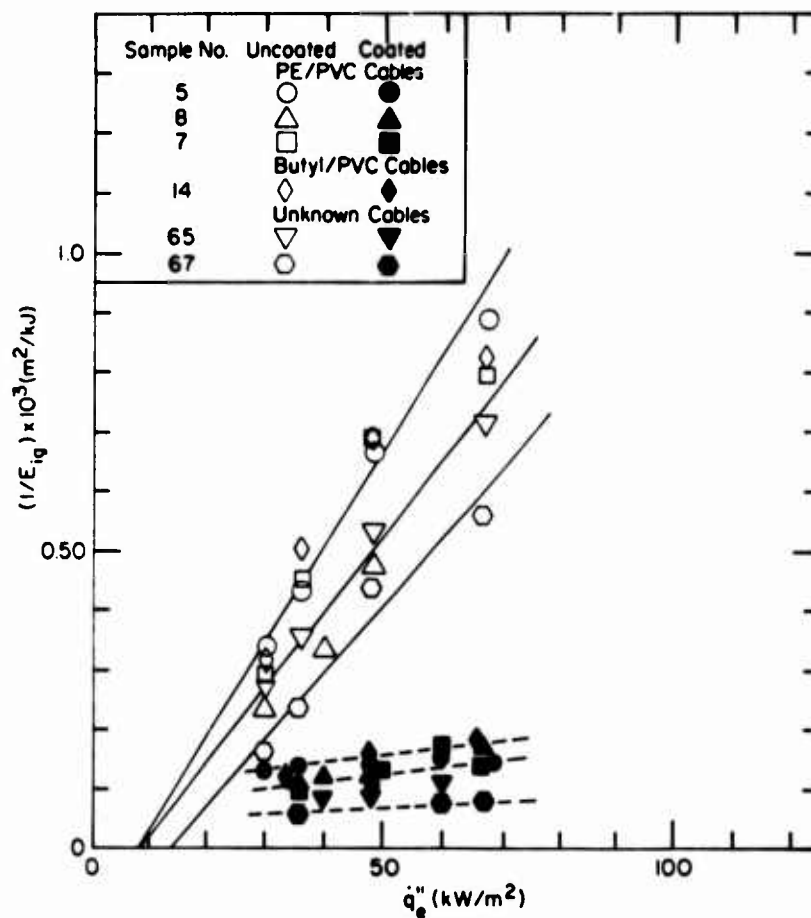


Figure 4. Inverse of ignition energy as a function of external radiant heat flux for piloted ignition under forced air flow for coated and uncoated cables (sample length ~ 0.06m, no correction for surface absorptivity)

The Acid Index — A Property of Polymer Combustion

P. C. Warren

Bell Communications Research, Inc.
Murray Hill, New Jersey 07974

ABSTRACT

Concern over acid evolution from burned fire retardant materials has prompted the development of a simple, precise, ten minute test to measure the phenomenon. The "acid index" (AI) is defined as the milliequivalents of acid (< pH 4.5) evolved per cc of original polymer when burned in pure oxygen. Poly(vinyl chloride) formulations as well as a variety of other wire and cable materials have been measured by this technique. Some of the principles involved in reducing the AI of polymeric materials while still maintaining low flammability and acceptable mechanical properties are discussed.

Introduction

The flammability of synthetic wire and cable materials is an important consideration since they are often utilized indoors or near dwellings. Ease of ignition, rate of flame spread, smoke development, and acidic or hazardous gas formation are the main areas of concern; the latter topics in particular have received increasing attention in recent years. An enormous amount of plasticized PVC has been incorporated into such products throughout the world, and much of it is more or less fire retardant. Nevertheless, PVC has come under attack because of its reputed heavy smoke and acidic byproducts encountered in incipient as well as mature fires.

PVC-based materials generate hydrogen chloride under pyrolytic or burning conditions. Indeed, it is well recognized that this process makes ignition difficult and slows the rate of combustion, which is one reason why the material is used in the first place. The purpose here is to document a simple experiment that can be used to quickly and accurately characterize the amount of acid gas that evolves from any plastic or rubber material. The further intent is to put the outgassing of PVC materials into perspective relative to other common fire retardant polymers. A basic assumption, of course, is that acidic gases or aerosols are generally not beneficial to nearby people or things.

Results and Discussion

1. Theory

The amount of hydrogen chloride or bromide liberated from burned polymers is typically determined by pyrolysis in air or nitrogen followed by titration to form insoluble silver halide, using either a specific (halide) electrode, or Mohr or Volhard wet methods to locate the endpoint. An alternative is to determine these materials by acid neutralization, which will be sensitive not only to the above elements but fluorine and sulfur as well. Since carbon dioxide is always a product of combustion, the equivalence point must be at a pH low enough to avoid interference by carbonic acid:



The quantitative treatment of carbonate systems is detailed in most introductory analytical chemistry texts.⁽¹⁾ Carbonic acid will not ionize

significantly until pH 4.5 is reached, so stronger acids will be preferentially neutralized by strong base. To give this equivalence point some practical meaning, one might arbitrarily say that evolved acid below about pH 4.5 has the potential of being interactive with people and/or things, while that above this number might be relatively innocuous. This statement refers only to the acid function of the molecule and says nothing about individual or collective combustion toxicities or corrosivities of these materials.

A fundamental combustion property of any synthetic or natural polymer is suggested based on the above experiment. The milliequivalents of evolved acid at or below pH 4.5 per cubic centimeter of original polymer burned in pure oxygen is defined as the acid index:

$$\text{acid index (mequiv/cc)} \equiv \frac{NV\rho}{w}$$

N = normality of base, mequiv/ml
V = volume of base, ml
 ρ = density of polymer, g/cc
w = weight of polymer, g

Milliequivalents of acid are determined because that is the only fundamental quantity that can be derived from a pH measurement. The procedure thus involves burning a known weight of material in pure oxygen, dissolving all evolved acid into water, titrating with standard base to pH 4.5 and correcting to mequiv/cc by multiplying by the specific gravity of the original material. This latter step allows comparison on a volume rather than a weight basis, thus avoiding errors when densities of materials vary greatly, as they often do when heavy inorganic fillers are incorporated. This concept also recognizes that materials are usually utilized in a given size rather than mass. Finally, given the amount of various materials in a container, room or building and knowing their individual acid indices, the total amount of acid evolved from total combustion is conveniently estimated.

2. Determination of Acid Index

Fifty milliliters of distilled water and a magnetic stirring bar are placed inside a Schoeniger combustion flask⁽²⁾ and the system is flushed with oxygen for about one minute. A 20 ± 5 mg sample of polymer, weighed to the nearest 0.1 mg, is wrapped in a piece of ashless filter paper and inserted into the platinum screen. The filter paper is ignited, the stopper placed in the flask, the assembly inverted and the sample totally combusted in 5-10 seconds. If there is no solid left in the platinum screen, the flask is simply shaken for thirty seconds or so. If some does remain, the solution must be magnetically stirred until the smoky atmosphere turns clear (~10 minutes); care must be taken that the residue not be allowed to contact the water below. After removal of the stopper, the contents of the flask are decanted into a 150 ml beaker, followed by a 10-20 ml distilled water rinse.

The solution is titrated with 0.1N NaOH to a pH 4.5 electrode or bromocresol green endpoint. If the latter method is used, 1 drop of a 1% phenol solution will be necessary to prevent possible bleaching of the indicator. For very small amounts of liberated acid, a blank reaction (combustion of filter paper only) should be determined and

this volume subtracted from that obtained from burned polymer. The acid index would be determined from the following relationship:

$$\text{acid index, mequiv/cc} = \frac{(0.1 \text{ mequiv/ml})(\text{volume of base, ml})(\text{density of polymer, g/cc})}{\text{weight of polymer, g}}$$

3. Quality Control Go/NoGo Test Using The Acid Index Method

A 20 ± 5 mg sample of polymer, weighed to the nearest 0.1 mg, is wrapped in a piece of ashless filter paper and placed in the platinum screen attached to the stopper of the Schoeniger flask. The 500 ml Schoeniger flask is filled with 50 ml distilled water, 5 drops of 0.04% bromocresol green indicator, 1 drop of 1% aqueous phenol and a volume of 0.1N NaOH as determined by the acid index desired:

$$\text{Volume, ml} = \frac{(\text{acid index, mequiv/cc})(\text{weight of polymer, g})}{(0.1 \text{ mequiv/ml})(\text{density of polymer, g/cc})}$$

The flask is then flushed with oxygen for about one minute, the filter paper ignited, the stopper placed in the flask, the assembly inverted and the sample completely combusted in 5-10 seconds. The flask is then shaken vigorously for 2-3 seconds, and the color of the solution is noted; a blue solution indicates that the polymer has an acid index lower than that specified above, a green one says that the acid indices are identical and a yellow one shows that the polymer acid index is higher than that selected. In short, a blue or green color would pass the test while a yellow one would fail it.

4. Acid Index Combustion Experiment

The combustion experiment itself is based on the Schoeniger combustion apparatus, which is nothing more than a sealed Erlenmeyer flask containing a small platinum screen to support the burning sample, pictured in Figure 1. Initial attempts to burn samples in

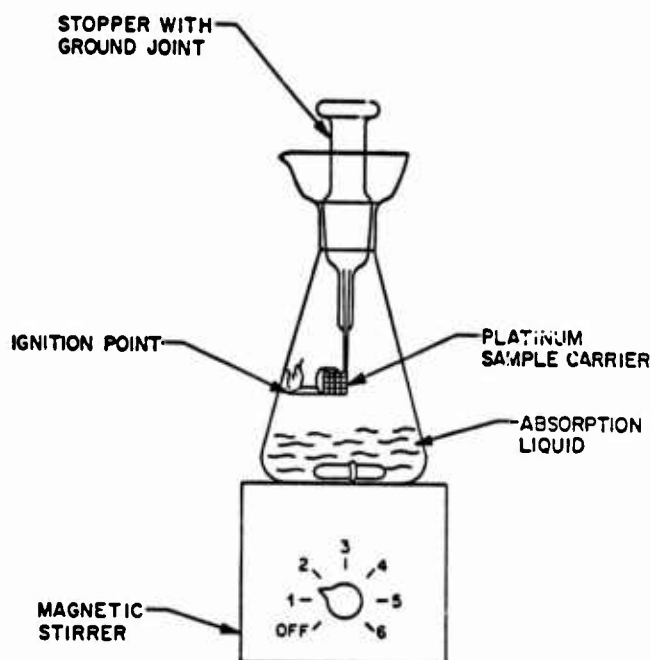


Figure 1

50/50 or 75/25 oxygen-nitrogen mixtures were unsuccessful because of poor sample ignition or incomplete combustion, hence all subsequent tests were run in 100% oxygen. All samples, including the bulky fluorocarbons, appeared to react completely under these conditions, at least from a macroscopic point of view. Once in a while the residue would obviously drop out of the screen during combustion into the

water below, necessitating a repeat experiment. Also, the sample size of 20 ± 5 mg seemed to be about optimum for the 500 ml flask. Too large a sample gave too vigorous a reaction resulting in an occasional spattering of unburned material, while a smaller amount gave too insensitive a test. Finally, in running hundreds of experiments in this apparatus there was never any obvious pressure buildup inside the flask and consequently never any sense of danger. The safety of the method has been verified in the literature.⁽³⁾

Real fires create hot, oxygen deficient conditions, quite unlike those inside the Schoeniger flask. In the laboratory experiment, a ~20 mg sample is consumed in a 500 cc flask, which translates to about a tenfold excess of required oxygen. Clearly the test will convert more of a given amount of sample to oxidized products than will occur in actual fires; accordingly the test should be viewed as a "worst case" condition. It should be kept in mind, however, that many halogenated fire retardants eliminate hydrogen halides early in the decomposition cycle, so that subsequent combustion conditions should not greatly affect the quantity of acid gases produced.

Table 1

Material	Density	(Experiment)	(Theoretical)
		AI	AI
PE	0.96	0	0
PE + 10 DBDPE ^a	0.97	0.9	1
PVC	1.40	21.5	22
PVC + 60 DOP ^{b,c}	1.22	12.0	12
PVC + 60 TCP ^{b,d}	1.33	13.0	13
PVC + 60 TPP ^{b,e}	1.37	13.5	14
PVC + 60 T23P ^{b,f}	1.66	19.5	21
PVF	1.50	28.0	33
PVF ₂	1.78	49.0	55
TFE/FEP	2.15	52.0	86
TFE	2.22	59.0	86
PPS ^g	1.34	12.0	12

^a DBDPE = decabromodiphenyl ether

^b PVC formulation: PVC; 60 phr plasticizer; 5 phr tribasic lead sulfate; 0.5 phr ethylene bis-stearamide; 0.5 phr dibasic lead stearate.

^c DOP = di-2-ethylhexyl phthalate

^d TCP = tricresyl phosphate, only $\text{H}_3\text{PO}_4 \rightarrow \text{H}_2\text{PO}_4^- + \text{H}^+$ and $\text{HCl} \rightarrow \text{H}^+ + \text{Cl}^-$ were considered in calculating total acidity.

^e TPP = triphenyl phosphate, only $\text{H}_3\text{PO}_4 \rightarrow \text{H}_2\text{PO}_4^- + \text{H}^+$ and $\text{HCl} \rightarrow \text{H}^+ + \text{Cl}^-$ were considered in calculating total acidity.

^f T23P = tris(2,3 dibromopropyl)phosphate, only $\text{H}_3\text{PO}_4 \rightarrow \text{H}^+ + \text{H}_2\text{PO}_4^-$, $\text{HBr} \rightarrow \text{H}^+ + \text{Br}^-$ and $\text{HCl} \rightarrow \text{H}^+ + \text{Cl}^-$ were considered in calculating total acidity.

^g PPS theoretical AI assumes only 1 titrable proton at <pH 4.5.

Table 1 compares the acid indices of some known compounds with the theoretical amount of acid they are capable of yielding. Only the elements Cl, Br, F, S and P were considered in calculating the total acidity. Iodine and selenium, as well as perhaps other elements, also give acid products but are found so infrequently in plastic materials that they were not considered. Carbon acids are not detected by this method because they are totally combusted. Unplasticized poly(vinyl chloride) (PVC) gave an acid index of 21.5 mequiv/cc, slightly but consistently less than a theoretical value of 22.4. There was always a

slight odor of chlorine when the flask was opened after combustion, suggesting that most, but not all, of the chlorine in PVC was converted to HCl. When pH indicators were used to determine the acid-base titration endpoint, their color was sometimes bleached clear, an observation also consistent with free halogen.

A di-2-ethylhexyl phthalate plasticized PVC showed a lower value of only 12 mequiv/cc because the acid-forming PVC matrix had been diluted with the non-acid forming liquid. The phosphate plasticized materials gave numbers very similar to the phthalate materials, because phosphorus adds almost nothing to the total acidity of the system. Not only does this element account for very little (<10%) of either plasticizer, but only the first proton of any phosphoric acid formed ($\text{H}_3\text{PO}_4 \rightarrow \text{H}^+ + \text{H}_2\text{PO}_4^-$) is acidic enough to be neutralized below pH 4.5.

Brominated materials are commonly incorporated into polymers as fire retardants and their effect on the acid index is substantial, as evidenced by the tris(2,3 dibromopropyl) phosphate (T23P) plasticized PVC. Combustion of bromine-containing compounds in 100% oxygen is reported to give free bromine as well as hydrogen bromide,⁽⁴⁾ while those combusted in air apparently produce only HBr.⁽⁵⁾ This suggests that the acid index measurement might underestimate the actual amount of acid produced in a real fire, but the T23P-plasticized PVC data indicate that the effect is probably only slight. Furthermore, there is evidence that while free bromine is definitely formed in the Schoeniger experiment it is usually outweighed by HBr.⁽⁶⁾ A second consideration is that the small amount of bromine rapidly bleaches any pH indicators used in the titration step, similar to the chlorine experience. This problem is circumvented by either using a pH electrode rather than an indicator, or by adding 1 drop of 1% aqueous phenol to the solution before indicator titration. Free bromine or hypobromite ion apparently reacts with phenol faster than it reacts with the indicator.⁽⁷⁾

Fluoropolymers give very large acid indices, as shown by the several examples in the table. They also give the least accurate values of any of the materials that produce acidic gases. While poly(vinyl fluoride) (PVF) and poly(vinylidene fluoride) (PVF₂) gave acid indices that were within 15% of expected numbers, perfluorinated materials showed only slightly more than half of their calculated values. Several possible reasons could account for these facts. First, perfluorinated materials usually pyrolyze rapidly down to monomer, some of which

probably escapes the combustion zone only partially oxidized. Second, the HF formed might react with the glassware, but this seems unlikely because a control experiment showed that identical results were obtained when the solution was titrated either five or thirty minutes after combustion. Third, at least some of the low values are due to the fact that HF, being a weak acid ($\text{pK}_a = 3.45$), is not totally neutralized at pH 4.5. Figure 2 compares the titration curves obtained from combustion of PVC (HCl titration) and PVF₂ (HF titration).

Finally, polyphenylene sulfide (PPS) was evaluated for its acid index and it agrees well with the theoretical value if only one proton is neutralized at a pH <4.5. Presumably SO₂ rapidly hydrolyzes to sulfurous acid (H₂SO₃); sulfuric acid is a strong acid that would yield two protons and apparently is not formed.

Table 2

Acid Index of Various Polymers

Material	Density	AI
red oak	0.66	0
polystyrene	1.04	0
6,6 polyamide	1.12	0
polyethylene terephthalate	1.34	0
polycarbonate	1.20	0
PVC/ABS blend	1.13	9
"low HCl" PVC jacket	1.52	2
PVC Type NM power cable jacket	1.36	9
PVC power cable insulation	1.32	12
FR ^a ethylene/EVA copolymer	1.50	8
40% glass filled PPS	1.60	9
FR ABS	1.20	3
FR polyamide, 25% glass filled	1.56	3
Neoprene rubber cable jacket	1.52	5
FR ^a polycarbonate	1.22	1
ethylene/chlorotrifluoroethylene copolymer	1.68	37
perfluoroalkoxy fluoropolymer	2.15	38
fluoroethylene/fluoropropylene copolymer	2.15	51

^aFR = fire retardant

Table 2 outlines some representative acid indices for various wire and cable materials and some molding resins. In general, fire retardant materials that incorporate any of the halogens or sulfur will have a non-zero value. Blends of PVC with either plasticizer or impact modifiers typically give numbers around 10 ± 3 . Vinyl materials that were highly loaded with basic fillers gave much lower AI values. In fact, PVC compounds formulated to provide minimum acid gas were in that sense no worse than other fire retardant materials.

5. Effect of Basic Fillers on Acid Index

Basic fillers such as CaCO₃, Li₂CO₃, K₂CO₃ etc., when added to PVC formulations, will react with gaseous hydrogen chloride during combustion and greatly reduce the acid evolved into the nearby environment.⁽⁸⁻¹⁰⁾ Figures 3 and 4 show the effect of added CaCO₃ on AI for unplasticized and phosphate plasticized PVC, respectively. In both cases, a reduction in acid evolution occurs because of volume dilution of the resin by filler and plasticizer, as well as by reaction to

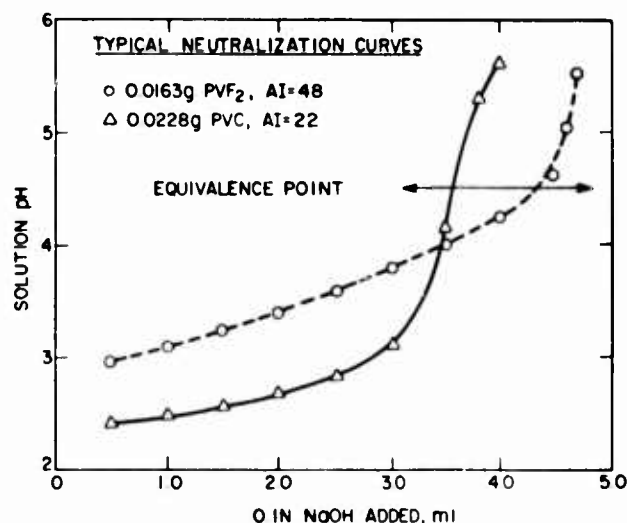


Figure 2

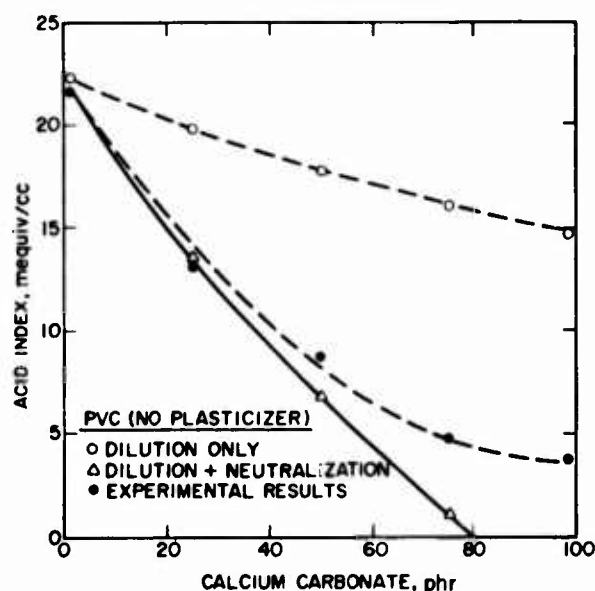


Figure 3

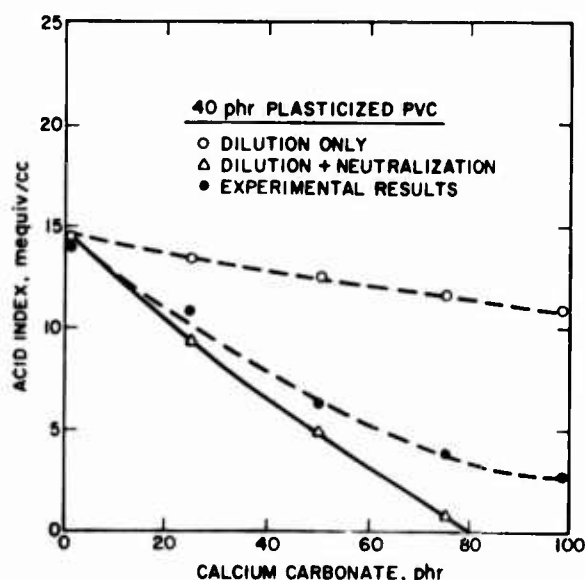


Figure 4

form stable and inert products:



From zero up to about 50 phr of added CaCO_3 , the experimental results emulate the theoretical numbers reasonably well but at higher concentrations the basic additive is less and less effective. The stoichiometric concentration is exactly 80 phr of additive, but fully 25% of the released HCl is unreacted at that loading. Even at

150 phr, only 90% of the acid is absorbed. The particle size of the CaCO_3 in these experiments averaged 1.2 μm . Smaller particles would improve these numbers⁽¹⁰⁾ but at the unacceptable cost of poor mechanical properties. High loadings of fillers are almost always detrimental to polymer performance, hence 80-100 phr may represent a practical concentration limit.

6. Effect of Plasticizer Content on Efficiency of Acid Neutralization

Since most PVC wire and cable materials are plasticized, the effect of the amount of plasticizer on acid scavenging of CaCO_3 was briefly investigated. Table 3 lists the milliequivalents of acid per gram of PVC resin incorporated into nine formulations, where CaCO_3 was varied between 0, 50 and 100 phr and plasticizer between 0, 30 and 60 phr,^a a range that encompasses most jacket and insulation compounds. Clearly the extent of reaction of basic salt with evolved hydrogen chloride is essentially unaffected by the presence of plasticizer. The acid index, then, is reduced by addition of plasticizer only because it increases the total volume of the system, not because of any subtle changes in the acid neutralization process.

Table 3

Effect of Plasticizer Content on Efficiency of Neutralization

PVC Formulation ^a plasticizer phr	Mequiv/g PVC Resin		
	0 phr CaCO_3	50 phr CaCO_3	100 phr CaCO_3
0	15.1	8.1	4.1
30	15.7	7.0	3.7
60	15.6	7.0	3.8

^a 100 phr 0.92 IV PVC resin; 0, 30 or 60 phr dialkyl phthalate plasticizer; 0, 50 or 100 phr 1.2 μm stearate coated CaCO_3 ; 5 phr tribasic lead sulfate; 0.5 phr dibasic lead stearate.

7. Effect of Basic Fillers on Fire Retardant Additives

Antimony oxide is essential in optimizing the fire resistance of PVC materials as well as those that employ chlorinated or brominated fire retardants. When basic fillers are added, they presumably compete with antimony oxide for hydrogen chloride, since it is well established that the antimony is primarily effective in the flame and chlorine is necessary to provide sufficient volatility for the heavy element. Figure 5 compares the flammability via the oxygen index measurement^b of 50 phr phthalate plasticized PVC compounds, one containing 100 phr of CaCO_3 (AI = 4) and one containing no filler (AI = 13). As antimony oxide is added to each formulation, it is clear that they respond similarly, albeit the filled material is considerably more flammable than the unfilled one. Clearly antimony oxide is just as effective in formulations where most of the HCl is absorbed by the basic filler as where it is not.

One way to circumvent the problem of higher flammability when large amounts of basic fillers are utilized is to incorporate some bromine-containing additives that release HBr. Since bromine is about five times as effective as a molar equivalent of chlorine in reducing the oxygen index,⁽¹¹⁾ a much smaller amount of volatile halogen acid is required to maintain low flammability. Again, one has to consider the

^a phr = parts per hundred of resin

^b The oxygen index is defined as the minimum percent concentration of oxygen that will just sustain downwards combustion of a vertically oriented polymer specimen.

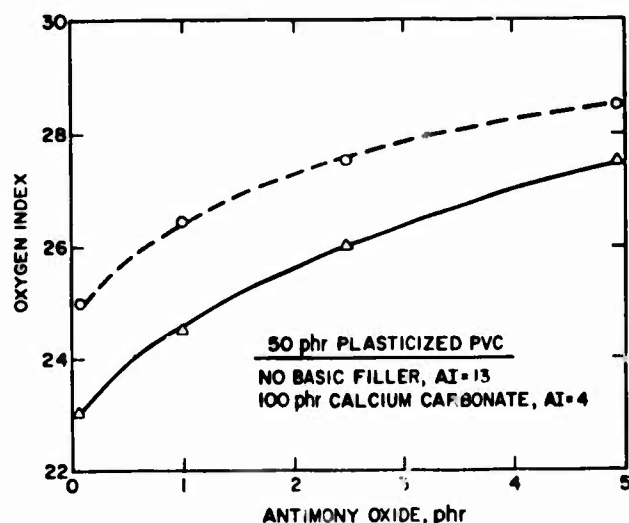


Figure 5

competition of HBr and the HCl for the basic filler, especially since the hydrogen bromide is probably liberated first. If all the HBr is totally neutralized by CaCO_3 , none will reach the flame where it is most active. Figure 6 shows the effect on the oxygen index of adding small amounts of the tetrabromide of 4-vinylcyclohexene to two 50 phr plasticized PVC formulations, one containing 100 phr of calcium carbonate (AI = 4) and one containing no basic filler (AI = 13). Clearly the heavier halogen works about as effectively in the low acid formulation as in the high acid one.

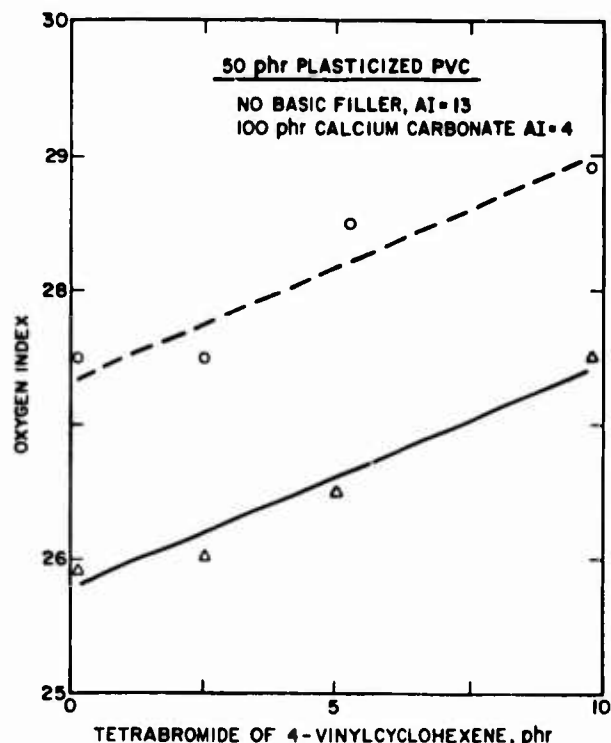


Figure 6

The criticism that basic fillers inhibit the full fire retardant properties of PVC formulations is reasonably well grounded, but the effect can be compensated by using the principles outlined above, among others. Table 4 lists some PVC cable jacket formulations along with several critical properties. Conventional PVC jacket compounds have relatively good resistance to combustion but at the expense of copious acid production during a fire. By filling conventional materials with CaCO_3 the acid production is reduced by at least two-thirds but the flammability is significantly enhanced. One example of a material that optimizes both properties consists of PVC lightly plasticized with a linear dicarboxylate combined with a fire retardant additive, tris(2,3 dibromopropyl) phosphate. The excellent performance has been accomplished without the usual trade-off in low temperature properties, although it comes at a somewhat higher price. This formulation is not necessarily recommended as the best one for the application, but serves to illustrate the principle that oxygen index, acid index and low temperature brittleness are not necessarily mutually exclusive properties.

Table 4

PVC Cable Jacket Compounds

Additive	Conventional Fire Retardant	Conventional Low Acid	Fire Retardant Low Acid
PVC	100	100	100
dialkyl phthalate	40	65	-
dialkyl adipate	-	-	35
1 μm coated CaCO_3	-	100	100
$\text{Al}_2\text{O}_3 \cdot 3\text{H}_2\text{O}$	15	-	-
Sb_2O_3	3	3	3
tris(2,3 dibromopropyl)phosphate	-	-	15
lead stabilizer	5	5	5
Properties			
oxygen index, % O	30.5	26.5	31
acid index, mequiv/cc	13	3.5	3.5
tensile strength, ASTM D412, psi	2800	1530	1950
elongation, ASTM D412, %	300	180	200
LTB,* ASTM D746, °C	-26	-25	-22
lb-vol cost, 1984 \$.61	.51	.74

* LTB = low temperature brittleness

Conclusions

Organic materials that incorporate any of the halogens and/or sulfur all produce relatively strong acids (pH < 4.5) when the gases from their combustion are combined with water. The extent of acid evolution can be measured by a simple test that yields the "acid index" (AI), defined as the milliequivalents of acid released per cc of original polymer after combustion in pure oxygen. The acid index is similar to the "oxygen index" (OI) in that both are derived from combustion experiments, each number is highly reproducible and unique to a given material, neither requires a knowledge of the polymer structure and either may or may not predict the outcome of a real fire. The AI will always represent the most oxidized and acidic products from combustion, and hence should always be treated as a worst case prediction. The OI, on the other hand, is never a worst case prediction because of its relatively mild test conditions.

The AI concept is useful because it quickly summarizes possible concerns about a given material relative to acids that may arise should

combustion occur. It says absolutely nothing about toxicity of products of combustion because acidity and toxicity are not simply related. It also says very little about corrosivity, because it does not distinguish between various acids. It also will not detect carbon acids that might arise from partial combustion. It does allow one to anticipate the maximum quantity of acids possible from an assembly of unknown materials in case of fire. It is easily adopted to quality control, since a go/no go AI can be determined in 5-10 minutes with simple, inexpensive equipment. Finally, and most important, it is a research tool with which materials can be formulated and quickly measured for liberated acid, thus providing a means towards a goal of negligible acid output.

How should acid gas evolution be treated in the overall picture of unwanted combustion of polymeric materials? Clearly the greatest priority should be the selection of materials that do not ignite or spread flame easily in the first place - where there is no fire there are usually no acidic gases. It is interesting to note, however, that PVC wire insulations have been criticized because acids may evolve from these materials in the realm of $>250^{\circ}\text{C}$, even though combustion may never occur.⁽¹²⁾ Also, why worry about acid gases from fluoropolymers when they are apparently so difficult to ignite or burn? One reason is that the mixed hydrocarbon/fluorocarbon materials such as polyvinyl fluoride, polyvinylidene fluoride, copolymers of ethylene and tetrafluoroethylene, etc. all yield HF when heated by any nearby source. Secondly, perfluorinated materials will still pyrolyze and combust in the heat from a large fire, as shown by the reported sharp temperature/oxygen index slope for polytetrafluoroethylene. Its oxygen index at room temperature is 95% oxygen, but at $\sim 250^{\circ}\text{C}$ it is well below 50% and not greatly different from unplasticized PVC.⁽¹³⁾

Reduction in smoke or particulate formation is probably second in priority, not only because it obscures visibility but may act as a carrier for irritating materials that can bypass normal bodily defenses. The extent to which acidic gases contribute to this mechanism depends on many parameters which may or may not develop in an actual fire, and in any case is outside the scope of this discussion.

Finally, it is apparent that acid evolution from burned, plasticized PVC compounds is not greatly different from other fire retardant plastics provided the material is formulated to minimize that property. While PVC has an AI value of 22, most commercial wire and cable formulations exhibit numbers about half of that. Incorporation of basic fillers will reduce the number by another factor of 3-5, so that the practical AI limit appears to be about an order of magnitude lower than the pure polymer. Further reductions in AI will be extraordinarily difficult in this system without compromising the other valuable properties that make PVC the workhorse that it is in the wire and cable industry.

REFERENCES

1. See, for example, A. R. Olson, C. W. Koch and G. C. Pimentel, *Introductory Quantitative Chemistry*, W. H. Freeman and Co. (San Francisco, 1956) pp. 214-227.
2. W. Schoeniger, *Mikrochim. Acta*, 123 (1955); 869 (1956).
3. A. M. G. MacDonald, *Analyst* 86 3 (1961).
4. C. E. Childs, E. E. Meyers, J. Cheng, E. Laframboise and R. B. Balodis, *Microchem. J.* 7 266 (1963).
5. A. W. Benbow and C. F. Cullis, *European Polym. J.* 11 723 (1975).
6. L. J. Anthony, B. E. Prescott, X. Quan, unpublished data.
7. P. J. M. Radford, "Oxyacids of Bromine and their Salts," in *Bromine and its Compounds*, Z. E. Jolles, ed., Academic Press (New York, 1966) p. 162.

8. O. Leuchs, "A New Self-Extinguishing Hydrogen Chloride Binding PVC Jacketing Compound for Cables," *Proceedings of the Nineteenth International Wire and Cable Symposium*, (Atlantic City, 1970) p. 239.
9. M. M. O'Mara, *J. Polym. Sci., A-1*, 9 1387 (1971).
10. G. Matthews and G. S. Plemper, *Brit. Polym. J.* 16 34 (1984); 15 95 (1983); 13 18 (1981).
11. P. C. Warren, "Mechanism of Inhibition of Poly(Vinyl Chloride)," *Technical Papers, SPE RETEC*, Newark, N.J., October 14, 1971, pp. 29-34.
12. D. Wallace, *J. Combust. Toxicology* 8 205 (1981).
13. C. P. Fenimore and G. W. Jones, *J. Appl. Polym. Sci.* 13 285 (1969).



Paul C. Warren is a district manager of the Plastics Chemistry Research group in Bell Communications Research, Inc., Murray Hill, N.J. After receiving a Ph.D. in organic chemistry from Cornell University in 1969, he joined Bell Laboratories where he pursued research in polymer flammability, test methods and PVC technology. He attained his present position in January, 1984 and his interests now center on the use and reliability of polymeric materials in telecommunications products.

Fire Safety of Wire and Cable Materials, Part III An Approach to Estimating Cable Fire Hazard

Frederic B. Clarke, Ph.D. and Philip J. DiNenno, P.E.

Benjamin/Clarke Associates, Inc.

Abstract

An assessment of the fire hazard of cable insulation materials, combining selected fire and smoke properties is presented. Using single relationships between heat release rate, flame spread rate, smoke obscuration and smoke toxicity, consistent cable performance requirements are developed. These requirements are based on rationally developed hazard criteria. The two approaches presented are intentionally simplified in order to demonstrate the relationships between the various fire and smoke properties. Comparisons between these properties and existing fire test methods for cable materials are drawn.

Introduction

In the first paper in this series, presented at the 32nd International Wire and Cable Symposium, it was shown that several cable fire properties contribute to the manner in which fire develops (1). These flammability properties are in turn closely coupled to the way in which a cable generates smoke. The set of cable fire variables required to describe fire hazard must therefore include data on the quantity and quality of the smoke. Smoke quantity is generally measured by smoke obscuration techniques, while smoke quality is generally measured in terms of its toxicity. The second paper in this series, presented at the Marine Cable Symposium, dealt with toxicity measurements of smoke (2). This paper, the third in the series, makes a first attempt to integrate cable fire properties into an assessment of hazard.

In any given situation, a cable fire's impact will depend as much on the environment in which the fire takes place, and the characteristics of the space in which the smoke is contained, as it does on the properties of the cable itself. Both smoke obscuration and toxicity are functions of the concentration of the smoke, so that the ratio of the amount of material burned to the volume to which the smoke is contained is very important.

The rate at which smoke is produced is also important. All smoke is toxic, so that the difference in smoke hazard posed by two materials under the same fire conditions is the relative time at which an intolerable amount of smoke has been produced. In general, ways of computing fire hazard involve calculating the time difference between fire initiation or detection and the onset of the first intolerable condition. It should be noted that this condition may be temperature, if the fire has a very rapid energy release rate or the volume in which it is contained is very small; or it may be the toxic effects of the smoke. Obscuration of the smoke by itself impedes escape but is not a killer. Rather, it causes the victims to remain in the smoke longer or perhaps to require rescue, where they could otherwise escape by themselves.

The purpose of this paper is to translate cable fire properties, as could be measured in the laboratory into estimates of the relative hazard they pose under actual fire conditions. The approach taken in this paper is to use specific examples rather than to treat the problem in the general case. We begin by simply envisioning a small cable run whose smoke is assumed to fill up the

floor of a small building. However, a more careful consideration of the problem reveals that the space in which the cables are contained can itself influence the rate at which they burn, and therefore the rate at which smoke is produced. Therefore, the second part of our approach is to modify a general case in light of common conditions of use and the lack of some of the desirable data.

Calculations of Smoke Hazard Criteria: An Illustration

Typical buildings are designed so that smoke from a fire is contained in the vicinity of the fire origin. The precise size of the smoke zone is dictated by the applicable building code. Typically, however, it may be a floor area of 2000 square feet (approximately 200 square meters). If the space is 8 feet high, this corresponds to a volume of 16,000 feet, or roughly 500 cubic meters.

For purposes of this illustration, let it be assumed that a cable bed 0.5 m in width runs through this compartment, (i.e. that the cable is not located in the plenum space) and that the scenario of ignition is one in which the cable is assumed to be ignitable, and to burn, by itself, i.e. without the necessary agency of another major fire. Finally, suppose that it is decided that the compartment should be safe for evacuation for 10 minutes after ignition of the fire. This requires:

- a. that visibility after the fire has burned for 10 minutes be sufficient that escape is not prevented; and

- b. that the concentration of smoke be not toxicologically incapacitating before that time.

Based on these parameters, limits can be set on the maximum concentration of smoke which such considerations would allow. From the allowable smoke concentration, sets of fire properties which give that concentration or less, can be determined.

Smoke Obscuration

There are differing opinions as to the level of visibility required for escape, but most experts agree that an acceptable level is no less than 1 meter -- and in some cases as much as 3.5 meter. If one chooses 1 meter visibility as the criterion, the allowable smoke density (in optical density per meter) can be calculated using a relationship determined by Rashbash and Pratt (3).

$$OD/m = \frac{1.3}{\left[\frac{1.4}{v} \right]}$$

where v is the visibility in meters. A visibility of 1 meter corresponds to a smoke optical density of 1.55/m. The optical density of the smoke in turn can be related to the mass of smoke through the "mass optical density" (MOD) of the burning material:

$$O.D./m = \frac{(MOD) (Smoke Mass, M)}{Compartment Volume}$$

For a volume of 500 cubic meters, the allowable mass of smoke, M, is any amount which does not block visibility. Hence,

$$M \leq \frac{1.5 \times 500}{(\text{MOD})} = \frac{750}{\text{MOD}(\text{in m/kg})}$$

The total mass of smoke produced as a function of time, t , is given by integrating the expression for mass burning rate, \dot{m} .

$$M = \int \dot{m} dt$$

It can readily be shown that a fire on a cable bed of width b loses mass in proportion to the area of cable burning. If fire spreads across the surface of the tray at a constant rate, f , then:

$$\text{Area burning} = bft \quad \text{and}$$

$$\dot{M} = \dot{q}'' \frac{bft}{H_c}, \quad \text{where } \dot{q}'' \text{ is the}$$

heat release rate per unit area and H_c is the heat of combustion. Thus,

$$M = \int \dot{m} dt = \dot{q}'' \frac{bft^2}{2H_c} \quad (1)$$

The allowable amount of smoke mass, M , has been determined by the allowable visibility and the mass optical density; the escape time criterion has been chosen as 10 minutes (600 sec) and the width of the cable run as .5 m. Substituting these values into the expression for smoke mass yields:

$$\frac{750}{\text{MOD}} \geq \frac{0.5 \dot{q}'' f(600 \text{ sec})^2}{2 H_c}, \quad \text{or}$$

$$\frac{(\dot{q}'')(\text{MOD})(f)}{H_c} \leq .0083 \text{ m/sec} \quad (2)$$

The intent of this expression is to provide that for this room volume and ignition scenario, cable having any combination of heat release rate, \dot{q}'' , flame spread, f , heat of combustion, H_c , and smoke mass optical density, MOD, which satisfies this inequality will

require 10 minutes or more to fill the room to a smoke density which substantially impedes escape.

Toxicological Incapacitation

In principle, the same logic can be used to calculate the toxicologically incapacitating level of smoke. However, existing animal smoke toxicity tests do not generally provide data in the correct form; rather, they report the dose which gives rise to an observed effect in half (50%) of the animals, usually for a 30-minute exposure. This dose, called the "EC50" of the smoke, is obviously dependent on the effect chosen to be monitored (4), as well as the time of exposure. A conservative approach is to require that the smoke concentration after 10 minutes of burning not exceed the EC50 for incapacitation in 30 minutes. The mass of smoke required to produce the incapacitating concentration in the 500 cu.m. volume is:

$$M = \text{EC50}(\text{in kg/m}) \times \text{Volume} = 500\text{m} \times \text{EC50}$$

And hence the allowable smoke produced in 10 minutes is any amount less than this level.

Substituting this value for M in expression (2) yields:

$$500 \times \text{EC50} \geq \frac{0.5 \dot{q}'' f(600)^2}{2 H_c}, \quad \text{or}$$

$$\frac{\dot{q}'' f}{(H_c)(\text{EC50})} \leq .0056 \frac{\text{m}}{\text{sec}} \quad (3)$$

This result is intended to mean that, for the chosen volume and ignition scenario, any combination of heat release rate, flame spread rate, heat of combustion and smoke EC50 which satisfies this expression will require 10 minutes or more to

produce toxicologically incapacitating conditions.

As an example of how the criteria could be used, Table 1 shows three different cables, all of which have properties which would meet the smoke criterion.

Note that the allowable mass optical density, a measure of smoke production potential can increase significantly if offset by comparatively lower values of flame spread and/or higher values of the heat of combustion.

If it is desired to set a smoke toxicity criterion for the same three cable samples, based on the requirement that the EC50 of the smoke not be exceeded in the same 10-minute period, the EC50 values are:

Cable a: $EC50 \geq .015 \text{ kg/m}^3$, or 15 mg/l
Cable b: $EC50 \geq .0075 \text{ kg/m}^3$, or 7.5 mg/l
Cable c: $EC50 \geq .006 \text{ kg/m}^3$, or 6 mg/l

It must be recalled that the EC50 is the incapacitating dose of smoke; hence, the bigger the allowable dose the less toxic the smoke. An apparently startling result of the calculation is that cable c, which produces the most smoke per unit weight of material burned, is also allowed to produce the most toxic smoke. This is because "cable c", by virtue of its low mass burning rate ($\dot{q}''f/H_c$), produces the lowest concentration of smoke, which offsets the higher toxicity.

Another option is to require that the compartment retain visibility for 10 minutes and that it be toxicologically tenable for an additional period of time; say, 5 minutes. The appropriate criterion is obtained by solving equation 2, where M is again set equal to the compartment volume times the EC50, and now $t = 15$

minutes (900 sec). This yields:

$$\frac{\dot{q}''f}{(H_c)(EC50)} \leq .0126$$

For the same three cable samples discussed above, the smoke toxicities would be:

Cable a: $EC50 \geq .034 \text{ kg/m}^3$, or 34 mg/l
Cable b: $EC50 \geq .017 \text{ kg/m}^3$, or 17 mg/l
Cable c: $EC50 \geq .014 \text{ kg/m}^3$, or 14 mg/l

This requirement is considerably more restrictive. The burning behavior assumed here dictates that the total smoke produced increases as the square of the burning time, so specifying a 50% increase in tenability time corresponds to requiring more than a twofold decrease in smoke toxicity, e.g. from 15 mg/l to 34 mg/l, as in cable a.

Limitations

The foregoing exercise is intended to show how criteria can be derived rationally. However, it is subject to a number of limitations which reflect both the complexities of fire and the current state of fire research. In order to avoid unrealistic expectations, it is important to identify some of these factors.

First, since most smoke toxicity tests were developed without regard to individual fire scenarios, it is not surprising that they often fail to measure the detailed effect of interest in a given situation. One cannot be sure that any presently available test give the "right" answer for cable fires and insulating materials. Combustion conditions, the choice of test animal, the choice of the biological effect to be a surrogate measure of "incapacitation" in an actual fire, extrapolating from measurements in a 30-minute exposure when a 10-

Table 1
CABLES MEETING SMOKE CRITERION

<u>Cable</u>	<u>MOD (smoke mass optical density, m/kg)</u>	<u>\dot{q}'' (heat release rate, MW/m of cable)</u>	<u>f (linear flame spread rate, m/sec)</u>	<u>Hc (heat of comb, MJ/kg)</u>
a	100	.20	.010 (23"/min)	25
b	200	.25	.0024 (5.5"/min)	15
c	250	.30	.0044 (10"/min)	40

Table 2
CRITICAL HEAT FLUX AND IGNITION TEMPERATURES
FOR CABLE SAMPLES -- FACTORY MUTUAL
FLAMMABILITY APPARATUS (Source: Reference 1)

<u>Cable Sample</u>	<u>Minimum Radiant Heat Flux For Piloted Ignition (W/CM²)</u>	<u>Ignition Temperature (Calculated) (C)</u>
1	1.4	430
2	2.2	520
3	2.2	520
4	2.5	540
5	2.5	540
6	3.4	730

Table 3
RADIANT FLUX TO HORIZONTAL SURFACES AS A FUNCTION OF FIRE SIZE

<u>Fire Size (kw)</u>	<u>Example</u>	<u>Radiant Flux (watts/sq. cm)</u>	
		<u>To Floor</u>	<u>In Upper Layer</u>
300	Upholstered Chair	.31	.55
620	Small Sofa	1.0	1.4
930	Foam Mattress	2.4	2.7
1130	28 inch Fuel Fire	3.6	4.2

Room Size: Length, 8 feet; Width, 10 feet; Height, 8 feet 30 inch doorway

a 30-minute exposure when a 10-minute exposure is desired -- all these are reasons why a good toxicity measurement for this purpose requires much additional work.

This difficulty remains even when toxicity is inferred by chemical analysis rather than by bioassay, since the allowable limits on the individual smoke components must be set by reference to some biologically-determined dose. In addition to the problems outlined for bioassays, one must recognize that reliance on chemical analysis requires an additional act of faith -- that the important toxic components are included in the list of analysis to be performed.

There are many simplifications of the fire process implicit in the previous analysis. First and most important is that all of the material properties have been assumed to be independent of each other. The complicated interactions between heat release rate and flame spread rate, for example have been neglected for clarity. All phenomena are assumed to be steady state, and this is an important simplification. No account has been taken of the effects of the enclosure in the burning behavior of the cable. These and many other simplifications are necessary for simple illustration of setting performance criteria for the cable, but may not always be admissible in practice.

This approach has also minimized some of the complexities of laboratory-based fire performance tests. One particularly important point is that flame spread rate and heat release rate are both heavily dependent on the radiant heat load felt by the sample. In fact, a number of cable insulations will

not burn readily unless an external heat flux is imposed (attempts to measure \dot{q}'' and f without an external flux applied to the sample would yield values of zero in such cases). Thus, the thermal conditions necessary to generate useful fire property data are ones which the material would seldom experience unless something else besides the cable were burning as well. These considerations led us to examine another approach.

A Modified Approach: Cable in Full-Scale Fires

In reality, wire and cable seldom start a fire or burn alone. Rather, they become involved as the result of exposure to an already-existing fire. Hence, predictions based on the production of smoke from burning cable alone are in some sense artificial, since there will usually be considerable quantities of smoke produced, with an adverse effect on life safety, regardless whether or not cable involvement occurs. This approach can be used to control or reduce the contribution of cable insulation to fire and smoke hazard, but whether the contribution is significant in any given case depends on the actual fire scenario. Estimates of hazard in more complex fire scenarios require more elaborate mathematical treatment (5,6) and, in some cases, full-scale experiments.

It has been assumed that test methods exist to measure precisely what is needed for these calculations. However, since existing methods for heat release and flame spread require that an imposed flux be selected, a level for same must be chosen. Values of 2-3 watts/cm represent the conditions a cable might experience in a developing fire, but they may be substantially higher than those required to inaugurate the burning

of cable materials. For example, Table 2 shows the critical flux required for ignition of a series of cables. Although all of these cable passed IEEE 383, the power density required to ignite them varies considerably.

The existence of a test such as IEEE 383 means that cables will not ignite readily. Indeed, Table 3 shows the size fire in a small room needed to produce various fluxes. Comparison of Tables 2 and 3 shows that, for the most readily ignited cable in a room of the size indicated, a 600 kw fire typical of that produced by a small sofa, is required, unless, of course, the cable run is placed very close to, or in, the fire plume. Other cables require even bigger exposure fires to become involved.

This gives rise to the question of how important the cables' contribution to the total smoke will be. Figures 1 and 2 compares the mass lost from a urethane foam pad (whose burning would typify the kind of exposure fire needed to involve the cables) with the mass lost by cables themselves when the cables are located on the floor of the room. The Figures show results for Sample 1 and Sample 2 or 3 (of Table 2) respectively. Note that, in neither case is any cable involved until the fire is well developed (the details of the fire calculations which give rise to Figures 2 and 3 are given in reference 1).

Indeed, if the fires exhaust themselves into the 2000 square feet space mentioned above, the smoke due to the foam alone will have obstructed visibility before the cable ignites. This is the case even for a low-smoke fuel (for example, one with a MOD value of 100m/kg). Such a fuel would

produce a smoke visibility of 1 meter (see above) at a concentration of .015 kg/cu.m., or a mass loss of 7.5 kg. The point at which 7.5 g of fuel has been lost is shown in Figure 1; it is before the cable becomes involved.

The same argument can be made for toxicity. Lethal smoke concentrations for urethane foams have been measured in the National Bureau of Standards' toxicity test method to have a 30-minute LC50 of 20-40 g/cu.m. (6). If a value of 30 g/cu m. is chosen, then the atmosphere will be lethal when 15 kg of foam has burned. Figure 2 shows that 15 kg of foam has burned before the cable is a significant contributor to the smoke. For the cable to be an important factor in the toxicity of the smoke at that time its toxicity must be vastly greater, gram for gram, than that of the foam. Stated the other way around, setting a stringent limit on the toxicity of smoke from the cable buys one essentially no safety at this point in the fire. Indeed, inspection of the entire time course shown in Figures 1 and 2 leads to the conclusion that the total smoke never contains cable smoke in large amounts. Somewhat larger fractions can perhaps be produced in smaller exposure fires, but it is difficult to envision circumstances in which the total smoke produced is contributed by the cable. If this be the case, it is difficult to see the necessity for toxicity controls on the cable which require the cable smoke to be considerably less toxic than that produced by typical (and necessarily present) fuels.

The mass-loss rate of the cable at elevated flux (e.g. 2.5 watts/sq cm) is the controller of how rapidly the cable insulation decomposes. Thus, when the cable is well-involved,

FIGURE 1 - TIME PROFILE OF RELATIVE CONTRIBUTION OF CABLE AND FOAM TO SMOKE, SHOWING ONSET OF SEVERE VISION OBSCURATION

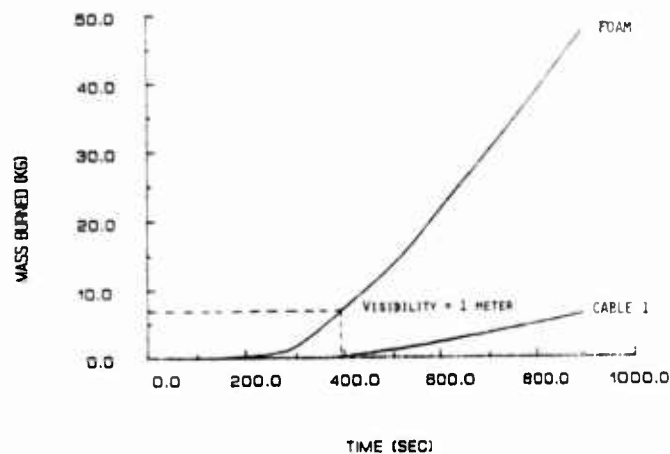


FIGURE 2 - TIME PROFILE OF RELATIVE CONTRIBUTION OF CABLE AND FOAM TO SMOKE, SHOWING ONSET OF SMOKE LETHALITY (FIRE CONDITIONS, SEE TABLE 1).

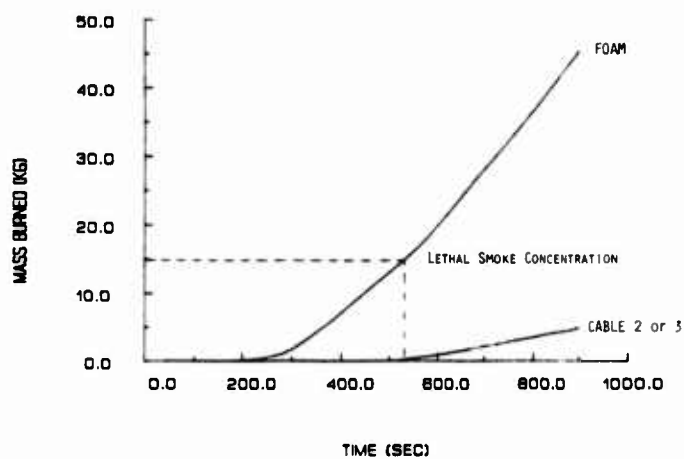
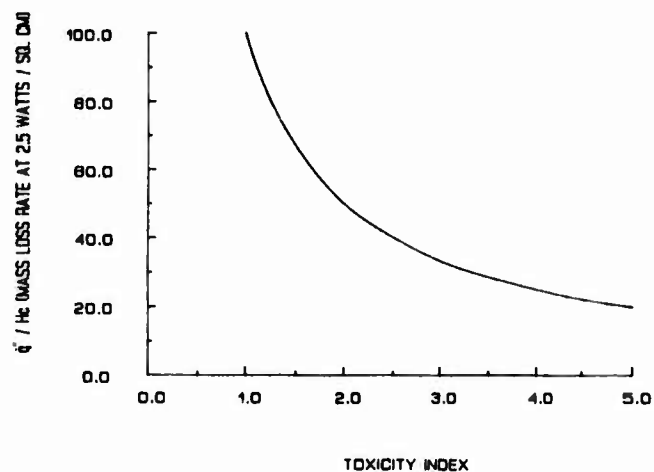


FIGURE 3 - RELATIONSHIP BETWEEN TOXICITY INDEX AND MASS LOSS RATE FOR CONSTANT AVAILABLE ESCAPE TIME.



$$\dot{M}(\text{cable}) = \dot{q}''/H_c,$$

where \dot{q}'' is its heat release rate per unit area at a previously established flux, and H_c is its heat of combustion. Reference to Table 1 will show that it requires about 900 kw to generate 2.5 watts/sq.m. in a typical room. The burning rate of a typical hydrocarbon fuel in a 900-kw fire is .03 kg/sec or 30 g/sec. It seems reasonable to require that smoke from the cable be no more toxic than that from the fuel. This condition is met if:

$$\frac{\dot{M}(\text{cable})}{LC50(\text{cable})} \leq \frac{\dot{M}(\text{fuel})}{LC50(\text{fuel})}$$

If we again assume an LC50 of 30 g/cu.m. this means that:

$$\frac{\dot{M}(\text{cable in g/sec at 2.5 w/cm})}{LC50(\text{cable})} \leq 1 \text{ m/sec}$$

The same criterion can also be expressed in terms of a toxicity index, such as is defined in current cable specifications, e.g. British Naval Engineering Standard 713 (8). A toxicity index of 1.0 is intended to correspond to smoke having an LC50 of 100 g/cu.m. In general, it can be shown (2) that toxicity index is formally related to LC50 by the following formula:

$$\text{Toxicity Index} = \frac{100 \text{ g/cu.m.}}{LC50}$$

The toxicity criterion developed above thus becomes:

$$\dot{M} \times \text{Toxicity Index} \leq 100, \text{ or}$$

$$\frac{(\dot{q}'')}{H_c} (\text{Toxicity Index}) \leq 100 \text{ g/sec}$$

A plot of this expression is shown in Figure 3. From a toxicity point of view, all materials whose smoke and mass loss properties fall on the curve are of equivalent safety; all which fall above the curve offer more toxic smoke; all which fall below offer less.

Summary

This paper concentrated on relating smoke properties, obscuration and toxicity, to fire properties, heat release rate, heat of combustion and flame spread rate. Two simplified approaches were taken: the first where the cable material itself was the only fuel burning in a space and, the more common situation, where the cable material is a secondary fuel item, exposed by a fire(s) in other materials in the room.

The expressions used show how one can relate smoke properties, fire properties, and characteristics of the space of interest to a common hazard criteria. The analysis process shows the importance of integrating all fire and smoke properties, with a set of expected fire scenarios and rationally developed performance criteria. The approaches taken, although necessarily simplified and be extended to include all of the detailed understanding of fire processes required.

References

1. Clarke, F., Benjamin, I., and DiNenno, P., "Overall Safety of Cable and Wiring Materials, Part I," 32nd IWCS, Conference Proceedings, p. 390 (1984).
2. Part II: Presented at Marine Cable Symposium, London, November 1, 1984.
3. Rasbash, D., Pratt. Fire

3. Rasbash, D., Pratt. Fire Safety Journal, Vol. 2, No. 23, 1977, p. 801
4. If the test measures lethality, the reported EC50 is usually designated "LC50" (read: Lethal concentration for 50% of the test animals). A number of different sublethal biological effects can be measured, and the reported EC50 will depend on the specific measurement technique.
5. Emmons, H., "The Prediction of Fire in Buildings," 17th Symposium (International) on Combustion, The Combustion Institute, Pittsburgh, PA. (1978).
6. Emmons, H., Mitler, H., A "Documentation for CFCV, The Fifth Harvard Computer Fire Code," NBS-GCR-81-344; National Bureau of Standards, Washington, D.C.; October 1981
7. Levin, B.C., et al, "Further Development of a Test Method for the Assessment of the Acute Inhalation Toxicity of Combustion Products", NBSIR 82-2532, U.S. Department of Commerce, NBS, Washington, D.C., June 1982
8. Determination of the Toxicity Index of the Products of Combustion from Small Specimens of materials, Naval Engineering Standard 713, Ministry of Defense (U.K.), 1983

FREDERIC B. CLARKE, III, Ph.D.

Frederic Clarke is President of Benjamin/Clarke Associates, Inc., a firm specializing in the characterization and analysis of fire safety problems. Until fall, 1981 he was director of the National Bureau of Standards' Center for Fire Research, the Nation's principal Federal fire laboratory. He was also Science Advisor to the United States Fire Administration.

Prior to coming to NBS, he spent three years in the research and marketing departments of Monsanto Company, St. Louis, Mo. In 1976, Clarke was one of twenty-three Federal executives chosen to receive a Congressional Fellowship. As a Congressional Fellow he served as legislative assistant to Senator John Culver (D.-Iowa), specializing in economic and product liability legislation; and as staff assistant to Congressman Jim Wright (D.-Texas), the House Majority Leader.



PHILIP J. DINENNO, P.E.

Philip DiNenno is a fire protection engineer with Benjamin/Clarke Associates Inc. He is primarily involved with the application of mathematical fire modeling and computer analysis techniques to the evaluation of fire safety problems. DiNenno has worked for five years as a consulting engineer in fire protection, specializing in applying research results, and utilizing models for the evaluation of fire protection problems. These applications have included power station safety analysis, nuclear fuel processing facility risk analysis, and the cost benefit analysis of fire protection solutions in industrial facilities. DiNenno has also worked as a research assistant and lecturer at the University of Maryland and as an engineering technician for NASA Goddard Space Flight Center. As a Research Assistant, DiNenno investigated over 50 fire incidents in residential and health care facilities, evaluating the aspects of fire development, smoke propagation, human behavior and their interactions.



FULLY-AUTOMATIC OPTICAL FIBER SPLICE MACHINE

Ryosuke ARIOKA, Tadashi HAIBARA, and Masao TACHIKURA

Ibaraki Electrical Communication Laboratory, N.T.T.
Tokai, Ibaraki-ken, 319-11, Japan

Summary

In practical high-density optical fiber cable transmission systems, high quality and efficient fiber splice techniques are required. This paper describes a newly developed fully-automatic arc-fusion splice machine, by which all splice processes such as stripping, cutting, alignment, fusion, and reinforcement are carried out sequentially without human intervention. To avoid mechanical damage, spliced fibers are gripped at the coated portion during all splice processes. The fibers with primary and buffer coats are cut just after secondary coat stripping. After that, the primary and buffer coats are removed completely by rotating felt-rollers. Then, the fibers are aligned by using movable arms with 2 μ m position accuracy controlled by microscopic image processing. The spliced portion is reinforced by a pair of plates with hot-melt adhesive. By using the new machine, an average splice loss of 0.07 dB and a median tensile strength of 1.2 GPa are obtained for graded-index multimode fibers.

1. Introduction

Optical fiber cable transmission systems have greatly been developed owing to rapid improvement in optical fiber and cable, laser diode, optical components, fiber connection techniques, and so on. For the construction of the systems, a large amount of fiber splices are required. Since the splice work requires much labor, high-efficient fiber splice techniques are indispensable for cost saving and shortening of the construction period. At present, several semi-automatic fusion splice machines have been developed[1]-[5]. However, in these machines, automatizing has been achieved only for fiber alignment and/or fusion splicing processes. There still remain some manual operations such as fiber cutting and fiber coat removing, which are influenced strongly by personnel skill. Accordingly, it is important for realizing efficient and reliable splices to make these operations be done automatically without human intervention.

We have analyzed the sequence of splice processes and have designed a system which is suitable for realizing automatic splice procedures. As a result of the analysis and design, we have developed a fully-automatic arc-fusion splice machine. This paper describes

a structure of the machine, mechanisms of individual operation processes, and experimental results on fusion splice using graded-index fibers.

2. Outline of Fully-Automatic Arc-Fusion Splice Machine

Fusion splicing procedure is generally divided into six processes; secondary coat stripping, primary coat removing, fiber cutting, fiber alignment, fusion splicing, and reinforcement. In the fully-automatic splice machine described here, these processes are rearranged and assigned to four functionally

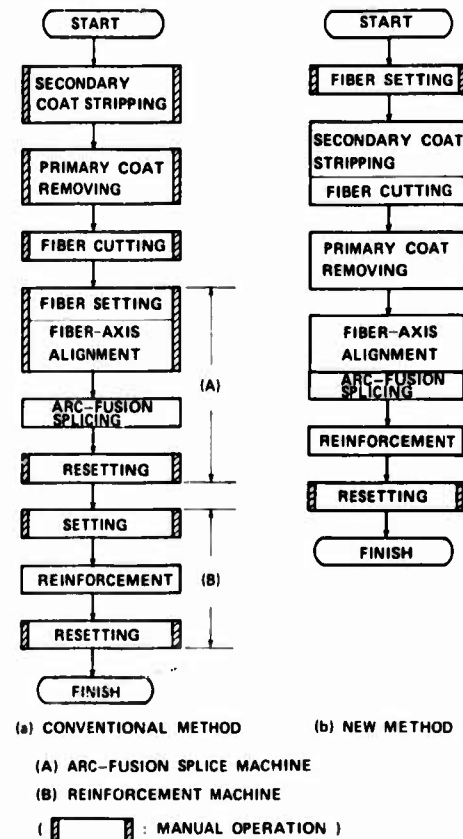
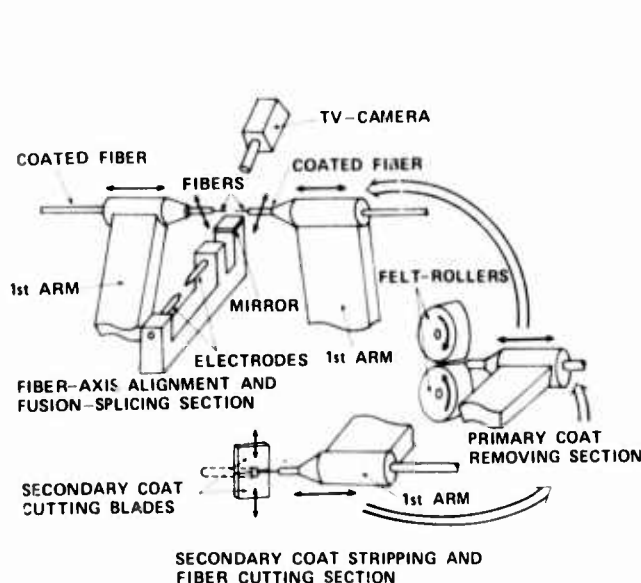
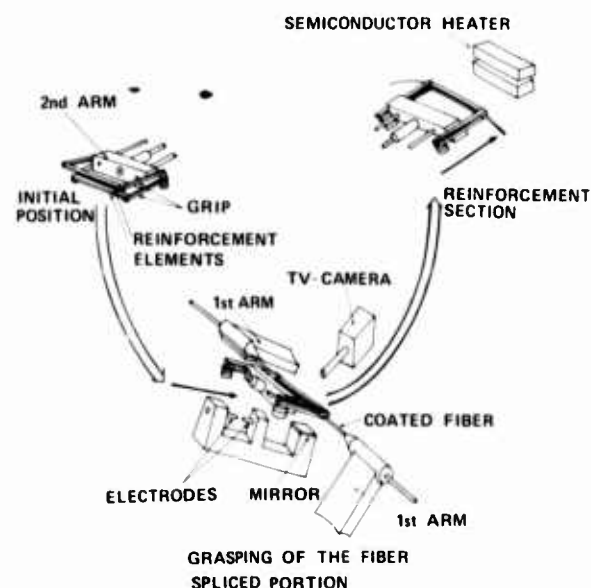


Fig.1 Arc-fusion splicing procedure



(1) MOVEMENT OF FIRST ARM



(2) MOVEMENT OF SECOND ARM

Fig.2 Outline of splicing processes

separated sections; secondary coat stripping and fiber cutting, primary coat removing, fiber alignment and fusion splicing, and reinforcement. The procedures of the conventional method[1] and new method are shown in Fig.1. In the conventional method, an operator has to intervene in all of these processes, even though the fusion splicing process(A) and reinforcement process(B) are automatically carried out on each independent machine. On the other hand, what an operator need to do with the fully-automatic splice machine are only to set the fibers and reinforcement elements, and to take out the spliced fiber from the machine. To perform two processes in the first section, the primary coat removing process and fiber cutting process are reversed in order.

In the present automatic machine, fiber ends are processed and spliced by the above-mentioned four sections. Outlines of operation processes in the machine are illustrated in Fig.2. To give compactness to the machine mechanism, the processing sections are three-dimensionally located. Fiber transfer between the sections is assigned to two types of rotational arms. The first arm grips a fiber at its coated portion continuously from the start to the completion of fusion splicing. Then, the second arm receives the spliced fiber and transfers it to the reinforcement section. Because of the presence of the second arm, the first arms can return to the first section and are ready for the splice of the next fiber pair.

Except for reinforcement, the fiber axial motion required in each processing is also assigned to the first arms. High-precision is required for positioning the first arms, because the arms also control fiber-axis alignment by their rotational motions. Therefore, only two degrees of freedom, rotational and axial motions, are given to the arms for lessening unavoidable errors in motion and for control ease.

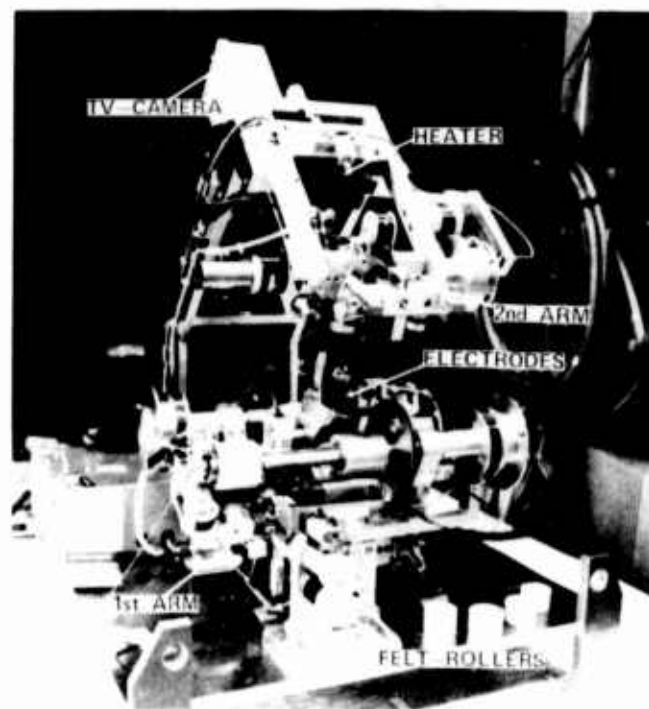


Fig.3 Photograph of the fully-automatic splice machine

Furthermore, mechanical damage on the fiber surface is avoided as much as possible by using a fiber primary coat removing technique with felt-rollers[6] and by the exclusion of fiber surface contact with other materials in the fiber-axis alignment process. Fiber-axis alignment is carried out by two-directional observation with a TV-camera.

A photograph of the fully-automatic arc-fusion splice machine is shown in Fig.3. The

machine is 50 cm long, 50 cm wide, and 70 cm high. All of its motions are controlled experimentally by a BASIC program on a personal computer.

3. Mechanism of Individual Processing Sections

3.1 Secondary coat stripping and fiber cutting section

The fully-automatic machine is designed for three layer coated fiber composed of primary, buffer, and secondary coats, as shown in Fig.4. Before splicing, it is necessary to remove the coats completely and cut the fiber to make a perpendicular endface. In the first processing section, the secondary coat is stripped and the fiber is cut. To start, an operator sets the coated fiber pair on a pair of first arms. This operation is only to insert each fiber end into a guide hole. Fiber ends are automatically guided to the pre-determined position in the first section. The fiber is nipped by a pair of blades with a semi-circular notch, and then is pulled out a suitable length for cutting. With this motion, the secondary coat is stripped from the fiber to a prescribed length. The fiber cutting is done after the secondary coat stripping, not after primary coat removing.

The fiber cutting mechanism is shown in Fig.5. A stripped fiber portion is scored by rotating broadax-shaped blade, while both sides are supported by the arm and the coat stripping parts. Then, the scored portion is pushed with a semicylindrical bed. At this moment, tensile stress occurs and causes a fiber fracture there. By this process, a perpendicular fiber end with a mirror surface is obtained. The remaining fiber chip is automatically scrapped.

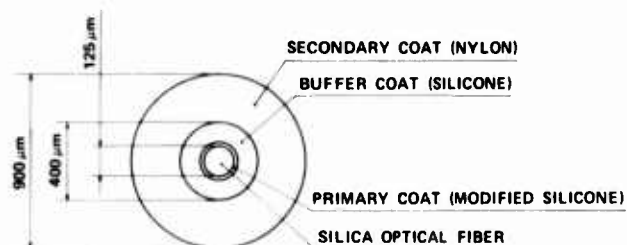


Fig.4 Three-layer coated fiber structure

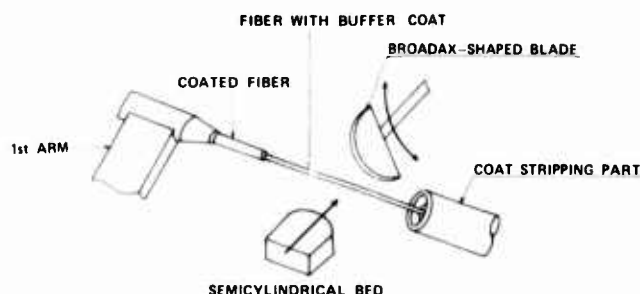


Fig.5 Fiber cutting mechanism

3.2 Primary and buffer coats removing section

When the plastic coats are mechanically stripped from the fiber by the conventional method, a number of cracks usually occur on the fiber surface, and fiber strength is greatly diminished. This strength reduction depends heavily on the force used to remove the primary and buffer coats. In order to prevent fiber strength reduction, we have developed a new coat remover[6] which consists of a pair of 25 mm diameter felt-rollers. The felt-rollers can remove primary and buffer coats with a small force for a few seconds without damaging the fiber surface. After cutting the fiber end, the fiber is transferred to this section and is inserted between the rotating rollers. In advance, the felt-rollers are wetted with ethanol, which is provided automatically. Then, the arm reciprocates in the fiber axial direction. The primary and buffer coats are removed completely by this method.

3.3 Fiber-axis alignment and arc-fusion splicing section

Usually, a V-groove has been used for fiber-axis alignment[1]. A pair of fibers are set in the V-groove, and butted together with small end separation for pre-fusion technique[7]. Therefore, there is a possibility of mechanical damage on the fiber surface by fiber contact with the V-groove. In the fully-automatic machine, to avoid mechanical damage, the fibers are gripped only at the coated portion by the arms, and aligned with a microscopic image of the fibers. Figure 6 shows a setup for fiber-axis alignment and arc-fusion splicing with microscopic image processing. The fiber images from two directions are picked up by a TV-camera, using a mirror. The personal computer calculates the position of each fiber from the video signals, and operates a pair of arms so as to minimize the transverse offset between two fibers. A photograph of the

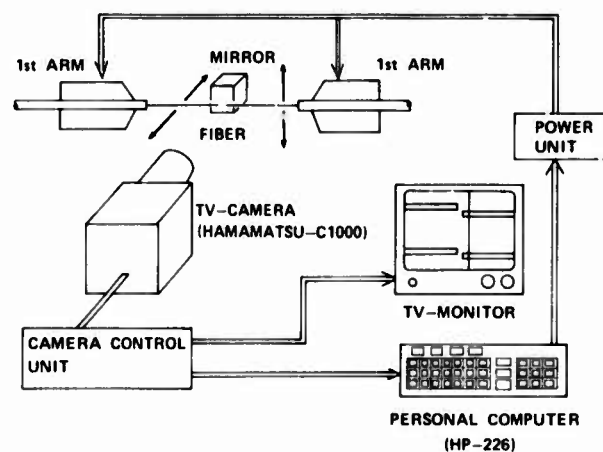


Fig.6 Setup for fiber-axis alignment with microscopic image processing

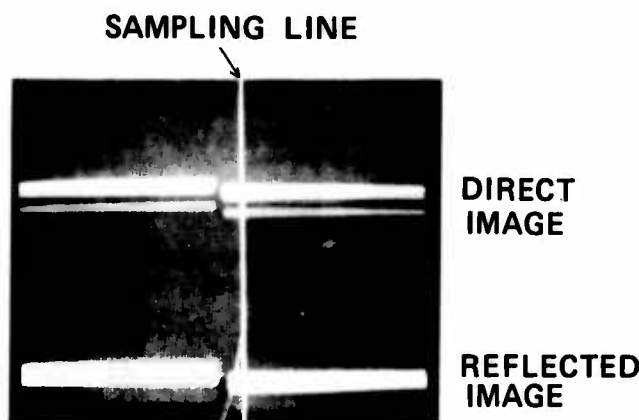


Fig.7 Photograph of TV-screen during alignment process

TV-screen during the alignment process is shown in Fig.7. An accuracy of $2\mu\text{m}$ has been obtained for the axis alignment, resulting from preciseness of the arm motion and high resolution of the TV-camera with 1024 scanning lines.

In the fiber splicing, pre-fusion technique[7] is used. In order to enlarge discharged region, high-frequency($\approx 20\text{ kHz}$) discharge[8][9] and 2 mm electrode gap are adopted. The position of the pair of electrodes is adjusted automatically in every trial to correspond to the change of splicing position.

3.4 Reinforcement section

It is necessary to reinforce the fusion-spliced portion for protection from mechanical damage. For the reinforcement, the heat-shrinkable tube method[10] is one of the approved methods. However, in this method, the mechanisms for setting and transferring reinforcement elements become complicated for automatizing. Therefore, in order to simplify the mechanisms, we adopted a sandwich-type reinforcement element composed of a pair of metal plates with hot-melt adhesive, similarly to that used for fusion mass-splices[9]. The structure of the sandwich-type reinforcement element is shown in Fig.8. The size of the element is 60 mm x 3 mm x 2 mm.

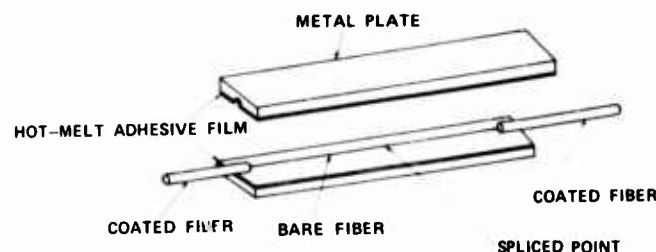


Fig.8 Structure of a sandwich-type reinforcement

The reinforcement process is as follows: A pair of elements for reinforcement are set beforehand on the grip of the second arm. After splicing, the spliced portion is sandwiched between the elements and is transferred to a heating part. In the heating part, the reinforcement elements are heated to about 150°C . The reinforcement process takes about 70 sec. After reinforcement, the spliced fiber is transferred by the second arm to an open space so that the operator can easily take it out of the machine.

4. Experimental Results

Performance tests were carried out for the machine, and the mechanisms of each processing section were regulated to have stable and sufficient characteristics. The fiber used in this experiment was graded-index multimode fiber with $50\mu\text{m}$ core diameter and $125\mu\text{m}$ outer diameter, coated by modified-silicone, silicone, and nylon in the order. The outer diameter of the nylon coat was 0.9 mm, as shown in Fig.4.

4.1 Secondary coat stripping and fiber cutting

Secondary coat was perfectly stripped by the required length in the first process. The fiber cutting process also exhibited good and stable performance, even though the cutting blade scored the fiber surface through the obstructive primary and buffer coats. The photograph shown in Fig.9 is an example of a fiber end-face. Figure 10 shows the fiber end-face angle histogram. An average end-face angle of 0.8° was obtained: The value is equivalent to that obtained with a conventional fiber cutting tool[11] by a skillful person.

In the cutting process, fiber tensile stress is given with bending deformation, in the same way as the method proposed by Gloge et al.[12]. Another method to give tension to the fiber without bending deformation, which is known as Chesler-Dabby technique[13], was also tried experimentally. However, fiber could not be cut well because the fiber was apt to slip from the stripping parts which support a tip of the fiber. It means that the bending deformation was

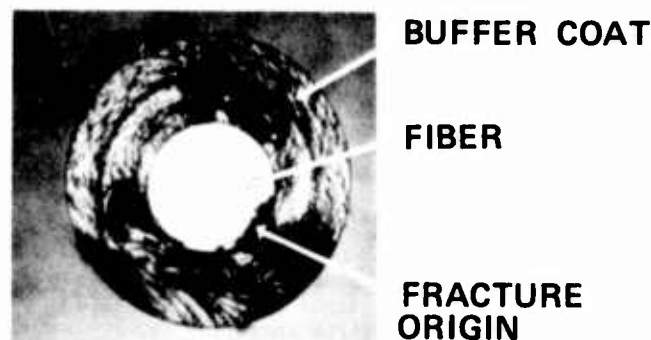


Fig.9 Photograph of fiber end-face with primary and buffer coats

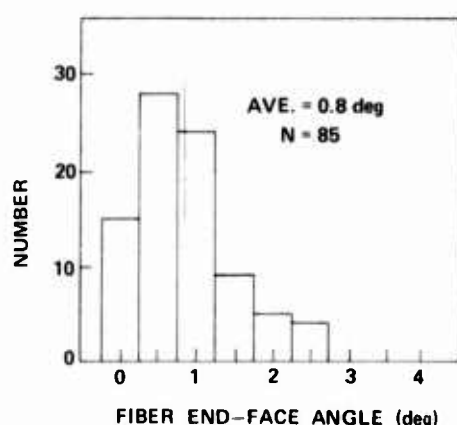


Fig.10 Histogram of fiber end-face angle

effective in increasing the fiber friction in the coat. Because of the effect, the fiber clamp could be omitted in the mechanism.

4.2 Primary and buffer coats removing

In the primary and buffer coats removing section, the buffer coat is removed at the instant when it is inserted between the rotating felt-rollers, and then primary coat is softly and gradually removed for a several seconds. Figure 11 shows the experimental relationship between the fiber coat removing force (i.e. fiber tension during primary coat removal) and the fiber tensile strength after removing. It is found that the required removing force of a few grams does not cause a remarkable reduction of fiber strength, while the force of several tens of grams, corresponding to the manually applied force, affects seriously the fiber strength reduction in the conventional method.

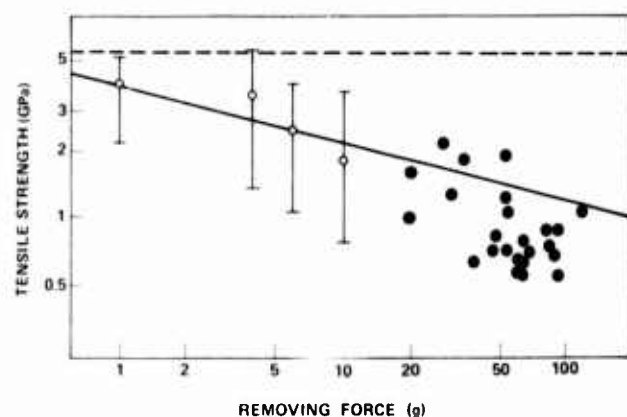


Fig.11 Experimental relationship between fiber coat removing force and fiber tensile strength after removing
 ● : stripped by conventional method
 ○ : stripped by felt-rollers
 ---- : median tensile strength of the coated fiber

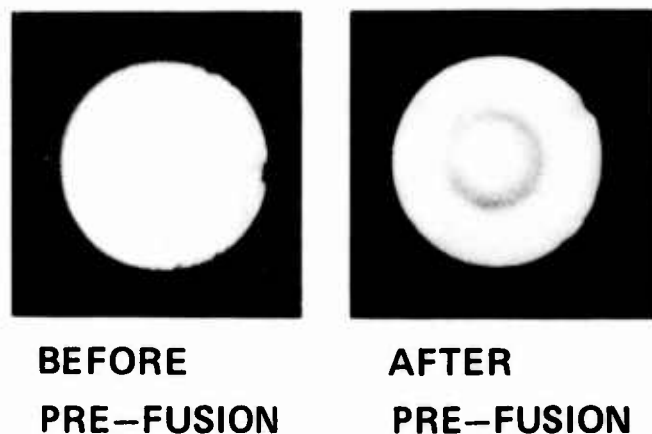


Fig.12 Photographs of the fiber end-face

In the coat removing process, coating material dusts adhered to the fiber end-face. However, it was found that the dusts disappeared at pre-fusion in the fusion splicing process, without any bad influence on spliced fiber.

Photographs of the fiber endface before and after pre-fusion are shown in Fig.12. Accordingly, fusion splicing does not suffer from the dust adhesion influence which inevitably originated from the inversion of the fiber cutting process and primary coat removing process.

4.3 Fiber alignment and splicing

In the fiber-axis alignment process, fibers are held by the first arms at coated portions. The method is certainly effective in avoiding mechanical damage, but cannot avoid fiber-axis inclination, which is one of the factors of splice loss. In the process, the inclination is not adjusted. Accordingly, the accuracy of

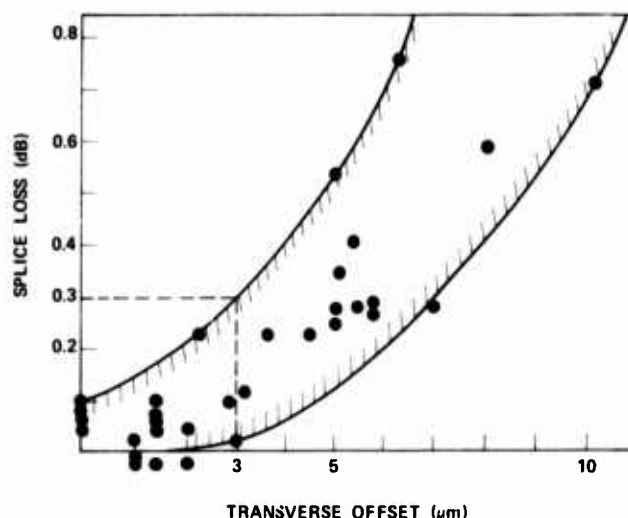


Fig.13 Relationship between transverse offset and splice loss

transverse axis alignment may be required to be higher, compared with other methods which utilize a fiber guide such as V-groove. In order to evaluate the required accuracy of axis alignment, the following experiment was carried out.

By using the machine, fibers were fusion-spliced intentionally with various transverse misalignments. The transverse offset was obtained by two-directional measurement utilizing the image processing operation used in the machine. The splice loss was measured by a LED light source ($\lambda = 0.85 \mu\text{m}$) under the steady-state mode condition. The relationship between the transverse offset and the splice loss is shown in Fig.13. The circles correspond to the experimental data. The hatched region shows the range of variational splice loss. It is clearly seen from this figure that fiber transverse offset can be allowed as far as $3 \mu\text{m}$ to get low splice loss below 0.3 dB. Accordingly, the transverse offset component observed from each direction is allowed to be as far as $2 \mu\text{m}$ (i.e. $3/\sqrt{2} \mu\text{m}$). This value was adopted for the judgement of alignment access completion.

Figure 14 shows examples of the changing of transverse offset during the alignment process. Fiber alignment is normally accomplished by the access within four times. The access of each arm was programmed to show asymptotic process without access direction inverse. This process is effective in avoiding positioning errors caused by the unstability of the mechanism.

A splice loss histogram obtained by using the fully-automatic machine shown in Fig.15. The average splice loss is 0.07 dB, and the value is equivalent to that by the conventional fusion splice method using V-groove[1]. Considering the value in the relationship shown in Fig.13, average alignment accuracy is estimated to be about $2 \mu\text{m}$.

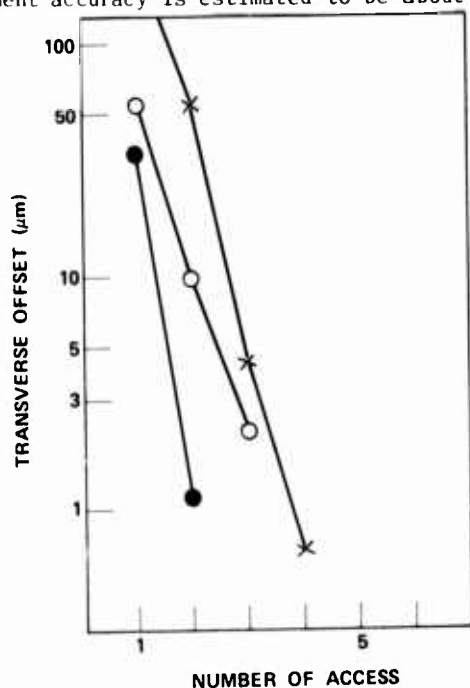


Fig.14 Examples of changing fiber-axis transverse offset

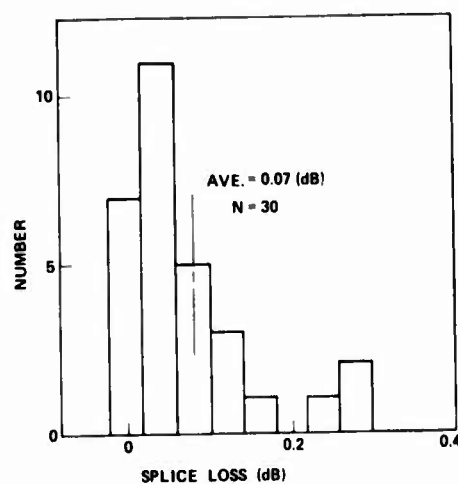


Fig.15 Splice loss histogram for graded-index optical fiber
outer diam.: $125 \mu\text{m}$
core diam.: $50 \mu\text{m}$
refractive-index difference: 1 %

4.4 Reinforcement

Tensile strength was evaluated for the spliced fibers before and after reinforcement. Figure 16 shows Weibull plots of the tensile strength, where curve a is coated fiber before splicing having a median strength of 5.4 GPa, and curves b and c represent the strengths after splicing by the conventional method and this method, respectively. Curve d shows the strength after reinforcement having a median value of 2.6 GPa. Before reinforcement, the median strength of 1.2 GPa obtained by this method is two times larger than that by the conventional method. This strength has a large merit for long-term reliability. From this result, it is found that

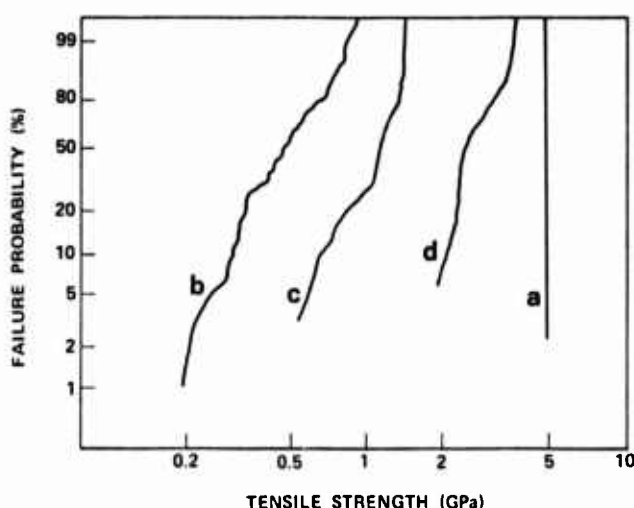


Fig.16 Weibull plots of tensile strength
a: coated fiber
b: spliced fiber by conventional method
c: spliced fiber by this machine
d: reinforced splice by this machine

gripping only at the secondary coat and the primary coat removal with felt-rollers are advantageous in preventing fiber strength reduction. Furthermore, by the reinforcement, the strength is improved to be more than twice before. The strength after the reinforcement is one and a half times larger than the conventional method[10].

4.5 Processing time

The working time of all processes used in this new machine is shown in Fig.17. The time required for fiber-end preparation(1)&(2), alignment and splicing(3), reinforcement(4), and transferring are 70 sec, 120 sec, 70 sec, and 230 sec, respectively. Total time from the initial fiber setting to pulling out the completed splice after reinforcement is about 8 min, which is comparable with that by the conventional method used in the field.

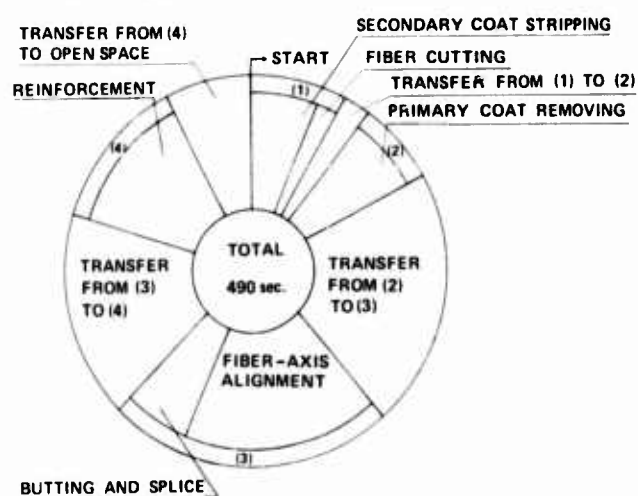


Fig.17 Processing time

The speed-up of the machine motion will easily be realized in the transferring process and in the fiber alignment process. In the former, the restriction to speed-up is in the lack of power to drive. By using frictionless bearings in the transmission mechanism, and by exchanging the motors for more powerful ones, a speed-up of two or three times will be realized. In the latter, time loss is mainly caused by the video signal input and data processing in the personal computer. By improving the interface and program used there, alignment speed will become better by three times or more. Accordingly, total time for all processes will be shortened to be as little as 5 min without any essential changes of the machine mechanism and process.

5. Conclusion

We have developed a fully-automatic arc-fusion splice machine for optical fibers, by which all splice processes are carried out sequentially without human intervention. The new method and mechanisms used for this machine are as follows;

- (1) rotational arms for both the fiber transfer among individual processing sections and the fiber-axis alignment,
- (2) a fiber cutting mechanism for buffer-coated fiber, and the primary and buffer coats removing mechanism using felt-rollers for the prevention of fiber strength reduction,
- (3) fiber aligning method by microscopic image processing in order to avoid any contact of bare fibers to other materials,
- (4) sandwich-type reinforcement method by a pair of plates with hot-melt adhesive.

By using this new machine, the following experimental results have been obtained:

- (1) The average endface angle was 0.8 deg, which is equivalent to that of the conventional method by a skillful person.
- (2) The average splice loss was 0.07 dB which is equivalent to conventional fusion splice method.
- (3) The median tensile strength of the spliced fibers was 1.2 GPa which is two times stronger than that from conventional fusion splice method.
- (4) Operation time for all processes was about 8 min in total, which is comparable to that by a conventional method in the field.

From the trial production of the fully-automatic machine, it can be concluded that practical fully-automatic splice machine for field use is realizable, because there are no serious problems in improving the speed and size of the total system.

Acknowledgment

The authors express their sincere appreciation to H.Fukutomi, N.Kojima, N.Uchida, A.Sakamoto, and M.Tokuda for their helpful discussions and suggestions.

References

- [1] M.Miyauchi, M.Matsumoto and T.Haibara: "Arc-fusion splice of optical fiber and its reliability in field", presented at 31st IWCS (1982)
- [2] G.K.Pacey and J.R.Scott: "Splicing system for optical fiber cables", presented at 30th IWCS (1981)
- [3] Y.Kato, S.Seikai, N.Shibata, S.Tachigami, Y.Toda, and O.Watanabe: "Arc-fusion splicing of single-mode fibers. 2", Appl. Opt. vol.21, pp.1916-1921 (1982)
- [4] O.Kawata, K.Hoshino and K.Ishihara: "Low-loss single-mode-fiber splicing technique using core direct monitoring", Electron. Lett. vol.19, pp.1048-1049 (1983)
- [5] A.Tardy, M.Jurczyczyn and L.Jeunhomme: "Automatic single mode fiber splicing machine without power monitoring", presented at 9th ECOC (1983)
- [6] T.Haibara, M.Matsumoto, T.Tanifuji, R.Arioka, and M.Tokuda: "New fiber coat stripping method for high-strength splicing", Appl. Opt. vol.22, pp.2945-2947 (1983)

- [7] M.Hirai and N.Uchida: "Melt splice of multimode optical fiber with an electric arc", Electron. Lett. vol.13, pp.123-125 (1977)
- [8] N.Kashima and F.Nihei: "Optical fiber fusion splice using high frequency discharge with high voltage trigger", Trans. IECE Japan vol.E64, pp.529-535, (1981)
- [9] M.Tachikura and N.Kashima: "Fusion mass-splices for optical fibers using high-frequency discharge", J. Lightwave Technol. vol.LT-2, pp.25-31 (1984)
- [10] M.Miyauchi, M.Matsumoto, Y.Toda, K.Matsuno, and Y.Tokumaru: "New reinforcement for arc-fusion spliced fiber", Electron. Lett. vol.17, pp.907-908 (1981)
- [11] M.Matsumoto, M.Miyauchi and M.Hirai: "A simple and practical cutting tool for optical fiber end preparation", Trans. IECE Japan vol.E66, pp.661-665 (1983)
- [12] D.Gloge, P.W.Smith, D.L.Bisbee, and E.L.Chinnock: "Optical fiber end preparation for low-loss splice", Bell Syst. Tech. J. vol.52, pp.1579-1588 (1973)
- [13] M.J.Sanders: "Torsion effects on fractured fiber ends", Appl. Opt. vol.18, pp.1480-1481 (1979)



Tadashi HAIBARA

Ibaraki Electrical
Communication Lab.,
N.T.T.
Tokai, Ibaraki-ken,
319-11, JAPAN

T. Haibara, Engineer of Cable and Material Section, Outside Plant Development Division, Ibaraki ECL, had been engaged in research and development of optical fiber splicing and its reliability. He is presently engaged in research and development of automatic optical fiber splice machine.

He was born in 1955 and received the BE and ME degrees from Hokkaido University in 1979 and 1981, respectively. He is a member of the Institute of Electronics and Communication Engineers of Japan, the Japan Society of Mechanical Engineers, and the Japan Society of Precision Engineering.



Ryosuke ARIOKA

Ibaraki Electrical
Communication Lab.,
N.T.T.
Tokai, Ibaraki-ken,
319-11, JAPAN

R. Arioka, Staff Engineer of Cable and Material Section, Outside Plant Development Division, Ibaraki ECL, had been engaged in development of tunnelling machine. Presently, he is engaged in research and development of automatic optical fiber splice machine.

He was born in 1945 and received the BE degree from Tokyo Metropolitan University in 1968. He is a member of the Institute of Electronics and Communication Engineers of Japan, and the Japan Society of Precision Engineering.



Masao TACHIKURA

Ibaraki Electrical
Communication Lab.,
N.T.T.
Tokai, Ibaraki-ken
319-11, JAPAN

M. Tachikura, Engineer of Cable and Material Section, Outside Plant Development Division, Ibaraki ECL, has been engaged in research and development on splices and connectors for optical fibers since he joined ECL in 1976.

He was born in 1950 and received the BE and ME degrees in Mechanical Engineering from Kyoto University in 1974 and 1976, respectively. He is a member of the Institute of Electronics and Communication Engineers of Japan and the Physical Society of Japan.

A PORTABLE SELF-ALIGNING FUSION SPLICER FOR SINGLE-MODE FIBRES

Patrick V. Andrews, Richard Grigsby, Roger J. Hazelden,
Martin T. McDonough and Sanjiv Saha.

BICC Research and Engineering Limited,
London, W12 7DX, UK.

Abstract

Increasing demand for the installation of single-mode fibre routes pointed the need for an easily portable self-contained self-aligning automated fusion splicer, and none was available commercially. The machine developed and reported here is microprocessor-controlled, with auto-alignment derived by maximising the core signal across the joint. The light from an LED is injected through the fibre coating into the core, and the detected light is similarly extracted from the core. Automatic fibre manipulation is by piezo-electric elements, allowing repeatable positioning to within 0.1 μm . Mean splicing losses of 0.058 dB were achieved on the first test run.

1. Introduction

For practical use in the field, a fusion splicer for single-mode fibre needs other qualities besides great accuracy of alignment of the fibres. It should be robust, readily portable, self-contained for power and joint transmission monitoring, have automatic fusion arc control and automatic fibre alignment. It should also be simple to service and simple to use. All of the few machines offered a year ago fell short in one or more of these respects, so the design of a practical machine was instigated.

There having been small numbers of two earlier models of single-mode splicer for use in-house, the new development, which is the subject of this report, is known as the Mark III for convenience.

2. General Design

The main requirements were:

- (1) A single portable unit.
- (2) A weight of not more than 20 kg complete.

(3) Durability.

- (4) Enough energy storage for 16 hours working, with recharging of the batteries in 8 hours.
- (5) High quality splices, with automatic control of fusion.
- (6) Provision of a means for local injection of light through the fibre wall for monitoring purposes.
- (7) Processor-controlled automatic alignment.
- (8) Easy access for servicing.

The weight limitation favours the use of piezoelectric elements for all fibre movements, rather than stepper motors. With all other components designed for low mass without sacrifice of robustness, the batteries become a major item of weight, and low power consumption becomes desirable.

Protection and rigidity of fixing of the comparatively delicate manipulation components of the splicer head are assured by fixing them to a small but thick chassis plate. This is supported by a comparatively malleable plate to absorb shocks.

Easy access to the control, power supply and monitoring components is assured by having them on printed circuit cards housed in a sub-rack beneath the malleable plate. The battery housing is also fastened beneath the plate.

A complete prototype machine is shown in Fig. 1.

3. Layout of the Splicer Head

The fibres to be spliced are held in mechanical chucks by magnetic clamps. The right-hand fibre has only one degree of freedom, which is in its axial direction; its movement is controlled by a manual micropositioner stage. The axis of this fibre, once set, is the reference to which

the left-hand fibre is adjusted. The latter fibre has three degrees of freedom; horizontal, vertical and axial, with coarse and fine adjustment in each direction. Coarse adjustment is by manual micropropositioners, while piezo-electric block translators provide fine control to within 0.1 μm as well as the essential drive in the axial direction during the fusion process itself. In addition, an adjustable mounting bracket makes it possible to zero the tilt angle of the left-hand fibre to its reference counterpart in the horizontal and vertical planes.

The left and right-hand manipulator assemblies are mounted on a substantial (15 mm thick) baseplate which also supports the electrode assembly for the fusion arc.

The electrodes with a gap of 0.85 - 0.90 mm, are disposed at 45° to the horizontal; the fibre viewing is by means of a split-view microscope, giving a magnification of 85 times, which enables the operator to view the fibres in either the horizontal or vertical planes by simply switching the illumination. The two views are distinguished by different coloured backlighting and all the micropositioner controls and microscope focussing adjusters are coded in corresponding colours for ease of operation.

4. Power Supply

Two 12 V 6 Ah batteries supply 24 V to the low voltage and high voltage power supply units which are housed with the microprocessor system, local light monitoring system and battery charger in the sub-rack. All components are accessible when the splicer is lifted out of its case.

The non-arcng full current drain of the splicer is 600 mA, and this reduces to 450 mA with the time switch control operated. Assuming the worst case of the splicer being switched on continuously making frequent splices, more than 9 hours operation is available. This increases to more than 12 hours when infrequent splices are made. The endurance for the full current mode may be expressed as 600 splicing minutes which, under normal conditions, is more than enough for 100 splices.

5. Microprocessor Control

The Mark III splicer uses a 6809 processor unit to provide control over the following functions:-

(1) Movement of the left hand chuck.

Movement in three mutually orthogonal axes is achieved by CPU control of three digital to analogue converters which supply voltage signals to the control inputs of the high voltage piezo supply. This provides outputs to each piezo element, giving a total displacement of 50 μm .

(2) Fusion arc power and duration.

Another digital to analogue converter is used for the power control of the arc high voltage supply. The arc is enabled and disabled with a digitally controlled relay switch.

(3) Monitoring of joint transmission

The output from the light detection system is read by the CPU using an analogue to digital converter and stored in the program for processing during either the manual or the automatic alignment phase.

(4) Interface with operator

The program is self-prompting, using the LCD to lead the operator through the steps of making a splice and reporting back the results as they occur. Control over the program is gained using the 16-key pad to reply to the CPU commands displayed.

(5) Battery energy economy

Using digitally-controlled relays the power supplies to parts of the equipment may be controlled from software. This can be used to conserve battery power after a period has elapsed without operator usage.

(6) Programs for arc control

Ten preset programs can be selected by the operator, these being permanently stored in the CPU ROM area. This set can be supplemented by the user entering his own program to be stored in the battery-backed RAM area. Should these RAM-based programs become standard, they can be put in as extra ROM-based programs, the number of which is only limited by the ROM space available (up to 16 k bytes).

(7) Battery care

The microprocessor also monitors the state of battery charge, informing the operator via the LCD. Warning is given as the battery approaches the minimum recommended charge, and automatic disablement of the alignment and splicing functions occurs when the voltage drops to the recommended limit.

6. Local Light Injection and Extraction

The technique used for local light injection is based on the propagation characteristics of curved single-mode fibres.

When an energised single-mode fibre is bent, below a certain radius of curvature, light is lost from the core due to energy transfer from the LP_{01} mode to the evanescent mode¹. It has been shown here, and by others², that the converse, light injection via a bend, is also possible.

Light is injected by focussing from a 940 nm LED onto a portion of the curved single-mode fibre, by means of a specially shaped rigid lens which contacts the fibre along the curve, the radius of which is 4.5 mm, and focusses most of the LED emission onto the surface of the coated fibre. The light focussing element and the LED are mounted in a clamp unit that enables fibres to be repeatably positioned with respect to the light collection and focussing element. Light on the fibre surface penetrates the coating, and some is converted into the guided mode. The fibre curvature used, 4.5 mm, is such that it provides efficient mode conversion, whilst at the same time is not deleterious to fibre strength. The probability of fibre failure during an exaggerated jointing period of 30 minutes³ is 1 in 8000, and the additional probability of failure during the next 40 years after release from the machine is less than 1 in 10^{13} .

To check the efficacy of using injected light at 940 nm for accurate core alignment, several tests were carried out. Light was injected near one end of a length of single-mode fibre, the other end being held in one of the chucks of the fusion splicer and scanned transversely by another piece of the same fibre; index matching liquid was used between the fibre ends to eliminate interference effects. The results of the test are shown in Fig. 2.

The output patterns from the injected fibre for both long and short lengths are very similar. This proves that only the fundamental mode is excited in the fibre, and that there is no cladding mode propagation. The plot obtained with direct launch is somewhat broader than the other two, as would be expected with high V numbers. Hence, even though the cut-off wavelength λ_c for the fibre is about 1100 nm, the injection technique used eliminates all modes higher than LP_{01} . The graphs further illustrate the high resolution of the system, allowing fibre core alignment to an accuracy of better than 0.1 μ m.

Local light extraction is carried out by leaking light out of the curved fibre, the radius of curvature again being 4.5 mm, and collecting by another shaped rigid lens, a major part of the light being focussed onto the active area of a silicon detector; again, a clamp unit is used to hold the fibre in relation to the extraction element.

A phase-sensitive detection system is required to amplify the weak signals from the detector photodiode and to produce a DC voltage output for the microprocessor with an acceptable signal/noise ratio. A modulation frequency of about 465 Hz is used, this frequency being far enough away from 50 Hz and 60 Hz mains frequencies and their harmonics to avoid interference, without requiring excessively high frequency response in the system.

The LED for the light injection is driven in synchronism with the detector circuit by a switch-mode constant current power supply, designed to minimise the power consumption.

The injection and extraction clamp units of the monitoring system which are incorporated in the splicer assembly were tested for the effects of vibration and temperature, with the result that:

- (1) There was no detectable change of performance after maintaining the temperature at 60°C for 3 hours and then 0°C for 3 hours.
- (2) Vibrations sweeping between 10 and 20 Hz at a rate of 5 s/cycle, with an amplitude of 6 mm peak to peak for a total of 600 cycles, induced no detectable change of performance.
- (3) There was no detectable change of performance during a period of 30 minutes under normal conditions.

The specially-shaped rigid lens employed for injection and extraction of light are the subject of pending patent applications.

7. Automatic Alignment of Fibres

To find the best alignment position automatically, the processor uses the simplex method on the alignment monitor output (a hill-climbing technique without constraints). A simplex is a geometric figure with one more vertex than the number of dimensions which contain the function that is to be maximised (or minimised). Thus in a two-dimensional search the simplex is a triangle. The two dimensions in this case are those orthogonal to the fibre axis.

The method works by laying a mesh of simplices over this surface in a manner that quickly encircles the maximum. The fibre being aligned is positioned at each vertex of the mesh in turn, starting at the first simplex, and the corresponding light transmission is monitored. The next simplex is then generated by reflecting the worst vertex in the centroid of the opposite side. When the simplex size becomes too coarse to allow a closer approach to the goal, the simplex size is reduced and the process repeated until eventually the desired resolution is attained.

A typical search pattern may be seen in Fig. 3, superimposed on a single-mode fibre cross-section. The offset has been exaggerated, as has the initial simplex size for the purposes of clarity.

During tests the success of the alignment routine was measured by comparing the auto-aligned maximum signal with the manually-aligned maximum signal - the results always fell within the noise limit of the aligning signal and appear in Fig. 4. The dB scale is referred to the best alignment attainable by hand at the start of the test.

8. Single-mode Splicing Technique

The basic techniques of single-mode arc fusion splicing are now well established, although each manufacturer of single-mode fusion splicing equipment incorporates variations on the basic theme^{4,5}.

The cleaved fibre ends are initially separated by a gap, typically 5-10 μm , large enough to allow unimpeded adjustment of offset. Once this alignment has been completed, the arc is struck at a power just sufficient to melt the fibre ends but not hot enough to distort the square end profiles. After a fixed delay the fibres are driven towards each other and as they pass the butting point the arc power is increased to a level at which a strong well-fused joint is formed, but not so high as to overheat the joint. Overheating would allow the surface tension in the molten cladding to distort the core alignment of fibres with eccentric cores. The arc is maintained at the higher level for a fixed interval, typically 1 second. The heated fibres, after reaching the butting point, fuse and continue to be driven together for a short distance, typically 5 μm . The splice is then complete and ready for protection.

9. Cleaving

Good cleaving is necessary before splicing. Bench-mounted cleavers can give excellent results, but are not really suited to field use. A hand-held cleaver is preferable.

Of hand-held single-mode cleavers, there were until recently only three makes on the market, and these were all to the same Japanese design. The multimode T402 cleaver from Biccotest could, with careful selection, give satisfactory cleaves with end angles better than 1° , but end angles of 0.5° or better are really called for, for low loss splices of better than 0.1 dB on single-mode fibre. A recent development of the T402, the Mark III single-mode cleaver, Fig. 5, gives end angles averaging better than 0.5° when correctly adjusted, Fig. 6. It is more robust than the T402 and does not easily go out of adjustment. There is also a fibre guide to govern the fibre position, with a trigger-operated fibre clamp. The cleaver may be used in the bench-mounted mode if required.

The T402 cleaver is the subject of British Patent No. 1519232 and the next development of this cleaver is the subject of a pending patent application.

The cleavers used for splicer assessment were the York Technology C007 bench-mounted cleaver and the Mark III cleaver just described.

10. Operation of the Mark III Fusion Splicing Machine

The operator is guided through the routine step by step, by means of the LCD display and, after each step is completed to the operator's satisfaction, depression of an indicated key gives the signal for the next stage. The steps are:

- (1) Select the program appropriate to the fibre to be spliced, or the operator's own program may be generated if desired.
- (2) Position the fibres in the chucks.
- (3) Check the fibre end angles and cleanliness using the split-view microscope.
- (4) Position the fibres in the Monitor clamps, if the monitor is to be used.
- (5) Roughly align the fibres, using the manual adjustment, to the satisfaction of the display.

- (6) Butt the fibres, so that they just touch.
- (7) Gap and prefuse, which is an automatic process.
- (8) Final alignment, either automatic or manual as appropriate.
- (9) Fuse, which is an automatic process.
- (10) Remove the spliced fibre and protect.

On pressing the 'fuse' button, the machine takes over to complete the joint, executing the steps described in section 8, and illustrated in Fig. 7.

These steps need little further explanation. The choice of manual alignment with the LCD able to act as a local monitor is provided but seldom needed. The whole routine need not take as long as five minutes to complete, of which less than one minute is taken for automatic alignment.

A series of test splices between identical fibres was made, using Corning acrylate-coated single-mode fibre. The losses were calculated from external monitor readings at 1300 nm. The results are shown in Fig. 8, and the mean splice loss is 0.058 dB. These results compare well with an earlier series made on a manually-aligned Mark II machine, Fig. 9, where the mean loss was 0.064 dB.

11. Collected Results and Conclusions

All of the original points in the outline target specification in section 2 have been met. The splicer is a single self-contained unit, weighing 19.95 kg. More than 100 splices can be made without recharging. A local monitoring system, with vibration-tested components, is included. Splicing is automatic, and the automatic alignment is accurate to 0.1 μ m, taking less than 1 minute. The mean splice loss is 0.058 dB.

The splicer is convenient to handle and simple to use. The mean splice loss is low and there is little further room for optimisation. Further gains in weight reduction could be made, particularly when a CMOS version of the CPU becomes available, permitting a large reduction of battery size.

References

- (1) W.A. Gambling, D.N. Payne and H. Matsumura, Radiation from curved single-mode fibres. *Electron. Lett.* 12 (1976), pp. 567-9.
- (2) C.M. de Blok and P. Matthijesse, Core alignment monitor for single-mode jointing. *Ibid* 20 (1984), pp. 109-10.
- (3) M. Fox, Private Communication.
- (4) Uwe Bottcher, Advanced splicing equipment for single mode fibre. FOC-LAN '83, Atlantic City USA, pp.21-25.
- (5) Yasuyuki Kato, Shigeyuki Seikai and Mitsuhiro Tateda, Arc-fusion splicing of single-mode fibers. 1: Optimum splice conditions. *Applied optics* 21 (1982), pp. 1332-1336.

Acknowledgements

The authors thank the Directors of BICC plc for permission to publish this paper, and colleagues for assistance with its preparation.



Patrick Andrews graduated from Faraday House, London, in 1954. After some years at British Thompson Houston, Rugby, and at Rolls Royce, Derby, he joined BICC Research and Engineering in 1963. There he was at first concerned with conductor physics until becoming enmeshed in optical fibres in 1977. At present he leads a team engaged in studies of jointing in optical fibres.



Roger Hazelden joined BICC in 1982 after graduating from Pembroke College, Cambridge with a BA(Hons) in Natural Sciences. He has been working on the development of automated fibre characterisation techniques and is now designing electronics for fibre-optic test, measurement and installation equipment.



Richard Grigsby has been with BICC Research and Engineering since 1961 and has been attached to the Optical Transmission Department since 1981, where he has been particularly concerned with optical fibre splicing.



Martin McDonough joined BICC in 1982 and is currently a member of the Optical Transmission Department. Martin holds a BSc in Mathematics and Philosophy from Keele University and an MSc in Microwaves and Modern Optics from University College London.



Sanjiv Saha obtained an MScTech degree in Materials from Sheffield University, UK, in 1978. He joined the Optical Transmission Department of BICC Research and Engineering soon after, and has worked in areas of fibre characterisation, fusion splicing, and fabrication of Y-couplers. He is currently working on local light injection and detection techniques.

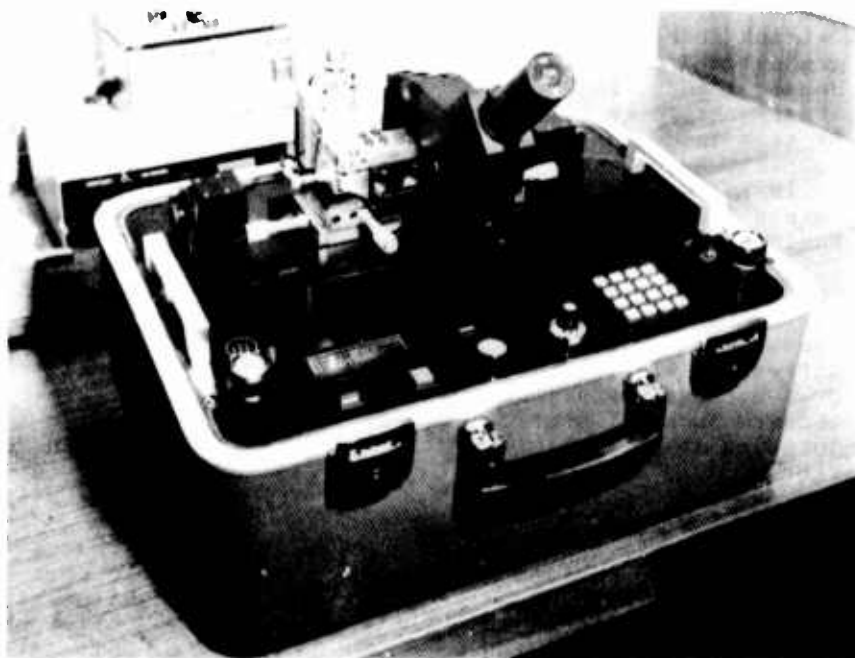


FIG. 1 PROTOTYPE SINGLE-MODE SPLICER

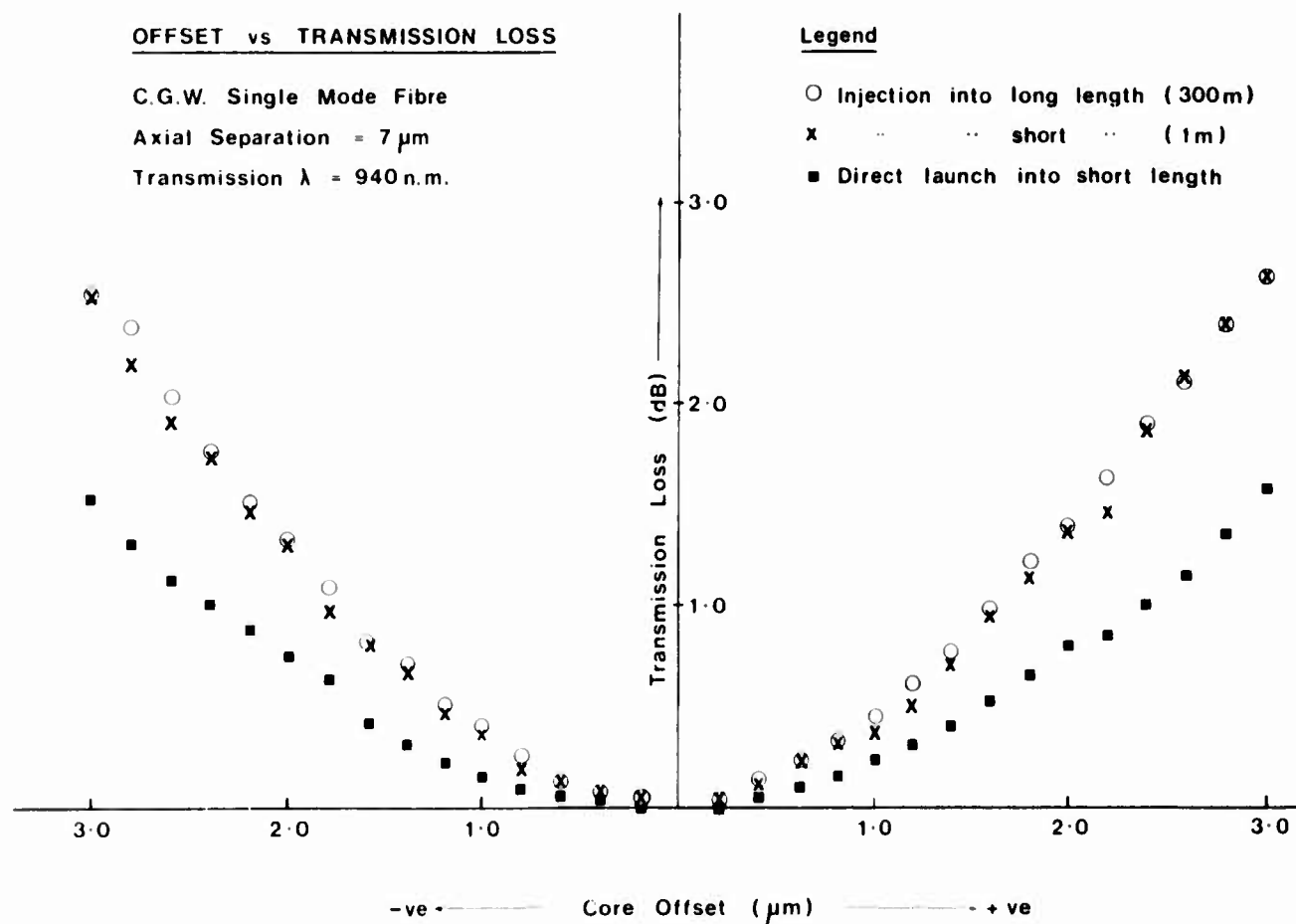


FIG. 2 ALIGNMENT BY LOCAL MONITOR

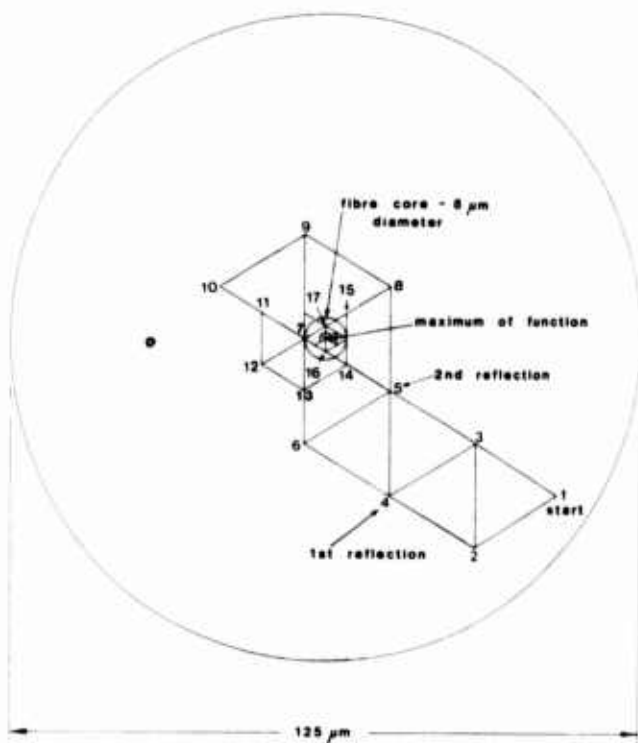


FIG. 3 A TYPICAL SIMPLEX SEARCH

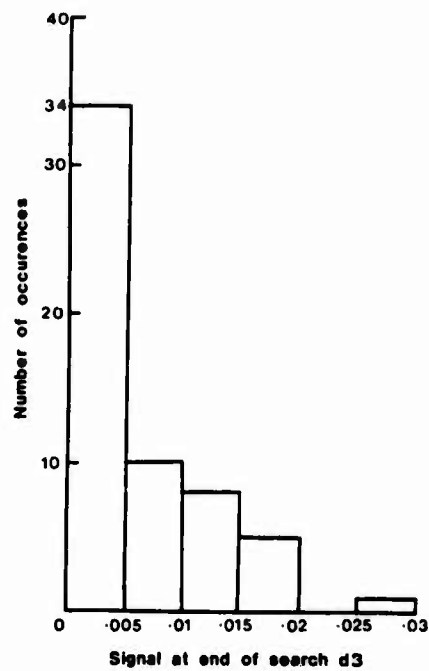


FIG. 4 SIMPLEX AUTOMATIC ALIGNMENT
TEST RESULTS



FIG. 5 MARK III SINGLE-MODE CLEAVER

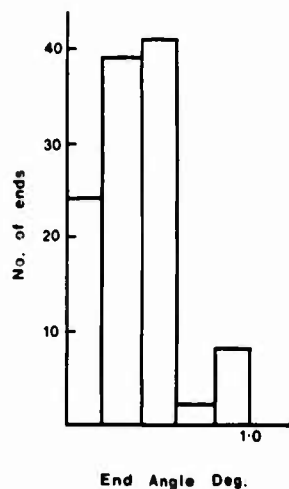


FIG. 6 THE COMBINED RESULTS OF
FOUR Mk III CLEAVERS

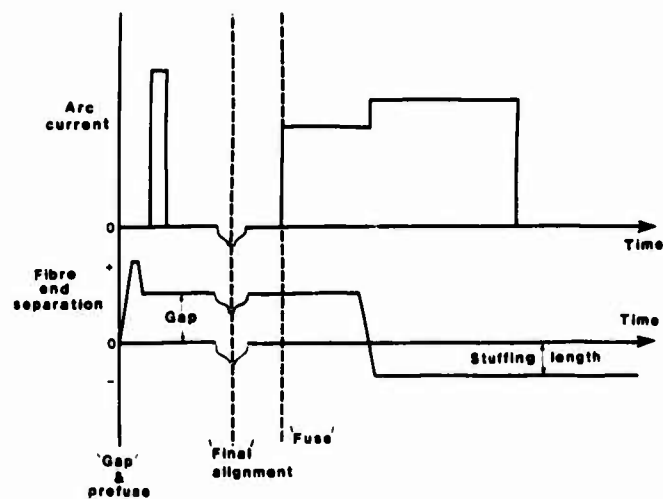


FIG. 7 SPLICING SEQUENCE FOR Mk III FUSION SPLICER

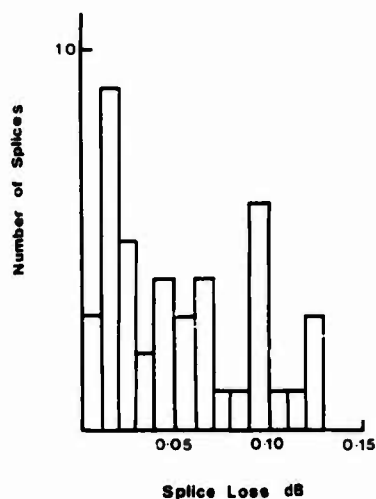


FIG. 8 FUSION SPLICE TEST RESULTS
FOR Mk III MACHINE

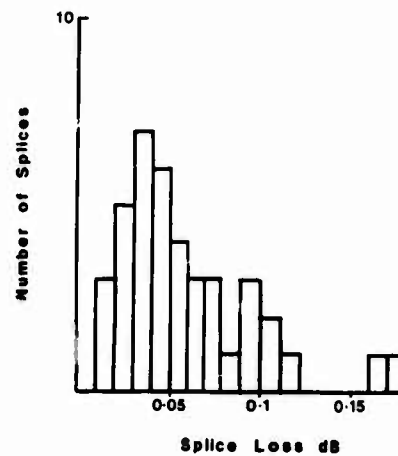


FIG. 9 FUSION SPLICE TEST RESULTS
FOR Mk II MACHINE

M. FUJISE Y. IWAMOTO

KDD Research & Development Laboratories
1-23, Nakameguro 2-Chome, Meguro-Ku, Tokyo 153, JAPAN

SUMMARY

This paper presents a new simple local monitoring method in core alignments of single-mode fibers and a newly developed self-core-alignment arc-fusion splicer. We have investigated cladding mode leakage light characteristics in the receiving fiber just behind the butt-joint point and designed a photo-receiver with high sensitivity for monitoring the leakage light power without bending the receiving fiber. Using the receiver and an arc-fusion splicer heretofore in use, we have obtained an extremely good result of an average splice loss of 0.03 dB for one hundred splices with transmitted optical power of only 1 μ W at the butt-joint point. Moreover, we have newly developed an arc-fusion splicer with self-core-alignment function based on the cladding mode leakage light power monitoring, which incorporates a microprocessor and piezoelectric elements. The design and the performance of the splicer and the results of splicing experiments are also presented.

1. Introduction

Core diameter of single mode optical fiber is small as 10 μ m and generally core axis deviates from that of cladding. Then, precise core alignment in splicing has been considered to be indispensable to achieving low loss splices. An optical power monitoring method, in which a light is excited in fibers through a splice point and its output light power at a far end of a receiving fiber is monitored, is widely adopted for core alignment and splice loss estimation.⁽¹⁾ In this method, in laying or repairing optical cables, it is necessary to send back the monitored information to the splicing point and consequently, splicing work is so complicated. Especially, this method cannot be applied to a final splicing in optical fiber digital transmission systems, since the information of transmitted optical power at butt-joint point is lost after the successional repeater.

As alternative method, Miller presented a local detection device utilizing a 10 cm long glass tube with an inner diameter of 0.3 mm and an InGaAs detector,⁽²⁾ and reported its application to field splicing with UV-curable cement.⁽³⁾ Moreover, another local monitoring

methods based on bending a receiving fiber just behind the butt-joint point were reported.⁽⁴⁾⁽⁵⁾⁽⁶⁾ Being different from that reported in reference(2), these methods have merits that the leakage light can be detected at one point in the receiving fiber and their detection devices fit different sizes of fibers. However, bending a fiber with a diameter of 4-10 mm² during the fiber jointing may cause a serious problem, because the local tension of fiber exceeds the usually accepted level in the fiber strength.

In this paper, we present a new simpler local monitoring method which makes precise core alignments possible by detecting cladding mode leakage light power at one point just behind a butt-joint point without bending a fiber. Firstly, this paper describes measurement results of cladding mode leakage light characteristics in a single-mode fiber coated with UV-curable resins, which is successfully used on commercial scale. Then, we discuss a photo-receiver design for cladding mode leakage light detection considering the results of the investigation of the fiber and the requirements from practical use. Using the photo-receiver, we have obtained an extremely good result of arc-fusion splicings.

Furthermore, we have newly developed an arc-fusion splicer with self-core-alignment function based on the cladding mode leakage light power monitoring, which incorporates a microprocessor and piezoelectric elements.

The transmitted optical power of the only 1 μ W at a butt-joint point makes precise core alignments possible and low loss splices must be made with the splicer at any point in a long length fiber over 50 Km between repeaters by driving a laser diode in a repeater as a light source.

2. Cladding mode leakage power measurements

If two fibers to be spliced are butt-jointed each other and light is excited in the incoming fiber, a guided mode in the core of incoming fiber is emitted into an air gap at the butt-joint and is coupled to both a guided mode and cladding modes in the outgoing fiber.

The cladding modes are confined in a cladding since buffer layers and a jacket of fiber end section of about 15 mm are stripped off and refractive index of air is lower than that of cladding. However, after cladding modes

get to the coated fiber section, they propagate in both a cladding and buffer layers since refractive index of the primary buffer layer is higher than that of cladding. Any kind of geometric imperfection of boundary surface between cladding and the primary buffer layer and their refractive index fluctuations cause cladding modes to leak out through the secondary buffer layer and the jacket as illustrated in Fig.1.

Figure 2 shows a set-up for leakage light power measurements. Single-mode fibers are energized through optical attenuator by a 1.3 μm laser diode modulated with 270Hz. The identical fibers are placed on movable fiber holders driven by micro-manipulators and are butt-jointed each other, where core axes are shifted relatively so that the most of emitted light is coupled into cladding modes. The cladding mode leakage light is detected with the 10 mm ϕ germanium photodiode on a side of the outgoing fiber stretched rectilinearly. Transverse offsets and a gap at the butt-joint are measured with electronic micrometers of which probes are attached to the movable fiber holders.

Table 1 shows the structural parameters of a UV-curable resin coated fiber used in the measurements and arc-fusion splices which will be mentioned later on. Coating materials are urethane-acrylate and epoxy-acrylate.

Figure 3 shows a measurement result of leakage light power distribution along the fiber, where P_t is the transmitted optical power at the butt-joint, P_l is the cladding mode leakage power at a distance l , dx is the transverse offset, dz is the gap length at the butt-joint and d is the length of the stripped fiber section.

As shown in Fig.3, the leakage light power decreases along the fiber and the power of about 20 dB below of the transmitted optical power at the butt-joint was obtained at the position of 100 mm from the cladding mode launched fiber end. Moreover, cladding mode loss of about 100 dB/m is induced from an inclination of the fitted line. We also measured leakage light powers around the fiber and obtained almost equally distributed leakage powers.

It may be said that the degree of the cladding mode stripping effect mainly depends on the refractive indexes of the coating materials. In this fiber, an outer layer have higher refractive index than that of an inner layer. Only the air guides several modes which propagate in cladding, buffer layers and a jacket. Hence, cladding modes leak out easily and the leakage light level decreases suddenly along a fiber.

On the other hand, we investigated a silicone resin coated fiber and the cladding mode loss in the fiber was estimated at about 30 dB/m. In this case, the secondary buffer layer of silicone rubber makes a role of guiding some modes, since its refractive index is lower than that of the primary buffer layer of modified-silicone.

3. Cladding mode power vs transverse offset

Assuming that electromagnetic fields of a guided mode in a single-mode fiber are Gaussian, we obtain a coupling coefficient of identical fibers between guided modes at the butt-joint point by the following equation:(7)

$$\eta_g = \frac{(n_1 k)^2 \omega_0^4}{(dz)^2 + (n_1 k)^2 \omega_0^4} \exp \left\{ -\frac{(n_1 k)^2 \omega_0^2 (dz)^2}{(dz)^2 + (n_1 k)^2 \omega_0^4} \right\}, \quad (1)$$

where dx is the transverse offset and dz is the air gap length. Note that only the transverse offset is considered in the equation (1). Here, ω_0 is the spot size of Gaussian beam in the core given by(8)

$$\omega_0 = a(0.650 + 1.619V^{-1.5} + 2.879V^{-6}), \quad (2)$$

where V parameter is defined as $V = ak\sqrt{n_1^2 - n_2^2}$, a is the core radius, $k = 2\pi/\lambda$ is the free space propagation constant of plane waves, λ is the light wavelength in vacua and n_1 and n_2 are core and cladding refractive index respectively.

Assuming that Gaussian beam except a portion confined in the core is coupled to cladding modes at the air gap, we obtain its coupling coefficient η_c as

$$\eta_c = 1 - \eta_g \quad (3)$$

Figure 4 shows theoretical curves of η_c for $dz = 10, 50$ and $100 \mu\text{m}$. η_c is the minimum when dx is zero. Then, the curves of η_c suggest that a core axis alignment can be made by monitoring cladding modes leakage light.

Figure 5 shows the logarithmic curves of equation (1),(3), which describe changes of guided mode power and cladding mode power vs. transverse offset of core axis. As shown in Fig.5, the transverse offset shift of dx from 1 to 0 μm causes change of over 10 dB in cladding mode power level and a change of only 0.2 dB in guided mode power level. Therefore, more precise alignment essentially can be achieved by monitoring the cladding mode leakage light power.

4. Detection system for monitoring

In a long-haul optical fiber transmission systems, a repeater interval is $\sim 50 \text{ Km}$, and output optical power of a laser diode in a repeater and loss of single-mode fiber are about -5 dFm and 0.5 dB/Km respectively. Hence, the lowest optical power in the fiber is about -30 dFm.

On the other hand, the leakage light power at $l = 100 \text{ mm}$ and $dz = 10 \mu\text{m}$ is experimentally estimated at 20 dB below that of transmitted optical power at a butt-joint point from Fig.3, and decreases about 25 dB down when dx goes zero as shown in Fig.5.

Therefore, in the case of 10 mm² detector is used, we need a photo-receiver with the minimum sensitivity of -75 dBm for precise core alignments in long-haul transmission systems.

Utilizing a 10 mm² Ge-PD and an ultra low noise operational amplifier, we developed a photo-receiver, that is, a transimpedance amplifier followed by a bandpass filter with variable bandwidth. The equivalent circuit diagram is shown in the inset of Fig.6. Here, P_i is incident light power.

R_d and R_f are dynamic resistance of the photodiode and feedback resistance of the transimpedance amplifier respectively. B is bandwidth of the bandpass filter and V_o is output voltage signal of the photo-receiver.

Considering signal current and various noise sources in the transimpedance amplifier, we obtain the output voltage signal of the photo-receiver as follows;

$$V_o = \left[\left(\frac{\eta e}{h\nu} P_i \right)^2 + \left\{ 2e \left(\frac{\eta e}{h\nu} P_i \right) + 2eI_d + \frac{4kT}{R_f} + \left(\frac{V_n}{R_n} \right)^2 + i_n^2 \right\} B \right]^{1/2} \cdot R_f \quad (4)$$

where η is quantum efficiency of the photodiode, e is electronic charge, h is Plank's constant, ν is light frequency, k is Boltzmann's constant, T is absolute temperature, B is frequency bandwidth of the filter, V_n and i_n are input noise voltage and input noise current of the operational amplifier respectively and I_d is dark current of the photodiode. In this equation,

is current due to the incident light signal. As noise sources in the photo-receiver of which output is limited by filtering to a bandwidth B , shot-noise current which has mean-squared amplitude as :

$$\left\{ 2e \left(\frac{\eta e}{h\nu} P_i \right) + 2eI_d \right\} B,$$

and thermal noise current of R_f which is described as

$$\sqrt{\frac{4kT}{R_f} B}$$

and a noise current which has a mean-squared amplitude of

$$\left\{ \left(\frac{V_n}{R_n} \right)^2 + i_n^2 \right\} B$$

due to the input voltage noise and the input current noise of the operational amplifier must be considered.

Both the dark current of the Ge-PD and the input voltage noise of the operational amplifier are main restrictive factors in the minimum sensitivity.

Figure 6 shows the responsivity and noise floor of the receiver, where open circles and crosses denote measured values and solid curves describe the calculation results obtained from equation(4) by using following parameters as

$$\eta = 0.6, \quad \nu = 2.31 \times 10^{14} \text{ Hz}, \quad I_d = 300 \mu\text{A},$$

$$T = 300\text{K}, \quad R_f = 1 \text{ M}\Omega, \quad R_d = 500 \Omega,$$

$$V_n = 3.2 \text{ nV}/\sqrt{\text{Hz}}, \quad i_n = 0.4 \text{ pA}/\sqrt{\text{Hz}}$$

$$\text{and } B = 4, 8 \text{ Hz}.$$

Figure 6 shows good overall agreements of measured and calculated relations between incident light power P_i and output voltage V_o .

In order to obtain a highly sensitive photo-receiver, it is necessary to use a high impedance feedback resistor and a narrow bandwidth filter. Choosing 1 M Ω as R_f and 4 Hz as B , we can obtain a photo-receiver whose responsivity and minimum detectable light level are about 0.63×10^6 V/W and about -75 dBm respectively.

Using this photo-receiver, we detected the cladding mode leakage light with changes of transverse offset of core axis. Figure 7 shows the changes of detected signal level against transverse offset of core axis in the UV-curable resin coated fiber. In this measurement, the transmitted optical power P_t was set -30 dBm. A photo detector was located at the position of $l = 120$ mm and air gap length Δz was set 10, 50 and 100 μm . The detected signal approached the minimum as the transverse offset of core axis converged towards zero in the similar way as cladding mode coupling coefficient curves as shown in Fig.4. Accordingly, pursuing the bottom by transversely moving a fiber holder performs an accurate core axis alignment.

From these measurements, it is cleared that the changes in detected signal agree with the theoretical curves as a whole. Further, clearness of the patterns obtained by using the photo-receiver is good enough for core alignments.

5. Arc-fusion splicings

We executed splicings of an UV-curable resin coated fiber, using the photo-receiver mentioned earlier. The result of splicings is shown in Fig.8, where transmitted optical power P_t at the butt-joint was set -30 dBm for each splicing. An average splice loss of 0.03 dB was obtained for one hundred samples.

Here, the splice loss was evaluated by monitoring the output optical power before cutting and after splicing. To attain a possibly accurate evaluation, we housed an optical attenuator and a sensor head of an optical power meter in a constant temperature box. In addition to that, a 1.3 μm InGaAsP/InP BH laser diode was attached to a constant temperature plate controlled by Peltier's thermo-device to stabilize the output optical power. Consequently, a stability within ± 0.0025 dB/hour was achieved.

We have carried out fusion splicings in a long optical fiber cables⁽⁹⁾ between repeaters by driving a laser diode installed in a repeater as a light source and gained confidence of the adaptability of this method in the final splicing work for the optical fiber digital transmission systems with repeater interval over 50 km.

6. Self-core-alignment arc-fusion splicer

As discussed so far, precise core alignment of single-mode fiber can be performed by monitoring cladding mode leakage light power. This new local monitoring method is efficient and of practical use. Therefore, we have newly developed a self-core-alignment arc-fusion splicer based on this monitoring method, which incorporates piezoelectric elements for positioning X, Y axis and an 8 bit μ -computer for controlling a sequence of alignment and arc-fusion splicing.

6.1 Piezoelectric element

For applications as in core alignments requiring a linear movement with extremely high resolution and good dynamic range, the converse piezoelectric effect offers an excellent positioning method. Since piezoelectric element converts electric energy directly to mechanical movement, it is free of backlash and has high speed responsivity.

As well known, hysteresis occurs between the applied voltage and expansion of piezoelectric element. The same operating voltage can give different expansions depending on whether the element previously had no applied voltage or the maximum applied voltage.

However, as shown in Fig.9, a fixed hysteresis curve is obtained under a constant temperature, a load and an cycle velocity. We made use of the rising branch characteristic of piezoelectric elements with full expansion range of 50 μ m at the applied voltage of 500 V.

Because of its direct conversion of an applied analog voltage to a mechanical movement, the resolution of piezoelectric element is determined by the stability of the applied voltage. Here, the minimum step of movement was controlled at 0.05 μ m by a μ -computer.

Figure 10 (a) shows another characteristic of piezoelectric element, that is, creeping. The piezoelectric element continues to change its expansion by a small amount, even if voltage is hold at a fixed point after being applied along the rising or the falling branch.

Figure 10 (a) illustrates displacement Cu and Cd by creeping and the creeping amount used in the splicer was about 1 % of absolute expansion length. This small amount of displacement can be compensated by applying an excess voltage V_F and reducing the applied voltage by V_B as shown in Fig. 10 (b). We set 25 V and 32 V as V_F and V_B respectively and obtained positioning precision less than 0.05 μ m.

6.2 Configuration of the splicer

Figure 11 shows the configuration of self-core-alignment arc-fusion splicer. The photoreceiver section is basically similar to that mentioned earlier. In order to supply a suitable input voltage to the A/D converter, the gain of an AC-amplifier is controlled automatically by autorange controller according

to power level of incident light. Its variable gain ranges from 0 to 60 dB. Detected leakage light signal is digitized by a 12 bit A/D converter and it is fed to an 8 bit μ -computer. The μ -computer controls drivers of piezoelectric elements for X, Y axis movement and also controls a driver of DC motor for Z axis movement.

The μ -computer automatically processes the sequence of core-alignment and arc-fusion splicing as shown in Fig. 12. Core-alignment sequence consists of 2 stages. The first stage is rough alignment sequence with 0.5 μ m step in a 20 μ m scan width and the second stage is fine alignment sequence with 0.05 μ m step in a 2 μ m scan width. The second stage is repeated 2 times to make sure of a sufficient alignment.

Various conditions in the arc-fusion splicing were set as followings : electrode gap was 1.5 mm, prefusion time was 0.01 sec, electric discharge duration was 2.0 sec, discharge current was 15 mA, pressing stroke of fiber end face was 35 μ m and its pressing velocity was 82 μ m/sec. Total time required to complete both core-alignment and arc-fusion splicing was 2.5 minutes.

Figure 13 shows a view of the newly developed arc-fusion splicer with a self-core alignment function. Using the splicer, we carried out arc-fusion splicings of same type of single-mode fibers as those spliced manually. Figure 14 shows the result of one hundred splicing trials where transmitted optical power at butt-joint point was set -25dBm. An average splicing loss of 0.05 dB was achieved in laboratory experiments.

7. Conclusion

A new simple local monitoring method and an arc-fusion splicer with self-core-alignment function have been reported. This local monitoring method ; cladding mode leakage light power monitoring, is desirable since it is not necessary to bend fibers. In addition to that, it essentially has the precedence in the preciseness of alignment over the conventional power monitoring method including local detection by bending fibers because the monitored signal excessively sensitive to the change of transverse offset.

The highly sensitive photo-receiver designed for the leakage light detection makes precise core alignments possible even in the case of that the transmitted optical power at a butt-joint is only 1 μ W. We have manually executed arc-fusion splicings of an UV-curable resin coated fiber using the photoreceiver and obtained a surprisingly good result, that is, an average splice loss of 0.03 dB for one hundred trials.

Then, we have presented a newly developed self-core-alignment arc-fusion splicer. This splicer performs automatically core-alignment and splicing in sequence. Its self-core-alignment function is based on the new local monitoring method. The splicer incorporates

piezoelectric elements for X, Y axis movement and a μ -computer for the signal processing and sequence control. The average splicing loss by the splicer was 0.05 dB in laboratory experiments.

This splicer can be used not only for usual splicing work but also for any splicings including a final splice in a long-haul digital transmission systems by sending a high bit-rate optical signal to comprise a low frequency component from the terminal equipment and driving a LD in the nearest repeater.

The authors wish to express their sincere thanks to Dr. H.Kaji and Dr. C.Ota of KDD Labs for their encouragement.

References

- (1) T.Tanifuji and Y.Kato, : "Realization of a low loss splice for single-mode fibers in the field using an automatic arc-fusion splicing machine" Proc. OFC'83, Feb. 1983, MG3, pp.14-15
- (2) C.M.Miller, : "Local detection device for single-mode fiber splicing", Proc. OFC'82, Apr. 1982, THAA2, pp.44-45
- (3) C.M.Miller, G.F.Deveau and M.Y.Smith, : "Low loss single mode fiber splices using ultraviolet curable cement", IOOC'83, July 1983, Tech. Digest, 30A3-6, pp.128-129
- (4) M.Fujise, K.Asakawa and Y.Shirasaki, : "Single-mode fiber arc-fusion splicing by monitoring the leakage light", National Conv. Rec. of IECE Japan, Aug. 1982, No. 389
- (5) Y.Kato, T.Tanifuji, M.Tokuda, and N.Uchida, : "New optical monitoring method for arc-fusion splice of single-mode fibres and high-precision estimation of splice loss", Electron. Lett., 1982, vol.18, No.22, pp.972-973
- (6) C.M.De Blok and P.Matthijsse, : "Core alignment procedure for single-mode-fibre jointing" ibid., 1984, vol.20, No.3, pp.109-110
- (7) I.Hatakeyama and H.Tsuchiya, : "Fusion splice loss for single-mode optical fiber", Trans. IECE Japan, Dec. 1979, vol.J62-C, No.12, pp.803-810
- (8) D.Marcuse, : "Loss analysis of single-mode fiber splices", Bell Syst. Tech. J., May 1977, vol.56, No.5, pp.703-718
- (9) Y.Ishikawa, Y.Niiro, K.Takai, and H.Wakabayashi, "7000 m deep sea trial of OS-280M optical-fiber submarine cable system", Electron. Lett., 1984, vol.20, No.13, PP.548-549



Masayuki Fujise received both the B.S. and the M.S. degrees in communication engineering from Kyushu University in 1973 and 1975, respectively, and the M. Eng. degree in electrical engineering from Cornell University in 1980. He joined KDD Laboratories and has been engaged in research on optical fiber measurements.



Yoshinao Iwamoto received his B.S. in Electronics Communication Engineering from Osaka University in 1964. After graduation he joined KDD.

Since 1969 he has been engaged in the development of the submarine coaxial cable systems. He is presently managing a group with responsibility for research and development of the optical fiber submarine cable systems in KDD Laboratories.

Core diameter	Cladding diameter	Core eccentricity	Refractive-index difference
(μm)	(μm)	(%)	(%)
10	125	1.0	0.32

Cutoff wavelength	Primary buffer layer	Secondary buffer layer	Jacket
(μm)	(Urethane-Acrylate) dia. (mm)/refr. index	(Epoxy-Acrylate) dia. (mm)/refr. index	(Urethane-Acrylate) dia. (mm)/refr. index
1.25	0.23/1.52	0.40/1.53	0.60/1.54

Table 1. Structural parameters of an UV-curable resin coated fiber

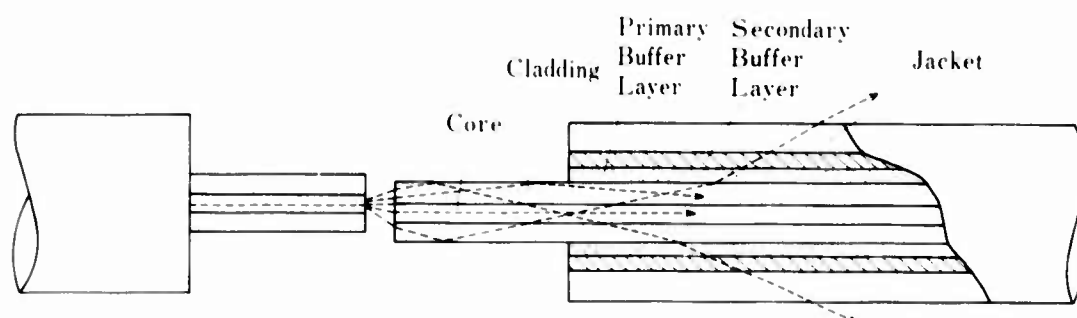


Fig. 1 Illustration of cladding mode leakage process

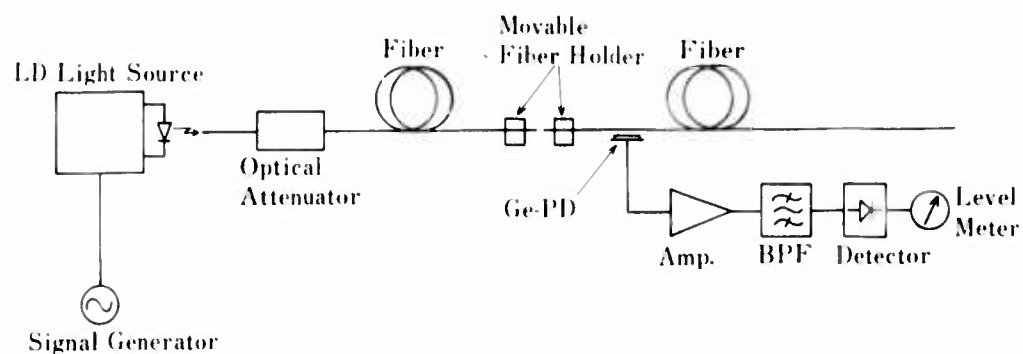


Fig. 2 Set-up for leakage light power measurements

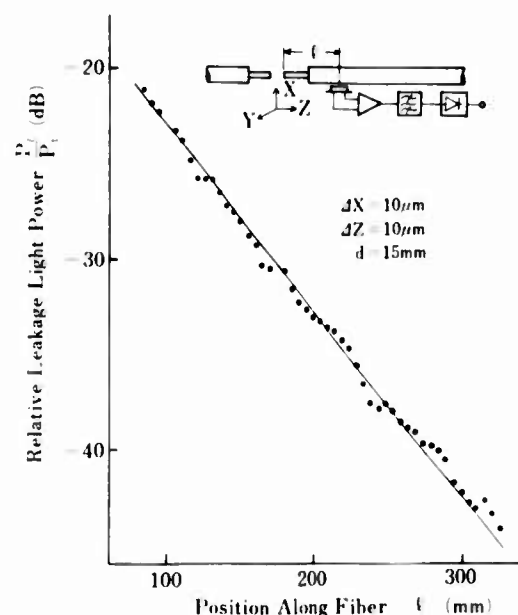


Fig. 3 Distribution of leakage light power along UV-curable resin coated fiber

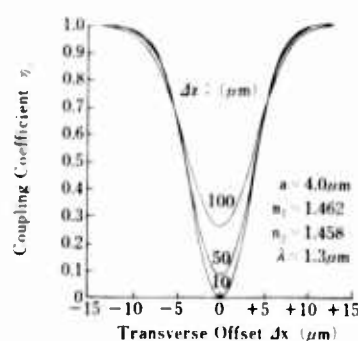


Fig. 4 Cladding mode coupling coefficient vs. transverse offset

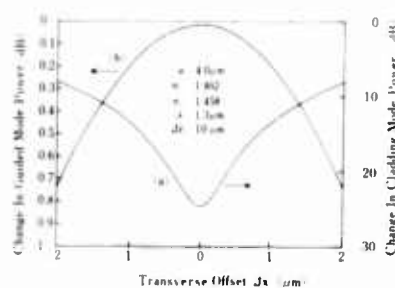


Fig. 5 Changes of monitored levels of cladding mode leakage light and far end output light against transverse offset of core axis

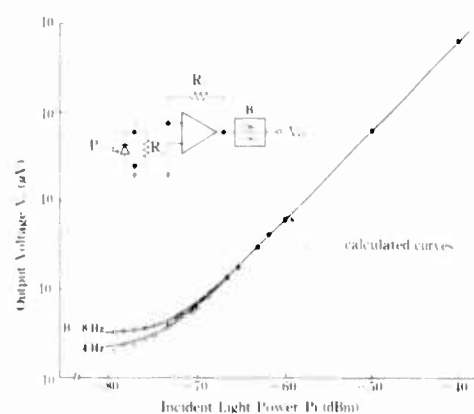


Fig. 6 Responsivity and noise floor of the photo receiver

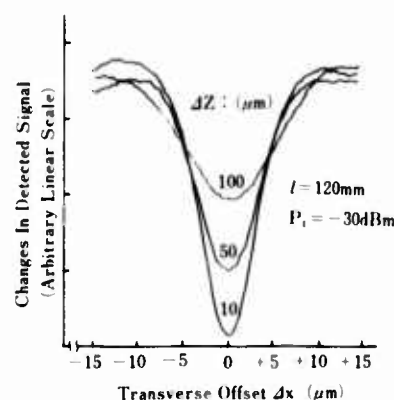


Fig. 7 Detected signal levels against transverse offset

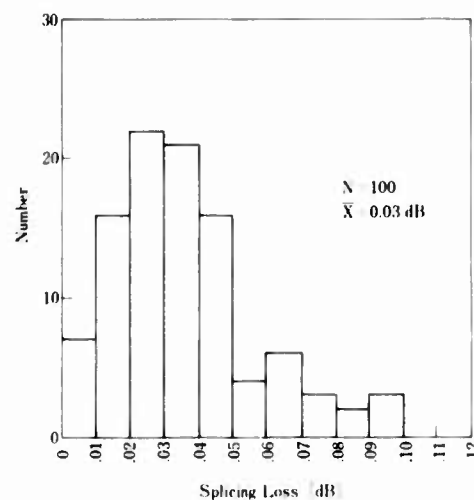


Fig. 8 Splice loss of UV-curable resin coated fiber

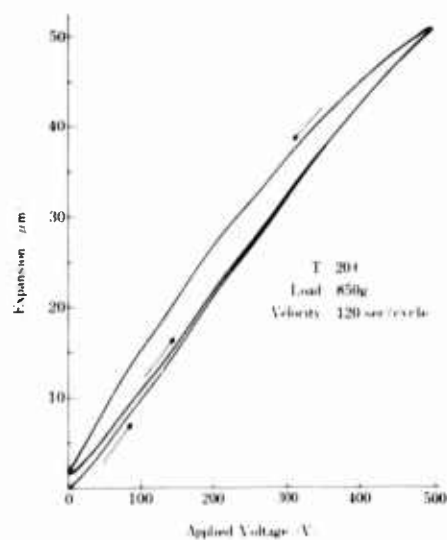


Fig. 9 Hysteresis characteristics and repeatability of piezoelectric element

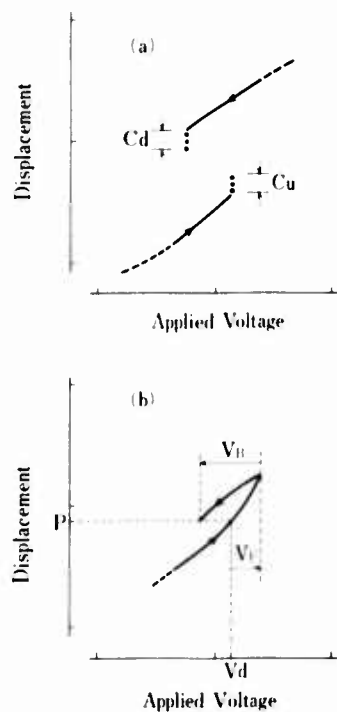


Fig. 10 Creeping and its compensation procedure

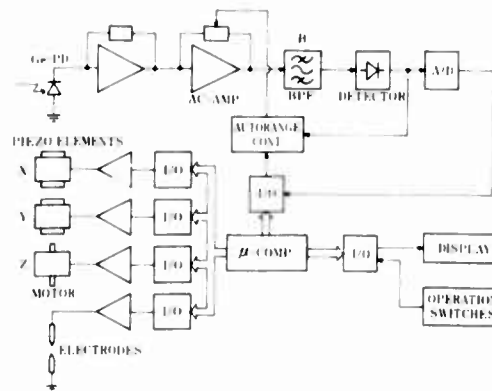


Fig. 11 Configuration of self-core-alignment arc-fusion splicer

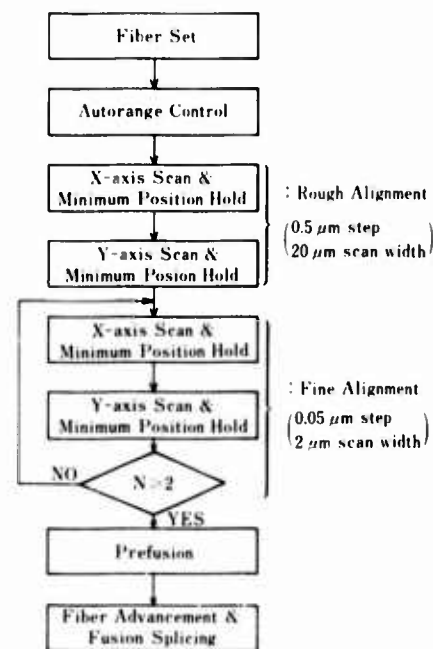


Fig. 12 Sequence of self-core-alignment and arc-fusion splicing



Fig. 13 Newly developed arc-fusion splicer
with self-core-alignment function

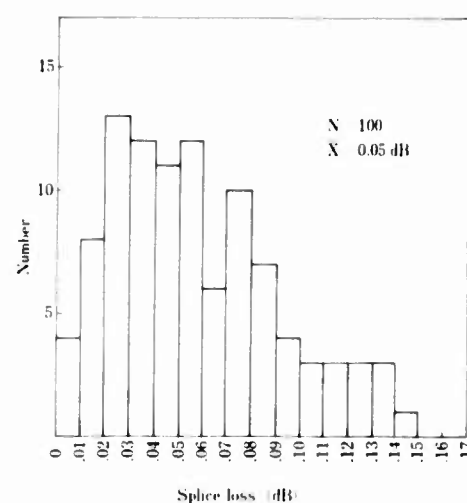


Fig. 14 Splice loss by self core-alignment
arc-fusion splicer

STATISTICAL MODELING OF MECHANICAL SPLICE AND CONNECTOR LOSSES FOR OPTICAL FIBERS

David E. Vokey
Tom Goldring

Siecor Corporation
Hickory, North Carolina

Abstract

The application of fiber optics in Local Area Networks and the feeder loop is receiving considerable attention. For ease in installation and subsequent reconfiguration the local applications require mechanical splicing methods and connectorized interfacing.

In this study, connector and splice losses for both step index single mode and graded index multimode fiber designs with Gaussian power distributions are analyzed. Losses are characterized statistically for the intrinsic and extrinsic parameters in the immediate area of the joint and at steady state long length distances.

The modeling is performed using a direct Monte Carlo method. Random populations are created representing the major intrinsic and extrinsic loss factors based upon distributions fitting the empirical data. Appropriate numerical analysis is then performed to predict connector and mechanical splice losses.

Introduction

Connectors and splices are integral elements in fiber optic applications. Connectors provide a rapid connect facility, coupling equipment to optical fiber cables. The connectors must withstand the rigors of frequent handling and mate repeatedly with low insertion loss. Splices are required to join successive cable lengths together in a durable manner. Splice losses should be as small as possible without involving complicated jointing techniques.

Connector and splice losses absorb a portion of the power budget. The demand for longer links with low loss fibers necessitates improved connector and splice performance. This paper reviews the various loss mechanisms and outlines analytical methods for characterizing splice and connector losses.

Loss Mechanisms.

The optical losses for a joint are frequently

referred to as intrinsic or extrinsic losses. Intrinsic losses are those losses at a joint which are a result of a mismatch of fiber transmission properties. Extrinsic losses are a result of mechanical misalignment of the fiber cores at the joint. For the purposes of this analysis, both loss categories are evaluated using a Gaussian power distribution. The Gaussian distribution assumption is appropriate for graded index multimode fiber and graded or step index single mode fiber (1), (2).

The multimode fiber analysis (1) describes both the loss in the immediate region of a joint and at a sufficient distance from the joint such that the optical power has reached a steady state distribution.

Normal manufacturing tolerances of optical fibers give rise to intrinsic mismatch losses at splice and connector interfaces.

The parameters with the most critical tolerances for multimode fibers are:

1. Numerical aperture
2. Core diameter

and for step index single mode fibers:

1. Cutoff wavelength
2. Refractive index difference

Fiber cladding diameter variations are of primary importance and can result in lateral offsets. Cladding tolerances are included in the lateral offset calculations.

There are several factors in addition to the intrinsic fiber related losses, which contribute to splice and connector loss. Tolerances on component manufacture and care in fiber preparation influence the coupling efficiency. The main extrinsic factors, as illustrated in Fig. 1, are:

1. Lateral offset
2. End separation
3. Angular misalignment

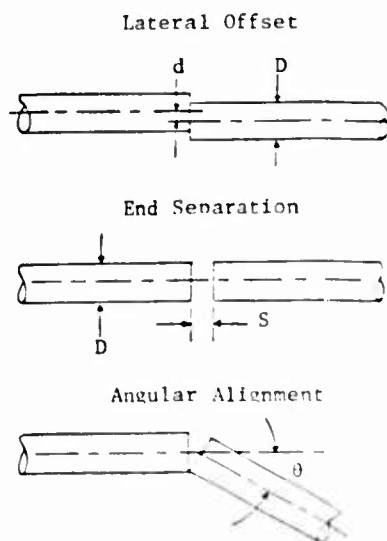


Fig. 1 Extrinsic Loss Factors

Achieving low loss connector and splice performance requires special consideration of these factors. Connectors are particularly difficult in that they must be rematable and withstand considerable handling.

Ideally, fibers in a joint should butt. In connectors or splices with no index matching fluid a small air gap exists. The gap gives rise to an additional reflection loss of about 0.32 dB.

Mathematical Modeling of Losses.

Loss models for multimode and single mode fibers have been reported (1), (2). Additionally, experiments describing extrinsic loss characteristics have been published (3). For this analysis, the various integrals associated with the models were either solved exactly or by numerical methods. Where no mathematical treatment was available, experimental results (3) were interpreted.

To aid in numerical analysis a set of polynomials were generated describing the various loss mechanisms for multimode fiber. Loss components are given for both the short length (S.L.) and steady state long length (L.L.).

The polynomials are of the general form

$$dB = a_1x + a_2x^2 + a_3x^3 \quad (1)$$

Coefficients for the polynomial representation are given in Table I.

Loss Component	x	a ₁	a ₂	a ₃
NA S.L.	$1-\Delta_2/\Delta_1$	1.8412	0.7229	3.5755
NA L.L.	$1-\Delta_2/\Delta_1$	3.7448	1.2036	3.6183
Core Dia.S.L.	$1-D_2/D_1$	1.7099	10.1097	2.8153
Core Dia.L.L.	$1-D_2/D_1$	3.688	8.7294	2.4456
Lateral Off-set S.L.	d/D	0.8660	3.2883	2.5114
Lateral Off-set L.L.	d/D	1.8660	2.9982	2.3235
End Separation	S/D	0.1249	0.2153	-0.0293
Angular Alignment	0	0.050	0.225	-0.025

The single mode analysis was reduced to a simple linear equation for mode field radius at 1300 nm (see appendix)

$$w = 2.052 \lambda_c - 856.3193 \Delta + 5.0198$$

$$\text{for } 1.21 \leq \lambda_c \leq 1.35$$

$$.0026 \leq \Delta \leq .0034$$

Connector Modeling.

To demonstrate the connector loss modeling algorithm a 4 rod multimode connector was chosen (Fig. 2). A total of 70 connectors were assembled with a 50/125/.2 core/clad/NA multimode fiber. The fiber position in the ferrules was measured directly. From the measurements a truncated normal distribution for the fiber position was developed. A direct Monte Carlo analysis was then performed using typical fiber tolerances with the analytical methods described in the appendix. The results for the simulation are given in Table II. (M = mean, S = standard deviation). The cumulative distributions of the simulation and the mandrel wrap launch insertion loss measurements are shown in Fig. 3.

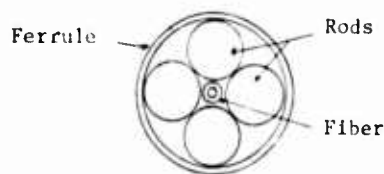


Fig. 2 4-Rod Connector

TABLE II. Connector Loss Analysis dB

	M	S	max
NA short length	.10	.07	.29
NA long length	.19	.14	.58
Diameter short length	.05	.03	.13
Diameter long length	.09	.06	.24
Lateral offset s.l.	.41	.29	1.12
Lateral offset l.l.	.60	.38	1.47
End separation	.06	.02	.14
Angle	.04	.05	.28
Fresnel	.32	-	-
Total -- short length	.97	.31	1.76
Total -- long length	1.31	.42	2.35

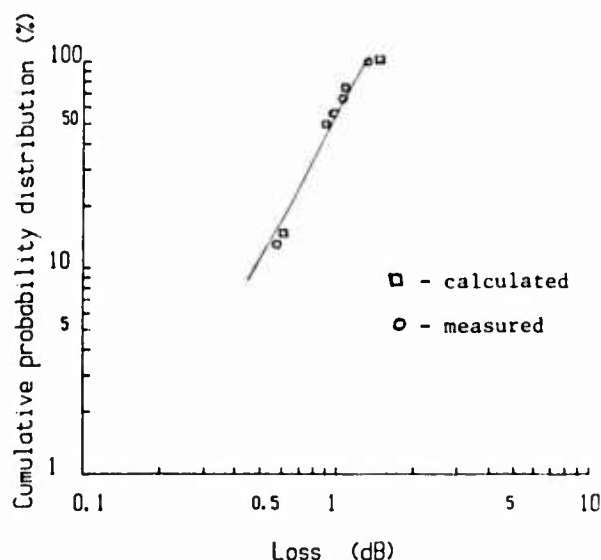


Fig. 3 Connector Loss Distributions

For comparative purposes a simulation for the same connector was performed with 85/125/.26 and 63/125/.29 fiber designs (Table III).

TABLE III. Fiber Comparisons

FIBER TYPE	CONNECTOR LOSS dB			
	SHORT LENGTH		LONG LENGTH	
	M	S	M	S
85/125/.26	.69	.14	.92	.22
63/125/.29	.79	.20	1.05	.29
50/125/.20	.97	.31	1.31	.42

With sufficiently rigorous mechanical analysis the connector components could be modeled and connector performance simulated and analyzed in greater detail.

V-Groove Connector Model

A simple V groove connector design was evaluated using a standard 10/125 step index single mode fiber design (Fig. 4). A 90° angle was assumed and the sensitivity of the splice loss to various tolerances calculated as described in the appendix. Loss statistics for various tolerances of fiber and angle, V-groove angle and combined vertical and horizontal displacements are shown in Table IV.

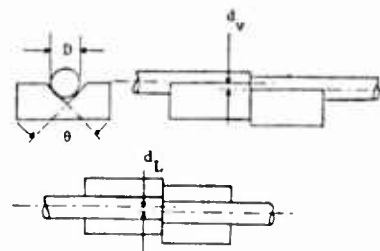


Fig. 4 V-Groove Connector

TABLE IV. Loss Estimates

Parameter Statistics		Loss Statistics dB	
		M	S
1. End Angle-degrees			
S	Max		
.5	1.5	.27	.31
.3	.9	.13	.14
.2	.6	.04	.04
2. V-Groove Angle-degrees			
S			
1		.23	.29
.5		.05	.06
.3		.02	.02
3. Vertical and Horizontal offset μm			
S			
1		.49	.43
.5		.16	.15
.3		.06	.05

Total splice loss distributions for the design using a typical fiber and varying connector tolerances (Table V.) are given in Figure 5.

TABLE V. V-Groove Simulation Statistics

Case	End Angle degrees		V-Groove degrees	Offset μm Horiz./Vert.
	S	Max	S	S
A	.5	1.5	1.0	1.0
B	.3	.9	.5	.5
C	.2	.6	.3	.3

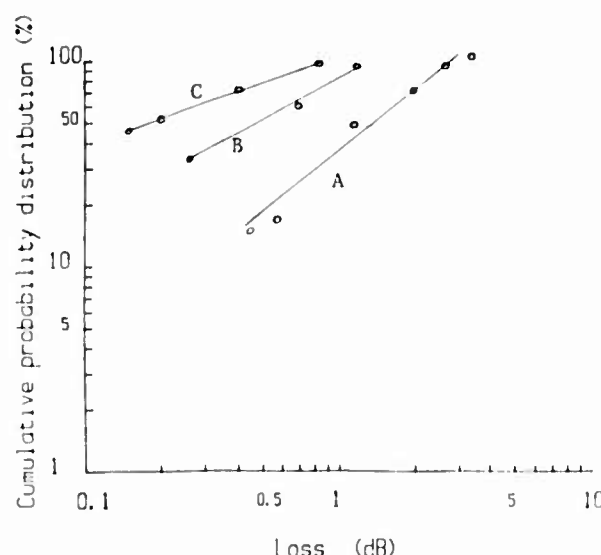


Fig. 5 V-Groove Simulation

Conclusion

Statistical modeling techniques applied to splice and connector designs can provide valuable insight to performance. The various loss mechanisms have been reported in the literature and provide the basis for the statistical techniques. Careful characterization of splice and connector components will allow loss modeling for design purposes.

Appendix

Generating random numbers with specified distributions.

i) Normal distribution: each element is the sum of k uniformly distributed pseudorandom integers between 0 and $n-1$. By the Central Limit Theorem of probability theory, these are asymptotically normal with mean $\mu = k(n-1)/2$, variance $\sigma^2 = k(n^2-1)/12$. In practice we used $k = 12$, $n = 32767$ (the largest two-byte integer). Dividing the results by σ and subtracting μ/σ we get a Z distribution (mean 0, variance 1).

ii) Truncated normal where one specifies $\bar{\mu}, \bar{\sigma}$ of the parent distribution and the limits a, b ($a < b$) of the derived distribution: if n is the desired sample size, we generate n elements from i). Suppose m of those do not lie between a and b : remove them and repeat the process as necessary.

iii) Truncated normal where one specifies a, b and μ, σ of the derived distribution: let $p = \sqrt{2\pi}$; then one may show that for the process described in ii),

$$\mu = \bar{\mu} + \frac{c\bar{\sigma}}{p} [e^{-\frac{1}{2}\bar{a}^2} - e^{-\frac{1}{2}\bar{b}^2}]$$

$$\sigma^2 = \bar{\sigma}^2 + \frac{c\bar{\sigma}}{p} [\bar{a}e^{-\frac{1}{2}\bar{a}^2} - \bar{b}e^{-\frac{1}{2}\bar{b}^2}] + \frac{2c\bar{\mu}\bar{\sigma}}{p} [e^{-\frac{1}{2}\bar{a}^2} - e^{-\frac{1}{2}\bar{b}^2}] + \bar{\mu}^2 - \mu^2$$

$$\text{Here, } \bar{a} = \frac{a - \bar{\mu}}{\bar{\sigma}}; \quad \bar{b} = \frac{b - \bar{\mu}}{\bar{\sigma}}$$

$$c = 1/(H(\bar{b}) - H(\bar{a}))$$

for H the distribution function of Z , i.e.

$$H(z) = \frac{1}{p} \int_{-\infty}^z e^{-\frac{1}{2}y^2} dy.$$

Thus given a, b, μ, σ we numerically invert these formulas to solve for $\bar{\mu}, \bar{\sigma}$ and then proceed as in ii).

iv) Symmetric truncated normal distribution ($\mu = a = b = \mu$): here $\mu = \bar{\mu}$ so one has the somewhat simpler task of inverting the equation for σ^2 .

v) Absolute value of a symmetric truncated normal with mean zero: this is a special case of iii) with $\mu = a = 0$. We have

$$\mu = \frac{c\bar{\sigma}}{p} [1 - e^{-\frac{1}{2}(\frac{b}{\bar{\sigma}})^2}]$$

$$\sigma^2 = \bar{\sigma}^2 - \mu^2 - \frac{c\bar{\sigma}b}{p} e^{-\frac{1}{2}(\frac{b}{\bar{\sigma}})^2},$$

$$\text{where } c = 1/(H(\frac{b}{\bar{\sigma}}) - \frac{1}{2}).$$

Thus one specifies b and either μ or σ (but not both), which allows one to solve for $\bar{\sigma}$. Then sample from ii) with mean 0, variance $\bar{\sigma}^2$, limits $\pm b$, and take the absolute value of the result.

vi) Weibull distribution: the cumulative distribution function is

$$G(z) = \text{Prob} [y \leq z] = 1 - e^{-\lambda z^\alpha}$$

Set $x = 1 - e^{-\lambda z^\alpha}$ and invert, giving

$$z = (\frac{1}{\lambda} \ln \frac{1}{1-x})^{\frac{1}{\alpha}}.$$

It is easy to show that if x is uniformly distributed, $0 \leq x < 1$ then z has the desired Weibull distribution. Given the mean and variance μ, σ^2 one may solve for λ, α by inverting the relations

$$\mu = \Gamma(\frac{1}{\alpha} + 1) - \frac{1}{\alpha}$$

$$\sigma^2 = \lambda^{-\frac{2}{\alpha}} [\Gamma(\frac{2}{\alpha} + 1) - \{\Gamma(\frac{1}{\alpha} + 1)\}^2].$$

(here Γ represents the Gamma function.)

Simulating a population of multimode fibers in four pin connectors.

Let n be the sample size. We create the following, to simulate the losses in a sample of n preconnectorized fibers measured against a reference fiber:

- n lateral offsets (distances from fiber core center to hole center)
- n values for numerical aperture
- n values for core diameter
- one value each for numerical aperture and core diameter of the reference fiber
- n values for end separation (distances between the ends of the opposing fibers)
- n values for angle between fiber axes.

Distributions used:

- iii)
- , c) - ii)
- the respective means used to generate b) and c)
- truncated version of vi)
- v).

Finally the losses are calculated as per (1).

Simulating a population of single mode step index fibers in a simple V-groove splice.

Create the following:

- two groups of n elements each representing ξ = angle of the V
- two groups of vertical offsets, n elements each
- two groups of horizontal offsets, n elements each
- n relative vertical offsets m_v
- n relative horizontal offsets m_h
- two groups of fiber outer (cladding) diameters, n elements each
- n values for relative lateral offset of group 1 vs. group 2 fibers
- n values for γ = cleave angle
- n values for α = rotation angle in tilt calculation

j) n values for θ = effective angle between cleaved faces = tilt angle

k) 2 groups of n values each for λ_c = cutoff wavelength

l) 2 groups of n values each for Δ = relative index difference

m) 2 groups of n values each for w = mode field radius

n) calculate transmission coefficients and corresponding losses as per (2).

Methodology.

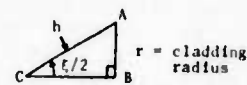
a), b), c), k), l) - sample from distribution iii) above

d) $m_v = |\text{vert.off.}_{gp.1} - \text{vert.off.}_{gp.2}|$

e) $m_h = |\text{hor.off.}_{gp.1} - \text{hor.off.}_{gp.2}|$

f) sample from distribution ii)

g) for a single V-groove:

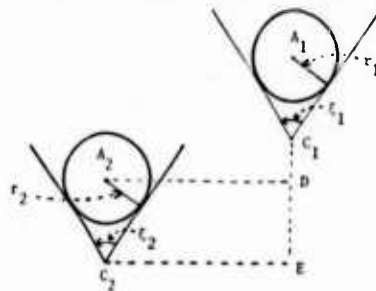


$$h = r / \sin(\xi/2).$$

Now given two V-grooves:

$$m_v = C_1 E \quad ; \quad h_1 = r_1 / \sin(\xi_1/2)$$

$$m_h = C_2 E \quad ; \quad h_2 = r_2 / \sin(\xi_2/2)$$



relative lateral offset

$$d = A_1 A_2$$

$$A_1 D = m_v + h_1 - h_2$$

$$A_2 D = m_h$$

$$d = \sqrt{(m_h)^2 + (m_v + h_1 - h_2)^2}.$$

h) sample from distribution v)

i) sample from uniform distribution with limits $0, 2\pi$



fiber 2 is rotated about its axis through an angle α , relative to fiber 1.

Let \vec{n}_1 = normal to face of fiber 1

for $i = 1, 2$. Then

θ = angle between \vec{n}_1 and \vec{n}_2 .

If we take the fibers as coaxial with z in xyz space, then without loss of generality

$$\vec{n}_1 = (\cos \alpha, \sin \alpha, \cot \gamma_1)$$

$$\vec{n}_2 = (1, 0, \cot \gamma_2)$$

$$\text{So } \theta = \cos^{-1} \frac{\vec{n}_1 \cdot \vec{n}_2}{|\vec{n}_1| |\vec{n}_2|}$$

$$= \cos^{-1}(\sin \gamma_1 \sin \gamma_2 \cos \alpha + \cos \gamma_1 \cos \gamma_2)$$

m) First calculate n_1 and n_2 , the effective

indices of refraction, and

a = core radius = $\lambda_c / 5.36 \sqrt{\Delta}$.

Let λ = operating wavelength, $k = 2\pi/\lambda$.

Solve the characteristic equation

$$u \frac{J_1(u)}{J_0(u)} = v \frac{K_1(v)}{K_0(v)} \quad \text{for } n$$

where $u = ka\sqrt{n_1^2 - n^2}$

$$v = ka\sqrt{n^2 - n_2^2},$$

and J_1, K_1 = Bessel functions.

Then $\beta = nk$ = propagation constant.

Now if r = radius then from (4), the power as a function of radius r is

$$p(r) = \begin{cases} \frac{n_1}{u^2} J_0^2\left(\frac{ur}{a}\right) & , r \leq a \\ \frac{n_2}{v^2} \left[\frac{J_1(u)}{K_1(v)} K_0\left(\frac{vr}{a}\right) \right]^2 & , r > a \end{cases}$$

where $u = a\sqrt{n_1^2 k^2 - \beta^2}$, $v = a\sqrt{\beta^2 - n_2^2 k^2}$.

We normalize $p(r)$ so that $p_{\text{norm}}(0) = 1$.

Then w is the number satisfying $p_{\text{norm}}(w) = .1$.

Observe that w is a function of λ , λ_c , and Δ .

For $\lambda = 1.3$ this function can be approximated to within an error $< 1\%$ by the linear function

$$w = 2.052 \lambda_c - 856.3193\Delta + 5.0198,$$

$$\text{for } 1.21 \leq \lambda_c \leq 1.35, .0026 \leq \Delta \leq .0034.$$

References

1. C.M. Miller, S.C. Mettler, "A Loss Model for Parabolic-Profile Fiber Splices", BSTJ, Vol. 57, No. 9, Nov. 1978, pp. 3167 - 3187.
2. D. Marcuse, "Loss Analysis of Single-Mode Fiber Splices", BSTJ, Vol. 56, May-June 1977, pp. 703 - 718.
3. T.C. Chu, A.R. McCormick, "Measurements of Loss Due to Offset, End Separation, and Angular Misalignment in Graded Index Fibers Excited by an Incoherent Source", BSTJ, Vol. 57, No. 3, March 1978, pp. 595 - 602.
4. H.G. Unger, Planar Optical Waveguides and Fibres, Clarendon Press, Oxford (1977), pp. 355, 366.



David Vokey

Siecor Corporation
489 Siecor Park
Hickory, NC 28603
U.S.A.

David Vokey is the Manager of Optical Engineering for Research and Development. He received his BSEE and MSEE from the University of Manitoba. He has been involved with the cable industry since 1969 and joined Siecor Corporation in 1983.



Tom Goldring

Siecor Corporation
489 Siecor Park
Hickory, NC 28603
U.S.A.

Tom Goldring is the Research and Development Mathematical and Scientific Computing Specialist. He received his B.S. (1969) and M.S. (1975) in mathematics from the University of Miami and his Ph.D. in mathematics from Yeshiva University (1977). He worked as an Assistant Professor of Mathematics at the University of North Carolina at Charlotte prior to joining Siecor in 1980.

IMPROVEMENT OF FIBER RELIABILITY IN SPLICE ENCLOSURES RESULTING FROM THE REDUCTION OF RELATIVE MOVEMENT BETWEEN CABLE CORE AND SHEATH

Yoshinori ISHIHATA, Satoshi KOSHIKA, Shyoichi HASEGAWA,
Eiji HAYASAKA, Yusuke TABATA and Fujio OHTSUKA

TOHOKU ELECTRIC POWER CO., INC. 7-1, 3-CHOME, ICHIBAN-CHO,
SENDAI 980, JAPAN

Abstract

At the cable end part of splice enclosures of optical cable, similar to the conventional copper communication cable, "phenomenon of cable core movement" of protrusion and draw inward of cable core in the longitudinal direction of cable sheath was observed. If the movement amount of optical cable core exceeds the allowance of the splice enclosure, bending stress and tensile stress are applied to the fibers causing the transmission loss increase and fiber break. Therefore to grasp the amount of cable core movement quantitatively, the theoretical and experimental study was conducted. And the proto-type cable were prepared and investigated with regard to the counter-measures for reducing the core movement. As the result, however, since it was impossible to set the core movement utterly zero, by the design of splice enclosure with the range of core movement taken into consideration, it was verified that a long service life of optical fiber at the cable splice part can be ensured.

1. Introduction

At the splice enclosures of the conventional copper communication cable, the phenomenon of cable core movement is well known.

On the other hand, similar to the conventional copper communication cable, we found the same phenomenon of cable core movement at the cable end part in splice enclosure of the aerial optical cable. After noticing the transmission loss increase of aerial optical cable that we have constructed, we investigated it in the field.

As the result, the cable core was observed protrusion or draw inward in the longitudinal direction of the cable sheath. However, the case of optical cable is different from that of the conventional copper communication cable in that the bend with a small radius due to core movement at the cable end part in splice enclosure causes an increase of the transmission loss of optical fiber and also the occurrence of the excessive

stress accelerates the static fatigue without fulfilling the long lifetime. Therefore, especially in the case of optical cable, the movement of the cable core can be considered to be an important factor that greatly governs its reliability.

The relationship between the movement amount of the optical cable core and the structures of optical cable and its splice enclosure was investigated and this report is given herein based on these results.

2. Investigation result of core movement at the field site

2.1 Phenomena of transmission loss increase at the field site

We designed and adopted 3 kinds of self-supporting optical cables as shown in Fig. 1.

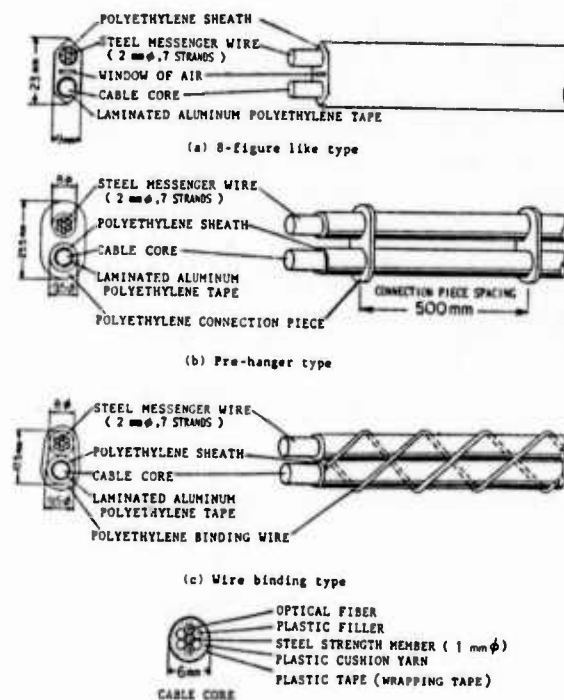


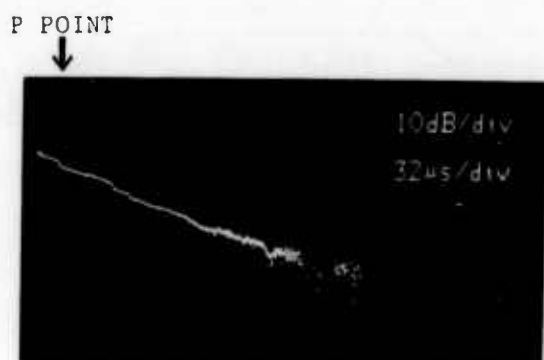
Fig. 1 Structure of Optical Cable for Aerial Use

These cables were put into practical use and have been installed as an information transmission line used for the electric power utilities since 1980. The total length of these cables has reached 400 km as of March 1984.

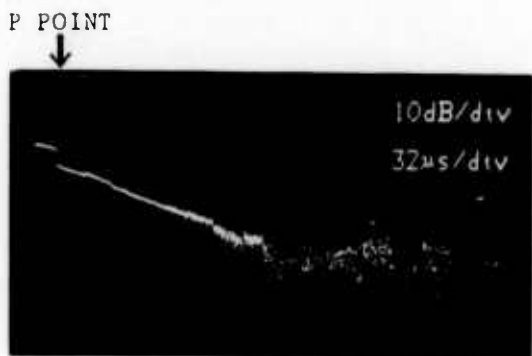
Last year, the transmission loss of the 8-figure like type optical cable shown in Fig. 1 (a) over the total link length of 27 km increased by some 4 dB after a lapse of about one and a half years since installation.

Therefore we measured the back scattered waveform of optical fiber using the OTDR (Optical Time Domain Reflectometer) and compared results with the back scattered waveform at the time of installing the optical cable.

Fig.2(a) shows the back scattered waveform at the time of installation and Fig.2(b) shows the back scattered waveform after the increase of transmission loss was produced. Since the local increase of transmission loss at P point was observed, we conducted an investigation of internal conditions by dismantling the splice enclosure at P point.



(a) At The Time of Installation



(b) After The Lapse of One And Half Year

Fig. 2 Backscatter Waveform Measured by OTDR

As a result, as shown in Photo 1, the phenomenon of cable core movement was observed, indicating extensive protrusion of optical cable core from the sheath. It was proved that by this movement, the optical fiber was pressed and bent at a few mm radius of curvature and transmission loss of optical cable was increased by the bending of this part.

Though cable core movement has been observed at the splice enclosures of the copper communication cable, since the core copper wire of the copper communication cable is strong to bending and elongation there are never serious problems.

However, in the case of optical cable, if there is a large core movement as above-mentioned, the increase of transmission loss or in the worst case, fiber break can be expected.

Therefore, as regards long-term reliability of optical cable, this phenomenon of cable core movement was found to be an important factor that governs the fiber reliability at optical cable splice enclosures.

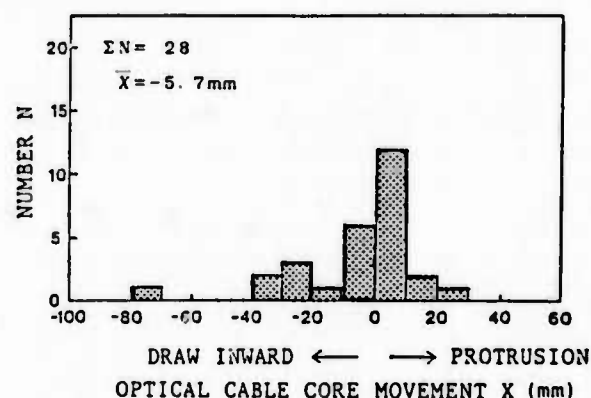


Photo.1 Internal View of Splice Enclosure of Type B at Point P

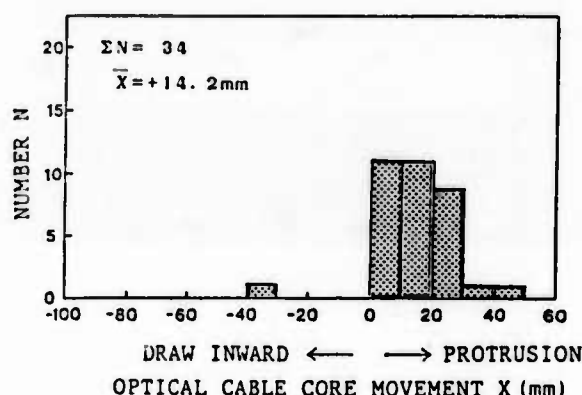
2.2 Investigation of core movement amount at the field site

To clarify the phenomenon of cable core movement, it can be considered necessary and indispensable to grasp the distribution of actual movement values. Therefore, we sampled the splice enclosure at the field site and investigated the movement values of the cable core.

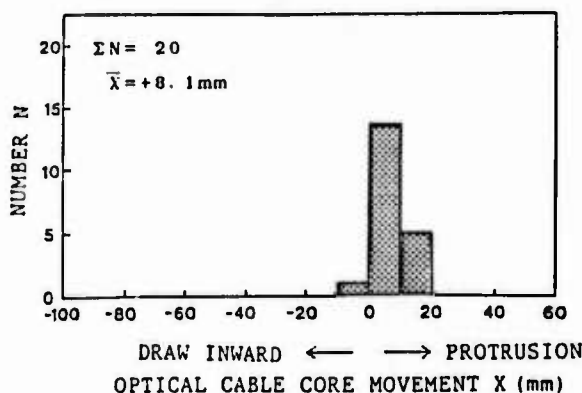
The result of investigation is shown in Fig.3. According to the figure, as regards the 3 kinds of cable types, the 8-figure like type shows the distribution of the widest range of cable core movement values thus being proved liable to produce core movement.



(a) 8-figure like type



(b) Pre-hanger type



(c) Wire binding type

Fig.3 Measured Result of Core Movement Amount

2.3 Relation of transmission loss increase to core movement and construction of splice enclosure

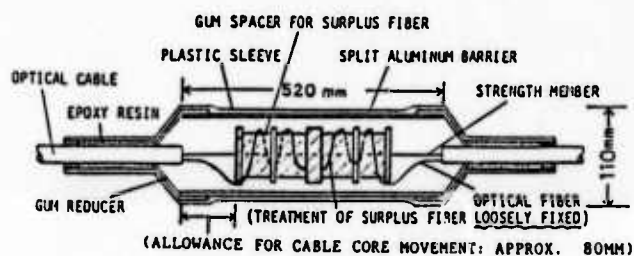
Fig. 4 shows the construction of 2 kinds of splice enclosures that we adopted.

In the investigation conducted so far, the splice enclosure of type B was used in entirety for the cable splice part of several locations where transmission loss increased.

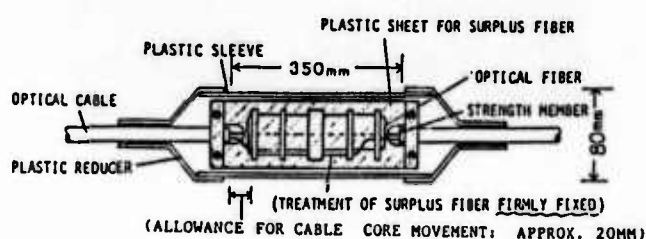
Since the core movement greatly exceeded the allowable value of 20mm of the splice enclosure against the core movement, the bend of optical fiber for a few mm radius was produced.

On the other hand, even in type A, which provides a large allowable value, although core movement occurred, the bend of optical fiber as seen in type B was not produced.

Therefore, it is proved that the movement of the cable core and construction of splice enclosures are closely related, that the allowable value of splice enclosure against movement of cable core can be considered to be an important factor.



(a) Type A



(b) Type B

Fig. 4 Construction of Splice Enclosures

3. Discussion

As the result of investigating the phenomenon of cable core movement at the field site, it was proved that the movement of cable core varies depending on the structure of cable and the increase of transmission loss depends on the relationship between the movement amount of the cable core and the construction of its splice enclosure.

Then, we studied the cause of movement of the cable core, its amount of movement and the countermeasures.

The phenomenon of cable core movement of self-supporting aerial optical cable can be considered to arise from the following 3 factors:

① Contraction of sheath: L_p

When the cable strain at the time of the manufacturing process is released, the sheath is contracted and correlatively the cable core protrudes.

② Contraction of sheath at cable slack: L_s

Since the main body of cables and messenger wires are separated at the splice part, the sheath loses the constraining force of messenger wire and contracts by the strain corresponding to the constraining force.

Thus correlatively the cable core protrudes.

③ Correlative movement of

core due to tension variation: L_E

After installing the cable, cable tension is subject to change by temperature variation and wind load. The messenger wire and cable sheath elongate and contract complying with such change of cable tension. The cable core joined with the messenger wire and the cable sheath with a finite friction force conducts the slip without being able to follow the elongation and contraction mentioned above. Thereby the sheath and core correlatively conduct the draw inward or the protrusion.

Thus, to grasp the movement amount of the cable core, the theoretical study and experimental study concerning the factors are conducted as described below.

3.1 Theoretical study [1]

3.1.1 Sheath contraction

The sheath residual process strain exists in the cable. It is assumed that this strain is released with the lapse of time. In this occasion, the sheath contraction amount L_p at the cable end can be given by the following equation:

$$L_p = \frac{\epsilon L}{2} - \frac{C \rho L^2}{8} \quad \text{for } L < 2L_1$$

$$= \frac{\epsilon^2}{2C\rho} \quad \text{for } L \geq 2L_1 \quad (1)$$

Where

- L : Cable length(m)
- ϵ : Sheath residual process strain
- C : Contraction coefficient(kg^{-1})
- ρ : Coefficient of friction in the longitudinal direction between sheath and cable core. (kg/m)
- L_1 : Cable range from the cable end with contracting of sheath.(m)

The cable range L_1 is given by:

$$L_1 = \frac{\epsilon}{C\rho} \quad (2)$$

Next, since the sheath contraction at the slack can be considered to depend on configuration and dimension of slack and the kind of optical cable, the value of this sheath contraction is expressed by L_s .

This value is a constant term that can be considered not to depend on the cable length. Therefore, the sheath contraction at the splice part of the optical cable L_M can be given by the following equation:

$$L_M = L_p + L_s \quad (3)$$

Since the cable end of the cable splice part is fixed to the splice enclosure, it can be considered to correlate to the phenomenon of protruding cable core.

3.1.2 Correlative movement of cable and sheath due to the change of tension

At first the tension T_1 is applied to the messenger wire of the cable, then the tension changes to T_2 . On this occasion the cable core movement amount L_E at the cable end due to the tension change, $T_2 - T_1$, can be given by the following equation when the cable is fully extended.

$$L_E = - \frac{E_T S_T (T_2^2 - T_1^2)}{2E_M^2 S_M^2 \rho} \quad \text{for } T_1 < T_2$$

$$= + \frac{E_T S_T (T_1^2 - T_2^2)}{4E_M^2 S_M^2 \rho} \quad \text{for } T_1 \geq T_2 \quad (4)$$

Where

- E_T : Young's Modulus of core tension member (kg/mm^2)
- S_T : Area of core tension member (mm^2)
- E_M : Young's Modulus of messenger wire (kg/mm^2)
- S_M : Area of messenger wire (mm^2)
- ρ : Coefficient of friction in the longitudinal direction between sheath and cable core(kg/m)

In the above equation, a plus value of L_E indicates protrusion and a minus value of L_E indicates draw inward.

Also the cable range L_2 from the cable end with the cable core movement due to the cable tension T is given by :

$$L_2 = \frac{E_T S_T T}{E_M S_M \rho} \quad (5)$$

In this case, the movement in the draw inward direction of the core appears in the case of tension increase and the movement in the protrusion direction of the core appears in the case of tension decrease.

From the above, in the case of self-supporting aerial optical cable, the total movement amount L_T of the cable core at the cable splice part can be given by the following equation:

$$L_T = L_P + L_S + L_E \quad (6)$$

3.2 Experimental study

To obtain the sheath contraction amount of self-supporting optical cable and the sheath contraction amount at the slack, a high temperature acceleration test of 80°C was conducted as the method of releasing the residual strain of the sheath. Also as the coefficient of frictions of sheath and core, the draw out force of the core was measured for obtaining the movement amount of cable core due to the change of cable tension.

3.2.1. Contraction amount of cable sheath

As for the high temperature acceleration test using the specimens of optical cable of 4m and 8m length, these cables were heated to 80°C and the contraction amount of cable sheath was measured.

Also a test was conducted using the 3 kinds of self-supporting optical cables of Fig. 1 as specimens.

Fig. 5 shows the cable end treatment configuration. The other end was tied with steel wire.

Fig. 6 shows the contraction amount of the sheath and Table 1 shows the draw out force of the cable core.

As a result, the sheath residual process strain ϵ , the contraction coefficient C and the cable range L_1 from the cable end with contracting of sheath are obtained as shown in Table 2.

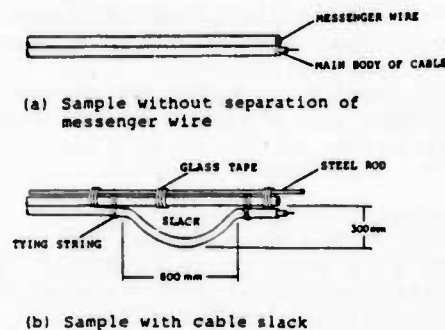
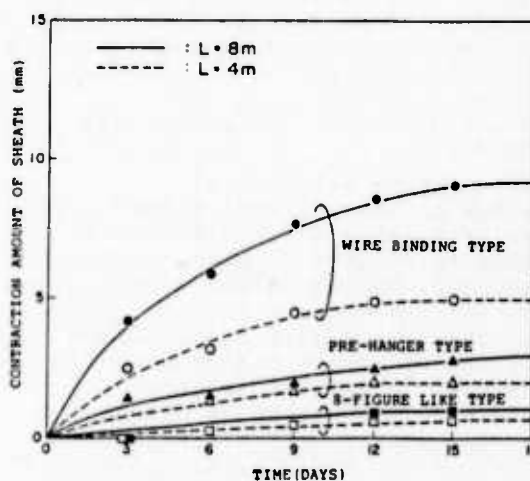
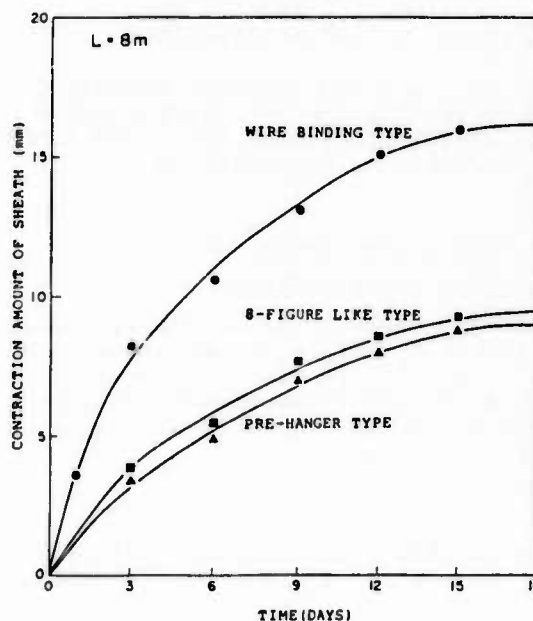


Fig. 5 Method of End Treatment of Self-supporting Aerial Optical Cable



(a) Sample without separation of messenger wire



(b) Sample with cable slack

Fig. 6 Contraction Amount of Sheath of Self-supporting Aerial Optical Cable

Table 1 Draw Out Force of Cable Core

Cable type	Draw out force of cable core (Coefficient of friction between sheath and cable core)
8-figure like type	0.1 kg/m
Pre-hanger type	1.9 kg/m
Wire binding type	2.7 kg/m

Table 2 Residual Process Strain, Contraction Coefficient and Cable Range With Contracting of Sheath

Cable type	Residual process strain ϵ	Contraction rate C	Cable range L_1
8-figure like type	2.3×10^{-4}	$2.5 \times 10^{-4} \text{ kg}^{-1}$	7.2m
Pre-hanger type	6.3×10^{-4}	$3.3 \times 10^{-5} \text{ kg}^{-1}$	10.0m
Wire binding type	1.4×10^{-3}	$1.9 \times 10^{-5} \text{ kg}^{-1}$	21.3m

Also the sheath contraction L_S at the slack can be obtained from the difference of the saturated sheath contraction amount between Fig. 6(a) and (b).

Table 3 shows the sheath contraction amount L_p , the sheath contraction amount L_S at the slack and the total value of sheath contraction amount L_M at the splice part of self-supporting optical cables.

Table 3 Sheath Contraction Amount at Splice Part

Cable type	Sheath contraction amount L_p	Slack contraction amount L_S	Contraction amount at splice part $L_M = L_p + L_S$
8-figure like type	1.0 mm	8.5 mm	9.5 mm
Pre-hanger type	3.1 mm	6.0 mm	9.1 mm
Wire binding type	17.8 mm	7.0 mm	24.8 mm

3.2.2. Correlative movement of cable core and sheath due to the change of tension

Substituting the core draw out force of Table 1 into equations (4) and (5), the core movement L_E produced by tension change and the cable range L_2 with cable core movement are as shown in Table 4. Whereas, the core movement was obtained for 2 conditions of tension change, that is, when the tension increased from zero tension to the designed maximum load 880kg and when

Table 4 Cable Core Movement Amount by Tension Change

Cable type	Tension change 0 → 200 kg		Tension change 0 → 880 kg	
	Core movement amount L_E	Cable range L_2	Core movement amount L_E	Cable range L_2
8-figure like type	-15.3 mm	67.0 m	-296.0 mm	296.0 m
Pre-hanger type	-0.8 mm	3.5 m	-15.6 mm	15.6 m
Wire binding type	-0.6 mm	2.5 m	-11.0 mm	11.0 m

Note: Minus symbol shows draw inward of core

the tension increased from zero tension to about 200kg, which is the value actually measured during the field site investigation.

When calculating the total movement L_T of the cable core using equation (6) from Table 3 and 4, the result becomes as shown in Table 5.

For comparison, the average values of core movement during the field site investigations are shown in Table 5.

Table 5 Field Investigated Value and Theoretical Calculated Value of Cable Core Movement Amount

Cable type	Theoretical calculated value of core movement amount L_T for the case tension change 0 → 200 kg	Field investigated value of core movement amount L_T
8-figure like type	-5.8 mm	-5.7 mm
Pre-hanger type	+8.3 mm	+14.2 mm
Wire binding type	+24.2 mm	+8.1 mm

Note: Plus symbol shows protrusion.

Minus symbol shows draw inward.

3.3 Study of countermeasures against core movement

From the results of theoretical study and experimental study, the following methods can be considered as the effective countermeasures against core movement at the splice part of optical cable.

- ① To reduce the sheath contraction, increasing the constraining force between messenger wire and the cable sheath and the friction force between the cable sheath and core.
- ② Increasing the friction force between the cable sheath and core, to reduce the core movement due to tension change.
- ③ Designing an allowable value against the core movement of splice enclosure larger than the core movement expected in the optical cable used.

We manufactured the prototype optical cables, adopting the method of ① - ② as shown in Table 6 and conducted an investigation.

Table 6 Prototype Optical Cable with the Countermeasures Against Core Movement that was adopted.

Cable type	Method of countermeasures against core movement	Content of prototype changing cable construction
8-figure like type	increase of draw out force of cable core.	Rubber coated cloth tape is used for upper Wrapping tape of cable core
Pre-hanger type	Integrity of messenger wire and main body of cable is strengthened.	Connection piece spacing is set at 400 mm.
	Integrity of messenger wire and main body of cable is strengthened.	Connection piece spacing is set at 300 mm.
Wire binding type	Integrity of messenger wire and main body of cable is strengthened.	Binding wire adopts round type PVC of large friction.
	Integrity of messenger wire and main body of cable is strengthened.	Binding wire adopts flat type PVC of large friction.

3.3.1 Acceleration test of high temperature and measurement of draw out force of core

The acceleration test of high temperature at 80°C was conducted using the prototype optical cables and the contraction amount of the cable sheath was measured. The length of optical cable used as a specimen was 8m. Moreover the measurement of draw out force of the core was conducted. Fig.7 shows the contraction amount of the cable sheath and Table 7 shows the draw out force of the core of optical cables prepared as prototypes.

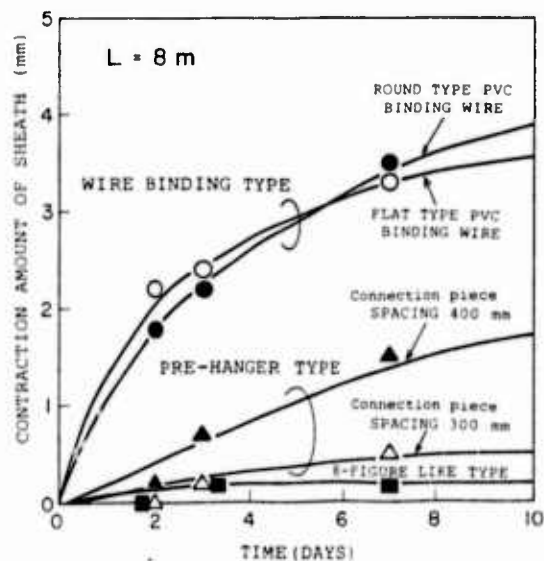


Fig. 7 Contraction Amount of Sheath of Prototype Cables

As a result, the contraction amount L_M of the cable sheath and the core movement amount L_F due to the change of cable tension at the splice part of the optical cable are as shown in Table 8. The core movement was obtained for the conditions regarding tension change, that is, when the tension increased from zero tension to the design maximum load 880kg and when the tension decreased from 880kg to zero tension.

Table 7 Draw out Force of Cable Core of Prototype Optical Cable with Counter-measures against Core Movement adopted.

Cable type	Draw out force of cable core
8-figure like type (Wrapping tape of rubber coated cloth)	4.0 kg/m
Pre-hanger type (Connection piece spacing 400 mm)	2.0 kg/m
Pre-hanger type (Connection piece spacing 300 mm)	2.6 kg/m
Wire binding type (round type PVC binding wire)	2.4 kg/m
Wire binding type (flat type PVC binding wire)	3.5 kg/m

Table 8 Contraction Amount of Cable Sheath and Core Movement Amount due to Tension Change

Cable type	Contraction amount of cable sheath L_M	Core movement amount due to tension change L_E	
		Tension decrease 880kg \rightarrow 0	Tension increase 0 \rightarrow 880kg
8-figure like type (Wrapping tape of rubber coated cloth)	9.0mm	+1.7mm	-7.4mm
Pre-hanger type (Connection piece spacing 400 mm)	7.8mm	+7.4mm	-14.8mm
Pre-hanger type (Connection piece spacing 300 mm)	6.6mm	+5.7mm	-11.4mm
Wire binding type (round type PVC binding wire)	13.8mm	+6.2mm	-12.3mm
Wire binding type (flat type PVC binding wire)	14.7mm	+4.2mm	-8.5mm

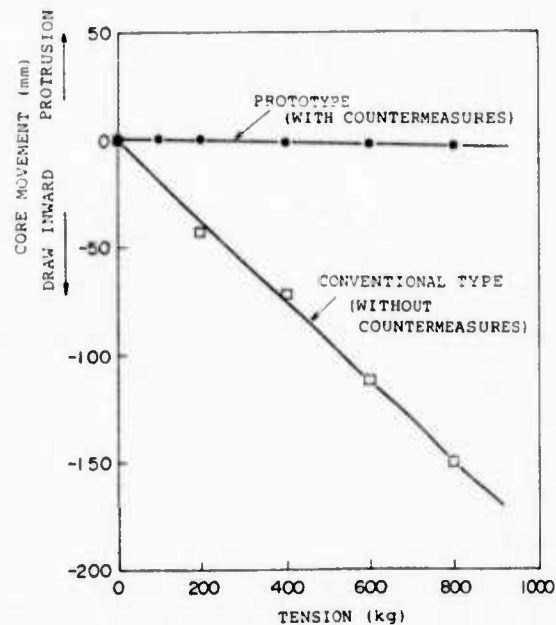


Fig. 8 Core Movement Amount of 8-figure Like Type Optical Cable due to Cable Tension Increase

3.3.2 Core movement amount due to the change of cable tension

An experiment to measure the core movement amount at the cable end due to tension change was conducted using the 8-figure like type optical cable prepared as a prototype and the conventional one without the countermeasures. In the experiment, each cable was 80 m long, and the applied tension was changed from zero to 800 kg. Fig. 8 shows the measured result of the core movement. In the case of the optical cable, the core movement amount due to the change of cable tension was about one fiftieth that of the conven-

tional one. As a result, counter-measures against the core movement of the 8-figure type proved to be effective. Summarizing the result of the study conducted as aforementioned, the total movement amount of cable core at the splice part of optical cable can be expected to be as shown in Table 9. From this result, by carrying out counter-measures against the movement of cable core, it is proved that the core movement can be set within a maximum of 20 mm.

Table 9 Range of Core Movement Amount of Prototype Optical Cable

Cable type	Range of cable core movement amount $L_T = L_P + L_S + L_E$	
	Maximum value of draw inward of core. Condition: Tension increase of 880kg and sheath contraction of zero arise.	Maximum value of protrusion of core. Condition: Tension decrease of 880kg and maximum sheath contraction arise.
8-figure like type (Wrapping tape of rubber coated cloth)	-7.4 mm	+12.7 mm
Pre-hanger type (Connection piece spacing 400 mm)	-14.8 mm	+15.2 mm
Pre-hanger type (Connection piece spacing 300 mm)	-11.4 mm	+12.3 mm
Wire binding type (round type PVC binding wire)	-12.3 mm	+20.0 mm
Wire binding type (flat type PVC binding wire)	-8.5 mm	+18.9 mm

Note: Plus symbol shows protrusion. Minus symbol shows draw inward.

4. Conclusion

Ever since the occasion of increasing transmission loss in self-supporting aerial optical cable, we recognized the importance of the phenomenon of cable core movement at the splice part of optical cable. Although this phenomenon is well known in the conventional copper communication cable, in the case of optical cable, it can be admitted that the impact on its reliability is great.

Thereby, in this report, the phenomenon of cable core movement of optical cable and the countermeasures against it were investigated.

As a result, in the self-supporting aerial optical cable, it was clarified that the following factors are important in designing the optical cable.

- ① Designing the friction force between the cable sheath and core to be appropriate.
- ② Designing the constraining force between messenger wire and the cable sheath to be tight enough.
- ③ Designing the splice enclosure with the amount of cable core movement taken into consideration.

The installation method of the optical cable to increase reliability is intended to be investigated hereafter.

Acknowledgements

We would like to thank H. Horima and S. Hisano, Sumitomo Electric Industries, Ltd. and T. Omori and A. Kurosawa, Kitanihon Electric Wire Co., Ltd. for the fruitful discussion.

Reference

- [1] M. MATSUMOTO, T. SAITO, M. HIROSE: IECE of Jpan, Vol.J65-B No.4, p.366, 1982

" Temperature Characteristics of Optical Fiber Cable Installed on Aerial Line."



Yoshinori Ishihata
Tohoku Electric Power Co., Inc.
7-1,3-chome,
Ichibancho,
Sendai, Japan

Yoshinori Ishihata was born in 1954 and received the M.S. degree from Tohoku University in 1979. He then joined Tohoku Electric Power Co., Inc., and has been engaged in the section of Telecommunications and Electronics Engineering. He is now an engineer in the Integrated Communication Network Development Office and a member of the Institute of Electronics and Communication Engineers of Japan.



Satoshi Koshika
Tohoku Electric Power Co., Inc.
7-1,3-chome,
Ichibancho,
Sendai, Japan

Satoshi Koshika was born in 1955 and received the M.S. degree from Waseda University in 1980. He then joined Tohoku Electric Power Co., Inc., and has been engaged in the section of Telecommunications and Electronics Engineering. He is now a researcher in the General Research and Development Center and member of the Institute of Electronics and Communication Engineers of Japan.



Shyoichi Hasegawa
Tohoku Electric Power Co., Inc.
7-1,3-chome,
Ichibancho,
Sendai, Japan

Shyoichi Hasegawa was born in 1947 and graduated from Taira Technical School in 1966. He then joined Tohoku Electric Power Co., Inc. and has been engaged in the section of Communications and Electronics Engineering. He is now an engineer of the Communication and Electronics Engineering Section of Tohoku Electric Power Co., Inc.



Eiji Hayasaka
Tohoku Electric Power
Co., Inc.
7-1,3-chome,
Ichibancho,
Sendai, Japan

Eiji Hayasaka was born in 1950 and received the M.S. degree from Tohoku University in 1974. He then joined Tohoku Electric Power Co., Inc. and has been engaged in the section of Communications and Electronics Engineering. He is now a senior staff member of the Integrated Communication Network Development Office and a member of the Institute of Electronics and Communication Engineers of Japan and the Institute of Electrical Engineers of Japan.



Fujio Ohtsuka
Tohoku Electric Power
Co., Inc.
7-1,3-chome,
Ichibancho
Sendai, Japan

Fujio Ohtsuka was born in 1931 and received the B.E. degree from Shinshu University in 1953. He then joined Tohoku Electric Power Co., Inc. and has been engaged in the investigation and design of Telecommunications systems for the electric power utilities. He is now a Chief Manager of the Integrated Communication Network Development Office and member of the Institute of Electrical Engineers of Japan.



Yusuke Tabata
Tohoku Electric Power
Co., Inc.
7-1,3-chome,
Ichibancho,
Sendai, Japan

Yusuke Tabata was born in 1934 and received the B.E. degree from Akita University in 1957. He then joined Tohoku Electric Power Co., Inc. and has been engaged in the section of Communications and Electronics Engineering. He is now a Manager of the Communications and Electronics Engineering Section and a member of the Institute of Electrical Engineers of Japan.

A TECHNIQUE FOR
THE RAPID CONFIRMATION OF THE WATER-TIGHTNESS OF BURIED PLANT CLOSURES

H. J. C. Spencer

Telspec Ltd. Rochester England

Summary

A method of testing the sealing of closures is described in which a very small volume of air between two concentric seals is pressurized, instead of complete closures. Inter-seal/closure volume ratios of 1 : 4000 are readily achieved, leading to a proportional reduction in the time required to detect a pressure fall due to a leaking seal.

Tests are made using a novel pneumatic/electronic device in the form of a small hand gun. This performs the functions of both pump and gauge in conventional test methods. In use the gun barrel is pressed into a test hole in the closure and the trigger pulled. The pressure in the inter-seal volume is reduced by about 5 psi below atmosphere. If it rises by as little as 0.03 psi in the next 10 seconds a red fail LED lights, otherwise a green LED lights. The fail signal indicates a leak rate of 0.5mm³/sec or more.

Introduction

Water and 'electrics' don't mix. This is true whether the electrics are individual metallic pairs of wires or sophisticated metal or glass high frequency conductors. A very high standard of water-tightness is, therefore, essential for telecommunications outside plant, particularly buried plant. This applies not just to the glamorous long-distance networks but also to the fringes of humble local distribution networks. The economic consequences of too frequent failures in the latter are particularly serious because of the very large number of closures at risk in local networks and because of the increasing pressure to place this plant under ground. This paper describes a new low-cost method for rapidly proving the water-tightness of the smallest closures.

Current Practices

Continuous Pressurization

Cable pressurization provides a ready means of protecting joints and closures from water ingress. It has enabled leaky cable networks to provide good service for many years, albeit at a considerable cost in preventive maintenance. Pressurization cannot, however, be applied economically to the vast numbers of joints and closures at the fringes of local networks. Also, the scope for protecting closures by cable pressure is now being reduced, even in the long distance networks, by the increasing use of filled cables.

Test on Installation

It is common practice to pressure test large or important closures when they are made. The tests are, however, slow to make and often require follow-up visits to confirm that pressure is retained. It is, therefore, uneconomic to extend the method to the much more numerous small closures.

Assemble and Hope

By far the greatest number of joints and closures in telecommunications networks are made and put into service without a test of any kind. They are assembled from sets of parts designed to ensure a high probability of a watertight closure being achieved if the correct works practices are followed faithfully.

Pressure Testing of Closures

The conventional method of pressure testing a cable joint or equipment housing is to raise the pressure within by a pump via a valve, to seal the valve, and to return after an interval to check with a gauge that pressure has been retained. Figure 1 shows how the pressure within a closure falls with time in the event of a small leak. The closure taken as an example is a small, 100 pair, reopenable joint used in large numbers in the UK and elsewhere. It has an internal volume of about 2000cm³ and for the test is assumed to be pressurized to

62kPa (9 psi). Air is assumed to leak from the closure at $1\text{mm}^3/\text{sec}$, measured at atmospheric pressure. This leak can be envisaged as equivalent to a bubble a second escaping in an immersion test and is of an operatively unacceptable magnitude. The curve of Figure 1 shows that the fall of pressure within the closure is slow. To detect it reliably in presence of possible changes in ambient temperature and pressure would require a wait of many hours. For larger closures waits of a day or more would be necessary.

A weakness of pressure testing closures, particularly those to be used in non-pressurized networks, is that it imposes stresses on them which are not typical of working conditions. This is particularly undesirable when closures use resilient seals as the stresses may deform these to give misleading indications of satisfactory sealing.

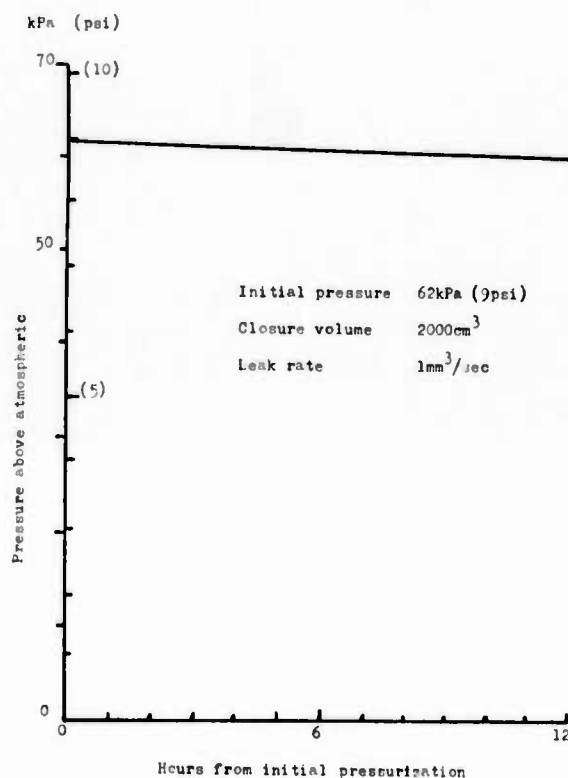


Fig. 1 Fall of pressure due to leak.

Double Seals

Double seals have been used for large and important equipment housings in the UK and elsewhere¹. Apart from the greater security of two seals in tandem concentric double seal arrangements provide the opportunity to test the effectiveness of closures without pressurizing whole housings. If both the seals are good the volume of air between them should be sealed from the atmosphere. The effectiveness of closures can, therefore, be tested by pressure testing this volume rather than complete housings. The advantage is that the volume of the inter-seal space is much less than that of complete housings so that the time required for a given leak to cause a detectable fall in pressure is considerably reduced.

A further advantage of pressurizing only the inter-seal space is that the stresses imposed on housings are much reduced. The stresses can be dangerous in large housings and this is a major reason for the double seal method having been used for them.

Development of the Double Seal Principle

The double-seals used for large housings have been generously dimensioned with relatively large volumes of air enclosed between the two seals. In consequence, although they have facilitated the testing of closures, a wait is still necessary between pressurization and test. Second visits are usually required and this is unacceptable for the less important applications. This paper describes the development of the double-seal principle to the point where the effectiveness of a closure can be confirmed virtually instantaneously at the time it is made. This dramatic advance is achieved by making the volume of the inter-seal space very small, and by the use of a novel testing device.²

A way of reducing the inter-seal space in the design of new equipment housings is illustrated in Figure 2. A resilient 'O' ring is pressed into contact with the edges of fine grooves cut into the surfaces to be sealed. The seal can be any shape in plan. Test access is given to one groove by a hole in the cover of the housing and to the other via a hole(s) pierced in the 'O' ring.

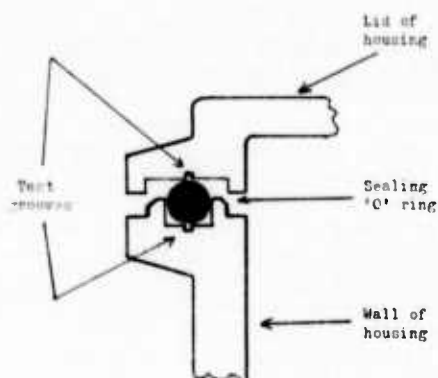


Fig. 2 Double seal arrangement for equipment housing.

Application to Existing Closures

The small closure used earlier as an example of pressure testing is of cylindrical form and makes use of a very common sealing method in which a rubber 'O' ring is compressed between surfaces forming a triangular section, as illustrated in Figures 3. This type of closure can be adapted to provide the annular test grooves required for the new method by replacing the 'O' ring by a ring having a figure-of-eight section, as illustrated in Figure 4. Occasional holes in the web of the ring provide an air path between the two grooves and test access to the outer one is given through a hole in the housing cover. The volume of the inter-seal space in this arrangement is only about 0.5cm^3 , to be compared with 2000cm^3 for the whole housing. The effect of reducing the volume by a factor of 4000 is to reduce the time for the fall in pressure due to a leak to become significant to seconds rather than hours, as indicated in Figure 5. There is a compounding effect in that changes in ambient pressure and temperature, which occur relatively slowly, become insignificant. For test times measured in seconds, therefore, it is possible to use much more sensitive testing devices, which allow test times to be reduced even further.

A new type of test device is necessary to exploit the possibilities revealed by Figure 5. It should be as sensitive as is practical but it is also important that it has a low internal volume because this is effectively added to the inter-seal volume of the closure under test and tends to nullify the advantage of making the latter low. The design of a novel test device meeting these requirements is described in the following paragraphs.

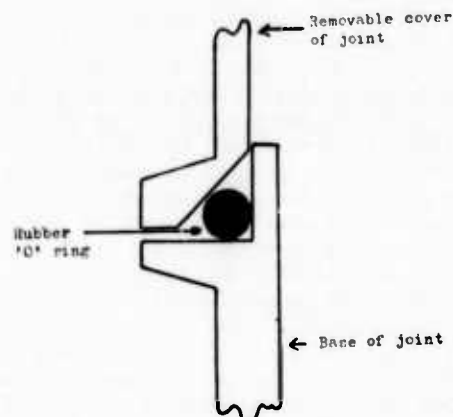


Fig. 3 Conventional joint seal.

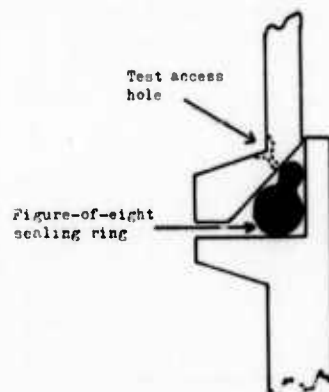


Fig. 4 Seal modified for testing.

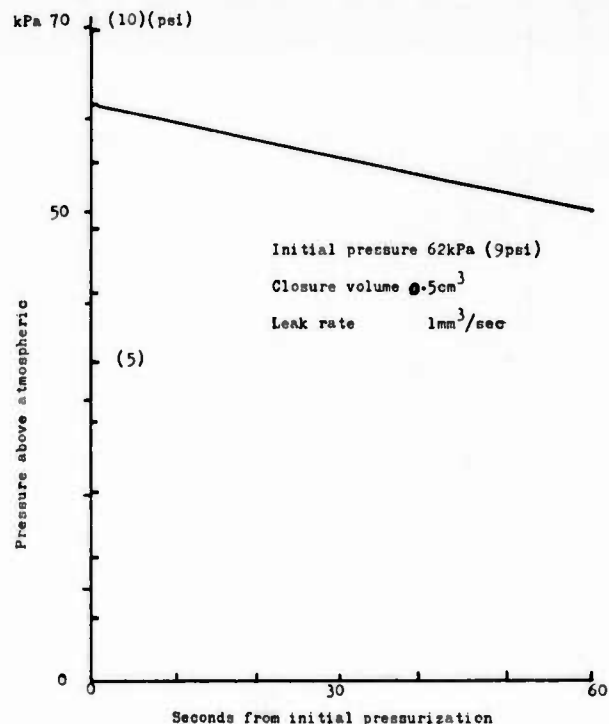


Fig. 5 Fall of pressure due to leak.

Design of a New Test Device

The tester is a small self contained pneumatic/electronic device taking the form of a hand-gun. It is illustrated in Figure 6. The gun is cocked by pressing in the knob protruding from the rear. It is then connected to the closure under test by pressing the rubber sealing ball at the end of the barrel into a conical hole in the closure. A more permanent screwed connection is unnecessary because of the short test time. The test is initiated by pulling the trigger of the gun. If either seal is defective a red LED at the rear of the gun is lit. Otherwise after an interval of 10 seconds a green LED lights. The way the gun is used is illustrated in Figure 7.

The basic principle of the test device is shown by Figure 8. It inverts the usual test method in that the pressure within the inter-seal volume of the closure is reduced relative to atmosphere rather than increased. The heart of the gun is a metal bellows. The bellows are latched in the fully compressed state when the gun is cocked. When the barrel of the gun is pressed into the hole in the closure and the trigger is pulled the bellows are released and expand, reducing the pressure within the bellows and the inter-seal space below atmosphere. The bellows expand to the point at which the force on them due to the difference between the internal and external air pressures equals the residual spring force of the bellows. Movement of the bellows should then cease. The interaction of the forces is illustrated in Figure 9. In the event of a defective seal, however, air leaks into the bellows and expansion continues. The circuitry of the gun detects this and lights the red LED. If, however, no movement of the bellows has been detected in 10 seconds the green LED is lit. The reduction in pressure caused by the the gun is of the order of 35kPa (5 psi). Adequate sensitivity is achieved with this relatively low pressure which has the advantage that the stresses placed upon the sealing members of the closure are reduced. The actual pressure for a particular application depends to some extent upon the volume of the inter-seal space. It is not very sensitive to this, however, because the volume of the bellows predominates, as can be deduced from Figure 9.

The sensitivity of the new test device is such that, subject to adjustment, a pressure change of about 21pa (0.03 psi) within the test cycle results in a fault indication. This corresponds to a leakage rate of 0.5mm^3 for closures with inter-seal volumes of the order of 1cm^3 . A practical demonstration of the sensitivity of the gun is that it can detect the presence of a human hair between the sealing ring and a mating surface well within the test cycle.



Fig. 6 Test gun.



Fig. 7 Test gun in use.

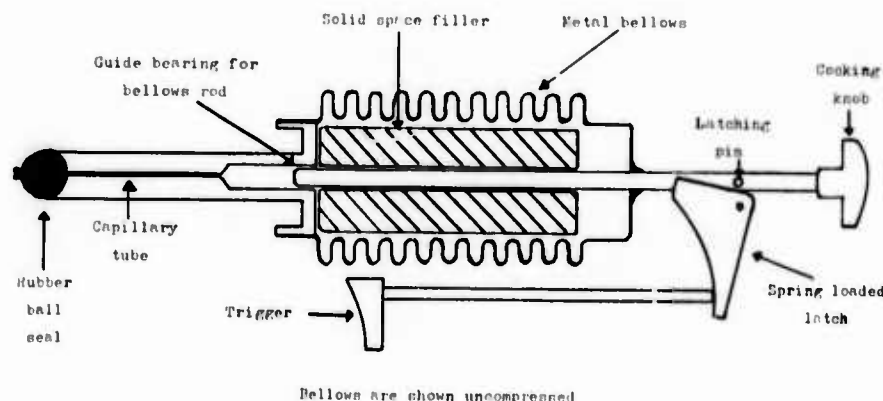


Fig. 8 Basic mechanism of test gun.

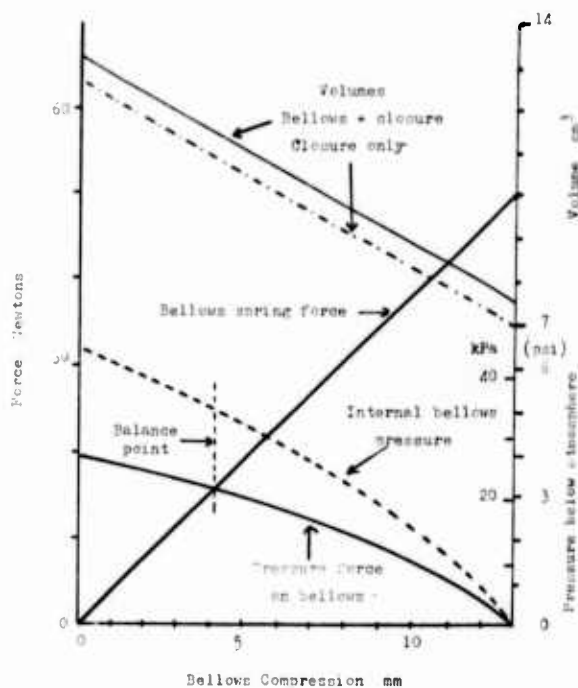


Fig. 9 Forces acting on bellows.

Closure Standards

The sensitivity of the new test method raises the question of whether it sets too high a standard. Outside Plant engineers have expressed concern over a test which is capable of detecting a leak caused by a hair. They fear the adverse working conditions under which closures often have to be made make the attainment of such a standard impractical. If this view prevailed the test gun can readily be desensitized.

It can be argued, however, that there is no such thing as a nearly watertight closure, and that because of the time plant is expected to give good service, possibly immersed under water, only perfection is acceptable. This point of view in turn raises the question of whether the method is sensitive enough. Experience is encouraging in this respect. It shows that most sealing defects are detected in much less than the 10 second test period. Also, experience has shown that leaks of the magnitude caused by a hair are effectively sealed if the sealing ring and mating surfaces are slightly greasy. This sets a threshold on the magnitude of leak it should be possible to detect which is within the range of the new method.

It is of interest that there should be no question of scaling acceptable leak rates to the size of closures. Given time, and in the outside plant field there is plenty, a small leak is as damaging to a large closure as to a small one. A common sensitivity of test is, therefore, required for all. It follows that the volume of the inter-seal space should be of the same order for all closures to which the method is to be applied, and that the same test device will be suitable.

One Seal or Two?

In the application of the new test method described in the paper, the hole giving access to the inter-seal space is left open after test, rendering the outer seal ineffective. This might be considered a disadvantage. The advantage of two seals however, really only applies to untested closures. In these both seals have a finite probability of failure and placing them in tandem greatly reduces the probability of total failure (unless a common

defect such as a surface scratch effects both). If both seals have been proved good it can be argued that there is no need for two. The test access hole for the new method could readily be closed after test, eg. by a pointed grub-screw within the hold which could be loosened for the test and then tightened. It was decided not to do this. The advantage of leaving the hole open is that a closure is tested, or re-tested, in exactly the condition in which it is to be left. This is not the case with present practices and experience has shown that faults due to faulty or improperly capped valves are not uncommon.

Further Applications

The closure considered in detail in the previous paragraphs is the archetype of a range of similar closures of varying diameters and lengths. The new sealing and testing technique can readily be applied to most of these. In many instances it can be applied retrospectively to plant already in service by changing easily replaceable parts.

The arrangement shown in Figure 2 is more suitable for new housings, particularly those of rectangular shape. Rectangular housings are better for equipment than cylindrical ones. In the past, however, cylindrical housings have been preferred because they are safer in a no-test design. The availability of a test facility should encourage the use of the more convenient rectangular shapes.

Cable entries are another field of use for the new technique. When these are made with entry glands with 'O' ring seals test-able double seals can be substituted.

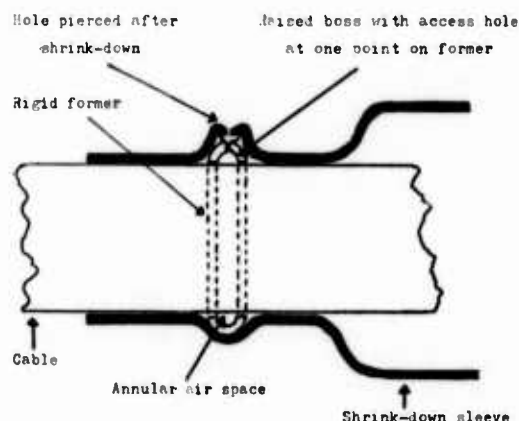


Fig. 10 Application to shrink down.

The technique can also be applied to shrink down closures, as illustrated in Figure 10. A rigid former is placed over the cable but under the sleeving prior to shrink-down. After shrink-down the position of the former is apparent through the sleeving and the sleeving can be pierced to provide access to an annular open space beneath the former.

Conclusions

A method has been developed for rapidly testing the water tightness of closures in telecommunications outside plant. It can be applied economically to the very large number of small closures used in distribution networks and can be applied retrospectively to many closures already in service. The new method has a number of advantages over current practices:-

- it enables the water tightness of closures to be confirmed within 10 seconds,
- it adds little to the cost of closures,
- it requires only a small, self-contained and relatively inexpensive test device,
- it is very suitable for closures used with filled cables because these do not enable closures to be protected by pressurization,
- it is particularly suitable for closures which have to be re-opened periodically during service,
- it provides an effective method for supervisors to carry out quality control checks of completed installations.

The new method is primarily intended for protecting closures in non-pressurized networks although it can be used in pressurized systems. The principle is capable of extension to all points in a network where water might penetrate and it is envisaged that ultimately every point will be protected by testable closures as a matter of course.

Acknowledgement

The Directors and Engineers of Telspec Ltd. Rochester, England are thanked for their contribution to this development.

References

1. Fletcher, N E. The 60 MHz Transmission Housings for Dependent Repeaters. IPOEEJ Vol 66 p 167, October 1973
2. British Patent Applications 8319497 and 8322096

H J C Spencer,
Telecommunications Consultant,
1, Oaklands Close,
Ascot,
Berks.,
England,
SL5 7NG.
Telephone: 0990 23983.



COMPOSITE BUFFERING FOR HIGH PERFORMANCE FIBER CABLES

P. R. Bark and D. O. Lawrence
Siecor Corporation, Hickory, NC
and

U. Oestreich and E. Mayr
Siemens AG, Munich, West Germany

This paper describes the design and performance of a newly developed composite fiber buffering that exhibits considerably improved microbending resistance compared to the conventional tight fiber buffering. The three-layer buffer consists of an acrylate coating surrounded by a low viscosity or softly cross-linked compound enclosed within a hard, double-layered plastic shell. A family of low fiber count cables has been designed to meet indoor and outdoor environmental requirements for data communications, industrial and military applications.

Introduction

High performance cable systems with long term stability under a variety of environments require a cable design minimizing microbending sensitivity. For multimode and singlemode telephone applications the well-proven single loose tube and Mini-Bundle™ buffering concept exhibits outstanding performance.^{1 2} For data communications, industrial and military applications, however, low fiber count cables are often required for even more severe environmental conditions:

- Wide temperature extremes
- High mechanical resistance against crush, impact, tensile shock and abrasion
- Great flexibility
- Small in size and weight

In many cases transmission rates are high, distances are long and both lasers and high efficiency LEDs are used as sources. This requires the use of all types of standard or radiation resistant fibers exhibiting different degrees of microbending sensitivity.

For example:

- 100/140 μm - 0.3 NA, short distance fiber
- 62/125 μm - 0.28 NA, data comm fiber
- 50/125 μm - 0.2 NA, long distance fiber
- 85/125 μm - 0.26 NA, data broad-band fiber
- 10/125 μm - 0.10 NA, singlemode fiber

Cables containing tightly buffered fibers have been used in the past for different applications and environments with somewhat unpredictable results. Considerably improved

microbending resistance can be achieved by using a composite fiber buffering that provides a degree of fiber to cable decoupling, makes buffer stripping easier, and because of its standardized outer diameter allows for compatibility with existing connector designs.³

Composite Fiber Buffering

In today's large scale, high speed fiber manufacturing coatings including ultraviolet cross-linked acrylate, silicone or epoxy are utilized. Such coatings are chosen to be easily strippable. For application in a composite buffer, the optical fiber (125 μm OD) is coated with a two-layer acrylate to an OD of 500 μm . This fiber then is surrounded by a 75 μm layer of low viscosity or softly cross-linked, nondripping compound. The Young's modulus of this compound has to be very low and is in the order of $<10^{-2}$ N/mm². An outer hard double-layer shell of extruded thermoplastic aramide and polyester encloses the fiber (see Figure 1). The Young's modulus of this hard shell is $>10^2$ N/mm². The outer diameter of the composite buffering is 0.9 mm and thus is compatible in size and appearance with tightly buffered fibers. This product shows excellent mechanical performance in respect to impact and crush resistance, allows for limited longitudinal and radial fiber movement and withstands a high number of cyclic flexes.

The thin layer of low modulus compound minimizes any possible deformation of the fiber coating that may be introduced by local forces onto the hard outer shell. This viscous compound also acts as a separation layer between fiber coating and outer shell facilitating easier buffer stripping.

Cable Designs

A family of low fiber count all-dielectric cables has been designed to meet either indoor intrabuilding (internal wiring) requirements or outdoor applications where compact, rugged and high performance cables are needed.

(a) Indoor Cables For Industrial and Data Communications Applications

Figure 2 shows the cross-sectional diagram of a one-fiber internal wiring or pigtail cable for use inside of transmitter/receiver housings or

on patch panels. A thin layer of Kevlar spun around the composite fiber buffering together with a thin PUR jacket results in a small cable which is easy to handle in wire-harnesses where a certain longitudinal stress is unavoidable.

In Figure 3 some typical performance characteristics for this cable are summarized. The fiber used for this cable evaluation is an 85/125 μm - 0.26 NA data broad-band fiber.

Two different designs of 2-fiber cables are depicted in Figure 4. For longer length tray, conduit or plenum installations a circular cable is proposed containing two composite buffered fibers, fillers, Kevlar, impregnated fiberglass yarns and outer jacket with an overall diameter of 4.5 mm. Installation load levels of 1000 N and operating temperature ranges from -20° to $+70^{\circ}\text{C}$ are easily achievable. The cable jacket consists of either flame retardant PUR or PVC.

Figure 5 summarizes the cable performance characteristics for 85/125 μm - 0.26 NA data broad-band fibers.

For even longer installation lengths and for applications where self-contained reinforced subunits are required, a more rugged fan-out cable with an overall diameter of 7 mm is available. This cable can withstand installation loads up to 1800 N and in a filled core version can be used in an outdoor environment, i.e., for connecting buildings with each other.

(b) Ruggedized Outdoor Cables

Figure 6 shows the cross-sectional diagram of a 2-fiber ruggedized field cable. Two composite buffered fibers are stranded together with Kevlar fillers and are jacketed with a thin layer of PUR. Alternating Kevlar yarns and impregnated fiberglass yarns are stranded around to provide tensile strength and temperature stability. An outer PUR jacket completes the cable with an overall diameter of 6 mm. This very compact cable design combines excellent mechanical and environmental performance with optical reliability as shown in Figure 7. Most of the performance data given is based on DOD-STD-1678 or EIA RS-455 standard test procedures. All performance characteristics are based on 50/125 μm - 0.2 NA multimode fibers. Of particular significance is the excellent temperature performance of this cable as shown in Figure 8. Over five cycles from -55° to $+85^{\circ}\text{C}$ the attenuation change is plotted. As can be seen, the maximum deviation from the starting attenuation is 0.2 dB/km, a value which even decreases with increasing number of cycles. In order to assure complete temperature conditioning at the extremes, the conditioning time of the 2 km cable samples was set to 12 hours, the cycle time to 36 hours.

For fiber counts between two and six a symmetrical cable design was chosen: six fibers

or dummies are stranded around a central Kevlar element. With additional Kevlar/impregnated fiberglass reinforcement and an outer PUR jacket, the cable OD is 7 mm.

These cables are especially suitable for military applications and field use, where ruggedness and performance under extreme temperature conditions are required. Due to negligible cabling losses and very little attenuation changes under extreme environmental conditions, it is possible to provide a cable design with low attenuation values, i.e., less than 1 dB/km at 1300 nm. This high performance is allowing for a long haul field communication system with fewer repeaters.

Connectorization experiments have shown that the composite buffer is readily compatible with existing connector designs. The 2-fiber ruggedized military cable has successfully been terminated with proven field connectors.

Summary

A newly design composite fiber buffering using different fiber types has been developed. Several hundred kilometers of this product have been manufactured in a production plant environment. Excellent performance with minimal microbending sensitivity has been demonstrated in different cable designs and field tests.

References

- 1 P. R. Bark, H. M. Liertz, U. Oestreich, G. H. Zeidler: "High Fiber Count Cables of the Mini-Bundle Design", 30th IWCS, 1981, Cherry Hill, NJ, pp. 255-258.
- 2 P. R. Bark, D. O. Lawrence: "Recent Developments in Mini-Unit Cable", 32nd IWCS, 1983, Cherry Hill, NJ, pp. 301-307.
- 3 U. Oestreich, G. Zeidler: "Development Trends in Fiber and Cable", Siemens Telecom Report 6 (1983); Special Issue "Optical Communications", pp. 198-201.

COMPOSITE BUFFER (8 mm OD)

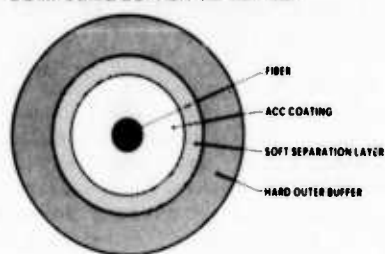


Figure 1

ONE FIBER WIRING CABLE (2 mm OD)

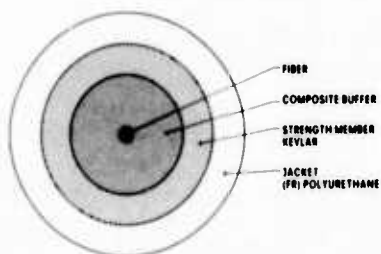
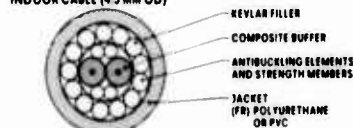


Figure 2

Characteristics	Performance
Tensile Strength @ 0.5% cable strain	300 N $\Delta\alpha = 0$ dB/km
Temperature Performance	(a) 0°C to 50°C $\Delta\alpha \leq 0.2$ dB/km (b) -40°C to +70°C $\Delta\alpha \leq 0.8$ dB/km
Crush	(a) ≤ 100 N/cm $\Delta\alpha = 0$ (b) ≤ 800 N/cm $\Delta\alpha > 0$ reversible
Impact	50 x 0.75 Nm no failure

Figure 3: Performance Characteristics of a Composite Buffered Fiber Indoor Cable Containing an 85/125 μm - 0.26 NA Data Broad-Band Fiber

TWO FIBER CABLES
INDOOR CABLE (4.5 mm OD)



RUGGEDIZED PAN-OUT CABLE (7.0 mm OD)

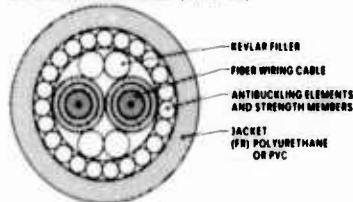


Figure 4

Characteristics	Performance
Tensile Strength @ 0.6% cable strain	1000 N $\Delta\alpha = 0.5$ dB/km reversible
Temperature Performance	(a) -20°C to +70°C $\Delta\alpha \leq 0.4$ dB/km (b) -40°C to +70°C $\Delta\alpha \leq 0.8$ dB/km
Crush	(a) ≤ 100 N/cm $\Delta\alpha = 0$ (b) ≤ 1000 N/cm $\Delta\alpha = 1.4$ dB/km reversible
Impact	50 x 2.2 Nm no failure

Figure 5: Performance Characteristics of a Composite Buffered 2-Fiber Intrabuilding Cable Containing 85/125 μm - 0.26 NA Data Broad-Band Fiber

TWO FIBER RUGGEDIZED CABLE (6 mm OD)

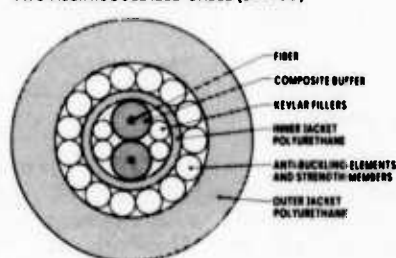


Figure 6

PERFORMANCE CHARACTERISTICS OF THE 2-FIBER RUGGEDIZED FIELD CABLE

CHARACTERISTICS	TEST PROCEDURE	CABLE PERFORMANCE	CRITERIA
TENSILE STRENGTH - OPERATING - INSTALLATION	EIA	500 N 1000 N	$\Delta\alpha = 0$ $\Delta\alpha = 0$ @ 500 N
TEMPERATURE - OPERATING - STORAGE	DOD	-55°/+95°C -70°/+95°C	$\Delta\alpha \leq 0.2$ dB/km $\Delta\alpha = 0$ @ RT
CYCLIC FLEXING	DOD	2000 X	$\Delta\alpha = 0$
IMPACT	DOD	100 X 3 Nm	$\Delta\alpha = 0$
COMPRESSION	DOD	2000 N/cm	$\Delta\alpha \leq 0.1$ dB
COLD BEND	DOD	-40°C/30 mm	$\Delta\alpha = 0$
TWIST BEND	DOD	1270 N/30 mm	NO FIBER BREAK
FREEZING WATER	DOD	-10°C/-2°C	$\Delta\alpha = 0$
KNOT TEST	EIA	KNOT/30 mm	$\Delta\alpha = 0$
FLAMMABILITY	IEEE	30 sec	$\Delta\alpha = 0$
COMPOUND DRIP	REA	+60°C/24 hrs	NO DRIP

Figure 7

TEMPERATURE CYCLING OF THE 2-FIBER RUGGEDIZED FIELD CABLE

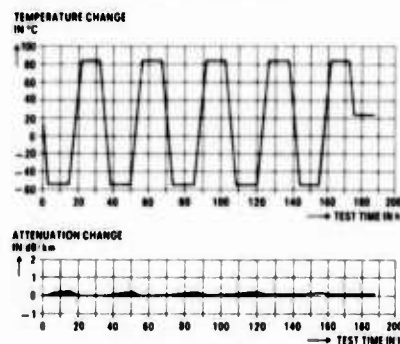


Figure 8



Peter R. Bark

Siecor Corporation
610 Siecor Park
Hickory, North Carolina

Peter Bark holds a Bachelor of Science degree from the Technical University at Munich. He also received his doctorate in engineering from the same institution in the field of molecular beam physics. He has been employed by Siemens AG in Munich, West Germany, since 1971, in several positions in the telecommunications cable field. His principal assignments were in the field of developing optical cables, interconnecting hardware and subsystems. Since 1977 Peter Bark has been with Siecor and holds the position of Vice-president for Engineering.



Derek O. Lawrence

Siecor Corporation
610 Siecor Park
Hickory, North Carolina

Derek Lawrence graduated from the City University, London, with a degree in Communications Engineering. He has been involved in the cable industry since 1970 and from 1975 has worked in optical fiber cable engineering, manufacturing and development. Since 1979 he has been with Siecor Corporation and is currently Engineering Manager.

Ulrich Oestreich

Siemens AG
Telecommunication Cables
Munich, West Germany

Ulrich Oestreich was born in 1928 in Berlin. He received a Dipl.-Ing. degree in electrical engineering at the Technical University in Berlin. In 1953 he joined the Siemens-Cabel-Works in Berlin and was involved in the development of high-voltage and telecommunication cables. Since 1974 he has been with the telecommunication cable department in Munich, where he holds a managing position for developing and manufacturing of fiber optic cables.

Ernst Mayr

Siemens AG
Munich, West Germany

Ernst Mayr was born in Munich in 1939. He received his engineering degree in Munich in 1966. He joined Siemens in 1966 and has since been involved with various aspects of cable systems development including gas pressure control and coaxial connections. Since 1978 he has been involved with the development of fiber optic cables, cable elements and technology.

DEVELOPMENT OF STRAIN-FREE OPTICAL FIBER CABLE

Shinichi Yonechi

Sumitomo Electric Industries, Ltd.
1, Taya-cho, Totsuka-ku, Yokohama, 244 Japan

Abstract

A new optical fiber cable in which the optical fibers do not significantly stretch during elongation of the whole cable by an external tension has been developed using a new design concept.

This design concept is based on some theoretical investigations concerning cable structure, in particular the lay length of fibers and the construction of the central member on which the fibers are wound helically.

Use of a particular central member having a stranded structure and of a special relationship between the lay lengths of the fibers and of the central member make it possible to keep the strain on the fiber lower than that on the whole cable.

The results of a tensile test on the newly developed cable showed good agreement with theoretical predictions.

One result was that the axial strain on the fibers was found to have been generated considerably smaller than the strain on the cable as a whole.

Results of other general mechanical tests on the trial cable and of a test of the cable's temperature-transmission loss property were also found to be satisfactory.

The next step in development is to widen application of this new design concept to practical cables and to establish design conditions for which further improvement in the strain delay can be realized.

1. Introduction

It is generally known that when external tension is applied to an optical fiber cable, the axial strain on optical fibers is equal to that on the entire cable¹. Even in spacer-type cables², in which optical fibers are housed in a rather loose fashion, almost the same elongations of the fibers and of the whole cable resulted during tensile tests.

This result stems from the fact that optical fibers lay along the bottom of the spacer in the cable without any extra slack.

A cable structure in which the optical fibers do not suffer any strain when the cable elongates due to tension would clearly be advantageous in terms of lengthening the fiber's lifetime.

We have successfully developed such a cable and have confirmed that its essential properties coincide with theoretical predictions.

The fundamental structure of this test cable can be utilized in many different kinds of optical fiber cables.

2. Theoretical Investigation

The strain-free cable structure used in the new cable is based on the following theoretical background. In a typical cable with a helically laid fiber, as shown in Fig. 1, axial expansion of the cable will always be accompanied by an increase in the lay length and a decrease in the helix radius.

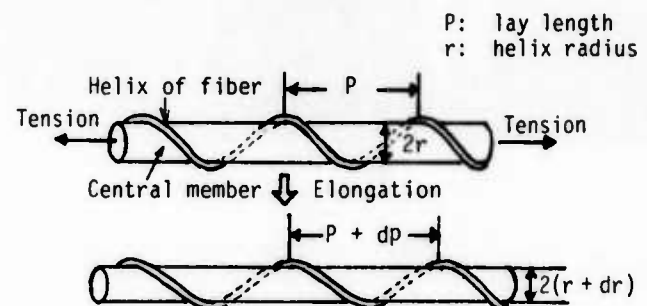


Fig. 1 Elongation model of typical optical fiber cable

The relationship between r and p in this deformation is described by the following equations:

$$\frac{dr}{dp} = -\frac{p}{4\pi^2 r} \quad \dots\dots\dots (1)$$

where the negative sign corresponds to the decrease in radius which occurs when the lay length increases.

On the other hand, a decrease in radius of the central member will also occur, amounting to:

$$\delta r = -\nu^* r \frac{\delta p}{p} \quad \dots\dots\dots (2)$$

where ν^* is the Poisson's ratio of the central member. From equations (1) and (2), if the condi-

tion

$$v^* > \left(\frac{p}{2\pi r}\right)^2 \quad \dots\dots\dots (3)$$

is satisfied, the optical fiber will not suffer any additional strain due to cable elongation, because the decrease of radius would be much faster for the central member than for the helix of the fiber. However, it seems highly impossible that the condition represented by equation (3) can be satisfied with practical values of r and p as long as the central member is made of a single material.

On the other hand, a central member of stranded structure is very effective for avoiding additional strain in the fiber. In the dual layer structure illustrated in Fig. 2, if the total elongation of the central member is $d1/l$, equation (1) yields:

$$\left. \begin{aligned} \frac{dr}{dl} &= -\frac{p^2}{4\pi^2 r l} \\ \frac{ds}{dl} &= -\frac{q^2}{4\pi^2 s l} \end{aligned} \right\} \dots\dots\dots (4)$$

where $dp = (dl/l)p$ and $dq = (dl/l)q$

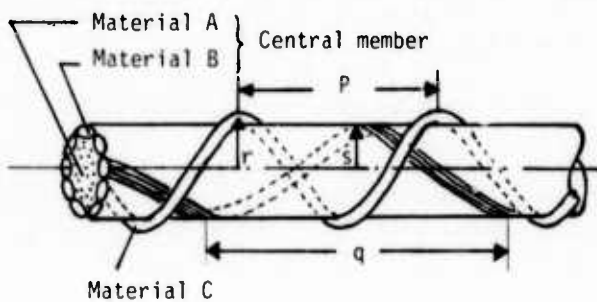


Fig. 2 Dual layer structure

Since r and s are nearly equal, the relation

$$q > p \quad \dots\dots\dots (5)$$

describes the condition in which the decrease in the radius occurs faster in the central member than in the helix of material C.

The strain-free cable structure is based on this principle. In actual application, the materials in Fig. 2 should be as follows:

- A: cushioning material
- B: strength member
- C: optical fiber

Since the general tendency of equation (1) will be as illustrated in Fig. 3, it can easily be understood that, the longer the lay length, the faster the radius decreases.

If the lay length of the fiber corresponds to γ in the graph, it is more preferable to have the lay length of the central member correspond to α than to β (of course, in the practical region for lay length).

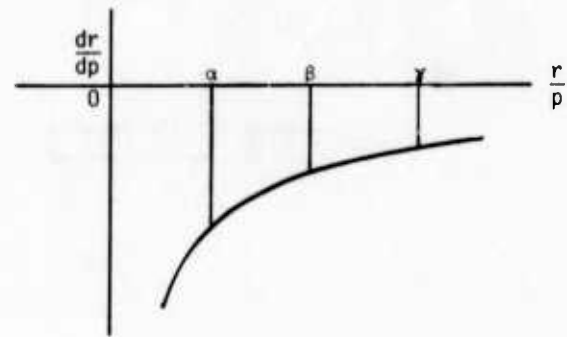


Fig. 3 Tendency for reduction of helix radius

3. Test Production

The design of the trial cable is based on the theoretical investigation described in the previous section. Fig. 4 shows the cross-sectional structure of the trial cable, whose construction is summarized in Table 1. Fig. 5 is a photograph of the cable.

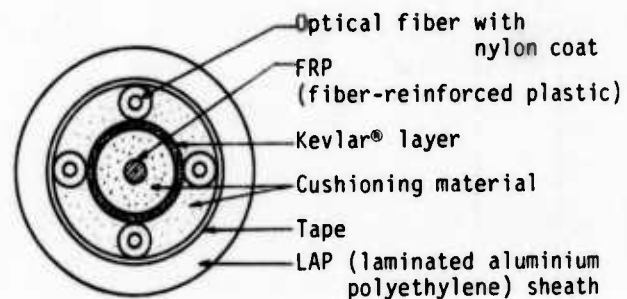


Fig. 4 Structure of trial cable

Table 1 Construction of the cable

Fiber	Type	Silica-type multi-mode fiber
	Core	50μm in diameter
	Cladding	125μm in diameter
	Buffer	Silicone resin 400μm in dia.
	Jacket	Nylon 0.9 mm in diameter
Cable	No. of fiber	4
	Sheath	LAP sheath 9 mm in diameter
	Weight	50 g/m

Because of its structure, when the cable is elongated by an external tension, the radius of the Kevlar® layer decreases faster than that of the optical fiber layer. Therefore, no additional strain is added to the optical fiber. The lay lengths were chosen to be 150 mm for the optical fiber and 325 mm for the Kevlar®. The cushioning material consists of plastic yarn, which makes it possible for the Kevlar® to shrink radially.

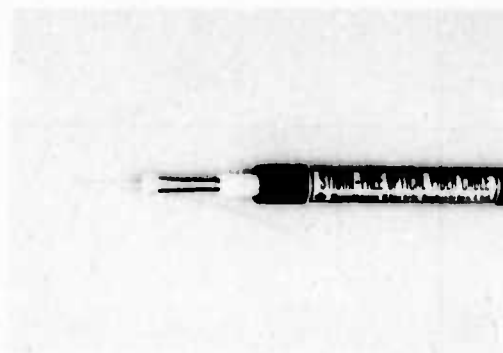


Fig. 5 The trial cable

The relationship between r/p and dr/dp for this case is shown in Fig. 6, and conforms with the condition of a strain-free effect mentioned in the previous section.

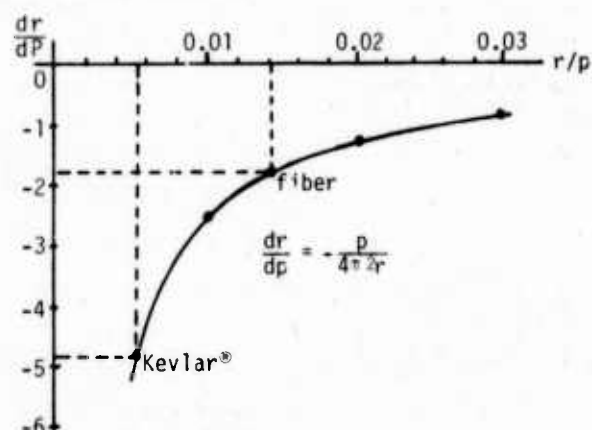


Fig. 6 r/p - dr/dp relation for the trial cable

A conventional stranding machine and sheathing machine were used without difficulty for production of the trial cable. Table 2 shows the final properties of the cable. No changes in the cable's transmission properties were observed through the manufacturing process.

Table 2 Transmission properties of final cable (wavelength = $0.85\mu\text{m}$)

Fiber (colour*)	Loss (dB/km)	Bandwidth (MHz·km)
No. 1 (blue)	2.93	411
No. 2 (yellow)	2.89	349
No. 3 (green)	2.53	450
No. 4 (red)	2.50	503

* colour of the nylon coating

4. Measurement of Fiber Elongation

A tensile test was carried out on the trial cable. The four fibers were jointed to each other to form an optical loop. Elongation of the fibers

was measured by the phase shift method³, as illustrated in Fig. 7.

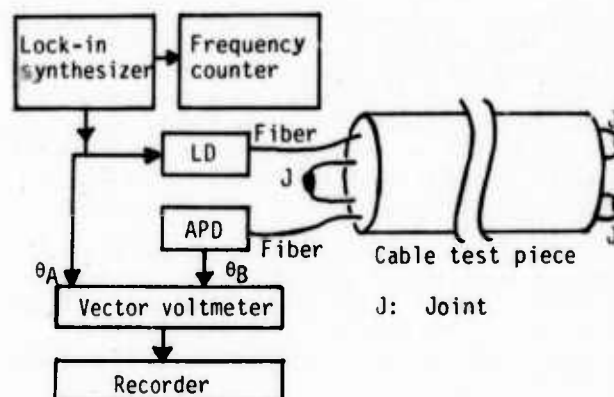


Fig. 7 Fiber elongation measurement system

A high-frequency LD optical source was connected to one fiber end. The phase shift of the high frequency electromagnetic wave observed at the other end corresponds to the fiber elongation.

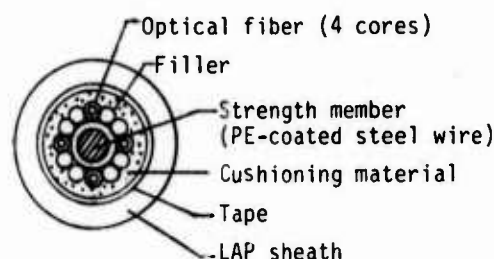
Both ends of the test cable were molded using resin to bond the cable elements to each other. The fiber elongation Δl , is described by the following equation:

$$\Delta l = k \frac{c}{fn} \frac{\theta_A - \theta_B}{2\pi} \quad \dots \dots \dots (6)$$

where $\theta_A - \theta_B$: phase shift (rad.)
 k : coefficient
 c : velocity of light
 f : frequency
 n : refractive index of fiber

The frequency, f , was chosen to be 900 MHz in this experiment.

For comparison, the conventional optical fiber cable in Fig. 8 was examined by the same testing method.



Diameter: 14mm, weight: 150 g/m

Fig. 8 Conventional optical fiber cable

The test results of both types of cables are shown in Fig. 9. Elongation of the cable (x axis) was measured by a scale directly attached to the cable, and elongation of the fiber (y axis) was calculated from the phase shift. It is clear that $\epsilon_c \approx \epsilon_f$ in the case of the conventional optical

fiber cable, while $\epsilon_f < \epsilon_c$ in the case of the trial cable. From the linear part of the graph for the trial cable, it can be seen that $\epsilon_c - \epsilon_f \approx 0.2(\%)$, which is the strain delay effect predicted by the theoretical considerations.

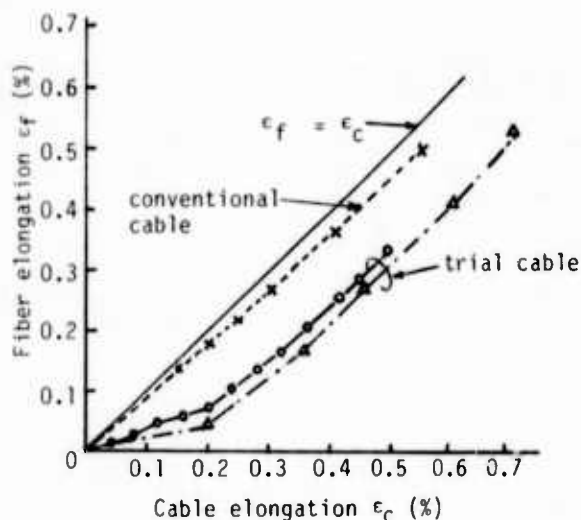


Fig. 9 Results of the tensile test (I)

Fig. 10 shows the linear relation between cable elongation (ϵ_c) and external tension for both types of cables. This relation confirms that the tensile test was carried out without any relaxation in the test pieces at the beginnings of the test.

It is also clear from the figure that the trial cable shows 4~5 times the elongation of the conventional cable under the same tension. This result is related to the make-up of their strength members.

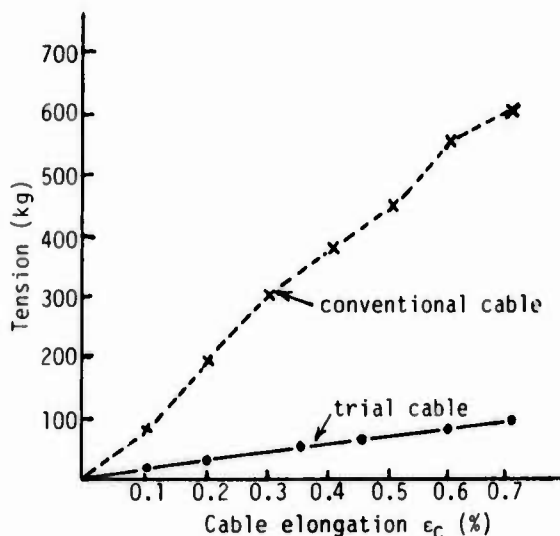


Fig. 10 Results of the tensile test (II)

The amount of $\epsilon_c - \epsilon_f$ in Fig. 9 can be explained by the following theoretical considerations. When an external tension acts on the trial cable, the helix radius of the fibers decreases toward some final value, as illustrated in Fig. 11, which shows the initial and final conditions of the fibers.

The final condition corresponds to the beginning point of the linear relationship between cable elongation and fiber elongation shown in Fig. 9. After reaching the final condition, both increments for ϵ_c and ϵ_f will be nearly equal. The lay length P_2 for fiber in the final condition is calculated as follows:

$$P_2 = P_1 + \int_{r_1}^{r_2} \frac{r^2}{L} \frac{dp}{dr} dr = P_1 + \frac{2\pi^2}{L} (r_1^2 - r_2^2) = 150.291(\text{mm}) \dots (7)$$

where $P_1 = 150\text{mm}$ is the initial lay length of the fibers and

$$L = \sqrt{P_1^2 + (2\pi r_1)^2} = \sqrt{P_2^2 + (2\pi r_2)^2} \text{ is the}$$

length of the fiber contained in one lay before the final condition and $r_2 = r_1 - 0.6$ (mm) is an estimation from the design.

Then, cable elongation ϵ_c will be

$$\epsilon_c = (P_2 - P_1)/P_1 = 0.0019 \dots (8)$$

i.e. in the final condition, ϵ_c will be about 0.2% and the value of $\epsilon_c - \epsilon_f$ remains at about 0.2%, in the range of $\epsilon_c > 0.2\%$.

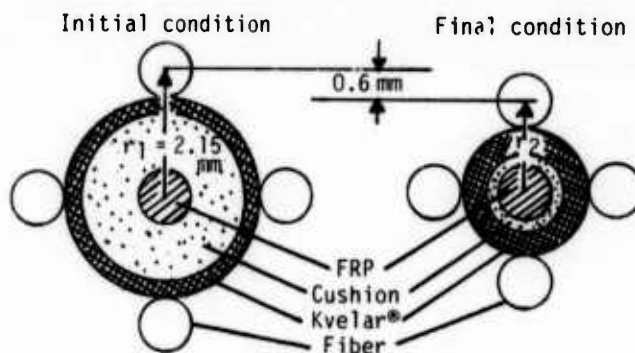


Fig. 11 Schematic view of crosssectional change under the tensile test

On the other hand, the decrease in the helix radius of the Kevlar® layer occurs considerably faster than that in the fibers. The similar calculation showed that the helix radius of the Kevlar® layer reaches to the final value when the cable elongates only by about 0.03%.

Namely, the Kevlar® layer is expected to act as a tensile strength member in the region of $\epsilon_c > 0.03\%$. This fact well explains the linear relation between the cable elongation and the tension for the trial cable in Fig. 10. Thus the theoretical predictions show good agreement with the experimental results shown in Fig. 9 and Fig. 10.

5. Other properties

We also checked the trial cable's general properties and achieved satisfactory results.

5.1 Mechanical properties

The mechanical properties of the new trial cable were investigated for several test items, using two samples of the new trial cable for each item. In spite of very small size of the strength member contained in the cable, it was confirmed that the strength of the new cable is greater than that of the conventional cable for each item. These results are due to the trial cable's strain-free structure and large amount of cushioning materials.

(1) Compression test: The transmission loss increase was measured while the cable was compressed by a 50mm width plate. The four fibers were joined to each other to form an optical loop for measuring the loss increase. The result of the compression test is shown in Fig. 12. The loss increase $\Delta\alpha$ was nearly equal to zero until the compressive force reached to 200 kg, and $\Delta\alpha$ is generated in the region of compressive loads more than 300 kg. This tendency is almost the same as that for the conventional layer cable.

The test was conducted for compressive loads up to 1000 kg, yet no fiber breakage occurred. The loss increase returned to zero when the compressive load was removed.

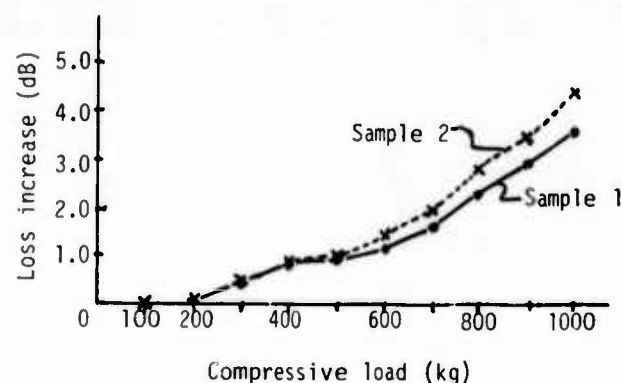


Fig. 12 Result of compression test

(2) Impact test: Cylindrical weights having a base of 1 inch diameter were dropped from a height of 1 meter to the cable surface and the loss increase $\Delta\alpha$ was measured for various weights. The results are summarized in Table 3. The trial cable shows a considerably higher level of performance than the conventional layer cable, which sometimes shows significant loss increase under an impact of about 1 kg x 1 m.

Table 3 Results of impact test

Sample Weight	No. 1	No. 2
< 3 kg	$\Delta\alpha \sim 0$	$\Delta\alpha \sim 0$
4.5 kg	$\Delta\alpha \sim 0.18\text{dB}$	$\Delta\alpha \rightarrow \infty$ (break)

(3) Bending test: The loss increase resulting from the bending radius was measured using mandrels of various sizes. The radius of the mandrels were ranged from 200mm to 30mm. Samples were bent one time, except for that used with the 30mm mandrel, which was bent 30 times.

As shown in Fig. 13, the loss increase first appeared as the radius of 30mm, while the loss increase generally appears at a radius of 50mm in the conventional layer cable. Thus, the new cable is superior to the conventional cable in this respect.

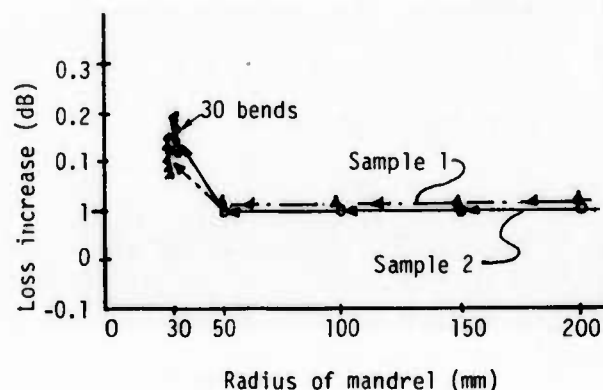


Fig. 13 Result of bending test

(4) Twisting test: A piece of cable of 1m length, hung vertically with 25 kg weight, was twisted in the direction in which the lay length shortens. The measured loss increase $\Delta\alpha$ versus number of twists is shown in Fig. 14. $\Delta\alpha$ first appeared at about 20 times of twists. Thus the new cable is again superior to the conventional one, for which $\Delta\alpha$ usually first appears at 10~15 of twists.

Releasing all twists, the loss increase returned to zero, the initial state.

(5) Squeezing test: A test cable of 1.5m length was hung over a roller of diameter 140mm at an angle of 135°. The loss increase $\Delta\alpha$ was measured against the tension which was gradually increased after every 5 times the cable was rolled back and forth. The test results are shown in Table 4. The loss increase $\Delta\alpha$ is nearly zero below 200 kg tension. In this characteristic as well, the new cable was more stable than the conventional one which generally first shows $\Delta\alpha$ in the tension range 150 kg to 200 kg.

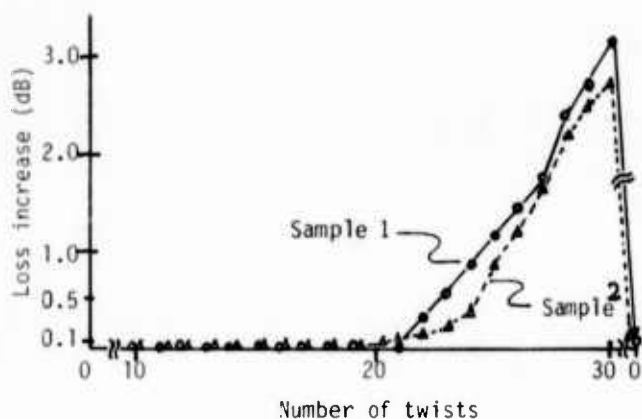


Fig. 14 Result of twisting test

Table 4 Result of squeezing test

Sample	No. 1	No. 2
Tension		
< 200 kg	$\Delta\alpha \sim 0$	$\Delta\alpha \sim 0$
250 kg	break* (at 1st jerk)	break* (at 2nd jerk)

*break occurred both in fiber and cable sheath

5.2 Temperature property

A trial cable of 230m length wound on a wooden drum was placed in a temperature controlled chamber. 2-fibers (blue & yellow) were spliced to form a 460m length optical loop, with the spliced part located out of the temperature controlled chamber. The loss increases at various temperatures were measured by the cut back method after leaving the cable at each temperature more than 3 hours.

The results are shown in Fig. 15. The property is more stable in the low temperature region than in the high temperature region.

The loss change in the high temperature region seems to be due to deformation of elements in the cable by thermal expansion or heat shrinkage.

The cable's stability in the low temperature region may be due to the LAP sheath structure, which prevents heat shrinkage of the cable in the low temperature region, both radially and longitudinally.

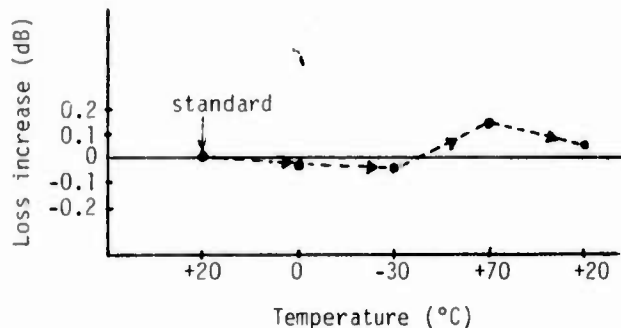


Fig. 15 Temperature property

6. Conclusion

In tests of the newly developed cable, it was clearly seen that, as predicted by theory, strain on the fibers was generated considerably smaller than that on the cable itself. This effect results from the cable's stranding structure, which uses a special relationship between the lay lengths of the members. This general principle can be utilized with the same effect for various kinds of cables. The difference in elongation between fiber and cable can be further increased by improving the cable design.

That the elongation of the fibers is less than that of the cable allows expanding the number of optical cable applications, and it also promises to increase fiber lifetime for all optical fiber cables.

The basic design concept by which the Strain-Free optical fiber cable was developed will be widely utilized in various applications of optical fiber cables.

References

- (1) Y. Katsuyama et al.: "Study on Mechanical and Transmission Characteristics of Optical Fiber Cable during Installation", J. Opt. Commun. 3 (1982) 1, 2-7
- (2) S. Yonechi et al.: "Application of Spacer Forming Technique to Communication Cables", 29th IWCS, Nov. 1980
- (3) S. Tanaka et al.: "Precise Measuring Method of Elongation and Residual Strain of Optical Fiber due to Cabling Process", 7th ECOC, Copenhagen, Sep. 1981, paper 6.6



Shinichi Yonechi
Sumitomo Electric
Industries, Ltd.
1, Taya-cho, Totsuka-ku
Yokohama 244 Japan

Shinichi Yonechi was born in 1945 and received a B.S. in 1966 from Tohoku University. He joined Sumitomo Electric Industries, Ltd. in 1971, and has been engaged in research and development of communication cables. He is an engineer in the Optical Fiber Cable Department, and is a member of the Institute of Electronics and Communication Engineers of Japan.

Evaluation of Shrinkage Forces and Thermal Transitions of Fluorinated Ethylene-Propylene (FEP) Cable Insulations and Buffered Optic Fibers at Low Temperatures

G. L. Grune
And
L.A. Hilliard

IBM Corp.
Polymers Group (E79)
Research Triangle Park, N.C. 27709

Abstract

In an attempt to further understand the effects of temperature cycling tight buffered optic fiber cables on proposed connector designs and attenuation losses, several experiments were performed in the IBM-RTP Polymers Laboratory. These initial experiments were made to quantify the amount of shrinkage (if any) which occurs when subjecting fiber optic cable materials to temperatures as low as -40 C.

Without any previous experience or known measurements involving shrinkage forces associated with cable insulations, the test procedure includes what is believed to be a novel approach. The cable jackets and fiber buffer insulations were fixed between stationary jaws in an Instron testing apparatus equipped with an environmental test chamber permitting temperature control.

Gauge lengths of 6.5 inches and 4.0 inches were used for the Fluorinated Ethylene-Propylene (FEP) tubular samples and polyester elastomer fiber buffers respectively. Typically the Instron chamber temperature was raised as rapidly as possible from ambient to the peak value (+60 C) and then lowered as rapidly as possible to the lowest temperature (0 or -40 C). The temperature cycle was completed by raising the temperature back to ambient conditions.

In addition to aiding our understanding of the jacket shrinkage which would affect fiber optic connectors, the experiment helped to develop a sense for the fiber buckling forces associated with temperature cycling. Along with the characteristic force curves which depict changes in force in the temperature ranges of -40 to +60 C, Differential Scanning Calorimetry (DSC) analysis was conducted on several of the FEP cable and single fiber unit jackets.

Introduction

The design requirements and functional specifications of both the indoor/outdoor and plenum indoor single fiber units (SFU's) for the IBM Cabling system (announced in May 1984), have been detailed in a previous paper¹. The use of UV-cured acrylate coated glass fibers buffered with a polyester elastomer coating, surrounded with polyamide strength members and jacketed with polyurethane, is a common choice of materials which have been used in some military cable applications^{2 and 3}.

This construction (see figure 1) consistently meets stringent cable requirements including tensile strength, maximum bend radius, compressive strength, impact resistance, flex, cold bend and humidity testing. An additional and even more stringent requirement includes an attenuation/temperature cycling test which calls for < 6 dB./Km. loss at 850 nm. during at least 5 cyclic excursions from +80 to -40 C.

The use of a lower molecular weight grade fluorinated ethylene-propylene (FEP) jacket for the single fiber unit (SFU) did not per-

form up to the standards set for the non-plenum polyurethane jacketed SFU. This paper outlines the major differences between the plenum (fluorinated jacketed fiber), and non-plenum (polyurethane jacketed fiber) constructions followed by a description of the test methods developed to distinguish the cause of excess attenuation loss in the plenum design. Next, test data extracted from actual plenum and non-plenum SFU samples is presented with some corollary data determined using Differential Scanning Calorimetry (DSC) techniques. Finally, a general conclusion based on the initial findings of this work, together with recommendations for future studies are detailed.

1. The Design and Functional Requirements for Non-Plenum and Plenum Single Fiber Units and Cables

Figures 1A and 1B below illustrate the similarities of the non-plenum and plenum single fiber units (SFU's) for the IBM cabling system.

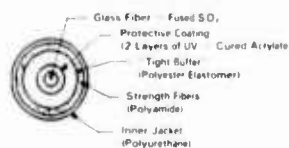


Figure 1A
Non-Plenum Single Fiber Unit
(SFU)

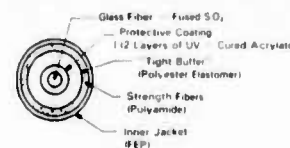


Figure 1B
Plenum Single Fiber Unit
(SFU)

The only difference at the time this testing was performed, was that the outer jacket material choice for the non-plenum cable was a polyester based polyurethane while the choice for the plenum cable was limited to a low molecular weight grade of FEP. These designs were limited by what were perceived to be U.L. (Underwriters Laboratories) flammability requirements. Although U.L. currently does not list any optic fiber cables as such, there is a requirement that cables intended for plenum usage (installed without conduit) meet U.L. 910. It is IBM's intent that any of the new cabling system plenum cables meet the stringent flammability requirements of U.L. 910. Thus even the SFU's were jacketed with FEP to insure that the overall cable would pass U.L. 910.

For the non-plenum SFU and subsequent cable construction, the use of polyurethane is allowable and desirable for many reasons. In addition to reduced cost (of PUR compared with FEP), the U.L. flammability requirements allow for a much less stringent U.L.

VW-1 test in cables which are intended for installation in metallic conduit. Also, the polyurethane is more flexible and as will be shown, more forgiving during temperature cycling of the total optic fiber cable construction, than is FEP.

The other specifications and functional requirements for the two SFU's are identical in most other respects including the same fiber dimensions (an outer diameter of $143 \pm 0, -6$ mm and an effective core diameter of 100 ± 4 mm, same cladding diameter (400 mm), and same SFU outer diameter (2.8 ± 0.3 mm). Other important fiber specifications are listed in Table 1.

Table 1

Optical Fiber Specifications

Numerical Aperature	=	0.29
Attenuation @ 850 nm	<	6 dB/Km
Attenuation @ 1300 nm	<	4 dB/Km
Bandwidth @ 850 nm	>	150 MHz • Km
Bandwidth @ 1300 nm	>	500 MHz • Km

The only other difference in requirements of the two SFU's (and overall cables) is that the FEP version (plenum), due to its tendency to crease during bending, was allowed a larger minimum bend radius of 15 cm. (compared with the PUR single fiber unit's 7 cm.) and only 10 flexes (compared with 1000) in the flex test, where the bend radius equals the minimum bend radius of the cable.

Figures 2A and 2B further illustrate the similarities with the total non-plenum and plenum cable designs.

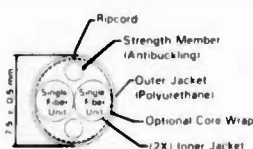


Figure 2A
Non Plenum 0 0 2 Type 5
Optic Fiber Cable

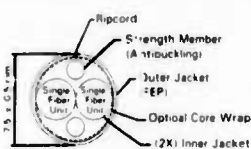


Figure 2B
Plenum 0 0 2 Type 5
Optic Fiber Cable

Again, the only substantial difference is the use of FEP for the 0-0-2 cable outer jacket. Other actual differences occurred with varying wall thicknesses which were allowed for the plenum version. Coding and other IBM cabling system designations have been published earlier. The two cables shown in Figures 2A and 2B above will be referred to in the remaining portion of this paper as Type 5 NP (non-plenum) or Type 5P (plenum) respectively.

II. Test Methods Developed to Determine the Cause of Excess Attenuation

2.1 Attenuation Loss Measurement During Required Temperature Cycling

For the Type 5NP and 5P cables described in Section I, the same temperature cycling test for both cables is performed as follows:

1. The cable is placed in a temperature chamber and optical monitoring equipment is set up. Recommended minimum cable length is 1000 meters.
2. The chamber is brought from ambient to +80 C and maintained at that temperature for 12 hours. The chamber temperature is then reduced to -40 C for 12 hours. This constitutes one cycle.
3. Readings are taken at each temperature starting with ambient for each test fiber and the source. The source should not vary by more than 0.5 dB throughout the test.
4. The number of cycles to be performed shall be determined as follows:
 - A minimum of 5 cycles shall be performed
 - After the minimum 5 cycles, the test may be terminated in the last two cycles if not more than 0.2 dB greater than the loss at the corresponding temperatures in the cycle prior to the last two cycles.
 - The test may be terminated any time that a fiber loss is above the specification limit.
5. If either fiber in a cable has a total loss (measured loss at ambient plus induced loss at any temperature) which exceeds the specification limit, this constitutes a failure.

The optical monitoring equipment set-up is shown in Figure 3.

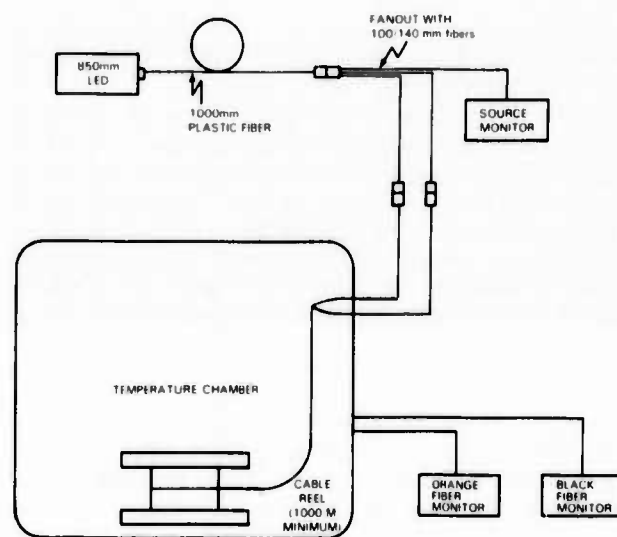


Figure 3
Optical Equipment
For
Temperature Cycling Test
(Power Monitors: Photodyne 11XE or Equivalent)

As mentioned before, the plenum (Type 5P) version shown in Figure 2B did not meet the requirements of the temperature cycling test detailed above. Figure 4 illustrates a typical plot for attenuation loss (in dB/Km.) with the number of temperature cycles for a typical Type 5P cable. The typical plot for a Type 5NP cable showed a "flat" curve - with no increase in attenuation loss during temperature cycling. It was the search for the cause of the phenomena shown in Figure 4, as well as the need to control and define shrinkback (often referred to as creep or cold flow in ASTM D2990) of insulation away from the optic fiber connector, which lead to the establishment of the shrinkage test described in the following section.

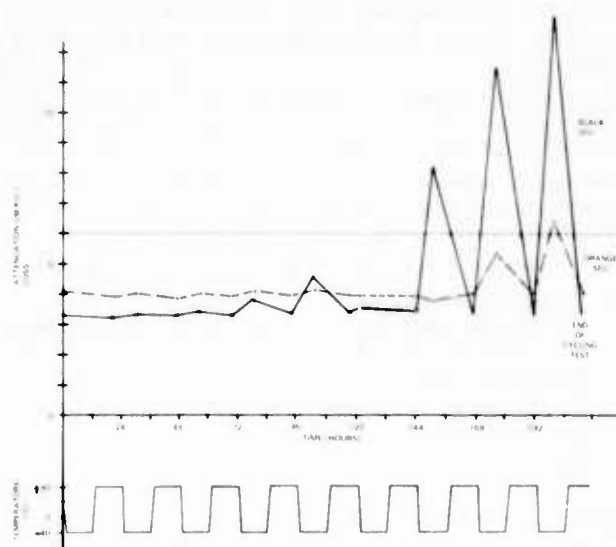


Figure 4
Typical Attenuation Loss For Type 5
Plenum Cable (1090M)

2.2 Thermal - Mechanical Shrinkage Force Test with the Instron Environmental Chamber

Figures 5A and 5B pictures the Instron Model 1125 (with Microcon I - microprocessor and data recorder unit) setup including the environmental chamber which surrounded the test specimen fixture in the geometry shown. Temperatures could be varied as desired within this apparatus. Originally, twenty-seven (27) different test specimens were temperature cycled to determine the shrinkage forces which occur throughout the temperature range of -40 to $+60$ C. Because the rate of heating and cooling was relatively slow, (about 30 minutes elapsed time for a full cycle from ambient to $+60$ C to -40 C), the polymer jacket (or buffered fiber) was assumed to equilibrate with the environmental chamber temperature. Test specimens of approximately 6" or 8" using gauge lengths of 4" or 6.5" were used for the polyester elastomer buffered fibers and FEP jackets respectively. The FEP jackets were hollow tubes from which the remaining cable members had been removed. The polyester buffered fibers were "whole" in that they were composed of the cladded $100/140$ μm glass fiber and two layers of acrylate. The temperature cycle included reaching the maximum temperature of $+60$ C rather than $+80$ C because originally we were interested in the response of the cable insulations with respect to fiber optic connector specifications which required excursions to only $+60$ C. Also, in the interest of time savings (usually only 3 tests/day could be run) and the fact that there was no measurable difference between the relaxation forces at $+60$ and $+80$ C, we continued with $+60$ C as the maximum temperature. Each FEP jacket was loaded with an initial tensile force of 0.75 lbs. after trial and error indicated this to be the maximum necessary to prevent significant relaxation due to the loading itself. The polyester elastomer fiber buffers were preloaded at 0.5 lbs. After preload, the jaws holding the ends of sample remained fixed. The force change was monitored and recorded on chart paper, the results of which are reported in Section III. Typically the chamber temperature was raised as rapidly as possible from ambient to the peak value ($+60$ C) and then lowered as rapidly as possible to the lowest temperature (0 or -40 C). The temperature cycle was completed by raising the temperature in the chamber back to ambient.

The Instron environmental chamber employs an electrical resistance heating element to increase temperature, while liquified CO_2 was forced in for cooling purposes. The flow of CO_2 into the chamber was dependent on the pressure inside the CO_2 tanks. The rate of cooling/heating was not monitored throughout the test.

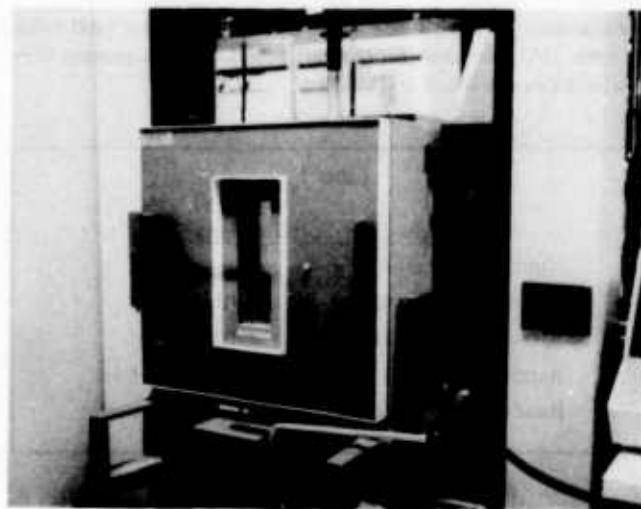


Figure 5A
Instron Model 1125 Environmental
Chamber

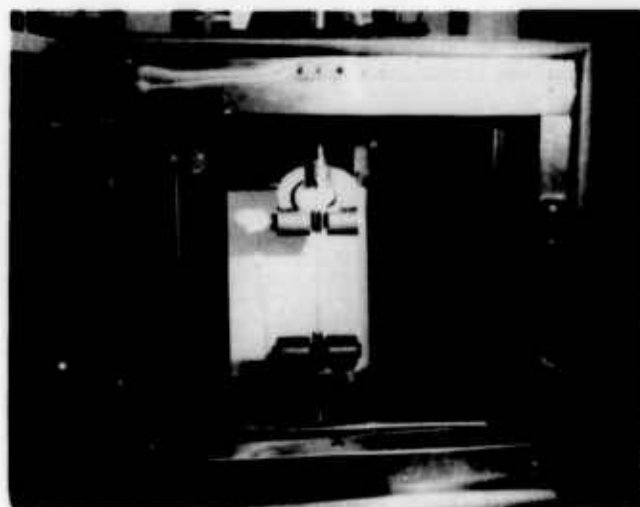


Figure 5B
Closeup View of Test Specimen
Geometry Within Instron
Environmental Chamber

III. Results and Discussion of Shrinkage and Thermal Transition Data

3.1 Shrinkage Data Measured With The Instron Environmental Test Chamber

It has been known and documented ^{4 and 5} for some time that, fiber macrobending can occur due to axial compressive forces generated

by compressive strain. This compressive strain develops due to the difference between the glass fiber and the buffer and jacket materials, which can lead to compressive strain and eventual fiber buckling and even fiber breakage. The shrinkage force test method described in Section II quantifies the shrinkage force, due to the plastic coatings being subjected to low temperatures, in a unique manner. As the following data will indicate, the shrinkage force is related to the total axial compressive force, which at some critical force, causes excess attenuation loss.

A list of thermal coefficients of expansion and secondary thermal transition temperatures for different polymer jackets which may be applicable for the SFU and Type 5 optic-fiber constructions, is given in Table 2.

Table 2

List Of Thermal Coefficients And Secondary Transition Temperatures Of Interest For Fiber Optic Cable Design

Material (Wire & Cable Grades)	Melting Pt. (T _m) °C	Thermal Expansion Coefficient ($\alpha = \Delta L / L \Delta T$) $\times 10^{-5}$			Secondary and Tertiary Transition Temperatures TMA 1(°C) DSC 2(°C)	
		-40 to 0°C	0 to 60°C	60 to 150°C		
Fluorinated Ethylene- Propylene (FEP)	265	6.5 - 7.0	7.1	9.0	-85, +18, +165	-60, +15
Ethylene- Tetrafluoroethylene (ETFE)	270	5.8 - 6.1	7.9	8.9	-120, -25, +110	+19, +30
Ethylene- Chlorotrifluoroethylene (ECTFE)	245	5.1	6.5	8.4	-50, 77, 127	—
Polyvinylidene Fluoride	161	7.1	7.1	7.1	—	—
Polyester Based PYR	195	8.3	10.5	9.4	—	-45
Polyester Elastomer	210	11.7	5.6	5.0	—	—
Flame-Retarded TPR	400 ^A	3.9	-0.81	-0.58	—	-27
Polyamide Fibers	400 ^A	-2.0	-2.2	-1.5	—	—
Epoxy Based UV Acrylate	100 ^B	—	2.2	—	—	—
Urethane Based UV Acrylate	85 ^B	5.5	11.0	—	—	—
Fused Silica (Glass) Fiber	700 ^B	440	440	440	?	?
Copper	1083	92	92	92	NA	NA
Aluminum	700	1.27	1.27	1.27	NA	NA

1—Determined via Thermal Mechanical Analysis
2—Determined via Differential Scanning Calorimetry
A—Decomposition Temperature
B—Softening Point

In the case of the SFU, the optical fiber exhibits a dual coating of UV-curable acrylates. The primary coating increases dramatically in modulus with decrease in temperature, which at low temperature provides little or no buffering to an external axial load. It is known (from earlier experimentation) that the compressive forces generated by subjecting the acrylate protective coatings to low temperatures alone, does not cause excessive attenuation loss. This enhanced our need to understand the contribution to compressive strain from the SFU and Type 5 cable jackets, which it was deduced, must be the primary contribution to excess attenuation loss.

All samples which were placed in the Instron environmental test chamber displayed an increase in shrinkage force with decrease in temperature. This surprising test result caused us to determine the reproducibility and reliability of our test. This was accomplished by performing a full temperature cycle (ambient to +60 to -40 C and back to ambient within 30 minutes) on three separate samples. The peak force (including the preload force of 0.75 lb.) was 4.25, 4.30, and 4.40 lbs. for the force traces shown in Figures 6, 7, and 8 respectively. With the mean value of 4.32 for these three experimentally determined loads, the standard deviation (σ) is 0.07 for an overall deviation of approximately 1.8%. This is well within experimental error. Interesting to note, is that the shape of the curves in these three figures are almost identical, indicating similar rates of heating and cooling, and similar thermal-mechanical transitions

each time. All three samples were hollow tubes extruded from low molecular weight grade FEP, filled with orange colorant. All of the test data exhibited the same type curves with approximately the same reproducibility.

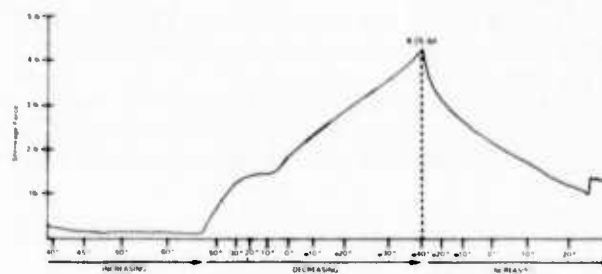


Figure 6

Force Curve For Single Fiber Unit (SFU) Outer Jacket Extruded from FEP w/ Orange Colorant. Temperature Cycle From Ambient to +60°C To -40°C Back To Ambient with 0.75 lb. Preload in Tension.

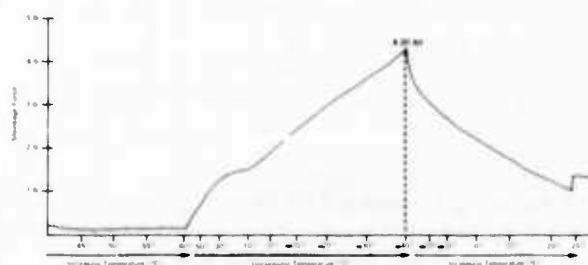


Figure 7

Force Curve For SFU Outer Jacket Extruded From FEP w/ Orange Colorant. Temperature Cycled As In Figure 6, With 0.75 lb. Preload in Tension

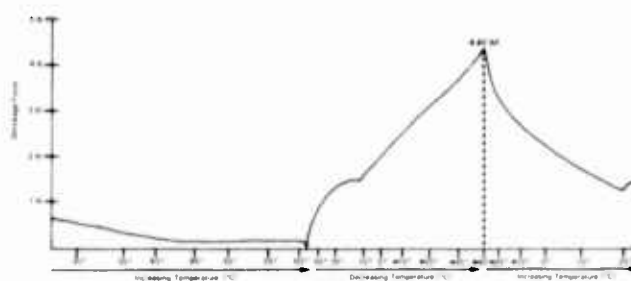


Figure 8

Force Curve For SFU Outer Jacket Extruded From FEP w/ Orange Colorant Temperature Cycled As In Figure 6, With 0.75 lb. Preload in Tension

The contrast between plenum and non-plenum SFU jacket shrinkages throughout the 0 to +60 C temperature range, is vivid-

ly shown when comparing Figures 9 and 10. Figure 9 is a typical force curve for a plenum orange colored FEP tubular section with approximately a .014" wall thickness, temperature cycled from ambient to +60 C and then cooled to only 0 C. The peak shrinkage force at the lowest temperature is 2.40 lbs. Figure 10 depicts a force curve obtained for the non-plenum orange colored polyurethane tubular section with the same approximate wall thickness, temperature cycled in the identical manner as the FEP tube. The peak shrinkage force at the same low temperature (0 C), is 0.5 lb. This is less than the original preload of 0.75 lb. It is obvious from this comparison that unlike the FEP, SFU jackets, the tendency is toward relaxation rather than shrinkage of the polyurethane jacket during temperature cycling from ambient to elevated temperatures.

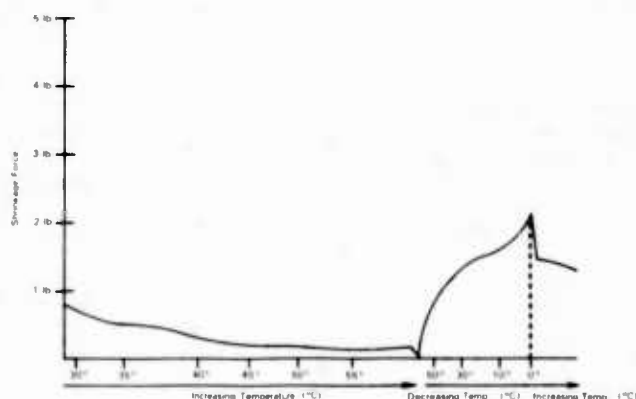


Figure 9
Typical Force Curve For SFU Jacket Extruded From FEP w/ Orange Colorant. Temperature Cycled From Ambient To +60°C To 0°C.

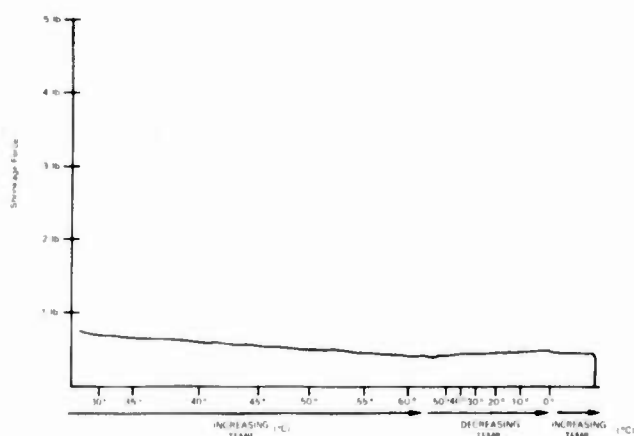


Figure 10
Typical Force Curve For SFU Jacket Extruded From Polyurethane w/ Orange Colorant. Temperature Cycled From Ambient To +60°C To 0°C.

When exposed to temperatures as low as -40 C, the polyurethane SFU jacket also displays a shrinkage force (see Figure 11). The peak

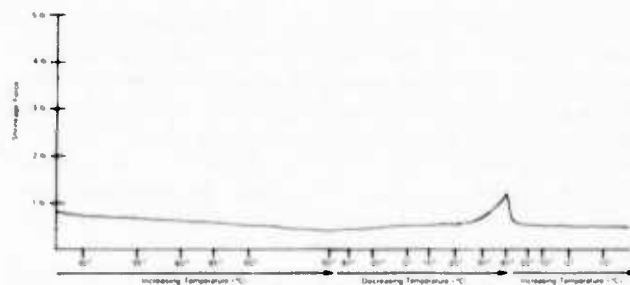


Figure 11
Force Curve For SFU Jacket Extruded From Polyurethane w/ Orange Colorant Temperature Cycled To -40°C.

force (at -40 C) occurs at 1.15 lb. - which includes the preload condition of .75 lb. The fact that some shrinkage force, which can act in a hysteresis type mode during repetitive temperature cycles, occurs with the polyurethane tube, reconfirms mathematical models and previous experiments^{4, and 12} which predict that even materials which exhibit low modulus at low temperatures can buckle due to shrinkage.

Next it was decided to look at a (previously thermally cycled) plenum SFU to determine changes that occur after temperature cycling from -40 to +60 C with the same sample over three continuous cycles. This data is presented in Figure 12 and illustrates the fact that each successive temperature cycle showed an increase in total shrinkage force from 4.30 to 4.85 to 4.95 lbs. on each excursion to -40 C. This is consistent with the attenuation loss during temperature cycling data found in Figure 4. After several temperature cycles (for the sample tested producing the force traces in Figure 12 the total number is unknown) to low temperatures, the shrinkage forces and attenuation losses seem to begin increasing. The critical value, in terms of this shrinkage force which leads to fiber buckling and subsequent macro/microbending and attenuation loss, is currently unknown. It is known, that without the use of proper antibuckling members as shown in the Type 5 cable constructions in Figures 2A and 2B, that fiber macrobending and fiber attenuation loss occurs. To determine the number of temperature cycles required to cause a successive increase in the shrinkage force measured in the Instron test fixture, a "virgin" (in terms of previous thermal history), sample of FEP plenum SFU tubing was temperature cycled three successive times. The results of this experiment are shown in Figure 13 and indicate that to reach the threshold of the shrinkage force increase with temperature cycling, requires greater than 3 full cycles. Again this is consistent with the typical attenuation loss findings depicted in Figure 4.

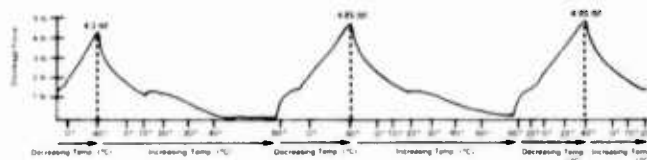


Figure 12
Force Curves For SFU Jacket Extruded From FEP w/ Orange Colorant With Previous Thermal Shock History. Three Successive Temperature Cycles From Ambient +60°C To -40°C To Ambient.

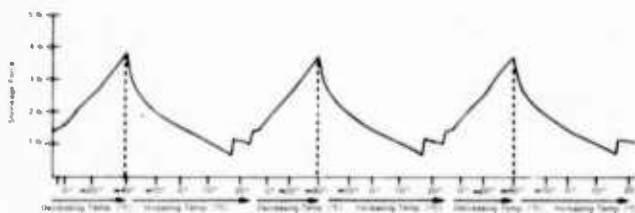


Figure 13
Force Curves for SFU Jacket Extruded From FEP w/Orange Colorant with No Previous Thermal Shock History. Three Successive Temperature Cycles Identical to Figure 12.

The last set of experiments with the FEP low molecular weight grade polymers were conducted on the outer jackets of the Type 5P cables. Temperature cycling in the Instron environmental chamber with a preload tension of 7.5, 4.0, 2.0, and 0.0 lbs., resulted in peak shrinkage force values which decreased from 30.0 to 27.5 to 21.0 to 18.2 lbs., respectively. All four measurements were made for jackets extruded under identical conditions by the same manufacturer, from the same cable reel. All samples were cycled in the Instron chamber in the usual, ambient to +60 to -40 C to ambient temperature cycle. The last two shrinkage force traces of the four measurements referred to above are shown in Figures 14A and B.

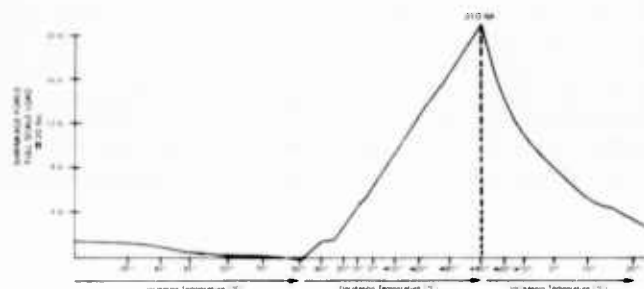


Figure 14 A
Force Curve for Type 5P Jacket Extruded From FEP w/Black Colorant. Temperature Cycled From Ambient to +60°C to -40°C to Ambient with 2.0 lb. Preload in Tension.

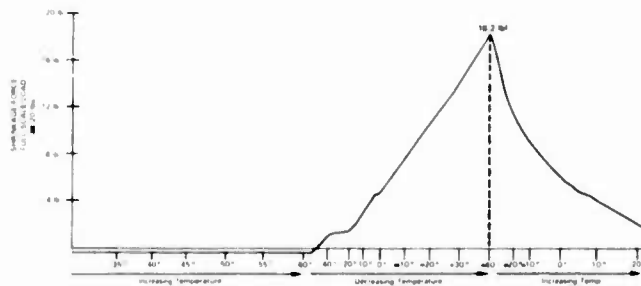


Figure 14B
Force Curve for Type 5P Jacket Extruded from FEP w/Black Colorant. Temperature Cycled from Ambient to +60°C to -40°C to Ambient with no Preload

A final point which correlates the magnitude of the shrinkage forces measured for the Type 5 outer jackets with those of the SFU jackets is seen by simple geometry calculations for the cross-sectional areas of the two tubes. Using the same sample lengths, the difference in magnitude of the cross-sectional area is identical with the total overall volume of FEP used in the tube. The example calculation which follows, shows a ratio of cross-sectional areas of the Type 5 outer jackets to the SFU's of approximately 6:1. The ratio of peak shrinkage forces of Type 5 outer jackets to the SFU's is approximately 5-6:1.

EXAMPLE CALCULATION

DIMENSIONS; Diam. of SFU = 2.8 mm;

Wall Thickness of SFU = .36 mm.

$$A_{\text{CROSS SECTIONAL}} = \pi r_o^2 - \pi r_i^2 = \pi (1.4)^2 - \pi [1.4 - .36]^2 \pm 2.76 \text{ mm.}$$

DIMENSIONS; Diam. of Type 5 Jacket = 7.5 mm;

Wall Thickness = .825 mm.

$$A_{\text{CROSS SECTIONAL}} = \pi r_o^2 - \pi r_i^2 = \pi (3.75)^2 - \pi [3.75 - .826]^2 \pm 17.30 \text{ mm.}$$

$$\text{Ratio} = 17.3/2.76 \pm 6:1$$

Final experiments were run using the polyester elastomer buffered fiber samples (located in the center of the SFU shown in Figures 1A and B). Using samples of 4" lengths including the full glass fiber construction, with a preload of 0.5 lb., four differently coated fibers were temperature cycled to -40 C in the now conventional manner. Figure 15 illustrates the shrinkage/relaxation curve for one of the typical buffered fibers which had no previous thermal history. The peak shrinkage force value for this sample was 1.55 lb., and careful inspection indicates that at high temperature (to 60 C), relaxation occurred (the force actually decreased). Comparison of this curve with curves of other polyester elastomer buffered fibers of different chemical morphology and with different thermal histories, revealed no significant differences.

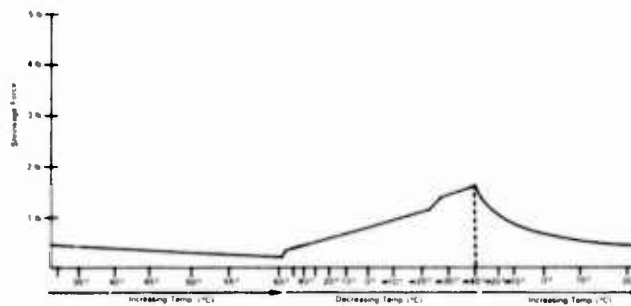


Figure 15
Typical Force Curve for "Virgin" Buffered Optic Fiber (Polyester Elastomer Buffer). Temperature Cycled from Ambient to +60°C to -40°C to Ambient with Preload of 0.5 Lbs. in Tension

3.2 Measurements of Thermal Transitions in Extruded, Filled Fluorinated Ethylene-Propylene Tubes Used in Single Fiber Unit (SFU) Constructions

Careful inspection of Figure 6, illustrating the force curve for a SFU jacket w/orange colorant, temperature cycled between +60 and -40 C, shows a significant change in the slope of the curve on cooling between 25 and 0 C. This is seen as well as on heating, where

the change is even more abrupt between 20 and 30 C. It is known that there is a change in thermal linear coefficient of expansion for FEP between the -40 to 0 C and 0 to 25 C temperature range and perhaps this phenomenon can be correlated with that change. More intriguing and perhaps just as important for long term optic fiber behavior, is the fact that Differential Scanning Calorimetry (DSC) on the same type SFU jacket, indicates a solid-solid secondary transition occurs between -10 and 10 C. This solid-solid transition has been reported by Eby and coworkers ¹³ and ¹⁴ at the National Bureau of Standards. They have found that two transitions, near 292 K (19 C) and 303 K (30 C), occur for the homopolymer of polytetrafluoroethylene (PTFE) when scanning with DSC, and that the two transitions apparently become one with addition of small concentrations of hexafluoropropylene comonomer units. The addition of 1.8-6.9 CF, units per 100 main-chain carbon atoms reduces the transition temperatures to 239-257 K (-34 to -16 C). Without any knowledge as to the specific CF, concentration in the low molecular weight FEP tubes extruded for SFU jackets, and only a logical guess (see figure 18 for DSC plot of recommended FEP colorant) that the addition of the orange inorganic pigment would raise the solid-solid transition temperature of our samples, it can only be theorized that the shifts in slope of the thermal-mechanical shrinkage force curves indicate this same transition.

Figure 16 A is a DSC plot for a typical "virgin" low molecular weight grade copolymer of polytetrafluoroethylene and hexafluoropropylene (FEP) extruded into a hollow jacket form with orange pigment as the only filler. This plot was obtained after taking a small cross-section of the hollow tube (weight of sample was approximately 25 mg.), encased in the aluminum pan, to +80 C and then quenching immediately to -40 C in liquid nitrogen. Due to the highly crystalline nature of the extruded, filled FEP sample, this was the only manner by which measurable thermal transitions occurred. Indium and Tin standards were used to calibrate the temperature shifts to within 1°C on the DuPont 1090 Thermal Analyzer throughout the course of these experiments. Figure 16B is just an enlargement of the transition area of interest.

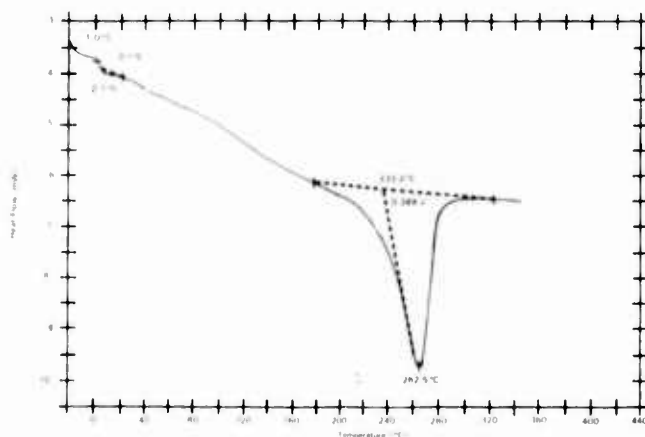


Figure 16A
DSC of "Virgin" SFU jacket (FEP)

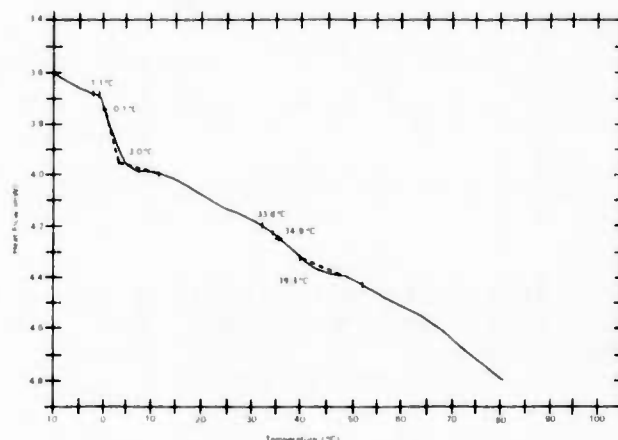


Figure 16B
DSC of "Virgin" SFU Jacket (FEP) Showing
Solid-Solid Crystal Transition Region.

Figure 17A is also a DSC plot, but for a typical SFU jacket FEP tube which had experienced several previous thermal cycles in the test setup diagrammed in Figure 3 and discussed in Section 2.1. An approximate 10 C temperature shift seems to occur in the solid-solid transition after temperature cycling. This same shift is seen by careful inspection of Figure 12. On heating from -40 C to +60 C in the Instron environmental chamber of the first versus the second and third cycles, the onset of the slope shifted from approximately 10 C to approximately 20 C. The precision of temperature measurement with this apparatus, as detailed before, was not sufficient to make direct comparisons with DSC results. Also interesting to note, and most prominently shown in Figure 17B, (an enlargement of the transition area in Fig. 17A) is the fact that pre-temperature cycling prior to DSC analysis seemed to sharpen the solid-solid transition.

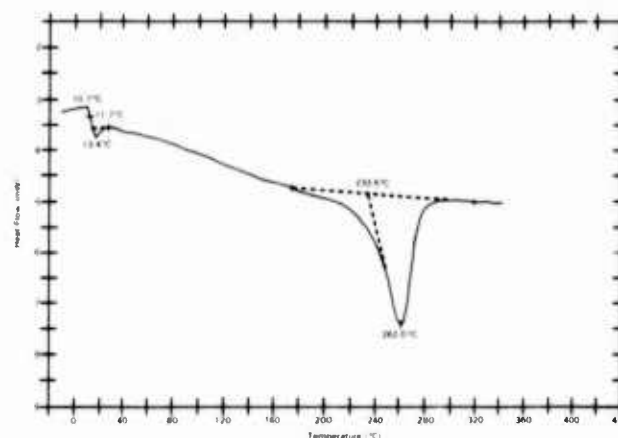


Figure 17A
DSC of Pre-Temperature Cycled SFU
Jacket (FEP)

Both figures 17A and B were obtained by first heating the sample to +80 C and then quenching immediately in liquid nitrogen to -40 C, as before. The sample was then heated at 10 C/min. through the meltpoint. Another laboratory¹⁵ has confirmed the presence of this solid-solid transition in the temperature range of -4 to -6.5 C. Their runs were made using 35 mg. samples which were heated to 290 C and left isothermally at that temperature for 60 minutes. The scans which produced transitions at the temperatures stated above, were from -60 to +100 C at a rate of 5 deg/min.

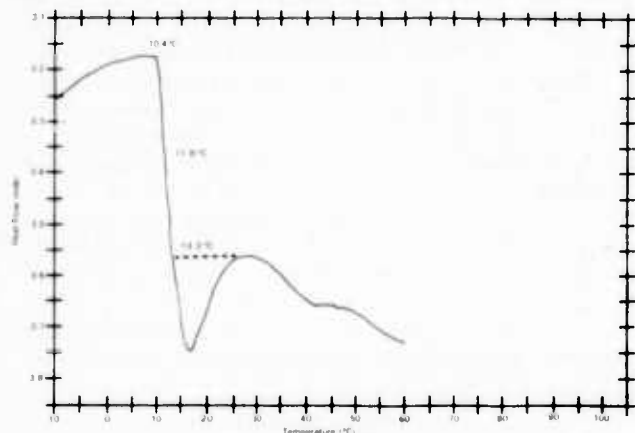


Figure 17B
DSC of Pre-Temp Cycled SFU Jacket (FEP)
Showing Solid-Solid Crystal Transition Region

Figures 18 and 19 are DSC plots most recently run on both the FEP orange pigment and the unfilled "virgin" resin respectively. It is evident that part of the difference between the temperature reported for solid-solid transitions in FEP and those seen for the extruded orange tubes, is explained by comparison of these two figures. Figure 18 illustrates an approximate +10 C shift in the solid-solid transition (17.9 C) compared with that of the virgin resin seen in Figure 19 (7.6° C). In addition to the fact that there may be greater than 6.9 CF₂ units per 100 main-chain carbon atoms in the orange pigmented extruded FEP tubes, (reported to have a -16 C solid-solid transition), the addition of orange pigment is partly responsible for the positive shift in the transition temperature.

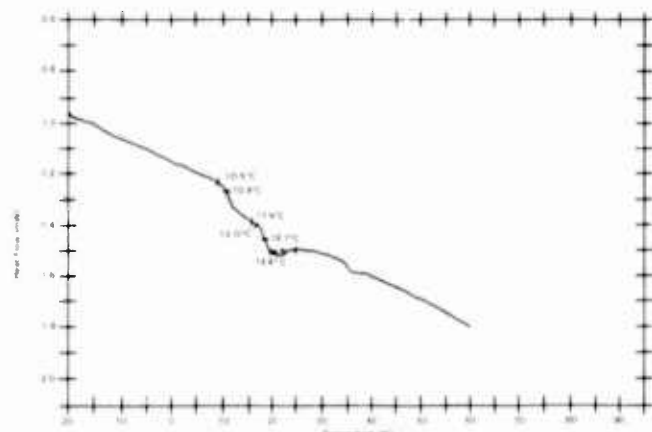


Figure 18
DSC Plot of Transition
Temperature Region for
Orange FEP Pigment

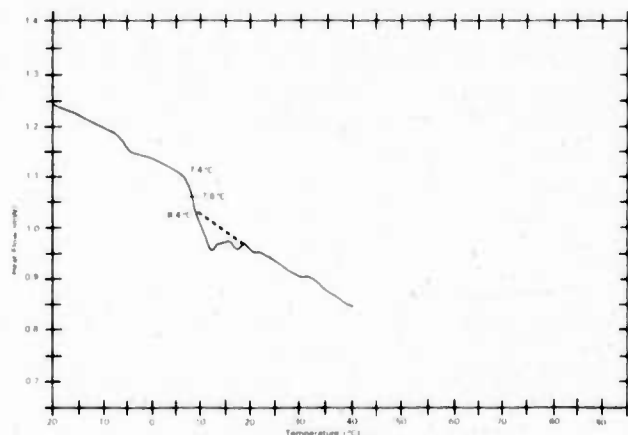


Figure 19
DSC Plot of Transition
Temperature Region for
"Virgin" FEP Resin

A final experiment was tried with a "virgin" FEP SFU jacket filled with the same orange pigment. This time the sample was temperature cycled from -40 to +80 C five successive times and scanned at a rate of 10 C/min. For the first four cycles no changes in the solid-solid transition occurred. On the fifth cycle, however, a downward shift of approximately 18 C was found. This data is reproduced in Figures 20 A, B, C, and D (cycles 2-5). In all, it is impossible to understand the effect of thermal cycling on the solid-solid transition in the orange pigmented FEP fiber jacket without additional studies. It is also difficult to understand what affect (if any), a temperature shift in the solid-solid crystal transition of FEP would have on overall fiber performance. Eby and coworkers¹³ reference several articles which state that this transition affects specific volume - as can be deduced from the shrinkage force curves presented here - as well as dielectric constant, heat capacity, N.M.R. spectrum, modulus of longitudinal ultrasonic waves, and other spectroscopic properties of PTFE. Based on these studies, it is important that further work be performed to more fully understand the effects of these transitions on FEP polymer properties. A final note of interest is that Eby and coworkers¹³ found that, with the exact same FEP

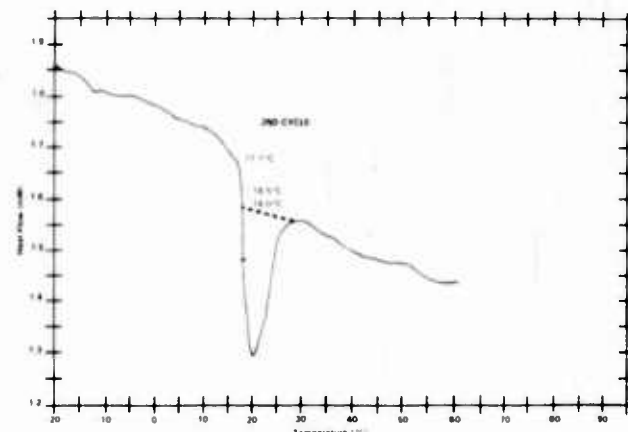


Figure 20A
Second Temp. Cycle for Orange Pigmented
FEP Single Fiber Unit (SFU) Jacket

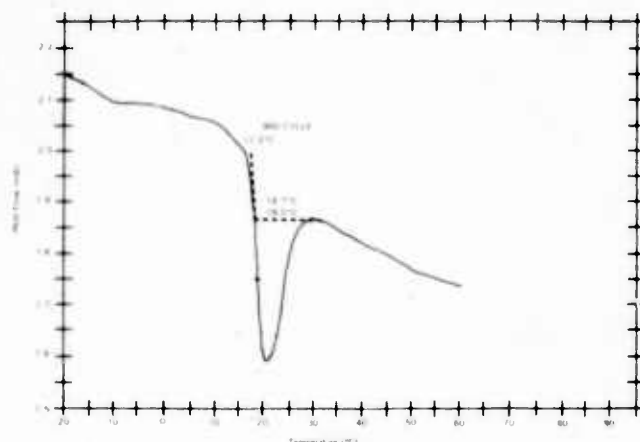


Figure 20B
Third Temp. Cycle for Orange Pigmented
FEP Single Fiber Unit (SFU) Jacket

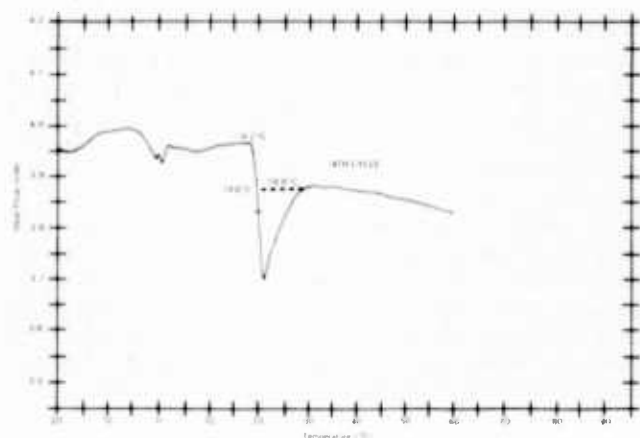


Figure 20C
Fourth Temp. Cycle for Orange Pigmented
FEP Single Fiber Unit (SFU) Jacket

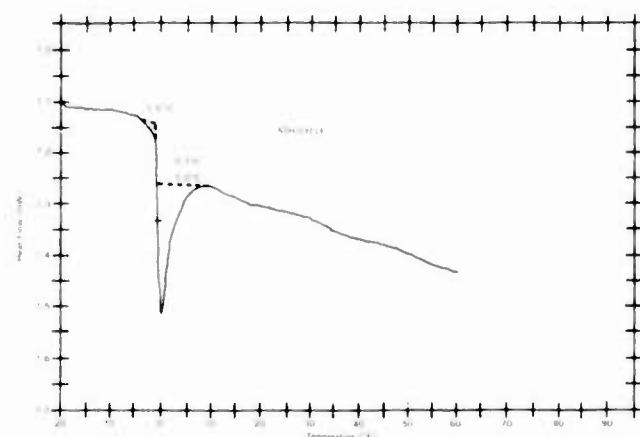


Figure 20D
Fifth Temp. Cycle for Orange Pigmented
FEP Single Fiber Unit (SFU) Jacket

copolymer composition, the rate of cooling from the melt changed the measured solid-solid transition as much as 8°C. Unless extrusion processes are controlled to a greater extent, there is no doubt that the crystal transition temperatures along a tube length of fluoropolymer will vary.

IV. Conclusions and Recommendations for Future Studies

4.1 Conclusions

Several different cable jackets extruded from a low molecular weight grade of FEP (fluorinated ethylene-propylene) were sectioned into approximate 8" (6.5" gauge lengths) lengths and temperature cycled from +60 to as low as -40°C. A novel measurement of shrinkage forces within the geometric configurations shown in Figure 5B seemed surprisingly high at the low end of the temperature scale. The increase in shrinkage force was found to be directly proportional to the diameter and wall thickness (i. e., total volume of FEP in the 6.5" gauge length tube) of the temperature cycled sample. Therefore a direct correlation with the thermal coefficient of expansion of the polymer in a specific temperature range was obtained. At the high end of the temperature range (above +40°C), the FEP jacketing expanded somewhat (indicating a positive thermal expansion coefficient) and resulted in reduction of the shrinkage force.

In testing to subzero temperatures with no preload, significant (order of magnitude) differences were not seen in shrinkage forces when compared with moderately preloaded (.5-.75 lbs. tension) samples. It was previously expected that the preload would have a large effect on the total measured shrinkage force. If any trend can be determined from the initial work performed (referring specifically to Figure 12), it seems as though the shrinkage forces increase after continuous temperature cycling of FEP jacketing. This trend is consistent with attenuation loss data collected for the plenum cable design (Figure 4).

All polyester elastomer buffered optical fiber samples shrink at low temperatures and relax at high temperatures, but the forces associated with these samples are significantly less than that found for the FEP jackets. Again, this is partially attributed to the smaller diameter of the polyester buffer ($0.9 \pm 0.5\text{mm}$).

In addition to the obvious volume changes of FEP based on shrinkage force testing of the various tubular jackets, solid-solid crystal transition temperatures, determined via Differential Scanning Calorimetry (DSC), correlate with change in slope of the shrinkage force curves. Whether these correlations indicate changes in the thermal expansion coefficient of the FEP in that temperature range or indicates the test method is sensitive enough to distinguish solid-solid crystal transitions in the polymer, is unclear.

4.2 Recommendations for Future Studies

Several experimental needs for further understanding became clear during the course of this work. First, it is important to measure the actual transmission of strain on the glass fiber during shrinkage of the FEP outer jackets as the temperature in the environment drops. Adequate fiber optic strain gauges must be developed to determine what actual axial critical force due to shrinkage (if any) can be tolerated.

Second, some initial work has been carried out, involving finite element analysis of the single fiber unit (SFU) construction, to determine mathematically, the ultimate stress-strain values transmitted to the glass fiber assuming linear relationships. Further work, requiring non-linear finite element analysis and subsequent laboratory tests could prove invaluable in future plenum tight buffer fiber optic cable designs.

Finally, a more detailed understanding of how thermal transitions, (such as the solid-solid crystal transitions reported for FEP), in various fluorinated polymer blends affect fiber attenuation (if at all) over time, is required.

List of Sources Cited

1. Grune, G.L. "Material Requirements for Multimedia Communications Cable", International Wire and Cable Symposium Proceedings, Nov. 1983, pp. 225-267.
2. Smith, J. "Manufacturing Methods and Technology Program for Ruggedized Tactical Fiber Optic Cable", Sixth Progress Report for Period April 1981 - June 1981, CORADCOM, Fort Monmouth, N.J., Report No. - 79-0789-6A.
3. Taylor, D. "Manufacturing Methods and Technology Program for Ruggedized Tactical Fiber Optic Cable", Seventh Progress Report for Period July 1981 - Sept. 1981, CORADCOM, Fort Monmouth, N.J., Report No. - 79-0789-7A.
4. Garmon, P., "Analysis of Excess Attenuation in Optical Fibers Subjected to Low Temperatures", International Wire and Cable Symposium Proceedings, Nov. 1983, pp. 134-143.
5. Katsuyama, Y., Mitsunaga, Y., Ishida, Y., and Ishihara, K., "Transmission Loss of Coated Single - Node Fiber at Low Temperatures", *Applied Optics* 19, 24, pp. 4200-4205, 1980.
6. Blyler, L. L., Gieniewski, C., Quan, X., and Ghoneim, H., "Buckling of Optical Fibers Within Elastomers Used in an Embedded - Core Cable Structure", International Wire and Cable Symposium Proceedings, Nov. 1983, pp. 144-150.
7. Wagatsuma, M., Okazaki, H., Kimura, T., and Yamakawa, S., "New Thermoplastic Dual Coextrusion - Coating System for Optical - Fiber Drawing", *Electronic Letters*, 20, No. 5, Mar. 1984, pp. 198-199.
8. Young, D. and Jun, R., "Environmental Effects on Acrylate Coated Optical Fibers", International Wire and Cable Symposium Proceedings, Nov. 1981, pp. 51-57.
9. Santana, M. R., and Lovelace, C. R., "Transmission - Loss Performance of Three Optical Fiber Coatings in a Ribbon Structure", 5th Optic Fibers Conference (OFC), 1982, p. 40.
10. Blyler, L., Jun, L., Hart, A., Jun, C., Levy, A., Santana, M. R., and Swift, L. L., "A New Dual Coating System for Optical Fibers", 8th ECOC, 1982, pp. 245-249.
11. Yamakawa, S., Shuto, Y., and Yamamoto, F., "A New Zero Linear Expansion Coefficient Tight Jacket Optical Fiber", 9th ECOC, 1983, pp. 227-230.
12. Yamakawa, S., Shuto, Y., and Yamamoto, F., "Transmission Loss of Thermotropic Liquid - Crystal Polyester - Jacketed Optical Fiber at Low Temperature", *Electronic Letters*, 20, No. 5, Mar. 1984, pp. 199-201.
13. Weeks, J. J., Sanchez, I. C., Eby, R. K., and Poser, C. I., "Order - Disorder Transitions in Polytetrafluoroethylene", *Polymer*, 21, Mar. 1980, pp. 325-331.
14. Weeks, J. J., Eby, R. K., and Clark, E. S., "Disorder in the Crystal Structures of Phases I and II of Copolymers of Tetrafluoroethylene and Hexafluoropropylene", *Polymer*, 22, Nov. 1981, pp. 1496-1499.
15. Personal Correspondence with Dr. L.W. Buxton, E.I. DuPont de Nemours Co., Fluoropolymers Research Laboratory, Washington Works Facility, Wilmington, DE.



G. L. Grune
IBM Corp.
Polymers Group (E79)
Research Triangle Park, N. C. 27709

About the Authors

Guerry L. Grune obtained his B.S.M.E. from Duke University, 1978 (graduation with distinction) with a double major (A.B.) in Chemistry the same year. After working for Fiber Industries Incorporated, a subsidiary of Celanese and ICI of Great Britain, from 1978-1980 in the heavy denier polyester filament and liquid crystal high modulus organic fiber groups, he returned to graduate school at the University of Massachusetts. There, he obtained his M.S.Ch.E. (1982) from the Departments of Chemical Engineering and Polymer Science and Engineering working under Dr. Robert W. Lenz in the area of thermotropic liquid crystals. Upon finishing his M.S. degree requirements in May, 1982, he joined the IBM-Raleigh Materials Laboratory, and has been associated with materials selection and development for LAN cable, fiber optics and the connector systems which will be used for the project.



L. A. Hilliard
IBM Corp.
Analytical Chemistry Group (E62)
Research Triangle Park, N. C. 27709

Leslie A. Hilliard attended North Carolina Central University majoring in Chemistry. He joined IBM in 1966 as a final tester for the IBM 1060. He is currently employed as a Senior Laboratory Specialist in the IBM-RTP Materials Laboratory.

Acknowledgements

The authors would like to acknowledge the diligence of Mr. Mark Young, who was responsible for development and testing of the shrinkage forces in the Instron environmental chamber. He helped create a novel approach to testing materials for plenum, tight buffered fiber optic applications.

Others who helped with discussions and suggestions for completion of this study, include Mr. R. Deveraux Munn — who initially requested this study in an effort to understand fiber optic connector problems. Also, the following deserve our gratitude;

Mr. Michael See — IBM, RTP
Mr. Bert Weidle — IBM, RTP
Mr. R. Benton Hobgood — IBM, RTP
Mr. Omer King — IBM, RTP
Mr. Sam Wallace — IBM, RTP
Mr. L. Douglas Hobgood — IBM, RTP
Dr. Roger C. Sanwald — IBM, RTP
Mr. Andrew Cooke — IBM, RTP
Mr. W. R. Wagner — IBM, RTP

IMPROVED COMPOSITE FIBER-OPTIC OVERHEAD GROUND WIRE

Yasunori Saito, Mahito Ishikawa, Saburo Kawabata, Yoshinobu Kitayama

Sumitomo Electric Industries, Ltd.
1, Taya-cho, Totsuka-ku, Yokohama, Japan

Abstract

A composite fiber-optic overhead ground wire (OPGW) containing single-mode optical fibers with a pure silica core and a fluorine-doped cladding, fixed within the spiral grooves of an aluminum spacer with an elastic material has been developed. As fibers in this OPGW are not susceptible to the local concentration of stresses caused by shrinkage, elongation and vibration of the OPGW, this new OPGW has higher reliability and possesses the following advantages: (1) The transmission characteristics of the optical fiber are extremely stable, (2) Longer lifetime of the optical fiber is expected.

1. Introduction

It is required in electrical power companies to establish digital communication systems for automatic control of power supplying networks. For this purpose, a composite fiber-optic overhead ground wire (OPGW)¹⁾ is an ideal transmission medium because of its low transmission loss, wide bandwidth, immunity to electromagnetic interference, etc. An OPGW is expected to be used not only for system protection and control of overhead transmission systems but also for new telecommunication networks. In this case single-mode fibers may be required for large capacity transmission. An OPGW has already been reported²⁾ to have sufficient performance to establish a high-speed digital transmission network which withstands actual operating conditions such as wide temperature variation, vibrations and large strain.

In this paper, a new design of OPGW is proposed for better performance. The OPGW contains single-mode fibers with a pure silica core and a fluorine-doped cladding. The optical fibers are fixed within the spiral grooves of an aluminum spacer with a heatresistant elastic material.

2. Cable design

Cable Structure

The optical fiber cable combined with a ground wire is exposed to severe conditions such as wide temperature variations, large strain and vibration. If an optical fiber cable is loosely

housed and can move freely longitudinally as shown in Figure 1, it is possible for the optical fibers to be subjected to the local concentration of stresses. In the conventional OPGW we chose spacer structure to prevent above problem. Figure 2 shows the cross section of the OPGW. Optical fibers are housed individually within a spiral groove of an aluminum spacer. In this composition uniform friction between optical fibers and aluminum spacer is important to prevent local concentration of distortion to the optical fibers against various kinds of external stresses, such as shrinkage, elongation and vibration. In the conventional OPGW, moderate friction exists between optical fibers and the aluminum spacer. This type of OPGW was confirmed through laboratory and field tests to have stable transmission characteristics in practical use. But it is preferable to fix the optical fibers to the aluminum spacer in case of

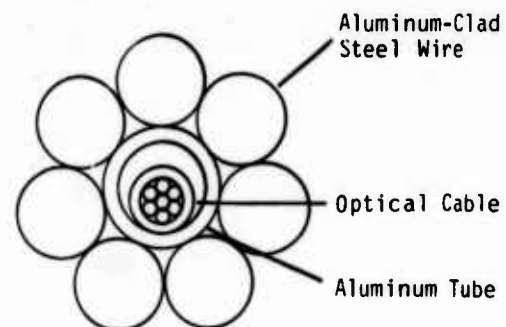


Fig. 1 Cross Section of OPGW (Non-Spacer Type)

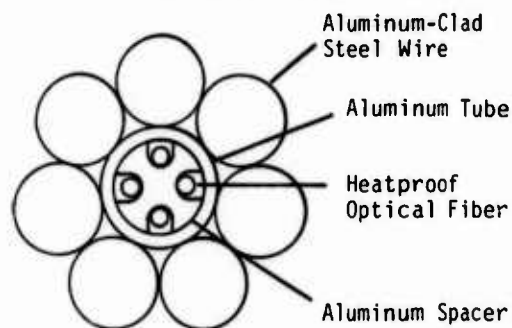


Fig. 2 Cross Section of OPGW (Spacer Type)

unexpected harsh conditions applied to the installed OPGW.

Based on this concept, the new OPGW featuring optical fibers and ground wires that move as a single body against external stress has been designed. Figure 3 shows the typical design of the new OPGW. This OPGW contains five doubly-coated single-mode fibers. Each of the five optical fibers is housed individually within the spiral grooves of an aluminum spacer and tightly fixed with a heatresistant elastic material filled within each groove. The aluminum spacer is covered with a hard aluminum tube. The optical fiber unit is then housed at the center of aluminum-clad steel wires.



Fig. 3 Photograph of New OPGW

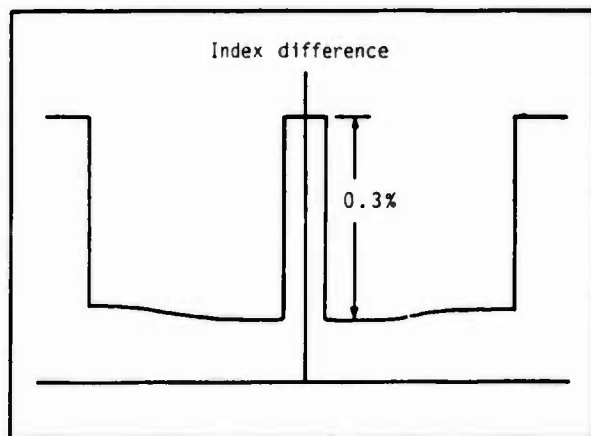


Fig. 4 Preform Refractive Index Profile

Optical Fiber

Single-mode fibers used in the OPGW have a pure silica core and a fluorine-doped cladding with a negative index difference $\Delta n = \sim 0.3\%$ and diameter $d = 125\mu\text{m}$. They are fabricated by the VAD method. The cladding to core diameter ratio is about 10. Figure 4 is an example of the fiber's refractive index profile. Transmission loss of the optical fiber is less than 0.5 dB/km at $1.3\mu\text{m}$.

The optical fiber is coated with an inner layer of room-temperature vulcanized silicon with a $400\mu\text{m}$ outer diameter and an outer layer of standard grade fluorocarbon polymer (ETFE) with a $700\mu\text{m}$ outer diameter to improve heatresistant properties of the optical fiber. This heatresistant optical fiber is able to withstand a continuous operating temperature of 100°C (momentary fluctuations to 250°C). By utilizing higher grade fluorocarbon polymer (PFA), the optical fiber can withstand a continuous operating temperature of 150°C (momentary fluctuations to 300°C)².

3. Cabling

Throughout the cabling process, no transmission loss deterioration was observed. Figure 5 shows an example of spectral transmission losses before and after the cabling process. Even at the longer wavelength of approximately $1.5\mu\text{m}$, when the V-value is decreased and the fiber is sensitive to the bend loss, there was no loss change.

4. OPGW Characteristics

Mechanical Characteristics

Lateral compression force was applied to 5cm optical fiber unit to estimate the compression force resistance. Figure 6 shows transmission loss increase against compression force for the

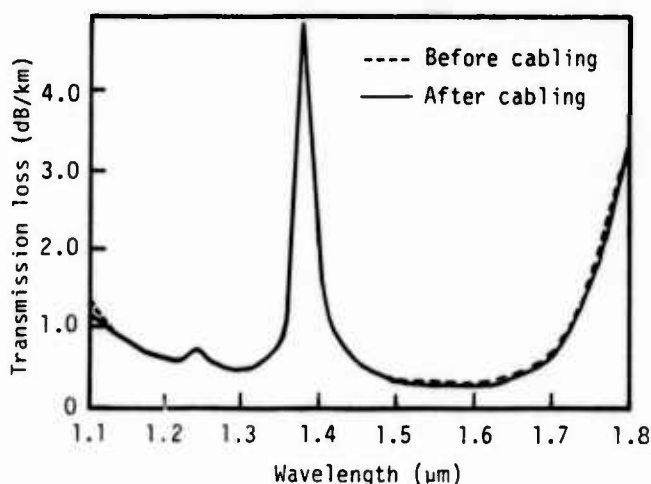


Fig. 5 Transmission Loss Change during Cabling

optical fiber unit. It was confirmed that the optical fiber unit can withstand compression force of more than 1000kg/5cm and provide rigid protection against external mechanical force.

A tensile test was conducted on an 80mm² OPGW. The length of the OPGW tested was 150m and tension was applied until the OPGW was broken. During this test procedure, the transmission loss of the optical fiber was monitored. The result of this test shows that no change in transmission loss occurred even just prior to the breaking point of OPGW because the optical fiber is uniformly elongated together with the aluminum spacer against tensile load and is not subject to local concentration of distortion.

Furthermore to confirm the endurance capability of OPGW against vibration after installation, a 30m OPGW was vibrated at 10⁶ times under a simulated turbulent condition (frequency: 10Hz, amplitude: 5mm). No change in transmission loss was observed during this test. It is confirmed that the optical fiber is not subjected to macro- and microbending during vibration of OPGW because it is fixed to the aluminum spacer and cannot move within the spiral groove.

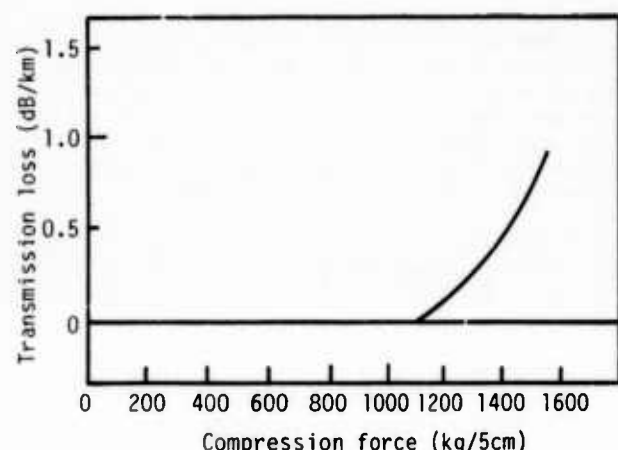


Fig. 6 Compression Force and Transmission Loss Change for Optical Fiber Unit

Temperature Characteristics

Temperature dependence of transmission loss at 1.3μm was measured on an optical fiber unit in a chamber. Transmission loss change is shown in Figure 7. The deterioration of transmission loss was less than 0.1 dB/km over the temperature range from -40°C to 100°C, which is well within the permissible range.

An arc discharge test was conducted on an 80mm² OPGW to investigate the effect of heat-shock stress and flashed light resulting from lightning on the OPGW. A 15m-long OPGW was subjected, in its midpoint, to an arc discharge with discharge currents up to 5.5kA and discharge holding time of 0.1 second. Although the stranded aluminum layer of the OPGW melted, there was no change at all in transmission loss of the optical fiber, nor any

6.3 Mb/s pseudo random pulse transmission error.

A short-circuit test was conducted to simulate accidental fault current in power transmission lines. Alternating current of 9kA was applied to the 2m-long OPGW for one second after the conductor temperature was raised and kept constant at 100°C by current. Although the conductor temperature rose to 230°C, no detectable loss change of the optical fiber was observed.

As the result of an arc discharge and a short circuit test, it was confirmed that the optical fiber was not susceptible to local concentration of stress and maintained stable transmission characteristics against heat shock stress.

To estimate infra-red loss increase in silica optical fiber due to the chemical reaction of hydrogen³⁾, an optical fiber unit was exposed to a temperature of 200°C for 24 hours. The mechanism of infra-red loss increase in coated

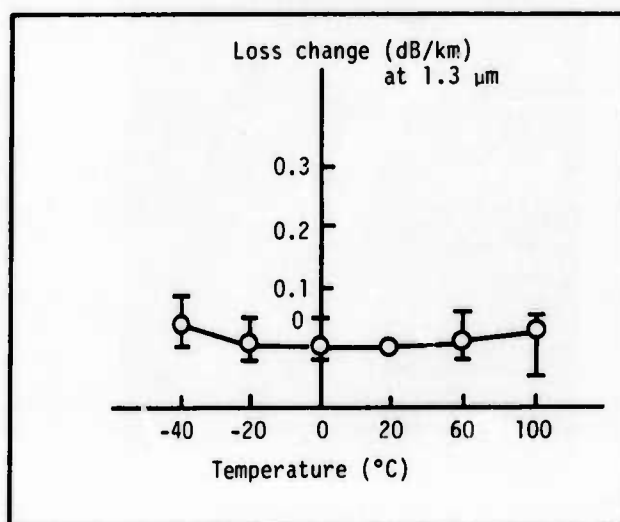


Fig. 7 Temperature Dependence of Transmission Loss Change for Optical Fiber Unit

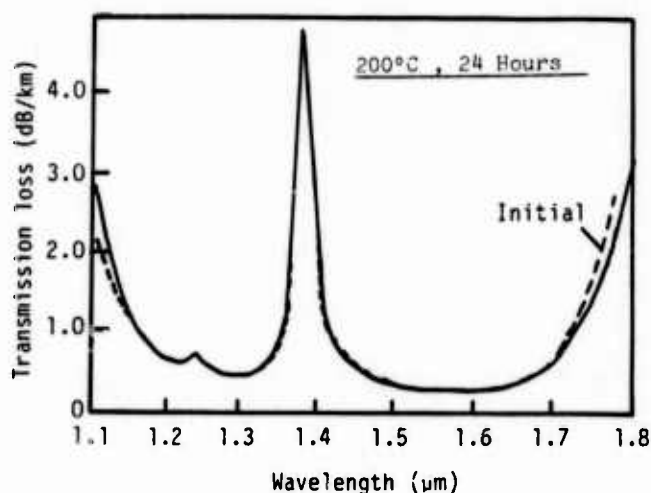


Fig. 8 Loss Spectra after Heat Treatment

fibers with heat treatment can be estimated as follows: Hydrogen atoms in the fiber, which are produced by diffusion of dissolved gas from coating and filling materials, or contained as impurities, are trapped to defects in the glass. As a result the glass structure changes, a new set of absorption peaks are observed, such as a peak at $1.4\mu\text{m}$ which corresponds to the overtones of Si-OH and Ge-OH absorption. A single-mode fiber with a pure silica core have fewer defects in the glass than a GeO_2 -doped fiber. Figure 8 shows loss spectra obtained by the heat treatment at 200°C . No significant infra-red loss change was observed even for an optical fiber unit with an airtight construction.

5. Conclusion

A composite fiber-optic overhead ground wire (OPGW) containing single-mode fibers with a pure silica core and a fluorine-doped cladding, fixed within the spiral grooves of an aluminum spacer with an elastic material has been developed. The OPGW has the advantageous feature of non-susceptibility to the local concentration of various kinds of stresses caused by shrinkage, elongation and vibration of the OPGW. This OPGW, which is expected to have high reliability, has extremely stable transmission properties.

Reference

- (1) M. Igarashi, J. Yokoyama, H. Iwamura, N. Mori, I. Matsubara, Y. Saito, "Composite Fiber-Optic Overhead Ground Wire", Proc. of 29th I.W.C.S., 1980
- (2) S. Kubota, H. Kawahira, T. Nakajima, I. Matsubara, Y. Saito, Y. Kitayama, "Field Trial of Composite Fiber-Optic Overhead Ground Wire", Proc. of 32nd I.W.C.S., 1983
- (3) N. Uchida, N. Uesugi, Y. Murakami, M. Nakahara, T. Tanifuji, N. Inagaki, "Infrared Loss Increase in Silica Optical Fiber due to Chemical Reaction of Hydrogen", 9th E.C.O.C. post deadline contents, 1983



Yasunori Saito
Sumitomo Electric
Research Triangle, Inc.
P.O. Box 13445
Research Triangle Park,
N.C.
27709, U.S.A.

Yasunori Saito received his B.S. degree in Electrical Communication Engineering from Tohoku Univ. in 1969. He then joined Sumitomo Electric Industries and has been engaged in research and development of high frequency transmission lines including fiber optics. Mr. Saito is a manager engineering of Sumitomo Electric Research Triangle, Inc., and a member of the Institute of Electronics & Communication Engineers of Japan



Mahito Ishikawa
Sumitomo Electric
Industries, Ltd.
1, Taya-cho,
Totsuka-ku,
Yokohama, Japan

Mahito Ishikawa received the B.E. degree in metalurgical engineering from Tohoku Univ. in 1969. He then joined Sumitomo Electric Industries and has been engaged in the development of production engineering of communication cable. Mr. Ishikawa is now a assistant manager of the production and plant engineering section of communication cable division.



Saburo Kawabata
Sumitomo Electric
Industries, Ltd.
1, Taya-cho,
Totsuka-ku,
Yokohama, Japan

Saburo Kawabata joined Sumitomo Electric Industries in 1968 and has been engaged in design and development of communication cable equipment. Mr. Kawabata is a member of production and plant engineering section of communication cable division.



Yoshinobu Kitayama
Sumitomo Electric
Industries, Ltd.
1, Taya-cho,
Totsuka-ku,
Yokohama, Japan

Yoshinobu Kitayama received his M.S. degree in Electrical Engineering from Kyoto Univ. in 1982. He then joined Sumitomo Electric Industries and has been engaged in research and development of optical fiber and cables. Mr. Kitayama is a member of Yokohama R & D Group, and a member of the Institute of Electronics & Communication Engineers of Japan.

PROGRESS IN THE DEVELOPMENT OF AN E-CFTE JACKETED HIGH TEMPERATURE FIBER OPTIC CABLE

David R. Maack

Stanley P. Dudek

Ted Allsworth

EOtec Corporation
West Haven, CT

Allied Chemical Co.
Morristown, NJ

Deutsch
Los Angeles, CA

SUMMARY

An E-CFTE fluoropolymer fiber-optic cable has been developed for use with an expanded beam optical pin which inserts directly into a Mil-C-38999 Series IV electrical connector. Change in loss at -65°C for 40 meters of cable and a splice is less than 2db even after multiple temperature cycles from room temperature. The upper temperature limit of the cable is currently 125°C due to the constraints imposed by the urethane-acrylate buffer coatings on the fiber.

This cable was developed in two stages. First, various E-CFTE formulations were run under a number of processing conditions in order to select the best formulation and its optimum process conditions. The second stage involved the design and testing of a cable to fit the optical connector pins.

I. INTRODUCTION

The high bandwidth-low loss fiber optic race so prevalent in telecommunications has dominated designers' thinking that proper perspective has sometimes been lost in a number of speciality areas where other parameters are more important. A good example of this is the aerospace and airframe industries where the need for kilometer length links is currently non-existent. Parameters which could be much more important than the absolute attenuation per kilometer are link stability, environmental resistance, mechanical parameters, temperature range, excess power budget, and ability to replace existing wire systems. In addition, the cable is only one part of an optical transmission system which includes connectors and as such should be specified and measured as a system.

The development of this cable began with the introduction of a series of expanded beam fiber optic pins designed to fit in the existing Mil-C-38999 Series IV electrical connector system thereby precluding the need for a special fiber optic connector. The design of these pins is such that no additional parts except the pins themselves and their backshells, and no additional tools except a scribe tool are required. It uses the same connector bodies, seals, assembly tools and procedures as the wire system. This placed the constraint on the fiber optic cable that it too had to look and act like its wire counterpart both in performance and dimensions. Consequently, existing wire and cable mil-specs with minor modifications may now be applicable to fiber optic cables. Figure 1 shows the system.



Figure 1 - Cable - Connector System

The mechanical, chemical, and temperature requirements of many of the potential applications dictate the use of a miniature, fluorocarbon cable construction whose dimensions would not only fit the new Mil-C-38999 type optical pins, but would allow retrofit to existing wire systems. None of the current available fiber optic cables fit all of these requirements, therefore, one had to be developed. Unfortunately, miniature fluorocarbon fiber optic cables which exhibit stable optical performance over wide environmental conditions are very difficult to produce. In addition, most work reported to date has been specifically targeted at the plenum cable market whose requirements are based, in part, on the need for long lengths.

When used in fiber optic cables, fluorocarbons have a number of intrinsic properties which can cause excessive microbending and a resultant increase in optical attenuation. This is due to two fundamental mechanisms generally observed in all thermoplastics. First is the thermal coefficient of expansion (ICE) difference between the plastic materials and the silica fiber. The second is a permanent post processing shrinkage phenomena that is highly dependent on the time-temperature history distribution of each increment of material. The major difference between the fluorocarbons and the more commonly used materials such as PVC and polyurethane is the magnitude of the shrinkage forces that can be generated. Typically, fluorocarbons are 10 to 100 times as strong as other materials.

The effect of the thermal coefficient of expansion is primarily observed as a reversible increase in loss as temperature is lowered. Consequently, a fluorocarbon with a low ICE is crucial. Complicating this issue, however, is a number of molecular transitions, or changes of state, that fluorocarbons go through over the temperature range of interest. Not only is the ICE above and below these transition temperatures different, it can change very rapidly about the transition temperature.

The permanent post processing shrinkage exhibited by thermoplastics is primarily due to stresses created and frozen into the compound during processing. These stresses are then slowly relaxed over time and manifest themselves as a gradual shrinkage. Temperature cycling, especially through a transition temperature accelerates this and can cause significant optical attenuation

increases. Minimization of this effect requires not only a fluorocarbon which exhibits low shrinkage, but processing parameters which minimize the formation of these stresses.

The selection of E-CIFE, as the material for this cable, was based on a comprehensive study of available fluorocarbon materials coupled with extensive cabling experience. The key properties of E-CIFE as they relate to use in a fiber optic cable are:

- Low moisture absorption
- Long term property stability
- Low coefficient of thermal expansion
- Broad range between transition temperatures
- Multiple-grade availability
- Lower post extrusion shrinkage
- High damping factor at transition temperatures

Fiber selection was extremely limited due to the few qualified sources of supply. Although the silica itself has no problem with any of the requirements, its coatings presently represent a serious limitation. Available coatings consist of urethane-acrylate or urethane-epoxy thermoset polymers whose upper temperature range is limited above 100°C. In addition, both of these coating materials exhibit a significant change in static and dynamic modulus as the temperature drops and cause increased microbend sensitivity. This coupled with the problems of the fluorocarbons can result in very large optical attenuation increases.

The fiber selected for the material-process portion of this study was double buffered Corning 100/140. It was chosen for its higher microbend sensitivity so that small and secondary cabling problems would result in large attenuation increases. The fiber that was fabricated into the final cable was double buffered Corning 85/125. It was chosen to match the optical requirements of the connector pins.

II. MATERIAL-PROCESS STUDY

Currently, most materials and processes used to make fiber optic cables originate out of the wire and cable industry and, as such, have been highly developed for the specific purpose to make wire. Since the constraints of an

optical fiber are significantly different than those of a copper conductor, i.e., microbending vs. dielectric strength, it stands to reason that these materials and processes are not optimized for fiber. Consequently, a study specifically designed to identify and optimize the material properties of the E-CIFE fluorocarbon was undertaken.

The details of the construction tested are shown in Figure II. Double buffered Corning 100/140 fiber was coated to a diameter of 900um with various formulations of E-CIFE. Multiple samples of each formulation were made under various processing conditions and then tested. Specific parameters examined were:

- o E-CIFE Formulation
- o Extrusion temperature profile
- o Extrusion tooling design
- o Post extrusion cooling

All extrusion work was performed on a 3/4" line specifically designed for fiber optics.

The evaluation procedure consisted of measuring optical loss on each sample between every operation on a Laser Precision OTDR. Multiple cleaves and readings were taken for each data point in order to reduce the possibility of errors. The specific operations were as follows:

1. Measure attenuation on received fiber and compare it to manufacturer's stated attenuation.

2. Extrude E-CIFE for a minimum of 500 meters-record all processing data.

3. Measure attenuation.

4. Respool onto small metal spool to increase stress between coating and fiber.

5. Measure attenuation.

6. Heat age spools of fiber at 100°C for 1/2 hour and let cool down to room temperature.

7. Measure attenuation.

8. Heat age spools of fiber at 125°C for 1/2 hour and let cool down to room temperature.

9. Measure attenuation.

10. Heat age spools of fiber at 150°C for 1 hour and let cool down to room temperature.

11. Measure attenuation.

This test cycle was selected so as to simulate the additional time temperature history which an inner jacket would be exposed to during subsequent extrusion operations.

TABLE I. MATERIAL - PROCESS RESULTS

Variable	Parameter	Change in Loss (from original fiber loss) - db/Km @ 812nm					
		As Extruded	Respool	100°C Age	125°C Age	150°C Age	Conclusion
Melt Index	High	0.68	3.45	2.35	1.83	2.28	Significant Factors
	Low	-0.64	2.00	3.53	8.20	9.97	
Shrinkage	Low	-0.66	1.23	2.88	3.15	5.54	Significant Factors
	High	-0.64	2.00	3.53	8.20	9.97	
Temp. Profile	Normal	0.49	0.37	0.30	0.53	2.99	Significant Factors
	Normal	0.68	3.45	2.35	1.83	2.28	
	Hot	0.47	0.35	0.83	0.07	1.61	
Tooling	Short Land	0.68	3.45	2.35	1.83	2.28	Significant Factors
	Long Land	0.49	0.37	0.30	0.53	2.99	
Cooling	Slow Cool	0.04	3.24	2.75	1.60	3.09	Secondary Factors
	Fast Cool	0.68	3.45	2.35	1.83	2.28	

III. MATERIAL - PROCESS RESULT

The results of the material-process study is outlined in Table I. The significant factors which affect the optical performance of the fibers are polymer melt index and post extrusion shrinkage, extruder temperature profile, and extruder tooling design. Cooling rate appears to be a secondary factor. It must be pointed out, however, that not only are there other important variables, but that singular variables usually cannot be changed without changing others.

IV. CABLE - CONNECTOR STUDY

Although the optical performance of the fiber on a per-kilometer basis is an important parameter, a more crucial issue is the performance of the fiber-cable-connector system. Consequently, the cable was designed with this system approach in mind using the results of the materials-process study and the dimensional needs of the optical pins. This cable, shown in Figure III, has the following design characteristics.

Mechanical

Fiber: Corning type 1519CSB
85/125 graded index
Coating Material: E-CTFE grade 500
Strength Member: Aramid
Outer Jacket: E-CTFE grade 500
Jacket Diameter: 1.725um 50um
Tensile Strength: 30 lbs.
Temperature Range:
-65°C to +105°C continuous
-65°C to +150°C intermittent

Optical

Attenuation: Less than 10db/km @ 25°C
NA: 0.26
Bandwidth: 100 MHz-km

Multiple samples of this cable were made during which manufacturing processes were optimized.

The testing and evaluation was done on seventeen short lengths of cable with a connector in the middle so as to simulate "real world" conditions. Figure IV is a schematic of the test set up. Cable length in the test chamber was 20

meters on each side of the connector. The test procedure consisted of 10 cycles from +20°C to -40°C and back to +20°C followed by 6 additional cycles to -65°C. Sufficient time was allowed at each temperature for the cable loss to stabilize after which the meters were read and recorded.

The test equipment consisted of a stabilized light source on the input side of a 1 x 20 multi-port coupler. Seventeen of the coupler outputs were fusion spliced to the seventeen cable-connector samples. Two additional ports were connectors fusion spliced to a pair of 40 meter cable lengths without splices for reference. The seventeen samples and one reference channel were placed in the test chamber. The output of every sample was coupled into a detector located outside the chamber. Each detector was then attached to its own optical multimeter.

V. CABLE - CONNECTOR RESULTS

The results of the cable-connector testing is summarized in Table II showing the average change in attenuation with its standard deviation at every temperature cycle. Figure V shows this data graphically. The number in the parenthesis under the temperature is the slope of that curve in db change per cycle and represents a permanent increase in loss at that temperature due to thermal cycling.

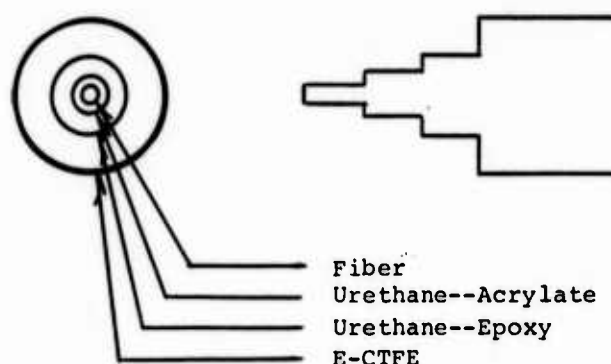


Figure II. Material Study Construction

TABLE II

Connector - Splice Results

		Attenuation Change db from original	
Cycle No.	Temp °C	Average	Variance
	+20	0	0
1	-40	0.79	0.18
	+20	-0.14	0.16
2	-40	0.78	0.19
	+20	-0.15	0.18
3	-40	0.83	0.19
	+20	-0.17	0.17
4	-40	0.78	0.29
	+20	-0.12	0.16
5	-40	0.84	0.24
	+20	-0.13	0.19
6	-40	0.96	0.25
	+20	-0.08	0.22
7	-40	1.04	0.29
	+20	-0.23	0.10
8	-40	0.97	0.26
	+20	-0.13	0.22
9	-40	1.03	0.27
	+20	-0.13	0.20
10	-40	1.09	0.28
	+20	-0.11	0.19
11	-65	-0.14	0.20
	+20	-0.14	0.20
12	-65	1.26	0.29
	+20	-0.08	0.22
13	-65	1.48	0.46
	+20	-0.07	0.22
14	-65	1.43	0.34
	+20	0.00	0.24
15	-65	1.56	0.37
	+20	0.02	0.24
16	-65	1.55	0.38
	+20	-0.05	0.22

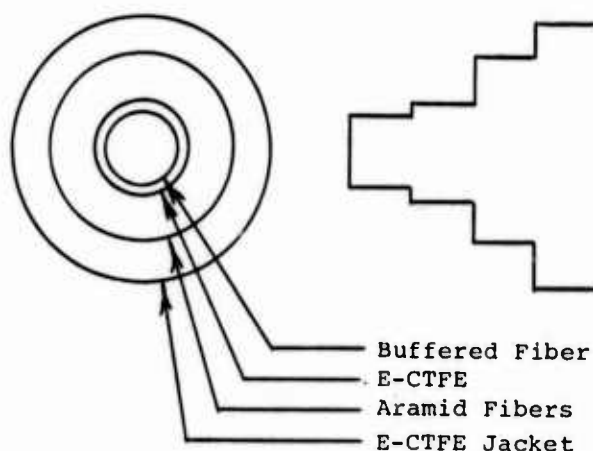


Figure III. Cable Construction

VI. DISCUSSION

The results of the material study demonstrated that both the E-CTFE formulation and the processing conditions have a significant effect on optical performance. The important properties of the E-CTFE were melt index and low shrinkage. The melt index relates to the basic polymer molecular structure and possibly to the forces generated during shrinkage. The low shrinkage can directly be measured with the thermal coefficient of expansion which is minimized in E-CTFE 500. In addition, the 500 grade has very good behavior around and at transition temperatures.

The important processing conditions were extruder temperature profile and tooling design. The best temperature profile was higher than normal for wire and cable. This suggests that the higher compound melt temperature reduces some of the molecular orientation which causes fiber microbending. Care must be taken, however, not to degrade the E-CTFE. Long land tooling also reduced increased loss for much the same reason as the higher temperatures. The long land and, therefore, longer transport time allows the molecules to relax more than allowed by short land tooling. The only problem is that this tooling design is expensive to machine and fragile when made of the proper materials.

The results of the connector-cable study demonstrate that change in loss can be minimized for a properly designed fiber optic interconnect system. In addition, analysis of the curve in Figure V. confirms that these changes are reversible at +20°C and self limiting at the low temperature extremes. The major loss contribution at the low temperature is most likely fiber microbending caused by the difference between the very low TCE of silica and the TCE of the E-CTFE jackets. The increase in modulus of the fiber buffers further contributes to the stresses coupled into the fiber.

Permanent shrinkage of the E-CTFE material has been minimized as evidenced by the reversible change in loss at +20°C and the relatively low slopes of the curves of the low temperature points. The curve of the +20°C measurements has a slope of .009 db/cycle up to the fourteenth cycle after which it goes to zero. The -40°C curve has a slope of .036 db/cycle and the -65°C curve has a slope of .040 db/cycle. Again, after the fourteenth cycle, these slopes approach zero.

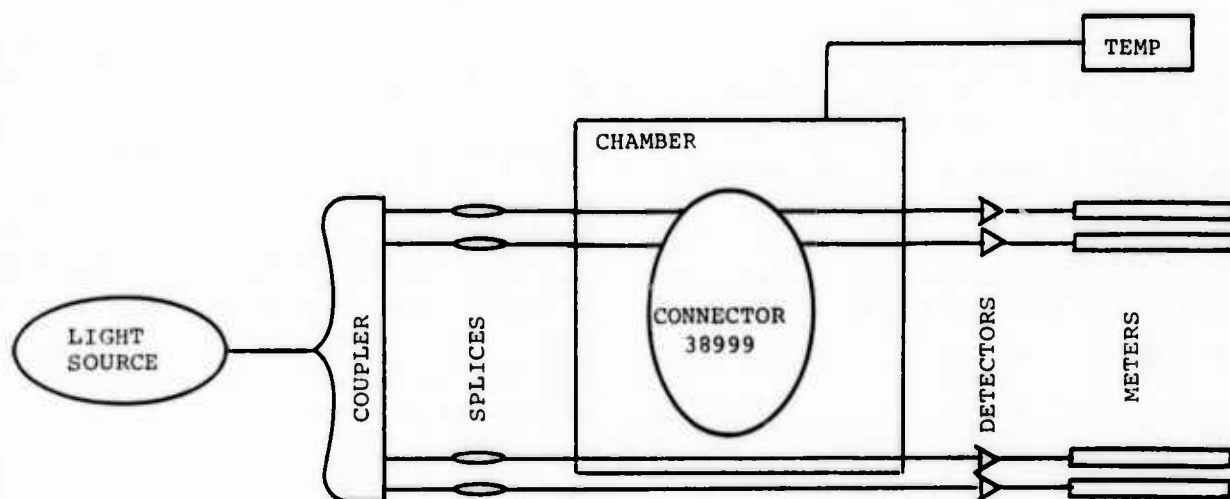


Figure IV. Cable Connector Test Set-Up

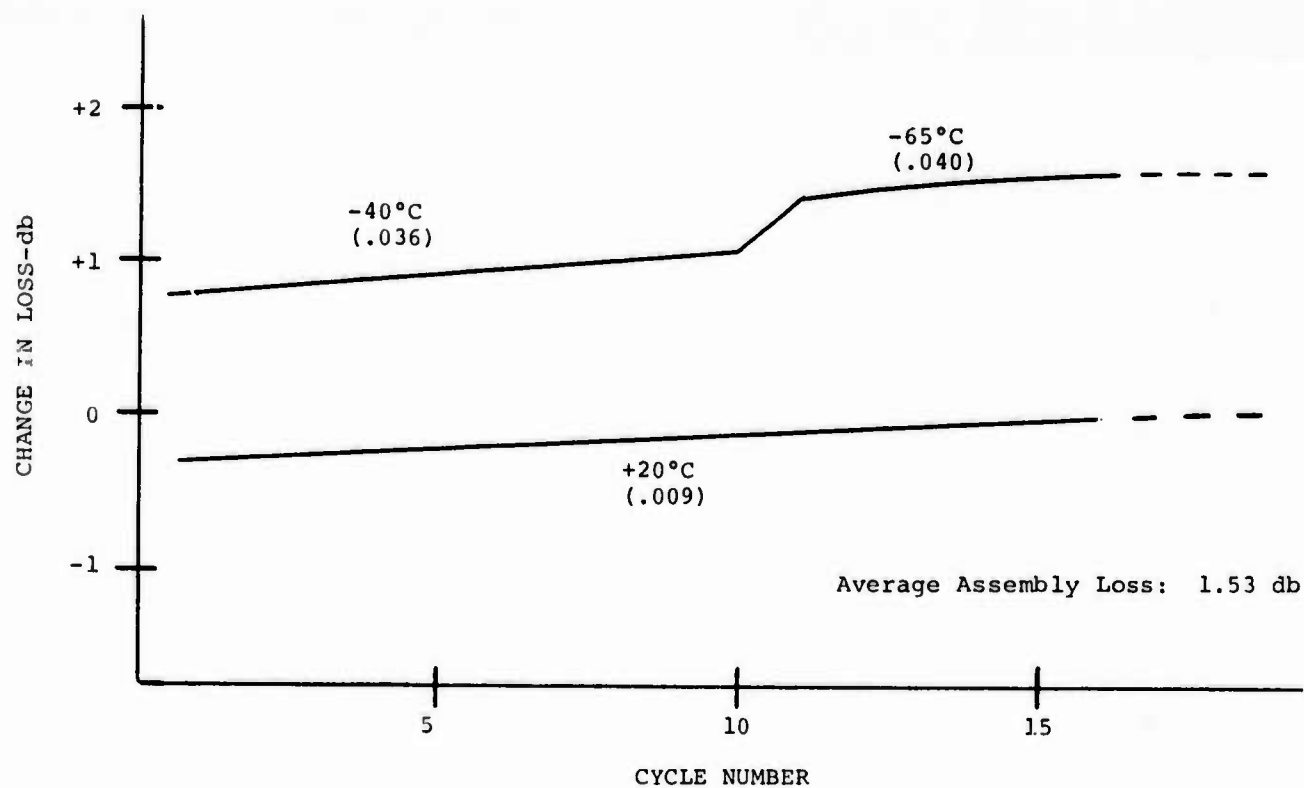


Figure V. Change in Loss vs Cycle Number

VII. CONCLUSIONS

A fiber optic interconnect system has been developed which exhibits acceptable performance even at -65°C . Average loss for 40 meters of cable and a connector is approximately 1.5 db at room temperature and less than 3.0 db at -65 even after extensive thermal cycling. Upper temperature is limited by the fiber buffers to 100°C continuous and 150°C intermittent. All other materials of construction are rated for a minimum of 150°C continuous. Currently work is under way to find sources of supply for high temperature buffered fibers, to develop a special grade of E-CFFE with improved properties, and to further optimize processing conditions.

REFERENCES

1. Tadmor, Zehev and Imrich Klein, Engineering Principles of Plasticating Extrusion, Van Nostrand Reinhold Company, New York, New York, 1970.
2. Billmeyer Jr., Fred W., Textbook of Polymer Science, Wiley-Interscience, New York, New York, 1971.
3. Glanvill, A.B., The Plastics Engineer's Data Book, Industrial Press, New York, New York, 1973.
4. Aloisio, C.J., "A Viscoelastic Analysis of Shrinkback," 31st International Wire and Cable Symposium (Nov. 1982).
5. Hale, P.G., et al, "A Refined Tight Design Duct Cable for Low Loss Monomode Fiber," 31st International Wire and Cable Symposium (Nov 1982).
6. Rabolt, John F., "Studies of Polymer Structure and Dynamics using the Ramam Active Longitudinal Acoustical Mode (LAM)," IBM Research Labs, San Jose.
7. Starkweather Jr., Howard, "Internal Motions in an Alternating Copolymer of Ethylene and Tetrafluoroethylene," Journal of Polymer Science, Volume II, 1973.

Mr. Maack is Director of Engineering at EOTec Corporation. He received concurrently a B.S. degree in Nuclear Science and a B.S. degree in Physics from Lowell Technological Institute in 1969, and a Masters in Business Administration from the University of New Haven in 1982. At present, he is pursuing his doctorate. His fiber optic experience began at Times Wire and Cable and continued at Galileo Electro Optics in 1977 through 1980 when he joined EOTec.

Mr. Dudek is Manager of Commercial Development - Wire and Cable Insulation Materials at Allied Corporation in Morristown, New Jersey. He received a B.S. degree in Biology from North Adams State College in 1971. He has fifteen years of plastics experience working at General Electric Company, Celanese Corporation, and Allied Chemical Corporation. For the past five years he has done considerable work with polymers for the fiber optic industry.

Mr. Allsworth is Vice President at the Deutsch Corporation. Currently, he is concentrating on new product and process development in the fields of optics, electrical components and refractory powdered metal component fabrication. He has over 20 years of engineering experience and is responsible for his companies line of fiber optic products. He has a degree in mechanical engineering from Purdue University.

APPLICATIONS AND COMPARATIVE PERFORMANCE OF LIGHTWAVE CABLE SHEATHS

K. Cornelison M. Fleck

Anaconda Wire and Cable Company, Overland Park, KS

ABSTRACT

Lightwave cables require a high degree of protection in any installation environment due to the high transmission rates and potential revenue losses associated with cable failure. Sheathing options are of prime concern in protecting these constructions under the full range of environmental conditions which may be encountered in the field. This paper discusses the performance of lightwave sheathing options including steel and stainless steel shields, single jacket, and welded aluminum armored constructions. The same basic cable core containing single mode optical fibers in loose filled buffer tubes was employed throughout this investigation for comparative purposes. The lightwave cable sheaths were evaluated for performance under a variety of mechanical and simulated environmental test conditions. Physical performance of the sheaths and optical stability of the fibers were monitored and the results are presented.

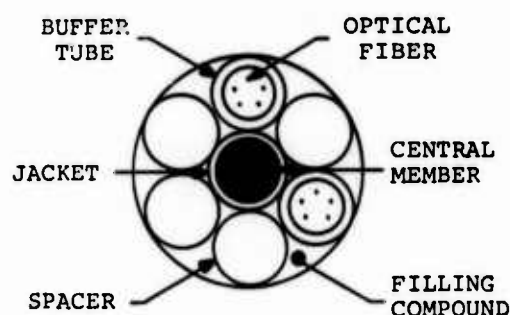
twisting, compressive loading, impacting, shotgun blasts, freezing, and induced currents. The results of this study along with other available sheath performance information is presented.

CABLE STRUCTURE

The same basic cable core structure was utilized throughout the test program to minimize variations of test results due to core design thus allowing for a more accurate comparison of the cable sheaths. The filled core, as seen in Figure 1, incorporates six tubes consisting of two filled buffer tubes, containing five optical fibers each, and four solid spacer rods helically stranded around a coated steel central member. The optical fibers were of a single longitudinal mode design having a mode field diameter of 10 microns, cladding diameter of 125 microns and outer diameter of 250 microns.

INTRODUCTION

The past year has seen an increasing demand for long-haul telephone systems incorporating single-mode optical fibers. Most of these cable systems are designed with life expectancies greater than 20 years and will thus encounter a variety of environmental conditions over their lifetimes. It is therefore of the utmost importance to determine the specific performance of lightwave cables under a variety of these environmental conditions thereby determining optimum applications of available sheathing options. This paper was undertaken to address some of the environmental and installation situations lightwave cables may be subjected to in the field. Five cable sheaths were evaluated for optical stability and sheath performance. Test procedures followed available documents from the Electronics Industries Association (EIA) and Department of Defense (DOD). Cables were subjected to flexing,



CORE STRUCTURE

FIGURE 1

A summary of the structure of the five cable constructions is listed in Table 1. The single jacket, steel and stainless steel construction consisted of high molecular weight polyethylene jackets. The two steel shields were coated on both sides with a 0.05mm ethylene acrylic copolymer. The cable construction utilizing a welded aluminum armor was tested with both a polyethylene and a heavier, 3mm PVC jacket.

OPTICAL TESTING

Most of the optical measurements were performed on an optical test bench capable of measuring up to 24 fibers at one time. This bench incorporates a feedback system to compensate for equipment drift while the mechanical portion of the test is being conducted. The optical measurements were obtained at a wavelength of 1500nm since the microbending effects of single mode fibers tend to be more pronounced at longer wavelengths. Cable transmission was initiated before beginning the mechanical test to establish a baseline after which optical stability was monitored during and after the performance of these tests. Some optical testings were also conducted on a spectral attenuation bench over a range of wavelengths, similar to the procedure outlined in EIA FOTP-78. Equipment drift and inherent noise in this system amounted to approximately 0.02dB.

MECHANICAL TESTING

Procedures

Mechanical testing consisted of performing a flex, twist, compression, and impact test upon the various constructions while monitoring the optical and physical performance of the cable. The mechanical test methods followed EIA and DOD documents which specify the test procedures, apparatus and set-up. Parameters not specified by these documents were taken from various telecommunication specifications of which the more rigorous test conditions were used. Mechanical testing was also performed to optical fiber and/or sheath failure. These mechanical tests are representative of the type of stress that occurs during installation and operation of the cable and thus help in predicting cable survival during and after installation in duct, buried and aerial applications.

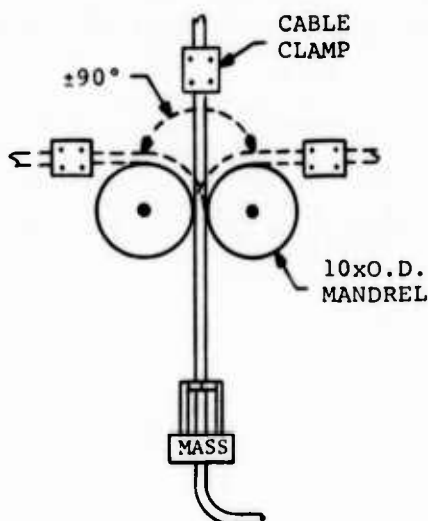
Flexing

The flexing test was performed per EIA FOTP-104 specification which states that the cable shall be flexed $\pm 90^\circ$ over mandrels having a diameter of ten times the cable diameter. A diagram of this apparatus can be found in Figure 2. A weight is attached to the cable to ensure the proper flexing action is achieved. Typical industry requirements have dictated that 10 flexes be performed for armored constructions and 100 flexes for unarmored constructions. Because of the small bend diameter of the cable, the metallic sheath is subjected to compression and elongation strains of about 8%.

Table 2 details the optical performance along with the jacket and shield performance. The data indicates that the optical performance is stable for all constructions and that no outer jacket damage occurs. Mechanically though, several breaks on the stainless steel shield at the overlap along with many points of buckling were noted. The welded aluminum armor also broke at several points along the lower portion of the corrugations. The observed failure mechanism of these metallic shields was fatigue fracture. Further testing was performed on these two constructions to determine the minimum flexing diameter necessary to achieve no shield breakage. It was found that the welded aluminum construction exhibited no breakage when flexed over mandrel diameters of 20 times the cable diameter while the stainless steel shield broke in less than $10 \pm 90^\circ$ flexes at this diameter. The stainless steel tape on the cable sample had relatively low corrugation depths and a lack of tape bonding at the overlap. Since the corrugation depth is important to allow repeated strain of the metal, the low corrugations contributed to the poor performance of this cable. The stainless tape may require more corrugations than carbon steel to achieve similar performance levels. Testing was also performed on the single jacket construction to determine the optical stability and sheath performance when subjected to additional cyclic flexes. No outer jacket damage and negligible attenuation changes were noted up to 1000 flexes.

Twist

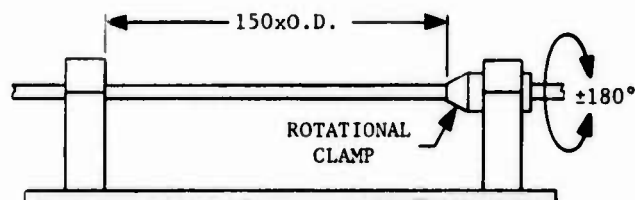
The twist test was performed per DOD-STD-1678. This document specifies twisting a cable section whose length is 150 times the cable diameter a total of $10 \pm 180^\circ$ rotations. Figure 3 illustrates the apparatus set-up.



FLEXING APPARATUS

FIGURE 2

The performance of the various constructions is listed in Table 3. All constructions exhibited negligible attenuation change and showed no visible deterioration of the jacket or shield. To differentiate shield performance, additional testing was performed up to $100 \pm 180^\circ$ twists. Optical measurements were obtained on the single jacket construction after 100 cycles demonstrating optical power is stable upon test completion. Mechanical testing of the shielded construction showed that only the aluminum armored construction failed before 100 cycles. Due to the large corrugation depth and higher torque required to twist this cable, the armor was deformed by the rotational clamp and premature armor breakage occurred.



TWISTING APPARATUS

FIGURE 3

Compression

The compression test was performed in accordance with EIA specification FOTP-41. The cable was mounted between two flat plates and a specified load applied. The change in attenuation after load removal and jacket appearance was monitored. The test apparatus is illustrated in Figure 4. More rigorous telecommunication specifications request compressive loads of 600N/cm and 750N/cm for unarmored and armored constructions respectively. Testing was performed at these specified values and also at higher compressive loads to determine points of failure. The compressive load was applied for 5 minutes and attenuation was monitored both during and after load removal.

Table 4 details the attenuation results and jacket performance at the specified loads. The attenuation change after load removal was negligible for all constructions. During compressive loading though, the single jacket, steel and stainless steel constructions exhibited dramatic changes in attenuation compared to the welded aluminum construction.

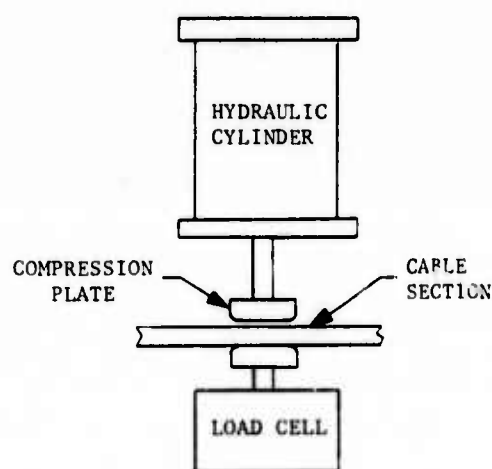
The cables were subjected to increasing loads until fiber breakage occurred. This data is summarized in Table 5. As expected, the cables with metallic shields withstood higher compression values than the cable with a single jacket. Fiber breakage started at approximately 760N/cm for the single jacket constructions, 1000N/cm for the steel tape sheaths, and no breaks occurred in the aluminum armored cables up to 1300N/cm.

The average attenuation change after load removal of the steel constructions, as seen in Table 6, was negligible while the aluminum armored construction exhibited attenuation increases at loads above 890 N/cm. The permanent deformation of the sheath apparently causes core and fiber stresses after load removal, although lightly compressing the cable at right angles to the original compressive force relieves these core stresses.

Additional data was gathered to determine why the aluminum construction allowed lower optical power changes at loads of 750 N/cm and exhibited no fiber failures at higher compressive loads. A graph of the percent cable deflection from the original diameter versus compressive loading is illustrated in Figure 5. The shielded constructions exhibited small incremental deflections beginning at compressive loads above 975 N/cm. As both the steel and stainless steel constructions exhibited fiber breakage close to this value, one

might also expect fiber breakage in the aluminum armored construction at similar values.

It was theorized that core variations with respect to fiber position play an important role in compression evaluations. To evaluate this theory, buffer tube compression tests were performed to determine the effects of compressive loads on multiple fibers versus single fiber tubes. Testing on the multiple fiber tube involved removing the fibers from the buffer tube, twisting the bundle together, then reinserting this fiber bundle into the tube. The results indicate that one fiber break occurred in the five fiber buffer tubes at 755 N/cm. These fibers, upon removal from the tube, showed dramatic deformations on the outer coating of the fibers due to the many fiber cross-overs in the tube. The single fiber tube exhibited no failure up to compressive loads of 1335 N/cm. An early study¹ indicated that single fiber per tube cables developed no fiber breakage at compressive loads up to 4450 N/cm. This data was also confirmed with our own single fiber per tube design.



COMPRESSION APPARATUS

FIGURE 4

From this data, it can be concluded that multiple fiber per tube cables undergoing increasing compressive loads exhibit increasing optical power losses due mainly to the overlapping of fibers thereby creating substantial fiber stresses and microbending losses. These stresses lead to a higher probability of fiber breakage. The amount of microbending losses and fiber stresses depend on the arrangement of the fibers in any given cable section

undergoing compressive loads. In general, cable constructions with optical fibers positioned with fewer overlaps exhibit lower attenuation changes and withstand higher compressive loads before fiber breakage. In reviewing the compressive loading data in Tables 4 and 5 for the welded aluminum construction, it seems likely that the fibers undergoing compressive loads in this cable were arranged with fewer fiber overlaps. This would explain the lower changes in attenuation during compressive load and the lack of fiber breakage at higher compression values.

The cable deflection graph previously discussed in Figure 5 also illustrates that the welded aluminum construction exhibits lower deflections than the other constructions at compressive load values less than 556 N/cm. At load values up to 330 N/cm, no deformation of the core or buffer tubes occurred in this construction. However, at the same compression load, core deformation in the steel shielded constructions were noted.

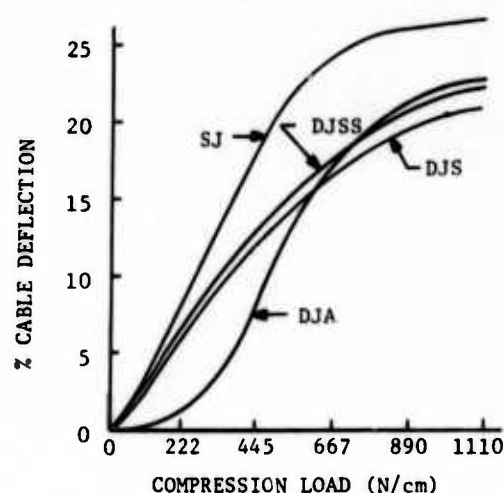
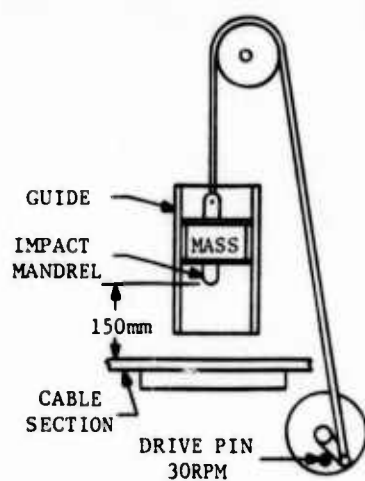


FIGURE 5

Impact

Impact testing was performed per EIA specification FOTP-25. This document states that a specified weight with a cylindrical impact hammer of radius 12.5mm shall be dropped from a height of 150 ± 5 mm for fifty cycles. An illustration of the impacting apparatus can be found in Figure 6.

The results of the impact study reveal that no fiber failures occur in 50 impacts although in some cases optical power losses were noted. It was determined that stress remained on the cable core after impacting due to the deformation of the shield but that the optical fiber micro-bending can be relieved by pinching the cable at right angles to the impact force relieving some of the residual compression forces. Data was also gathered to compare the number of impacts to optical fiber failure. The data revealed a fairly wide range in the number of impacts to optical fiber breakage. It was determined that optical fibers positioned directly under the impacting forces exhibited attenuation changes sooner than fibers positioned otherwise. As the five constructions tested possessed only two buffer tubes, the tubes may not have been positioned directly under the impacting force in all trials. Due to the random positioning of the buffer tubes, the sheaths were compared by utilizing a graph of the percent cable deflection versus number of impacts. This graph is illustrated in Figure 7. For this test, an impacting weight of 6.22kg was selected. The graph reveals that the three shielded constructions exhibit almost identical deflections and perform significantly better than the single jacket cable.



IMPACT APPARATUS

FIGURE 6

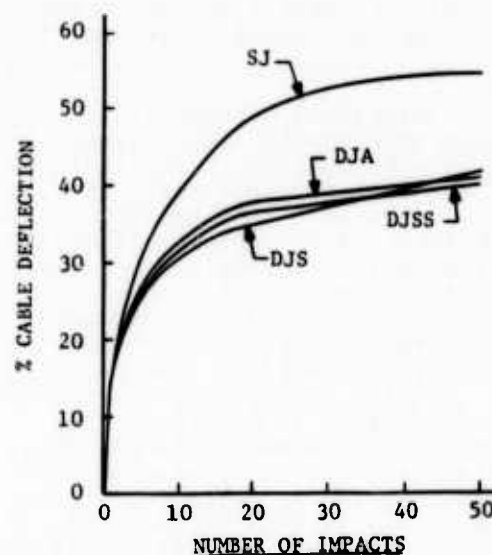


FIGURE 7

Discussion

The mechanical test data indicates that attenuation changes due to cyclic flexing and twisting are negligible unless catastrophic shield failure occurs causing damage to the inner jacket and cable core. The single jacket construction exhibits excellent flexibility properties thereby presenting few problems in duct installations whereas, if shielded constructions are necessary in duct applications, one must consider the payoff sheave sizes, duct curvatures, and minimum cable bend radius at the maximum rated pulling tension to avoid shield breakage. The twisting data suggests that torsional forces as would be found in side payout installations and in aerial applications should not affect shield performance.

The compression data indicates that shielded cables enhance compressive resistance to optical fiber breakage. These constructions can also withstand loads up to 890 N/cm with only minor attenuation changes after load removal although during compressive loading significant power losses are noted. The welded aluminum construction should exhibit lower optical power changes during compressive loads up to 555 N/cm while the steel and stainless steel cables would perform better after load removal when subjected to compressive forces above 890 N/cm. The impact data demonstrates that shielded cables have similar performances when subjected to impacting forces and therefore cable performance is more a function of the cable core design than of the sheathing options.

SHOTGUN RESISTANCE

Procedures

Aerially installed lightwave cables may at some point in their lifetimes encounter accidental or intentional shotgun blasts. For this reason, testing was undertaken to determine lightwave cable resistance to shotgun impacts. Specific test procedures were not available for these tests therefore we devised a test to simulate shotgun impacts on aerially installed cables from various distances. This test was designed to evaluate the effects of shotgun blasts with regards to physical performance (pellet penetration depth) and optical attenuation. The physical testing consisted of firing at short sections of the cable from distances of twenty, forty, and sixty feet. Only one shot was fired at any one section of cable. The data obtained from the physical test was then used to determine the cable constructions and firing distances for the optical attenuation test.

Impact Area and Shell Type

The physical and optical test consisted of the same set-up for the cable impact area (See Figure 8). An eight-foot cable section was pulled taut between two clamps and positioned with no other supports surrounding the immediate vicinity of the cable impact area. A twelve gauge shotgun was employed to fire at the cables. This shotgun gauge seemed to be a reasonable worst case shotgun owned by most hunters. Four different shotgun loads were fired at the various cable constructions and are listed in Table 7. The magnum loads consisted of at least fifty percent more shot than the game loads thereby increasing the amount of shot striking the lightwave cable. The magnum shell designated as M6 was assumed to be a reasonable worst case shell type and was employed in the attenuation test.

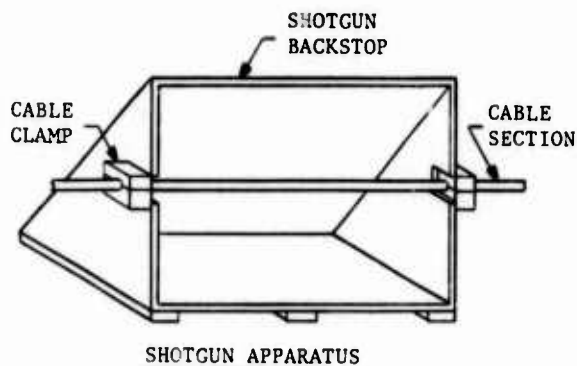


FIGURE 8

Physical and Optical Results

The results of the physical tests are listed in Table 8 with respect to the various constructions, firing distances and shell types. The welded aluminum construction with PVC jacket showed no penetration through the armor while all other constructions exhibited penetrations through the shield at distances of 60 feet. Only half of the DJA cable samples exhibited core penetrations for the various shells fired at 60 feet, while all the steel shielded constructions exhibited core penetrations at this distance.

At distances of forty feet, the welded aluminum construction with PVC outer jacket was found to allow no pellet penetrations when the four shell types were fired. A game load was also fired from twenty feet at this construction with no shot penetration through the armor although small cracks in the aluminum armor were noted. The armor was also crushed to approximately sixty percent of its original diameter. Overall, this construction exhibited superior performance while undergoing shotgun impacts and was subsequently used in the attenuation test.

The optical testing consisted of measuring the attenuation before and after the shotgun blast. The fibers in the welded aluminum PVC construction were connected to the attenuation test equipment and monitored before and after the shotgun blast. Shotgun shell loads were fired at distances from 30 to 60 feet with no pellet penetration through the armor and, as would therefore be expected, the average attenuation change was negligible.

Discussion

The effects of shotgun blasts on aerially installed lightwave cables depend on a variety of factors including cable construction, shotgun gauge and load type. The shotgun data demonstrates that steel and stainless steel shields are not effective in deterring shotgun pellets from entering the cable core. It can also be surmised that other constructions without metallic shield and increased jacket thickness will not perform any better in this test. The welded aluminum armor construction with polyethylene jacket offers somewhat better protection although pellets penetrated the core in half of the cables tested at 60 feet. The aluminum construction with PVC jacket offers superior performance due to the combination of armoring and higher outer jacket wall thickness. It is believed

that jacket materials exhibiting high elasticity and density will absorb more of the pellet momentum thus contributing significantly to the resistance of light-wave cables to shotgun blasts. Future developmental work should concentrate on jacket materials to determine optimum cable designs resisting shotgun pellet penetrations.

FREEZING

Procedures and Results

The freezing test was performed per EIA specification FOTP-98. This document specifies freezing a minimum length of 50 meters of cable placed in a tank of water. The optical attenuation and jacket performance shall be monitored.

The results showed that no visible outer jacket damage occurred and the attenuation changes for all constructions were minimal while frozen in water. Similar performance of the shielded and single jacket constructions were observed in this test. Therefore, the single jacket construction should provide adequate protection in duct applications where standing water is allowed free expansion under freezing conditions.

CURRENT CAPACITY

The current capacity of the metallic sheaths were compared for steady state and short duration fault conditions. Steady state current can be induced into the cable from adjacent power lines, and short duration fault current can be induced by faults in adjacent power systems or by lightning strokes.

The temperature rise in steady state conditions is determined by the balance of the heat generated within the sheath and the heat dissipated to the environment². The temperature rise during fault conditions is determined by the energy of the fault and the thermal storage capacity of the sheath³, since the heat generated within the sheath does not have a chance to dissipate to the environment during the fault.

Testing was performed to verify the calculated steady state current load, and the results are summarized in Table 9. The calculations and current test were based on a 40°C rise in temperature. The aluminum armor, with its larger area and lower resistivity has a greater current capacity than the steel tapes.

However, because of the low shield resistance, the amount of current induced in the cable with a given voltage gradient can be greater than in cables with the steel tape sheaths.

The fault current capabilities were also calculated for the three sheaths. based on a 130°C temperature rise for the metallic sheath component. The values indicate the ability to withstand short term current surges without damage due to overheating and melting of the cable components or metallic sheath. The aluminum armor has significantly higher fault current capacity due to its high conductivity and cross sectional area. Since the stainless steel tape has the lowest fault current capacity, it is often incorporated with aluminum or copper tapes to improve the conductivity of the sheath.⁴

Other Considerations

The data presented thus far in this paper quantifies some of the performance parameters of lightwave cables. Other parameters such as rodent resistance and shield corrosion must be considered to determine specific applications of light-wave cables. Previous studies^{5,6,7} have been performed to determine the resistance of cables to rodent attacks. Squirrels and gopher attacks may be prevalent in aerial and direct buried application respectively of which the cable damage, which occurs by the gnawing animals, is similar for both species. Most of the rodent studies have concentrated on the pocket gopher, *Geomys bursarius*, indicating that in the small size ranges of lightwave cables, low carbon steel .15 m thick and stainless steel .13mm thick are excellent shields resisting gopher attack while aluminum shielding is not adequate to prevent gophers from penetrating into the cable cores. These studies have also indicated that the outer jacket and shield coating are generally removed in these attacks thus subjecting the shield to the corrosive effects of nature. Long term corrosion studies^{8,9} of metal tapes have indicated that stainless steel shields exhibit excellent corrosion resistance properties in a variety of soil composition while aluminum shields are also excellent performers with the exclusion of cables placed in poor drainage clay and tidal marsh soils. It was also determined that low carbon steel directly exposed to the various soil compositions offers poor long term performance in most of these soils.

SUMMARY

Lightwave cables will encounter a variety of environmental conditions during installation and cable operation. This paper demonstrated that in many instances the various lightwave cable sheathing options evaluated offer significantly different performance while undergoing mechanical and environmental tests. The welded aluminum construction offers enhanced performance in situations such as shotgun resistance, compressive loading and fault current capacities. The stainless steel construction performs very similar to the low carbon steel construction in mechanical testing while also exhibiting excellent performance in rodent attacks and corrosion resistance. To determine the optimum applications of lightwave sheaths, consideration of the specific installation parameters, individual sheath performance and cost comparisons such as initial variances between sheaths and predicted maintenance payments and revenue losses due to cable failure must be examined. All of these factors must be analyzed before deciding upon the lightwave cable sheathing option best suited for the installation and environment.

REFERENCES

1. P.S. Venkatesan, K. Korbelak, "Characterization of Ruggedized Fiber Optic Dual Wavelength Cables," Proceedings of the 31st International Wire and Cable Symposium, 1982.
2. J.H. Neher, M.H. Grath, "The Calculation of the Temperature Rise and Load Capability of Cable Systems," Proc. AIEE Conference, June 24-28, 1957.
3. Insulated Cable Engineers Association. Short Circuit Performance of Metallic Shields and Sheaths of Insulated Cable (2nd Edition), Insulated Cable Engineers Association, 1979.
4. W. Weinraub, D. Davis, M. Kinard, "A Rodent and Lightning Protective Sheath for Fiber Optic Cables," Proceedings of the 32nd International Wire and Cable Symposium, 1983, pp 243-249.
5. R.A. Connolly and N.J. Cogelia, "The Gopher and Buried Cable," Bell Telephone Laboratories RECORD, April, 1970.
6. Weinraub et al.
7. N.J. Cogelia, G.K. LaVoie, J.F. Glahn, "Rodent Biting Pressure and Chewing Action and Their Effects on Wire and Cable Sheaths," Proceedings of the 25th International Wire and Cable Symposium, 1976.
8. W.F. Gerhold, J.P. McCann, "Corrosion Evaluation of Underground Telephone Cable Shielding Materials," Paper No. 31, National Association of Corrosion Engineers, Houston, TX, 1976.
9. J.L. Fink, E. Escalante, W.F. Gerhold, "Corrosion Evaluation of Underground Telephone Cable Shielding Materials," Published by U.S. Department of Commerce, June, 1982.



Ken Cornelison is a Supervisor of Product Development at the Telecommunication Product Engineering Center in Overland Park, KS. He received a degree in Electrical Engineering in 1974 from Rose-Hulman Institute of Technology in 1974, and joined Anaconda in 1976. He received an MBA from Ball State University in 1982. In 1982 he joined the Lightwave Cable Division to design and develop optical cables for the telecommunication industry.



Mike Fleck is a Senior Product Engineer at Anaconda's Telecommunication Product Engineering Center in Overland Park, KS. He received a B.S. degree in Mechanical Engineering in 1981 from the University of Illinois. After graduation he joined Anaconda and has been involved in cable manufacturing processes and product design.

Table 1

Cable Structure

Construction	Outer Diameter mm(inch)	Inner Jacket Thickness mm(inch)	Shield Thickness mm(inch)	Corrugation Depth mm(inch)	Outer Jacket Thickness mm(inch)
Single Jacket(SJ)	9.6(.38)	--	--	--	1.0(0.040)
Double Jacket Steel (DJS)	14.0(0.55)	1.0(0.040)	0.15 (0.006)	0.81 (0.032)	1.4 (0.055)
Double Jacket Stainless Steel (DJSS)	13.7(0.54)	1.0(0.04)	0.13 (0.005)	0.63 (0.025)	1.4 (0.055)
Double Jacketed Welded Aluminum (DJA)	18.0(0.71)	1.0(0.04)	0.58 (0.023)	3.0 (0.12)	1.4 (0.055)
Double Jacket Welded Aluminum (DJA-PVC)	21.2(0.83)	1.0(0.04)	0.58 (0.12)	3.0 (0.12)	3.0 (0.120)

Table 2

Cyclic Flexing Results

Cable Type	Number of Flexes	Weight kg(lbs)	Average Attenuation Change(dB)	Jacket/Shield Performance
SJ	100	4.75(10.5)	<.02	Pass
DJS	10	5.75(12.7)	<.02	Pass/Pass
DJSS	10	5.75(12.7)	<.02	Pass/Broke
DJA	10	5.75(12.7)	<.02	Pass/Broke
DJA-PVC	10	5.75(12.7)	<.02	Pass/Broke

Table 3

Twist Results

Cable Type	Number of Twist ± 180	Average Attenuation Change (dB)	Jacket/Shield Performance
SJ	10	<.02	Pass
DJS	10	<.02	Pass/Pass
DJSS	10	<.02	Pass/Pass
DJA	10	<.02	Pass/Pass
DJA-PVC	10	<.02	Pass/Pass

Table 4

Compression Results
After Load Removal

Cable Type	Compressive Load N/cm(lbs))	Average Attenuation Change (dB)	Jacket Performance
SJ	600 (1350)	<.02	Pass
DJS	750 (1685)	<.02	Pass
DJSS	750 (1685)	<.02	Pass
DJA	750 (1685)	<.02	Pass
DJA-PVC	750 (1685)	<.02	Pass

Table 5

Minimum Compression To Fiber Breakage

Cable Type	Compressive Load N/cm (lbs)	Number of Trials	Results
SJ	756 (1700)	2	One Fiber break in one trial
DJS	980 (2200)	2	One Fiber break in one trial
DJSS	1070 (2400)	2	One Fiber break in one trial
DJA	1070 (2400)	2	No Fiber breakage
DJA	1290 (2900)	1	No Fiber Breakage

Table 6

Attenuation Recovery After Load Removal

Compressive Load N/cm (lbs)	Average Attenuation Change (dB)		
	DJS	DJA	DJSS
800 (1800)	<.02	<.02	<.02
890 (2000)	<.02	0.15	<.02
980 (2200)	<.02	0.91	<.02
1070 (2400)	<.02	1.23	<.02

Table 7

Shotgun Shell Designation

Designation	Shell Length (in)	Load Type	Shot Size	Shot Weight (oz)	Powder Weight (drams)
G6	2 3/4	Game	*6	1.000	3.25
G7.5	2 3/4	Game	*7.5	1.000	3.25
M6	2 3/4	Magnum	*6	1.500	4.00
M6-3	3	Magnum	*6	1.625	4.25

Table 8

Shotgun Impacts - Physical Results

Cable Type	Shell Designation	Distance (feet)	Results
DJS	G7.5	40	Penetration to Core
DJS	G6	40	Penetration to Core
DJS	M6	60	Penetration to Core
DJS	G6	60	Penetration to Core
DJSS	M6	60	Penetration to Core
DJSS	G6	60	Penetration to Core
DJSS	M6	60	Penetration to Core
DJA	M6	40	Penetration to Core
DJA	G7.5	60	Penetration to Core
DJA	G6	60	Penetration through Armor
DJA	M6	60	Penetration to Core
DJA-PVC	G7.5	40	No Penetration through Armor
DJA-PVC	G6	40	No Penetration through Armor
DJA-PVC	M6	40	No Penetration through Armor
DJA-PVC	M6-3	40	No Penetration through Armor
DJA-PVC	G6	20	Cable Crushed

TABLE 9

CURRENT CAPACITY

Loading Conditions	Steel	Stainless Steel	Aluminum Armor
<u>Steady State:</u> 40°C rise in air			
Calculated (Amp)	30	12	115
Measured (Amp)	35	14	117
<u>Fault Capacity</u>			
130°C rise			
Calculated (A ² -sec)	104 x 10 ³	16 x 10 ³	2.4 x 10 ⁶

COMPOSITE CONDUCTORS FOR CABLE ELECTROMAGNETIC COMPATIBILITY

Dennis Chalk

Lyle E. McBride

Brand Rex Company
Willimantic, Conn. 06226

Texas Instruments Incorporated
Attleboro, Mass. 02703

Abstract

Nearly all shielding methods for cables have been based on the use of conductive materials to carry away unwanted signal currents. The purpose of this work is to investigate the behavior of a conductive material, copper, coated with a magnetic alloy, Invar, when used as a shielding braid. Performance, as measured by the surface transfer impedance of the shield, is compared to that of a similar copper braid.

Test results indicate that the expected fall-off in transfer impedance at low frequencies (below 1 MHz) because of the small penetration depth in Invar is not observed. In fact, the mutual inductance due to coupling through the shield appears to be increased. However, there is a rapid improvement in performance beyond 20 MHz. This phenomenon is shown to be due to high-frequency losses in the Invar surface.

Introduction

Cables carrying analogue and digital signals, essential links in computer and communications systems, are natural antennas. Well-shielded equipment may fail to meet EMC requirements because interconnecting cables are susceptible to outside interference, or are guilty of broadcasting the signals they carry. Twisted pairs, copper braids, aluminum foil, corrugated or spiral-wrapped strips and a variety of other techniques have been used to attack this perennial problem.

Nearly all shielding methods for cables have been based on the use of conductive materials--copper or aluminum--to carry away unwanted signal currents to ground. The shielding effects of conductors have been investigated and analyzed for over half a century [1]. The value of magnetically permeable metals in combination with conductors has been recognized nearly as long [2] although such shields have been little used in cables until recently.

The purpose of this work is to investigate the use of composite conductors containing both copper and a magnetically permeable alloy. For this initial investigation, the alloy chosen was Invar (36% nickel, balance iron), because of its low cost, high ductility and relatively high magnetic permeability. Earlier studies [3,4] have covered the effectiveness of such materials in strip form because of the reduced penetration of alternating fields in conductive-magnetic composites, and one report [5] revealed a similar effect when a copper clad steel wire braid was sandwiched between an inner brass tube and an outer copper braid. The shielding effectiveness of such multilayer composites can be approximately predicted by surface impedance equations [4]; however, a single layer braid composed of clad wire does not fit the multilayer strip model.

The material selected for the tests reported here was made by bonding a layer of Invar on the surface of a copper rod and drawing the resulting composite to final gauge. The finished wire has an outside diameter of 0.0071 in (0.18 mm); it is roughly 17% Invar by cross-sectional area.

The Invar clad copper wire was applied to a typical multi-conductor cable as a braided shield. The braid angles, coverage and other parameters were chosen to be the same as those of the optimized tinned copper braid normally used with this particular cable design.

Because the test results with this first design appeared to indicate an over-optimal braid condition, a second cable sample was prepared having a lower braid density. The change did not, however, produce a significantly different result. In an attempt to reduce the surface transfer impedance and demonstrate the reduction (due to skin effect) typical of composite strip shields at intermediate frequencies, a further sample was prepared, similar to the first except that the Invar surface was pickled in ferric chloride to remove most of the surface oxide; the Invar was then coated with solder to give the same

surface as that of a conventional copper braid.

Experimental Procedure

The test fixture used was that specified in MIL-C-85485 [6], made by placing a length of tubular braid over a 1 m length of jacketed cable, attaching it to the braided shield of the sample cable at one end and using it as the ground at the other. MIL-C-85485 has detailed instructions for preparing this sample/test fixture. Figure 1 shows the sample arrangement.

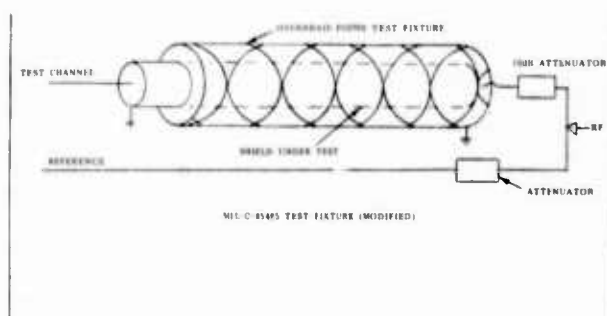


Figure 1--Sample Arrangement

The excitation voltage was connected to the shield under test by means of the 10 dB attenuator specified by MIL-C-85485. The center conductor of the cable was connected at one end to the test channel of the computer-controlled data acquisition system described in reference [7] by means of an impedance matching network; the other end was connected directly to the cable shield being tested. Two network analyzers, both under computer control, were used to cover the frequency range from 1 KHz to 1 GHz.

Test Results

Figure 2 shows the results of the test with the first sample, converted to the units of surface transfer impedance by means of the equations of MIL-C-85485. At 1 KHz the transfer impedance is 4.6 milliohm; it begins to rise linearly at about 300 KHz, reaches a peak of 315 milliohm at 27 MHz, and then declines as frequency continues to increase.

Tests of the sample with lower optical coverage showed that its performance was essentially unchanged; the surface trans-

fer impedance curve was the same as that shown in figure 2. The tinned (solder coated) sample's performance is shown in figure 3.

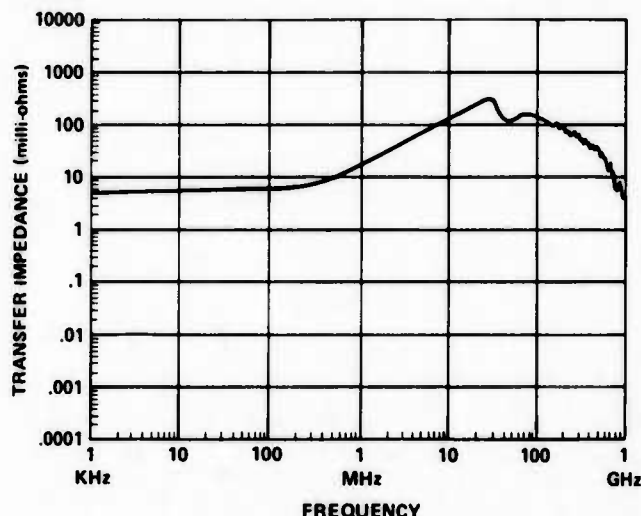


Figure 2--Clad Braid Surface Transfer Impedance

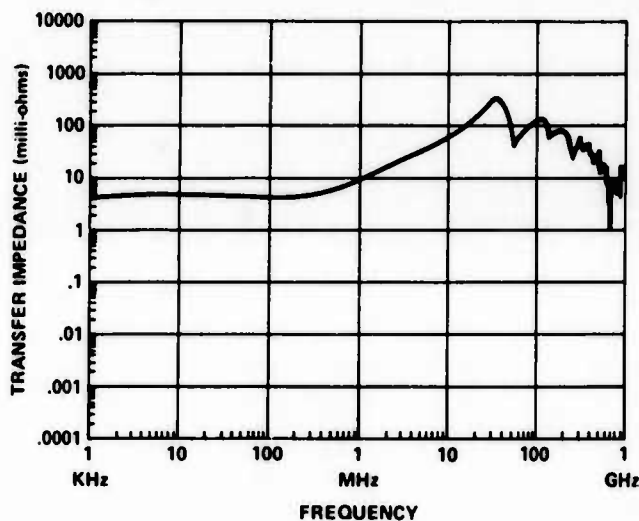


Figure 3--Tinned Clad Braid Surface Transfer Impedance

Discussion

The Invar clad braid's behavior is quite different from that of an essentially identical shield made from tinned copper (a typical test curve for copper optimized braid is shown in figure 4).

The low-frequency asymptote (equivalent to the d-c resistance of the shield) is slightly higher for the clad shield, because of its reduced copper content. The copper's transfer impedance begins to fall sharply at 500 KHz and reaches a minimum at 2 MHz, presumably because of reduced penetration of the metal due to skin ef-

fect. The clad shield's impedance might be expected to fall at a lower frequency because of the enhancement of skin effect by its magnetic properties.

The fact that, instead of falling, the transfer impedance of the composite rises in this frequency range shows our initial assumption--that a clad wire braid would behave much like a clad strip shield--to be fundamentally incorrect. Instead, the test data are consistent with a conclusion that the coupling coefficient between shield wires and internal conductors remains the same (the geometry is, of course, identical) but because the self-inductance of the shield wires is increased by the Invar cladding, the mutual inductance between shield and center conductors is increased in the same ratio.

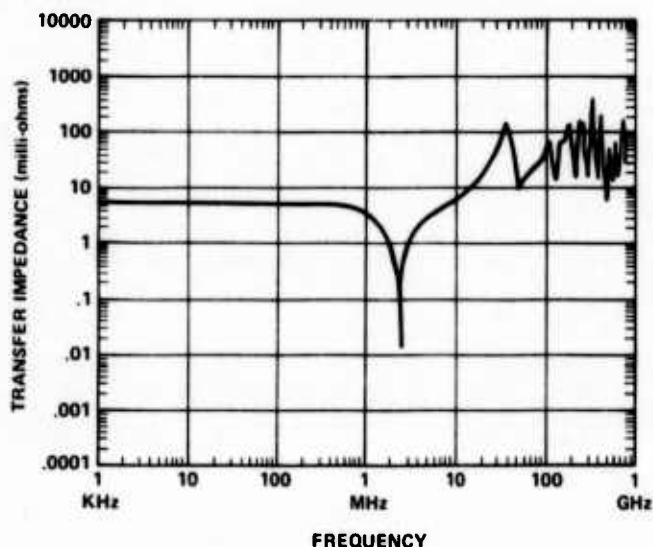


Figure 4--Tinned Copper Braid Surface Transfer Impedance

A similar region of linear increase appears in the curve for the tinned copper braid, but at about an order of magnitude lower amplitude level. It appears, then, that the magnetic surface layer has increased the mutual inductance component of surface transfer impedance by a factor of ten--hardly a desirable change.

In the region above 10 MHz, energy transfer by this mutual inductance (due to aperture coupling and the "porpoising" effect) would be expected to dominate the transfer impedance; the two shields in that case should behave similarly at high frequencies except for the amplitude increase due to the Invar's added inductance. However, it is clear that the shapes of the two curves are significantly different above about 20 MHz. While the copper curve oscillates violently, the curve representing the clad wire is

smooth, and falls off rapidly as the frequency increases. This fall-off in transfer impedance to levels below those of tinned copper is particularly unexpected in view of the higher mutual inductance noted above.

The most likely explanation appears to be based on the dependence of transmission-line losses on the surface impedance of the shield. The same skin-effect phenomenon that leads to a reduction in the transfer impedance of a metal tape shield produces a rise in both the surface resistance and the surface inductance of the clad conductor. The analysis of reference [2] shows that when the thickness of a conductor is larger than the depth of penetration at a particular frequency, the surface impedance approaches the characteristic impedance of the metal, and has equal resistive and inductive elements.

Because the characteristic impedance is proportional to the square root of permeability divided by conductivity, an Invar surface has several orders of magnitude more surface impedance than a copper surface at high frequencies. Calculation of magnetic metals' impedance is questionable at high frequencies, because of the change of permeability with frequency; however, the equations of [2] can be used to estimate the effect that might be expected from this cause.

Figure 5 (based on the losses of a calculated one-meter transmission line having an Invar conductor and an assumed characteristic impedance of 50 ohms) illustrates the probable difference in attenuation between a copper shield and one of clad wire under the conditions of test.

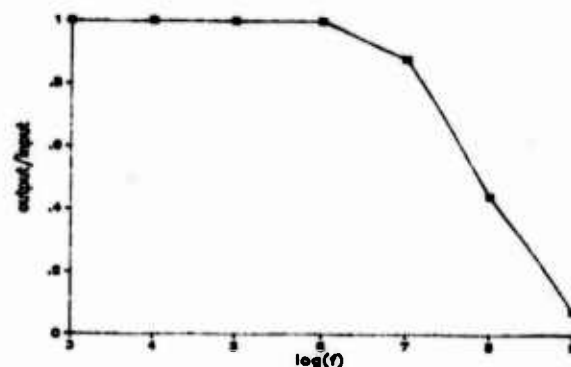


Figure 5--Signal Reduction due to Invar Surface Resistance

This calculated curve is at least qualitatively consistent with the differences between figures 2 and 4; the reduction in both cases begins to appear at about 10

MHz, and is more than an order of magnitude at 1 GHz. (In fact, the reduction in figure 2 is more than two orders of magnitude, considering the factor of ten increase in the mutual inductance referred to above.)

An even stronger corroboration of the assumption that the differences are due to attenuation by the Invar surface resistance is the elimination of the sharp peaks or resonances apparent in figure 4 above 10 MHz. These peaks are caused by standing waves in the short-circuited transmission line made up by the shield and the outer braid (Figure 1). The high attenuation in this transmission line due to Invar's surface resistance has eliminated the reflections from the short-circuited end; the peaks and valleys above 100 MHz have vanished completely in Figure 2.

When the Invar wire surface was tinned, the result (Figure 3) also supports the above explanations. Below 20 MHz, the curve is almost identical to that of Figure 2 (although there is a slight decrease in the mutual inductance, probably due to improved contact between wires at the points of crossing, and hence smaller effective orifices). Beyond 20 MHz, however, there is a gradual transition from the behavior of the Invar braid to something very like the tinned copper of Figure 4.

The change is apparently due to the conductivity of the solder coating. As the resistance of the Invar surface increases because of skin effect, the effect of the solder layer's conductance begins to appear, and the curve begins to approach that of the tinned copper (which is also dominated by the effect of the solder coating at high frequencies). It appears that at some frequency beyond the capability of the tests conducted here the curves of Figures 3 and 4 would merge, because the field is confined by skin effect to the solder surface in both cases.

Conclusions

The sharp reduction in surface transfer impedance observed at relatively low frequencies in clad strip shields does not occur with braided shields made from Invar clad copper wire; in fact the clad shield is less effective than plain copper around 1 MHz.

There is, however, a very large improvement in measured shielding effectiveness at frequencies above 100 MHz because the high surface resistivity of the Invar absorbs interference energy before it can be transferred to the shielded conductors. While this effect is probably not, theoretically speaking, a reduction in surface transfer impedance, it does represent a real improvement in the ability of the shield to protect the cable against high frequency interference. The gain appears to be as much as 20 to 40 dB.

Tinning the Invar surface appears to negate the advantages of the clad shield at high frequencies without doing very much to improve low frequency performance.

References

1. Edison Electric Institute and Bell Telephone System--Joint Subcommittee on Development and Research, "Shielding of Ground-return Circuits at Low Frequencies", Engineering Report No. 26, 1934.
2. Schelkunoff, S. A., "The Electromagnetic Theory of Coaxial Transmission Lines and Cylindrical Shields", Bell System Technical Journal, 13, pp. 539-579, 1934.
3. McBride, L. E., Trenkler, Y., Delagi, R. G., "Shielding Effectiveness of Composite Metals at Voice and Carrier Frequencies", Proc. 31st Int. Wire and Cable Symp., pp. 193-197, 1982.
4. McBride, L. E., Trenkler, Y., "Clad Metals--Permeability Plus Conductivity for Effective Shielding", Proc. IEEE Natl. Symp. on EMC, pp. 261-265, 1984.
5. Merrell, J. E., Hoeft, L. O., Hofstra, J. S., "Measured Transfer Impedance of Metallic and Non-Metallic Conduits Covered with Tinned Copper and SnCuFe Braids", Proc. IEEE Natl. Symp. on EMC, pp. 39-42, 1984.
6. Military Standard, "Cable, Electric, Filter Line, Radio Frequency Absorptive", MIL-C-85485, 1981.
7. Chalk, D., Hoeft, L. O., Hofstra, J. S., "Comparison of Surface Transfer Impedance Measured with Quadaxial and Triaxial (IEC 96-1 and MIL-C-85485) Test Fixtures", Proc. IEEE Int. Symp. on EMC, pp. 518-520, 1983.



Dennis Chalk is a Senior Product Engineer for Military Products at Brand-Rex. He attended Westchester Community College in Valhalla, NY and joined Brand-Rex in 1982. Prior to his employment at Brand-Rex, Chalk was a Technical Services Representative for Tensolite Company in Buchanan, NY.

He is a member of S.A.E. and ASNE and co-author of a technical paper "Comparison of Surface Transfer Impedance Measured with Quadraxial and Triaxial (IEC 96-1 and Mil-C-85485) Test Fixtures," with Dr. Lothar Hoeft and Joseph Hofstra of the BDM Corporation in Albuquerque, NM.



Lyle E. McBride is a Senior Member of the Technical Staff of Texas Instruments Incorporated, New Business Development. He received the B.E.E. degree from Cornell University in 1952, and the A.M. and Ph.D. degrees from Harvard University in 1961 and 1963 respectively.

He has been employed by TI since 1966; his current responsibilities include electromagnetic compatibility and analysis of the electrical properties of clad metal strip and wire. He is a member of IEEE and the Society of Cable Television Engineers. His patents are in the areas of electronics and automatic controls.

THE ADAPTATION OF AN AIR-DIELECTRIC RF CABLE FOR USE AS AN OIL-FILLED HIGH VOLTAGE PULSE TRANSMISSION LINE *

W.C. Weiss R.L. Copp L.L. Reginato J.A. Schmidt

Lawrence Livermore National Laboratory
Livermore, California

Abstract

This paper describes the specifications, conceptual design, prototype testing and operating experience of an oil-filled high voltage pulse transmission cable adapted from commercially available air-dielectric RF components.

Lawrence Livermore National Laboratory's Advanced Test Accelerator (ATA) requires a method of transmitting 250kV, 70 nanosecond pulses from the power conditioning equipment to the accelerator. The oil-filled cable approach was chosen over alternative concepts because of its high voltage holding capability, long life and flexibility. The criteria for cable and connector design are discussed. The results of prototype testing and performance of the final design are presented.

Introduction

Pulsed power requirements for components occasionally exceed the specifications of commercially available components used in conventional applications. This necessitates either developing new components in cooperation with manufacturers or modifying standard components. This latter course was followed in meeting the ATA requirement of transmitting high voltage pulses from pulse generating equipment located in an area safe for personnel access into a hazardous radiation area.

ATA is a 10 kiloamp electron beam accelerator with an output energy of 50 MeV. This energy is added to the beam in 250kV increments as the beam passes through a linear array of 200 accelerating stages or cells. Each 70 nanosecond accelerating pulse is carefully timed to arrive at a cell as the beam begins its transit through it.

Figure 1 shows one accelerating stage consisting of a pulse generator, accelerating cell and one of the two interconnecting transmission lines. The paralleled 24 ohm transmission lines carry the pulse from the 12 ohm generator to the accelerating gap within the cell. The impedance the cell presents to the transmission

lines is 250kV/10kA or 25 ohms. To match the 12 ohm equivalent transmission line impedance terminating resistors are connected in parallel with the cell input terminals.

In addition to the electrical specifications the transmission lines are required to have enough mechanical flexibility to permit their installation and removal from the conduits which cross the radiation barrier. Flexibility is also necessary to eliminate the alignment difficulties caused by multiple transmission line connections between the support structure, which mounts the 200 pulse generators, and the accelerating cell array.

Selection of Cable Dielectric

Solid, gas and liquid media were considered as dielectric choices for the cables. A solid dielectric has a problem similar to that of a solid dielectric capacitor. They both have a limited charge-discharge cycle lifetime in pulsed operation. The dielectric invariably contains voids resulting from the polymerization and extrusion processes and possible separation spaces at electrode surfaces. Air or residual polymerization gases ionize during each high voltage pulse and enlarge the voids by erosion. Eventually the reduced dielectric thickness is unable to withstand the electric field stress and dielectric puncture follows. Reference 1 presents empirical formulae indicating that breakdown field stress is inversely proportional to the one-tenth power of the dielectric volume. This relationship is based on the probability of the occurrence of potentially destructive voids being proportional to the volume of stressed dielectric. The reference also shows that, similar to capacitors, cable pulsed lifetime is proportional to the eighth power of the ratio of breakdown field stress to the maximum operating field stress. Using these criteria the calculations for a polyethylene cable of the specified electrical characteristics and a 30 million pulse lifetime resulted in a center conductor diameter of 2.75 inches and a shield diameter of 5.0 inches. A cable dielectric of these dimensions is difficult to fabricate with an assurance of a minimum of voids and it is doubtful that the flexibility requirement could be met.

Gas filled cables avoid the pulse lifetime

*Work performed jointly under the auspices of the U.S. Department of Energy by Lawrence Livermore National Laboratory under contract W-7405-ENG-48 and for the Department of Defense under Defense Advanced Research Projects Agency ARPA Order No. 4395, monitored by Naval Surface Weapons Center under document number N60921-84-WR-W0095.

limitation of solid dielectrics, but because of the lower dielectric constants of gases compared to those of the solid dielectrics, the conductor separations must be smaller to produce the increased capacitance per unit length needed for low impedances. For example, the conductor separation for a 24 ohm gas filled cable is 37.7% of that of a 50 ohm cable with the same shield outer diameter. To compensate for the reduced separation the insulating gas would require high pressurization at 250kV operating levels.

Liquid dielectrics also are free of lifetime limitations and while investigating the characteristics of gas filled cables it became obvious that the low dielectric constant problem of gases could be overcome by substituting a liquid dielectric such as water (relative permittivity of 80) or transformer oil (relative permittivity of 2.3) in cables originally intended for gas filling.

Using a liquid dielectric also offered the possibility of compatibility with the high energy density storage water dielectric of the pulse generator or the combination insulating and cooling transformer oil dielectric of the accelerating cell. The transformer oil was chosen over water on the basis of calculations which showed that the oil permittivity allowed the use of standard gas filled cable components to obtain the 24 ohm impedance. A second factor in favor of oil was the use of the cables as return lines for the accelerator cell cooling system.

Cable Design Criteria

The cable design factors include the impedance which determines the ratio of outer-to-inner conductor radii and the selection of an inner conductor radius sufficiently large to give a reasonable breakdown safety factor.

The characteristic impedance equation for a coaxial cable is:

$$Z_0 = (1/2 \pi)(u/e)^{1/2} (\ln r_0/r_i)$$

$$r_0/r_i = \exp [2 \pi Z_0 (e/u)^{1/2}] \quad (1)$$

where u = dielectric permeability, H/M
 e = dielectric permittivity, F/M
 r_0 = outer conductor radius, cm
 r_i = inner conductor radius, cm
 π = 3.14

The maximum electric field occurs at the surface of the inner conductor and is given in reference 2 by:

$$E_{\max} = \frac{V}{r_i \ln(r_0/r_i)} \text{ MV/cm} \quad (2)$$

where V = cable voltage in megavolts

The breakdown field at an electrode surface for liquid dielectrics under pulsed conditions is a function of the surface area and the time the field is present. The empirical equation for the breakdown field is given in Reference 1 as:

$$E_{bd} = \frac{K}{t^{1/3} A^{1/10}} \text{ MV/cm} \quad (3)$$

where K is an experimentally determined constant for the dielectric.

t = time that field is present in microseconds

A = Surface area of electrode stressed to 90% or more of the maximum field on the electrode - in square centimeters. For a round conductor coaxial cable $A = 2 \pi r_i L$ where L = cable length in centimeters.

Setting the maximum field of equation (2) equal to the breakdown field of equation (3) and substituting the conductor radius ratio of equation (1)

$$r_i = \left(\frac{V t^{1/3} (2 \pi L)^{1/10}}{2 \pi K Z_0 (e/u)^{1/2}} \right)^{10/9} \text{ cm} \quad (4)$$

For the ATA application:

L = 686 cm (22.5 ft.)
 V = 0.750 megavolts (using a safety factor of $3 \times 250\text{kV}$)
 K = 0.50 for transformer oil
 u = 4×10^{-7} Henries/meter
 e = $2.3 (8.84 \times 10^{-12})$ Farads/meter (2.3 is the relative dielectric constant of transformer oil)
 Z_0 = 24 ohms
 t = 0.070 microseconds (70 nanoseconds)

r_i is calculated to be 2.6 cm (1.0 inch)

Substituting this value into equation (1)

$$r_0 = 4.7 \text{ cm (1.85 inch)}$$

For the polyethylene separator, which holds the inner conductor in position (Figure 4), the maximum field will occur at the center conductor interface and can be calculated from equation (2). For a safety factor-included cable voltage of 750kV $E_{\max} = 481\text{kV/cm}$ or 1220V/mil . Polyethylene is rated in Reference 3 at 1200V/mil . Since the volume of separator material is small compared to the oil volume, the lifetime predicted by the equations of Reference 2 is well beyond the specified 30 million pulses.

The calculated outer conductor radius, r_0 , approximates that of the RF cable manufacturers nominal 4 inch O.D. 50 ohm cable and the inner conductor radius approximates that of the inner conductor of his 5 inch O.D. cable. (Since both conductors are corrugated, the manufacturer recommends using an average of the peaks and valleys of the corrugations for dimensions used in impedance calculations.) The separator required for this combination of conductors was non-standard but the manufacturer agreed to design and fabricate one for

several lengths of prototype cable.

Cable Construction

The details of the cable construction are shown in figures 2, 3, and 4. Both the center conductor and shield are made of corrugated copper sheet with a seam running the length of the cable and welded to hold a specified 10lb/sq.in. The center conductor is supported by a serrated polyethylene separator, 1/4 inch thick, wound around the center conductor in a 4 inch pitch spiral. The minimum bending radius for the cable is recommended by the manufacturer as 35 inches, although later tests showed that the cable would operate successfully with a 20 inch bend. The connector fittings are hard soldered by the manufacturer to the outer shield and center conductors and provide liquid-tight seals. The polyethylene anchor insulator, shown in figure 3, gives additional center conductor support at the connector.

Cable Test Procedure

Figure 5 shows the test stand assembled for evaluating the prototype cable. A 10 ohm, 50 nanosecond, 250kV water-dielectric pulse generator was connected by a water-to-oil interface to the test cable. The cable was essentially unterminated since the center conductor was loaded only by a small capacitance to the capacitive voltage divider and the divider housing.

At the 10 ohm-to-24 ohm interface the transmission coefficient is 1.4 and with the cable unterminated the reflected pulse amplitude added to the incident pulse amplitude results in a voltage doubling. Therefore, the total voltage step-up is 2.8 and for a generator output of 250kV the maximum available test voltage is 700kV. Without a matched terminating load pulse reflections from the end of the cable will produce a series of alternate positive and negative pulses which will continue until the energy injected by the pulse generator is dissipated by transmission line losses. This effect subjects the cable to a more severe test than it would experience in normal terminated operation where the negative pulse from the generator transits the cable and is absorbed in the load without further reflection. However, with a series of reflected pulses, voltage is present for a longer time and equation (3) indicates that the breakdown voltage rating will be lowered.

The cable was suspended as shown with the specified bend radius and filled with de-aerated and filtered oil. Oil at equilibrium with the atmosphere will contain 10% by volume of absorbed air. When subjected to a low vacuum most of the air will be removed. If the de-aerated oil is used to fill a system with trapped air pockets, the oil will gradually absorb the trapped air and if arcing occurs the released gases, consisting predominantly of hydrogen and smaller amounts of methane and acetylene, will also be absorbed. Filtering is used to remove carbon particles resulting from the arcing, although in pulsed systems an appreciable amount of carbon can be accumulated before dielectric strength is significantly affected.

During the initial test series the cable voltage was raised in small increments from a 250kV level until the first breakdown occurred at 525kV. The cable was allowed to "recover" for 30 minutes which was hoped to be sufficient time to absorb gases released during the breakdown. The next series of pulses started at 250kV and the level was increased in small increments until breakdown occurred at over 600kV. Again the cable was given time to recover. The cycle of repeating the test series with breakdowns occurring at higher levels and allowing for cable recovery was repeated until the 700kV maximum available voltage was reached without further breakdown. The oil in the cable was then exposed to the atmosphere overnight and a test series was repeated to the 700kV level with no further breakdown.

Several additional tests were conducted. A section of cable was tested in the horizontal position to determine if the de-aerated oil could successfully remove air or breakdown gases more likely to be trapped in this position. The test results showed no significant difference in performance over inclined or completely vertical sections. The bending radius was reduced to 20 inches with no degradation of performance. The radius was further reduced until a crease developed in the outer shield. Repeated breakdowns took place at the crease but when the cable was returned to the recommended bend radius the breakdowns stopped.

The entire test procedure was repeated on a second cable sample. The initial breakdown occurred at a level slightly higher than the first sample (575kV) but after repeating the breakdown-recovery cycle eventually 700kV was reached without breakdown.

Test Analysis

After completing the tests a dissection of the cable showed that each breakdown appeared to have taken place at a different location. Each arc either punctured the dielectric separator or tracked along its edge. At the site of each breakdown the arc discharge energy produced a depression or dent, occurring most frequently in the center conductor but occasionally in the outer conductor. Although the pulse supplied by the generator was negative, oscilloscope traces showed that breakdowns were likely to occur on a subsequent positive reflection. This is to be expected because with a positive center conductor free electrons will be drawn into a region of higher field gradient, gaining energy at an accelerated rate as they approach the center conductor. Thus, the avalanching effect is enhanced with positive voltage on the center conductor. Normally, when there is an option, pulse energy is generated and transmitted with a negative polarity.

The improvement in the cable's voltage handling capability after the breakdown "conditioning" process can be attributed to the probability that oil, which fills in dielectric punctures, replaces weak dielectric material. Oil also fills the dented spaces between conductors and the dielectric which effectively increases the conductor spacing with a resulting decrease in electric field stress.

Accelerator Cable Performance

The cables installed between the pulse generators and accelerating cells operate under conditions less severe than those of the test stand. The maximum bend radius is 30 inches with inclinations no less than 45 degrees. Prior to filling with de-aerated oil the cables are evacuated. During accelerator operation the oil is continuously circulated and filtered while a vacuum is maintained on the oil reservoir. In routine operation a 250kV negative pulse is transmitted to the accelerating cell which appears to be a matched load when a beam is passing through the cell. If the cell is pulsed without a beam present the cell impedance is mismatched upward with a transmission coefficient of 1.35 and reflected voltage pulse of $1.35 \times 250\text{kV}$ or 337kV.

The accelerator was brought on line and up to its rated energy output in small increments of accelerating stages as experience with beam propagation permitted increased energy levels to be attempted. Consequently, not all cables have accumulated the same number of pulses. At a pulse-per-second repetition rate the cables with the largest pulse totals have about 5 million pulses. Of the four hundred cables in service only one has required replacement and this was due to a wrench socket found in the cable which caused repeated arcing until the outer shield was punctured. During the start-up period cables which had breakdowns were allowed to continue breaking down with the assumption that, as in the prototype test, the voltage holding capability would improve. Eventually, breakdowns stopped in all cables except the one with the socket.

Conclusion

Adapting commercially available air-dielectric cables to high voltage pulse applications by filling with a liquid dielectric is feasible where the impedance and voltage requirements can be met with existing components or minor modifications to those components. The cable's long life and ability to recover from breakdowns is valuable where reliable operation is important.

The disadvantages include the requirement for a sealed connector, a circulating de-aerated oil supply and possibly a means of evacuating the cable before filling. However, if the cable is operated at conservative levels, without breakdowns, it could be treated as a permanently sealed system and be as reliable as oil-filled power transformers.

References

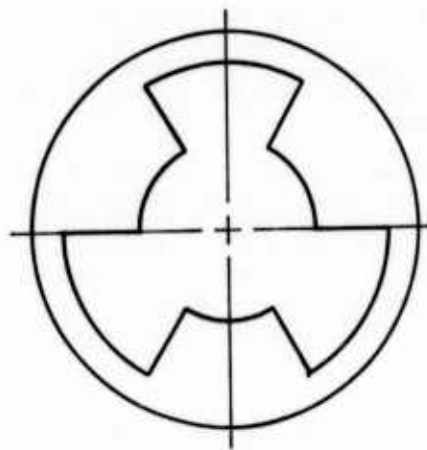
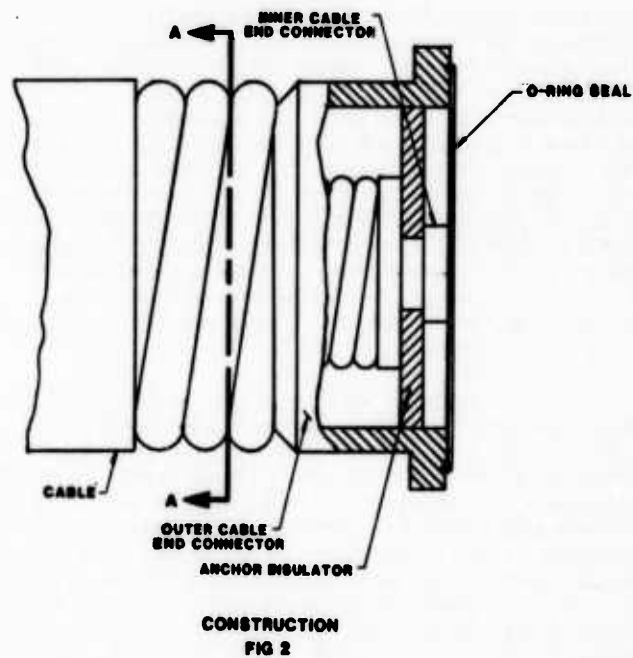
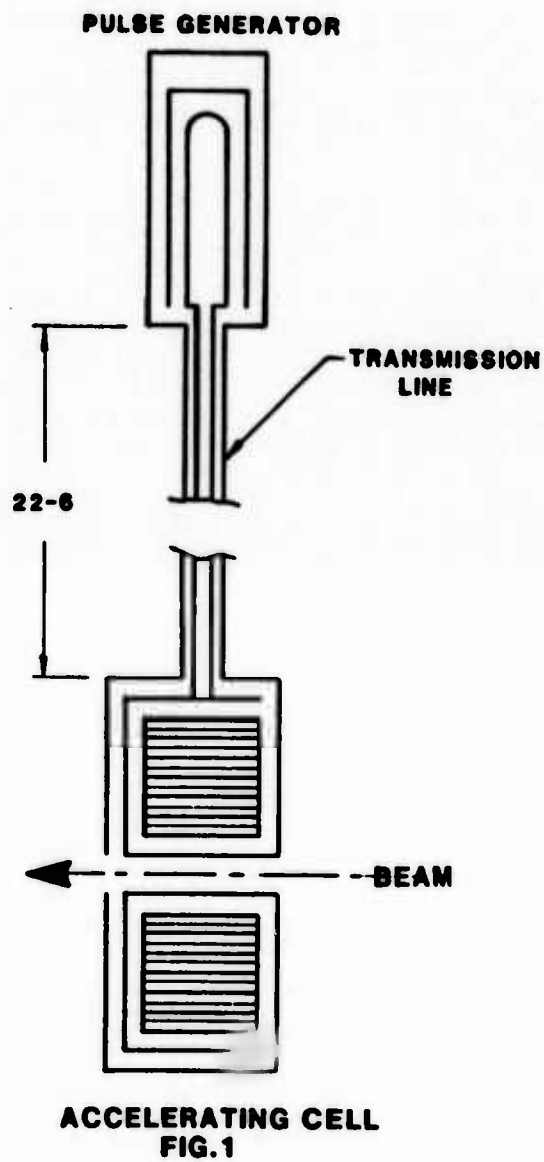
1. J.C. Martin, Nanosecond Pulse Techniques, Circuit and Electromagnetic System Design, Note 4, Atomic Weapons Research Establishment, April 1970
2. L.L. Alston, High Voltage Technology, Oxford University Press, 1968
3. F.M. Clark, Insulating Materials for Design and Engineering Practice. John Wiley and Sons, Inc. 1962.

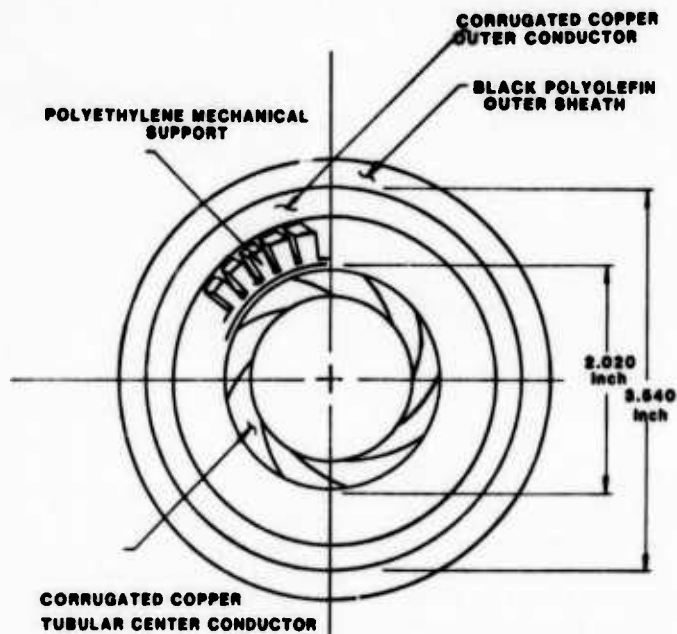


W. C. Weiss is an Engineering Associate with the Beam Research Group at LLNL. He has been active in the design and testing of pulsed power equipment for several accelerators and flash x-ray machines at LLNL and formerly at the Physics International Company.

DISCLAIMER

This document was prepared as an account of work sponsored by an agency of the United States Government. Neither the United States Government nor the University of California nor any of their employees, makes any warranty, express or implied, or assumes any legal liability or responsibility for the accuracy, completeness, or usefulness of any information, apparatus, product, or process disclosed, or represents that its use would not infringe privately owned rights. Reference herein to any specific commercial products, process, or service by trade name, trademark, manufacturer, or otherwise, does not necessarily constitute or imply its endorsement, recommendation, or favoring by the United States Government or the University of California. The views and opinions of authors expressed herein do not necessarily state or reflect those of the United States Government thereof, and shall not be used for advertising or product endorsement purposes.





CABLE
SECTION A-A
FIG 4

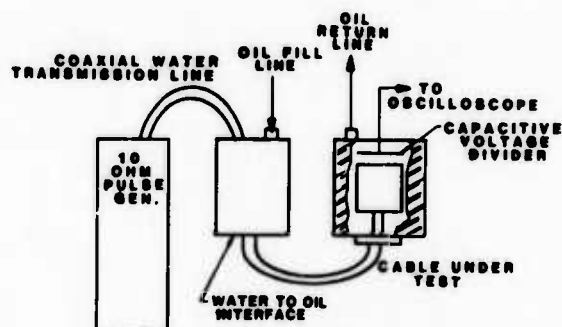


FIGURE 5

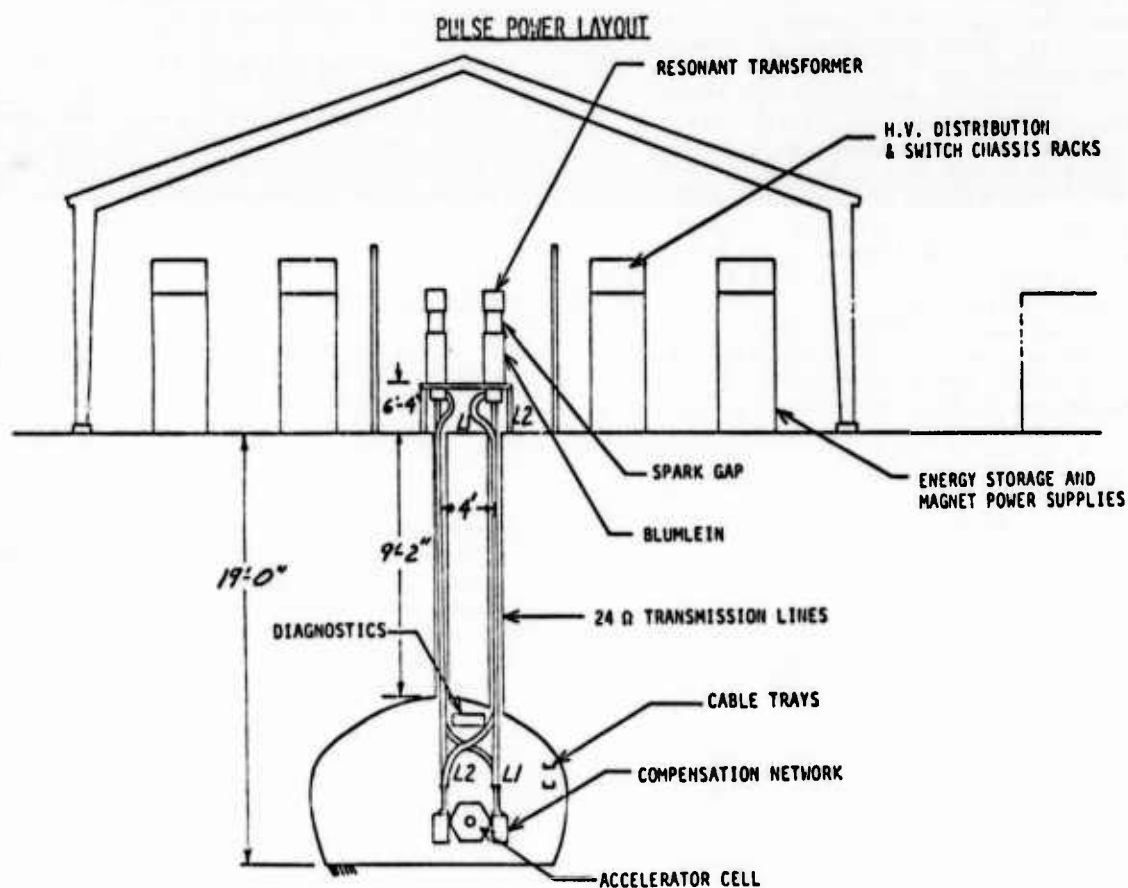


FIG. 6

FILLING COMPOUND FLOW TEST

C. K. Eoll

Siecor Corporation
Hickory, North Carolina

Abstract

The Rural Electrification Administration and others specify that filled telephone cable must pass a "compound flow test". This "drip test" involves hanging a short sample of cable in a hot oven for a specified period of time; filling compound must not drip from the sample. According to the version of REA PE-89 described in the Federal Register dated July 9, 1984, cable with copper conductors and cellular insulation must be tested for 24 hours at 80°C. The results of extensive drip testing are reported. Two different modes of failure are identified and traced to different sources in the processing. The results show that some cable susceptible to one of the two failure modes can pass at 80°C but fail at lower temperatures such as 71°C. In addition, the method of sample preparation is shown to affect the outcome of drip tests.

Introduction

The relation between drip performance and processing conditions in the filling operation was investigated for filled, foam-skin telephone cables.

Drip testing was performed at four test temperatures from 71 to 85°C, using samples prepared by each of two methods. For every combination of temperature and method of preparation, several samples of each experimental cable were tested.

Included in the results were some surprises.

Procedure

The filling trials were carried out using 25x19, 100x26 and 50x26 AWG foam-skin cores that had been manufactured earlier. All cores were filled in tandem with jacketing, using experimental pressure filling equipment.

About 300 to 500 ft of core was needed to make each 30-foot test cable. In all, twelve such cables were manufactured under various conditions of processing.

Choice of Filling Compound.

For this experiment a grease was chosen that was known to be relatively susceptible to drip failure at the highest test temperatures. Without a significant number of failures the results would contain little of the information sought.

Filling Equipment.

The experimental equipment included a pressure filling chamber 30 inches in length. Grease was supplied to the head by a positive-displacement pump with a continuously variable output.

Provision was made to allow grease overflowing the head to be collected whenever necessary to measure the rate and temperature of the overflow. (A small amount of material escaped collection. This led to systematic errors in the measurements - errors which were small, but for which no quantitative estimates of magnitude were available.)

Processing Conditions.

For the 19 AWG core, the temperature of the grease in the pot at the filling station as well as the overflow rate were varied from run to run. Only the overflow rate was changed for the 26 AWG cores. The particular conditions chosen were extreme in some cases, again to help ensure a significant number of drip failures.

For all runs of any particular core, all other conditions were kept essentially the same.

"Start-up" line speeds were used in this set of trials.

Equilibrium Conditions: It was assumed that equilibrium conditions in the filling head were quickly established once the line reached its intended speed and the appropriate overflow rate was set. Data was available to prove that this was at least approximately true under some processing conditions.

In most cases at least 120 ft. of core was run through the head to allow equilibrium to be established. To help in reaching such a condition quickly, the filling head was not allowed to cool off between trials; grease was kept circulating through the head.

Only under equilibrium conditions would a test cable be made in the same way throughout its length.

Actual Temperature of Grease Filling Cores: The grease loses a significant amount of heat as it is pumped from the pot to the head. Heat is lost to the pipes, the pump and the head itself. One may estimate the temperature drop associated with this loss as follows. If the line is stopped with the core still in the filling head and with the temperature of the grease in the pot unchanged, overflow temperature drop as a function of overflow rate may be measured. The temperature drop due to cooling by the equipment under the original processing conditions is approximated by the zero-line-speed temperature drop at an overflow rate equal to the original total rate of flow through the pump. (Since flow patterns and temperature distributions in the head are different at zero line speed than at normal running speeds, the rate of heat loss to the head itself can be different. Therefore the zero-line-speed data cannot provide more than an estimate of the loss under normal running conditions.)

Heat loss at zero line speed was measured for two overflow rates for each of the three cores used in this experiment. Using this data the temperature of the grease actually involved in filling and heating each core during the experimental runs was estimated.

Test Conditions.

Sample Preparation: Except for the method of flaring the pairs, all drip samples were prepared according to the REA compound flow test procedure in PE-89. Each test sample was one foot in length, with 5 inches of jacket and 3 inches of shield and core wrap removed from one end.

Roughly half the samples had the exposed pairs flared according to the REA method, where each pair is separated from every other pair. In the remaining samples the pairs were flared in a way that will be designated the XXX method, where all pairs are flared at 45° to form a hollow cone.

Definition of Drip Failure: The presence of an oily spot or spots on the paper under a sample after 24 hours at the test temperature constituted a failure for the purposes of this investigation. Sometimes at the end of a test there would be what looked like droplets of liquid on the flared conductors. If the paper underneath was clean, however, the sample was not considered a failure.

Occasionally, a blob of solid-looking material was found on the paper under a sample. Such a blob typically appeared within the first hour or so of a test. If there was no other evidence of dripping within the 24 hour test period, the sample was considered to have passed. (Sometimes when pairs are flared during sample preparation, a blob of filling compound is left hanging from a conductor by only a thread of grease. The weight of the blob and/or air motion in the oven can cause such a thread to break during testing. The dropping of such a blob was not deemed to be a true failure.)

Results

The drip performance of 347 samples of the various test cables is presented in Table I.

For each test cable the final temperature of the filled core as it left the filling head is calculated in Appendix II using a formula given in Appendix I.

Table I provides only some of the processing information pertinent to each test cable. Table VII in Appendix II provides further data.

TABLE I: Drip Performance

Pair Count & Gauge (AWG)	Cable #	Approx. Temp. of Grease in Pot (°F)	Flow Rate into Head = W + G (lbs/min)	Temperature and Type of Drip Test *							
				71°C		75°C		80°C		85°C	
				XXX	REA	XXX	REA	XXX	REA	XXX	REA
25x19	1	220	6.5	PP	PPP	PPPP	PPP F	PPPP	PPP F	PPPP	PPPP
"	2	"	14	PP	PPP	PPPP	PPPP	PPPP	PPP F	PPPP	PPPP
"	3	"	32	PP	PP F	PPPP	PPPP	PPPP	PPPP	PPP F	PPP F
"	4	235	6.5	PP	PPP	PPPP	PPPP	PPPP	PPPP	PPPP	PPPP
"	5	"	14	PP	PP	PPPP	PPPP	PPPP	PPPP	PPPP	PPP F
"	6	"	26	PP	PPP	PPP F	PPPP	PP FF	PPP F	FFFF	FFFF
"	7	"	33	PP	PPPP	PP	PP	P FFF	P FFF	FFFF	FFFF
100x26	8	220	4.6	PPP	P FF	PPPP	PP FF	PPPP	PPPP	PPP F	PPPP
"	9	"	16	PPP	P FF	PPPP	PPPP	PPPP	PPPP	PPPP	PPPP
50x26	10	220	8.2	PP	PP F	PPPP	PPP F	PPPP	PPPP	PPPP	PPPP
"	11	"	18	PP	PPP	PPPP	PPPP	PPPP	PPPP	PPPP	PPPP
"	12	"	83	PP	PP FF	P FFF	FFFF	PP FF	P FFF	P FFF	FFFF

* XXX = pairs in 45° hollow cone; REA = each pair separated from others; P = Pass, F = Fail

Interpretation of Results

Two Types of Drip Failure.

Drip failures in Table I fall naturally into two distinct classes. One class, the "random" failures, includes relatively isolated failures scattered across the four test temperatures. The other class, the "non-random" failures, includes those that cluster at the higher test temperatures: if non-random failures occur at some test temperature, then non-random failures will occur at all higher test temperatures. In the case of cable #7, for example, the majority of samples tested at 80° and 85°C failed; but there were no failures at 71° or 75°C. In only one or two cases is there any doubt about which class a failure belongs to.

Melt Failures.

The non-random failures (Table II) are associated with those trials with the hottest grease and/or the highest overflow rates. Cable #12, for example, was made with an extremely high overflow rate; and the failure rate at 71° was 33% while at all higher test temperatures the failure rate was at least 63%.

Table VII in Appendix II indicates that, generally speaking, increasing either the overflow rate or the greasing temperature increases the temperature of the core as it leaves the filling head. Table III compares core temperature to drip performance. Noting that possible experimental errors make the core temperatures only approximate, no

TABLE II:

Melt (Non-random) Failures in Table I

No. of failures in 4 test samples:

Test Temp. (°C)	71	75	80	85
Method	XXX REA	XXX REA	XXX REA	XXX REA
Cable # 3				1 1
# 5				0 1
# 6		1** 0	2 1	4 4
# 7			3 3	4 4
# 12	0* 2	3 4	2 3	3 4
Total	0 2	4 4	7 7	12 14

* Only 2 samples tested.

** Identification of failure type uncertain - tentatively taken as a non-random failure.

TABLE III:

Melt (Non-random) Failures

Gauge (AWG)	Cable #	Approx. Core Temp. after Filling (°F)	Lowest Temp. at which Failures Occurred (°C)
19	1	157	None
"	2	185	None
"	3	194	85
19	4	173	None
"	5	194	85
"	6	189	75*
"	7	200	80*
26	8	155	None
"	9	179	None
26	10	170	None
"	11	186	None
"	12	215	71

* One cannot be certain that the single failure of cable #6 at 75°C was a non-random failure. In addition, only four samples of cable #7 were tested at 75°C; it is possible that failure(s) of that cable at 75°C would have occurred if eight samples had been tested as in the case of cable #6 at 75°C.

cable that had a core temperature of 186°F or lower exhibited non-random failures, while every cable where the core temperature was 189°F or higher did show such failures.

Shock-cooled grease is known to have a higher melting point than grease that cools slowly from the molten state. Conventional wisdom says that filling compound in a core must cool rapidly through some congealing point in order to end up with good drip properties, and the above results* provide supporting evidence in the case of non-random failures. By implication, unless the temperature of the core is already below this congealing point when the core leaves the filling head, the subsequent slow cooling will yield a grease with a suppressed melting point. Then this grease simply melts in the drip tests, producing non-random failures at all test temperatures at or above its melting point. With this reasoning in mind, the non-random failures are being called "melt failures".

Shear Failures.

The random failures almost all occurred in samples tested using the REA method. With only one unequivocal exception - one of the samples of Cable #8 tested at 85°C - none of the samples tested using the XXX method of flaring the pairs exhibited random style failures.

When the random failures at each test temperature are all considered together regardless of core type or processing conditions, rate of failure is found to go up as test temperature goes down. As shown in Table IV, for samples from the six cables exhibiting random failures and prepared by the REA method, the failure rate goes from 0% at 85°C to 33% at 71°C. (This behavior is even more exaggerated for 26 AWG cable considered alone: 56% of the samples tested at 71°C failed, and there were no failures at 80 or 85°C.)

Table V relates the number of random failures exhibited by each core to the approximate core temperature immediately after filling. In contrast to the case of melt failures, there is no simple overall relationship between failures and core temperatures. Fixing attention on the cables made with the 220°F grease and considering only one core type at a time, however, the number of random failures typically fell with increasing core

* Perhaps the congealing point appropriate to filling with the experimental grease should be defined to be between 186 and 189°F. The congealing point measured by the particular method of ASTM D-938 was 181.5 °F. Since the absolute accuracy of the calculated core temperatures is possibly poor, the two congealing points might even be closely related.

TABLE IV:

Shear (Random) Failures in Table I

No. of Failures Using REA Method:

Cable #	Gauge (AWG)	Test Temperature (°C)			
		71	75	80	85
1	19	0	1	1	0
2	"	0	0	1	0
3	"	1	0	0	
8	26	2	2	0	0
9	"	2	0	0	0
10	"	1	1	0	0
Total		6	4	2	0
No. of samples of each cable tested		3	4	4	4
% failure rate		33	17	8	0

Note: Using XXX method, only one out of 86 samples of these same cables at the same test temperatures exhibited a definitely random style failure.

temperature. The number of random failures also dropped when 235° instead of 220° grease was used to fill the 19 AWG core. Thus, for a given core, increasing the pot temperature and/or the overflow rate will reduce the number of random failures.

Many filling compounds are known to be shear sensitive. According to conventional wisdom their drip properties are degraded by shearing forces, acting on the partially or wholly solidified materials. Such working of a grease would be involved if it was squeezed between the conductors in a core after it had congealed. Since random failures are associated with lower core temperatures, it is natural to connect the random failures with degradation through shear; so random failures are being called "shear failures".

Earlier Work.

Several papers^{1,2,3} in the literature of the early seventies addressed subjects related to drip testing. Since then, further understanding has been gained but little has been published. The "conventional wisdom" referred to in the last two sections is, of course, the author's interpretation of recent information that has been available through private communications.

ConclusionsThe Experimental Grease.

For cable made by using a particular grease to pressure fill preassembled cores, two distinct drip failure mechanisms were identified. Melt failures are associated with cores that are too hot as they leave the filling head, and shear failures are associated with cores that are too cold.

The XXX method of flaring the pairs in drip samples was unsuitable for identifying cable susceptible to shear failures.

For 26 AWG cable tested using the REA method of flaring the pairs, shear failures were found only at the lower test temperatures of 71 and 75°C. Considering cables #8 and #9 in particular, the results were startling: amongst samples prepared by the REA method none failed at 80°C, whereas the failure rate at 71° was 67%.

According to the version of REA PE-89 described in the Federal Register published on July 9, 1984 (pages 27,952 to 27,954), cables with cellular insulation must be tested for drip at 80°C; according to the discussion in the

TABLE V:

Shear (Random) Failures

Gauge (AWG)	Cable #	Approx. Temp. of Grease in Pot (°F)	Approx. Core Temp. after Filling (°F)	No. of Failures*
19	1	220	157	2
"	2	"	185	1
"	3	"	194	1
19	4	235	173	None
"	5	"	194	None
"	6	"	189	None
"	7	"	200	None
26	8	220	155	5
"	9	"	179	2
26	10	220	170	2
"	11	"	186	None

* amongst all samples, whether prepared by REA or XXX method.

Register, if a filling compound passes the 80° requirement then separation of the material will be avoided in aerial installations. Cables #8 and #9, for example, show that passing an 80° test provides no such guarantee, assuming that poor behavior in drip tests really can imply a higher susceptibility to compound separation.

By tailoring process conditions to ensure that shear failures will not occur - i.e. by processing at relatively hot temperatures - one increases the risk of melt failures at 80°C. Susceptibility to drip at lower test temperatures would, however, be avoided.

A better product could be assured by a 71°C requirement than by an 80°C requirement.

Other Greases.

Other filling compounds have been found to be prone to shear failures to varying degrees. Extensive experimental work with several members of one widely used class of compounds found some susceptibility to shear failure in every one of those members - and the best materials with respect to melt failure are not necessarily the best from the point of view of shear. At least some of these compounds can be used to make products that pass drip tests both at 80°C and lower temperatures; in all cases, however, temperatures in processing must be kept under relatively tight control if melt and shear failures are both to be avoided.

Acknowledgements

The author should like to thank Siercor Corporation for permission to publish this paper.

He is also indebted to the many fellow employees, including G. Williamson and L. Davis, who helped with the factory trials and/or the drip testing.

Finally, thanks are due to M. Armstrong for typing the manuscript.

References

1. R.A. Conser, T.A. Heim and L.D. Moody, "Manufacturing Waterproof Telephone Cable", Proc. of the 19th International Wire & Cable Symposium, p. 270, 1970.
2. R.G. Schneider and E.L. Franke, "Vacuum-pressure Impregnation of Waterproof Cable & Associated In-line Compound Mixing System", Proc. of the 20th International Wire & Cable Symposium, p. 134, 1971.

3. J.J. Kaufman and T.E. Luisi, "Shear & Flow Characteristics of Waterproof Petrolatum-based Cable Filler Compounds", Proc. of the 23rd International Wire & Cable Symposium, p. 76, 1974.

Appendix I:

Formula for Core Temperature

The final temperature of a core, T_f^c (°F), as it leaves the filling head is given by the

$$T_f^c = \left(\frac{1}{1 + \alpha} \right) \left[T_1^g + \frac{1,000W}{gL} (T_1^g - T_f^g) + \alpha T_1^c \right],$$

where T_1^c = the initial temperature of the core as it enters the filling head, i.e. the temperature of the unfilled core (°F);

T_1^g = the initial temperature of the grease that fills and heats the core, and it is defined to be the temperature of the grease in the pot (T_p^g) less the temperature drop due to heat loss to the equipment (°F);

T_f^g = the final temperature of the grease that only heats the core, i.e. the temperature of the overflow (°F);

W = overflow rate (lb/min);

L = line speed (ft/min);

g = rate of consumption of grease by core, i.e. the amount of grease within the core wrap tape in the final cable (lb/1,000 ft).

The parameter α is dimensionless, and it is defined by the formula

$$\alpha = \frac{c_c c + c_i i}{c_g g},$$

where c_c , c_i and c_g are the heat capacities of copper, the insulation and the grease, respectively, in BTU/(lb·°F); and c and i are the amounts of copper and insulation, respectively, in lb/1,000 ft.

The above formula for T_f^c may be easily derived by noting that the core is heated by the grease which remains in the core as well as the grease which overflows the head, and assuming that the core is uniform in temperature as it leaves the head.

Appendix II:

Temperature of Filled Cores

The temperature of each core as it left the filling head may be found in the last column of Table VII. These temperatures were calculated by means of the formula in Appendix I, using the input data provided in Tables VI and VII.

The only "possible experimental errors" that were taken into account in the calculations were some of the possible errors in temperature. Other possible errors were ignored, either because they had a relatively small impact, or because they could significantly affect only the absolute, not the relative, accuracy of the calculated core temperatures.

Estimating Heat Loss to Equipment.

The line drawn through the experimental points in Graph I was used to provide the estimates of the drop in grease temperature due to heat loss to the piping, pump and head.

The six points plotted for flow rates between 6 and 36 lb/min give the measured amounts by which the temperature dropped at zero line speed. Within experimental error, the temperature drop was independent of core type and pot temperature here.

As for the point at a flow rate of about 83 lb/min, the estimate of the temperature drop of the grease due to heat loss to the equipment was calculated using data from cable # 12 where the core was moving at 30 ft/min. Since 141 times as much grease was being pumped through the head as was being consumed by the core one could assume that the insulated conductors must have become almost as hot as the overflowing grease. At 30 ft/min this would have required about 61 BTU/min; and with grease flowing at 83 lb/min, 56 BTU/min would have been provided for each degree Fahrenheit drop in grease temperature. Thus about 1°F of the drop in temperature of the overflow was attributed to the cooling of the grease by the core. Since the overflow was $5 \pm 1^\circ\text{F}$ cooler than the grease in the pot, heat loss to the equipment resulted in a temperature drop of about $4 \pm 1^\circ\text{F}$.

TABLE VI:

Parameters for Calculating Core Temperatures

Material	Heat Capacity in BTU/(lb.°F)
Grease	0.674*
Copper	0.093
High density polyethylene insulation	0.55

* average from 163 to 235°F.

Core Type	** α
25 x 19 FS	1.06
100 x 26 FS	1.21
50 x 26 FS	1.15

** defined in Appendix I, and calculated using nominal values for weights per 1000 ft of copper, insulation and grease in each core type.

Temperature in plant = 82°F; unfilled cores assumed to have same temperature.

GRAPH I:

Drop in Temperature of Grease Due to Loss of Heat to Equipment

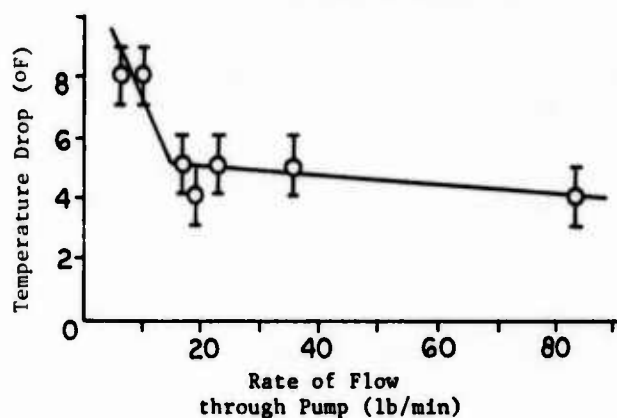


TABLE VII : Core Temperatures after Filling

Cable #	Type of Core	Temp. of Grease in Pot (°F)	Line Speed (ft/min)	Measured Head Over-flow Rate (lb/min)	Temp. of Head Overflow (°F)	Calculated Consumption by Core (lb/min)	Estimate of Temp. Drop in Piping, etc. (°F)	Cooling of Overflow by Core (°F)	Final Core Temp. (°F)
1	25x19	220	40	4.58	200	1.96	9.0 ± 1.0	11 ± 2	157 ± 3
2	"	222	40	11.8	204	1.96	5.0 + 0.7 - 0.5	13 + 1.7 - 1.5	185 ± 5
3	"	222	40	30.3	211	1.96	4.8 ± 0.5	6.2 ± 1.5	194 ± 12
4	"	234	40	4.51	206	1.96	9.0 + 2.0 - 1.0	19 + 3 - 2	173 + 4 - 3
5	"	235	42	11.7	215.5	2.05	5.0 + 1.0 - 0.5	14.5 + 2 - 1.5	194 + 6 - 5
6	"	235	40	23.5	224	1.96	4.9 ± 0.5	6.1 ± 1.5	189 ± 9
7	"	235	41	30.7	224	2.00	4.8 ± 0.5	6.2 ± 1.5	200 ± 12
8	100x26	220	29	3.50	199	1.08	10.0 ± 1.5	11 ± 2.5	155 ± 5
9	"	220	28	14.5	209	1.04	5.0 ± 0.5	6.0 ± 1.5	179 ± 10
10	50x26	220	29	7.58	207.5	0.57	8.0 ± 1.0	4.5 ± 1.6	170 ± 10
11	"	220	29	17.3	212	0.57	5.0 ± 0.5	3.0 ± 1.5	186 ± 21
12	"	220	30	82.5	215	0.59	4.0 ± 1.0*	1*	215*

Symbol or formula T_p^g L W T_f^g $\frac{Lg}{1,000} \equiv G$ $T_p^g - T_i^g$ $T_i^g - T_f^g$ T_f^c

Possible error in each reading ±0.5 ±0.5**

* Here the final core temperature is assumed, not calculated. Details are provided in text.

** Except for cable # 10 where the possible error is ±0.1.



C.K. Eoll

Siecor Corporation
489 Siecor Park
Hickory, NC 28603
U.S.A.

Christopher K. Eoll was born in Thunder Bay, Ont., Canada in 1940. He received a B. Sc. degree in physics and an M. Sc. degree

in theoretical physics from Queen's University, Kingston, Ont., Canada in 1962 and 1964, respectively. Then in 1967 he was granted a Ph. D. degree in mathematical physics by the University of Toronto, Toronto, Ont., Canada. Subsequently, he spent two years as a Post-doctoral Fellow at the University of Sussex, Brighton, England and the International Centre for Theoretical Physics, Trieste, Italy.

From 1969 to 1977 he was employed by Canada Wire and Cable Ltd., where his final position was Product Development Manager for the Communications Products Div. He joined Superior Cable Corp. in 1977 as Technical Director. At present, he is a Senior Scientist for Siecor Corporation.

Water Blocking Optical Fiber Cable Filled with Grease Compound

T. Kaneko, S. Yamaguchi, H. Tanaka, T. Maeda,
Y. Ijiri, K. Mio and Y. Hayashi

Dainichi-Nippon Cables, Ltd., Itami, Japan

Abstract

In order to improve reliability of the optical fiber cable and lower maintenance cost, an optical fiber cable using a new water blocking material has been developed. The water blocking compound consists of urea grease as a filler and starch modified with acrylic acid as a water absorbent and sweller. This material has the advantages of being easily injected, inexpensive and soft at room temperature.

Two types of optical fiber cables, one incorporating ten and the other thirty VAD-GI optical fibers, were made with this water blocking compound. There was no degradation of fiber properties due to cable fabrication. The test results of optical and mechanical properties were the same as or better than those of the air core cable. No compound dropping was observed in flow experiment at 110 °C for 24 hours. The excellent water blocking capability of the compound was proved.

1. Introduction

Water seepage into optical fiber cable causes an increase in transmission loss and deterioration of fiber strength.¹⁾ To overcome this problem, the gas maintenance system has been conventionally used. This system, however, involves protective measures and equipment leading to much complicated maintenance and high cost. Therefore, the development of a new water blocking optical fiber cable has been required. In the past, water blocking materials used in metallic cables have been experimented with, but a material which sufficiently meets the demands of optical fiber cable was not developed.

We have considered a new compound consisting of urea grease as a filler and starch modified with acrylic acid as a water absorbent and sweller. With this new blocking compound we prepared layer type and unit type cables.

This paper reports the characteristics of the water blocking compound itself. Also included are the

results of tests of these cables for loss increase by cabling, water blocking, roll bending, and heat cycle properties as well as loss under lateral pressure.

2. New Water Blocking Material

2.1 Water Blocking Test

The water blocking compound we have developed is a mixture of urea grease and starch modified with acrylic acid which act as an absorbent and sweller. This material, soft at room temperature, is easily injected and does not affect the fibers when the cable is pressed by external force such as bending, lateral pressure and so on. Table 1 shows the characteristics of various grease compounds: water blocking capability, dropping point, cone penetration of samples with varying proportions of urea grease and starch modified with acrylic acid. The water blocking test was carried out by spreading a 10⁰ x 10⁰ x 0.1⁰ cm sample on a glass plate, and by placing a 0.9 mm thick metal mesh on top and another glass plate over the mesh. One of the edges was placed in water and the amount of seepage was measured. The use of starch as a water absorbent is very efficient.

Table 1 Characteristics of Various Grease Compounds

Ratio of urea grease and Starch	1:0	2:1	1:1	1:2
Water blocking capability	None	Good	Good	Good
Dropping point (°C)	>200	>200	>200	>200
Cone penetration	272	255	207	152

A dropping point over 200 °C is a characteristic not found in the conventional water blocking material used in metallic cables. The urea grease to starch ratio of 2:1 seems better, in consideration of the influence of the compound on the fibers and ease of filling, as the compound softens in proportion to the amount of grease mixed in.

2.2 Absorption Test

On the assumption that water seepage and drying are repeated, the water absorption capability of the compound was tested. Testing was conducted on the compound (urea grease: starch = 2:1) by the following procedure and the absorption and drying process was repeated five times.

(1) An envelope was made with a filter paper and weighed. (w)

(2) The compound (about 1 g) was placed in the envelope and weighed. (w_0)

(3) The envelopes were allowed to absorb de-ionized water, tap water, or 5 % salt water for an hour and weighed. (w_1)

(4) The envelopes were dried for 48 hours at 50 °C and weighed. (w_2)

Then absorption was calculated with the following formulae:

(A) : the amount of water absorbed by starch

(W_A) : the amount of water absorbed by the filter paper

$$A = W_1 - W_0 - W_A$$

(B) : water left after drying

$$B = W_2 - W_0$$

The results of the test as shown in Fig. 1 indicate no deterioration in absorption capability of the samples allowed to absorb de-ionized water, tap water or salt water.

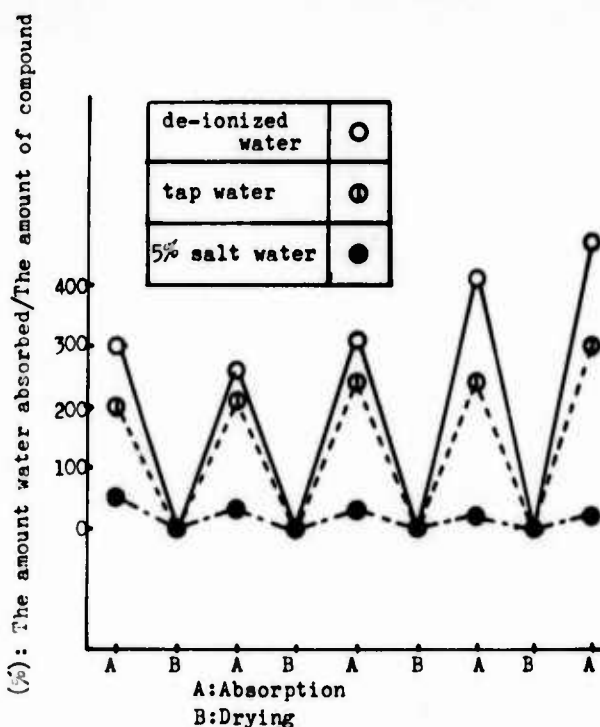


Fig.1 The Results of Repeated Absorption Test

2.3 Compound Reliability Test

Another test was performed to check whether seeped water can be blocked in the developed compound over a long period of time.

Glass tubes 7.5 mm in diameter and 1,000 mm in length were filled with samples (urea grease, starch or the compound) to 550 mm, then 300 mm of colored water was poured onto the samples and they were allowed to stand for two months. The length of water permeation was measured.

As shown in Table 2, the sample with the compound consisting of urea grease and starch with a 2:1 ratio stopped the permeation.

Table 2 Length of Water Permeation (mm)

Sample Time	Urea grease	Compound	Starch
Initial	0	0	0
1 hr.	290	0	0
2 hrs.	310	0	0
3 hrs.	400	1	11
6 hrs.	550	2	12
2 days	leaked	8	15
4 days	-	13	18
10 days	-	22	22
20 days	-	22	42
40 days	-	22	42
60 days	-	22	42

n.b Samples were not fully-filled in consideration of the practical application to cables.

Finally, the effect of this compound on fiber coating materials such as nylon and epoxy was tested by leaving these materials placed in the compound at 100 °C for 72 hours. The stability of the compound was proved by the absence of swelling and chemical reaction.

3. Optical Fiber Cables Using the Water Blocking Grease Compound

A layer type cable with ten fibers and a unit type cable with thirty fibers were made with the developed compound and tested. The optical fibers 50/125 μm in diameter were graded-index type VAD fibers with silicone buffer 0.4 mm in diameter and nylon jacketing 0.9 mm in diameter.

3.1 Layer Type Ten Fiber Cable

Two layer type ten fiber cables as shown in Fig. 2 were made: one was filled with the compound and the other with pp-yarn. Comparison of test results revealed the following:

(1) No loss increase due to compound filling was seen because the compound is soft at room temperature.

(2) The water blocking test performed at 1.2 m water pressure for 24 hours showed that a cable filled to 80% with the

new compound was more than able to stop seepage. However, the use of urea grease only as a filler requires filling the cable 100 %.

(3) Fig. 3 shows results of roll bending tests. The cable filled with the grease compound showed results similar to those of the pp-yarn cable.

(4) Fig. 4 shows the comparison of lateral pressure resistance of these cables. Loss increase incurred by sandwiching the cable with iron plates 50 mm wide as shown in Fig. 5 was measured. The results show the grease compound cable had the better lateral pressure resistance.

(5) The bending test was also carried out with a mandrel and loss increase was measured. As shown in Fig. 6, results were satisfactory.

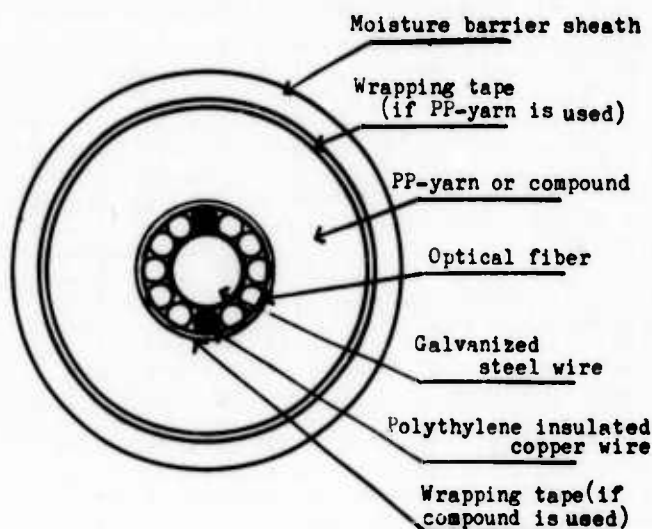


Fig. 2 Cross-section of Layer Type Ten Fiber Cable

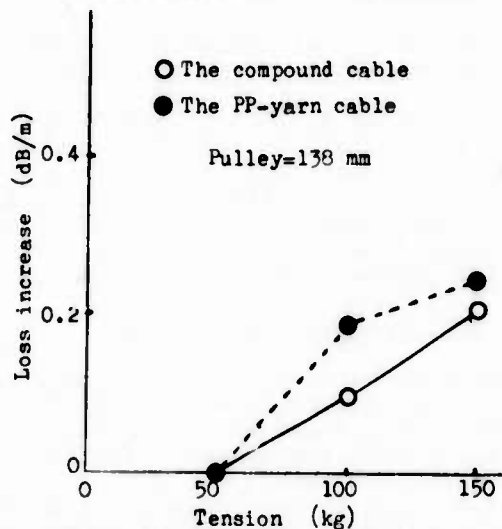


Fig. 3 Roll Bending Characteristics of Layer Type Ten Fiber Cable

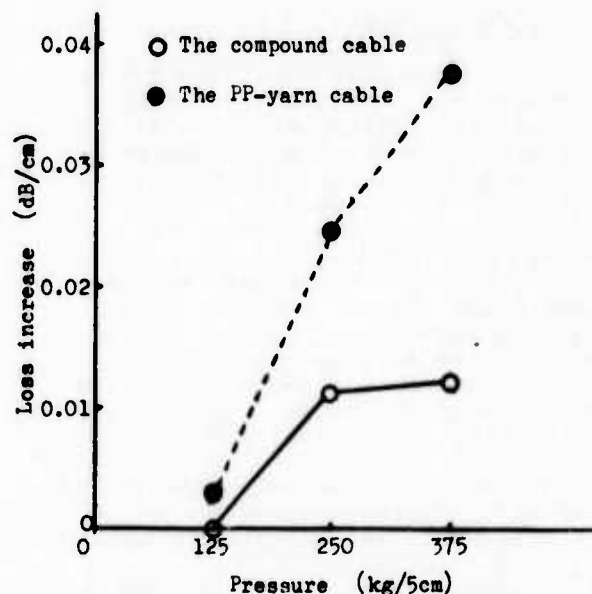


Fig. 4 Lateral Pressure Resistance

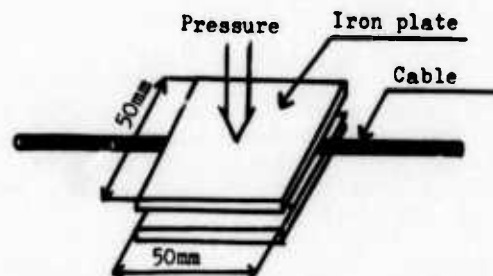


Fig. 5 The Method of Lateral Pressure Test

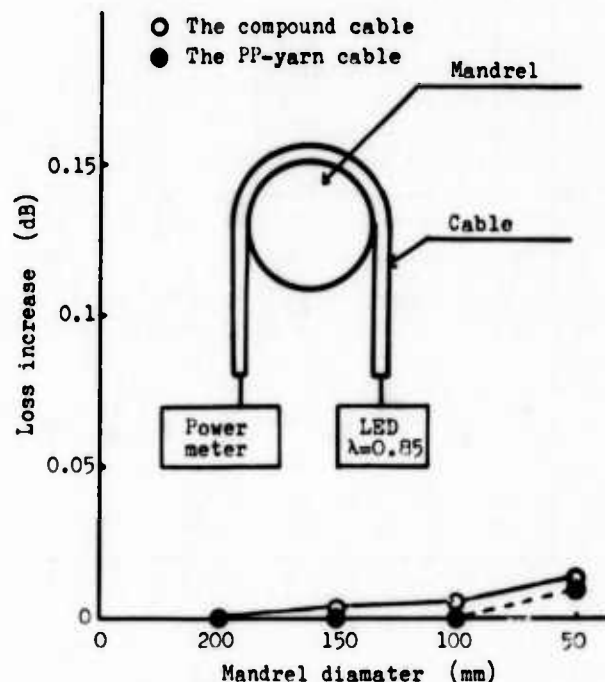


Fig. 6 The Method and the Results of the Bending Test

3.2 Unit Type Thirty Fiber cable

The applicability of the developed grease compound to optical fiber cable was confirmed in the section 3.1. Next, a unit type thirty fiber cable with a spacer having spiral grooves to enhance protection against roll bending and lateral pressure as shown in Fig. 7 was tested.

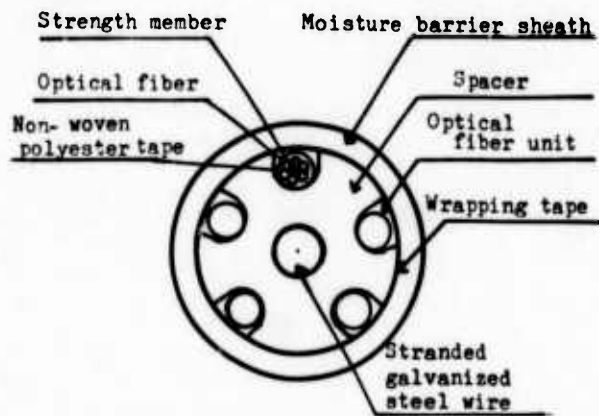


Fig. 7 Construction of Unit Type Thirty Fiber Cable

In order to increase the number of fibers each groove can contain a six-fiber unit. Non-woven polyester tape with mesh was used as support wrapping to facilitate filling of the compound. Evaluation tests showed the following results:

- (1) No loss increase was observed after fiber stranding, unit stranding and compound filling.
- (2) Fig. 8 shows the results of the roll bending test. At 200 kg tension, a loss increase less than 0.01 dB/km was recorded. There was no change in stranding pitch after the test.
- (3) Fig. 9 shows the results of the lateral pressure test. There was no loss increase by lateral pressure up to 500 kg/5 cm owing to the high protectiveness of the spacer.
- (4) A heat cycling test (-30°C for 6 hours - 60°C for 6 hours) was carried out. Loss increase was less than 0.04 dB/km, indicating little influence of temperature on cable performance. This is because the compound itself remains soft even in low temperatures.
- (5) The results of water blocking, dropping, bending, flexibility, and torsion tests summarized in Table 3 were satisfactory.

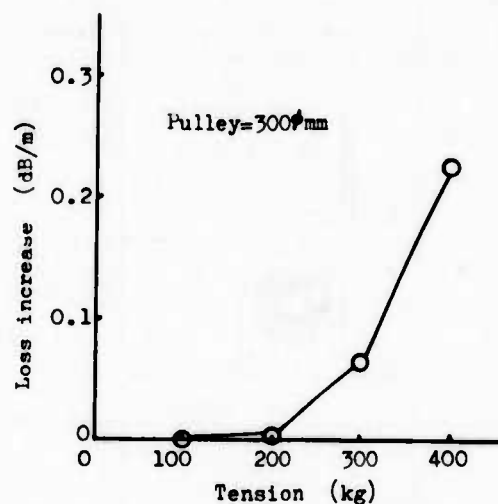


Fig. 8 Roll Bending Characteristics of Unit Type Thirty Fiber Cable

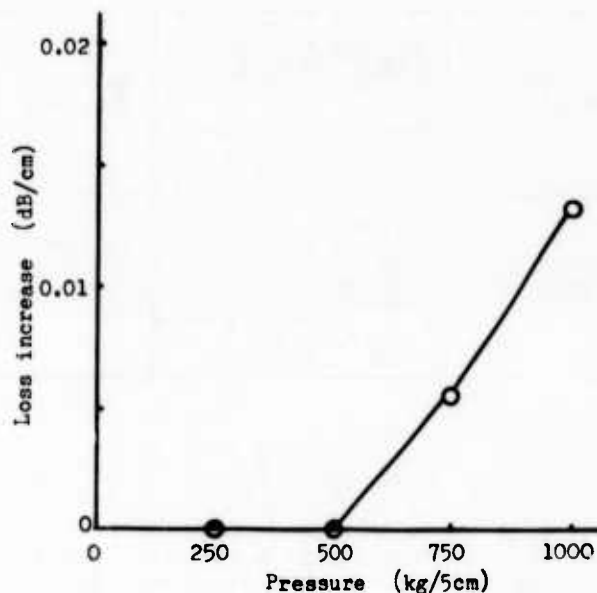
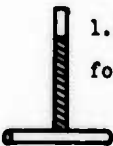

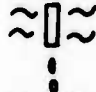




Fig. 9 Lateral Pressure Resistance of Unit Type Thirty Fiber Cable

Table 3 Test Conditions and Results

Item	Test condition	Results
Water-blocking	 1.2m Pressure for 24 hours	1cm length of water permeation
Bending	 Mandrel diameter=200mm 2 Times of reciprocation	No loss increase
Dropping	 Sample length=13cm 110°C x 24 hours	No dropping
Flexibility	 Sample length=50cm	14cm/1kg
Torsion	 Sample length=1m Torsional angle=±180°	No loss increase

4. Summary

As a water blocking compound for optical fiber cable we have developed a mixture consisting of urea grease and starch modified with acrylic acid as an absorbent. A layer type ten fiber cable and a unit type thirty fiber cable incorporating the developed compound were test-produced and their excellent optical and mechanical properties were confirmed. The water blocking capability of this compound greatly enhances the reliability of optical fibers.

Reference

- 1) B. R. Eichenbaum, M. R. Santana, L. D. Tate, and R. Sabia, "Design and Performance of a Filled High-fiber-count Multimode Optical Cable", International Wire & Cable Symposium Proceedings, (1982) pp 396 - 400



Takashi Kaneko
DAINICHI-NIPPON
CABLES, Ltd.
4-3, Ikejiri, Itami
664, Japan

Mr. Kaneko joined DAINICHI-NIPPON CABLES, Ltd., in 1974 and is currently engaged in design of optical fiber cable. He received B. E. degree in electronics engineering from Sophia University in 1974.



Shunichiro Yamaguchi
DAINICHI-NIPPON
CABLES, Ltd.
4-3, Ikejiri, Itami
664, Japan

Mr. Yamaguchi joined DAINICHI-NIPPON CABLES, Ltd., in 1975 and has been engaged in research and development of telecommunication cables. He received B. E. degree in electrical communication engineering from Waseda University in 1975.



Hiroyuki Tanaka
DAINICHI-NIPPON
CABLES, Ltd.
4-3, Ikejiri, Itami
664, Japan

Mr. Tanaka joined DAINICHI-NIPPON CABLES, Ltd., in 1971 and has been engaged in research and development of optical fiber cables. He received M. S. degree in electric engineering from Osaka University in 1971.



Tsutomu Maeda
DAINICHI-NIPPON
CABLES, Ltd.
4-3, Ikejiri, Itami
664, Japan

Mr. Maeda, manager of Electronics and Communication R & D Department, joined DAINICHI-NIPPON CABLES, Ltd., in 1978. He received B. E. degree in electrical communication engineering from Osaka University in 1958.



Yuichi Hayashi
DAINICHI-NIPPON
CABLES, LTD.
1008, Niibori
Kumagaya,
Japan

Mr. Hayashi, senior engineer of Production Engineering Department, joined DAINICHI-NIPPON CABLES, Ltd., in 1970. He received B. E. degree from Waseda University in 1970.



Yasuo Ijiri
DAINICHI-NIPPON
CABLES, LTD.
8, Nishonocho
Higashimukaijima
Amagasaki, 660
Japan

Mr. Ijiri, senior engineer of Materials Research Laboratory joined DAINICHI-NIPPON CABLES, Ltd., in 1969 after graduation from Osaka Prefectural Technical College.



Kotaro Mio
DAINICHI-NIPPON
CABLES, LTD.
8, Nishinocho
Higashimukaijima
Amagasaki, 660,
Japan

Mr. Mio, chief engineer of Materials Research Laboratory joined DAINICHI-NIPPON CABLES, Ltd., in 1966. He received B. E. degree in chemical engineering from Osaka Prefectural University in 1966.

A HIGHLY EFFECTIVE APPROACH TO WATERPROOFING CABLE

H HUGHES

R A HUNN

J T JOUBERT

SOUTH AFRICAN INVENTIONS DEVELOPMENT CORPORATION
SCIENTIA, PRETORIA, SOUTH AFRICA

ABSTRACT

The existing methods of cable waterproofing such as petroleum jelly filling, discrete water blocks, etc, are mentioned and their drawbacks are noted. This new patented approach uses coated yarn which is laid between the conductors in the cable. The effect of the coated yarn on the electrical and water resistant properties of the cable is discussed. Manufacture on conventional production equipment is easy and does not slow the production process down. Cable laying is done in the conventional manner with no danger of moisture ingress during field installation even under wet conditions. Jointing is clean and can be carried out at sub-zero temperatures if need be. There are no material incompatibility problems and the cable parameters are hardly affected by the waterproofing. In addition the cost penalty of waterproofing is less than 6%.

1. CURRENT SITUATION

The importance of providing plastic insulated cables with some form of protection against water ingress from sheath permeation, sheath damage or leaking joints is well documented (1) (2) (3). Among the methods that have been tried or adopted are:

- * Gas pressurization
- * Aluminium polyethylene laminate (APL) sheaths
- * Discrete water blocks
- * Petroleum jelly (pj) filling
- * Polyurethane filling
- * Water-swellable powder filling
- * Water-swellable tapes

All these have significant shortcomings of one form or another such as:

- * High capital cost of production or operating plant
- * Only partial protection
- * Non-uniformity of fillings due to manufacturing difficulties
- * Cable flexibility limitations

- * A degree of incompatibility of materials precluding the use of certain polymeric
- * A need to alter the cable design to maintain electrical properties
- * Jointing difficulties caused by the nature of the materials under service conditions.

2. NEW APPROACH

2.1 Description

Of all the existing methods of cable waterproofing the water-swellable powder appears to be the most promising solution, but it is difficult to obtain a uniform distribution of the powder in the cable. To incorporate the water-active agent into the cable with sufficient uniformity the idea was conceived to use a suitable yarn as a carrier and to include these coated yarns into the cable construction during the twinning stage of cable manufacture.

In this way the coating material is retained uniformly throughout the length and cross-section of the cable. In the presence of moisture, the active ingredient on the yarn reacts rapidly to produce a water block capable of remaining effective for many years even in the event of complete cable severance.

Beyond this, cable design and manufacture are entirely normal, involving negligible penalty in cable dimensions, electrical performance, production speed or cost.

2.2 Waterproofing effectiveness

The volume of the water-swellable compound increases about 16-fold when wet. In fact by observation of the mechanism of blocking in glass-tube models it would appear that the block is not formed by a mechanical pressure blocking of the interstices so much as by an increase in the viscosity of the penetrating water to the point where it can no longer flow through the interstices. This happens very quickly with the chosen material so that under a metre head of water, the block stabilises, restricting the presence of water to within 900 mm from the point of entry, as can be seen from the limiting boundary in Fig. 1.

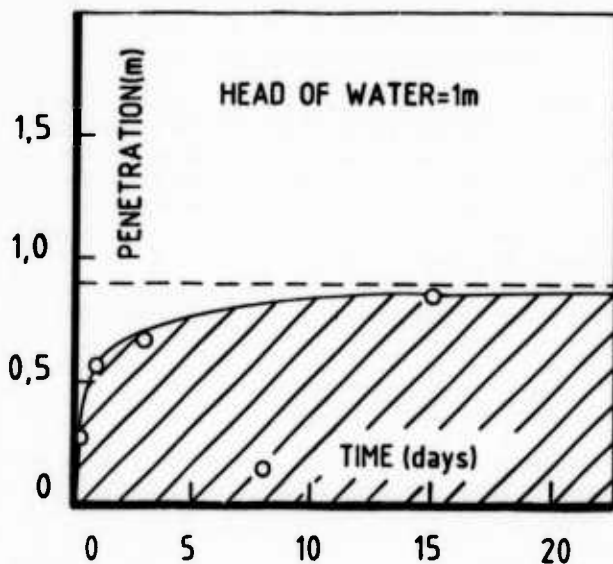


Fig 1. Formation of Water Block in Cable.

Early cable samples have withstood 1 m head of water, end-applied, for over four years to date without signs of deterioration or failure under normal ambient conditions.

2.3 Stage of development

Production-scale lengths have been made and are being tested in a local telephone distribution network in South Africa.

3. CABLE DESIGN

It was decided to base this design on a standard 50-pair APL-sheathed subscriber distribution cable. Conductors would be 0,5 mm insulated with solid polyethylene to a diameter of 0,92 mm, and assembled in 5x10-pair units. The diameter of the coated yarn is selected to fit into the interstice between conductors. The APL is omitted, and there is virtually no change to the outside diameter of the cable.

It is known that the omission of the APL reduces the pair capacitance by approximately 5%.

To determine the effect of the coated yarn on pair capacitance, it was estimated by reference to tables of material properties that the coated yarn would have a permittivity of between 3 and 4. If the yarn were perfectly circular in section, a yarn diameter of 0,62 mm would fit the pair interstice and still only occupy 60% of the total existing interstitial area of the cable. If it is then assumed that the dilution effect of the air is simply proportional to area, the nett increase in permittivity of the interstices would increase the pair capacitance by about 24%. However, in a preliminary experiment it was found that the pair capacitance increased by only about 8%. Consequently it is clear that the permittivity of the interstice is not diluted in the simple proportion of material to air. We have therefore approached the design as follows:

The average pair capacitance of a screened multipair cable can be calculated from the well-tried empirical relationship based on Spencer's derivation (4):

$$C = \frac{31K}{\ln[1,22(2x - 1)]} \quad \text{nF/km}$$

x = the ratio of insulation to wire diameter, D/d . For unscreened cables the factor 31 becomes 29,5. This equation has been found to be accurate to 1% over a wide range of x .

An empirical approach to determine K , the effective cable permittivity, which appears to fit the measurements over the range investigated so far is:

$$K_i = 1 + 0,45 (K_s - 1) (ds/D)^2$$

$$K = 0,7 (K_d - K_i) + K_i$$

where ds , K_s are the diameter and permittivity of the coated yarn and D , K_d are the diameter and permittivity of the wire insulation.

These relations can be used to investigate the probable effects of varying coated yarn parameters. In Fig. 2 the percentage increase in K with variation of K_s is shown for the theoretical coated yarn diameter of 0,67 D . It will be seen that a permittivity of 3,5 would correspond with the 8% increase in K observed in the early trials.

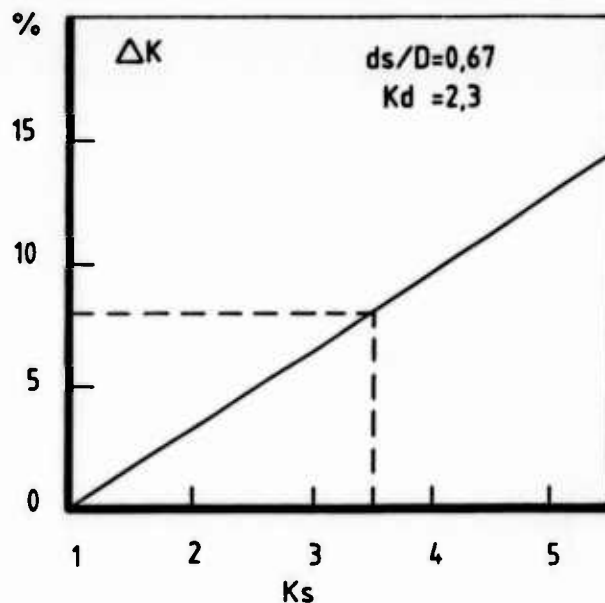


Fig. 2: Total Permittivity Increase vs Coated Yarn Permittivity

In Fig. 3 it can be seen how K_s can be increased by reducing coated yarn diameter, for a constant 8% increase in K . The yarns we used were deliberately left untwisted hence the diameter ds is somewhat notional. If twisted they would form into a diameter of 0,6 mm.

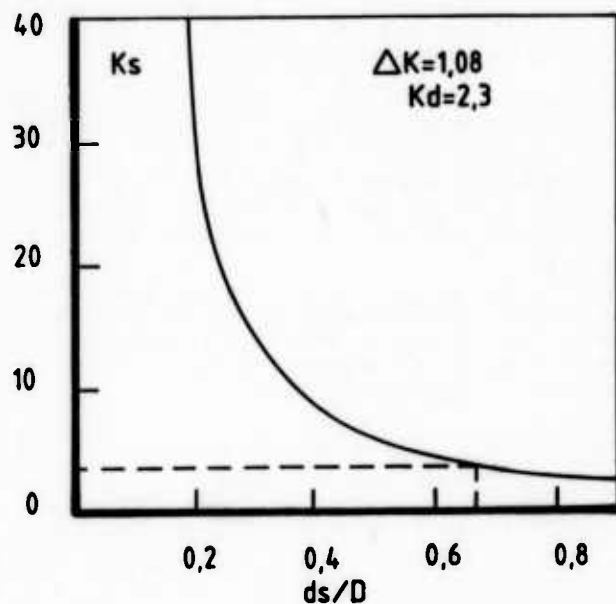


Fig. 3: Coated Yarn Permittivity vs Yarn Diameter

Applying the above we would expect a cable constructed from 0,5 mm wire insulated to 0,92 mm with polyethylene to have an average pair capacitance of 50 nF/km if sheathed with APL and 51,4 nF/km if provided with two 0,6 mm coated yarns per pair and left unscreened. With an expected standard deviation of 2 nF/km both these designs would meet our specification maximum of 56 nF/km for pair capacitance.

Approximately 5 000 m of 50-pair cable were made to this design for evaluation.

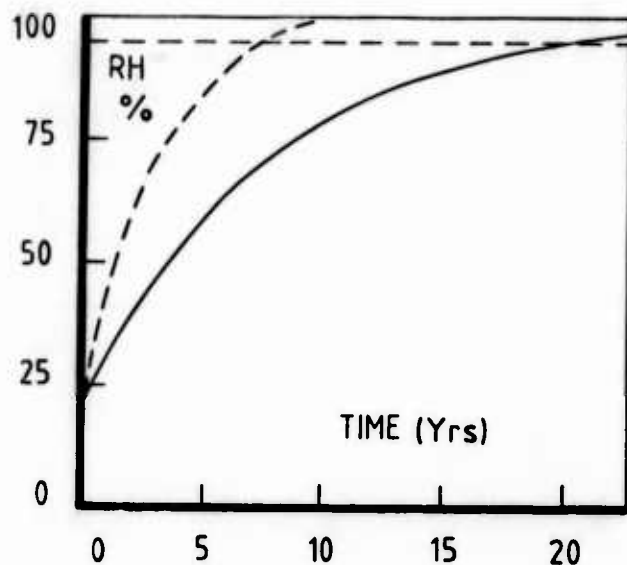


Fig. 4: Moisture Accumulation in Cable due to Permeation of Water through the Sheath.

4. CABLE CHARACTERISTICS

4.1 Effect of water permeation through sheath

Following the approach used by Dr J C Harrison (5) the effect of water permeation on this cable construction was calculated. As will be seen in Fig. 4, the increased mass of water absorbent material considerably delays the build-up of moisture in the cable air spaces. If the end-of-life point is taken as Harrison's 95% Relative Humidity limit the lifetime of the cable is extended to 20 years compared with 8 years for a similar cable without the coated yarn protection.

4.2 Electrical effect of water block and fault location

When water enters the cable through a hole in the sheath, it is assumed that the length of the water block is about 900 mm to either side of the hole. The capacitance of this section would rise from 51,5 nF/km to 105 nF/km. The effect of this on a 1 000 m length of cable would be to raise the effective capacitance to 51,60 nF/km i.e. by 0,2%. This would be unnoticeable to voice frequency transmissions but would represent a 'point' impedance increase of 17% at higher frequencies. The reflection coefficient would be 0,085.

This corresponds to -21,5 dB reflection. However the discontinuity is only 12 nsec long compared with a 500 nsec pulse in a 2 M bit/sec system. Thus the effective reflection is at a relative level of -45dB at the point of discontinuity. This is illustrated in Fig. 5.

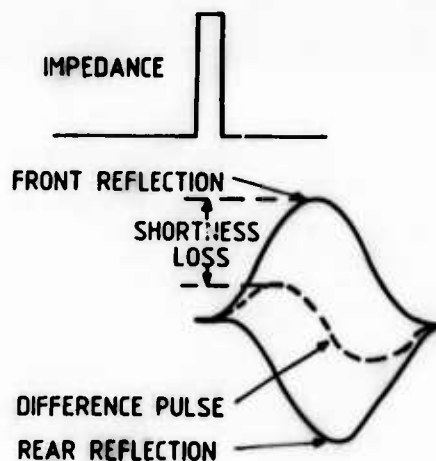


Fig. 5: Effect of Block-length on Pulse Reflection.

Although the size of the impedance change is insufficient to affect PCM transmission materially, it is more than sufficient to permit exact location of the fault by pulse reflection techniques when necessary.

4.3 Low Frequency Characteristics

In Fig. 6 is shown a histogram of the pair capacitance measured on four 1 000 m lengths of cable. The mean value is 51,5 nF/km and the standard deviation is

1,94 nF/km as expected. Normal APL-sheathed production cables show the same spread of pair capacitance but have a mean value of 50 nF/km.

The pair-to-pair capacitance unbalance histogram in Fig. 7 has a standard deviation of 26 pF/1 000 m which is 62% of the value found in normal APL production cables. This is due to the coated yarn cables having a mean pair twist-length only 70% of the normal cables. This reduction is due to limiting the maximum twist-length to 100 mm as noted later under Cable Manufacture.

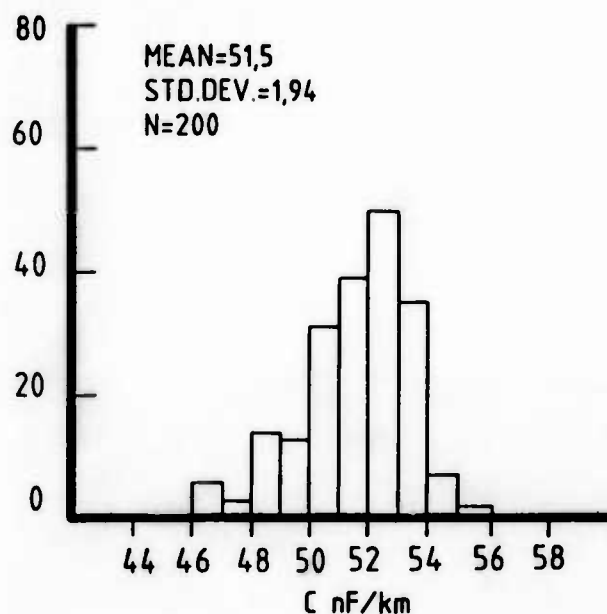


Fig 6: Pair Capacitance Distribution

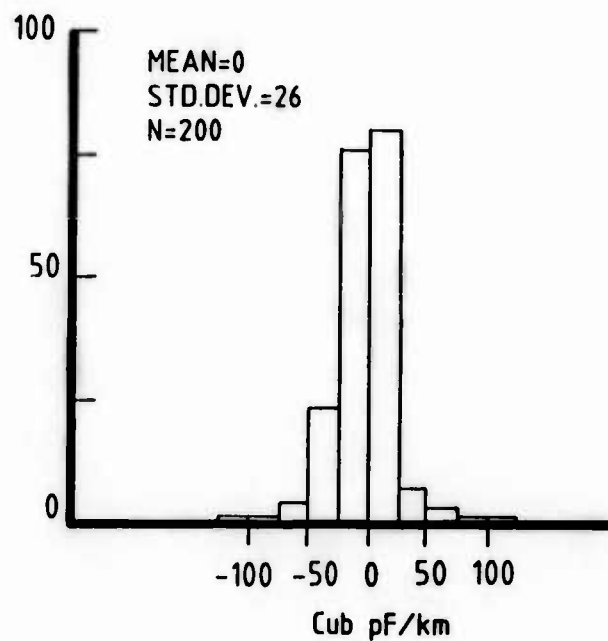


Fig. 7: Distribution of Pair-to-Pair Capacitance

4.4 High Frequency Characteristics

In order to ascertain whether there were any unexpected effects at higher frequencies due to inclusion of the coated yarn, the primary transmission parameters were measured directly on a 6 m length of cable over the frequency range of 1 kHz to 1 MHz using a Siemens and Halske balanced impedance bridge. These results are shown as discrete points in Fig. 8. The continuous lines represent the parameter values calculated using the measured dimensions of the tested pairs. Good agreement was found except for the capacitance parameter where the measured value showed an unexpected steady decline as frequency increased, reaching 8% below the calculated value at 800 kHz. To check that this was not a test arrangement peculiarity, a 6 m length of a standard APL cable was measured in exactly the same way. The capacitance values were constant with frequency. The same behaviour was shown by an unscreened bundle of pairs. We therefore conclude that the permittivity of the coated yarn drops with rising frequency from about 3,5 to 2,3. The expected and measured values of impedance and attenuation for the coated yarn cable are shown in Fig. 9 where the effect of the reducing capacitance is seen as an increase of impedance and a reduction of attenuation from the expected values as the frequency rises.

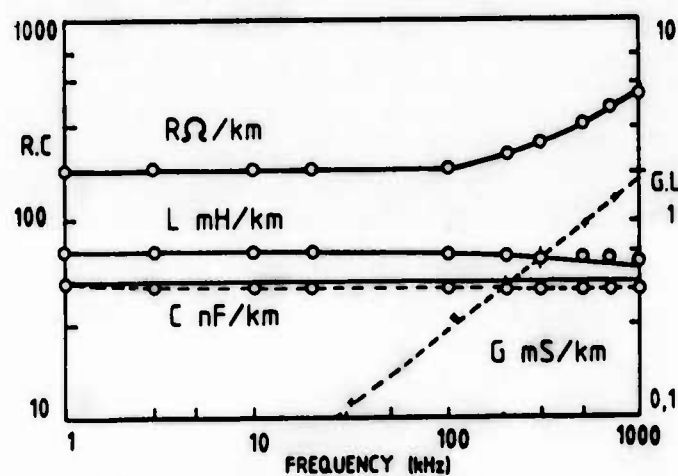


Fig. 8: Primary Transmission Constants.

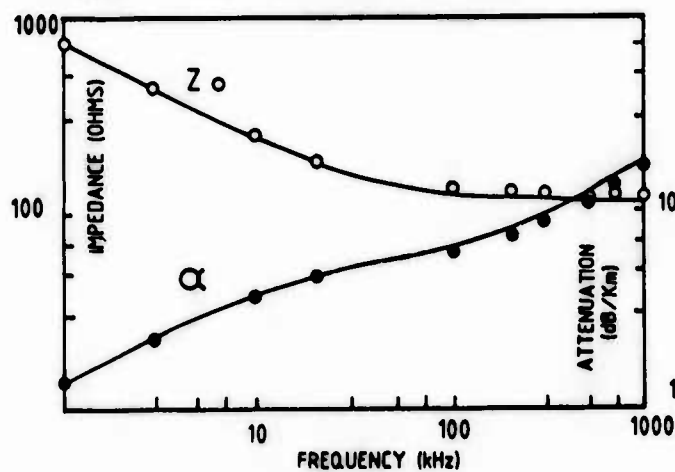


Fig 9: Secondary Transmission Constants

5. PHYSICAL AND CHEMICAL CHARACTERISTICS OF THE COATED YARN

5.1 Temperature range

Laboratory tests on coated yarn show that it is stable from -20°C to at least 60°C, and it is believed that, with the new generation coatings being developed, water blocking to 80°C will be achieved.

5.2 Storage

We have no reason to suspect a limited storage life provided a normal level of control of ambient conditions is maintained.

The bobbins with coated yarn should be kept dry because the coating on the yarn is hygroscopic. At approximately 25°C the extent of water pick-up is of the order of 15% when the relative humidity changes from 30% to 100%. While the yarn may easily be dried out again, the use of moist yarn increases the pair capacitance of the cable.

From general principles one would expect the change of pair capacitance to be significantly less than would be the case with paper insulation, for example.

5.3 Flammability

The major constituent of the coating is inorganic with the result that continuous burning of the coated yarn can only be achieved after exposure to a naked flame. The flammability risk level of the coated yarn is however, less than that of the polyethylene insulation.

5.4 Compatibility

The coated yarn in either the dry or wet state is completely compatible not only with polyethylene and polypropylene but also with PVC. The range of cables that can be waterproofed by this method is therefore greater than if pJ is used.

5.5 Toxicity

The hydrophilic ingredient in the coating is a food grade product. The preservative and all other components are also non-toxic.

5.6 Weight variation in string manufacture

Although the plant producing the coated yarn is still undergoing development and may therefore be regarded as somewhat experimental, coating weights can be controlled to what field trials have shown to be an acceptable level of about 10%. As we gain more experience both in yarn coating and also in the manufacture of the coating solution, we confidently expect this level to be improved further.

6. CABLE MANUFACTURE AND INSTALLATION

6.1 Cable Manufacture

The manufacture of the cable presented no problems.

The only difference to normal cable manufacture was the provision of two spindle carriers with simple braking to hold the bobbins of coated yarn at the back of a double-twist twinner. Because of an improvised yarn guide some coating material was lost by scraping as can be seen in Fig. 10, but this was estimated to be less than 0.5% by weight. When a proper guide was installed there was no noticeable dusting during twinning or at any other stage of manufacture.

A significant change to the design was to restrict the pair twist lengths to a maximum of 100 mm to prevent the coated yarns looping out of the pair interstices. The speed of the twinners was not reduced from the normal 1500 rpm bow speed.

After twinning the cable was formed in one operation in 5 x 10 pair units on a drum twister running at 120 rpm.

No special precautions were taken during manufacture to prevent atmospheric humidity affecting the coated yarn.

Various stages of manufacture are shown in Figures 11 to 16.

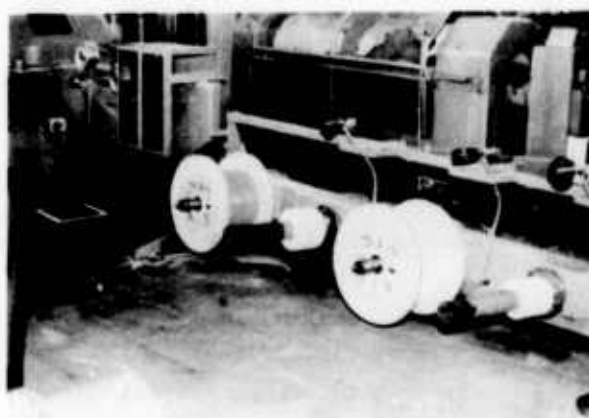


Fig. 10: Insulated Conductor and Coated Yarn Input stand to Twinner.

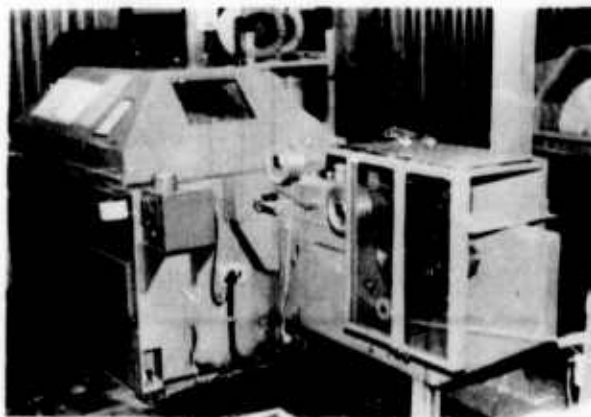


Fig. 11: Input to Twinner

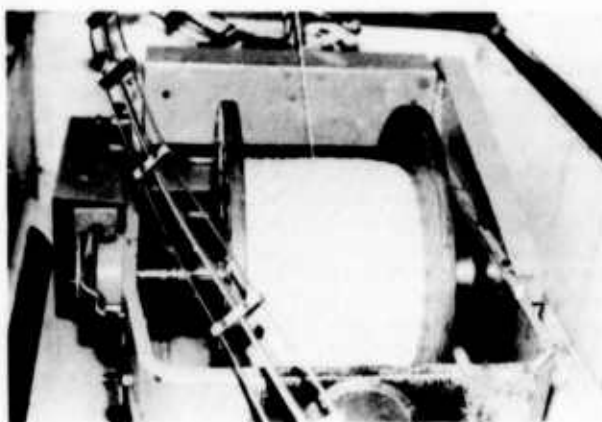


Fig. 12: Take-up inside Twinner

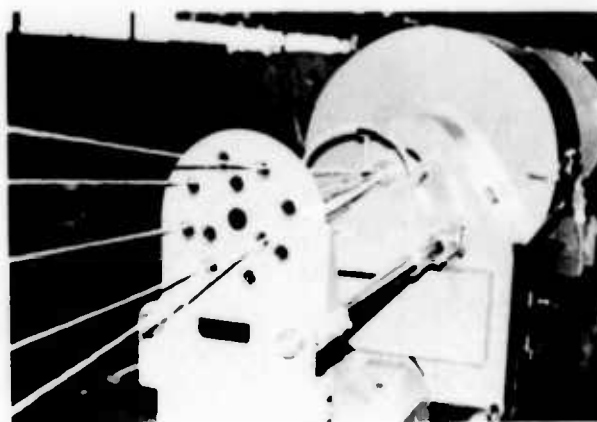


Fig. 15: Ten-pair Unit Closure on Drum Twister

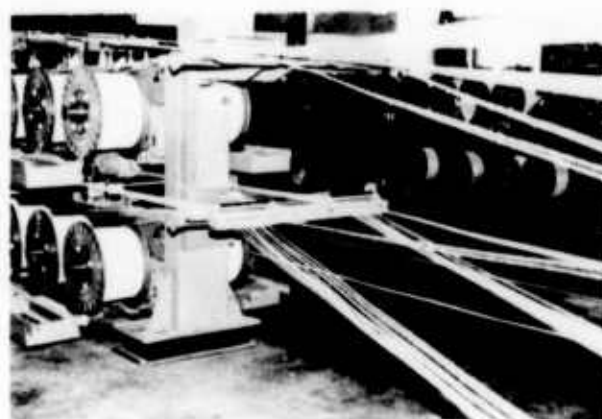


Fig. 13: Pay-off to Drum Twister



Fig. 16: Paper Tape Lapping of Cable on the Drum Twister

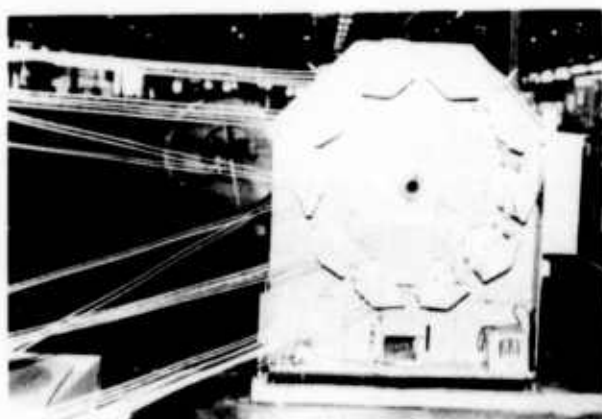


Fig. 14: Input Lay-plates to Drum Twister

6.2 Cable installation and jointing

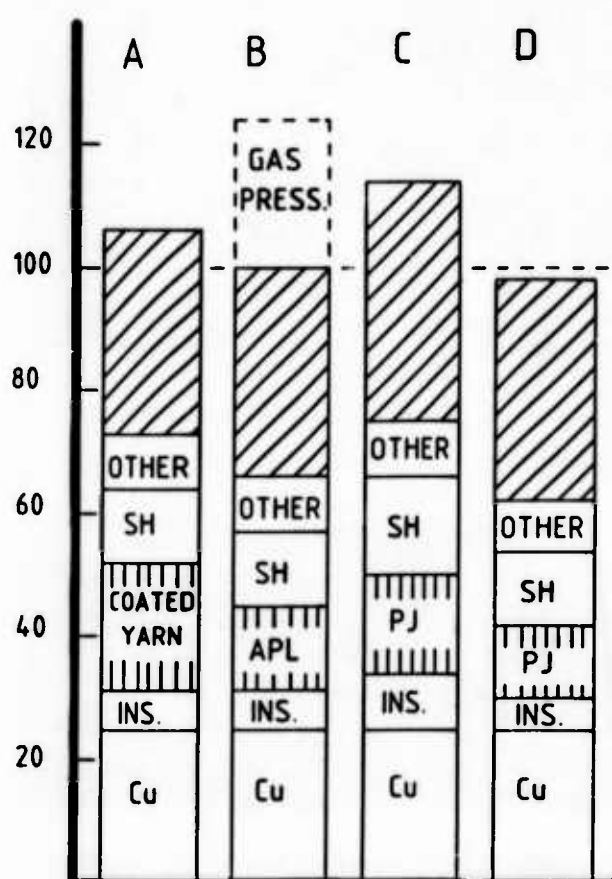
Cable laying is done in the conventional manner with no danger of moisture ingress during field installation even under wet conditions. Jointing is a clean operation and could be done at near-zero temperatures if necessary.

7. COSTS

The bar-chart in Fig. 17 illustrates the relative costs of typical constructions of 50-pair 0,5 mm cables using common forms of water protection. The costs are those applicable in South Africa and are normalised to the APL sheath construction. All the cables are designed for a common electrical specification viz:

- * Pair capacitance 56 nF/km maximum
- * Capacitance Unbalance 570 pF/km maximum
- * Loop resistance 180 ohms/km maximum
- * Insulation resistance 40 Gohms. km minimum
- * HV withstand (Pr-Pr) 6 kVdc minimum

Note that the cellular polyethylene insulation construction would not normally be guaranteed to withstand 6kVdc.



A = Solid Pe. + Coated Yarn
 B = Solid Pe. + APL
 C = Solid Pe. + PJ
 D = Cellular Pe. + PJ

Fig. 17: Cost Comparison of Waterproofed Cables of Similar Electrical Properties.

The cross-hatched portions of the bars represent the processing costs and the vertical shading highlights the material cost of the water-protective element of the cables. The estimated cost per kilometer of cable of adding gas-pressure protection to the APL cable is also shown. The relative total cable costs are:

* APL-sheathed cable without gas pressure	100
* APL-sheathed cable with gas pressure	124
* Pj-filled solid polyethylene insulated cable	114
* Pj-filled cellular polyethylene insulated cable	98
* Solid polyethylene insulated cable with coated yarn	106

All the cables have the same diameter except for the solid polyethylene pj-filled cable which is 15% larger in diameter to maintain the pair capacitance at the required level.

It will be seen that in South Africa cable waterproofed by the new method costs only 6% more than the APL-sheathed cable which is the present standard and 8% less than the nearest electrically equivalent waterproofing method.

8. CONCLUSIONS

In contrast to the existing methods of cable waterproofing which tend to have disadvantages in some respects, this proposed new approach proposed features well in all the aspects of cable manufacture, installation, use and costs.

In this new approach:

- * The cable pairs are effectively protected against radial and longitudinal water penetration and permeating water is absorbed.
- * There is no incompatibility between materials.
- * The transmission parameters and high voltage withstand of the cable are hardly affected by the introduction of coated yarn.
- * The cable is not physically deformed by the ingress of water.
- * The coated yarn is easy to introduce in manufacture without costly extra plant, extra processes or reduced speed of production.
- * There are no objectionable handling problems in manufacture or installation
- * The overall dimensions and cost of the cable are minimally affected.

REFERENCES

1. FRIESEN, H W and WINDELER, A S: "Moisture Permeation and its Effects on Communication Cable"; Proceedings of the Fifteenth International Wire and Cable Symposium; Dec. 1966.
2. PRICHETT, J, MATHER, E L and VERNE, S: "Fully-filled Telephone Cable with Cellular Polyethylene Insulation after Ten Years' Service"; Proceedings of the Twenty fourth International Wire and Cable Symposium; Nov. 1975.
3. DEAN, N S: "The Development of fully filled cables for the telephone distribution network"; Proceedings of the Seventeenth International Wire and Cable Symposium; Dec. 1968.
4. SPENCER, H J C: "Optimum Design of Local Twin Telephone Cables with Aluminium Conductors"; Proceedings of the Institution of Electrical Engineers; April 1969.
5. HARRISON, Dr J C: "The Metal Foil-Polythene Cable Sheath and its use in the BPO"; Journal of the Institution of Post Office Electrical Engineers; 1967.

Harold Hughes graduated in Natural Sciences and Electrical Engineering in 1948 from Corpus Christi College, Cambridge, England, and was awarded his Masters degree in 1960 and Membership of IEE in 1961. He worked on test, design and development of telephone cables for 17 years with BICC, Prescott, England, and was involved inter alia in the original development of water blocking and p/j filling of telephone cables. Since 1972 he has been Chief Engineer at ATC (Pty) Ltd in South Africa, concerned with all types of telecommunication cables and optical fibre manufacture, design and development.



Reg Hunn is a Member of the Institution of Electrical Engineers and a Fellow of the Institution of Electrical and Electronics Incorporated Engineers. He worked for twenty years in the UK on development work related to petroleum-based saturants for high voltage paper cables and projects associated with communication cables before joining Chemical Services Limited in South Africa in 1974. He currently holds the position of Managing Director of a company supplying high voltage paper cable dielectrics in South Africa and also that of Special Projects Manager of Chemical Services Limited. It is in the context of the latter position that he is working with the South African Inventions Development Corporation on this project.



Theo Joubert graduated in Electrical and Mechanical Engineering in 1960 from the University of Stellenbosch and obtained an MBA from the University of Cape Town in 1970. He has since been involved mainly in technical and economic optimisations, planning and industrial financing. At present he is the Deputy General Manager of the South African Inventions Development Corporation, which holds the patents to this new approach to cable waterproofing.



DYNAMIC SPLICING OF PROTECTED OPTICAL FIBERS

Th. TOUCHAIS

J.P. HULIN

M. de VECCHIS

RAYCHEM PONTOISE SA
ST OEN L'AUMONE
FRANCE

THOMSON/CSF
CONFLANS-SIE HONORINE
FRANCE

THOMSON/CSF
CONFLANS SIE HONORINE
FRANCE

ABSTRACT

A fiber optic connection system which isolates, protects, and splices individual fibers from a multifiber grooved core cable is described. This system was developed to meet the specific cable design and field installation requirements of the French videocommunication network.

Two steps are involved in the process. First the fibers from the grooved core cable are individually pulled out of the cable and inserted into loose protective tubes. Then a splicing instrument is used to align the fiber cores, to check the efficiency of the splice by introducing optical power into the core without any fiber discontinuity, and to achieve and protect the splice with an ultra-violet polymerizable adhesive. The special splicing instrument, which was developed earlier, was adapted to this application.

INTRODUCTION

Optical fiber videocommunication networks require accurate, efficient, and durable splices for the optical fibers. These splices must be performed in the field, and their ability to carry the signal with minimal signal loss must be verified. During the splicing operation, the fibers must be protected from damage and from contamination from the field environment. The present splicing system was designed to satisfy these requirements.

This splicing system has two major components: a cable termination device (SECO) and an adhesive splicing instrument (FIBERPACK). These components have been previously presented as independent items (See References 1 and 2), but they will be briefly summarized here. The design adaptations that were made in order to ensure their compatibility will also be described.

The cable termination device (SECO) consists of loose plastic tubes to protect the fibers and a heat shrinkable sleeve to hold the tubes in place and to protect the end of the cable core. The fibers are pulled out of the cable one at a time, and a special tool is used to insert them into individual loose protective tubes without having to splice the fibers. This isolates and protects the fibers while they are being spliced.

The adhesive splicing system is based on optimum alignment of fiber cores which is accomplished by finding the maximum optical power transmitted through the splice. The optical power is launched into and detected from macrobends in the fibers without removing the fibers from their protective tubes. The splice is made by inserting the fiber ends into a transparent tube filled with an ultra-violet polymerizable resin. Since the system monitors the signal across the splice, it provides an immediate loss reading for the finished splice.

Extensive laboratory testing has been performed on splices made with ten fiber cables. The tests include attenuation measurements and attenuation monitoring during environmental cycling, humidity exposure, and temperature aging.

GROOVED CORE CABLE TERMINATION DEVICE (SECO)

A cylindrical grooved core cable has been selected for use in the French videocommunication network. This cable, which is shown in Figure 1., has excellent mechanical and thermal properties because the fibers are located in the grooves loosely, without tension but with a slight excess length.

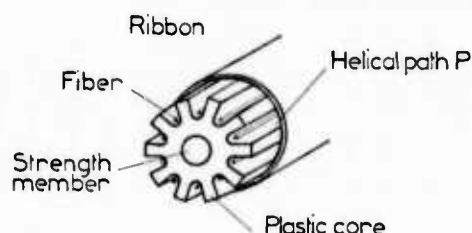


Fig. 1. Fibers in a Grooved Core Cable.

Any time the cable element comes to an end (at a termination box or a splicing point), all its advantages must be kept, and the fibers must be protected while craftsmen manipulate them during splicing. A cable termination device (SECO) shown in Figure 2 has been designed to meet these requirements. It has two components: (a) small plastic tubes which allow easy fiber recognition and handling and which protect the fiber against abrasion or any sharp edge in the final layout, and (b) a heat shrinkable transparent sleeve which holds the protective tubes in place at the cut end of the cable. The tool which is used to insert the fibers into individual loose protective tubes is shown in Figure 3.

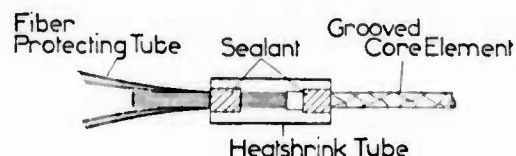


Fig. 2. Cable Termination Device (SECO) Attached to a Cable

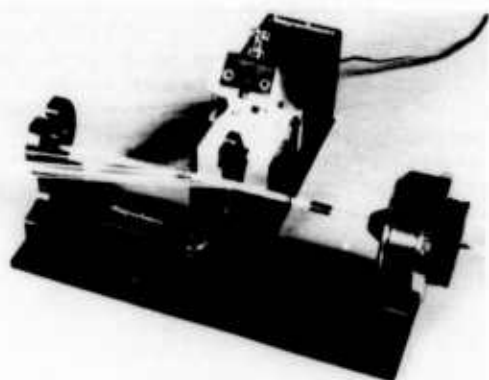


Fig. 3. Instrument Used to Insert Fibers into Protective Tubes.

Two different versions of the cable termination device have been designed for the French videocommunication network. One version is used with termination boxes where the tube end is linked to a dematable connector which allows the network to connect or disconnect any subscriber. The other version is used with cable splices to ensure complete fiber protection from grooved core cable to grooved core cable. This paper describes the second version.

The cable termination device consists of a number of tubes equal to the number of fibers (typically ten) and of a heat shrinkable sleeve made of irradiated polyolefin with two thermoplastic adhesive strips. The first adhesive strip locks the protective tubes into the grooves of the cable and joins them to the sleeve. The second adhesive strip joins the cable element to the same sleeve.

The important design parameters for such a device are all concerned with minimizing signal loss. First of all, the device must create a minimum of signal loss during its installation over the fibers. In addition, the device must not create any further signal loss over the life of the fiber.

Since the linear coefficient of thermal expansion of the polyolefin material in the protective tube is orders of magnitude higher than that of glass, the differential elongation during temperature cycles must be compensated for in order to avoid any losses.

The design characteristics which have been incorporated into this product to ensure its reliability include:

- * The coefficient of thermal expansion of the protective tube is kept as low as possible through basic material properties, well controlled extrusion conditions and stabilization by irradiation.
- * The inside diameter and wall thickness of the protective tube are selected to provide freedom for the fiber to move inside the tube and to allow the maximum permitted excess length of fiber in the tube.

ADHESIVE SPLICING SYSTEM

- * The material and the smoothness of the inner surface of the protective tube are designed to minimize the friction between the tube and the outer coating of the fiber. The friction coefficient is kept low to allow any differential dimensional value to be spread over the entire fiber/tube length and to keep any stresses well distributed.
- * The protective tubes must be flexible enough to remain in an 80mm diameter coil for the lifetime of the fiber.
- * The tensile strength of the protective tube/grooved core cable/heat shrinkable sleeve link is very high in order to avoid any disbonding during lifetime use.

The procedure used to separate and protect the fibers was designed to lower both craft sensitivity and installation time. The two opposed pitch terphane ribbons which protect and hold the fibers in the grooved core are only removed over an 80mm length of cable where the core will eventually be cut. This spot is located approximately 1.3 meters away from the end of the cable. Each fiber is then pulled back out of the cable individually and inserted into its protective tube before the next fiber is pulled and protected. Insertion and threading of the fibers into the protective tubes is done by means of an easy to operate tool which pulls the fiber between a motor driven roller and a rubbery counter roller. The second roller is spring loaded to regulate the tension force and to avoid taking up any of the excess length of fiber which must remain inside the cable.

The total installation time of a cable termination device has been reduced to only fifteen minutes, and the ten fibers remain protected except during the short time when they are individually pulled out of the cable element and threaded into their protective tube.

The adhesive splicing system is designed to minimize the signal loss across the splice by aligning the fiber cores and to maximize the strength and integrity of the splice through the use of an adhesive resin encased in a protective tube. The instrument which is used to make the splice incorporates the ability to introduce a signal into the fiber on one side of the splice and read the signal on the other side of the splice. This instrument is shown in Figure 4.



Fig. 4. Dynamic Splicing Instrument.

Normally, it is impossible to check the quality of a splice in a fiber optic field operation without sending a signal from the beginning of the cable. As a result, splices are usually made by one crew and then either measured for signal loss by the same crew after it returns to the central office or checked by a different crew using the optical time domain reflectometer (OTDR) in the office. The ability to obtain a splice qualification at the site and without cutting the fiber represents an important breakthrough. This new system can take advantage of its signal launching and decoupling feature to measure the signal loss at the splice before and/or after curing the adhesive.

The incoming fiber, encased in its loose protective tube, is secured around a mandrel which creates a macrobend in the fiber. The mandrel is then positioned in front of a signal device containing a light emitting diode (LED). This LED can send optical power through the protective tube into the fiber core without any need for a fiber discontinuity. The outgoing fiber is secured around another mandrel which also creates a macrobend in the fiber. This fiber is then positioned in front of a PIN diode which will monitor the signal delivered from the LED.

After stripping and cleaving the fiber end, each fiber is positioned into a holder which includes two methods of fiber alignment: (a) The fiber can be moved along its longitudinal axis using manual controls, or (b) a motor can be used to move the fiber in any direction parallel to the end of the fiber. The directions of fiber alignment are shown in Figure 5.

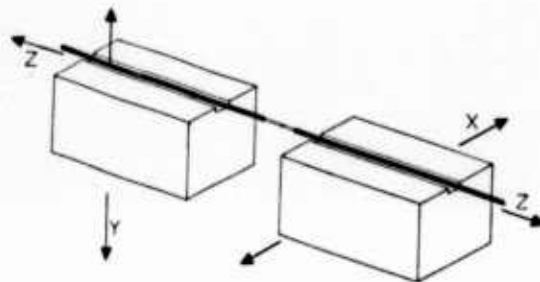


Fig. 5. Fiber Alignment Stages.

Once the fibers are fixed in the holders, the signal sent by the LED and received by the PIN diode is input into a microcomputer. The microcomputer commands the motors which reposition the holders until the maximum signal is received, thus indicating that the optimum core alignment has been made. The resolution of the complete mechanism is 0.3 microns. The automatic alignment capability is illustrated in the block diagram in Figure 6.

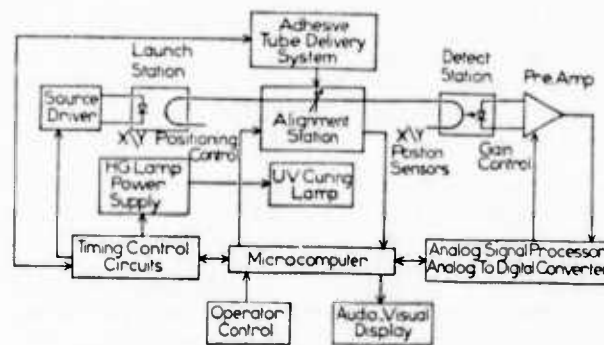


Fig. 6. Auto-Alignment Capability.

Once the fibers have been aligned, the holders are locked into position so that the fibers can only be moved apart longitudinally; their core alignment can not be altered. The operator then uses the manual controls to separate the fibers far enough to allow the splice tube to be moved into place. Once the splice tube is in place, the operator moves the fibers back together, and now they are inside the splice tube.

Measuring the signal loss is a procedure which involves two main steps: calculating the power in the source fiber and determining the signal loss caused by the splice. These two steps are described below.

After the fibers have been automatically aligned, and before the splice tube has been put in place, the operator uses the reticle of the microscope to position the fiber ends at a predetermined optimum distance from each other. The microcomputer routine will then monitor the signal strength for different X and Y coordinates and derive a numerical aperture for the incoming fiber. This reference measurement is stored in the microcomputer.

For the second step, the splice tube is in place and the fibers are aligned within it. The operator positions the fibers at two different distances apart and records the signal readings at the two distances or end gaps. The ratio of the two readings is then correlated with the dB loss of the splice. This can be done and/or after the curing step, and therefore the splice can be reworked before it is completed if the signal loss is too great. (Such a situation could be caused by poorly prepared fiber ends or by impurities.)

The resolution of the system is within 0.1 dB, and the time to complete a splice, including preparing the fiber ends, is 12 to 15 minutes.

The splice tube is precision molded out of transparent plastic, and it contains a resin whose index of refraction closely matches the index of refraction of the fiber core. The resin is in its liquid state, but its viscosity is such that its surface tension will hold it within the tube and yet will allow the fibers to move during the core alignment operation. After this is done, the resin is cured by means of two ultraviolet sources. Once the resin is cured, it locks the fibers in their final position and environmentally protects the connection. A typical splice tube is shown in Figure 7.

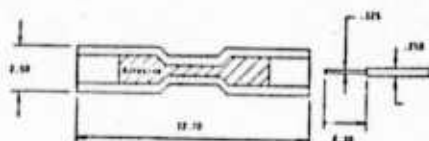


Fig. 7. A Splice Tube.

This adhesive splicing technique allows different types of fibers to be spliced as long as the outer coating diameter of the fiber is small enough to allow the fiber cores to be aligned within the 500 micron bore tube. The splice tubes are supplied in ultraviolet protected micro cassettes which contain ten units each, and their shelf life is over one year. A splice tube cassette is illustrated in Figure 8.

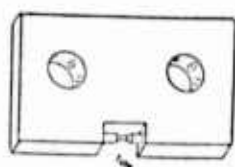


Fig. 8. Splice Tube Cassette.

SYSTEM INTEGRATION

The cable termination system and the adhesive splicing system were developed independently. In order to use them together, some design modifications had to be made. The splicing equipment had to be able to align the cores of the fibers while they were inside their individual loose protective tubes. This implied the ability to launch optical power into the fiber core through the protective tube wall and across the air gap between the inner wall surface and the fiber surface. Furthermore, on the receiving fiber side, the signal that was received had to be strong enough to get a microcomputer processable signal/noise ratio.

In order to meet these requirements, the coupling length has been increased by coiling the loose tube containing the fiber around a mandrel. The signal can then be introduced into each of the coils. The same concept has been used on the monitoring side: the mandrel is located at the focal point of a reflecting ellipsoid, whose second focal point is occupied by the PIN diode.

Using the cable termination device with the adhesive splicing system created some new design criteria for the protective tubes, such as:

- * The tubes must provide optical clarity at the 840 micron wavelength of the LED.
- * The tubes must have mechanical properties which will allow them to be coiled around a small diameter mandrel without any kinking effect which would create sharp edges and damage the optical fiber.

The flexibility requirements for the tube influence many of its design parameters including its Young's modulus E , its diameter, and its wall thickness. The tube must be able to return to its original shape after the splicing procedure and must avoid any remaining small curvature radius that would create a signal loss.

The splicing operation subjects the fiber to some bending stresses, and the possibility of fiber failure during splicing or during the lifetime of the fiber has been considered. The result presented is the continuation of D.V Nelson's study (See Reference 3) for this particular application.

The results shown in Figure 9 are plotted for a lifetime of 10 years. The probability of a break occurring is minimized because the fiber is only bent around the mandrel for a few minutes during the splicing operation. In addition, the mandrel diameter has been optimized to allow maximum coupling and decoupling of power at minimum fiber stress levels. The present coiling mandrels have a 6mm diameter.

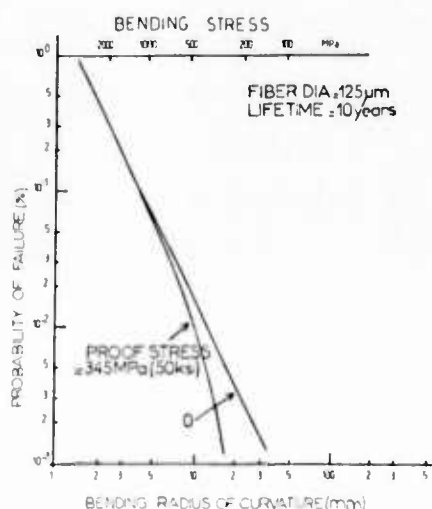


Fig. 9. Bending Stress.

EXPERIMENTAL RESULTS

Several tests have been performed on graded index fiber of 50/125/250 microns to qualify the ultraviolet curable splice under different environmental conditions. The measurement methods are described below, and then the results are presented for splice attenuation, temperature cycling, humidity exposure, temperature aging and tensile strength tests.

Measurement Method

Signal attenuation is measured either by direct insertion loss or by the backscattering method.

The insertion loss system, which is illustrated in Figure 10, was designed to insure long term stability of the base line signal. The light source is a tungsten ribbon filament lamp contained in a housing. Light is collimated by an achromatic condensing lens, modulated mechanically, and refocused at the fiber by a microscope objective. The focussed spot size is 1mm in diameter. One of the common sources of long term drift in a system of this sort is misalignment of the injection optics caused by differences in thermal expansion and contraction between the separate optical mounts. The use of the large focussed spot size has minimized this source of error.

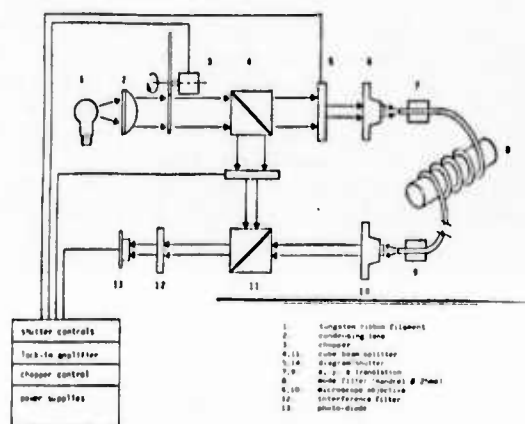


Fig. 10. Insertion Loss System.

On the receiver side, light leaving the fiber is collimated and projected onto a silicon photodiode contained in a housing. This housing also contains a series of ten nanometer bandpass interference filters. All of our tests thus far have been done at 0.85 micron. The signal from the photodiode is fed to a lock-in amplifier and read-out digitally on a front panel meter.

The maximum rate of baseline drift of the system is less than 0.008 dB/hour. This was achieved with no correction for drift in the electronics. For longer term tests requiring greater stability, beam splitters are mounted in two locations and a portion of the optical signal is shunted directly from the source to the detector. This is used to correct for long term degradation of the lamp and thermal drift of the detector and amplifier circuitry. The backscattering technique asks for two measurements to avoid any error which could be due to the different fiber diffusivities. The splices are made between two cable reels with at least 800 meters of cable on each. The OTDR is then used from both ends of the spliced cables and the final attenuation value is the average of both readings. When paper graphs of the backscattered curves are used, the resolution of the method is considered to be 0.05 dB.

Attenuation Histograms

The first set of results from the splicing equipment was gathered with the optical power launched directly into the fibers. The Corning glass fibers were broken and respliced, then attenuation was measured by insertion loss. The mean value for 141 splices is 0.07 dB with a maximum loss of 0.16 dB, as shown in Figure 11.

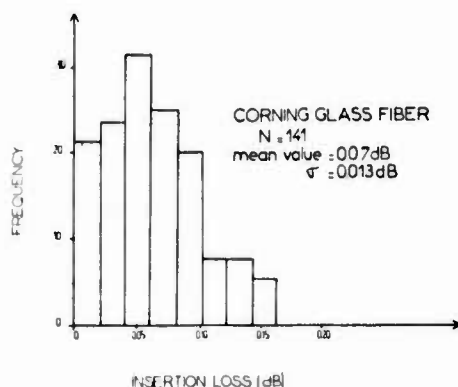


Fig. 11. Histogram 1.

The attenuation measurements with the light launched into the fiber through its protective loose tube were done on Fibres Optiques Industries (FOI) fibers, which will be used in the French videocommunication network. Measurements were made with the backscattering method using two cable elements.

A first group of measurements was done mating the fibers of one element to their corresponding fibers in the other cable element as shown in Figure 12. The second group was measured from randomly spliced fibers thus including the optical and geometrical parameter in the attenuation value. These results are shown in Figure 13.

The mean value of 0.22 dB from histogram 3 (Figure 13), with a standard deviation of 0.11 dB and a maximum attenuation of 0.5 dB, shows that the proposed dynamic core alignment concept ensures a high quality splice with any two fibers being spliced.

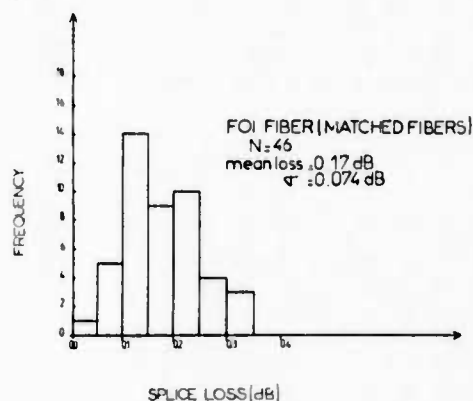


Fig. 12. Histogram 2.

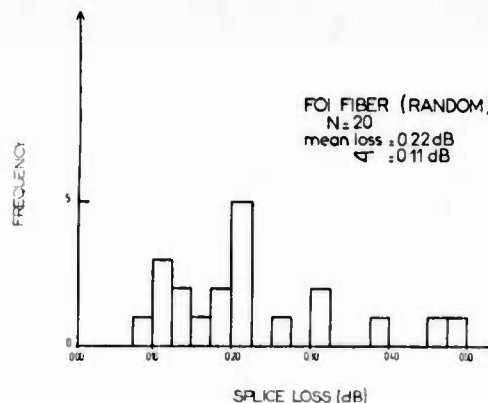


Fig. 13. Histogram 3.

Temperature Cycling

Several cycles can be used to test the thermal behavior of a splice. The two temperature ranges that were used were - 40 deg to + 70 deg C and - 25 deg to + 80 deg C. The signal loss across the splice was measured by the direct insertion loss method which was described earlier.

The French Telecommunications administration has recommended the use of the - 25 deg to + 80 deg C cycle in order to better understand the behaviour of optical splices. Three different signal loss excursion limits have been set:

- * 0.1 dB max in the - 15 deg to + 55 deg C cycle (hour 0 to hour 11)
- * 0.2 dB max in the - 25 deg to + 70 deg C cycle (hour 11 to hour 24)
- * 1.0 dB max in the + 55 deg to + 80 deg C cycle (hour 24 to hour 42)

Furthermore, the final signal loss after six cycles should not be more than 0.2 dB above the original value.

Typical graphs of the signal loss variations with time are shown in Figure 14. The ultraviolet polymerizable splice meets the requirements set for both thermal cycles.

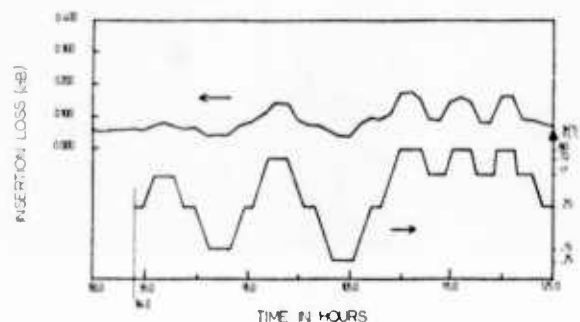


Fig. 14. Results of Temperature Cycling Tests.

Humidity Exposure and Temperature Aging

The tested splices were either soaked in 50 deg C water for 100 hours or were put into an oven with circulating air at 80 deg C for 100 hours. In both cases, the signal loss was monitored by the direct insertion loss method.

The results are presented in Figures 15 and 16, and they show no variation greater than 0.2 dB throughout the test time.

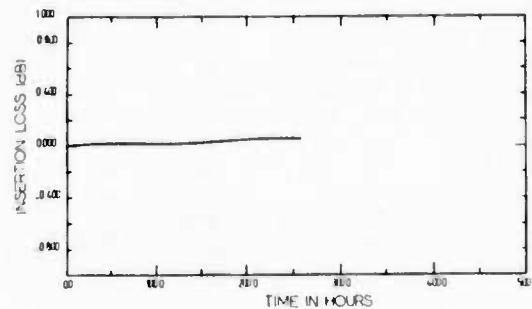


Fig. 15. Results of Water Soak Test.

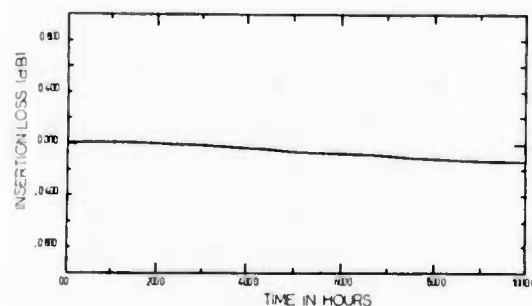


Fig. 16. Results of Heat Ageing Tests.

Tensile Strength

A tensile test apparatus was used to measure the strength of the splice. The strength is the force needed either to break the splice or to pull one of the fibers out of the polymerized adhesive material.

The jaw separation speed was 5 mm per minute. Two sets of measurements were made on the splices, one before and one after a - 40 deg to + 70 deg C temperature cycle.

The 0.5 daN average value achieved in this test is an acceptable value, but it is on the low side of the acceptance range. Consequently, a new splice has been designed and is presently undergoing final qualification tests in our laboratories. The outside shape of the splice tube has not been changed, but the average tensile strength has been increased to 1 daN.

System Temperature Cycling

Once the characteristics of the splice had been established, it was time to test the splice in operation with a complete fiber protection and cable termination system installed. The first temperature cycles were performed between -40 deg C and $+70$ deg C. Fibres Optiques Industries (FOI) fibers were used, and the direct insertion loss method was employed.

The results, which are presented in Figure 17, show no transmission changes greater than 0.2 dB during the test. The next step is to test with the -25 deg to $+80$ deg C temperature cycle.

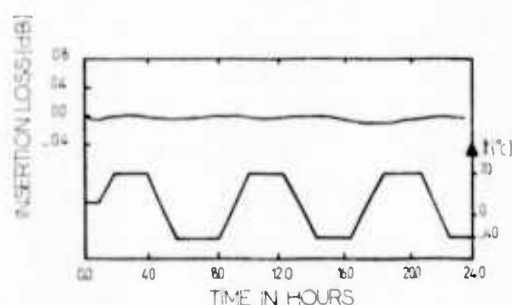


Fig. 17. System Temperature Cycling.

CONCLUSION

A splicing system has been developed which provides protection for the optical fibers from the time they leave one grooved core cable until they enter the other grooved core cable. The fibers are individually inserted into loose tubes which protect them from damage and contamination. The fiber cores are aligned, which provides the optimum power transmission through the splice, and because the index of refraction of the adhesive resin closely matches the index of refraction of the optical fiber, fibers of different brands and different optical quality can be spliced. Furthermore, since the splicing system is capable of introducing a signal into the fiber and reading that signal across the splice, the quality of the final splice can be monitored in the field without any need for extra crews or extra measuring equipment.

REFERENCES

1. B.D. Campbell, et al., "Fiber Optic Connection System," 31st IWCS, 1982, pp. 149 - 152.
2. De Vecchis, et al., "Termination Device for Grooved Core Cables," IWCS, 1983.
3. D.V. Nelson, and V.A. Fentress, "Fracture Mechanics Evaluation of the Static Fatigue Life of Optical Fibers in Bending," IWCS, 1983.



Thierry TOUCHAIS received his engineering degree from Ecole Centrale de Lyon in 1976 and his MS in Mechanical Engineering at UC Berkeley in 1977. After some years spent in process R&D, in 1981, he joined the RAYCHEM Telecom product development group located in Belgium. Since 1984, he has been heading the technical group in the French Telecom Division.



Michel de VECCHIS was born in 1946. He received his engineering degree from Ecole Nationale Supérieure des Télécommunications, PARIS, in 1969. He joined L.T.T. in 1970 and was first engaged in research and development work in the field of microwave components and subsystems. He is now the technical director of L.T.T. Cable Division.



Jean Pierre HULIN was born in 1946. He received his engineering degree from Ecole d'Electricité et de Mécanique Industrielle (Ecole Violet), PARIS, in 1971. After some years devoted to production of special purpose cables, he joined L.T.T. fibre optic group in 1977. He has been the head of the optical fiber cable and splice group and is now the assistant technical director of L.T.T. Cable Division.

ARC FUSION SPLICING MACHINE WITH AN APPLICATION OF LOCAL MONITORING METHOD

Naoshi Hakamata, Shuzo Suzuki, Yuichi Usui, Toshiaki Kakii

Sumitomo Electric Industries, Ltd.
1, Taya-cho, Totsuka-ku, Yokohama, Japan

Abstract

In single-mode fiber splicing, optimum core alignment is required for obtaining minimum splice loss. In practical field splicing, it can be achieved by positioning the fiber ends so as to maximize the transmitted power. But this method has the disadvantage that technicians must be readied at the far end of the receiving fiber in order to monitor the transmitted power.

To solve this problem, a new arc-fusion splicing machine with the ability to achieve the optimum core alignment only at the splicing point has been developed. This paper describes the basic study, configuration, and performance of the new machine. We are convinced by the following test results that this new system will have wide-ranging practical applications.

1. Introduction

Recently, optical transmission systems using single-mode fibers have been applied in many areas. In the construction of single-mode fiber transmission lines, splicing technique, especially for the optimum core alignment, is very important. Conventionally, optimum core alignment is achieved by positioning the fiber ends at the splicing point so as to maximize the transmitted power. This method has the following disadvantages:

- (1) Test technicians are required at the far end of the receiving fiber.
- (2) The above test data must be collated continuously at the site of splicing point.

The new arc-fusion splicing machine solves these problems by monitoring scattered power only at the splicing point to achieve the optimum core alignment. Data access to the far end of the fiber is not necessary.

2. Basic study on the new local monitoring method

2.1 Experiment

When misalignment of the core axes of two fibers occurs at the splicing point, partial transmission power in the tranceiving fiber is coupled with the power of cladding modes of the receiving fiber. It is known that^[1] the power of cladding modes is easily scattered out of the fiber. Thus, we expect that the optimum core alignment could be obtained by minimizing the power scattered from the receiving fiber at the splicing point.

Fig. 1 shows the schematic view of the experimental set-up. A 1.3 μ m laser diode was used as a light source. Each fiber end was connected using matched-index fluid. The partially scattered light power was detected by a InGaAs photo diode through a 1mm ϕ glass rod which was attached to the bare part of the receiving fiber with matched-index fluid. Fig. 2 shows the relationship between the partially scattered power and the butt joint loss as a function of the fiber offset. The results of the experiment indicate that the scattered power is minimized at the offset which delivers maximum transmitted power.

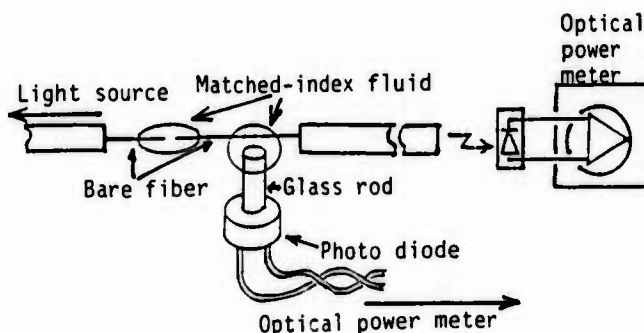


Fig. 1 Experimental set-up for the scattered power measurement.

In order to detect the scattered light with high efficiency, we have recently developed the unique V-groove which has a piece of glass rod (1.0mm-o.d.) at the bottom as shown in Fig. 3. A photo detector is connected with its glass rod through a large core fiber. Fig. 3 illustrates the scattered power detection system. The receiving fiber is set on this V-groove. When misalignment of the core axes of two fibers occurs at the butt joint point, the light scattered out of the receiving fiber is partially guided to the photo detector through the glass rod and the large core fiber. Fig. 4 plots the local monitored power detected by this photo detector as a function of the butt joint loss. A light source with -15dBm output from the tranceiving fiber was used.

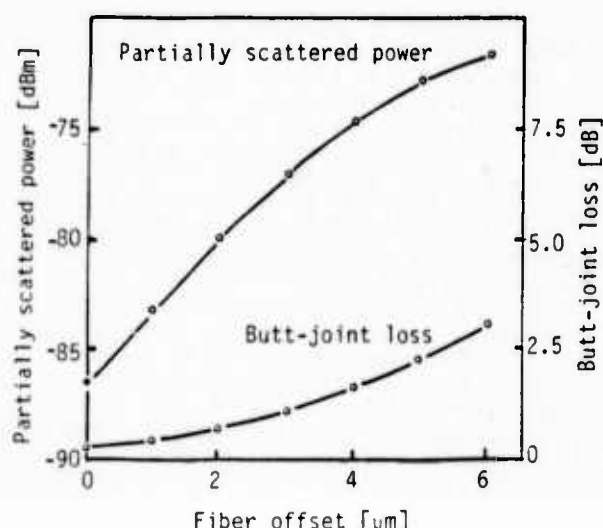


Fig. 2 Relationship between partially scattered power and the butt-joint loss.

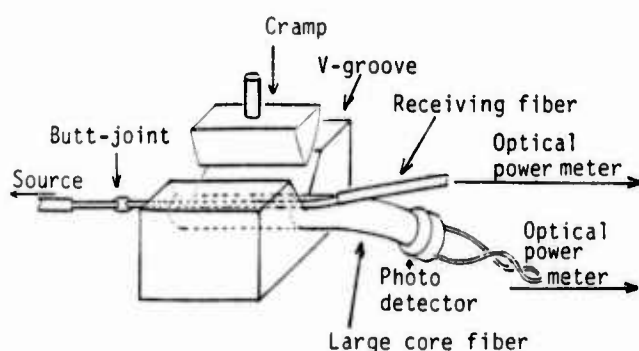


Fig. 3 Schematic view of the scattered power detection method.

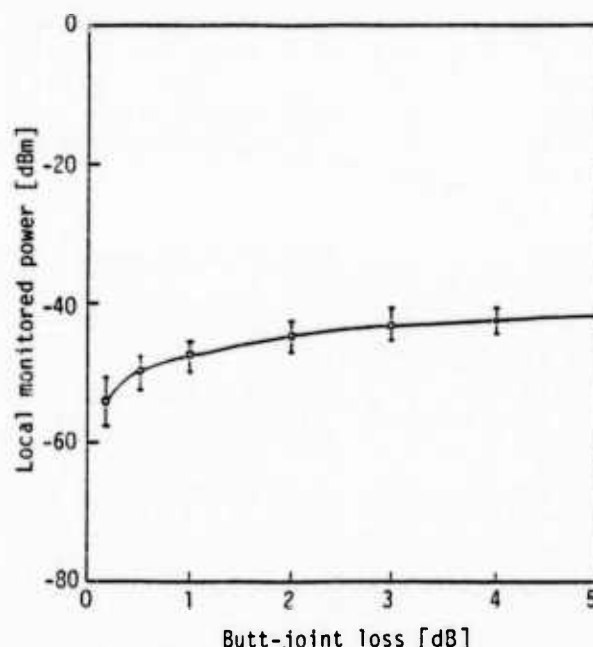


Fig. 4 Local monitored power as a function of the butt-joint loss.

2.2 Discussion

The butt-joint loss (α) and the scattered power (β) are related with the power transmission coefficient $T^{[2]}$, that is,

$$\alpha = |10 \log T|, \quad \dots \dots \dots (1)$$

$$\beta = 10 \log(1 - T), \quad \dots \dots \dots (2)$$

The monitored power γ is expressed by

$$\gamma = \beta + K + P_L, \quad \dots \dots \dots (3)$$

where, K = coupling loss in the scattered power detection system,

P_L = fiber output level from light source.

From Eq. (1), (2), and (3), the local monitored power γ is expressed by

$$\gamma = 10 \log(1 - 10^{-0.1\alpha}) + K + P_L \quad \dots \dots (4)$$

Fig. 5 indicates the calculated value of Eq. (4) for several values of K and $P_L = -15\text{dBm}$. After comparing the tendency of the line shown in Fig. 4, with those of lines in Fig. 5, it is estimated that the coupling loss (K) in our local monitoring system is about -24dBm .

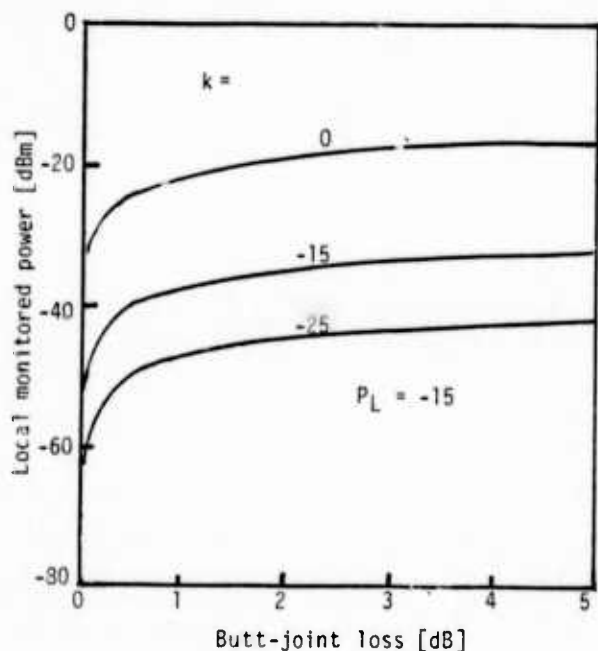


Fig. 5 Local monitored power as a function of the butt-joint loss for several values of K defined by Eq. (3).

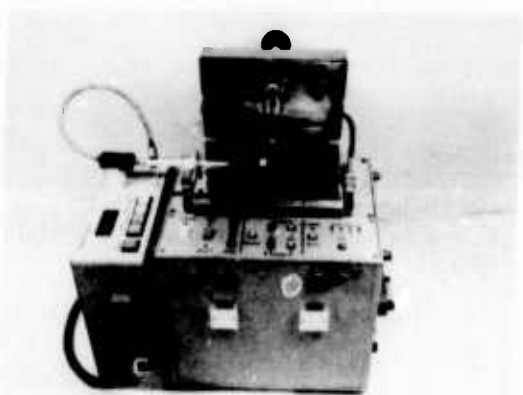


Fig. 6 New splicing machine and optical power meter.

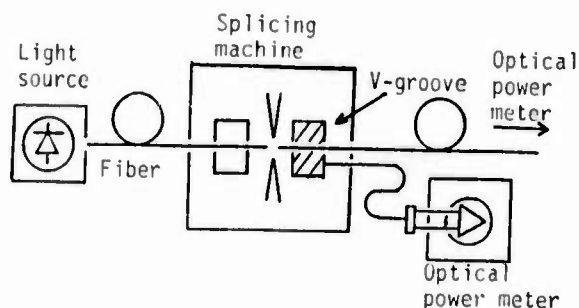


Fig. 7 Experimental set-up for the splicing test.

3. Design and Performance

3.1 Design

On the basis of the experimental results, we have developed a new splicing machine with an application of local monitoring system which consists of a unique V-groove and an optical power meter which has been newly developed and has high sensitivity. Fig. 6 shows a photograph of the new splicing machine and the optical power meter. Table 1 shows the specifications of this splicing machine and the optical power meter.

3.2 Performance of the local monitoring splicing machine

(1) Splice loss of identical fibers

For the purpose of evaluating the splicing loss between identical fibers, we set up the system as shown in Fig. 7 with a $1.3\mu\text{m}$ laser diode with -15dBm output from a single-mode fiber, the new splicing machine, the new optical power meter for detecting local monitored power, and an optical power meter for detecting the transmitted power. Table 2 shows the parameters of a single-mode fiber used in this experiment. Fig. 8 shows a histogram of the coupling loss (K) defined by Eq. (3). It is found that the coupling loss (K) is fairly stabilized at about -24dBm . When the local monitored power (Y) after the optimum core alignment is much higher than that derived from Eq. (4), we can judge that the fiber setting is very poor before splicing. Fig. 9 shows a histogram of splice losses by using this local monitoring method. An average splice loss of 0.07dB was obtained.

(2) Splice loss of different fibers

Table 3 shows the parameters of single-mode fibers used in the splicing test. After splicing, an optical time domain reflectometer (OTDR) was used for splice loss measurements. The OTDR

Splicing machine	
Size (mm)	240W x 200D x 250H
Weight (kg)	12
Power	12V DC
Optical power meter	
Size (mm)	200W x 200D x 80H
Weight (kg)	3
Power	12V DC

Table 1 Specifications

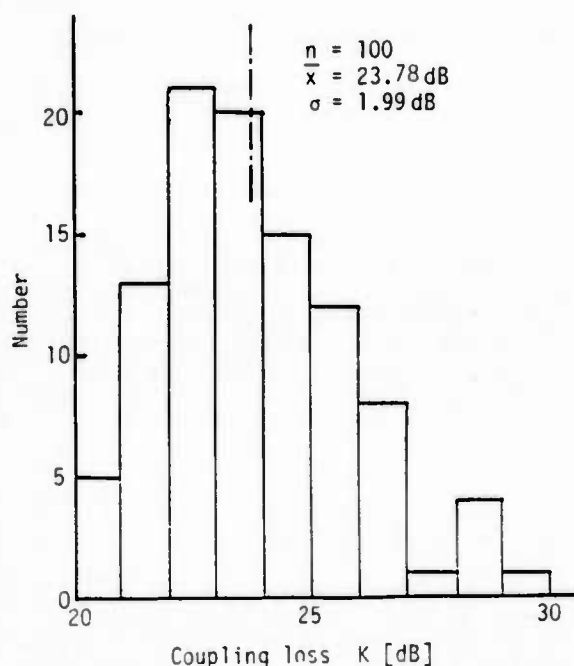


Fig. 8 Histogram of coupling loss in the scattered power detection system

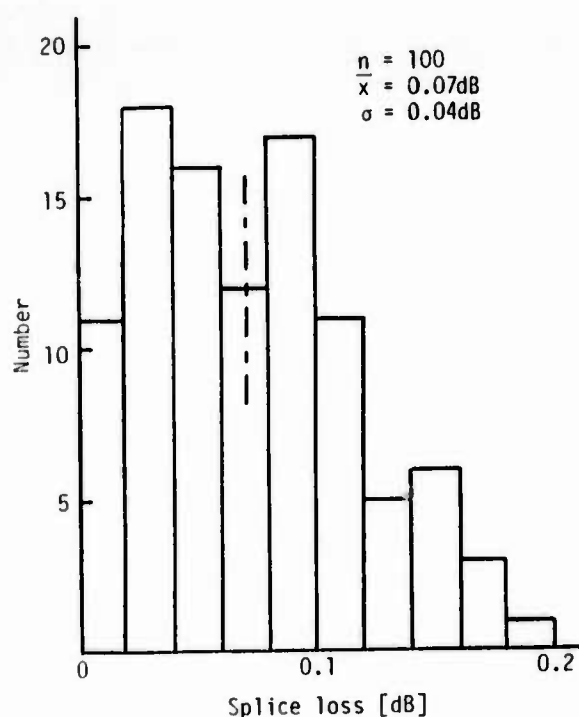


Fig. 9 Histogram of splice loss for identical fibers using a new splicing machine

measurements were made in both directions. Fig. 10 shows a histogram of splice losses for different fibers. An average splice loss of 0.11 dB was obtained.

Fiber diameter [μm]	125.1
Core diameter [μm]	8.0
Spot size [μm]	5.1
Core eccentricity [%]	1.0

Table 2 Fiber parameters

	Fiber diameter [μm]	Core diameter [μm]	Spot size [μm]	Core eccentricity [%]	Fiber length [km]
No. 1	125.5	8.2	5.04	1.2	1.31
No. 2	125.5	8.1	5.22	2.0	1.36
No. 3	125.0	8.4	5.20	0.7	1.33
No. 4	124.9	8.2	5.07	0.5	1.30
No. 5	125.1	8.1	5.19	3.0	1.16
No. 6	125.0	8.4	5.05	1.0	0.92
No. 7	125.7	8.2	5.02	2.3	1.54
No. 8	125.1	8.1	4.98	2.7	0.92

Table 3 Fiber parameters

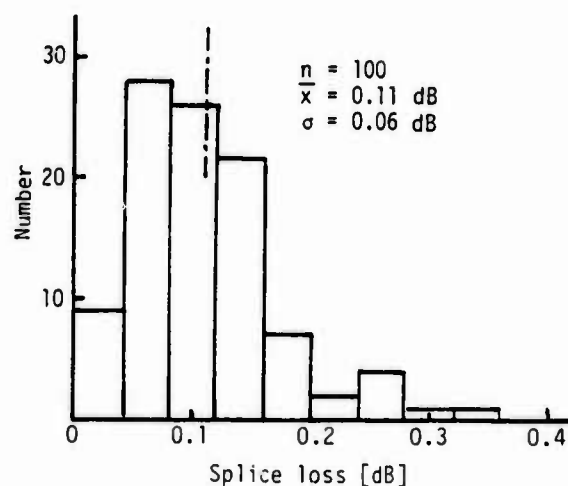


Fig. 10 Histogram of splice loss measured by OTDR for different fibers

(3) Discussion on the estimation of splice loss

When the butt-joint loss is known, we can estimate the splice loss by using the local monitored power difference between before and after splicing (ΔP). From Eq. (4), ΔP is expressed as

$$\Delta P = \gamma_2 - \gamma_1 = 10 \log \left(\frac{1 - 10^{-0.1\alpha_2}}{1 - 10^{-0.1\alpha_1}} \right) \dots\dots\dots (5)$$

where, γ_2 = the local monitored power after splicing,

γ_1 = the local monitored power before splicing,

α_2 = the splice loss,

α_1 = the butt-joint loss.

A splice loss (α_2) is derived from Eq. (5) as

$$\alpha_2 = \{10 \log \{1 - 10^{0.1\Delta P} (1 - 10^{-0.1\alpha_1})\}\} \dots\dots (6)$$

The solid line in Fig. 11 indicates the calculated splice loss as a function of ΔP by assuming $\alpha_1 = 0.1$ dB. The dots of Fig. 11 indicate the measured splice losses, which were obtained by arranging the fiber axis purposely, as a function of ΔP . The measured splice losses agree with the one calculated within an error range of 0.1dB. From these results, splice loss can be estimated within an error range of 0.1dB by measuring ΔP and using Eq. (6).

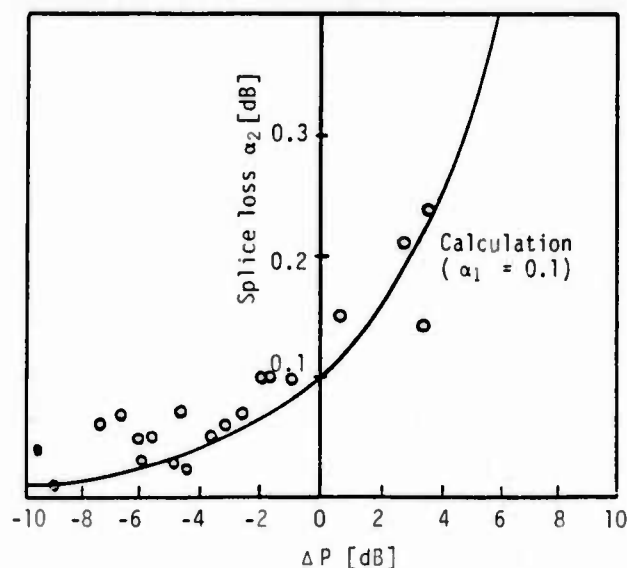


Fig. 11 Relationship between splice loss and coupling loss (ΔP)

3.3 Features of the local monitoring system

The features of the splicing machine and the optical power meter which we have developed are summarized as follows:

- (1) The optimum core alignment can be achieved automatically within approximately one minute.
- (2) Each fiber end at the butt-joint is automatically immersed in matched-index fluid.
- (3) No additional operation is needed for detecting the scattered power.
- (4) The minimum detectable power level of the optical power meter is -90dBm, the value of which is obtained mainly by using the InGaAs photo detector that we have developed.

4. Conclusion

We have developed a new-arc fusion splicing machine with an application of local monitoring method. In use, an average splice loss of 0.07dB for identical fibers is obtained, and splice loss can be calculated with in an error range of ± 0.1 dB.

References

- [1] C. M. Miller, "Local detection device for single-mode fiber splicing", OFC '82, THAA2
- [2] D. Marcuse, "Loss analysis of single-mode fiber splices", Bell Syst. Tech. Jour., Vol. 56, No. 5, P. 703, 1977



Naoshi Hakamata
Sumitomo Electric
Industries, Ltd.
1, Taya-cho,
Totsuka-ku,
Yokohama, Japan

Naoshi Hakamata was born in 1960 and received a B.S. degree from Nagoya University in 1983. He joined Sumitomo Electric Industries, Ltd. in 1983, and has been engaged in research and development of optical fiber splice. He is a member of the Institute of Electronics and Communication Engineers of Japan



Toshiaki Kakii
Sumitomo Electric
Industries, Ltd.
1, Taya-cho,
Totsuka-ku,
Yokohama, Japan

Toshiaki Kakii was born in 1955 and received a M.E. degree from Keio University in 1980. He joined Sumitomo Electric Industries, Ltd. in 1980 and has been engaged in research and development of optical fiber jointing method. He is a member of the Institute of Electronics and Communication Engineers of Japan



Shuzo Suzuki
Sumitomo Electric
Industries, Ltd.
1, Taya-cho,
Totsuka-ku,
Yokohama, Japan

Shuzo Suzuki received a M.S. in 1972 from Tokyo University. He joined Sumitomo Electric Industries, Ltd. in 1972, and has been engaged in research and development of optical fiber and cable. He is a member of the Institute of Electronics and Communication Engineers of Japan.



Yuichi Usui
Sumitomo Electric
Industries, Ltd.
1, Taya-cho,
Totsuka-ku,
Yokohama, Japan

Yuichi Usui was born in Nagano Prefecture, Japan, on February 2, 1950. He received the B.E. degree in mechanical engineering from Kyoto University, Kyoto, Japan, in 1973. In 1973 he joined Sumitomo Electric Industries, Ltd., Yokohama, Japan, and has been engaged in developmental research on optical fiber splice. Mr. Usui is a member of the Institute of Electronics and Communication Engineers of Japan.

SHORT-HAUL FIBER-OPTIC-LINK CONNECTOR LOSS

D. H. Rice and G. E. Keiser

GTE Government Systems Corporation
77 A Street
Needham Heights, Massachusetts 02194

Abstract

For a short-haul multimode, four-connector fiber-optic transmission system with an LED source, it is shown that the effects of mode filtering and mixing at connectors are very important in determining connector loss. It is shown that connector loss is position dependent, being highest at the first connection, lowest at the second and between these values in the third and fourth positions. Based upon the data observed, a meaningful production test set-up was devised with good correlation between predicted and in-system observed path loss.

Point-to-point fiber-optic transmission systems may be conveniently categorized as either short- or long-distance systems. A short-distance (short-haul) system is often a tactical or moveable system and therefore generally uses multimode fiber with several connectors. Because of its simplicity an LED rather than a laser source is used. A short-haul system can be defined as one where connector loss determines path loss.

Connector loss in such a system is a complicated function of the modal power distribution in the transmitting fiber as well as misalignment and mismatching of mating

fibers. Fiber modal-power distribution depends upon source power launch conditions and subsequent mode mixing and filtering which can occur at connectors. Thus, the manufacturer is confronted with the difficulty of making meaningful tests on fabricated connectorized cable assemblies and the system designer with estimating path loss and its variations.

The system to be considered here (Figure 1) is made up of three concatenated cable assemblies (four connectors), using 50- μ m core, all-glass, graded-index fiber with Hughes epoxied pin/socket connectors. The source is an LED. It is shown that connector loss is different for different connector locations in the path, being highest for the first connector and lowest for the second connector, that connector loss approaches an equilibrium value for the last two connectors and that a meaningful manufacturing test may be devised for connector loss in a short-haul system.

Table I shows measured values of total path loss and individual connector losses for the system of Figure 1. Note that the sum of individual connector losses equals the mea-

Table I
Measured Values

Path	L_{C1} (dB)	L_{C2} (dB)	L_{C3} (dB)	L_{C4} (dB)	L_{TOT} (dB)	$\sum_{n=1}^4 L_{Cn}$ (dB)
1	2.4	1.00	1.42	0.67	5.49	5.49
2	2.4	1.02	2.52	2.54	8.47	8.48
3	2.4	0.68	1.03	0.93	5.04	5.04
4	2.4	1.32	2.01	1.50	7.22	7.21
5	2.4	1.12	1.00	1.35	5.87	5.87
6	2.4	1.14	1.05	1.77	6.36	6.36

Average Loss L_{C1} = 2.4 dB
Average Loss L_{C2} = 1.04 dB
Average Loss L_{C3} = 1.50 dB
Average Loss L_{C4} = 1.46 dB

Average Loss (all connectors) = 1.52 dB
Note: L_{C1} = Loss at connector nearest source
 L_{C4} = Loss at connector nearest receiver

8.611-84

sured total path loss and that the loss is different for each connector position. Figure 2 shows a plot of average connector loss as a function of position. Note that the first connector position has the highest loss, the second position exhibits lowest loss and that the difference between the losses for the third and last position is very small. Assuming that total connector loss is made up of geometric misalignment effects, mismatches between transmitting and receiving fiber characteristics (core radius, numerical aperture and index gradient), and cladding and higher order mode removal by the connector's epoxy, the following explanation for the position-dependent loss is presented.

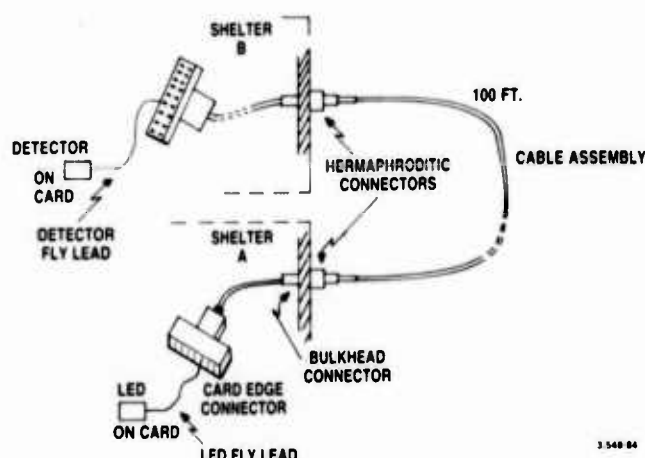


Figure 1. Typical Signal Path

For the first connector (nearest the source) coupling loss is highest because of the removal of higher-order and cladding modes by the epoxy, in addition to normal misalignment and mismatch losses. In the second connector, the loss is lowest because of the predominance of lower-order modes in the transmitting fiber resulting from the mode filtering in the first connector. Transmitting-fiber modal power is now concentrated into a smaller diameter spot in the center of the fiber, thereby reducing the effects of misalignment and mismatching. In the third and fourth connectors, connector loss is somewhat higher than for the second position because of the generation of some higher-order modes (mode mixing) at the second connector. However, the loss difference between the third and fourth connections is small indicating the approach of modal equilibrium condition. It is also important to note that the average loss for the last connector is very close to the average connector loss for the path (i.e. total loss divided by the number of connectors), indicating that a connector-loss test setup based upon an equilibrium modal condition would be realistic for this system.

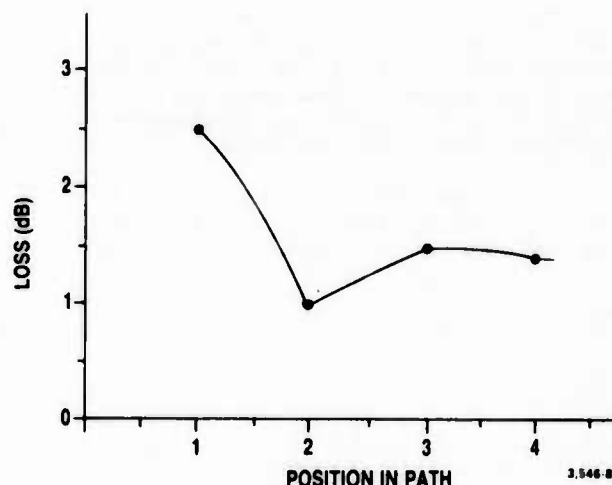
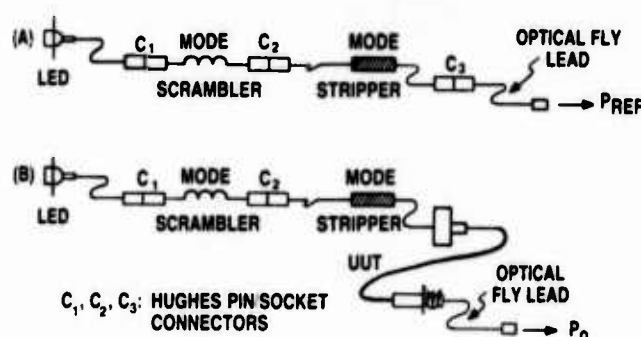


Figure 2. Average Connector Loss Vs. Path Position

Figure 3 shows the connector loss test set which uses a mode filter between the LED source and the optical output. The mode filter consists of a mode mixer (scrambler) followed by a cladding mode stripper. The mode mixer was constructed by winding two hundred feet of the system fiber on a 2" diameter mandrel, and the mode stripper consisted of a fiber lead with approximately one inch of bare fiber covered with index matching gel. Figure 4 represents the distribution of connector losses measured using this test set. Good agreement is seen between average loss for the system and measured connector loss. Note that this data is skewed because no loss values greater than 1.6 dB were recorded. Any unit with a loss greater than 1.6 dB was discarded or reworked, as this value represents the production pass/fail value. If one assumes symmetry about the 1.6 dB axis, a reasonably normal distribution can be approximated.



1. MEASURE P_{REF} IN (a)
2. MEASURE P_0 IN (b)
3. CALCULATE LOSS: $L_c(dB) = 10 \log \frac{P_{REF}}{P_0}$

Figure 3. Loss Measurement System

Figure 5 depicts a smoothed, filtered curve of connector loss for 31 connectors measured with the LED source, but with the mode filter removed. This shows there is an average loss value which is the same as for the first connector in the system.

It has been demonstrated that the effects of connector mode mixing and filtering are very important in determining path loss

in a multimode, LED-excited, short-haul fiber-optic system. Mode mixing and filtering not only makes connector loss sensitive to connector position, but makes meaningful tests and system design estimates very difficult. However, using judiciously applied mode filtering in the loss measurement system, the manufacturing engineer can give the system design engineer meaningful data.

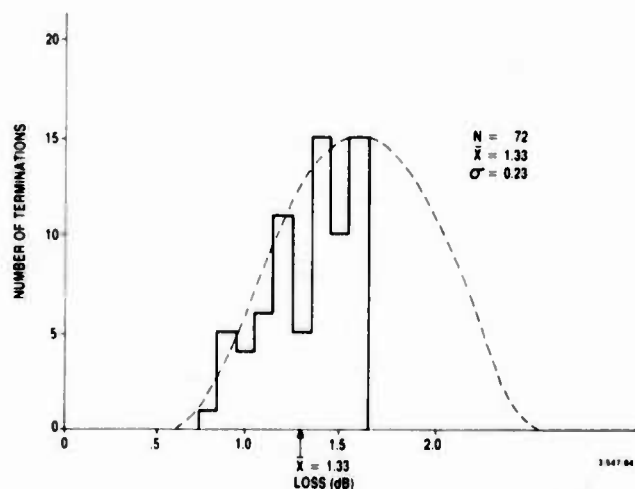


Figure 4. Loss (dB) Distribution LED Source with Mode Filtering

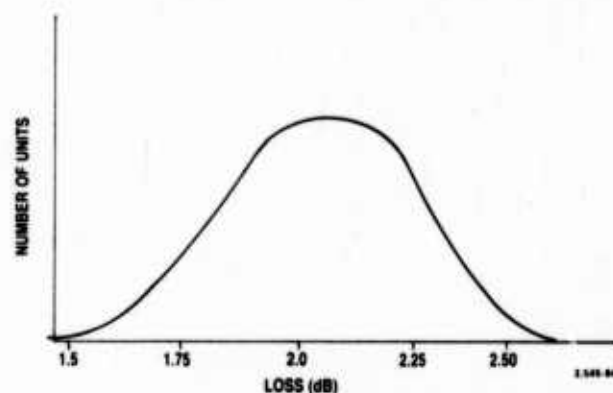


Figure 5. Loss (dB) Distribution LED Source, No Mode Filtering



Gerd E. Keiser is the Manager of the Fiber Optic Equipment Unit of GTE Communication Systems Division of GTE Government Systems Corporation. He has been employed by GTE since 1974. He holds BA and MS degrees in physics at the University of Wisconsin, Milwaukee and his Ph.D. degree in physics from Northeastern University in Boston.



Donald H. Rice is a Senior Member of the Technical Staff of GTE Communication Systems Division of the GTE Government Systems Corporation. He has been employed by GTE since 1953. He holds a BS degree in Chemistry and a BS in Electrical Engineering from the University of Illinois and an MS in Electrical Engineering from Northeastern University.

FIELD USABLE SINGLE MODE FIBRE SPLICING APPLYING LOCAL CORE ALIGNMENT

C.M. de Blok and P. Matthijsse

PTT, Dr. Neher Laboratories

Leidschendam, Netherlands

Abstract

In the spring of this year two single mode fibre cables, each with six fibres, have been installed in the Netherlands. Splicing was done by electric glow discharge fusion applying a core alignment system based on the local injection and detection of an optical signal by means of a bend in both fibre ends. In addition, the received signal level was used as a check on the fusion and protection process by demanding an increase of the transmitted signal just after fusion and no change during protection of the splice. A modified multimode splicing set was used including a manually controlled piezo-electric fibre translator. The splicing was done by a regular jointing crew trained for about one month. The obtained mean value of the splice loss was 0.13 dB. Splicing was rather time consuming and bothering for the jointers, primarily due to the preparation of the end faces. No specific problems were caused by the application of the local alignment. It offers a great flexibility in the installation procedure as sequential splicing is no longer required and simultaneous splicing on different splicing points, which was done on several occasions, can be performed without any interference problems.

Introduction

Concerning the introduction of optical systems into the transmission network, fibre splicing is of great importance for the Dutch PTT from the point of view of both the splice loss as a part of the total loss budget and the operational conditions resulting from the splicing procedure. Based on the fault statistics of the conventional buried long distance cables about three additional splices per kilometer are expected during a 25 years' period. Assuming provisionally the same number of additional splices for optical cables, the repeaterless operation of 25 km links with single mode fibres during this period, which is the intention, requires a mean splicing loss of 0.15 dB at most. Most of these additional splices will be due to cable damage or change of the cable routing caused by road diversions. Therefore, restrictive conditions with respect to the sequence of splicing or the necessity of far-end monitoring equipment are hardly acceptable. Both considerations lead to the conclusion that the application of local core alignment will be a necessity in the future. In this paper the experiences with the application of a local alignment system, which has been developed in the PTT laboratories and has been used for the

splicing of two single mode fibre cables in Rotterdam will be described.

Alignment unit

Most local core alignment systems for single mode fibres, which have been proposed till now are based on a precise detection of the mutual position of the cores in both fibre ends. This can be done e.g. by means of fluorescence^{1,2} or a precise video detection system^{3,4}. In reference 5 a transmission method has been described, based on the local injection and detection of an optical signal guided by the core of both fibres. This method is very simple, especially when using loose tube cabled fibres with a cladding mode stripping coating as in our cables. For this reason this method was chosen and made suitable for field use. Injection and detection of the optical signal is done by bending both fibres at a distance of about 40 cm from the splicing point ($R = 4$ mm) and without removal of the coating material (figure 1).

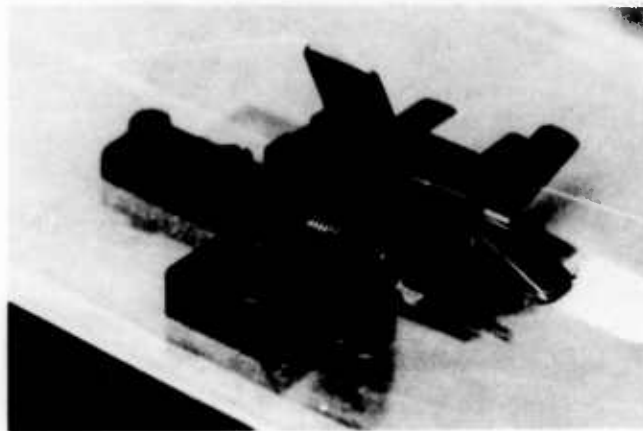


Figure 1: Fibre in one of the bending clamps

The launched signal emerges from a 0.200 mm core diameter SI fibre, which was inserted in a metal tube and ground at a sharp edge of 15° . The coated fibre is pressed against this oblique fibre end with a reflecting clamp and bent over 180° just behind this launching region. Loosening of the clamp activates a microswitch to switch off the launching source for safety reasons. Detection is done with the same arrangement. Only the metal tube is replaced by a quartz rod with a diameter of 1.8 mm provided with a reflecting coating.

The optical source is a 12 W, 904 nm pulsed GaAs single heterostructure diode laser. The driving signal is used as a reference signal for the synchronous detection circuit, which is preceded by a commercially available low frequency detector amplifier module. The received signal level is indicated on a pointer instrument. At each moment in the alignment procedure the signal level can be stored in a memory. The increase of the received signal relative to the stored value is indicated by the lighting of a number of lamps from a row of 12 lamps situated besides the pointer instrument. Each lamp represents a 0.05 dB increase in optical signal level. The alignment unit is shown in figure 2 with the splicing set in front of it. In figure 3 the transmission of a fibre joint as a function of the transverse offset of the fibre ends is shown.

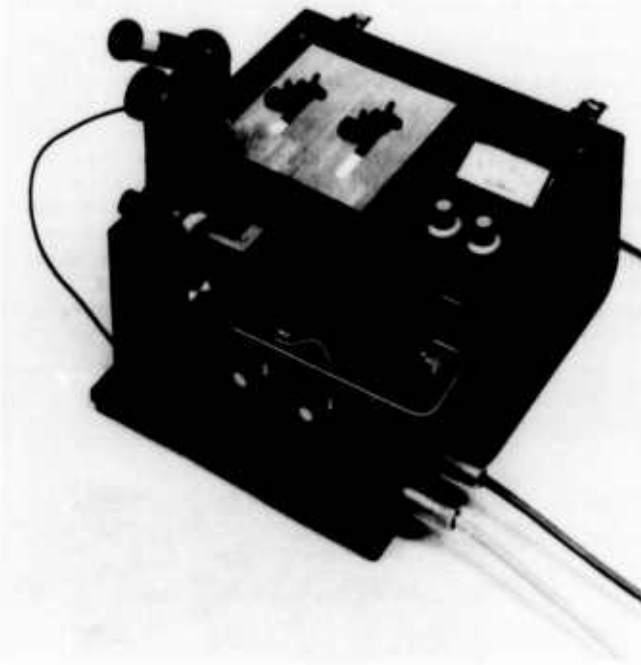


Figure 2: Alignment unit with splicing set in front of it

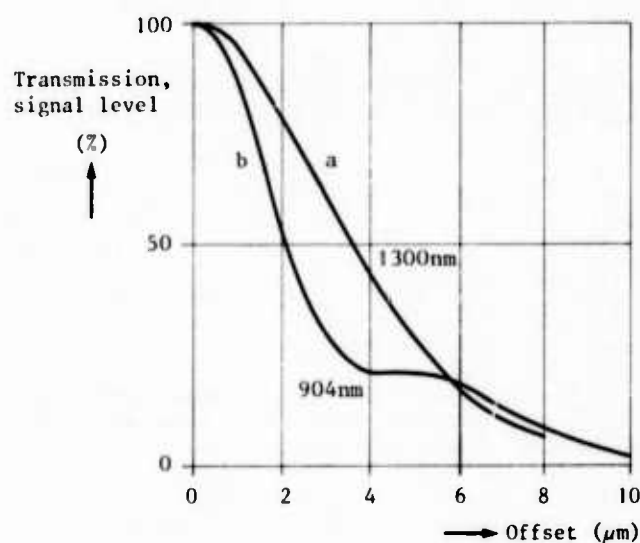


Figure 3: Transmission of a fibre joint at 1300 nm and detected signal level of the alignment system at 904 nm versus offset

Curve a represents the loss of the joint at 1300 nm as measured with a far end transmitter and receiver, without bends in the fibre, whereas curve b represents the signal as produced by the alignment system. From this figure it will be clear that no cladding modes are present as the transmission has decreased to an negligible level for an offset larger than the core diameter. It also shows that for the used fibre type the alignment at 904 nm is more sensitive to offset errors than at 1300 nm as the transmission curve is much more peaked in the optimum region.

Splicing equipment

For the first installations in Rotterdam it was decided to use a modified multimode splicing set based on fusion by a glow discharge. The reasons for this decision were:

- i) these sets are well-proven, rather cheap and were easily available unlike possible alternative single mode fibre splicing sets,
- ii) in a preliminary stage it was shown in our laboratories that with this set low loss single mode fibre splices could be made.

The modifications included a decrease of the gap between the electrodes, a shortening of the discharge time and the lengths of the automatic movements of one of the fibre ends during the fusion process and the mounting of a piezo-electric fibre translator in one of the fibre clamps. In February of this year three of these sets, each together with an alignment unit, became available for training purposes.

Splicing procedure

In the applied splicing procedure nothing was very specific besides the alignment and the check of the splice loss. Cleaving was done with a commercially available fibre cutter. After insertion of the fibres in the alignment unit and the clamps of the splicing set the fibre ends were aligned visually by using the mechanical translators and the viewer on the splicing set. This rough alignment resulted in a signal from the alignment unit, which was sufficient to start the fine alignment. This was done manually by means of the piezo-electric fibre translator while observing the signal level indicated by the pointer. The optimum signal level was stored in the memory in the alignment unit. After fusion there should be a signal increase indicated by the lighting of a number of lamps and originating from the vanishing of the Fresnel losses and the decrease of an occasional loss due to lightly slant fibre end faces. By correlating the measured 1300 nm loss of a number of splices with the corresponding number of lighted lamps it was found that the lighting of at least six lamps suffices for a splice loss better than 0.15 dB. If less than six lamps were lighted the jointer had to renew the splice. In case of a good splice it is protected, taken from the alignment unit and fastened in the fibre organiser. No check of the splice loss by means of a far end measurement (e.g. an OTDR measurement) is performed. The only problem encountered in this procedure is that if the fibre ends are prepared in such a way that a good splice will be impossible (e.g. too slant end faces) the transmitted alignment signal nevertheless will increase after splicing, because the joint loss becomes less bad. In most of these cases, observed in the training period, all lamps lighted, which gives the jointer a warning that something can be wrong. A second warning can come from the optimum level of the transmitted signal, which is usually lower than for the other splices. Trials to measure the splice loss with the alignment unit by inserting the detecting clamp both after and before the splice were not successful up till now due to a lack of reproducibility and the complexity of this procedure for the jointer. Besides, the measured loss should be correlated to the loss at 1300 nm.

Results

After a training period of about one month four jointers, none of which had any experience with fibres before, started with the splicing of the two six fibre cables in Rotterdam. In the last week of their training two splicing sleeves were completed in a realistic field environment alongside a busy street. The mean value of the resulting splice loss, measured in the laboratories, was 0.15 dB. Three months later the splicing of the two Rotterdam cables was completed. The cables had a length of 7.6 and 9.4 km respectively, and were installed in an urban area in an air compressurized duct system. The total number of splicing points was 33. Measurement of the total attenuation at 1300 nm resulted in a mean splice loss of 0.15 dB for the first cable and 0.11 dB for the second one. The mean losses per

route are shown in table I.

Route	1	2	3	4	5	6
Mean splice loss	0.11	0.19	0.19	0.09	0.18	0.15
Route	7	8	9	10	11	12
Mean splice loss	0.08	0.14	0.09	0.12	0.09	0.13

Table I: Mean splice losses in two six fibre cables. The routes 1 to 6 are in the first installed cable.

It appears that there is a considerable variation in mean splice loss. Evaluation of the OTDR curves, which will be made from the two ends of each of the routes, probably will show whether these differences are due to incidental bad splices.

Important other experiences were:

- The preparation of the fibre ends had to be done very careful. Especially the fibre end faces must be perpendicular to the fibre axis. In practice it appeared that the used cleaving tool was rather sensitive to temperature variations. As the temperature in the tent where the splicing was done (see figure 4), varied from about 0 to 25 °C many initial problems arose. This problem was solved to a greater part by laying this tool on a temperature stabilized plate.

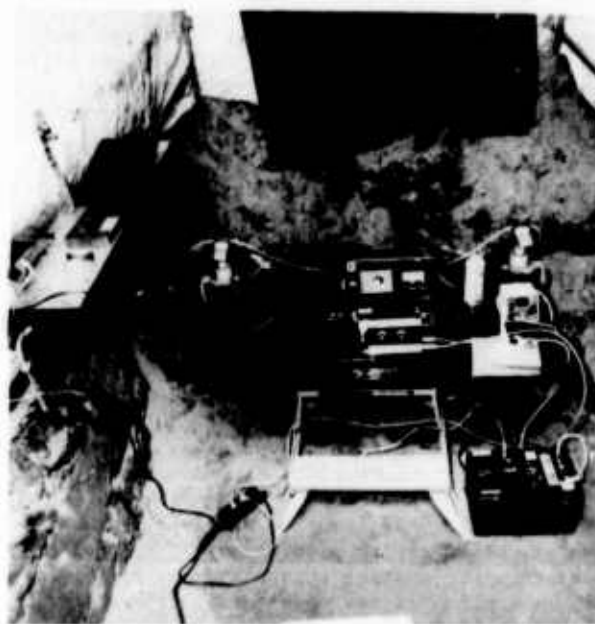


Figure 4: Interior of the splicing tent

- For three splices it was found afterwards that the corresponding discontinuity in the OTDR curve, which was measured for other reasons, was greater than 2 dB. Renewal resulted in a much better result. Probably these splices were due to the reasons described above. Although this only involves 1.5 % of all splices this effect requires special attention.
- The application of the alignment system requires that a rather long length of primary coated fibre has to be handled and stored in the organiser. This did not lead to any specific problem.
- For most splices the splicing procedure had to be repeated several times. This was most probably due to the non optimized splicing set or to an end face preparation, which was not satisfactory.
- The total time needed to make a complete splice varied considerably and sometimes was very long. Although this result is rather negative as for the splicing procedure it also shows that the check by means of the alignment system is rather severe.
- The simultaneous working on the same route by two or even three splicing crews did not raise any problems for the splicing. Also the sequence of the splicing is not determined by the splicing procedure as in the case of using far end equipment.

Conclusions

The principle conclusion which can be drawn from these installations is that the local core alignment using the bending method can be applied very well in a field environment. It can be combined with any splicing method, and showing from the total result obtained in the Rotterdam routes, it can even be combined with a splicing set which is developed for multimode fibres. Points of concern for the next installations are especially the choice of a splicing set which is more suitable for single mode fibres i.e. a set with a mechanical stability in the sub micron region, and a further improvement of the check on the splice loss. Important points which require continuous attention are the bending of the fibre and the transparency of the cladding mode stripping fibre coating. As for the first point, the signal level can be increased considerably by a more optimal launching and detection method, on which we are working now, resulting in less deformation of the fibre. The second point, the transparency of the fibre coating, is especially relevant when painting is considered as a method for fibre identification. Intermittent painting or the choice of a material which is transparent for the launched wavelength or can be removed easily can be a solution. In case of a non mode stripping coating this alignment principle can only be applied if very concentric fibres are spliced or if special provisions are made for additional cladding mode stripping near the fibre ends⁵.

References

- 1) K. Katekura, H. Yamamoto and M. Nunakawa, Novel core alignment method for low-loss splicing of single mode fibres utilising UV excited fluorescence of Ge-doped silica core, *Electr. Lett.*, 1982, Vol. 18, pp. 712-713.
- 2) G.D. Khoe, J.A. Luijendijk and A.C. Jacobs, Application of UV excited fluorescence for the preparation of single mode fibre connectors and splices, *Proc. 9th Europ. Conf. on Opt. Comm.*, Geneva, September 1983, pp. 413-416.
- 3) O. Kawata, K. Hoshino, Y. Miyajima, M. Ohnishi and K. Ishihara, A splicing technique for single mode fibres using direct core monitoring, *Journal of Lightwave Techn.*, 1984, Vol. 2, pp. 185-191.
- 4) O. Kawata, K. Hoshino and K. Ishihara, Core axis alignment method to achieve ultra low loss fusion splicing for single mode optical fibres, *Optics Letter*, 1984, Vol. 9, pp. 255-256.
- 5) C.M. de Blok and P. Matthijsse, Core alignment procedure for single mode fibre jointing, *Electr. Letters*, 1984, Vol. 20, pp. 109-110.



C.M. de Blok
Dr. Neher Laboratories
Netherlands PTT
2260 AK LEIDSCHENDAM

Cornelis M. de Blok was born in 1954. He joined the Dr. Neher Laboratories in 1971 and has been engaged in the development of various subscriber services on metallic cable, passive fibre optic devices and measurement techniques for fibre optic cables. Now he is an engineer in the digital transmission department of the Dr. Neher Laboratories.



P. Matthijsse
Dr. Neher Laboratories

Pieter Matthijsse was born in 1945. He graduated as an electrical engineer at the Eindhoven University of Technology in 1971 and obtained his PhD degree in applied sciences in 1976 at the University of Leuven (Belgium). He then joined the Dr. Neher Laboratories where he has worked on various subjects in the field of optical fibre transmission: measurement techniques, passive components, splicing and systems. Now he is a senior staff engineer of the digital transmission department.

A CUSTOMER DESIGNED SPLICE CLOSURE

G. S. Cobb, J. F. Malluck, J. R. Massey and
A. H. Williamson, Jr.

AT&T Bell Laboratories
2000 Northeast Expressway
Norcross, Georgia 30071

ABSTRACT

AT&T Bell Laboratories has conducted a Closure Development Study whose goal was to organize a Plan for the design and development of new closures meeting the telephone companies' needs for the 80's and beyond. Data were gathered by means of indepth interviews with fifteen BOC's and then were combined with information generated "in house" to establish a list of Design Objectives. Summarizing, the customer requires a universal closure design having a high degree of reliability, easy to assemble, with little need of training and having a low initial cost. The result of our effort is the 2000 Series Splice Closure. Its design is applicable in all plant types and can accommodate cable sizes and types from the largest to the smallest. This paper presents results of the BOC study leading to the 2000 Closure and details of the design that address the customers' needs.

I. Introduction

In the early 1980's, AT&T Bell Laboratories established a Plan to guide its efforts in developing a new splice closure. The Plan consisted of four steps, namely:

1. Identify all the significant influences on closure design, usage, and applications.
2. Determine the impact of each of these influences on future closure development.
3. Compile a broad set of specific objectives for closure development.
4. Design the closure.

This paper will discuss each of these steps in detail. It will begin with basic inputs and end by describing the finished product. In between, will be discussions of feasibility studies and an illustration of how the finite ele-

ment analysis method was used as a design tool.

It was in the execution of Step 1 that the customer's input was so vital and hence the title of this paper, "A Customer Designed Splice Closure."

II. Influences on Closure Design

If given the opportunity to design a new product from scratch, the natural first step would be to identify all those variables or influences which affect the product. In the area of splice closures, eight such influences were identified:

1. Present Performance -
How well are current closures meeting field needs?
2. Future Requirements -
What will the outside plant require of closures in the future?
3. Human Factors -
What should the closure designer expect of the closure user?
4. Tools
Under what circumstances might specialized closure assembly tools be desired?
5. Closure Reliability
What are the fundamental failure mechanisms for closures?
6. Materials Technology
What materials should be used in future closure designs?
7. Manufacturing Technology
What manufacturing processes should be used in future closure designs?
8. Economics
How is the economic worth of a new closure evaluated?

Having identified the influences, the next task was to identify the best

source(s) of information applicable to each influence. Only data having a direct bearing on closure design was desired. Generalized information was not sought. With these guidelines, it was concluded that the Bell Operating Companies (BOC) were the best source of information concerning the first four listed influences. Input on the last four would come from AT&T Bell Laboratories and AT&T Technologies. The remainder of this section will be devoted to describing the methods used to gather information from the BOC and a discussion of some of those results.

The method selected to gather the BOC information was an interview process. A list of possible management interviewees was established from suggestions submitted by the AT&T Bell Laboratories Transmission Media Laboratory. Two qualifications were required to be included on the list. First, the person should have some experience and understanding of closure requirements. Secondly, and most important, the interviewee had to have a reputation of interacting candidly with AT&T Bell Laboratories, i.e. someone who will "tell it like it is."

Each interviewee was contacted and an interview requested. The survey purpose was explained to each interviewee and anonymity, to the best of our ability, was pledged.

Fifty-seven (57) management interviewees were thus selected from fifteen BOC's. Twenty-two (22) interviewees had line responsibility and the remaining thirty-five (35) were staff positions. Table 1 shows the management interviewee distribution by Level and Job Type.

TABLE 1
Distribution by Level and Job Type

. By Level	
1st	9
2nd	24
3rd	23
4th	1
. By Job Type	
Construction	42
Maintenance	4
Const. & Maint.	8
Engineering	3

Two craft crews, one construction and one maintenance, were interviewed for every management interview, resulting in a total of 300 craft interviews. Table 2 lists the craft demographics. There was a good balance between construction and maintenance with the craft, but it was not the 50-50 split desired. Except for buildings, the

craft were about evenly distributed with experience in the different plant types; typically the experience level was very high. Seventy-seven (77%) percent of the craft interviewed had two or more years experience. Further, this same level of experience was present for all BOC's, not just the slower growth companies.

TABLE 2
Craft Demographics

. Work Area	
Construction	65%
Maintenance	31%
Const. & Maint.	4%
. Plant Type	
Aerial	32%
Underground	37%
Buried	28%
Buildings	3%
. Work Experience	
<6 months	7%
6 Months - 1 Year	6%
1 Year - 2 Years	10%
2 Years - 5 Years	9%
>5 Years	68%

There was no attempt by the BOC to have only experienced craft available. This high level of experience is a positive factor when establishing credence of the data.

The management people were individually interviewed using an established questionnaire. The craft people were interviewed in small groups using a second questionnaire. Each question was discussed in order and then the craft marked their responses.

The management questionnaire contained thirty-six (36) objective type questions, twenty (20) open-ended type questions, and five (5) bibliographical questions. A similar number and type of question(s) were used on the craft questionnaire.

Present Performance

How do closures fail was one of the major results being sought on "present performance." Data requested was: relative frequency of failure modes, relative significance, and the effect of geography and topography on closure failures. Relative frequency data is shown in Table 3. UG, B, and A stand for underground plant, buried plant, and aerial plant respectively. Data shown is from the management interviews.

TABLE 3
"Please rank the closure failure modes listed below as to their relative frequency"

Failure Mode	Plant Type		
	UG	B	A
Reentry activity	1	3	1
Poor craftsmanship	2	2	2
Water entry	4	1	4
Use of too small of closure	3	8	7
Poor bonding	6	6	3
Poor adhesion of sealing tapes	7	4	8
Complexity of seal design	5	5	6
Other	8	7	5

The rankings shown are based on the numerical average recorded for each factor. Reentry activity and poor craftsmanship rank #1 and #2 for underground and aerial plant. The actual numerical average in the underground plant was 2.23 for #1 and 2.31 for #2 compared to 4.02 for the 3rd ranked factor, "use of too small a closure." The difference between #1 and #2 in aerial plant was 0.27 compared to the .08 for UG.

In buried plant, #1 was, as expected, water entry. Second ranked poor craftsmanship was quite close to #1 with a difference (delta) of .09. Reentry was a distant third. This was most likely because buried splices are encapsulated and are generally not meant to be reentered.

Bonding only appears to be a problem (relatively speaking) in aerial plant. Feedback during the interviews and a craft question concerning bonding, shows the problem to be associated primarily with metal splice closures.

Closure design attributes received relatively good "marks" except for the previously mentioned bonding in aerial plant. However, examination of the "other" responses showed design was considered a problem in buried plant and was ranked #1 in two questionnaires. Additional factors ranked either #1, #2 or #3 in the "other" category were: poor BOC engineering design (3 instances), reaction between

sealing tape and encapsulant (2 instances) and temperature effects of metallic closures in aerial plant (2 instances). A final observation about the "other" data. It was only designated 8% of the time for the first three choices. This indicates that the factors listed were in fact the most common and important factors as viewed by both AT&T Bell Laboratories, the source of the factors, and the BOC's.

When asked to list the major closure shortcomings in the underground plant, data shown in Table 4 was recorded.

TABLE 4
UG Closure "Shortcomings"

Item	Number of Time Noted
Craft Sensitive	9
Bolts and Bar	8
Too Large for Manholes	6
Difficult and/or Slow Reentry	5
Too Many Piece Parts	5
Size Limitations	4
Metal Cases Too Heavy	4
Bonding on Metal Closures	4
Alignment of End Plates	3

Although many questions were answered by assigning the problem to a material, i.e., bolts breaking, only the data shown in Table 5 was gathered purely from a material failure viewpoint. The data was taken from the management survey via the question, "What are the most frequent closure material failures that you have encountered?"

TABLE 5
Material Failure Modes

Material(s)	Instances Noted
Bolt and bolt strips	13
B-Sealing Tape	10
Inserts in End Plates	7
Cracks in metallic closures	6
Corrosion of metallic closures	4
Sealing Tape/Encapsulant	4
Sealing Tapes	4

Except for the metallic closure problems, all instances noted in Table 5 refer to fasteners or seals.

Human Factors

"Does a great reduction in the skill required to put on a closure tend to interfere with job satisfaction or craftsman pride?" Eight-four percent of the BOC management said no, nine percent said yes, and the remaining seven percent offered an opinion between yes and no. The reasoning behind this overwhelming endorsement of "goof-proofing" was the splicer is paid for and takes pride in wire work, i.e., the talking path. Productivity with good quality are their motivation and thus they look at closure installation as a necessary evil, the same as cleaning up the work site which must be accomplished at or near the end of the work day.

Is the craftsman's capability changing and what impact will this have on closure design was addressed by asking both management and craft to rate characteristics that best describe the outside plant craftsman. Table 6 lists the data by trait or characteristic. Not all traits were on the craft

TABLE 6
Craft Characteristics

Trait	Management	Craft
More Manual dexterity	12%	34%
Same	32%	30%
Less manual dexterity	56%	36%
Physically larger	25%	42%
Same	25%	41%
Physically smaller	50%	16%
Stronger	13%	13%
Same	29%	47%
Weaker	59%	40%
More intelligent	51%	44%
Same	39%	33%
Less intelligent	11%	23%
Better attitude	23%	18%
Same	30%	25%
Worse attitude	47%	56%
More trainable	51%	-
Same	26%	-
Less trainable	23%	-
Slower turnover	5%	-
Same	19%	-
Rapid turnover	75%	-

questionnaire. The first three traits are physical while the last four are mental or personality oriented. If the

response "same" is considered positive, then management views craft in a more negative manner than craft views itself on the physical traits, but more positively on the mental traits than craft. All of these traits impact on closure design especially manual dexterity and strength.

Tools

The basic questions the interviews sought to answer concerning tools were:

1. What are the valid objections to closure tools?
2. What are the motivations for introducing closure tools?

When asked how valid are the given objections to new closures tools, cost was ranked #1 as could be expected. It received thirty-two first choices while #2 ranked maintenance received only twelve first choices. Thus, cost is by far the most valid objection to introducing new closure tools. These results are in Table 7.

TABLE 7
Valid Objections to New Tools

Objection	Average Rank
Cost	1.78
Maintenance & Repair	2.57
Training	2.94
Inventory	2.98
Other	3.80
Manpower Reduction	4.50

Motivations for introducing new closure tools are ranked in Table 8.

TABLE 8
Motivation for Introducing Closure Tools

Motivation	Average Rank
Make Closure More Reliable	1.85
Make Job Easier	2.53
Make Job Safer	2.65
Make Job Faster	2.74
Make Closure Less Expensive	3.85
Other	6.00

Reliability was a firm #1 choice followed by easier, safer, faster and last cost considerations. Cost was a distant fifth place when compared to the fourth place of "faster".

Future Requirements

BOC data on future closure requirements covered a wide range of topics from reentry considerations to environmental concerns to the changes brought about by fiber optics and electronic pair gain systems.

Perhaps the most important question asked because it goes straight to the point is, "What closure attributes should be considered to assure BOC acceptance?"

Reliability was the overwhelming #1 choice. This coincides exactly with AT&T Bell Laboratories design philosophy. First cost was a distant ranked third, although it is used by many BOC's when determining which closure will be purchased. Ease of assembly was ranked #2 and had an average response of 2.67 compared to 4.20 for first cost. Ease of reentry, even with its associated problems, was considered important and ranked fourth. The data is clear, make it reliable, easy to assemble and then cost effective.

The above results were examples of the data gathered from the BOC's. This information was combined with in-house studies of reliability, manufacturing processes, materials technology and economics. From the gathered data, the Design Objectives shown in Table 9 were established completing steps 1, 2, and 3 of the Closure Development Plan.

TABLE 9
Design Objectives

High Reliability
Universal Applications
First Cost Advantage
Simple to Assemble
Ease of Reentry
Compliant Seals Preferred
Avoid Threaded Fasteners
Alignment Aids Required
Special Tool(s) Only to Decrease
Craft Sensitivity and Only if Tool is
Inexpensive
Fewer Parts

III. Splice Closure Design

Step 4 was stated simply, "Design the Closure." It was in fact a series of smaller steps consisting of material and process feasibility studies, design concepts, and preliminary trade-offs between design objectives and cost considerations.

Material and Process Studies

The purpose of these studies was to select a material-process combination that would economically provide a product to meet the established Design Objectives. Initially, the constraint was imposed that the selection of both the material and the process would have to be taken from those currently available and well-established in order to avoid probable lengthy development programs prior to actual product design. Further constraints were placed on material choice in the form of environmental and associated material compatibility, Bell System and REA performance requirements; with these constraints and requirements in mind, the vast array of possible material-process combinations were reduced to:

Hot stamped glass mat reinforced polypropylene

Injection molded polypropylene

Die cast aluminum

Sand cast galvanized cast iron

Extruded polypropylene

Roll formed nylon coated steel

Roll formed low carbon coated stainless steel

The first four of these processes were currently in use in existing closure manufacture.

In order to conduct a comparative economic study, a simple representative physical model was established. It consisted of three sizes of semi-circular parts providing a reasonable simulation of the proposed family of closures. These models would be required to maintain 10 psi pressurization for a period of 40 years using a standard pressurization system under all environmental conditions found in aerial, buried and underground plant and 20 psi for a short time during flash testing. Accordingly, the model thickness was determined by material

property and/or process limitation; eg, for example, the minimum practical wall thickness in sand cast iron is 5/32 inch, even though this greatly exceeds the pressurization requirement. These models were then subjected to part cost analysis and a study to determine capital investment required for the manufacture of the estimated annual demands of the three sizes. These studies resulted in the selection of the hot stamp process as the preferred manufacturing method.

To describe the hot stamped process, we must first describe the material. It is a laminate of polypropylene and fiberglass mat. It is supplied in a rigid sheet approximately one-eighth inch thick.

Preforms or blanks are then cut from this sheet stock and placed in an oven with the necessary controls to bring the material up to a formable temperature. At this point the heated blanks are placed in matched die sets, or molds, mounted in a hydraulic press of sufficient capacity to deform the material to the desired shape. After an adequate chill to allow cooling to a structurally stable state, the mold is opened and the finished part removed.

Design Concepts

The basic assumptions used to generate design concepts where the closure would consist of either a one or two piece cover surrounding a two piece endplate (1 cable entry). The cover would be sealed to itself or a second cover piece with a non-mastic material. Likewise the seal between each endplate and cover would be a non-mastic and finally the seal between the endplate and the cable would be of a non-mastic material.

Fasteners would be one piece and preferably integral with the covers and endplates.

From a strength consideration, the closure would have to withstand pressurization to 10 psi and then temperature cycling from -40°F to 140°F in an eight hour period. Further, it would have to withstand an overpressure of 20 psi for thirty minutes and possess an impact resistance of 120 inch-lbs. at 0°F.

The cover seal concept was a tongue and groove sealing configuration using a sealant. It was successful as a sealing system but manufacturing cost and durability were unattractive. These developments lead to a groove-groove geometry and a solid compliant seal member.

Fasteners were originally conceived as one piece non-metallic structures. Feasibility studies showed this approach to be unacceptable. The fastener concept then turned to a more efficient use of metals as fasteners. This direction lead to wire forms.

Traditional mastic sealing techniques were chosen for the cable to endplate seal after considering a number of alternatives. These seals have had a history of high reliability, rarely need to be disturbed during reentry and permit endplate designs which do not require special tools.

Resulting Design

The result of the above described steps was a splice closure that is applicable to all plant types. Table 10 lists the range of sizes available. The closure can be utilized with lightguide and copper cable with diameters up to 3.5 inch.

Figure 1 shows the design features of the closure. Key to uniqueness of this design is the use of two compliant seals and a wire form as an over center fastener. Such a system permits very fast reentry and closing times on the order of one minute. This compares to like tasks of 14 to 20 minutes for existing product.

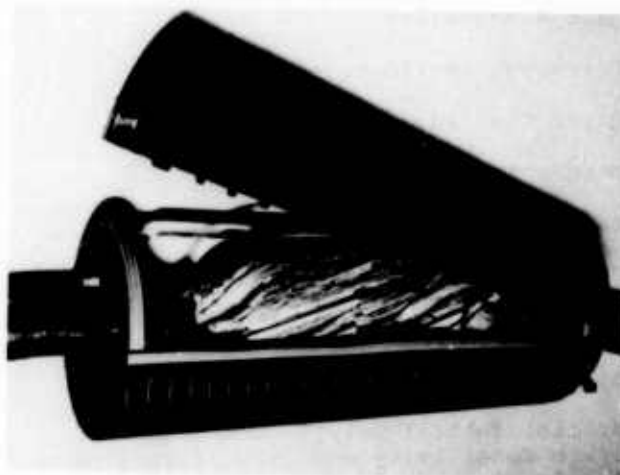


FIGURE 1. 2000 CLOSURE

The compliant endplate seal and flange seal meet at each corner of the closure half. By properly selecting the seal geometry, seal groove geometry and seal material properties, the system when brought together with the spring latch forms a pressure tight seal capable of withstanding 10 psi

TABLE 10
Closure Sizes

Closure Inner Diameter	Sheath Opening		
	20 inch	28 inch	36 inch
5.5 inch	X	X	
7.0 inch	X	X	
8.5 inch	X	X	X
10.0 inch	X	X	X
12.0 inch	X		

for forty years in a standard pressurization system. It was in the design of this seal system that the finite element method of analysis was utilized.

The closure seals were extensively analyzed as they are a critical component in a pressurized closure design, and must reliably seal the closure over the design life. In addition, analysis of a particular successful design could then be exploited in the design of an entire family of closure diameters, by parametrically varying the analytical model to predict seal performance for each closure diameter to be manufactured.

The endplate to cover seal makes use of compliant ribs to seal between the closure cover and endplate. Figure 2 shows a cross-section of the seal which is formed by extrusion, cut to proper length, and then bonded into a closed circle. When the closure cover is installed the ring is compressed such that the three upper ribs seal against

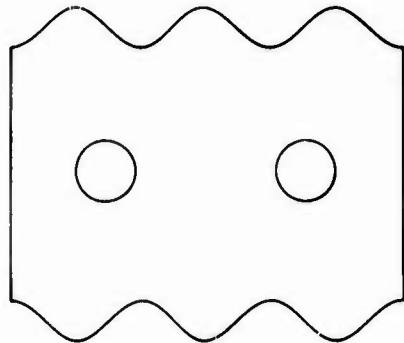


FIGURE 2. ENDPLATE SEAL PROFILE

the cover, and the three lower ribs seal against the endplate. Sufficient contact stress then exists between the seal ribs and the cover and endplate to adequately maintain internal pressure. The contact stress must be maintained over a range of part tolerances, and thermal environment which may alter part dimensions. Bear in mind that substantial deformation of the ribs is required to accommodate the dimensional variations.

The relatively complex geometry of the seal lends itself to analysis by use of the finite-element method. Figure 3 depicts the finite-element model generated to represent a portion of the actual seal cross-section. Symmetry allows this model to adequately represent the entire structure. Axisymmetry is employed to represent the three dimensional ring. Four node isoparametric solid elements were used for the seal model. In addition, gap elements were employed in the analysis to ade-

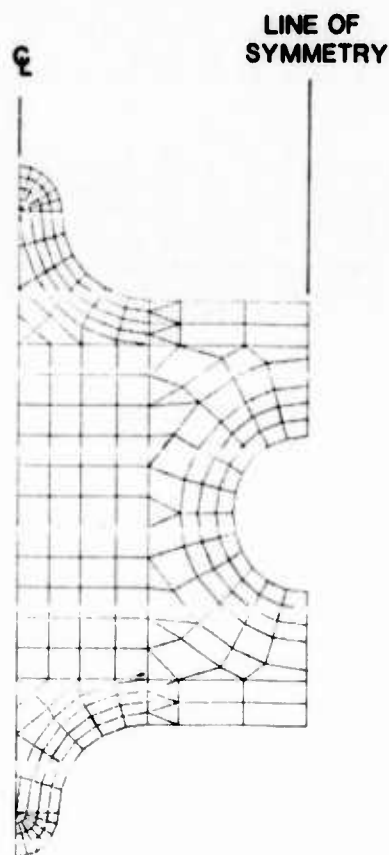


FIGURE 3. FINITE ELEMENT MODEL OF ENDPLATE SEAL

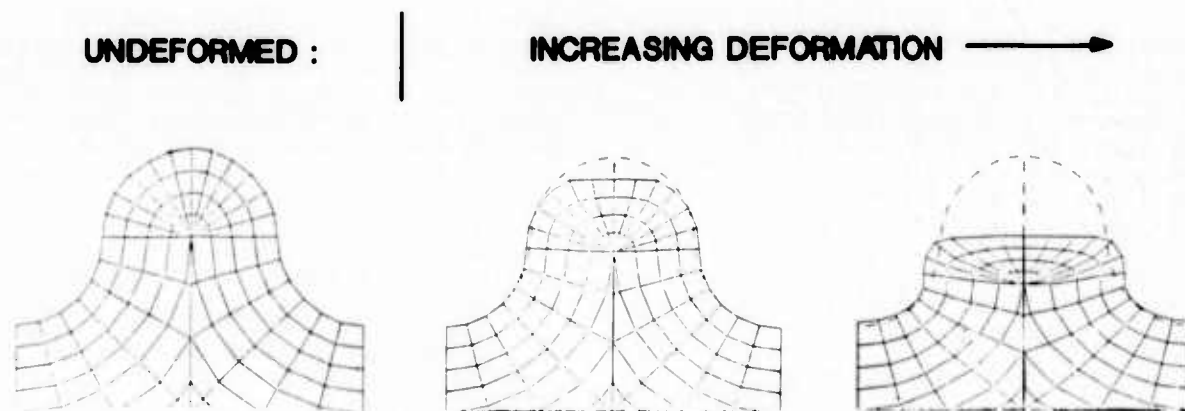


FIGURE 4. ILLUSTRATION OF CONTACT SURFACE DEVELOPMENT

quately represent the interaction of the seal and sealing surfaces that is, the development of the contact surface. The sequence of pictures in Figure 4 illustrates the non-linear development of the contact surface as one displaces the gap elements. The contact stress which exists on this flat surface is the actual mechanism for maintaining an adequate seal.

The contact stress is a non-linear function of the seal deformation, that is, there is a rapid rise in contact stress with the initial deformation, but the rate of increase diminishes as the deformation proceeds as shown in Figure 5. These data were translated into a range of contact stresses upon which to base the design. This information can then be exploited in the design of seals for a range of additional closure sizes.

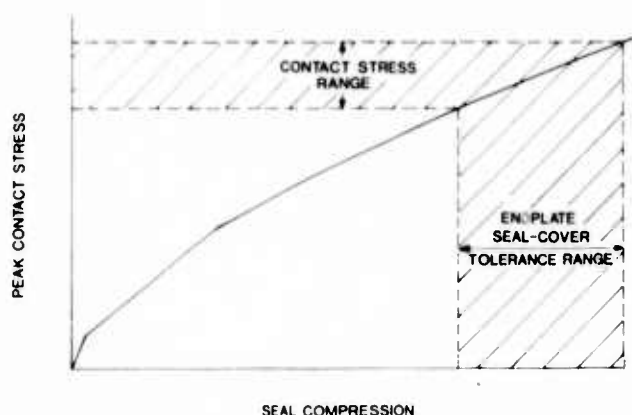


FIGURE 5. FINITE ELEMENT PREDICTIONS OF CONTACT STRESS

Instead of further detailed description of the design, its features can be best appreciated by examining the design against the customer generated Design Objectives listed in Table 9.

- **High Reliability**
The basis of demonstrating reliability is embodied in meeting the requirements of PUB 55003.¹ Such requirements as impact strength, cable pullout, flex testing, electrical tests, overpressure tests, chemical resistance and temperature cycling are typical of those specified in this document.
- **Universal Applications**
These were covered in Table 10 from a size consideration. The design is applicable to all plant types. Lightguide cable is accommodated with the use of grommets. Vault applications use the same grommet techniques as existing technology in conjunction with a fire retardant cover and endplate material.
- **First Cost Advantage**
Prices of the closure are available through AT&T Technologies and they are competitive.
- **Simple to Assemble • Ease of Reentry • Compliant Seals • Avoid Threaded Fasteners**
These objectives were met as previously discussed. There are only four threaded fasteners in the closure, two in each endplate. This compares to twenty-six in existing designs. Further, the bolt torque requirement has been eliminated by careful location of the fastener with respect to the sealant.

- **Alignment Aids**
Two aluminum alignment bars are provided to insure alignment of endplates. They further serve as a measurement device to establish the sheath opening and locate the endplate collars prior to splicing.
- **Special Tools**
No special tools are required to install or reenter this new closure. Only hand tools typically carried by a craftsperson are necessary.
- **Fewer Parts**
Basically the closure consists of two covers, two endplates, two alignment bars and four seals. All fasteners, latches, etc. are in place and ready to be used.

IV. Summary

An indepth interviewing processing was conducted among fifteen BOC's to explore and document the customer's opinion concerning the present performance and future requirements of splice closures, the necessity of closure tools and their view of human factors relating to the craft. These data were combined with in-depth studies of materials and manufacturing technology, reliability and economic and a list of Design Objectives were established to guide the design and development of a new series of splice closures.

The design that resulted has been named the 2000 Series Closure. It is universal in its application and is available in a wide range of sizes and configurations.

The message received during the BOC interview process was design a closure that is very reliable, simple to install, go on right the first time and inexpensive. The 2000 Closure meets these criteria.

Reference

1. Bell System Technical Reference, Pressuretight Splice Closure, PUB 55003, Issue 1, October 1981.



Gary S. Cobb is a Member of Technical Staff in the Cable Joining Department of AT&T Bell Laboratories, located in Norcross, Georgia. He is presently the Project Engineer for the 2000 Closure. Prior to this assignment, he was the Project Engineer for CONECS. Mr. Cobb was active in the development of Sea Plow IV, a vehicle for burying ocean cable. Before that he was involved in the design and development of ocean cable and associated hardware. Mr. Cobb received his BSME degree from Virginia Polytechnic Institute and State University and an MSME from the University of Maryland.



John F. Malluck is a Member of Technical Staff in the Cable Joining Department of AT&T Bell Laboratories. His present duties include detailed structural analysis for the 2000 series closure project. Prior to this assignment, he was employed in the aerospace industry with a specialization in structural dynamics and fracture mechanics. Dr. Malluck received his Ph.D in Engineering Mechanics from the Georgia Institute of Technology.



John R. Massey is a Senior Technical Associate in the Cable Joining Department of AT&T Bell Laboratories. He is presently the design engineer on the seal, fasteners and covers for the 2000 closure. Prior to this assignment, he designed grommets for tip cable and assisted in design of grommet and seals for lightguide cables and closures. Before that, he was active in mechanical design of the ARSB system. Years prior to that he was a development engineer on Hercules, Zeus, Sprint and Sparten missile guidance sets. Mr. Massey attended Guilford College in Greensboro, North Carolina.



A. H. Williamson, Jr. is a Member of Technical Staff in the Cable Joining Department of AT&T Bell Laboratories. He is presently one of the design engineers on the 2000 closure project. He has been active in apparatus design in both central office and outside plant since 1967. Prior to that, he was involved in the design and development of radar antenna systems and underwater sound hydrophone support structures. Mr. Williamson received his BSME from Union College in Schenectady, New York.

BONDED ASP: A SUPERIOR SHEATH FOR BURIED
AND UNDERGROUND FILLED CABLES

D. M. Mitchell and R. P. Collins
AT&T Bell Laboratories - Norcross, GA

D. E. West and M. D. Kinard
AT&T Technologies, Inc. - Norcross, GA

ABSTRACT

A new primary sheath has been developed for filled cables which improves the cable handling and sheath strength characteristics, enabling installation in ducts. The new sheath, called Bonded ASP, utilizes the Bonded Sheath Technology developed for pressurized cables and extends it to the fully flooded sheath of filled cables. The resulting composite, in which the steel outer member is adhesively bonded to the polyethylene jacket, exhibits greater strength, greater flexibility, and improved handling characteristics. Sheath buckling in cold weather installation, and jacket slippage in hot weather are virtually eliminated. This results in a cable which is, for the first time, rated for installation in underground plant, traditionally the domain of pressurized cable.

1. INTRODUCTION

1.1 Filled Cable Evolution

Filled Cable was introduced into the U. S. telephone industry in 1969 by Western Electric. Since that time it has grown to be the cable of choice for buried use in all independent and former Bell operating companies in this country. Today, well over half of all cable manufactured and placed is filled design.

The first filled cables were very small, partly for manufacturing reasons, and partly because the premiums for filling compounds and larger cross sections could not be justified above about 200 pair. However, with the advent of cost and size reductions of foam-skin insulation (1), and the outstanding maintenance performance of filled cable, the demand for filled cables of larger and larger size has continued to grow. Today a substantial amount of filled cable over 3.0 inches in diameter with pair counts up to 3600 is being made. These

cables are not only being buried, but we know that many are being pulled into underground conduit. There are cases, particularly in smaller telephone offices, where the conversion of the last few hundred or thousand feet of a long buried route from filled to pressurized air-core would be complicated and expensive. Moreover, in areas where new routes are just developing, many operating companies find the exchange of slightly higher cable cost for the elimination of the first cost and long term maintenance of air pressurization a very attractive choice.

1.2 Limitations of Filled Cables for Underground Use

This general success of filled cable, and the concern for long term maintenance of air pressure systems, has led to rising demand for underground filled cable. However, from the design standpoint, there have been several objections to the endorsement and widespread usage of filled cable in the underground. These objections have been based on a number of factors related to filling compound and sheath limitations.

1.2.1 Filling Compound Limitations Up until 1980 all filled cable had a petroleum jelly (PJ) based grease-like filling compound. While these compounds had excellent processing and cable waterproofing properties, they have been a constant source of complaint from craftspeople. Because of their crystalline nature, they stiffen greatly below 30 deg. F, and large cables can become difficult or impossible to handle in the winter. In addition, PJ based compounds are rather incompatible with most splice encapsulants such that low viscosity oily interfaces are formed between conductors and the encapsulant mass. This has been the basis for the requirement within the Bell companies that the exposed cable core be well cleaned of filling compound prior to splicing. Adequate cleaning is only achieved with the use of petroleum based solvents, and while these can be safely used in open

splice pits, their use in the manholes of underground plant is generally considered undesirable. The greasy nature of PJ compounds has also been a concern. Many users feel that PJ is very difficult to clean up and remove from clothing, tools, etc., and that it can actually become a hazard when it becomes a slippery coating on ladders and equipment.

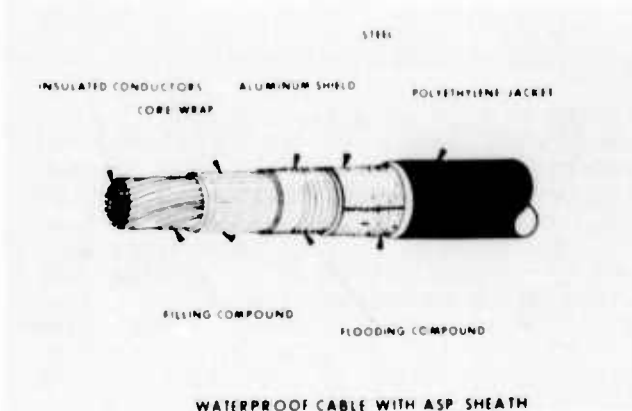


FIG. 1

1.2.2 Sheath Limitations Filled cable has always been provided with a fairly conventional composite sheath, and for the Bell companies the standard has been ASP, Figure 1. This sheath has an inner shield of corrugated aluminum, a protective layer of corrugated steel, and an outer jacket of black low density polyethylene. The metal layers are well flooded with thermoplastic compound for corrosion protection and longitudinal water blocking. ASP sheath has evolved as the most suitable and economic design for direct plowing and trenching of buried filled cable in all regions of the U.S. However, in spite of its outstanding performance history in buried applications, it has not been optimum for very large cables, particularly in underground applications. As the unit weight and cross-sectioned size of cable increases, conventional ASP sheath is more susceptible to buckling, jacket slip, cable flattening, and opening of the overlapped seam in the metallic shield. These characteristics increased the possibility of interference or jamming in the cable ducts and of resultant hidden sheath damage.

2. DEVELOPMENT OF BONDED ASP SHEATH

2.1 General Design Criteria

Improved mechanical performance from bonded construction in stalpeth sheath has been reported previously (2). Increased resistance to jacket slip and

sheath buckling reduce the possibility of handling problems and sheath damage as cables are pulled into underground ducts. The use of bonding in ASP sheath results in similar improvements, particularly in cables exceeding 2.5 inches in diameter.

FLEXGEL[™] filling compound has also been described (3). This material, developed by AT&T Technologies, is a thermoplastic rubber dispersed (or extended) in mineral oil; it is now widely used in the industry and has proved to have excellent waterproofing, handling, and performance properties. FLEXGEL[™] is more compatible with encapsulating compounds than PJ so that no cleaning is required prior to splicing, thus eliminating the solvent-in-manhole problem. Because of its non-crystalline nature, it does not stiffen significantly at low temperatures, so that handling of large cables, and wire separation for splicing are no more difficult in winter than summer. FLEXGEL[™] has a somewhat crumbly nature, Figure 2, which many people feel makes it much easier than PJ to manage, clean up, and remove from clothing. The advent of FLEXGEL[™] has virtually eliminated filling compound as an obstruction to use of filled cable in the underground.



FIG. 2 FLEXGEL[™] FILLING COMPOUND IN OPEN CORE END

Filled cable with bonded ASP sheath and FLEXGEL[™] filling compound thus provides a combination of properties suited to underground applications:

- High jacket slip strength.
- Sheath buckling resistance.
- Simplified and reliable encapsulated splicing.

FLEXGEL[™] is a trademark of AT&T Technologies, Inc.

2.2 Manufacturing Considerations

Bonding between the jacket and underlying metal must be sound and continuous. Mechanical strain resulting from bending or torsion tends to concentrate in a region in which bonding is interrupted, resulting in serious local weakening of the sheath. Adhesion can be prevented in an area in which the coated metal surface is contaminated prior to application of the jacket. For this reason, flooding compound, used to seal the inner sheath layers of filled cable, must be excluded from the bonded interface. When the outer metal is closed by a simple overlapped joint, seepage of flooding compound through the open seam during jacketing must be prevented. AT&T Technologies has developed means to accomplish this reliably in a continuous sheathing process (5).



FIG. 3 COMPARATIVE BENDING OF ASP SHEATHS

2.3 Bending Performance

Figure 3 illustrates the difference in bending performance observed in bonded ASP versus unbonded ASP sheath. Both cables had 26-gauge 1800-pair DEPIC cores and outside diameters were from 2.62 to 2.68 inches. Free bend tests were performed, consecutively, at room temperature. Since the overlapped seam is most susceptible to buckling when placed in compression, it was positioned along the inner or concave surface. The cables were retained in final bend configuration for the photograph. Data obtained from separate tests are shown in the following table:

Bend Radius for Buckle Formation*

Temperature deg. F	Sheath Type**	Cable O.D. Ins.	Radius Ins.
15	ASP	2.70	19
	B-ASP	2.65	10
70	ASP	2.98	30
	B-ASP	2.98	14
110	ASP	3.00	20
	B-ASP	3.00	7

* Overlapped seam in compression.

** Asp = Unbonded B-ASP = Bonded

Although the cables bent at 15 deg. F are somewhat smaller in diameter than those tested at the higher temperatures, significantly improved performance of bonded ASP is apparent in all cases.

2.4 Torsional Performance

Torsional stability is of equal importance to the mechanical performance of cable sheath for duct installation. Bonded ASP sheath on filled 1800-pair, 26-gauge DEPIC cable tested at 15 deg. F has been found to withstand 1 full axial twist in 6 feet without torsional buckle. In addition, with selection of the proper jacketing material, the construction has demonstrated excellent toughness across the overlapped seam in the metal at the bonded interface to resist jacket splitting.

2.5 Electrical Bonding

As in the case of bonded stalpeth, standard electrical bonding hardware and installation methods can be used to provide continuity when sections of bonded ASP sheaths are joined.

2.6 Water Resistance

In underground cable plant, the presence of filling compound replaces pressurization as the means for resisting water entry. The effectiveness of FLEXGEL filling compound for this purpose has been established through its extensive use in feeder and distribution cable for buried applications.

3. CABLE APPLICATION

3.1 Field Experience

Twenty six gauge cables up to 2700 pair containing FLEXGEL[™] filling compound and having bonded ASP sheath have been manufactured by AT&T Technologies, Inc., and successfully pulled into underground concrete ducts of the local telephone system in Oklahoma City, Oklahoma. Standard pulling eyes were furnished, exposed cable ends were capped, and standard installation methods were used. The ducts were from 6 to 8 years old, 4-inch and 3-1/2 inch I.D. runs were included, and rodding was done prior to placement.

Air temperature ranged from 70 deg. F to 80 deg. F. Cables entered the manholes in C-bend, but some reverse bending occurred at reel pay-off. Sheath lubricant was applied and guide collars were used at duct entry; pulling speeds reached 85 to 90 feet/minute. Excess length was furnished in some sections to permit some cable to be completely pulled through for inspection of the sheath after duct passage. Figure 4 shows a cable end emerging from a pull in excess of 600 feet; no indication of jacket slip or sheath buckling was observed.



FIG. 4 BONDED ASP EMERGING FROM CABLE DUCT

Bonded sheath reduces cable ovality, lessening concerns for interference as the nominal cable diameter approaches the limiting duct clearance. Cable having bonded ASP sheath and 3.4 inch maximum diameter was successfully placed in 3-1/2 inch I.D. duct without incident.

All splices below ground were encapsulated. Western Electric 710 modular connectors, 23-type closures, and D-encapsulant were used. Wire joining, closure assembly, and encapsulation of typical splices in 1800 pair cable were completed by two splicers in 3 hours. Figures 5, 6, and 7, show stages in splicing.



FIG. 5 CABLE SPLICE IN PROGRESS



FIG. 6 COMPLETED SPLICE

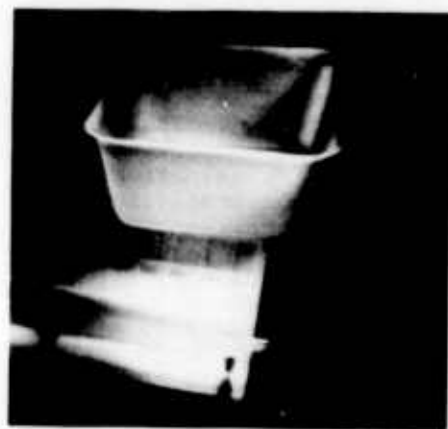


FIG. 7 CLOSURE ASSEMBLED & READY TO POUR ENCAPSULANT

Although it is not required that FLEXGEL™ be cleaned from wire work prior to encapsulation, some material is unavoidably dislodged during splice preparation. Debris and waste materials were confined in receptacles, and hand wipes were used periodically to minimize deposits of filling compound on clothing, tools, and working surfaces. Safe and satisfactory working conditions were maintained without difficulty throughout the splicing operation.

3.2 Recommendations for Underground Use

The combination of FLEXGEL™ filling compound and bonded ASP sheath make filled cable a fully satisfactory candidate for use in underground duct or conduit. Based on our past experience with this cable in underground applications, the following guidelines for its use have been developed.

- The choice of filled cable should be economically justified. Often its somewhat higher cost is readily offset by savings of construction and maintenance of air pressure systems.
- Filled cable should not be randomly substituted into existing underground plant. Plant continuity should be maintained within individual cable routes, using filled or pressurized cable exclusively.
- Where filled cable interconnects with pressurized cable, pneumatic isolation of the filled cable is required.
- Filled cable should not be used in underground locations where maximum duct or manhole temperatures are expected to exceed 140 deg. F.
- All splices of filled cable below grade should be encapsulated.
- Avoid accumulating filling compound on platforms, ladders, or tools.
- Encapsulant should be compatible with cable filling compound in order to seal to the wire surface effectively. Incompatibility between filling compound and encapsulant may result in leakage paths along wire surfaces.
- Complete removal of incompatible cable filling compound prior to encapsulation is required, and this may necessitate solvent cleaning of the wire work. The use of flammable or toxic solvents in manholes should be avoided.

- Re-enterable encapsulants are preferred, however, the need for entering and re-encapsulation of splices in manholes should be minimized. Initial planning and construction should anticipate growth and modifications to avoid encapsulated splice re-entry insofar as possible.
- Cable ends below grade level should remain sealed until spliced, and open wire work should be protected in a sealed enclosure if left temporarily exposed.

4. SUMMARY

Bonded ASP sheath has been developed as a substantial improvement over the conventional unbonded designs for filled cable. Explicit manufacturing methods were developed to reliably produce uniform bonding without contamination from internal filling and flooding materials. In combination with FLEXGEL™ filling compound, this results in a filled cable which can be fully recommended for pulling into underground ducts as well as direct burial.

REFERENCES

1. McCann, J. P., R. Sabia, and B. Wargotz, Eighteenth International Wire and Cable Symposium, 1969.
2. Mitchell, D. M. and G. H. Webster, Twenty-Third International Wire and Cable Symposium, 1974.
3. Yanizeski, G. M., E. L. Johnson, and R. G. Schneider, Twenty-ninth International Wire and Cable Symposium, 1980.
4. Mitchell, D. M. and R. Sabia, Twenty-ninth International Wire and Cable Symposium, 1980.
5. Patent applied for.
6. Clock, G. E., G. A. Klumb and R. C. Mildner, Twelfth International Wire and Cable Symposium, 1963.
7. Mildner, R. C., W. E. Ropp, and J. H. Snow, Fifteenth International Wire and Cable Symposium, 1966.

ACKNOWLEDGEMENTS

The work of R. C. Mildner, et al, (6, 7) in the development of polymer coatings to promote the adhesion of polyethylene jacket compounds to metallic substrates has been instrumental in the development of bonded sheath technology.



D. M. Mitchell
AT&T Bell Laboratories
2000 N. E. Expwy
Norcross, GA 30071

Mr. Mitchell is a Member of Technical Staff at AT&T Bell Laboratories in Norcross, GA. He is a graduate of Newark College of Engineering (now New Jersey Inst. of Technology), BS-ME. He joined AT&T Bell Laboratories in 1954. Much of his early career was devoted to ocean cable development. Since 1971 he has been associated with the Transmission Media Laboratory with principal responsibilities in the development and application of multipair cable.



R. P. Collins
AT&T Bell Laboratories
2000 N. E. Expwy
Norcross, GA 30071

Mr. Collins joined AT&T Bell Laboratories in Baltimore in 1962 with a B.S. in Mechanical Engineering from Miss. State University. In 1965 he received the M.S. in Engineering at the University of Maryland. He is presently Supervisor of the Feeder and Distribution Cable Development Group in Atlanta where he is responsible for product development and application engineering of multipair telephone cables.



D. E. West
AT&T Technologies, Inc.
2000 N. E. Expwy
Norcross, GA 30071

Mr. West is a Development Engineer at the AT&T Technologies Product Engineering and Control Center in Norcross, GA. He received his B.S. in Mechanical Engineering from North Carolina State University in 1980. He joined Western Electric in 1980 and has been involved in the development of cable sheathing and jacketing processes.



M. D. Kinard
AT&T Technologies, Inc.
2000 N. E. Expwy
Norcross, GA

Mr. Kinard is a Senior Development Engineer at the AT&T Technologies Product Engineering Control Center in Norcross, GA. He received his B.S. in Mechanical Engineering from Old Dominion University in 1974. He joined Western Electric in 1979, and is currently responsible for cable sheath design and development. He has a background in power plant design and overhaul, and in thermal and heat transfer analysis.

ADVANCEMENT IN PULP CABLE DESIGN AND MANUFACTURE

by

P.P. Kish

P.A. McGettigan

Northern Telecom Canada Limited
Montreal, Quebec

ABSTRACT

This technical paper covers the development of multi-unit pulp (MUP) cables with improved crosstalk performance manufactured on a new computer-controlled, tandem twisting and unit stranding facility. During the process development and introduction of new cable designs, extensive, comparative testing was performed under controlled conditions. In every such test, several important transmission parameters were significantly improved.

A fully identifiable MUP design using a staggered 25-pair twist lay scheme provides the capability for color-to-color splicing without incurring a sensible crosstalk impairment compared with random splicing. Both actual splicing tests and computer simulations have shown that the difference in the worst-case Far End Crosstalk performance is less than 1 dB. Likewise, the larger 100-pair units for the 22 gauge "true" MUP design resulted in a significant improvement in the Near End Crosstalk characteristics.

INTRODUCTION

This paper describes the development of a new multiple unit design pulp insulated communications cable with improved transmission characteristics. A cornerstone in the development of the new product is an integrated twisting and stranding process called tandem twisting. Essentially, it is a process that combines the twisting of single conductors and the stranding of twisted pairs into cable units in one operation. The new process provides more uniform twisting tensions and also design flexibility in the selection of twist lays and the layup of pairs within a unit. As a result, the crosstalk performance has been significantly improved compared with conventional designs.

This paper divides naturally into two sections. The first part covers the operation and capabilities of the tandem twisting equipment. The second part covers the evolution of pulp insulated cable designs and the resulting improvement in product performance.

TRANSITION TO TANDEM TWIST

The conventional method of manufacturing a stranded pulp unit follows a two-step process. In the first operation, two insulated conductors are selected from reel racks and loaded into a vertical twister. The twist lays are determined by manually changing a gear ratio. The twisted pairs are then off-loaded and grouped in sets by gauge and color. In a separate operation, the twisted pairs are transferred to give-ups on "table tops" with 100 positions. The pairs are then guided through a faceplate, stranded, bound and taken up through a rotating cradle.

Tandem twisting eliminates one process step. The twisted pair is manufactured in the same operation as the stranded unit and does not exist as a separate entity. Fig. 1 illustrates the tandem twisting process and its main components: the loading system, the rows of twister modules, the control system, and the stranding machine.

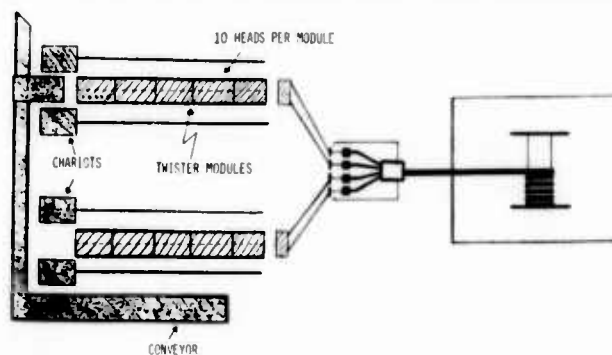


FIG. 1 TANDEM TWISTING PROCESS

First, at the back of the machine, up to 200 reels of pulp insulated conductors are selected from reel racks in the proper color sequence. They are then semi-automatically loaded with chariots into the respective twister head positions of each module. The twister modules are arranged in rows. There are five (5) modules in a row with ten (10) twister heads per module for a total of 100 twister heads capable of producing 100 pairs of output.

Each twister head is independently driven by an induction motor through a micro-processor controlled variable frequency drive. A central computer controls the frequency of rotation of the flybar as a function of the line speed (i.e., number of twists per unit length). The twist frequency is set in accordance with a programmed twist scheme. Any number of different twist lays can be assigned to a given twister head position including a continuously varying twist lay pattern. This arrangement provides complete flexibility in the design and manufacture of different types of units.

The pairs coming from each twister head are then routed through guides, pulleys, grouped together and pulled by a helper capstan which is slaved to the strander line speed. The pairs then pass through a faceplate and into a conventional unit stranding machine.

The main benefits derived from tandem twisting are product related and are of particular significance in the digital world:

- Improved transmission characteristics of the product, namely a lower capacitance deviation and a better crosstalk performance which results from a more uniform control of twisting tensions and a wider spectrum of available twist lays.
- The identification of all pairs in a multiple unit design pulp cable.
- The potential increase in the number of T1 carrier circuits in a full-sized, 22 AWG, "true" MUP cable.

PULP CABLE DESIGN

Large pair count pulp insulated cables are generally used as feeder and trunk cables which radiate from and connect switching centers. For such applications they are normally installed in underground ducts in urban areas.

Pulp insulated cables have undergone a number of design improvements over the years. For example, a more compact pulp cable was introduced in the mid 70's which enabled telephone utilities to increase underground duct efficiency. This was later followed with the development of modular unit design pulp cable which permitted easy division of the cable into 25-pair groups for modular splicing systems. Behind the scenes, the computerization of the pulp insulating process and the advent of tandem twisting have provided an extended capability for product design optimization and performance enhancement. This has led to the development of a new multiple unit pulp (MUP) design with improved pair-to-pair capacitance unbalance and equal level far end crosstalk (ELFEXT) characteristics.

Fig. 2 illustrates the construction of the new 100-pair MUP unit design compared with the concentric modular unit design (MOD) layout. The

100-pair multi-unit construction consists of four units of 25 pairs which are identified by blue, orange, green and brown binders.

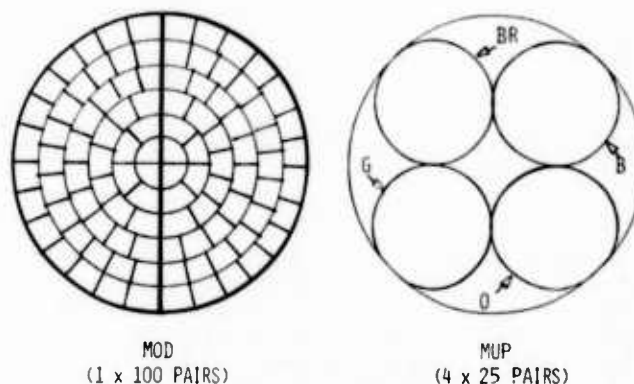


FIG. 2 UNIT DESIGN

The unique feature which distinguishes the new MUP design from other pulp unit constructions is the fully identifiable color coding system in which all 25 pairs in a 25-pair group are positively identified by colors of insulation and stains on the white conductor. The color coding scheme for the twisted pairs is shown in Table 1. It is particularly noteworthy that the tandem twisting method of assembly permits this to be accomplished while providing the desired crosstalk characteristics on all gauges. Full pair identification provides the capability for color-to-color splicing when required for cut-overs and in the restoration of a severed cable.

TABLE 1

COLOR CODE FOR TWISTED PAIRS

Ring	Tip	Ring	Tip
Blue	White	Green	White
"	" /Orange	"	" /Orange
"	" /Black	"	" /Black
"	" /Red	"	" /Red
"	" /Blue	"	" /Blue
"	" /Green	"	" /Green
Orange	White	Red	White
"	" /Orange	"	" /Orange
"	" /Black	"	" /Black
"	" /Red	"	" /Red
"	" /Blue	"	" /Blue
"	" /Green	"	" /Green
		Red	Blue

CROSSTALK CHARACTERISTICS

Traditionally, standard design pulp cables are made using only nine different twist lays (13 for MOD). The result is that for most pairs in a large unit of 100 pairs, there are 11 (seven for MOD) or more pairs in the same unit with the same lay. Crosstalk measurements on cables indicate that two pairs with the same twist length at any given distance apart have values of ELFEXT which are 6 to 10 dB worse on average than pairs the same distance apart but differing in twist length by only 2% to 4%. This result is illustrated in Fig. 3 which shows the variation of crosstalk as a function of distance between pairs in the same layer for a 100-pair pre-"MOD" unit design. Note the dips of about 8 dB in the curves when the combination of pairs are separated by 2, 5 or 8 other pairs in the same layer. These are the combinations of pairs which have the same twist lay. Also, it should be noted that pairs with any given twist lays tend to have values of ELFEXT about 7 dB worse if they are adjacent compared with those pair combinations which are separated by one intervening pair.

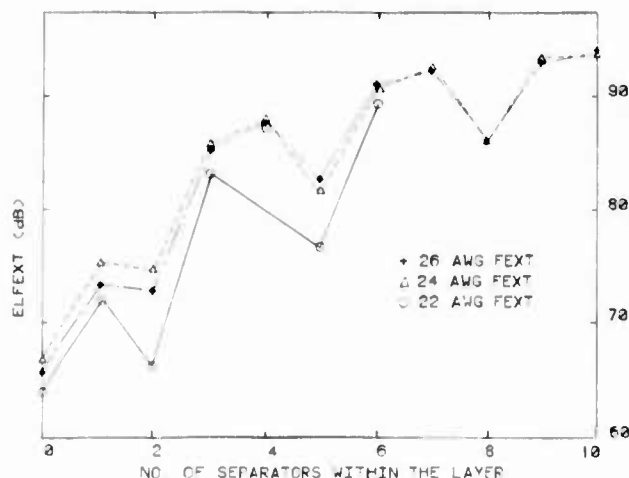


FIG. 3 VARIATION OF dB AVERAGE WITH SEPARATION AT 772 kHz FOR PULP CABLE

In conventional manufacturing practice, pairs are threaded through holes in faceplates such that pairs having the same twist length are separated from one another by at least two other pairs within a layer or between layers in a unit. Short stranding lays also help to maintain the pairs in their desired positions in the unit. However, there is always a small probability that pairs can become displaced or transposed due to uneven tension variations, process vibrations, or operator error. In such cases this can lead to a high pair-to-pair capacitance unbalance and detrimental crosstalk couplings between pairs with like twists which become adjacent for a significant distance along the length of the cable. Within the limitations of the manufacturing process, these abnormal crosstalk couplings could be effectively eliminated if the twist lengths of all pairs in close proximity were sufficiently different from each other.

The new tandem twisting facility has the capability of providing any number of different twist lays according to the position of pairs within a unit and independent of the pair color code. This capability has been exploited fully in the new multiple unit pulp design. Each pair within a 25-pair binder group is assigned a different twist lay with a minimum difference of 0.1 inch between pairs. Likewise, adjacent layers of pairs between 25-pair binder groups which are located side-by-side have a different twist length assignment and are also oscillated with respect to each other. Thus, the likelihood of any like pairs becoming adjacent is virtually eliminated.

Typical within-unit Equal Level Far End Crosstalk characteristics are presented in Fig. 4 for 100-pair, 26 AWG MUP units of the new design compared with the regular MOD design. These characteristics were compiled from a large number of measurements on representative cables from regular production. Both cable types have similar average crosstalk values. However, in the worst-case (i.e., < 0.01% of pair combinations), the crosstalk coupling loss is significantly better for MUP units manufactured on the tandem twisting facility. Poor crosstalk combinations in this region are probably due to displaced pairs or wrong twist lays which are unlikely to be a problem with the new design and/or process. For example, in one unusual instance on the tandem twister where a pulp unit was manufactured with the wrong twist scheme, it seemed that even when the twist lays on adjacent pairs were nominally the same, in practice they were actually different enough to avoid a worsening in ELFEXT. This is because the slip of any two induction motors which drive the twister heads are never identical.

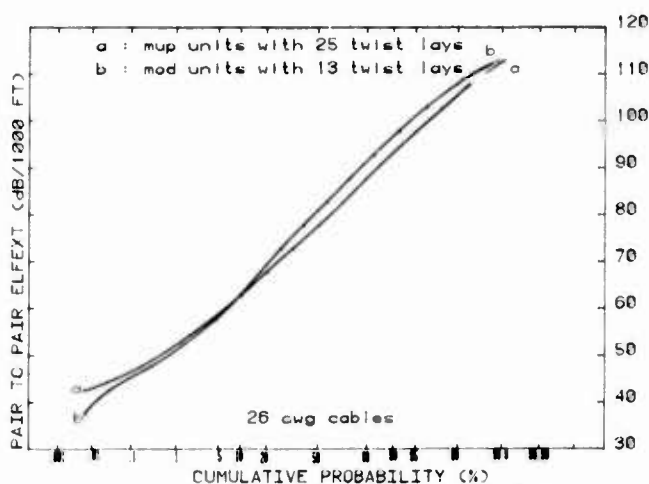


FIG. 4 EQUAL LEVEL FAR END CROSSTALK CHARACTERISTICS @ 772 kHz

COLOR-TO-COLOR vs. RANDOM SPLICING

The three main variables influencing the Equal Level Far End Crosstalk (ELFEXT) of any two combinations of pairs in a pulp unit are:

- (1) The effective distance separating the two pairs from each other, i.e., the greater the distance separating any two pairs, the better the crosstalk.
- (2) The quality of the insulated conductors making up the two pairs, i.e., for best crosstalk characteristics, the dimensions of the insulated conductors should be as concentric and as uniform as possible.
- (3) The length of twist lays, i.e., the shorter the average twist lay and the greater the difference in twist lays between the two pairs, the better the crosstalk characteristics.

For any cable type, the splicing procedure can influence variable (1), while variables (2) and (3) are controlled to the degree technically and economically feasible by good design and manufacturing processes. In any unit, it is inevitable that some pair combinations are worse than others. Random splicing increases the odds that the worst combinations will be spliced to good combinations, thus resulting in an averaging effect.

Fig. 5 shows the effect of random splicing on the Power Sum ELFEXT results for two 50-pair, 22 AWG MUP unit designs with 13 and 25 twist lays respectively. The Power Sum of ELFEXT in dB is a measure of the total interference on any pair from all the other pairs within a unit combined. The higher the value the better the result. A computer program was written to simulate a random splicing interconnection matrix for a full repeater section comprised of several lengths of spliced cable. The Power Sum was then calculated from individual crosstalk measurements on all pair combinations within a number of units of each design.

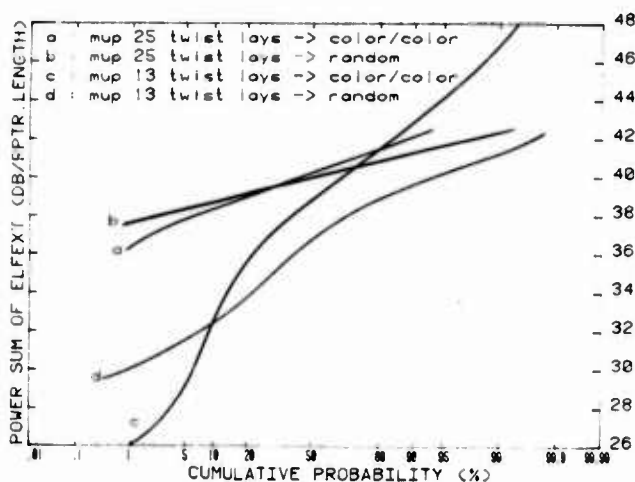


FIG. 5 EFFECT OF RANDOM vs. COLOR-TO-COLOR SPLICING

From Fig. 5, it is apparent that random splicing provides an improvement in the 1% Worst Power Sum compared with color-to-color splicing. This improvement is greatest when a spliced length in a repeater section has abnormally poor crosstalk characteristics, as was measured for 50-pair MUP units with only 13 twist lays. A plausible explanation of this is that the 1% Worst Power Sum is dominated by a very small number of poor combinations (1 to 5 out of 1225) and, with random splicing, the probability is low of a poor combination being spliced to another poor combination in a repeater section. Thus, the worst combinations tend to show the greatest improvement. On the other hand, the total ELFEXT power remains unchanged - it is essentially distributed more uniformly among the circuits.

In the case of the MUP design with the 25 twist lays, the improvement in the 1% Worst Power Sum due to random splicing is less significant, typically less than 1 dB in a repeater section with six randomly spliced lengths. Also, it is noted that for both random and color-to-color splicing, the average and the 1% Worst Power Sum are much higher than the corresponding values obtained for MUP units with a limited twist scheme.

From these results, it can be concluded that color-to-color splicing of MUP units with 25 twist lays is technically feasible without incurring any significant impairment in crosstalk performance compared with random splicing. These results have been verified by splicing trials on a full-sized 22 AWG identifiable MUP cable where some of the units were random spliced and other units spliced color-to-color. The results of these trials are summarized in Table 2 and show virtually no difference in the ELFEXT statistics between the splicing methods.

TABLE 2
CROSSTALK RESULTS
ON A 900-PR./22 AWG MUP CABLE MANUFACTURED
ON THE TANDEM TWISTER

ELFEXT @ 772 kHz WITHIN 50-PAIR UNITS		
	Random Splicing (dB/1000 ft)	Color-to-Color Splicing (dB/1000 ft)
Min.	47.9	47.6
Avg	71.9	73.2
Std. Dev.	9.0	9.9
RMS dB	64.2	64.1
PSUM Avg	47.7	47.6
PSUM Worst Pr.	43.8	43.8

MUP RANGE EXTENSION

A principal objective which has been realized through the new design and process is the manufacturing capability for so-called true MUP 22 AWG pulp cables as a replacement for psuedo-MUP. Large sized 22 AWG pulp cores are usually assembled from units of 50 pairs. In the psuedo-MUP design, the pairs within a unit are arranged in concentric layers using a limited number of dominant pair colors, usually green, blue and red. For such units it is possible to separate the pairs within a unit into two color groups of 25 pairs, one group comprising of one color and the other group comprising of the remaining two colors. The construction of a 50-pair MOD unit design is similar to psuedo-MUP, except that only two colors are used, namely green and orange. It is not usual practice to provide complete color coding of pairs in such units because of design and manufacturing restrictions. For normal splicing operations, complete pair identification is not important because of the productivity and performance benefits provided by random splicing. Nevertheless complete color coding of pairs is desirable after installation for cut-overs or where a cable is accidentally cut, then restoration of the cable requires matching up of the conductor pairs for splicing.

A 50-pair true MUP unit design is comprised of two 25-pair binder groups made up from 12-pair and 13-pair subunits. As discussed in the previous section, a substandard crosstalk performance was measured on 50-pair MUP units with 13 or fewer twist lays as a result of the close proximity of pairs with like twists, either within or between the subunits. However, it was also shown that the crosstalk performance is substantially improved by an identifiable MUP design which incorporates 25 different twist lays.

A comparison of the within unit ELFEXT characteristics between the different designs is illustrated in Fig. 6.

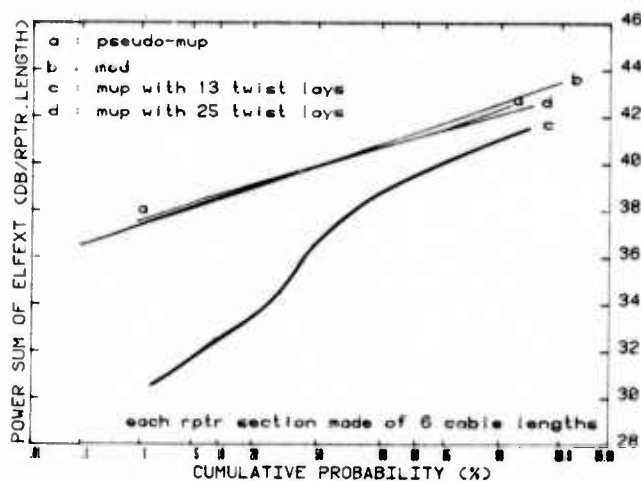


FIG. 6 WITHIN UNIT ELFEXT CHARACTERISTICS FOR DIFFERENT DESIGNS

The distribution of Power Sums is plotted for a full repeater section consisting of six randomly spliced lengths of cable. The results indicate that the psuedo-MUP, the MOD, and the identifiable MUP design with 25 twist lays, all have essentially identical within-unit crosstalk characteristics.

T1 CARRIER FILL

The capacity of a large sized 22 AWG pulp insulated cable for digital carrier applications is limited by the Near End Crosstalk interference between groups of T1 carrier circuits in opposite directions of transmission. In accordance with T1 engineering guidelines for single cable operation, such oppositely directed transmission groups are assigned in non adjacent units from the outer layer of units in the cable core. For example, in a 900-pair 22 AWG pulp cable which contains eleven (11) 50-pair units in the outer layer, only eight (8) units can be assigned for T1 carrier, four (4) in each direction of transmission, for a total of 400 pairs which is equivalent to a 44% T1 carrier fill. The Near End Crosstalk characteristics between adjacent 50-pair units of standard pulp insulated cables do not have sufficient crosstalk isolation to maintain acceptable error margins for T1 carrier applications. However, significant improvements in the Near End Crosstalk characteristics between adjacent units have been achieved with a larger 100-pair 22 AWG true MUP design manufactured on the tandem twister.

The layup of a 900-pair 22 AWG pulp core with 100-pair MUP units is illustrated in Fig. 7. With this design, 600 of the 900 pairs can be used for T1 carrier yielding a maximum 67% fill. This is possible since improved Near End Crosstalk characteristics allow adjacent units in the outer layer to carry TRANSMIT and RECEIVE signals. The result is a 50% increase in digital transmission capacity compared with a standard pulp insulated cable.

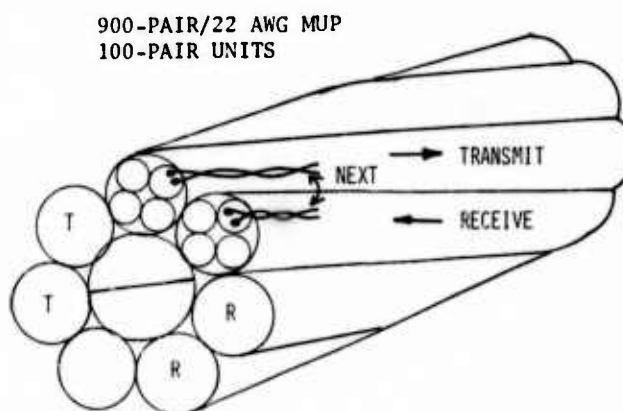


FIG. 7 PAIR ASSIGNMENT FOR T1 CARRIER APPLICATIONS

The Power Sum distribution of Near End Crosstalk (NEXT) between adjacent units on the outside layer is shown in Fig. 8 for different unit designs, including 50-pair MOD, 50-pair MUP, and 100-pair MUP units. The results indicate a 3 dB improvement in the 1% Worst Power Sum for 100-pair MUP units compared with either of the 50-pair unit designs, in spite of a doubling of the number of interfering pairs. This result translates into a worst case error margin of 12 dB which meets the T1 carrier design criterion.

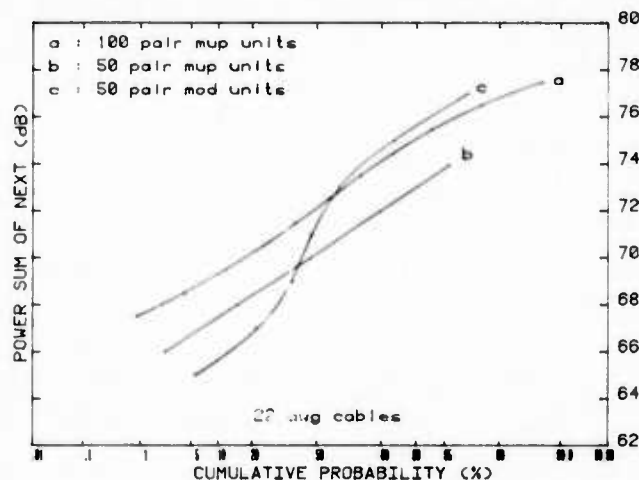


FIG. 8 NEXT BETWEEN ADJACENT UNITS ON OUTSIDE LAYER

At first glance, the distribution of Power Sum NEXT for 50-pair MOD units might look rather unusual, however, on closer scrutiny, the results are readily explained. The distribution is bi-modal in nature. The pairs with the worst Power Sums correspond with the outer layer pairs of adjacent units. These pairs tend to come together once every stranding lay and can give rise to poor crosstalk couplings due to their proximity to each other. On the other hand, the pairs with the better power sums correspond with the inner layer pairs within the units. These pairs are effectively screened through the intervening pairs in the outer layers. This effect does not occur in either the 50-pair or the 100-pair multi-unit designs because each of the subunits is oscillated and stranded independently. There is less likelihood of any two pairs in different subunits coming together for any appreciable distance over the length of cable.

SUMMARY AND CONCLUSIONS

A large number of controlled trials and comparative tests have been performed on different pulp insulated cable designs manufactured on conventional equipment and the new tandem twisting facility. In all these tests, the material, process, and design parameters were kept constant except for those being evaluated. From this work, a valuable insight was gained on the effect of design and process parameters on cable performance.

These results have led to the development of a new Multiple Unit Pulp (MUP) cable design with improved transmission characteristics.

Some of the results that have been achieved are summarized below:

- (1) "True" MUP 22 AWG cables using 25 different twist lays provide within unit crosstalk characteristics as good as MOD or psuedo-MUP designs.
- (2) "True" MUP 22 AWG cables with larger 100-pair multi-units provide a 6 dB improvement in the RMS dB NEXT coupling loss between adjacent units, thus permitting adjacent units to be used for opposite directions of transmission for T1 carrier systems. This increases the T1 carrier fill by up to 50%.
- (3) The new Multiple Unit Pulp design provides full pair identification in a 25-pair binder group by colors of insulation and stains on the white conductor. This permits color-to-color splicing when required for cable restoration or relocation.
- (4) A significant improvement in the worst case Far End Crosstalk performance makes color-to-color splicing feasible within 25-pair binder groups as for PIC cables. The expected crosstalk impairment compared to random spliced cable is 1 dB for the 1% Worst Power Sum of ELFEXT in a repeater section of cable.

ACKNOWLEDGEMENT

Many people within Northern Telecom, Cable Division, have contributed to the successful realization of the tandem twisting project. Special thanks are extended to the tandem twisting design team for their dedicated efforts. Also, the authors are indebted to Jon Green and Fernand Loiseau for their valuable assistance in the performance of the experiments and in the analysis of the measured data presented in this paper.

REFERENCES

- (1) Engineering of T1 Carrier System Repeated Lines by H. Cravis and T.V. Crater, The Bell System Technical Journal, Vol. 42, No. 2, March 1963.
- (2) A Study into Paired Cable Crosstalk by R.J. Oakley and R. Jarr, 22nd International Wire and Cable Symposium, 1973.
- (3) Modular Unit Design Pulp Cable by J.-P. Waucheul and R.L. Beauchamp, 28th International Wire and Cable Symposium, 1979.

REFERENCES (cont'd)

- (4) Paired Cable Performance Evaluation for Digital Transmission Systems by P.P. Kish and J.A. McDade, Intel Expo-81, Los Angeles.
- (5) T1 Characterization-Field Measurement Results by T.C. Kaup, D.G. Leeper, A.K. Reilly and P.E. Scheffler, The Bell System Technical Journal, Vol. 60, No. 6, July-August 1981.



Paul P. Kish received a B.A.Sc. degree in electrical engineering in 1971 and a M.A.Sc. degree in 1972, both from the University of Waterloo, Ontario. He joined Bell-Northern Research and later Northern Telecom Canada Limited as a member of Cable Research and Development Staff. He has been working primarily on the design and development of paired communication cables for analog and digital carrier applications. He is presently Manager of Cable Development, Research and Development, Cable Division.



Philip A. McGettigan is a member of the Research and Development Staff, Cable Division, Northern Telecom Canada Limited. He is currently involved in wire and cable design and in the evaluation of new products and processes. He graduated in 1956 from University College Dublin with the degree of Bachelor of Engineering (Mechanical and Electrical). After working with Canadian Westinghouse, he joined Northern in 1959. Since then he has worked on the design, development and manufacture of communications and power wires and cables.

DIGITAL PULSE TRANSMISSION CHARACTERISTICS OF INSIDE WIRE AND CABLE

J. C. Hyder
J. T. Loadholt

AT&T Bell Laboratories
Norcross, Georgia 30071

ABSTRACT

The digital data transmission capability of twisted pair cables used in customer premises applications is of great interest to designers and users of digital communications networks. Our empirical studies indicate that inside wiring cables of conventional materials and construction have considerable potential for carrying digital signals at rates of 1 Megabit per second or higher for distances great enough to include many intrabuilding cable runs. A single parameter such as capacitance can provide some insight into cable performance, but does not model the absolute capability of the cable. Conventional transmission line analysis, which considers all cable parameters, can be used to assess a cable's usefulness for a particular application.

INTRODUCTION

The capability of twisted pair cable to transmit digital signals without error is of great interest to local area network designers and users who must understand the capability of available media to provide the simplest and most economical transmission system. Twisted pair cable is the most commonly used customer premises media with over fifty years service for voice and low speed data communications. It is a low cost, easy to install media that can be an excellent transmission line when used efficiently. This report is based on laboratory experiments which are part of an ongoing study to assess the data transmission capability of available inside wiring cable designs.

Current inside wire and cable designs for telephone communications represent an evolution in materials and cable development considering transmission, electromagnetic interference (EMI), mechanical and fire safety criteria. Polyvinyl chloride (PVC) insulation is

the most often used insulation since it provides reliable performance in all respects at low cost. In situations where stringent fire resistant requirements apply, fluoropolymers are often used in addition to PVC based designs. The several common insulations used on pairs (with or without various forms of shields) are capable of producing a wide selection of cable designs for data transmission.

Digital transmission is not, of course, a new usage of twisted pair cable. Digital carrier has been operating on telephone trunking, feeder and distribution twisted pairs for a number of years. T2 carrier, for example, is a 6.3 Megabit/second system capable of transmitting 13000 feet on 22 AWG twisted pair cable.¹ Cable designs are optimized for such systems and the example makes the point that there is significant bandwidth capability in twisted pair media if systems designers take advantage of it. Another excellent example of optimization is found in Reference 2, "D.C. Welcomes MAT," the story of Metropolitan Area Trunk cables.

Studies of telephone loop plant intended for "voice" communications have also concluded that extensive opportunity exists for wideband applications, and utilization of in place cables can provide cost effective service.³ The study reported here addresses the same question for building cables.

It is likely that optimized designs will appear for premises applications. The optimization must consider many factors: bandwidth-length needs, signaling format, loss, phase distortion, crosstalk, EMI, physical characteristics, size and cost. The user will often need to address the question of adequacy versus optimization as well, particularly when a decision must be made to use or replace existing media. In addition to directions for specifying new and special cables, there is a

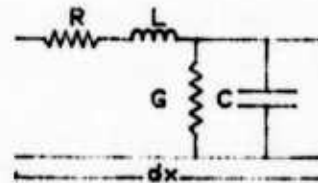
need for guidelines for assessing a particular cable's capability.

The work reported here began as empirical tests to evaluate the distance potential of several commercially available twisted pair cables as a function of bit-rate. The bit-rates were chosen for convenience because of available equipment, but they represent a wide range of rates. The data are presented with discussions which relate the result to cable characteristics. Expected trends are evident in that cables with coarser gauge copper, larger conductor-to-conductor spacing, and lower effective dielectric constants have greater ultimate capability. The results show, however, that all cables tested, including PVC insulated ones labeled as "voice" cables, have significant digital data transmission capability. The differences among cables are only of concern as the user plans applications that greatly exceed the typical station runs (250 ft.). Standards placing strong importance on a single parameter (such as RS-232C does capacitance) correctly recognize trends, but may unnecessarily exclude perfectly adequate cables for particular applications.

TRANSMISSION ANALYSIS

With complete transmission characteristics we can assess signal impairment due to the media. The signal is degraded by three mechanisms as it travels through the cable. The first mechanism is attenuation, which reduces the level. The limit on signal quality occurs when the level is too low to detect accurately. Secondly, the frequency dependence of loss, phase velocity, group velocity and delay (related parameters) distorts the signal. For digital signals, this second mechanism spreads the pulse with the limiting condition being intersymbol interference. The third effect is crosstalk coupling from adjacent circuits in the same cable. All three mechanisms are functions of cable geometry as well as materials selection. The crosstalk especially is a function of manufacturing quality since deviations from design intent can degrade pair to pair isolation. Crosstalk performance is also a function of signaling format. For the majority of building applications, crosstalk and interference will likely be the primary mechanisms of signal impairment. Woodard's treatment of crosstalk between pairs with unbalanced signals exemplifies the limitations that can occur (in a case with inefficient signaling).⁴

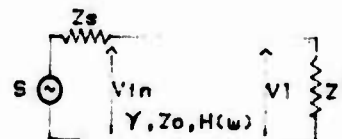
The transmission characteristics of twisted pair media are accurately modeled by a distributed circuit for most applications. Figure 1 shows the model and defines the primary constants of the transmission line.



R=DISTRIBUTED RESISTANCE
L=DISTRIBUTED INDUCTANCE
G=DISTRIBUTED CONDUCTANCE
C=DISTRIBUTED CAPACITANCE
dx=INCREMENTAL LENGTH

FIGURE 1

Figure 2 illustrates the modeling of a cable by a transfer function $H(\omega)$, (where ω is radian frequency), which operates on an input signal V_{in} and delivers an output signal V_{out} at the end of the cable. The quality of the model depends on how well the secondary parameters are measured and how well they truly represent the manner in which the cable is interconnected and signaled in practice. Most published transmission data assumes that each pair will be used according to the cable design intent which is with a balanced mode signal on each pair. Our data agrees with this assumption.



S= SIGNAL SOURCE
 Z_s =SOURCE IMPEDANCE
 Z_1 =LOAD IMPEDANCE
 V_{in} =SIGNAL PRESENTED TO CABLE
 V_1 =SIGNAL AT LOAD
 $H(\omega)$ =TRANSFER FUNCTION OF CABLE
 $V_1(\omega)=H(\omega)*V_{in}(\omega)$
 $H(\omega)=\text{EXP}(-\gamma z)$

FIGURE 2

The transfer function for a cable of length x is given by

$$H(\omega) = e^{-\gamma x} \\ = e^{-\alpha x} e^{-j\beta x} \quad (1)$$

where γ , the propagation factor is composed of a real part α , the attenuation factor, and an imaginary part β , the phase factor.

Figures 3A, B and C show attenuation, capacitance and phase data for several cables. The numerals labeling the curves refer to the "Sample Number" in Table I. Table I identifies the important features of each cable.

Two observations from Figure 3 are pertinent to later discussions. First, the cable capacitances are not ordered in magnitude exactly according to the magnitude of their respective insulation dielectric constants. This demonstrates the significance of conductor and dielectric diameters as factors in determining the cable capacitance. Second, while attenuation and phase factors generally correlate with capacitances, the differences in α or β are not necessarily as significant as the differences in capacitance alone and it is the attenuation and phase that control transmission impairment.

The effects of attenuation and phase can be predicted by constructing the cable transfer function from the primary constants R , L , G and C . This analysis follows and the accompanying discussion emphasizes which parameters contribute to distortion and how they vary with frequency.

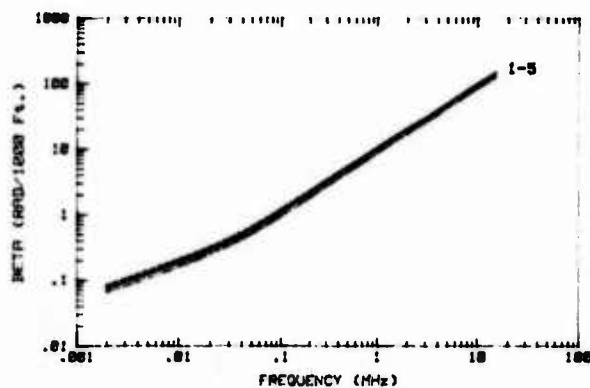


FIGURE 3A

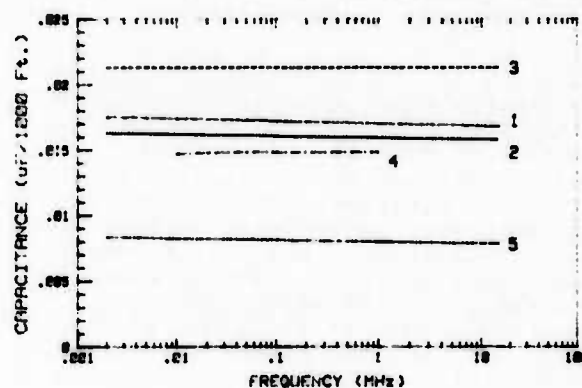


FIGURE 3B

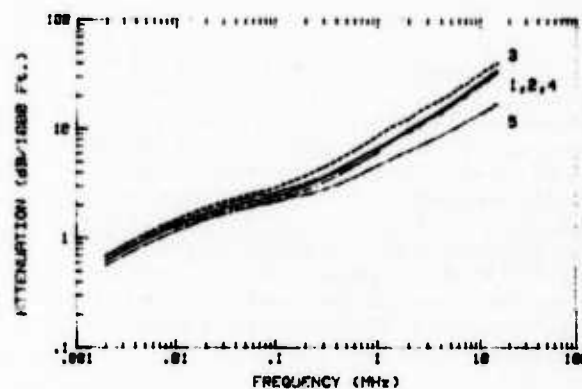


FIGURE 3C

TABLE I
CABLE DIMENSIONS AND MATERIALS
(All Cables Contain Four Pairs)

Sample	d	DOD	er	Insulation
1	.019	.0345	3.8	PVC #1
2	.019	.0345	3.8	PVC #2
3	.019	.0312	2.6	Fluoropolymer #1
4	.020	.0350	2.1	Fluoropolymer #2
5	.0159	.0005	1.0	Expanded Polyolefin

d=conductor diameter
DOD=Diameter over the dielectric
er=insulation dielectric constant

The propagation parameter γ is related to R , L , G and C by

$$\gamma = \alpha + j\beta = \sqrt{(R+j\omega L)(G+j\omega C)} \quad (2)$$

With copper conductors and reasonably low loss dielectrics, low frequency (LF) and high frequency (HF) approximations for α and β can be made. (Impedance formulas are included for completeness.)

$$\alpha_{LF} = \sqrt{\frac{\omega RC}{2}} \quad (3)$$

$$\alpha_{HF} = \frac{R}{2} \sqrt{\frac{C}{L}} + \frac{G}{2} \sqrt{\frac{L}{C}} \quad (4)$$

$$\beta_{LF} = \sqrt{\frac{\omega RC}{2}} \quad (5)$$

$$\beta_{HF} = \omega \left[\sqrt{LC} + \frac{R^2}{\omega} \sqrt{\frac{C}{L}} \frac{1}{8L} \right] \quad (6)$$

$$Z_{OLF} = \sqrt{\frac{R}{\omega C}} \angle -45^\circ \quad (7)$$

$$Z_{OHF} = \sqrt{\frac{L}{C}} \quad (8)$$

From Equations (3)-(6), resistance, inductance and capacitance are all significant factors in the attenuation and phase parameters. The high frequency response is dominated by the resistance, which increases as the square root of frequency. Capacitance and inductance are relatively flat in the frequency range of interest. Obviously, lower resistance and lower capacitance will lower attenuation. The limiting consideration is, however, that one cannot build an arbitrarily large pair. Once a size or space is allocated for a pair, optimizations can be done and comparisons such as these are of value.

For applications that require an extension of the capability of existing designs, the same equations can be used to optimize and compare designs. A twisted pair cable is optimized by selecting a set of dimensions and materials that produces an extremum in a desired property such as attenuation. The geometry of multipair cable is too complex for a closed form solution but individual pairs are often modeled as balanced shielded pairs (see Figure 4) with an effective shield diameter representing the surrounding pairs (sized to agree with proximity effects on R, L and C) and an effective dielec-

tric constant ($\epsilon_{r \text{ eff}}$) accounting for interstitial spaces. If D (effective shield diameter) is fixed, then for each d (conductor gauge) there is an optimum choice of S (conductor spacing). It is calculated from

$$\frac{\partial \alpha}{\partial (S/d)} = 0 \quad (9)$$

with loss approximated from Eq. 6 as

$$\alpha \approx \frac{R}{2Z_0} \quad (10)$$

where⁵

$$R = \frac{2R_s}{\pi d} \left[1 + \frac{1 + 2p^2}{4p^4} (1 - 4q^2) \right] + \frac{8R_s}{\pi D} q^2 \left[1 + q^2 - \frac{1 + 4p^2}{16p^4} \right] \quad (11)$$

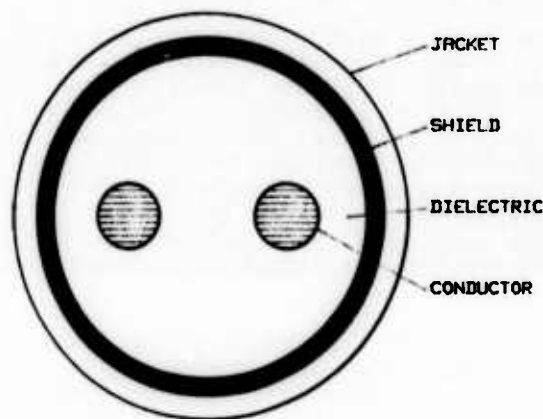


FIGURE 4
SHIELDED BALANCED PAIR

and

$$Z_0 = \frac{1}{\pi} \sqrt{\frac{\mu_0}{\epsilon_{\text{eff}}}} \left\{ \log \left[2p \frac{(1-q^2)}{1+q^2} \right] - \frac{1+4p^2}{16p^4} (1-4q^2) \right\} \quad (12)$$

and $p = S/d$, $q = S/D$, μ_0 = permeability of free space and R_s , (R_{s_c}) are the surface resistivities of the conductor and shield, respectively.

Using these closed form equations a plot of α versus S/d can be generated as shown in Figure 5.

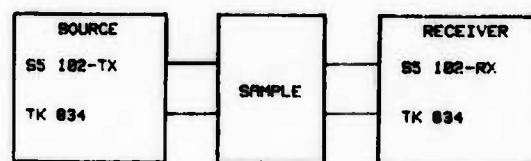
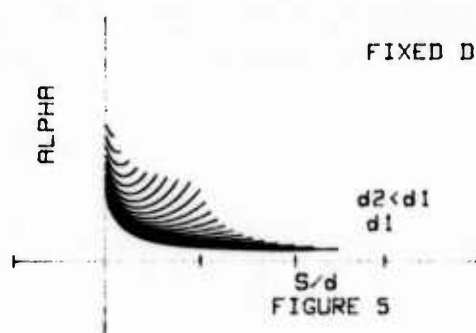


FIGURE 6

It is noteworthy that with the assumption of a good dielectric, the optimum S/d ratio is independent of the insulation dielectric constant, but the absolute level of attenuation varies with the square root of ϵ_{eff} . Different choices of ϵ_{eff} give different impedances.

EMPIRICAL RESULTS

The data transmission capability has been evaluated empirically for several generally available inside wiring cables with different insulation materials and slightly different dimensions as seen in Table I. The intent was to study how material and dimensional variations influence the properties of the completed cable and relate the results to the transmission analysis above.

The initial experiment was to simply determine the maximum distance a balanced mode digital signal could be transmitted without errors. Cable sections were concatenated in lengths of 200 feet. Send and receive circuits were looped within the same cable sheath on adjacent pairs. Figure 6 shows the setup and Figure 7 shows the results. Number labels correspond to Table I. Figure 8 shows the fundamental pulse shape representing a "1" or "0" for the higher bit rate transmission. The lower bit-rate data is not optimum in that RS-232 unbalanced format was used. The empirical results were related to the analysis above by convolving the signal transform with the cable transfer function of Figure 2.[6]. The results of doing this on cables of lengths corresponding to those at which errors were noted are shown in Figure 9 along with measured results. The user or designer may evaluate cable empirically or analytically.

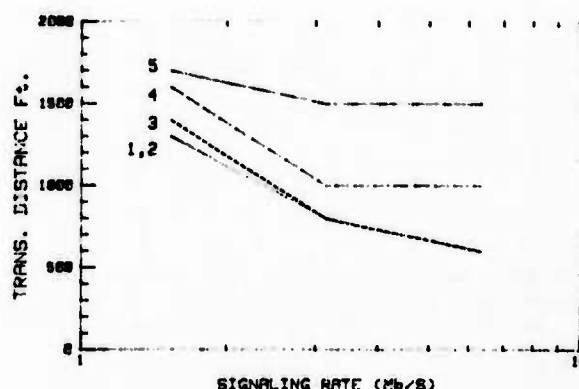


FIGURE 7

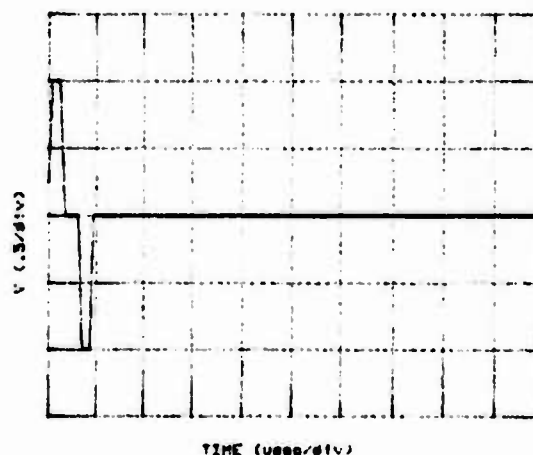
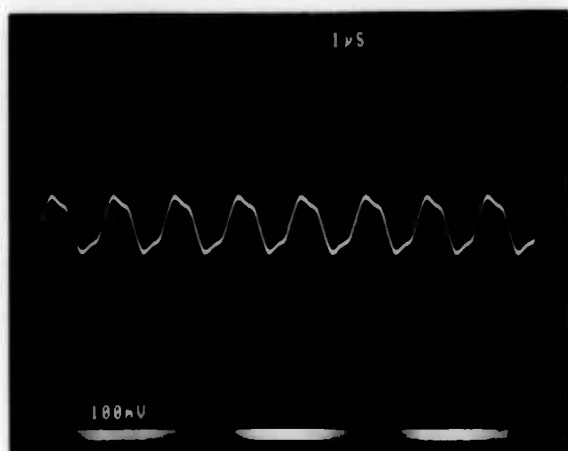
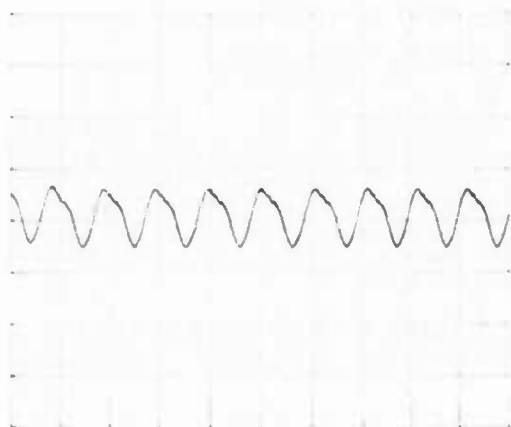


FIGURE 8



(A) MEASURED



(B) CALCULATED

FIGURE 9

Of several observations that might be made from the results, two are of particular interest. First, the fact that the effective dielectric constant is a function of both the primary insulation and the air space around it significantly helps lower delay by diluting the effect of the primary insulation dielectric constant. With the common methods of making twisted pair cable, reducing the dielectric constant of the insulation material does not reduce the effective dielectric constant of the cable in a one-to-one fashion. Figure 10 shows effective dielectric constant (as derived from signal velocity) versus primary insulation dielectric constant. This explains in part why the distance performance of the several cables does not differ as much as might be anticipated from material characteristics alone. It might be correctly noted that tightness of twisting and stranding greatly affects this observa-

tion. However, the results of Figure 10 describe typically available cables, and there is little reason to believe that production methods will change in the near future. Second, the lengths for successful transmission are very long compared to typical building cable runs. On a single floor of a multi-floor building, runs for telecommunications typically be under 250 feet [6]. Figure 11 shows that even the "poorest" cables exceeded this length by a factor of two at the highest bit-rate tested.

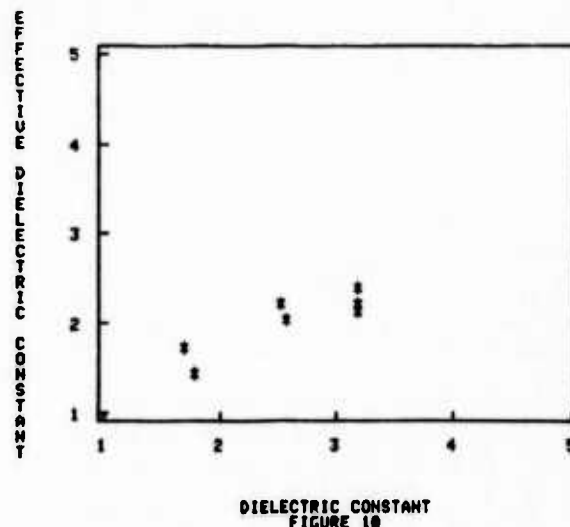


FIGURE 10

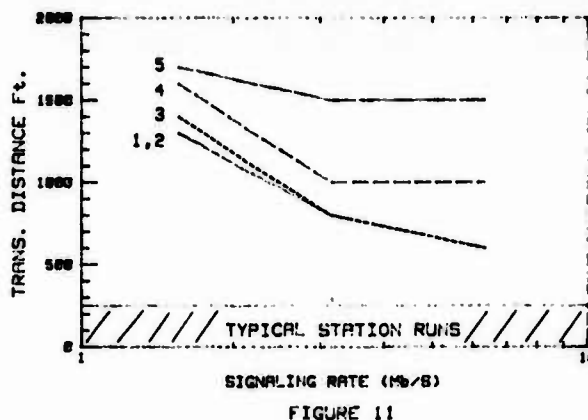


FIGURE 11

A second experiment added crosstalk impairment. Signals of the same bit-rate were applied to previously quiet pairs. For four pair cables this meant, for example, the two remaining pairs were used as a send and receive loop. The results show some degradation in the attained distance as seen in Figure 12. An interesting observation with crosstalk in these four pair cables is that the usable distance can be independent of the transmission properties of the cable under test.

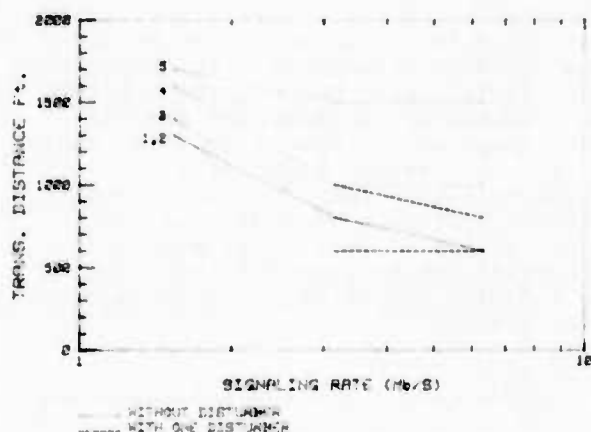


FIGURE 12

This probably points to the impreciseness of multipair cables in that variations in manufacturing control of pair-balance can outweigh the potential benefits of careful material and dimensional selection. The distances obtained are still, however, more than adequate for many building applications.

To pursue crosstalk effects in more detail requires an in-depth understanding of pair usage for a particular system. Such detail was beyond the scope of these initial experiments. The results show the capability of the cables which is available to the system designer. Carefully designed and controlled twisting schemes, or even shields if performance justifies the cost can, of course, do much to minimize crosstalk interference.

CONCLUSIONS

Empirical data from laboratory experiments demonstrated significant capability for information transmission in typical inside wiring cables. The results show expected trends in that the bit rate-distance product (or capability) decreases with higher resistance, capacitance, loss, delay and nonlinearity in delay. The use of convolution demonstrates (again) that proven techniques are available to help judge a given cable's capability (based on available and complete transmission characteristics) when questions arise. The most important conclusion is, however, that even with low cost inside wiring cable, there is much capability that can be exploited.

Systems designers, of course, must eventually decide if the differences among these cables are significant in view of their overall capability. The work presented here admittedly is a partial study of a complex problem. As wideband applications develop in complexity, studies such as this will become more essential. Such studies will have to consider the effects of such practical necessities as cross-connects or transitions to other media. As always, proven performance at the lowest cost will eventually become the guideline for selecting cabling.

REFERENCES

1. Setzer, D. E. and Windler, A. S., "A Low Capacitance Cable for the Tz Digital Transmission Line," Proceedings of Nineteenth International Wire and Cable Symposium, December 1, 1970, Atlantic City, New Jersey.
2. Brosius, B. S., and Webster, G. H., "D. C. Welcomes MAT," Telephony, January 1, 1979.
3. McIntosh, T. F., Nutt, W. G., "Wideband Transmission in the Distribution Network," Proceedings of the Thirtieth International Wire and Cable Symposium, November 17, 1981, Cherry Hill, New Jersey.
4. Woodard, D. P., Jr., "Unbalanced Digital Crosstalk in Balanced, Twisted Pair, Inside Wiring Cable," Proceedings of the 32nd International Wire and Cable Symposium, November 15, 1983, Cherry Hill, New Jersey.
5. Ramo, S., Whinnery, J. R., Van Duzer, T., Fields and Waves in Communication Electronics, John Wiley and Sons, New York, 1967.
6. Woodard, D. P., Jr., unpublished work.
7. _____, Bell System Practices, AT&T Std., 917-454-000, May 1972.



J. C. Hyder is a member of the Building Cable Group at AT&T Bell Laboratories in Norcross Georgia.



J. T. Loadholt is a Member of Technical Staff at AT&T Bell Laboratories, Norcross, Georgia. He received a B. E. E. degree from Georgia Institute of Technology in 1970 and an M. S. in Electrical Engineering from the University of Illinois in 1971. He joined Bell Laboratories in 1970 and is a member of the Building Cable Group.

DIGITAL PERFORMANCE OF METALLIC TWISTED PAIR TRANSMISSION MEDIA

J.W. Kincaid, Jr.

D. Johnson

BELDEN TECHNICAL RESEARCH CENTER
GENEVA, ILLINOIS

ABSTRACT

The figure of merit, F_m , concept is extended to the low frequency or long line case. F_m according to first order approximation theory is presented. The theoretical transient response for this case is compared to empirical results for multi-pair cable. An algorithm for calculating intersymbol interference is derived for the skin effect limited case as well as the low frequency case according to the first order approximation theory. Theoretical results for both Manchester and NRZ encoded data are compared to empirical results for multi-pair cable.

INTRODUCTION

The digital performance of twisted pair cable is often deduced from empirical performance data measured on specific cable designs. This may be accomplished first hand with available cable or taken from readily available charts¹ of bit rate versus cable length for a specific digital coding technique and distortion criteria.

A second approach to determine digital performance is the use of approximate^{2,3} theoretical relationships between frequency domain performance parameters (phase velocity, attenuation characteristic impedance) and time domain parameters, (impulse response overlap, step response 0-50%, 10-90% rise time).

Both approaches have shortcomings. Not only is empirical data expensive to acquire, but its usefulness is ultimately limited by such considerations as: how similar is the complicated real world digital application to the laboratory set-up, or how much different will the performance be if the cable actually installed (due to the vagaries of purchasing/contracting) is different from the specific design referenced for empirical performance data?

The theoretical approach, on the other hand, is limited by the simplifying first order approximations which are often made. These approximations are justified to the extent that they provide qualitative understanding of performance relationships. Correspondingly simple frequency domain relationships do quite accurately predict frequency

domain performance. To approach this accuracy in the time domain, however, requires computer techniques to solve the rigorous theoretical relationships.⁴

The figure of merit⁵ concept is an example of the second approach. This is an interesting way of specifying the digital performance of diverse transmission media such as fiber optics, coaxial cable, and twisted pair cable. For metallic media, the figure of merit, F_m , is derived from first order approximations (it is assumed that signal degradation or pulse dispersion is caused by skin effect impedance, $f \geq 100$ KHz, and that dielectric losses are negligible) and is a function of media geometry, materials, and length. The units of F_m are bit rate multiplied by length raised to the exponent γ .

The exponent γ has values of 2 for metallic media and from $\frac{1}{2}$ to 1 for optical media. The practical application of F_m involves selecting the media with

F_m greater than $P \cdot L^\gamma$ where P and L are the system parameters bit rate and transmission distance respectively. In addition to the parameters bit rate and transmission distance, the allowable signal distortion is also a significant systems parameter. Thus for a given metallic line there is not a unique F_m . Starting with an eye pattern⁶, F_m has been derived for the case where signal degradation is limited to 5% peak to peak time jitter (isochronous distortion). If higher amounts of jitter would not unacceptably degrade system performance, larger values of F_m could be assigned than for the 5% limiting case.

This paper extends the figure of merit concept to the low frequency or long line case. At low frequencies, ($f \leq 100$ KHz) the skin effect is not well developed and does not account for signal degradation. Over long lines the normal low pass filtering characteristics diminish the high frequency signal content in favor of the low frequency content. Consequently a figure of merit based on low frequency relationships is of interest.

The paper also compares the step response predicted by the first order approximation models with empirical results. Finally, the empirical step response is used to calculate peak to peak time jitter for Manchester and NRZ encoded data.

LOW FREQUENCY FIGURE OF MERIT

GENERAL MODEL

A frequently used model for a data transmission system is given in Figure 1.

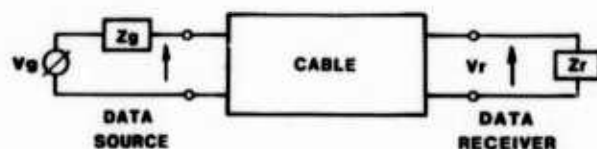


Figure 1. Data transmission system model.

The signal, V_r , appearing at the receiver is determined by the receiver impedance Z_r , the cable characteristics, the source impedance Z_g , and the signal V_g . In general, both the source and receiver impedances and the cable contribute to signal distortion - V_r is not a replica of V_g .

The various relationships may be expressed in the frequency domain.⁷

$$V_r(s) = V_g(s) \frac{Z(s)}{Z(s) + Z_g(s)} \times$$

$$\frac{1 + \rho_1(s)}{1 + \rho_1(s)\rho_2(s)} e^{-\gamma(s)l} e^{-2\gamma(s)l} \quad (1)$$

$$\text{where } Z(s) = \sqrt{\frac{R + sL}{G + sC}}, \text{ the cable characteristic impedance} \quad (2)$$

$$\gamma(s) = \sqrt{(R + sL)(G + sC)}, \text{ the cable propagation constant} \quad (3)$$

$$\rho_1(s) = \frac{Z_r(s) - Z(s)}{Z_r(s) + Z(s)}, \text{ the receiver reflection coefficient} \quad (4)$$

$$\rho_2(s) = \frac{Z_g(s) - Z(s)}{Z_g(s) + Z(s)}, \text{ the source reflection coefficient} \quad (5)$$

l = cable length
 s = $j\omega$

R, L, G, C are the primary transmission line constants Resistance, Inductance, Conductance, and Capacitance, respectively.

APPROXIMATIONS

The following simplifying assumptions will be made.

- (1) Source impedance equals zero and receiver impedance matches the cable impedance:
 $Z(s) = Z_r(s), Z_g(s) = 0$

- (2) Conductance, G , is negligible

$$G = 0$$

- (3) R, L , and C , do not change with frequency.

With these assumptions equation (1) reduces to:

$$V_r(s) = V_g(s) e^{-\gamma(s)l} \quad (6)$$

Under these conditions signal distortion is attributed to the factor $e^{-\gamma(s)l}$. Additional simplifying assumptions are required before proceeding to the figure of merit.

By factoring out \sqrt{RCs} from (3) and setting $G = 0$ the propagation constant $\gamma(s)$ can be expressed as follows:

$$\gamma(s) = \sqrt{RCs} \sqrt{1 + s \frac{L}{R}} \quad (7)$$

To a first order approximation (by retaining the

first term in the binomial expansion of $\sqrt{1 + s \frac{L}{R}}$ the propagation constant reduces to the following expression.

$$\gamma(s) = \sqrt{RCs} \quad (8)$$

The real and imaginary parts of this expression agree with known voice frequency expressions⁸ for attenuation α , and phase constant β , respectively.

UNIT IMPULSE RESPONSE

Using (8) in (6) and solving for the unit impulse response ($V_g(s) = 1$) the following result is obtained.

$$V_{r1}(s) = e^{-\sqrt{RC} l \sqrt{s}} \quad (9)$$

The inverse of (9) is listed in standard tables.⁹

$$V_{r1}(t) = \frac{A}{2\sqrt{\pi t^3}} e^{-\frac{A^2}{4t}} \quad (10)$$

$$\text{where } A = l\sqrt{RC}.$$

Comparison of (9) and (10) with the impulse response for the high frequency approximation case⁵ reveals the same form of equation except:

$$1) A = l \frac{K}{2\sqrt{\frac{L}{C}}} = \frac{l}{2} \frac{K}{Z_0}$$

2) linear time shift factor = $e^{-l\sqrt{LC}} s$

Here K is a constant determined by the skin effect and may be evaluated from cable geometry or high frequency attenuation. Thus A is dependent on length, and high frequency attenuation and impedance Zo.

In a similar fashion the A of equation (10) may be expressed as a constant determined by length and low frequency attenuation and impedance. These relationships are summarized in Table 1.

Table 1

FREQUENCY RANGE	Z	α	A
LOW	$\sqrt{\frac{R}{\omega C}}$	$\sqrt{\frac{R\omega C}{2}}$	$l\sqrt{RC}$ OR $\sqrt{2} \frac{\alpha}{\omega} l$
HIGH	$\sqrt{\frac{L}{C}}$	$\frac{K}{2} \sqrt{\frac{\omega}{8}}$ OR $R = K\sqrt{\omega}$	$l \frac{K}{2Z}$ OR $\sqrt{2} \frac{\alpha}{\omega} l$

The impulse response equation (10) may be normalized⁵ by the change of variable

$$\rho = t \frac{4}{A^2} \quad (11)$$

where β in the reference is identical to $A^2/4$. Thus the normalized response plotted in Figure 2 can be used for high or low frequency approximations by selecting the appropriate expression for A from Table 1.

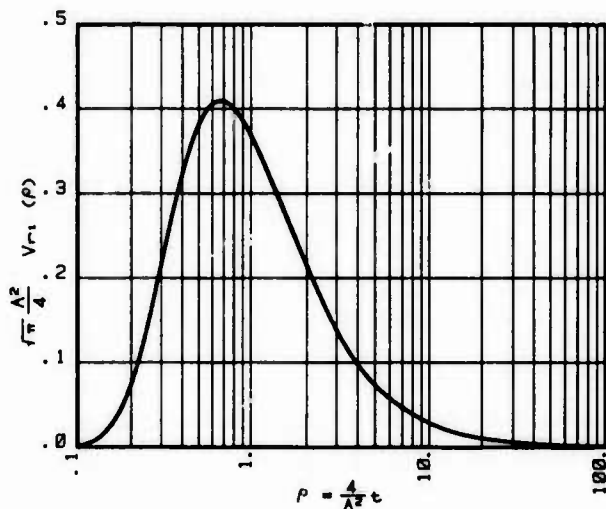


Figure 2. Normalized impulse response.

UNIT STEP RESPONSE

The unit step response is obtained by substituting (8) in (6) with $V_g(s) = \frac{1}{s}$.

$$V_{r2}(s) = \frac{1}{s} e^{-\sqrt{RC} l \sqrt{s}} \quad (12)$$

the inverse of (12) is listed in standard tables⁹. Alternately the inverse is given as the integral of (10).

$$V_{r2}(t) = \operatorname{erfc} \frac{A}{2\sqrt{t}} \quad (13)$$

where $A = l\sqrt{RC}$.

Equation (13) gives the step response for high or low frequencies with the appropriate choice of A from table 1. The normalized step response is plotted in Figure 3 along with the impulse response.

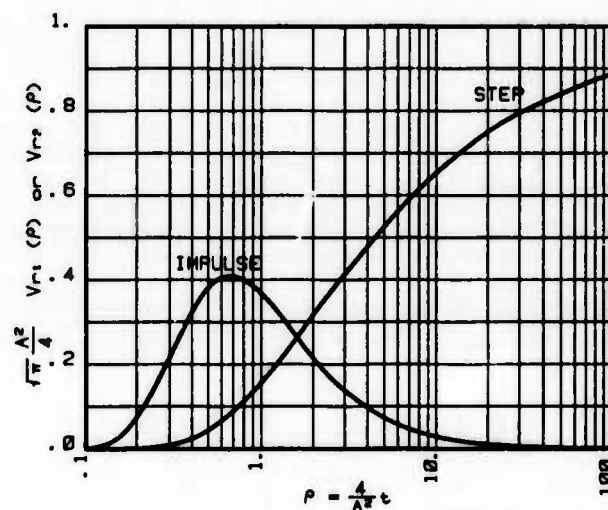


Figure 3. Normalized responses. Unit step and impulse response.

DISTORTION CRITERIA

Two arbitrary criteria for distortion have been proposed for the high frequency case.⁵ These are:

- 1) Limit the minimum pulse spacing to the value of time required for the impulse response to decay to 10 percent of maximum value.
- 2) Limit the minimum pulse spacing to twice the value of time required for the step response to reach 50% of final value.

The values of normalized time, ρ , from equation (11) which fulfill these criteria are 7.715 and 8.70 respectively.

For the low frequency case the appropriate value of ρ is deduced from empirical data. (The cable parameters are given in Figure 6) Figure 4 gives the measured 0-50% and 10-90% rise time as well as the values predicted by equation (13) when A is given by Table 1. It is seen that the 0-50% measured data approximates the predicted values for lengths shorter than 3000 feet. However, measured and predicted values of 10-90% rise time diverge for lengths greater than 130 feet.

Clearly the empirical step response is quicker than that predicted by the complementary error function once cable length exceeds a certain value. The implication of a quicker step response is that the impulse response is also quicker. This has been substantiated by extracting the impulse response from the measured step response. With eye patterns it has been empirically shown that the condition for 5% isochronous distortion corresponds approximately to a unit interval equal to the 10-90% rise time. Therefore a figure of merit relationship based on 5% isochronous distortion should utilize a ρ scaled for the 10-90% rise time.

FIGURE OF MERIT

The maximum bit rate, P, is given by

$$P = \frac{1}{t_{\min}} \quad (14)$$

where t_{\min} is the minimum pulse spacing. The value of t_{\min} is determined from the values of ρ which meet the distortion criteria.

From equation (11) bit rate is then given by.

$$P = \frac{4}{A^2 \rho_{\min}} \quad (15)$$

From Table 1 the attenuation form for A may be substituted into equation (15).

The maximum bit rate then becomes

$$P = \frac{2}{\rho_{\min}} \cdot \frac{\omega}{\alpha^2} \cdot \frac{1}{l^2} \quad (16)$$

The figure of merit, F_m , is readily seen from equation (16) to be given by

$$F_m = P \cdot l^2 = \frac{2}{\rho_{\min}} \cdot \frac{\omega}{\alpha^2} \quad (17)$$

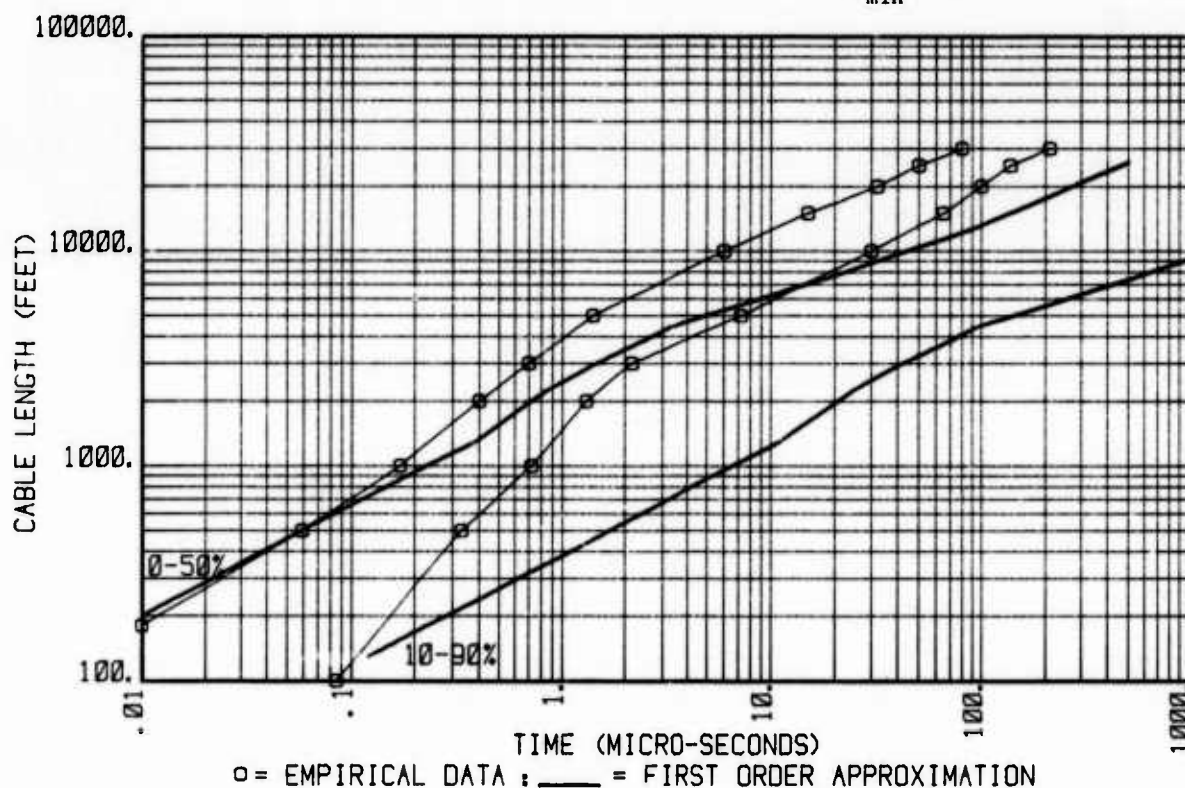


Figure 4. Rise time versus cable length. A comparison of first order model predictions with empirical results for 0-50% and 10-90% rise time of the step response.

Here p_{\min} is specified by the distortion criteria. The factor ω/α^2 is the ratio of a given frequency to the square of attenuation at the given frequency. Equation (17) is valid for both the high and low frequency cases. Alternately equivalent expressions for A from Table 1 can be substituted into (15) and equivalent figures of merit for high or low frequency can be derived. The various relationships are summarized in Table 2.

Table 2

FREQUENCY RANGE	$F_m = P \cdot Q^2 = \frac{4}{A^2 P} Q^2$	
LOW	$\frac{4}{RC} \cdot \frac{1}{P}$	$\frac{2\omega}{a^2} \cdot \frac{1}{P}$
HIGH	$\frac{16 Z^2}{K^2} \cdot \frac{1}{P}$	$\frac{2\omega}{a^2} \cdot \frac{1}{P}$

BIT RATE VERSUS CABLE LENGTH

The empirical data presented in Figure 5 was measured on #24 AWG twisted pair cable with 100 ohm characteristic impedance. The cable parameters are given in Figure 6.

The data source consisted of a pseudo-random bit generator, NRZ/Manchester circuitry, and a pulse generator with complementary outputs. The equipment output rise time was less than 5 nanoseconds with source impedance equal to 50 ohms. At the data receiver the twisted pairs were terminated with a 100 ohm resistor and connected to a wide band oscilloscope via a differential probe.

Isochronous distortion was determined from the eye pattern displayed on the oscilloscope. Typical NRZ and Manchester eye patterns are presented in Figure 7. The bit rate was adjusted for conditions of 5% or 10% peak to peak time jitter for twisted pair lengths ranging from 100 feet to 30,000 feet.

Comparison of NRZ to Manchester bit rate performance does not indicate one coding technique to consistently achieve greater bit rates than the other for the same cable length and isochronous distortion.

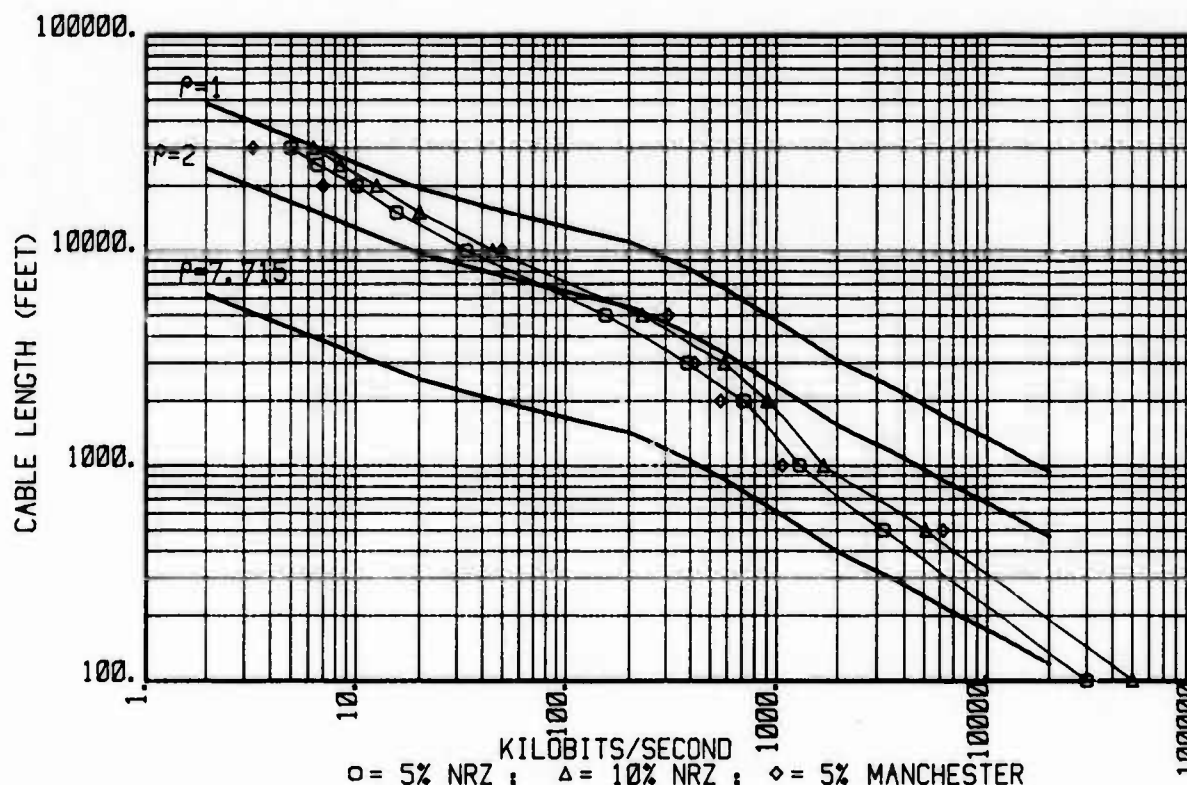


Figure 5. Bit rate versus cable length. A comparison of first order model predictions with empirical results for NRZ and Manchester coded data.

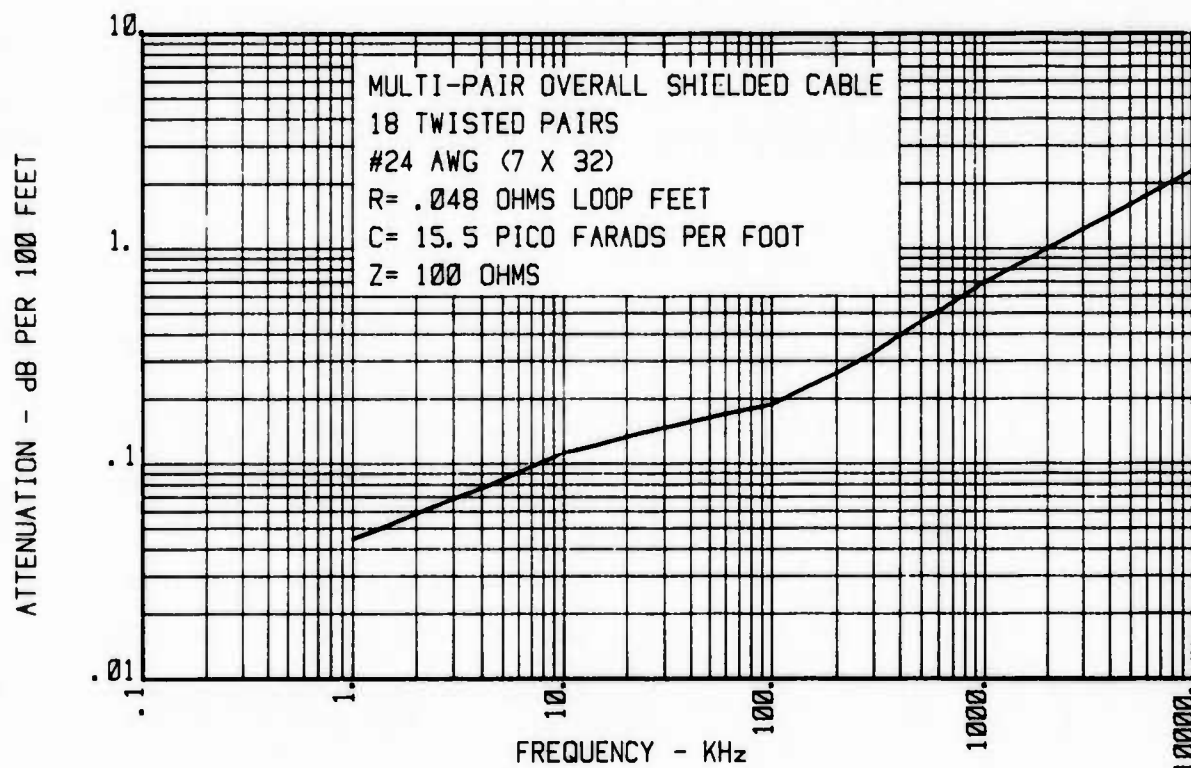
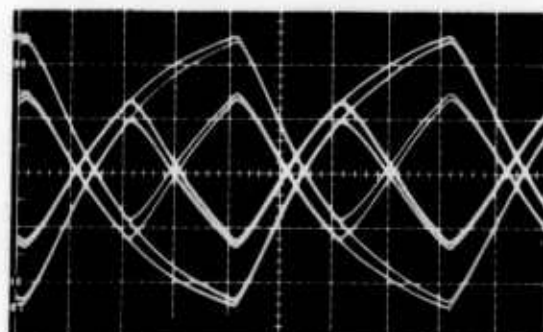
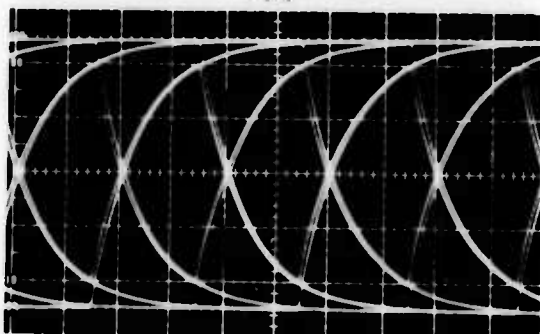


Figure 6. Attenuation versus frequency. Parameters of multi-pair overall shielded cable.



(a)



(b)

Figure 7. (a) Manchester code eye pattern
 (b) NRZ code eye pattern

For example, at 500 feet the Manchester bit rate is approximately twice that achieved with NRZ. However, at 3000 feet, both Manchester and NRZ result in approximately the same bit rate for equal isochronous distortion.

The first order approximation models for bit rate versus distance are plotted in Figure 5 for values of ρ equal to 1, 2, and 7.715. This data was calculated from the attenuation form of the figure of merit, F_m , listed in Table 2. Attenuation values at frequencies equal to one half P , the bit rate, were used at low, high and intermediate frequencies.

The high frequency model with $\rho = 7.715$ approaches the empirical performance for very short lengths--for example 100 feet. For long lengths the high frequency model is too conservative, compared to actual performance.

The low frequency model with $\rho = 1$ or 2 approximates bit rate performance for long cable lengths. The choice of $\rho = 1$ or 2 is somewhat arbitrary. However, this may be rationalized by comparing the empirical step response to the first order approximation step response in Figure 4. For lengths greater than 7000 feet the calculated 0-50% rise time is actually greater than the measured 10-90% rise time. With $\rho = 2$ the low frequency model underestimates cable performance for lengths greater than 7000 feet and overestimates performance for lengths less than 7000 feet.

PERCENT JITTER ALGORITHM

For NRZ code the percent jitter was determined from the difference in threshold crossing times for two bit patterns. These are illustrated in Figure 8. The function $f(t)$ represents the step response of a given length of cable.

The equations in Figure 8 may be solved iteratively to determine the percent jitter for a given bit rate, (I/T) , or the bit rate at which a given value of percent jitter occurs.

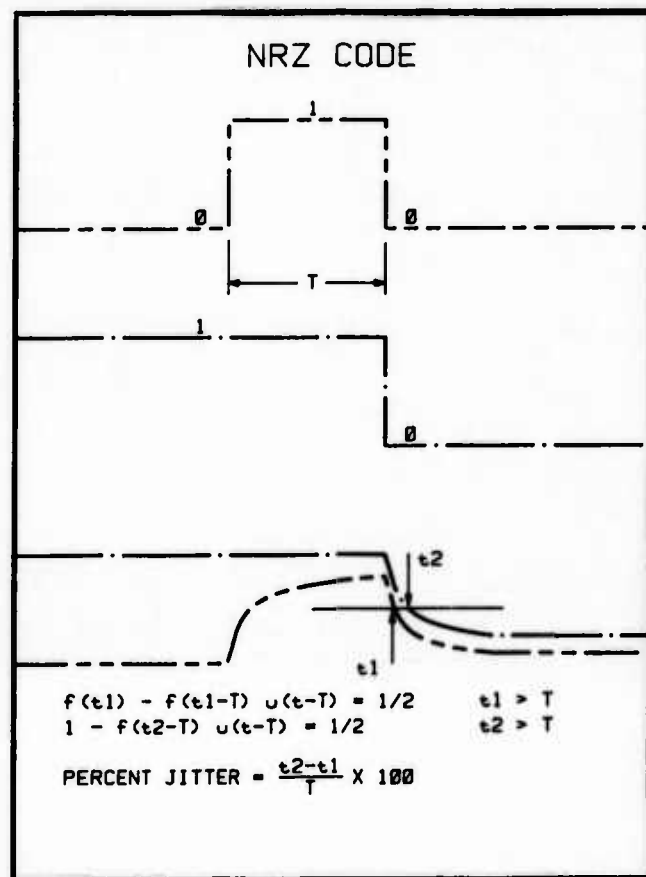


Figure 8. NRZ code definition.
Percent jitter algorithm

Table 3 summarizes the results for the following cases (cable parameters given in Figure 6)

- (1) $f(t)$ extracted from eye pattern photographs
- (2) percent jitter produced by a pseudo-random bit sequence

Table 3

CABLE LENGTH FEET	$\frac{I}{T}$ FOR 5% JITTER	
	(1)	(2)
1000'	1350	1290
2000'	770	717
10000'	38	34
30000'	4.8	5

The bit rates agree within 12%. The accuracy of the algorithm is dependent on the accuracy with which $f(t)$ represents the actual step response. Determining the step response from eye pattern photographs is inherently error prone. A direct digital interface to the oscilloscope trace would allow accuracy enhancement beyond the 12% figure determined in this work. Use of the complementary error function for $f(t)$ produces overly conservative estimates of bit rate for a given percent jitter.

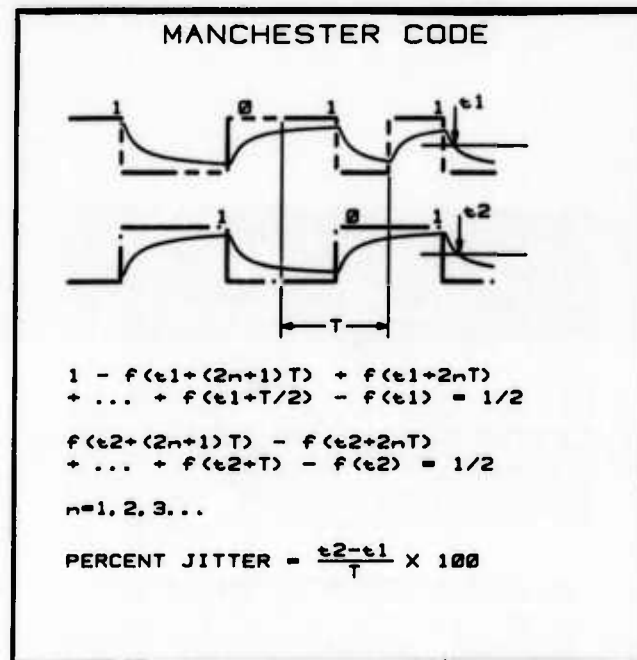


Figure 9. Manchester code definition.
Percent jitter algorithm

An algorithm for calculating percent jitter at a specified bit rate (I/T) , for a step response $f(t)$ is given in Figure 9. In Manchester code there may or may not be a transition between unit interval cells (I/T) . However, there is always a transition within the unit interval--the midpoint in Figure 9. The algorithm gives the difference in threshold crossing times at the unit interval mid-point.

The algorithm may be solved iteratively, as in the case of NRZ code. For values of $n = 4$, which corresponds to nine terms, the calculated values of jitter averaged out to 3% for the cable lengths and bit rates corresponding to case (2) in Table 3. Again, it is believed the inherent inaccuracy of extracting the step response from eye pattern photographs causes the relatively poor agreement between measured and calculated results.

CONCLUSION

The low frequency figure of merit was derived and expressed in terms of attenuation, frequency and the parameter, ρ . Although the form of the equation is similar to that of the high frequency figure of merit the parameter ρ was set equal to one or two for low frequencies, whereas the value 7.715, or 8.7 has been suggested for the high frequency model. With $\rho = 2$ the predicted bit rate (based on the figure of merit) was compared to empirical results for a 24 AWG twisted pair cable. The prediction was conservative for lengths greater than 7000 feet and optimistic for lengths less than 7000 feet.

Future work should compare figure of merit predictions with empirical data for twisted pair cable of varying wire gage and characteristic impedance.

The measured step response was compared to the first order approximation model. The complementary error function does not accurately predict 0-50% or 10-90% rise once the cable length exceeds approximately 3000 feet and 130 feet respectively. Future work should improve the accuracy of the step response prediction for long cable lengths.

Algorithms may be used to calculate percent jitter if the step response is accurately known. A more accurate step response prediction for long cable lengths could eliminate the need for testing to determine the empirical bit rate/percent jitter characteristics for NRZ or Manchester code. Alternatively direct digital acquisition of the empirical step response could improve the accuracy of results when the bit rate/percent jitter characteristics are calculated from an algorithm.

REFERENCES

1. Belden Electronic Wire and Cable Catalog No. 882.
2. R.L. Wigington and N.S. Nahman, "Transient Analysis of Coaxial Cables Considering Skin Effect," Proc. IRE, Vol. 45, pp. 166-174, Feb. 1957.
3. N.S. Nahman and D.R. Holt, "Transient Analysis of Coaxial Cables Using the Skin Effect Approximation $A + B\sqrt{S}$," IEEE Transactions on Circuit Theory, Vol. 19, pp. 443-451, Sept 1972.

4. D.R. Holt, "Expansions with Coefficient Algorithms for Time Domain Responses of Skin-Effect Lossy Coaxial Cables," J. Res. Nat. Bur. Stand., B.(Math. Sci.), Vol. 74B, No. 3, July-Sept. 1970.
5. R.L. Gallawa, "Conventional and Optical Transmission Lines for Digital Systems in a Noisy Environment," OT Report 77-114, March, 1977.
6. J.A. Hull, "Characterization of Transmission Media," Telecommunications, pp-70-72, Feb. 1984.
7. J.I. Potter and S. Fich, "Theory of Networks and Lines," Prentice Hall Electrical Engineering Series, New Jersey, 1963.
8. G.S. Eager, I. Kolodny, L. Jachimowicz, and D.E. Robinson, "Transmission Properties of Polyethylene-Insulated Telephone Cables at Voice and Carrier Frequencies," AIEE Trans. (Commun. Electron.), Vol. 78, pp. 618-639, Nov. 1959.
9. Standard Mathematical Tables, Chemical Rubber Publishing Company.

ACKNOWLEDGEMENTS

The authors wish to thank T. Weberg for the many eye pattern measurements which were expertly performed and B. Calkins for the excellent graphics programming techniques. Discussions with J. Hull of NTIA-ITS regarding the figure of merit concept were enlightening and stimulated work on this paper.



John Kincaid received the MSEE and BSEE degrees from the University of Oklahoma in 1967 and 1966, respectively. He joined Belden in 1972 as a Product Development Engineer with our Electronic Division. John is presently Chief Engineer - Advanced Electronic Product Development at Belden's Technical Research Center in Geneva, Illinois. Mr. Kincaid is a member of EIA Subcommittee TR 30.1



Dave Johnson completed his undergraduate work at Augustana College receiving a B.A. degree in Mathematics and Chemistry in 1969. An M.A. degree in Mathematics was received from the University of Illinois in 1970. Dave joined the Engineering Computer Services Group at Belden's Technical Research Center in 1979. Mr. Johnson is a member of the Association for Computer Machinery.

The Inelastica: The Effect of Internal Friction on the Shape and Tension of a Bent Cable

A. L. Hale

AT&T Bell Laboratories
Whippany, New Jersey 07981

ABSTRACT

In many applications, the interaction of tension and bending in a cable having significant flexural stiffness has important practical consequences. A perfectly flexible cable pulled over a roller fairlead would conform to the throat curvature of each roller. For a real cable, maximum curvature depends on tension; for sufficiently low tension, the specified limit of permissible curvature will be satisfied regardless of roller size. This paper considers the equilibrium of a stiff but weightless cable as it passes through a bend around a frictionless sheave. During approach, cable curvature and bending moment increase steadily; during departure, both decrease but not necessarily along the same path in the moment-curvature plane. The path traversed is related in a simple way, useful with experimental data, to the tension change due to internal energy dissipation. A model based on the internal friction mechanism associated with a particular cable design (one having a sheath reinforced by wires laid in a helical pattern) yields results that agree reasonably well with available experimental data and provides a means to discriminate among alternative unloading characteristics on a plot of moment vs. curvature.

INTRODUCTION

Figure 1 shows an aerial line truck being used to place lightguide cable by the moving-reel method. The cable passes from the rear-mounted reel to the cable guide ahead of the lasher by way of the "main sheave", a pair of back-to-back quadrant blocks or roller fairleads free to swing independently about a vertical shaft near the right



Figure 1. Line Truck Placing Aerial Lightguide Cable.

rear corner of the truck cab. Each quadrant block contains three deep-throat rollers with a root radius of about 1.2 in., which is much less than the minimum permissible cable bending radius. How nearly

the cable curvature approaches that of the rollers depends, in part, upon the cable tension due to friction in the reel supports.

Figure 2 shows two extreme conditions for cable on a roller fairlead. For the optimistic extreme shown in part (a), the cable has a constant radius of curvature equal to the large "pitch" radius R of the fairlead. For the pessimistic extreme in part (b), however, the cable

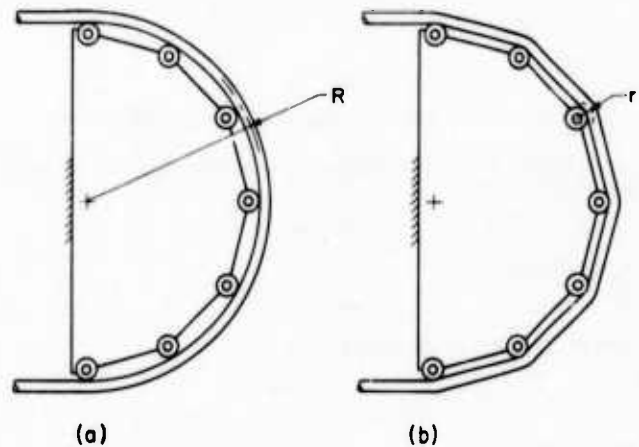


Figure 2. Extreme Pictures of Cable Action on Roller Fairlead.

conforms to the pitch radius r of each roller. In (a) the cable curve is consistent with pure bending, the effect of tension being negligible. In (b) the effect of cable flexural stiffness is negligible, and the cable behaves as a perfectly flexible rope. Where does the truth lie between these extremes?

THEORY

General

To examine this question consider the equilibrium of a weightless, initially straight cable passing steadily around a single small, freely turning roller at P (Fig. 3(a)). "Initially straight" means that the cable is straight when free of any bending moment. (The effect of reel "set" will be considered later.) "Freely turning" signifies that the bearings of the roller are frictionless. The force F_1 acting along the left-hand asymptote is the unique force resultant of the tension, bending moment, and shear force acting on the left-hand end of cable at any cross section. If the cable curves sharply enough about the roller to acquire a set, the right-hand resultant F_2 acts along a line parallel to but offset from the asymptote. The total angle of bend β is the sum of the angle θ_1 through which the cable bends during its approach (up to the single point of contact with the roller) and the angle θ_2 for the bend of the receding cable.

Figure 3(b) shows the free-body diagram for a differential cable element of length ds . The x axis is positioned along the line of action

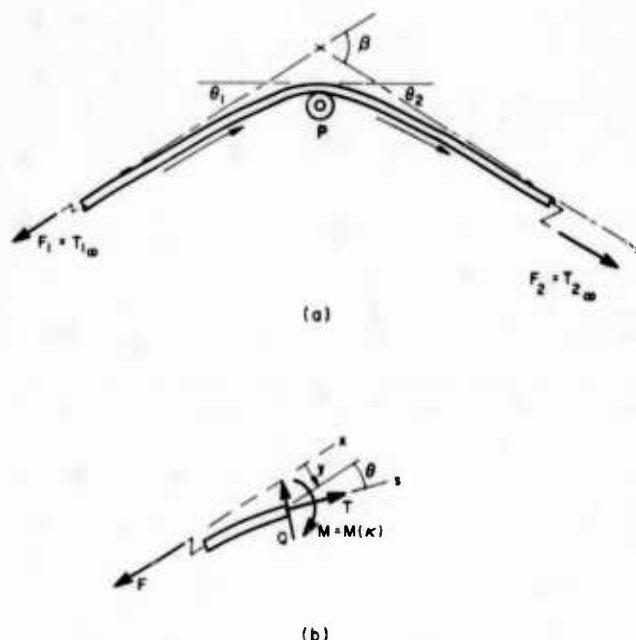


Figure 3. Cable Bent in Passage over a Single Small Roller.

of the resultant F . From equilibrium of moments about the right-hand end of the element,

$$M = Fy$$

or, in differential form,

$$dM = F dy. \quad (1)$$

From the geometry of the element,

$$dx = ds \cos \theta, \quad (2)$$

$$dy = ds \sin \theta, \quad (3)$$

and

$$\frac{ds}{d\theta} = \rho = \frac{1}{\kappa}, \quad (4)$$

where ρ is the radius of curvature (and κ is the curvature) of the cable center line. Combining (1), (3), and (4) gives

$$\begin{aligned} \kappa dM &= F \sin \theta d\theta \\ &= d(-F \cos \theta) \\ &= -dT \end{aligned} \quad (5)$$

from force equilibrium in the x direction. In integrated form (5) becomes

$$\Delta T = - \int_{M_1}^{M_2} \kappa dM, \quad (6)$$

where $\Delta T (= T_2 - T_1)$ is the change in tension from any point, 1, to any other point, 2.

These equations apply independently of the nature of the moment-curvature relation. In the case of linear thin-rod elastostatics they describe the classical elastica.^[1] Large-curvature bending of a real cable, however, is neither linear nor elastic. Figure 4 shows the moment-curvature characteristic for the bending of a cross-ply lightguide cable. The loading relation, with curvature increasing from the origin to point P , was experimentally determined,^[2] while the unloading and reverse-loading portions are inferred theoretically from the loading curve.

The loading path is initially linear but then bends over and follows a curve of much lower slope to the end of loading at P . In the unloading region beyond point P , the initial incremental loading and de-

formation are linearly related and reversible. Nonlinear, inelastic behavior resumes, however, before the bending moment is reduced to zero. At this point a large curvature remains. Straightening the cable requires application of a reverse (negative) bending moment, as shown at the lower axis crossing.

Given the moment-curvature characteristic of the cable as shown in Fig. 4, the interpretation of Eq. (6) is particularly simple. The integrand κdM is the area of the horizontal strip shown between the

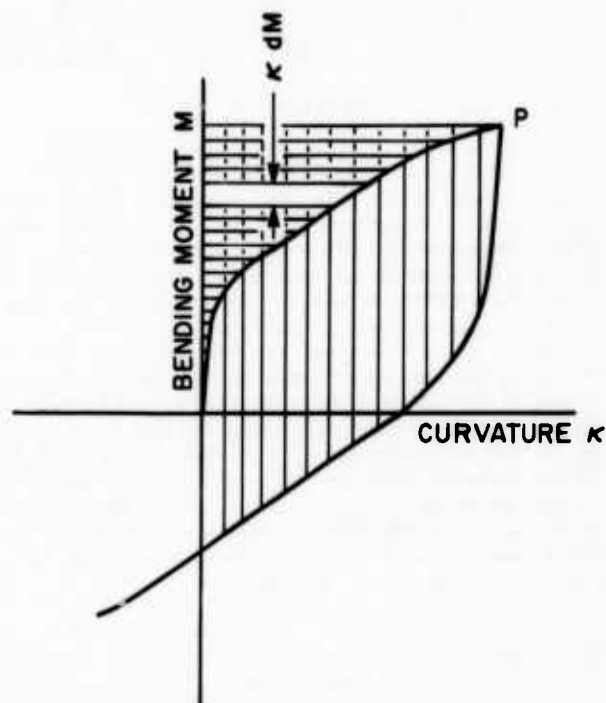


Figure 4. Bending Moment and Curvature in Passage over Small Roller.

M - κ curve and the moment axis, positive when (for example) the curvature is positive and the moment is increasing. Hence, according to (6), the tension increase between an undeformed cable element (zero curvature, zero moment) and an element loaded to the maximum curvature and moment at point P equals the negative of the horizontally shaded area in Fig. 4. (The area is positive, and so the tension change is a decrease.) This is a remarkable result: the tension change between two points of a cable is completely determined by the moment-curvature characteristic of the intervening cable. Knowledge of other quantities such as length or angle of bend is not required.

For a particular cable characteristic the areas of interest can be measured with a planimeter. Experimental data are available for loading and unloading but not reverse loading. Filling this gap requires examination of the behavior of the cable itself, in the form of a simple model.

Friction Model

The model is based upon the slippage of helically disposed reinforcing wires (strength members) embedded in the plastic material of the cable sheath. (Each wire may be imagined to occupy its own channel or tunnel formed in the surrounding material.) When a long section of a cable so constructed is bent into a circular arc, the part of the cable toward the inside of the bend is shortened and that toward the outside is lengthened. If the wires are firmly attached to the surrounding material, they will share this deformation as the radius of the arc is gradually decreased. If, on the other hand, the wires are perfectly free to slip, they will remain free of strain and will slide along their chan-

nels toward the outside of the bend. By symmetry, no sliding motion will occur at those points, on the outside and inside of the bend, that are farthest from the neutral surface. The maximum relative displacement toward the outside will occur at the neutral surface. Lutchansky^[3] illustrated this motion with photographs of a demonstration model. He analyzed the wire stresses in a cable having a compliant core, considering the extreme cases of no friction and of no relative motion at the core-wire interface. Levy^[4] extended the model by considering slippage with friction. Both authors focused on stress; here the goal is to determine the bending-moment contributions of the wires and the surrounding material. The nature of the unloading and reverse-loading process is of particular interest.

Wire Stresses Figure 5(a,b) shows one reinforcing wire spiraled about the core of a bent cable. The phantom lines represent the out-

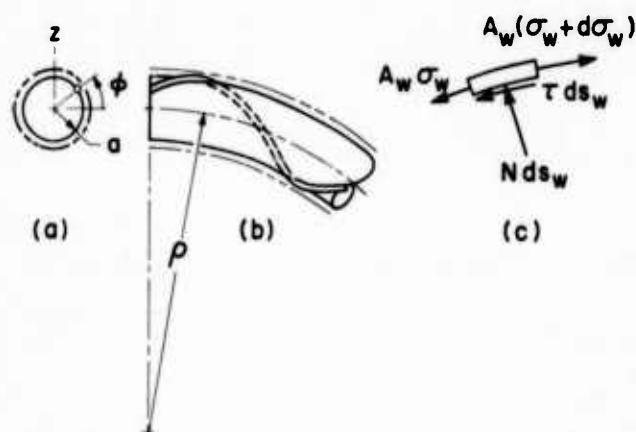


Figure 5. Geometry and Forces for a Single Reinforcing Wire.

side of the cable jacket. In the absence of slippage the wire stress at the cross section shown is

$$\sigma_w = E_w \frac{z}{\rho} = E_w \kappa a \sin \phi, \quad (7)$$

where E_w is Young's modulus for the wire material, other symbols are defined by Fig. 5, and the effect of the small helix angle between the wire and the cable axis is neglected. From Fig. 5(c) the shear force τ per unit length of the wire is

$$\tau = A_w \frac{d\sigma_w}{ds_w}, \quad (8)$$

where A_w is the wire cross-sectional area and s_w is arc length measured along the wire:

$$s_w \approx l \frac{\phi}{2\pi}, \quad (9)$$

where l is the pitch of the undeformed helix. Hence, approximately,

$$\tau = \frac{2\pi}{l} A_w E_w \kappa a \cos \phi \quad (10)$$

when the wire has not slipped.

The maximum shear stress occurs at $\phi=0$, the neutral axis. Slippage will begin there when $\tau_{\phi=0} = \tau_{\max}$, the maximum shear force per unit length that the interface can support, and will then spread in both directions along the wire. Figure 6 shows τ and σ_w plotted over a half-turn of the wire, from the inside of the bend at $\phi=-\pi/2$ to the outside at $\phi=\pi/2$, when the region of slippage extends from $\phi=-\phi_T$ to $\phi=\phi_T$. At every point the slope of the tensile-stress curve is proportional to τ , as required by (8) and (9). Within the region of slippage the slope is uniform. At $\phi=\phi_T$ the tensile stress is continuous because a discontinuity would require the existence of a concentrated axial force, which the interface cannot support. Outside the slippage region σ_w is given by (7). At $\phi=\phi_T$, σ_w has an abrupt change of slope, and τ

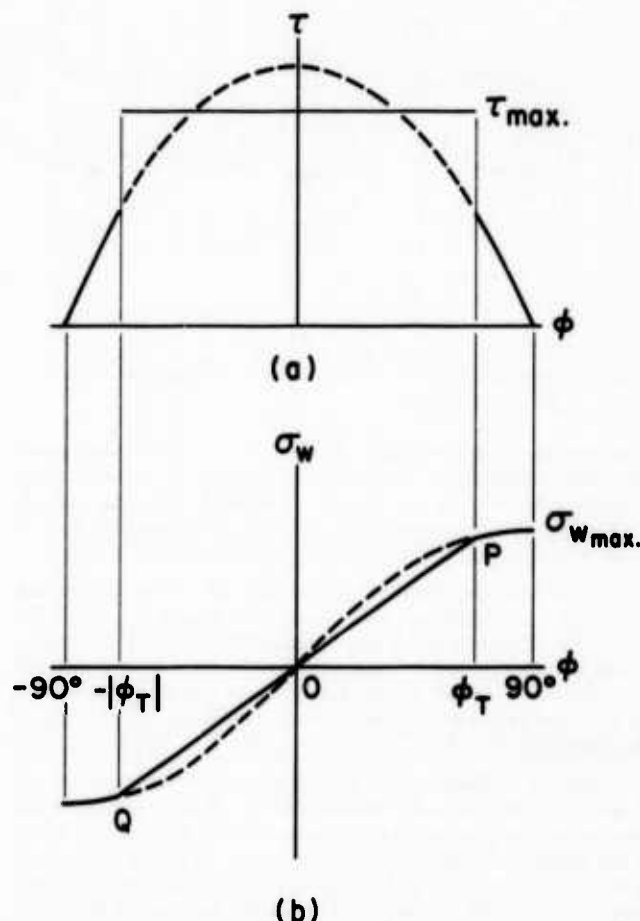


Figure 6. Stresses for One Wire During Transition from Elastic to Inelastic Bending.

is discontinuous. Hence, during spread of the slippage region, σ_w is given by

$$\sigma_w = \begin{cases} \frac{\tau_{\max} l \phi}{2\pi}, & |\phi| \leq \phi_T \\ E_w \kappa a \sin \phi, & \phi_T \leq \phi \leq \frac{\pi}{2} \end{cases} \quad (11)$$

Continuity at $\phi=\phi_T$ gives κ in terms of ϕ_T :

$$\kappa = \frac{l}{2\pi} \frac{\tau_{\max}}{E_w A_w a \sin \phi_T}, \quad 0 < \phi_T < \frac{\pi}{2}. \quad (12)$$

as the transition from no slippage to "almost complete"¹ slippage proceeds during loading. Curvature increases by a factor of $\pi/2$ during the transition. Once the transition is complete, the wires continue to slip almost everywhere with no increase in stress as κ increases further.

The process of unloading and reverse loading after initial loading into the inelastic range determines the size and shape of the lower curve in Fig. 4 and, hence, the tension increase in a cable as it recedes from a sheave. The process is most easily described graphically, by considering superimposed stresses. Figure 7(a) shows the stress in one wire at the start of unloading (solid curve with maximum of $\sigma_{w_{\max}}$). Figure 7(b) shows superimposed negative stresses for two levels of negative curvature change $\Delta\kappa$, and Fig. 7(c) shows the resultant stresses, which cannot go below the lower inclined line representing reversed sliding. Reverse sliding begins when the curve of resultant

1. Slippage "almost everywhere"—everywhere except at the points $\phi=\pm\pi/2$ farthest from the neutral surface.

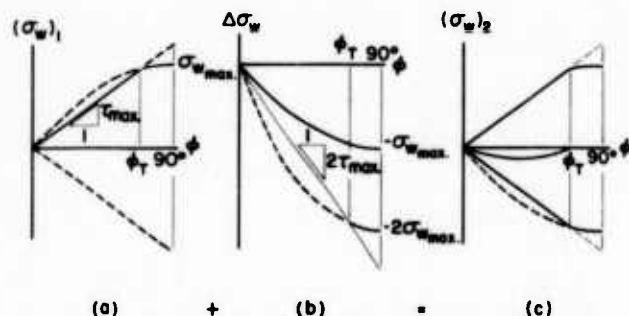


Figure 7. Superposition of Tensile Stresses During Unloading and Reverse Loading.

stress becomes tangent to the limit line, and the superimposed-stress curve becomes tangent to the inclined line in part (b). At that stage $|\Delta\sigma_w|$ is twice the stress that first caused sliding in the initial loading. The same conclusion applies to any later stage of reverse loading, such as that shown by the lower curves in parts (b) and (c) of the figure.

Thus, at any stage during the unloading and reverse loading, the magnitudes of the superimposed curvature and stresses are *double* the curvature and stresses at the same stage of initial loading. This conclusion is made plausible by the realization that initial loading starts at the midpoint of the full range of elastic—and subsequent inelastic—action, while unloading and load reversal traverse the full range from one extreme to the other.

Bending Moments The bending-moment contribution M_w of n equally-spaced reinforcing wires is the sum of the moments of the wire tensions $A_w \sigma_w$ about the neutral axis of the cable cross section. In the elastic range the result is independent of the angular orientation of the collection of n areas (as long as $n > 2$). In the inelastic range there is a small cyclic variation, which will be neglected; in effect, the wire areas will be considered "smeared out" into a thin ring for which $dA_w = n A_w d\phi/2\pi$. For two layers of wires the difference in radii of the layers will also be neglected.

The moment contribution from each of the four quadrants of the cable cross section during the transition from nonsliding to sliding is, then,

$$\frac{M_w}{4} = \frac{n A_w}{2\pi} \left\{ \int_0^{\phi_T} a \sin \phi \frac{\tau_{\max} l \phi}{2\pi A_w} d\phi + \int_{\phi_T}^{\pi/2} a^2 \sin^2 \phi \frac{l}{2\pi} \frac{\tau_{\max}}{A_w a} \frac{\phi_T}{\sin \phi_T} d\phi \right\}$$

when κ is expressed in terms of ϕ_T . Integration gives

$$M_w = \frac{n a l \tau_{\max}}{\pi^2} \Phi(\phi_T), \quad 0 < \phi_T < \frac{\pi}{2}, \quad (13)$$

where

$$\Phi(\phi_T) = \sin \phi_T + \frac{\phi_T}{\sin \phi_T} \left[\frac{\pi}{4} - \frac{\phi_T}{2} \right] - \frac{\phi_T \cos \phi_T}{2}. \quad (14)$$

The maximum contribution of the wires is

$$M_{w_{\max}} = \frac{n a l \tau_{\max}}{\pi^2}, \quad \kappa \geq \frac{l}{2\pi} \frac{\tau_{\max}}{E_w A_w a}; \quad (15)$$

(14) shows that M_w increases by the factor $4/\pi$ during the transition.

From the limits of M_w and κ as $\phi_T \rightarrow 0$ the elastic bending-stiffness contribution K_w of the wires is

$$K_w = \frac{n A_w a^2}{2} E_w, \quad (16)$$

or $I_w E_w$ as expected. If the cable sheath exclusive of the wires is assumed to behave elastically with a flexural stiffness K_p , then the complete theoretical M - κ characteristic of the cable is obtained as shown in Fig. 8. In Fig. 9 the model is fitted to experimental data² for

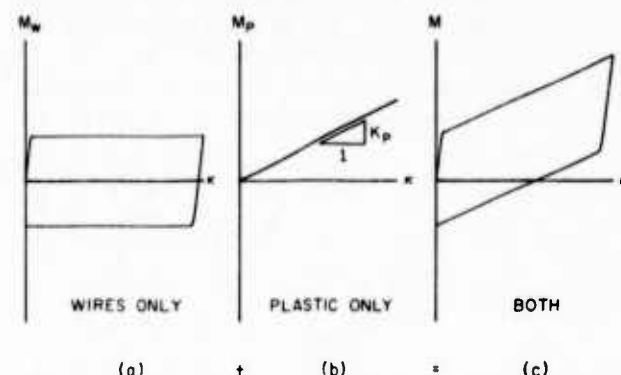


Figure 8. Theoretical Bending Moments During the Loading, Unloading, and Reverse-Loading Process.

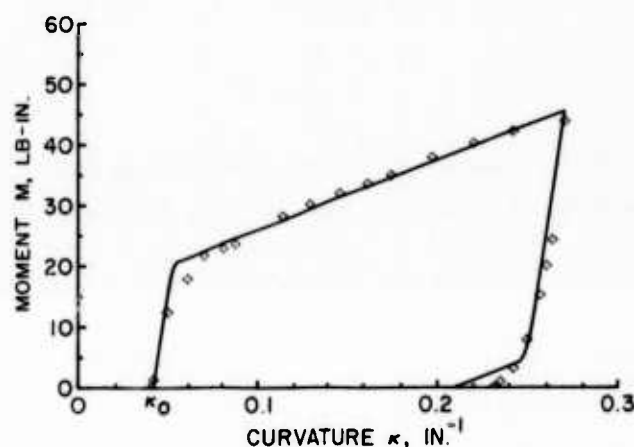


Figure 9. Comparison of Friction Model with Loading-Unloading Data.

a cross-ply lightguide cable sample. The fitted parameters are $K_p + K_w$ (common slope of both steep line segments), K_w (shallow slope), and $M_{w_{\max}}$ (intercept of shallow incline at line $\kappa = \kappa_0$; κ_0 is the initial curvature, or reel set, of the cable sample). Maximum shear force τ_{\max} per unit length for each wire follows from $M_{w_{\max}}$ through (15), and the shape of the transition portion of the characteristic is determined by (12) and (13) with ϕ_T varying from 0 to $\pi/2$. Except for the sharper knees of the theoretical curve, the agreement is startlingly good. In the model, wire slippage at the neutral surface starts simultaneously at all points along the length of the uniformly curved cable. In the experiment—and in practice—curvature varies along the length of the sample, and the onset of slippage at different locations occurs at different stages of the loading.

The friction model of inelastic cable bending is the basis for the extension of the cable characteristic in Fig. 4 into the unloading and

2. Courtesy of P. D. Patel, AT&T Bell Laboratories, Norcross, Georgia.

reverse-loading ranges. Since the changes, in both curvature and moment, necessary to reverse the sliding direction are double the values required for initial sliding, the lower curve in Fig. 4 is obtained from the loading curve by first doubling both dimensions and then turning the replica and joining it to the end of the loading curve.

APPLICATIONS

Single Roller

Given the angle of bend β in Fig. 3 and the minimum radius of curvature for the cable whose loading and reverse-loading curves are shown in Fig. 4,³ what are the maximum permissible tensions T_{1m} and T_{2m} ? From (6), the tension change during cable approach is

$$T_P - T_{1m} = -A_1, \quad (17)$$

where A_1 is the magnitude of the horizontally-shaded area. Similarly,

$$T_{2m} - T_P = A_2, \quad (18)$$

the area shaded vertically, overlapping area A_1 . The areas are measured on a plot of the loading curve and its enlarged replica. Equilibrium of forces parallel to the tangent at P gives

$$T_P = T_{1m} \cos \theta_1 \quad (19)$$

$$= T_{2m} \cos \theta_2. \quad (20)$$

The fifth equation in the five unknowns T_{1m} , T_{2m} , T_P , θ_1 , and θ_2 is

$$\theta_1 + \theta_2 = \beta. \quad (21)$$

Eliminating all unknowns but θ_1 gives

$$\frac{\sec(\beta - \theta_1) - 1}{\sec \theta_1 - 1} = \frac{A_2}{A_1}, \quad (22)$$

which shows that $\beta - \theta_1 (= \theta_2) > \theta_1$ (except when $\beta = 180^\circ$); (22) can be solved numerically for θ_1 . When $\beta = 180^\circ$, $\cos \theta_2 = -\cos \theta_1$ so that (19) and (20) give $(T_{2m} + T_{1m}) \cos \theta_1 = 0$; hence $\theta_1 = \theta_2 = 90^\circ$, $T_P = 0$, $T_{1m} = A_1$, and $T_{2m} = A_2$.

Table 1 lists some results for bend angles β of 180° and 27° ; the latter approximates conditions for cable passing the first and last rollers of the main sheave in Fig. 1. The 5-in. radius of curvature is the

TABLE 1. Angles and Tensions for Bends Around a Single Small Roller

β degrees	ρ_{min} in.	θ_1 degrees	θ_2 degrees	T_{1m} lb	T_{2m} lb
180	5	90	90	2.68	10.15
180	3.6	90	90	4.00	16.12
27	5	9.26	17.74	206	213
27	3.6	9.07	17.93	320	332

minimum permissible for the cable at tensions well below the rated load, and 3.6 in. was the minimum radius of curvature when the sample buckled. For either radius the tension increase $T_{2m} - T_{1m}$ is independent of β because the net area $A_2 - A_1$ enclosed between the M - κ characteristic and the moment axis depends on ρ_{min} (or κ_{max}) only. For $\rho_{min} = 5$ in. the increase is about 7.5 lb; for $\rho_{min} = 3.6$ in., it is about 12 lb. A change of this magnitude is unlikely to be important in itself except at low tensions (see next application).

Criteria for permissible cable-handling conditions often include some combination of tension and radius of curvature. In that context the solution just outlined is convenient and practical: given ρ_{min} and β , is T_P acceptably low? Is the value of T_{1m} that produces these conditions higher than is to be expected in normal practice (e.g., from reel-support friction)?

If some other variable is prescribed in place of ρ_{min} , however, another layer of iteration is added in the solution; in effect, ρ_{min} must be repeatedly assumed and the replacement variable repeatedly determined until the prescribed value is matched within an acceptable tolerance. Plots of A_1 , A_2 , and A_2/A_1 as functions of ρ_{min} are useful. For rough calculations an algebraic approximation derived from the friction model neglecting the rounding of the knees and the compliance of the wires is $A_2/A_1 = 1 + 4 M_{w_{max}} \rho_{min} / K_P$. This facilitates but does not eliminate the second layer of iteration.

Running-Line Dynamometer

The results for the single roller indicate that the act of measuring low tension with a running-line dynamometer will itself cause a tension change. Figure 10 shows a setup for measuring the tension in a light-guide cable while it is being lashed to an aerial strand. (Passing a lightguide cable over sheaves this small—the cable bending radius is



Figure 10. Use of Running-Line Dynamometer to Measure Low Cable Tension.

slightly less than the 3.6 in. of the previous application—is not recommended. The cable in the picture is a dummy—a standard sheath containing no optical fibers.) Figure 11(a) represents the dynamometer schematically, on the presumption that the cable makes arc contact with the first sheave. Figure 11(b) shows the cycle of moment vs. curvature for a cable element passing through the device. During the approach, bending moment follows the path from O to A in part (b) of the figure. The entire contact with the sheave in arc A , at constant M and constant κ , corresponds to a single point on the M - κ path. From the first sheave the cable passes to the second through the inflection point I_1 , completing a half turn around the M - κ loop. The tension increase is the same as for the same maximum curvature in passage over a single roller. Again, arc B is represented by a single point in the M - κ plane; the cable is not flexing as it hugs the sheave. Between I_1 and I_2 the tension increase is slightly greater than that for the approach to I_1 . The tension increase in the passage over the third sheave is the same as that for the second. (Additional sheaves alternated in the same regular pattern would all cause equal increases.) From the single-roller application we can infer a tension increase of slightly more than 36 lb due to the dynamometer.

The dynamometer load cell senses the vertical component of force on the middle sheave—the sum of the vertical components of the tensions and shear forces at I_1 and I_2 . The load sensed is greater than would exist for the same approach tension T_0 without internal friction in the cable, but is still related uniquely to T_0 for a particular cable in motion. It is only necessary to calibrate the load-cell output, in terms of the tension to be measured, with the cable in question passing

3. Santana and Yanizeski,¹² cross-ply sample 1 of Fig. 14.

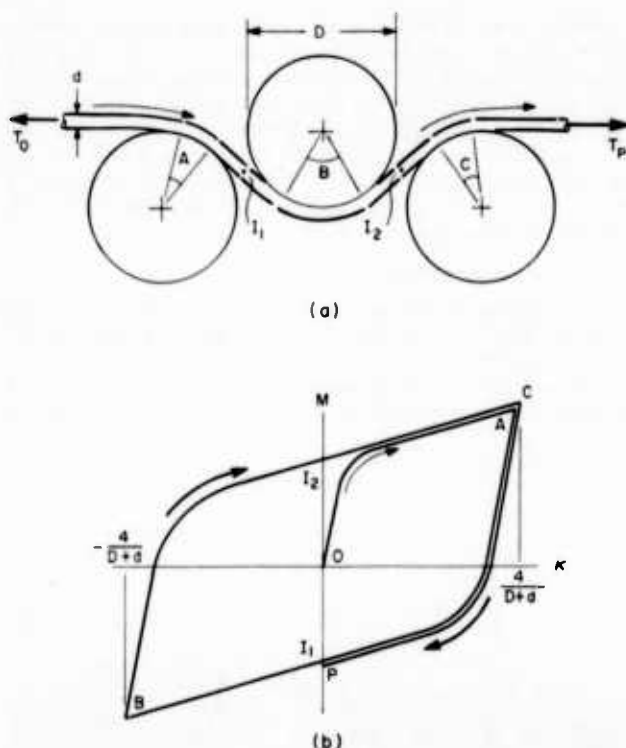


Figure 11. Cable Passing Through Running-Line Dynamometer.

steadily through the dynamometer. A static calibration in a testing machine will not suffice.

Effect of Initial Curvature

Figure 12 shows the M - κ cycle for the running-line dynamometer taking into account an initial curvature κ_0 of the cable stored on the supply reel. The distance and the cable tension between that reel and the dynamometer are assumed to be sufficient so that some cable between the two is essentially straight. The straightening, represented by the path leading to point O on the diagram, occurs before the cable reaches the dynamometer. Bending by the dynamometer thus begins at O . The tension increase on the first sheave is the area enclosed by the loop from O to A to I_1 . This area is slightly smaller than the

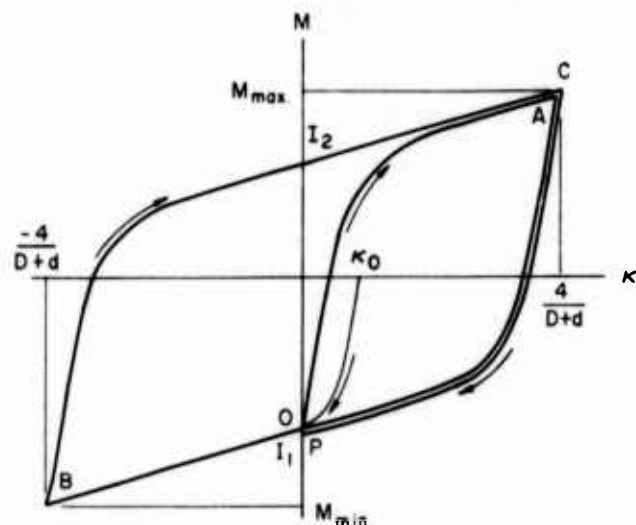


Figure 12. Effect of Initial Cable Curvature (Reel Set).

corresponding area in Fig. 11(b), the difference being three times the area enclosed there by the vertical axis and the paths OA and I_2C . That area is only about 0.1 lb for a cable that is initially straight (as in Fig. 11) but otherwise the same as the sample in Fig. 9. Thus the direct effect of initial curvature on cable tension is insignificant in this application.

There is, however, one significant but unavoidable indirect effect, namely, a change in the shear forces at I_1 and I_2 , which depends on the cable orientation (concave up or concave down). To the extent that the cable consistently assumes the preferred orientation, the effect can be calibrated for.

Roller Fairlead

A return to the roller-fairlead question concludes the applications. Figure 13(a) shows the fairlead geometry, where the roller spacing is defined by the pitch radius R and the angular increment $\Delta\beta$. If cable flexing between rollers is inelastic, the cable shape can be shown to

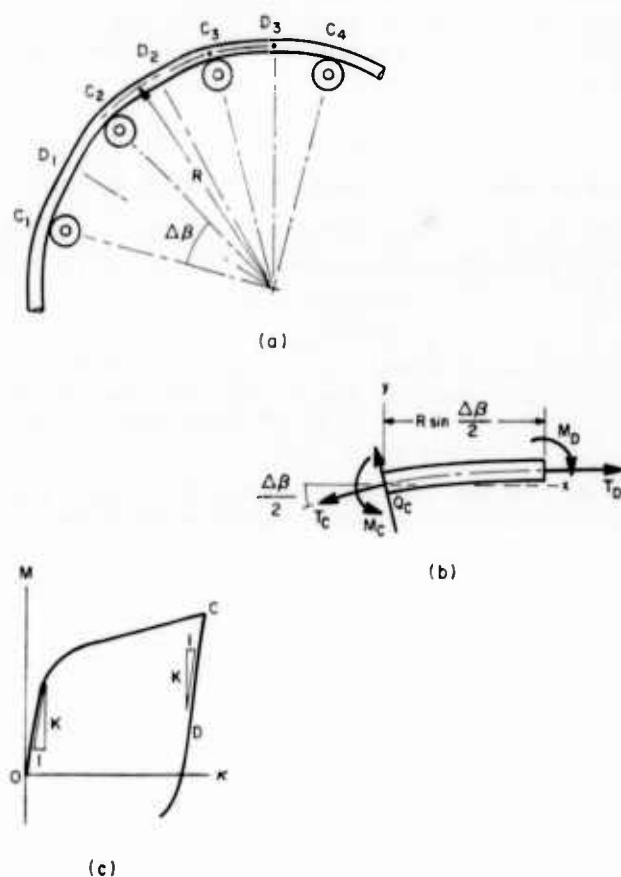


Figure 13. Cable Passing over Roller Fairlead; Elastic Action Between Rollers.

change from interval to interval, becoming flatter as tension builds up. The result is a formidable problem involving numerous transcendental equations in as many unknowns—an unwelcome prospect.

A relatively simple and limited but suggestive and useful solution is sought instead, based upon a retreat to elastic cable behavior between rollers, with inelastic action confined to the approach to the first roller and the departure from the last. What are the maximum tensions, at and between the rollers, that meet this restriction for various roller spacings?

In Fig. 13(c) the path OC represents the inelastic loading stage as a cable element approaches the first roller. If the unloading and

reloading action between rollers is elastic, a configuration that repeats itself from roller to roller is possible, with a linear decrease in moment and curvature from the point C_i at each roller to the point D_i halfway to the next, followed by linear reloading from there to the next point C_{i+1} .

The symmetry of this situation leads to the free-body diagram in Fig. 13(b), where the x axis now joins the points on the cable pitch line at successive rollers. The boundary conditions expressing the symmetry are

$$\theta = \frac{\Delta\beta}{2} \text{ at } x=0 \quad (23a)$$

and

$$\theta = 0 \text{ at } x = R \sin \frac{\Delta\beta}{2}. \quad (24a)$$

Maximum tension in the span is T_D , upon which the curvature κ_C depends:

$$\kappa = \kappa_C \text{ at } x=0, \quad (23b)$$

$$T = T_D \text{ at } x = R \sin \frac{\Delta\beta}{2}. \quad (24b)$$

Bending moment at a general point between C and D is (from Fig. 13(c))

$$M = M_C - K(\kappa_C - \kappa), \quad (25)$$

where $K = K_p + K_w$; substituting into the first form of (5)—where $F = T_D$ —and integrating from C to a general point using (23a) yield

$$K(\kappa_C^2 - \kappa^2) = 2T_D(\cos\theta - \cos\frac{\Delta\beta}{2}), \quad (26)$$

relating κ to θ . Using this result to integrate dx (as given by (2) and (4)) from C to D produces the transcendental equation

$$R \sin \frac{\Delta\beta}{2} = \int_0^{\Delta\beta/2} \frac{\cos\theta d\theta}{\left\{ \kappa_C^2 - \frac{2T_D}{K} (\cos\theta - \cos\frac{\Delta\beta}{2}) \right\}^{1/2}} \quad (27)$$

relating κ_C to T_D with R and $\Delta\beta$ as parameters.

The results of a solution by numerical quadrature and iteration are shown in Fig. 14. Because the cable behaves elastically between rollers, the curve there is in fact a form of the classical elastica for an initially-curved thin rod (the cable acquires a set as it approaches C_1). The equation is expressible in terms of elliptic integrals but must still be solved by numerical approximation.

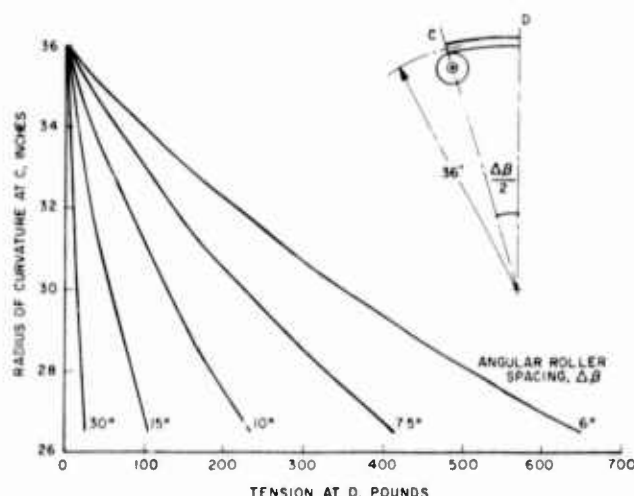


Figure 14. Minimum Radius of Curvature vs. Maximum Tension for Cross-Ply Cable on Roller Fairlead.

Each curve in Fig. 14 relates the minimum radius of curvature to the maximum tension for a particular roller spacing. (For $\Delta\beta = 6^\circ$, corresponding to 15 rollers uniformly spaced over a quadrant, the roller centers are about 3.6 in. apart.) As T_D increases, ρ_C decreases from 36 in. for the pure-bending condition to $\rho_C \approx 26.5$ in. at the limit of elastic action, when wire slippage impends at point D . Tension at that limit depends strongly upon the roller spacing. For $\Delta\beta = 30^\circ$, wire slippage begins at an interroller tension of only about 26 lb; for $\Delta\beta = 6^\circ$, cable flexing is still elastic at a tension of 650 lb. Thus, with a sufficient number of closely spaced, freely turning rollers—both conditions are essential—, operation up to the rated load of 600 lb for the cross-ply cable is possible. Wider roller spacing would entail inelastic action and progressively increasing tension in passage over the fairlead. It is not clear that repeated inelastic flexing of cable passing over a fairlead is desirable, and the problem has not yet been attempted.

CONCLUSION

Inelastic behavior of a cable in motion through bends around rollers and sheaves is described by a large-deflection theory that employs the experimentally determined nonlinear, inelastic moment-curvature characteristic of the cable. At present, data are readily available for loading and recovery only; extension into the reverse-loading range is needed. Meanwhile a friction model of inelastic bending based on slippage of helically disposed reinforcing wires separately embedded in the surrounding sheath material provides the needed extrapolation into the load-reversal range. The theory provides guidance in such practical problems as the measurement of low cable tensions and the design or evaluation of roller fairleads.

REFERENCES

1. Love, A. E. H., *A Treatise on the Mathematical Theory of Elasticity*, 4th Edition (New York: Dover), 1927, pp. 401-5.
2. Santana, M. R., and G. M. Yanizeski, "Bending Performance of Fiber-Optic Cable Sheaths: Application of New Apparatus and Techniques", *Trans. ASME*, Vol. 104, pp. 578-86, July 1982.
3. Lutchansky, M., "Axial Stresses in Armor Wires of Bent Submarine Cables", *ASME Journal of Engineering for Industry*, Vol. 91, No. 3, August 1969.
4. Levy, H. J., AT&T Bell Laboratories, unpublished work.



The author received B. S., M. S., and Ph. D. degrees in mechanical engineering at the University of California at Berkeley in 1947, 1949, and 1956, respectively. In 1956 he began work at Bell Telephone Laboratories in submarine cable systems development, studying gripping and tension-transfer stresses in armorless cable passing through a linear cable engine. He has developed cable-handling information for use with the series of AT&T Sea Plows and, in recent years, has been part of a group responsible for methods of installing lightguide cable in buried, underground, and aerial telephone plant.

DEVELOPMENT OF RADIATION RESISTANT MULTI-FIBER OPTICAL CABLE INCORPORATING GRADED INDEX TYPE FIBERS

M. DAZAI, H. YOKOTA, M. NAKASUJI, H. HORIMA and M. WATANABE

SUMITOMO ELECTRIC INDUSTRIES, LTD. 1, TAYA, TOTSUKA-KU, YOKOHAMA 244, JAPAN

Abstract

We have successfully developed a multi-fiber optical cable with a large transmission capacity, incorporating graded index type fibers and featuring high resistance to radiation. With fiber-optic communication systems becoming more and more widely applied recently, nuclear power plants have begun to consider installing data- and video-transmission systems using optical fibers. The fibers in such systems are often required to be resistant to radiation while at the same time capable of carrying large amounts of information signals. This report describes the first cabling of graded index fibers with fluorine-containing core and cladding which have both radiation resistance and large transmission capacity. We evaluated the radiation resistant characteristics and mechanical properties of both the fibers and the developed cable, fire retardant characteristics of the cable, and other properties. And we confirmed the reliability and applicability of the newly developed cable for radiation-filled environment.

1. Introduction

With fiber-optic communication system becoming more and more widely applied recently, data- and video-transmission systems which use optical fibers are being considered for installation in nuclear power stations. The optical fibers in such systems, depending on where they are installed, are often required to provide not only wide bandwidth but also radiation resistant characteristics. The typical optical fiber added with germanium (Ge) in its core, on the other hand, has a marked increase of transmission loss by radiation. Hence it was difficult to use these fibers in radiation-filled environment.

Accordingly as the optical fiber for such use, we developed a step index (SI) type optical fiber with pure silica core and fluorine added cladding which offers vastly improved radiation resistance(1)(2). In the case of SI type fiber, however, the demerit of small transmission capacity is involved.

In the optical cable developed this time, the graded index (GI) type fiber(3) added with fluorine in its core has made it possible to provide both radiation resistant and wide bandwidth characteristics. Besides these fundamental characteristics, as the principal features of this optical cable, the following features are available.

(1) A very stable mechanical characteristics are provided by the construction of spacer type(4).

(2) By adopting the "fire retardant" material, the "fire retardant" characteristics is provided that passes the vertical tray flame test of IEEE Standard 383.

In this paper, as the result of evaluating the transmission, mechanical and fire retardant characteristics of GI type fluorine added optical fiber cable, as well as the radiation resistant characteristics, it was verified that there was no problem at all for practical use. The report therefore is given in this paper.

2. Various characteristics of GI type optical fiber added with fluorine

2.1 Fiber construction

The construction parameters of GI type fiber added with fluorine which was developed and produced as cable this time are shown in Table 1. And the outline of the refractive index profile is shown in Fig. 1. NA is about 0.18 in average indicating the value somewhat smaller than that of the standard GI type fiber added with Ge (about 0.2). The fiber is of double coating with silicon resin and nylon similar to the standard case.

Table 1 Parameters of GI type fiber added with fluorine

Item		Typical value
Core diameter		50 μm
Outer diameter		125 μm
NA		0.18
Coating	Material	Silicone and nylon
	Outer diameter	0.9 mm

2.2 Transmission characteristics of fiber

As the result of measuring the transmission loss and transmission bandwidth of fluorine added GI type optical fiber at the wavelength of 0.85 μm , the values of average loss of less than 3 dB/km and the bandwidth of over 350 MHz·km were obtained. Also,

the result of measurement for the length dependence of bandwidth is shown in Fig. 2. The measurement was conducted at the wavelength $0.85\ \mu\text{m}$ while cutting off in order the fiber of continuous length 1,400 m.

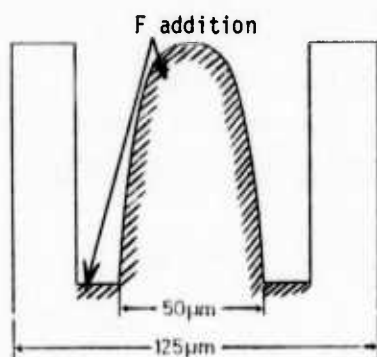


Fig. 1 Outline of refractive index profile of GI type optical fiber added with fluorine

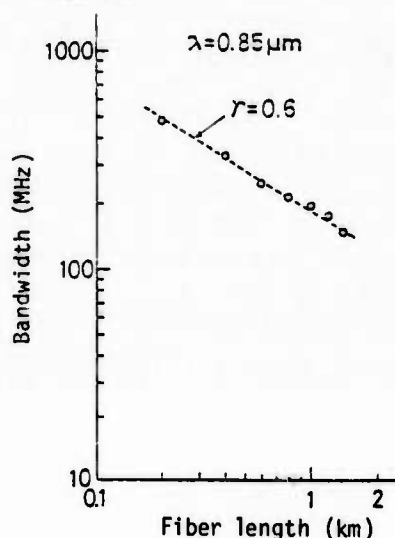


Fig. 2 Length dependence of bandwidth of fluorine added GI type fiber

As shown in Fig. 2, the length dependent coefficient γ of the bandwidth becomes the value of about 0.6. This value is smaller than the value (≈ 1) at $0.85\ \mu\text{m}$ of the standard GI type fiber.

2.3 Radiation resistant characteristics

1) Radiation resistant characteristics of fiber

The evaluation of radiation resistant characteristics of fiber was conducted at the condition of coiled sample of about 100 m length with respect to several kinds of fibers using γ ray with ^{60}Co set as the radiation source. The gamma ray dose rate was 10^4R/h . In the one hour irradiation, the loss increase during and after irradiation (wavelength $0.85\ \mu\text{m}$) was continuously monitored. Fig. 3 shows the outline of measuring system.

The test result is shown in Fig. 4. The test

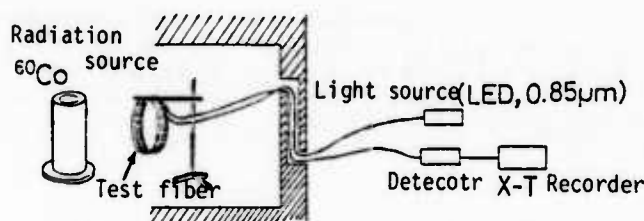


Fig. 3 Measuring system of radiation resistant characteristics

fibers are, as shown in Fig. 4, GI type fiber added with fluorine (shown in Fig. 1), SI type fiber added with fluorine (shown in Fig. 5(a)) and standard type GI fiber added with Ge (shown in Fig. 5(b)).

While the loss increase due to irradiation is significant in fiber added with Ge, in the case of fiber added with fluorine, although the trend differs somewhat between GI type and SI type, the loss increase for both of these types after one hour irradiation is less than 5 dB/km restoring to the increase of about 1 dB/km after stopping the irradiation.

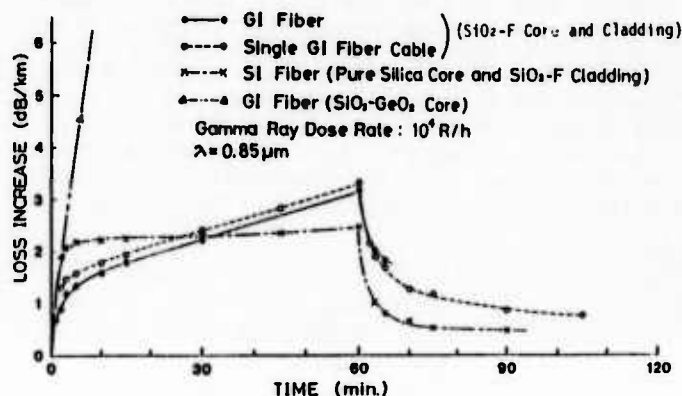


Fig. 4 Radiation resistant characteristics of various types of fibers

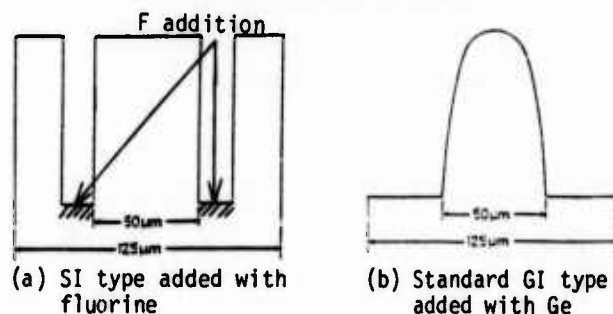


Fig. 5 Refractive index profiles of fibers

2) Radiation resistant characteristics of cable

Fig. 4 shows together the result of evaluating the radiation resistant characteristics of the cable containing the fluorine added GI type fiber. The single fiber cable shown in Fig. 6 was used and evaluation was conducted at the same condition as that of the case of fiber itself.

As the result, the characteristics approximately the same as the result of fiber condition was obtained and the deterioration of characteristics by the irradiation of γ ray stemming from the cable material other than optical fiber was not created at all.

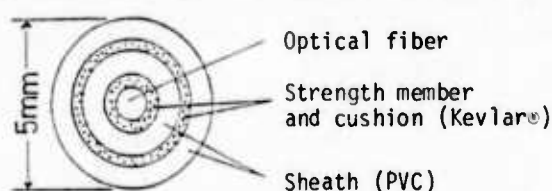


Fig. 6 Structure of single fiber cable

2.4 Mechanical characteristics of fiber

As the mechanical characteristics of fluorine containing GI type optical fiber, evaluation of loss change due to side compression and bending was conducted. The measuring method and loss change are shown in Fig. 7 and Fig. 8, respectively. In both cases, GI fiber added with fluorine and GI fiber added with Ge were compared.

As regards the result of side compression test, the fluorine added GI fiber presents a somewhat larger loss increase than standard GI fiber. And as regards bending test, although a larger loss increase occurs in fluorine containing fiber in the case of mandrel diameter $D=10\text{ mm}\phi$, in the cases of $D=20\text{ mm}\phi$ and $D=30\text{ mm}\phi$ results for both fibers, fluorine containing fiber and Ge containing fiber, were almost the same. The difference between the results of fluorine added GI fiber and Ge added standard GI fiber is consider-

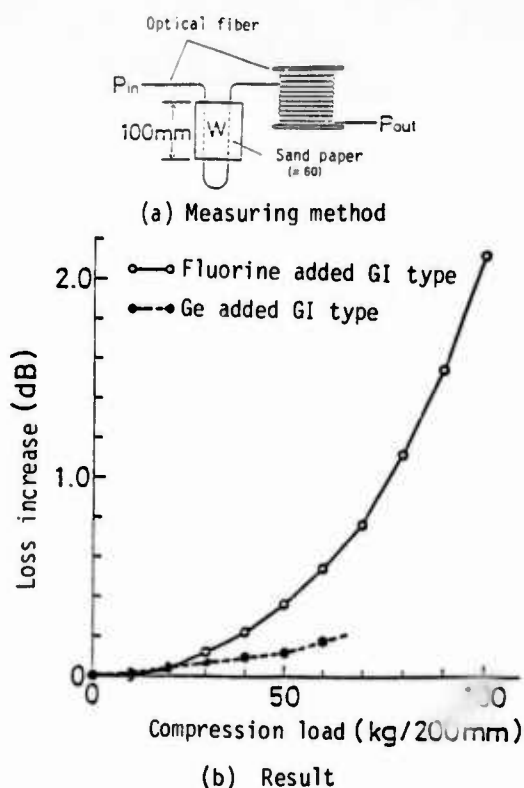
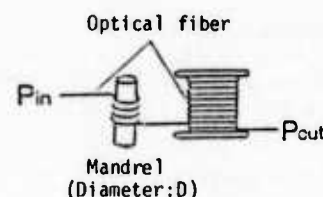
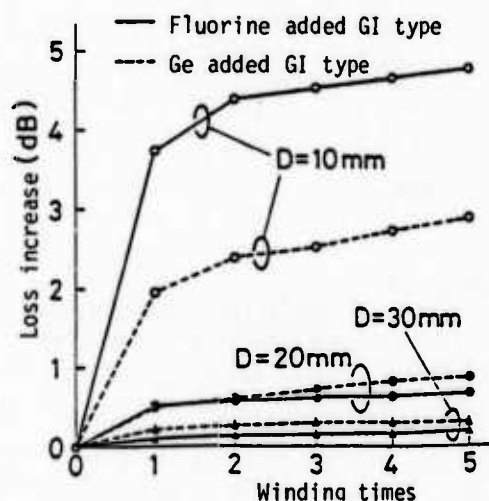


Fig. 7 Result of side compression test of fluorine added GI type fibers



(a) Measuring method



(b) Result

Fig. 8 Result of bending test of fluorine added GI type fibers

ed to arise mainly from the difference of refractive index profile and NA value.

2.5 Fiber splice characteristics

In actual system, the possibility of splice between radiation resistant cable with fluorine added fiber and standard cable with Ge added fiber can be considered. Thereby with the standard GI fiber added with Ge ($NA=0.2$) and newly developed GI fiber added with fluorine ($NA=0.18$) offered as the sample, evaluation of splice loss and the strength and reliability of spliced part was conducted. Core diameter of fiber used for the test was $50\text{ }\mu\text{m}$ for both types.

Measuring method is shown in Fig. 9 and fiber combination and the result are shown in Table 2. As shown in Fig. 9, the splice loss is defined as the ratio of output power of 1 km length fiber (P_{in}) and the output power after splicing 2 m fiber to the above fiber (P_{out}). And after splicing, the strength of spliced part was evaluated by screening of 260 g weight before reinforcement.

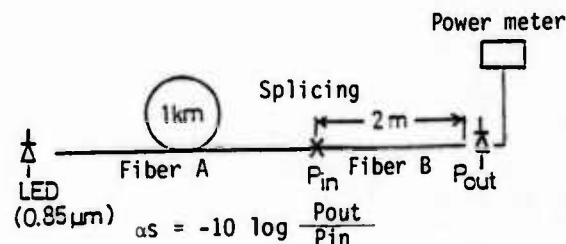


Fig. 9 Measuring method of fiber splicing loss

Table 2 Splice loss of fibers with fluorine and with Ge

(a) Fiber combination

	Fiber A	Fiber B
Measurement 1	GI type added with Ge (NA=0.2)	GI type added with fluorine (NA=0.18)
Measurement 2	GI type added with fluorine (NA=0.18)	GI type added with Ge (NA=0.2)

(b) Result of measurement 1 (N=10)

	Splice loss (dB)	Screening of 260 g
Ave.	0.17	1/10 break

(c) Result of measurement 2 (N=10)

	Splice loss (dB)	Screening of 260 g
Ave.	0.03	1/10 break

From the result of Table 2, despite the appearance of rather large splice loss in the case of measurement 1 (NA large \rightarrow NA small), no problem is considered for practical use. Also the result obtained by conducting the heat cycle test ($-20^{\circ}\text{C} \sim +60^{\circ}\text{C}$, 30 cycles) for all the samples after splicing and reinforcement indicated no occurrence of fiber break. It is concluded that the splice of both fibers can be conducted without problem from the aspects of strength and reliability.

3. Various characteristics of GI type radiation resistant multi-fiber cable

3.1 Construction of cable

The construction cross section of GI type radiation resistant 42-fiber cable developed this time is shown in Fig. 10 and its appearance is shown in Photo 1.

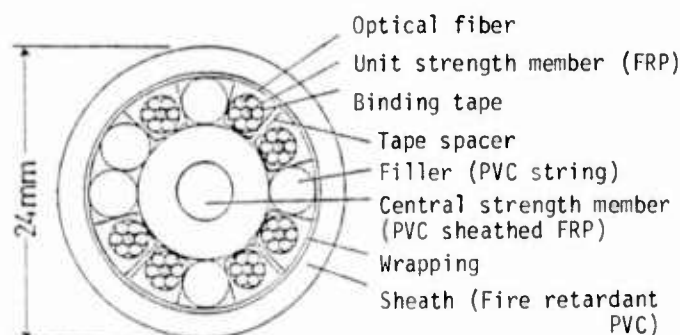


Fig. 10 Construction of 42-fiber radiation resistant optical cable

Cable is of the construction containing 6-fiber optical unit in the plastic spacer offering the non-metallic type that does not use metal material at all. Also taking the "fire retardant" characteristics into consideration, the jacket of cable tension member (FRP) and the material of interstitial string are in entirety set as PVC (polyvinyl chloride). Furthermore the "fire retardant" PVC is used as the sheath material. Outer diameter of cable is about 24 mm and the weight is about 500 kg/km.

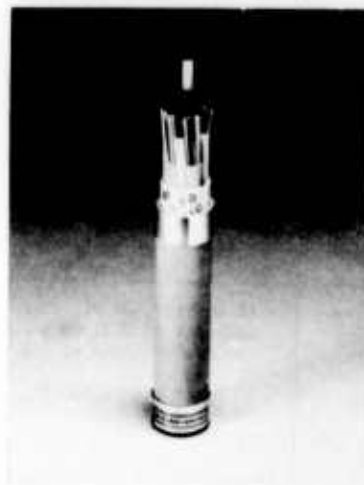


Photo 1

Appearance of radiation resistant optical cable

3.2 Mechanical characteristics of cable

To evaluate the basic mechanical characteristics requested in the cable, using the multi-fiber cable developed, tests as to respective items of tension, bending, compression and impact were conducted. The outline of testing method and result is summarized in Table 3. Also the relationship between tension and loss increase and between tension and cable elongation are shown in Fig. 11 while the relationship between side compression load and loss increase and between side compression load and cable non-circularity are shown in Fig. 12.

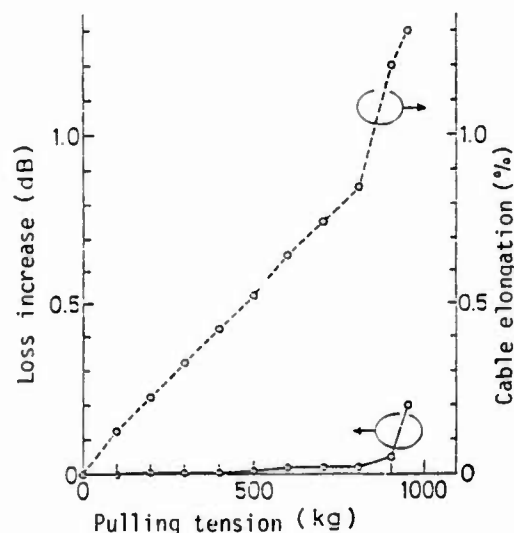


Fig. 11 Result of cable pulling test

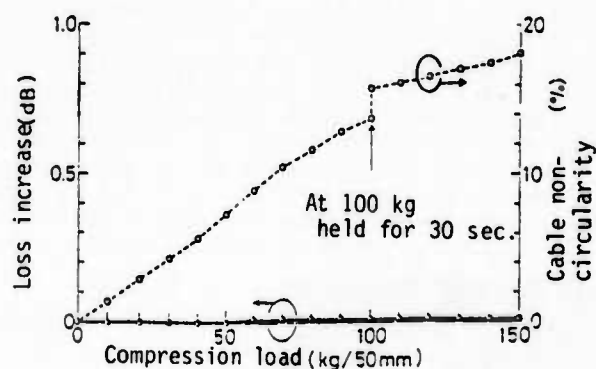
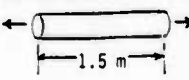

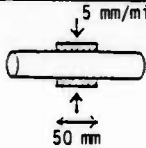
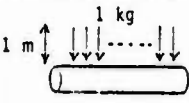


Fig. 12 Result of cable compression test

Table 3 Mechanical characteristics of radiation-resistant optical cable

Item	Testing method	Test result
Tension	 <p>20 mm/min. Max. 1,000 kg</p>	<ul style="list-style-type: none"> At tension 500 kg, loss increase is 0.01 dB and cable elongation is 0.5 %. Up to tension 1,000 kg, no break of fiber.
Bending	 <p>Mandrel diameter: 280 mm 10 times bendings</p>	<ul style="list-style-type: none"> Loss increase at bending max. +0.03 dB. No loss change after test. No break of fiber.
Compression	 <p>5 mm/min. 50 mm Max. 150 kg/50 mm (at 100 kg, held for 30 sec.)</p>	<ul style="list-style-type: none"> Loss increase during test max. +0.01 dB. No loss change after test. No break of fiber
Impact	 <p>1 kg 1 m Impact body: metal pillar of 25 mm Drop at 10 different locations</p>	<ul style="list-style-type: none"> No loss change.

3.3 "Fire retardant" characteristics of cable

As for the cable used in nuclear power stations, there are many cases of requirement to provide the "fire retardant" characteristics in addition. As aforementioned, in the development this time, the improvement of the characteristics was implemented by not only using "fire retardant" PVC in the outer sheath but also using PVC material for the interstitial material. Also the characteristic was evaluated by actually conducting the burning test on the cable manufactured.

As for the testing method, vertical tray flame test of IEEE Standard 383 simulating the actual scale of fire was adopted. The outline of measuring system is shown in Fig. 13. In the test, when extinguishing the fire by letting the burner to burn for 20 minutes, cable that extinguished for itself without prolonging the burning is qualified.

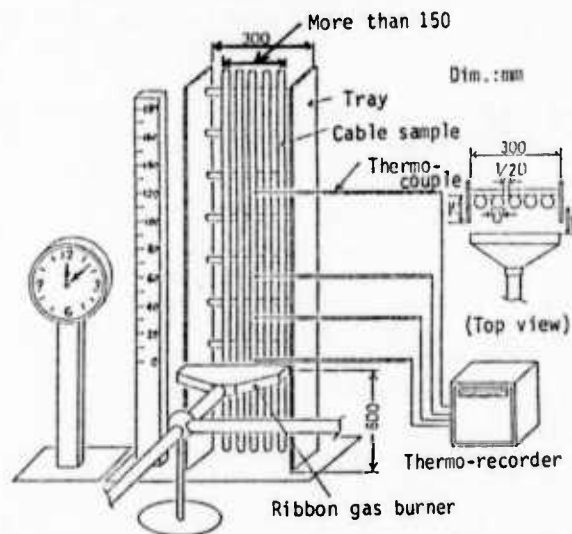


Fig. 13 Vertical tray flame test equipment

Although the result of evaluation indicated that the cable was burnt and impaired to about 60 cm above the burner, the burning of the cable itself was stopped at 15 minutes after starting the burning. Therefore the prolonged burning after extinguishing the burner was utterly unable to be recognized confirming that the "fire retardant" characteristics that fully satisfied this standard was provided. The situation of burning test is shown in Photo 2.

4. Conclusion

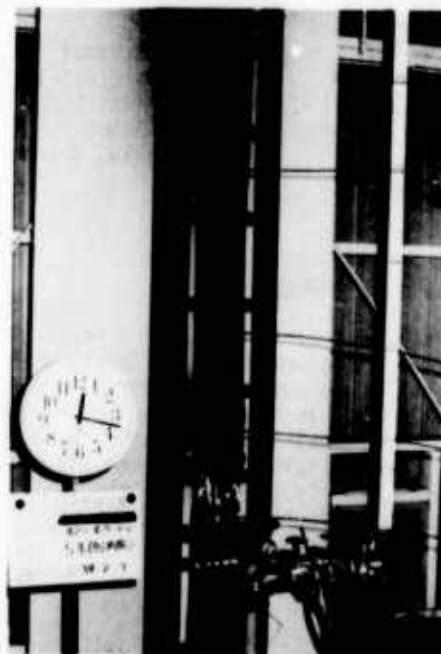
At the time of developing radiation resistant large capacity multi-fiber optical cable for the use in optical communication system for nuclear power stations, various characteristics of GI type fiber added with fluorine and the cable newly developed this time were evaluated. As the result the following items described were verified clarifying that there was utterly no problem for practical use.

(1) In the evaluation of radiation resistant characteristics, evaluation was conducted not only on the fiber but also on the cable condition (1 fiber optical cable). Also the comparison of fiber condition was conducted indicating no occurrence of deterioration.

(2) As regards the splicing of GI type fiber added with fluorine and the standard GI type fiber added with Ge, there was no problem for practical use from the viewpoints of splice loss, strength and reliability.



(a) After lapse of about 5 minutes



(b) After lapse of about 17 minutes

Photo 2 Scene of cable burning test

(3) As regards the side compression and bending characteristics of fluorine added GI fiber, compared with the standard GI fiber, the loss increase was somewhat larger (this can be considered to stem chiefly from the speciality of refractive index profile and from NA being somewhat low). However, in the evaluation of mechanical evaluation after completing as cable product, there was no problem in particular.

(4) As the cable characteristics the evaluation of "fire retardant" characteristics besides mechanical characteristics was conducted and the study of material constituting the cable was conducted. Thereby it was confirmed that the superior characteristics was provided and it was found that there was no problem at all for the practical use.

Acknowledgement

The writers wish to express his deep acknowledgement to Mr. Shishido, Manager of Communication Department of KITANIHON ELECTRIC WIRE CO., LTD. as well as other persons concerned who have offered cooperation in developing this optical cable.

References

- (1) S. Kurosaki et al., National Conference IECE Japan, 1866, March 1980.
- (2) M. Hoshikawa et al., National Conference IECE Japan, 964, March 1981.

- (3) M. Nakasuji et al., IEE Japan, EIM-83-23, March 1983.
- (4) S. Yonechi et al., IWCS Proceedings, PP101-110, 1980



Masahiko Dazai
Sumitomo Electric
Industries, Ltd.
1, Taya-cho,
Totsuka-ku, Yokohama
Japan

Masahiko Dazai was born in 1955 and received the M.S. degree for engineering from Tohoku University in 1982. He joined Sumitomo Electric Industries, Ltd. in 1982, and has been engaged in development and design of optical fiber cables. He is a member of Fiber Optics Division in Sumitomo Electric Industries Ltd., and is a member of the Institute of Electronics and Communication Engineers of Japan.



Hiroaki Horima
Sumitomo Electric
Industries, Ltd.
1, Taya-cho,
Totsuka-ku, Yokohama
Japan

Hiroaki Horima was born in 1947. He received the M.S. degree for engineering from Osaka University in 1972.

He joined Sumitomo Electric Industries Ltd. and worked on the development of CATV coaxial cables, multi-pair PEF-insulated junction cables and low loss unbalanced type cables.

Thereafter he concentrated on the development of optical fiber cables. He is now Senior Engineer of Fiber Optics Division in Sumitomo Electric Industries Ltd. He is a member of the Institute of Electronics and Communication Engineers of Japan.



Hiroshi Yokota
Sumitomo Electric
Industries, Ltd.
1, Taya-cho,
Totsuka-ku, Yokohama
Japan

Hiroshi Yokota received a B.S. degree in physical engineering from Tokyo University. He joined Sumitomo Electric Industries, Ltd. in 1975, where he has been engaged in research and development of optical fiber fabrication. He is a member of the Institute of Electronics and Communication Engineers of Japan.



Minoru Watanabe
Sumitomo Electric
Industries, Ltd.
1, Taya-cho,
Totsuka-ku, Yokohama
Japan

Minoru Watanabe was born in 1946 and received a Ph.D. degrees in chemistry from Kyoto University in 1977. He joined Sumitomo Electric Industries, Ltd. in 1977, and has been engaged in research and development of optical fiber fabrication. He is a senior engineer of Yokohama Research and Development Department and is a member of the Institute of Electronics and Communication Engineers of Japan, the chemical Society of Japan, the Japan Society of Applied Physics and the Ceramic Society of Japan.



Masaaki Nakasuji
Sumitomo Electric
Industries, Ltd.
1, Taya-cho,
Totsuka-ku, Yokohama
Japan

Masaaki Nakasuji received a B.S. degree in Chemical Engineering from Kyoto University in 1981. He joined Sumitomo Electric Industries, Ltd. in 1981, and has been engaged in research and development of optical fiber fabrication. He is a member of Yokohama R & D Group, and is a member of the Institute of Electronics and Communication Engineers of Japan.

ENVIRONMENTAL CHARACTERISTICS OF OPTICAL FIBER CABLE
FOR USE IN NUCLEAR POWER PLANTS

K. Shibuya S. Ohashi Y. Kumazawa F. Nakane and T. Kojima

Showa Electric Wire and Cable Co., Ltd.
4-1-1, Minamihashimoto, Sagami-hara, Kanagawa, 229 Japan

ABSTRACT

In order to use the optical fiber cable in nuclear power plants, the various environmental characteristics such as flame retardant, heat aging, radiation and mechanical characteristics were investigated.

As the flame retardant test, oxygen index, vertical tray flame and HCl gas trapping tests were made. From these results, it became clear that this optical fiber cable has sufficient flame retardant characteristics because of choosing optimum flame retardant materials.

Heat aging test was made at 121°C for 7 days. The induced loss during the test was 0.1 dB/km or less.

Radiation characteristics were investigated by irradiation of ^{60}Co γ -ray under the condition of 100R(Roentgen)/hr. x 100hr. after heat aging test. The radiation-induced loss at 10^4R was only about 1 dB/km on account of using pure silica core fibers. Furthermore, from these data, the radiation-induced loss at 10^6R was estimated less than 2 dB/km.

In order to investigate the mechanical characteristics, tensile, bending, twisting, compression, impact, pulling on pulley and vibration tests were made. During these tests, loss increase of optical fibers were scarcely found.

INTRODUCTION

In the interest of safety and reliability, nuclear power and the related plants employ a high technical measuring control system which requires a number of control cables. At the same time, with the recent development of optical fiber technology, there has been a trend to apply optical fibers to nuclear power related fields. Optical fibers have many advantages over the conventional copper cable: the low loss characteristics can increase the transmission distance, the broad bandwidth permits multiplex data transmission and reduction of cables in number, the cable is reduced in weight, and the electromagnetic immunity reduces signal errors.

Few studies have been made on environmental characteristics of optical fibers except those concerning radiation characteristics. We have made flame retardant, environmental and mechanical tests on optical fiber cable to investigate their overall environmental characteristics.

This paper is a report of our results.

SAMPLES

Figure 1 illustrates the crosssection of optical fiber cable used in the tests and Table 1 shows the specification of the cable.

This optical fiber cable is a non-metallic type cable which strands together 6 nylon coated fibers and spacers around a FRP tensionmember. The optical fibers are made of pure silica core having excellent radiation resistance. All cable materials are flame retardant. The tensionmember is constructed of 2.5mm diameter FRP on which flame retardant noncorrosive PVC is coated, and is 3.3mm in outside diameter. The outside diameter of the cable is about 11mm.

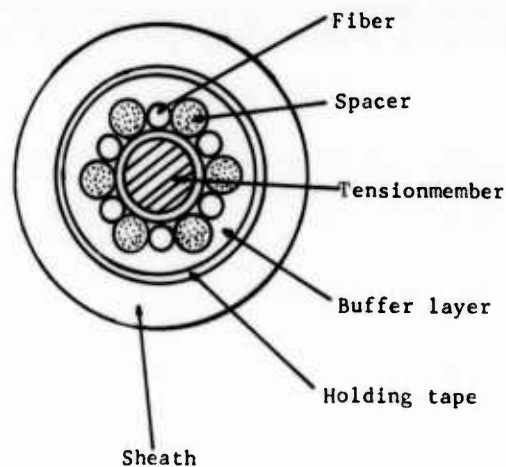


Fig.1 Crosssection of the cable

Table 1 Specification of the cable

Optical fiber	Core diameter;	50 μ m
	Cladding diameter;	125 μ m
	Refractive index profile;	SI type
	Relative index difference;	0.8%
	Core material;	Pure silica
	OH content of the core; About	100ppm
	Initial loss(0.85 μ m);	3.8dB/km(ave.)
	Secondary coating;	Nylon
Tension-member	Flame retardant noncorrosive PVC coated FRP	
Spacer	Flame retardant noncorrosive PVC	
Buffer layer	Kynol [®] yarn	
Holding tape	Flame retardant rubbered tape	
Sheath	Flame retardant noncorrosive PVC	

TEST METHODS AND RESULTS

We made oxygen index, vertical tray flame, and HCl gas trapping tests as flame retardant tests, heat aging and ⁶⁰Co γ -ray irradiation tests as environmental tests. We also made tensile, bending, twisting, compression, impact, pulling on pulley and vibration tests as mechanical tests which simulate external forces that may be applied to the cable during installation. The test methods and results will be described below.

FLAME RETARDANT TEST^{1), 2)}

1. Oxygen Index test

Oxygen index refers to the minimum oxygen concentration in an oxygen-nitrogen mixture gas, expressed in volume %, required to maintain combustion of a cable material under specific conditions. Therefore, the greater the index, the higher the flame resistance.

Figure 2 shows the method for measuring an oxygen index. The oxygen index measurement was made in accordance with JIS-K-7201(1972). In this measurement, four kinds of materials were used: a sheath, tensionmember, buffer layer and holding tape. For each material, three samples were measured.

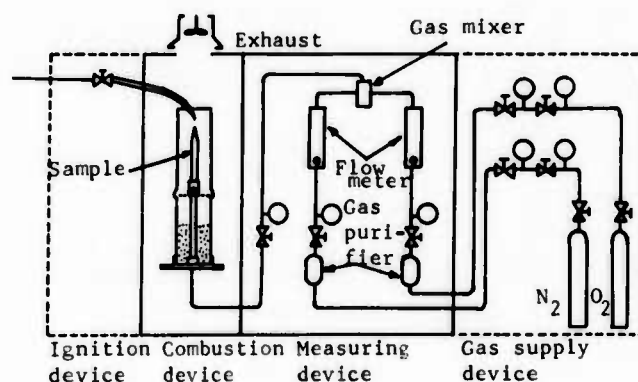


Fig.2 Oxygen Index measuring method

Table 2 shows the test results. It is generally considered that a sheath needs an oxygen index of 27 or more and the other materials 25 or more. However, the test revealed that all the materials have an oxygen index of 27 or more.

2. Vertical tray flame test

Figure 3 shows the outline of the vertical tray flame test equipment. The test method used is in accordance with IEEE 383-1974. The sample cables were set on the vertical ladder tray at intervals of the cable radius so that the cable array has a width of 150 mm, and the burner was placed at 600 mm height above the floor. The flame temperature was adjusted to 840°C and the burning time was 20 minutes. The burner flame energy was 70,000 BTU/hr. The cable temperature was continuously measured with thermocouples A, B, C and D.

Table 3 shows the test results, and Photo. 1 and Photo. 2 show the cable conditions during combustion and immediately after extinction. The above standard prescribes that the flame shall not spread to the upper end of the cable during combustion or after extinction. In any of three trials, the flame did not reach the upper end of the cable and extinguished itself as soon as the burner was turned off.

Table 2 Results of Oxygen Index test

Material	Sheath			Tensionmember			Buffer layer			Holding tape		
Oxygen index (n = 3)	27.8	27.6	28.3	48.6	48.3	48.7	29.2	30.1	29.6	41.8	42.2	42.1
Average	27.9			48.5			29.6			42.0		

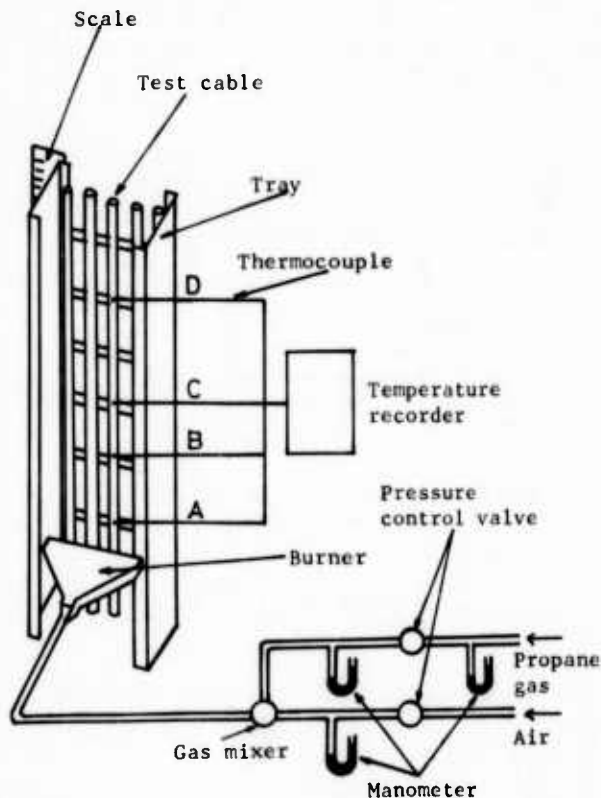


Fig.3 Vertical tray flame test equipment

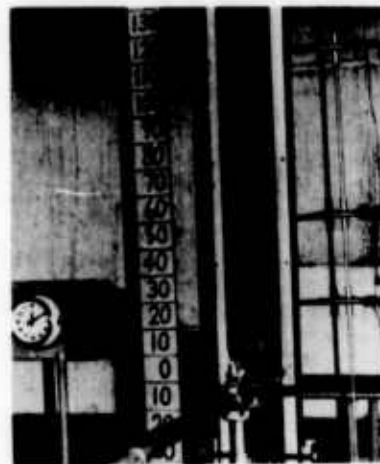


Photo. 1 Cable condition during combustion

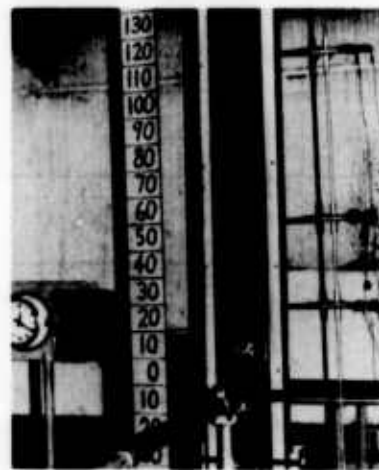


Photo. 2 Cable condition immediately after extinction

Table 3 Results of vertical tray flame test

Test time	Burning time after fire extinguishing (sec.)	Burning out length of the cable (m)
1	0	0.76 ~ 0.91
2	0	0.75 ~ 0.93
3	0	0.73 ~ 0.96

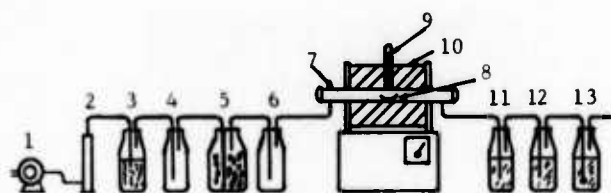
3. HCl gas trapping test

The HCl gas generated when a cable is burned out shall be not more than 100 mg for each gram of sheath, since this corrosive gas has a bad influence upon the human body and surrounding equipment.

Figure 4 shows the method for the HCl gas measurement. The measurement conditions are as follows:

Sample weight ; 0.5 g
 Preheat temperature ; 300 to 400°C
 Preheat time ; 5 minutes
 Burning temperature ; 800±30°C
 Burning time ; 30 minutes
 Air flow ; 0.5±0.1 l/min.

Table 4 shows the test results. The HCl gas generation of the three samples were all less than 100 mg.



- 1 Air pump
2 Flow meter
3 Glass bottle for drying air
4 Glass bottle contains conc H_2SO_4
5 Glass bottle contains silica gel
6 Quartz tube
7 Quartz tube
8 Quartz boat (Sample)
9 Thermocouple
10 Electrical furnace
11 Gas washing bottle for trapping HCl
12 Gas washing bottle
13 Gas

Fig.4 HCl trapping test method

Table 4 Results of HCl trapping test

Sample (Sheath)	1	2	3
Weight of HCl generation (mg/g*)	86.7	89.3	87.4
Average (mg/g*)	87.8		

Remark* mg/g (weight of HCl gas/lg of sheath)

ENVIRONMENTAL TEST

Heat aging and ^{60}Co γ -ray irradiation tests were successively made on the same samples. As indicated in Figure 5, the 6 fibers of each sample were grouped into two and 3 fibers in each group were spliced to form a loop, and the induced loss was continuously measured for each loop.

1. Heat aging test

The sample was heated at $121^\circ C$ for 7 days. These accelerated deterioration conditions correspond to the design life of a common nuclear power plant.

Figure 6 shows the test results. The induced loss was extremely stable during heating. For both loops, the induced loss was within 0.1 dB/km. In addition, the cable after heating exhibited no apparent changes.

2. ^{60}Co γ -ray irradiation test

Subsequently to the heat aging test, the sample cable was placed in the irradiation room where the sample was exposed to ^{60}Co γ -ray. The desired value of radiation-induced loss was set at a total dose 10^6 R in order to ensuring the system margin. However, because of the great dose rate dependency of optical fibers, ³⁾ the irradiation was made under the condition of 100 R/hr. x 100 hr. and the value at 10^6 R was estimated by extrapolation.

Figure 7 shows the radiation-induced loss characteristics during irradiation. As the pure silica core fiber has extremely radiation resistance, the radiation-induced loss was about 1 dB/km at a total dose of 10^4 R, and it was estimated less than 2 dB/km at 10^6 R on the basis of the steady state increase in the region between 2×10^3 R and 10^4 R.

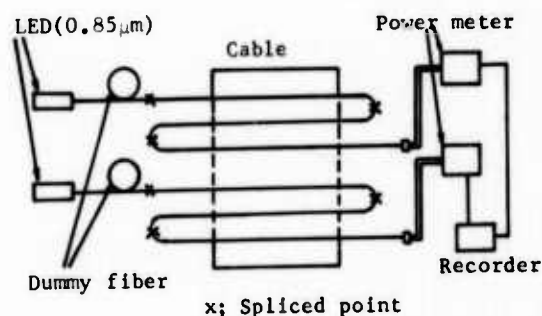


Fig.5 Measuring set-up of heat aging and ^{60}Co γ irradiation tests

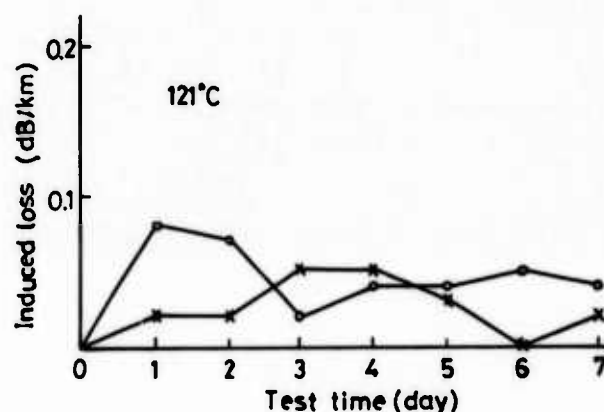


Fig.6 Heat aging characteristics

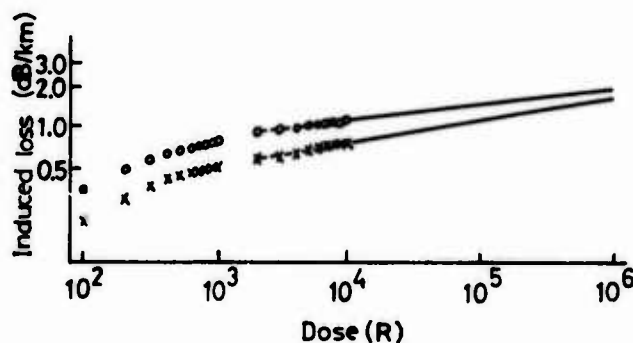


Fig.7 Induced loss by ^{60}Co γ irradiation

MECHANICAL TEST

The mechanical tests simulate external forces that the cable is expected to encounter during installation. The mechanical tests were made with the following aims.

1. Tensile test

The tensile force during installation is estimated, and the two times force of the allowable tension is applied to the sample cable.

2. Bending test

This test examines the cable state when the cable is sharply bent in pipe.

3. Twisting test

Cables are easily twisted when they are frequently bent during installation. This test examines the cable state when the cable is twisted.

4. Compression test

This test examines the cable state when the cable is trod by a person.

5. Impact test

This test examines the cable state when a tool or any other instrument is dropped on the cable.

6. Pulling on pulley test

This test examines the cable state, simulating a tension to which the cable may be subjected at a bend during installation.

7. Vibration test

This test examines the cable state when the cable installed is subjected to vibration caused by a motor, etc.

All fibers of the cable were spliced to form loops and the loss increase during test was measured. In all tests except the compression and impact tests, the sheath, fiber and tension member at the cable ends were combined in one using epoxy resin so that the cable elongation in the longitudinal direction is equal to that in normal installation.

Table 5 shows the test methods and results. Any of the tests showed that the optical fiber cable exhibits almost no loss increase and has mechanical characteristics equal to or more than those of conventional copper cables.

CONCLUSION

We made flame retardant, environmental and mechanical tests to investigate overall characteristics of optical fiber cable developed for use in radiation environments, such as in nuclear power plants.

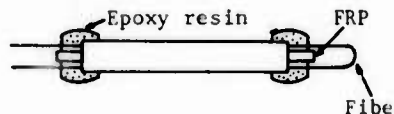
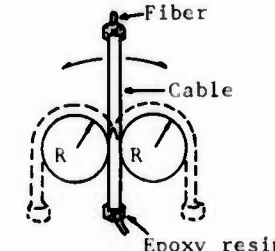
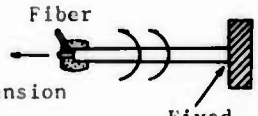
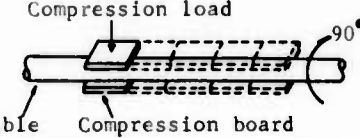
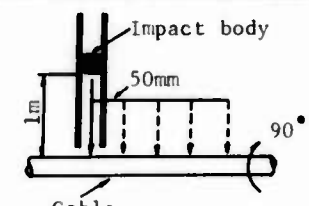
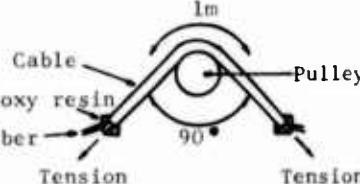
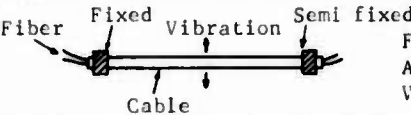
The tests revealed that this cable is sufficiently flame retardant and has extremely stable characteristics.

This type of cable has been already installed in nuclear power plant, contributing to the improvement of data transmission reliability.

REFERENCES

- 1) J.Matsuo, et al; Proceedings of the 26th IWCS p216 - 227 (1977)
- 2) M.Ike, et al; Showa Electric Wire and Cable Review, Vol.28, No.2 p3 - 68 (1978) (in Japanese)
- 3) K.Shibuya, et al; Proceedings of the 31st IWCS p51 - 62 (1982)

Table 5 Mechanical characteristics

Test item	Test method	Test result
Tensile test	 <p>Tensile load; 100kg Tensile time; 5 min.</p>	No loss increase
Bending test	 <p>Mandrel radius(R); 100mm Bending angle; ± 180 deg. Bending time ; 30 times</p>	No loss increase
Twisting test	 <p>Tensile load ; 25kg Twisting angle; ± 180 deg. Twisting time ; 10 times</p>	No loss increase
Compression test	 <p>Compression load ; 100kg Compression time ; 1 min. Compression board size; 50x50(mm) Compression place ; 5 continuous places and 2 directions of 90° at 1 place</p>	0.01dB 0.0dB after test
Impact test	 <p>Impact body size; 25mm³ Impact weight ; 1kg Impact height ; 1m Impact point ; 5 continuous points at 50mm pitch and 2 directions of 90° at 1 point</p>	No loss increase
Pulling on pulley test	 <p>Pulling length ; 1m Pulley diameter; 135mm³ Tensile load ; 50kg Pulling angle ; 90 deg. Pulling times ; 10 times</p>	No loss increase
Vibration test	 <p>Frequency ; 10Hz Amplitude ; ± 5mm Vibration time; 10⁶ times</p>	No loss increase



Kiyoshi Shibuya

Kiyoshi Shibuya was born in 1947. He joined Showa Electric Wire and Cable Co., Ltd. after his graduation from Tohoku University in 1972. He has been engaged in research and development of aluminum conductors, superconductors and optical fibers. He is now a senior engineer of optical fiber and system division. He is a member of the Institute of Electronics and Communication Engineers of Japan.



Fumoto Nakane

Fumoto Nakane was born in 1945. He joined Showa Electric Wire and Cable Co., Ltd. after his graduation from Waseda University in 1969. He has been engaged in research and development of metallic materials of the cable, superconductors and optical fibers. He is now a chief engineer of optical fiber and system division. He is a member of the Institute of Electronics and Communication Engineers of Japan.



Shogo Ohashi

Shogo Ohashi was born in 1954. He received his B.E. degree from Shizuoka University in 1976 and M.E. degree from Tohoku University in 1978. He joined Showa Electric Wire and Cable Co., Ltd. in 1978. He has been engaged in design of communication cables and optical fiber cables. He is now a staff engineer of communication cable division. He is a member of the Institute of Electronics and Communication Engineers of Japan.



Takeshi Kojima

Takeshi Kojima was born in 1934. He joined Showa Electric Wire and Cable Co., Ltd. after his graduation from College of Tokyo Science in 1958. He has been engaged in research and development of dielectric materials for extra high voltage cable and optical fibers. He is now a manager of optical fiber and system division. He is a member of the Institute of Electrical Engineers of Japan.



Yoshio Kumazawa

Yoshio Kumazawa was born in 1943. He joined Showa Electric Wire and Cable Co., Ltd. after his graduation from Showa First Technical High School in 1962. He has been engaged in research and development of communication cables and optical fiber cables. He is now an assistant chief engineer of optical fiber and system division.

FIBER OPTIC CABLE FOR APPLICATIONS IN THERMAL RADIATION ENVIRONMENTS

G. Anderson,* J. C. Smith,* J. McAlarney,* S. Share,** and A. Baba**

ITT Electro-Optical Products Division, Roanoke, VA 24019-0065*
Harry Diamond Laboratory, Adelphi, MD 20783**

ABSTRACT

A fiber optic cable has been developed for use in thermal radiation environments. This cable is a lightweight, ruggedized structure that uses a heat barrier for protection from thermal radiation and is fabricated from commercially available, easily obtainable materials.

This paper presents fiber and cable performance data derived from several years of cable development and experimentation. Optical performance at low, room, and high temperatures is given on the optical fiber and finished cable. Data on the mechanical performance (impact, twist bend, cyclic flex, and tensile load) of the cable at low, room, and high temperatures are provided for unirradiated and thermally irradiated cables. Finally, thermally irradiated cables are compared with cables subjected to a flame test.

INTRODUCTION

The many uses of fiber optics make it necessary for them to operate in various environments. A fiber optic cable can have applications in thermal radiation environments, as well as in climactic environments where temperature varies from approximately -50°C to 70°C. This paper describes a rugged fiber optic cable structure used in thermal radiation environments. Included are optical and mechanical characteristics of the fiber optic cable at low, high, and room temperatures, the mechanical integrity of the cable after thermal radiation, and the response of the cable to a flame test.

DESIGN AND MANUFACTURE

The cable design standards address optical performance, mechanical integrity, ruggedness, and thermal radiation integrity. The cable is composed of a rugged cable core protected by an expendable thermal barrier and outer jacket. This two-part concept helps to ensure that thermal radiation will be absorbed or dissipated before reaching the cable core. Therefore, the core will survive intact, and the surviving cable core will retain its ruggedness. The cable core is designed to withstand a rugged field environment.

The core consists of two optical fibers, strength members and an inner jacket. The fibers are bound tightly to the buffer, secondary coating, and cable strength members. The fibers are stranded together in one operation and the inner jacket is extruded in a second operation. The fibers are thus embedded in a fibrous matrix allowing the fibers to reorient external forces to relieve stress. At the same time, the matrix and tightness of the inner jacket hold the fibers, thus preventing retraction. The total outside diameter (od) of the cable is 6 mm.

The cable was fabricated with dual-window, graded-index fibers. The composition of these fibers specified the removal of and/or substitution of specific cladding and core dopants. Various aspects of the preform fabrication process needed to be adjusted. Adjustment was required to efficiently deposit the dopants, control the refractive index profile and reduce migration of hydroxyl ion (OH-) in the preform. These process developments were optimized by using preform profiling techniques and process control of chemical

vapor deposition (CVD). Process control of CVD helps to ensure a reproducible fiber. The fibers, which have a 50- μ m core diameter and a 125- μ m (od), were proof-tested at 100 kpsi.

The fiber has a low-modulus primary coating and secondary coating of thermoplastic material. The secondary coating, which puts additional stresses on the fiber, causes increased attenuation. Additional attenuation occurs especially at low temperature if the refractive-index profile and numerical aperture of the fiber are not optimized. The fiber, therefore, has been designed with a minimum numerical aperture of 0.23 along with an alpha profile that exhibits good dual-window performance.

The optical performance of the two-part cable with the fibers described above is given in Table 1. Data are presented on 11 1-km lengths of cable (denoted A through K). Table 1 shows

Table 1. Optical Performance.

Attenuation, 850 nm (dB/km)										
Cable	Secondary Coated Fiber (25°C)				Cable (25°C)		Cable (-57°C)		Bandwidth 850 nm (MHz-km)	
	Fiber	a	b	a	b	a	b	a	b	
A		3.37	3.44	3.08	3.35					
B		3.10	3.10	6.26	5.10			503	508	
C		4.00	3.62	4.04	3.61	4.28 4.14	3.74	599	416	
		1300 nm		1300 nm		1300 nm -46°C		1300 nm		
D		1.41*	1.50*	1.10	2.13	1.82	2.37	248	534	
E		1.93	2.10	1.56	1.91	1.60	2.17	385	540	
F		1.49	2.49	2.09	1.44	2.62	2.80	497	458	
G		1.55	1.59	1.09	1.35	2.14	2.10	521	372	
H		1.30	0.86	1.49	1.23	1.82	1.92	472	386	
I		1.93	1.34	1.13	1.19	--	--	740	701	
J		1.39	1.52	1.02	0.76	2.42	2.56	372	489	
K		0.44	0.79	0.43	0.69	1.99	2.11	816	886	

*Without secondary coating.

the attenuation of the secondary coated fiber and of the cabled fiber at 850 nm and 1300 nm. Data are given for the two optical fibers in each cable (labeled a and b in the table) at room temperature (25°C) and low temperature. The table shows a relatively small increase in cable loss (<1 dB/km in all the cables except one) from room temperature to low temperature. The cable losses at 1300 nm and -46°C were less than 3 dB/km. Four cables (half the group) had losses less than 2.2 dB/km. Most of the fiber bandwidths were 400 MHz-km or greater.

TEST RESULTS

The fiber optic cable was subjected to several tests to evaluate mechanical integrity. The tests conducted were cyclic flexing, twist bend, and impact. In the cyclic flexing test, one end of the cable was rotated through 90 degrees on each side of a 15-mm diameter mandrel (180° arc) while a 10-kg weight was hung from the other end. Two thousand cycles were performed at room temperature and 1000 cycles were performed at 71°C and at -46°C.

The cable was suspended over a 3-cm diameter pulley for twist bend testing. One side of the cable was cycled up and down, while the other side of the cable was rotated 180 degrees clockwise. It then was returned to the starting position and rotated 180 degrees counter-clockwise. Throughout the test a 10-kg weight was hung from the end of the cable. Two thousand cycles were performed at room temperature and 100 cycles were performed at 71°C and -46°C.

In the impact test, a 1.5-kg hammer with a 10-mm radius of curvature dropped 150 mm onto the cable. Two hundred impacts were performed at room temperature and 100 were performed at 71°C and at -46°C.

Table 2 lists these test results. All the tests were performed at low, room, and high temperatures. The core

Table 2. Mechanical Integrity Tests and Results.

Test	Temperature	Test Results
Cyclic-flexing	Room Temperature -46°C, 71°C	No damage to cable core Outer jacket splits at 71°C, -46°C All fibers transmitted
Twist-bend	Room Temperature -46°C, 71°C	No damage to cable core Outer jacket split at 71°C, -46°C All fibers transmitted
Impact	Room Temperature -46°C, 71°C	No damage to cable core Outer jacket splits at 71°C, -46°C All fibers transmitted

was not damaged by any of the tests for all temperatures. However, the outer jacket did split at low and high temperatures. All the fibers passed the tests without breaking.

The ruggedness of the cable core was tested by laying the cable in soil and subjecting it to crossings, pivot turns, and high-speed turns by a 23-ton tracked vehicle. First, the optical cable core with fibers was subjected to and survived 26 crossings without

failure. Next the tracked vehicle was positioned on the cables for static pivot turns. After 10 to 12 cycles, the cable was captured in the tracks of the vehicle and looped three turns around the axle. The cable suffered severe shear which ripped the jacket and exposed the fibers. The fibers remained conductive until the cable was badly strained in removing the cable from the gearing. Finally the tracked vehicle made high-speed right-angle turns on the cables. The optical cable survived this test.

THERMAL RADIATION TEST RESULTS

The next test series measured the thermal radiation integrity of the cable in a thermal radiation environment. The fiber optic cable was exposed to thermal radiation environments at the White Sands Solar Facility (WSSF). The WSSF uses a 12.2 by 11 m heliostat to reflect solar radiation onto a spherical concentrator. The spectral output of the facility, similar to the solar spectrum, peaks at about 500 nm, with an infrared component extending to about 2500 nm and an ultraviolet component extending down to 330 nm.

Tested cable samples were irradiated at the focal plane of the facility concentrator, where the peak thermal irradiance, Q_p , is 72 cal/cm²-s over a 3.8-cm diameter. The thermal irradiance at the cable position (the focal plane) is measured with a Hycal asymptotic calorimeter. The total thermal fluence, Q , of the irradiation is given by $Q = 2.1t_r Q_p$, where t_r is the rise time of the irradiation to the peak irradiance, Q_p .

The cables were irradiated to a total thermal fluence sufficient to completely breach the outer cable jacket. At this fluence, the heat barrier was not breached, and the underlying jacket of the cable core was charred only lightly on the surface. Cutting the cable in half showed that at least three quarters of the inner-jacket thickness was not affected by the thermal radiation. The strength members and the secondary coated fibers also were unaffected.

The thermally irradiated samples were subjected to various mechanical tests -- impact and tensile load -- after thermal testing. The impact tests (described in the previous section) were performed on the cable at the point of maximum thermal exposure, i.e., where the jacket was breached. In the tensile load test, the thermally irradiated section of cable was subjected to a 100-kg

load for five minutes (strain rate was 10 mm/min). All fibers in the thermally irradiated cables survived the impact test and the tensile load test without breaking. Moreover, the cable was stressed to the point of fiber failure after reaching the 100-kg stress (of 5-minute duration) for the tensile load test. Of the five cables tested, the minimum failure level was 284 kg; however, several cables survived levels exceeding 400 kg without failure.

FLAME TEST RESULTS AND COMPARISON WITH THERMAL RADIATION TEST RESULTS

A final test series compared the thermal radiation integrity of the cable to that measured in the flame tests. Flame tests performed on irradiated cables were compared with the thermally irradiated cables. Several unirradiated cables were exposed to a 30-second torch flame application. The length of cable exposed to the flame was 20 mm. The temperature of the torch flame was about 950°C. The cables were held at a 50-degree angle. (Note: the cable was held at a 90-degree angle during the thermal radiation exposure.) When exposed to the flame, the outer cable jacket completely burned off and the underlying heat barrier blackened. No cable material dripped. The cable core was intact. Flaming lasted 50 to 75 seconds after removal of the torch. The cable charred and the lengths of charred cable were 38 to 60 mm.

These flame tests showed minimal flame propagation and minimal burning following removal of the flame. The thermal radiation exposures exhibited qualitatively similar results. Namely, the outer cable jacket was breached, but the inner jacket was not significantly affected. The cable did ignite during the WSSF exposure, but the flame did not persist more than 10 seconds after reaching the peak thermal irradiance. The length of charred cable was about 100 mm.

SUMMARY

A fiber-optic cable designed for use in thermal radiation environments was described. The cable was rugged, had high-bandwidth, and displayed good optical loss characteristics over a wide range of temperatures. The cable had good mechanical stability both before and after thermal exposure. Finally, the cable showed very little burning and flame propagation after being subjected to both a flame test and thermal radiation tests.

BANDWIDTH AND CUT-OFF WAVELENGTH OF SINGLE-MODE LIGHTGUIDE - SYSTEM CONSIDERATIONS

R. W. Tarwater,* M. J. Maslaney,**† D. L. Philen,* F. T. Stone,* and D. G. Duff***

*AT&T Bell Laboratories
2000 N. E. Expressway
Norcross, GA 30071

**Tau-Tron, Inc.
3000 Northwoods Parkway
Norcross, GA 30071

***AT&T Bell Laboratories
Crawfords Corner Road
Holmdel, NJ 07733

ABSTRACT

Measurements on installed single-mode lightguide cables confirm the validity of the straightforward relationships between system bandwidth, fiber dispersion, and laser spectral width predicted by theory. Concatenation measurements of dispersion show that system bandwidth scales inversely with span length, thus eliminating the bandwidth length concatenation uncertainties associated with multimode bandwidth. Field bandwidth measurements using commercially available lasers (FWHM spectral width ≈ 4 nm) showed average bandwidth on 30 km spans of 2.3 GHz at 1316 nm and 256 MHz at 1515 nm. When single longitudinal mode lasers (with spectral widths one to two orders of magnitude narrower than present lasers) become available it will be possible to upgrade system bandwidth by a corresponding one to two orders of magnitude by replacing only the electronics - new cables will not be required. This will make multigigabit upgrades possible on existing cables in either the 1300 or 1500 nm window.

Modal noise measurements were made on systems with lasers transmitting well below the cut-off wavelength of a short fiber section at data rates up to 1.7 Gb/sec and splice losses as high as 3 dB. These measurements show that systems can operate tens of nm below the 5-meter cut-off wavelength of the fiber and still have negligible modal noise even with short lengths of fiber.

1. INTRODUCTION

With the increasingly prevalent use of single-mode lightguide, transmission engineers are faced with new media parameters that define the transmission properties of the media. Each of these must be understood and specified correctly for the overall system transmission performance to be assured. This paper examines two single-mode lightguide media parameters, dispersion (bandwidth) and cut-off wavelength, and their respective impact on system performance.

2. BANDWIDTH

2.1 THEORY

In lightguide media the system bandwidth is a function of the dispersion (pulse broadening) that occurs as light propagates along the fiber. In multimode lightguide there are two dominant types of dispersion - intermodal dispersion and material dispersion. Intermodal dispersion is caused by the various modes having different propagation characteristics. Material dispersion is caused by the wavelength

dependence of the refractive index of the materials in the fiber - that is, the different wavelengths of light present in the source will propagate at different speeds. Single-mode lightguide inherently eliminates intermodal dispersion by eliminating all but a single mode of propagation, leaving material dispersion as the dominant contributor to system bandwidth. The effect of material dispersion can be minimized by selecting a fiber design such that material dispersion passes through zero at the nominal system operating wavelength. The dispersion characteristics of a fiber are typically expressed by specifying a maximum value (in psec/nm-km) for the dispersion over a specified wavelength range and by specifying the maximum, nominal, and minimum values for the zero dispersion wavelength. The total dispersion (in psec) for a given span length (in km) utilizing a source with a given spectral width (Full Width Half Maximum, in nm) is equal to fiber dispersion times source spectral width times span length. This total dispersion (in psec) can also be expressed as bandwidth (in GHz), by assuming a Gaussian response. Equation 1 summarizes.

$$BW = \frac{441}{dWL} \quad (1)$$

Where: BW = System Bandwidth in GHz
d = Fiber Dispersion in psec/nm-km
W = Source FWHM Spectral Width in nm
L = Span Length in km.

Observe that bandwidth scales inversely with length (unlike multimode lightguide bandwidth where the length scaling varies). Also note that system bandwidth is inversely proportional to the source spectral width. Thus, the bandwidth of an installed single-mode system could be upgraded in the future simply by replacing the electronics as narrow-spectrum lasers become available - new cables would not be required.

The following sections summarize the results of two studies that confirm these relationships.

2.2 LENGTH CONCATENATION MEASUREMENTS

The design of long repeater spans of single mode fiber requires that the dispersion and zero dispersion wavelength be well characterized. However, measuring these long lengths may be technically difficult. Usually, one has information on the dispersion for individual fibers that compose a repeater span. This study shows that the dispersion information from individual fibers can be used to predict the dispersion properties of longer concatenated lengths.

The dispersion of the single mode fibers was measured using the pulse delay technique and a fiber-Raman laser. The laser provides narrow pulses that are tunable from 1180 to 1700 nm. The transit time, τ , of a pulse through a fiber of length L is determined as a function of wavelength, and a delay curve calculated by fitting the data to:

† Formerly with AT&T Bell Laboratories.

$$\frac{\tau}{L} = A + B\lambda^2 + C\lambda^{-2} \quad (2)$$

The dispersion is given by the first derivative of the delay curve as:

$$d = 2B\lambda - 2C\lambda^{-3} \quad (3)$$

The dispersion of a concatenated fiber length should be given by a length weighted average of the individual fiber dispersions comprising the span.

$$D = \frac{(L_1 d_1 + L_2 d_2 + \dots + L_n d_n)}{(L_1 + L_2 + \dots + L_n)} \quad (4)$$

This also holds for the zero dispersion wavelength if one is only interested in that parameter.

Fibers used for this concatenation study consisted of two cables each 1.16 km long and each containing 36 fibers. These two cables were spliced together and the zero dispersion wavelength of each 2.32 km fiber path measured. A total of 36 individual fiber paths were available for concatenating into longer lengths. The distribution of zero dispersion wavelengths of the 36 fibers was centered at 1312 nm with no fibers lower than 1306 nm nor higher than 1318 nm. From this set, five concatenated lengths were assembled. These were 6.96 km, 9.28 km, 13.92 km, 20.88 km, and 27.84 km. The zero dispersion wavelength was determined experimentally for each of these five spans. The results of these measurements are shown in Table 1. The estimated uncertainty in the measured zero dispersion wavelength is 2 nm. Table 1 compares the measured and calculated zero dispersion wavelengths for the five spans, and the uncertainty listed for the calculation is the statistical uncertainty obtained by calculating the algebraic sum (one standard deviation). Also listed in Table 1 is the difference between the calculated value and the measured value. In every case, this difference is smaller than the one sigma uncertainty in the calculated value.

The results of this study show that the zero dispersion wavelength (or dispersion curve) of long fiber spans may be accurately predicted from dispersion data from the individual fibers comprising the span.

TABLE 1 Summary of Zero Dispersion Wavelengths for Concatenated Single-Mode Fibers			
Fiber Length (km)	Zero Dispersion Wavelength (nm)		
	Measured	Calculated	Difference
6.96	1311.7	1312.3 ± 1.6	+0.6
9.28	1309.1	1309.6 ± 1.5	+0.5
13.92	1314.2	1314.1 ± 2.6	-0.1
20.88	1311.3	1311.4 ± 1.3	-0.1
27.84	1310.7	1311.5 ± 2.6	-0.8

2.3 FIELD BANDWIDTH MEASUREMENTS

Single-mode bandwidth measurements were performed in the field on a 12-fiber cable section 15 km long. The fibers were spliced together at one end to provide six 30 km lengths.

The fibers were measured using the equipment shown in Figure 1. Measurements were taken with two different laser sources. One laser had a nominal wavelength of 1316 nm and a Full Width Half Maximum (FWHM) spectral width of 3.8 nm. The second laser had a nominal wavelength of 1515 nm and a FWHM spectral width of 5.5

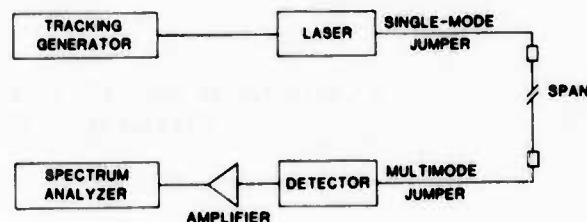


FIGURE 1. BANDWIDTH MEASUREMENT SYSTEM

nm. Measurements with a short strap indicated a measurement system response which was flat to within ± 3 dB out to 1500 MHz. All six 30 km paths were measured with each laser. The fiber loss was low enough at 1515 nm to permit measurements on 60 km lengths also. Thus, three 60 km spans were constructed using the six 30 km sections and measured with the 1515 nm laser.

The measurement procedure consisted of a calibration of the system and then a measurement of each fiber path. The calibration was performed with either a short strap or an optical attenuator inserted between the transmit jumper and the receive jumper. A sweep was then made by the tracking generator and the resulting response stored in the spectrum analyzer's memory. The fiber under test was then inserted between the jumpers and another sweep performed by the tracking generator. The results of this sweep were subtracted from the stored calibration response to produce the fiber response. A reference frequency of 10 MHz was used as baseband, from which the 6 dB (electrical) down point was located. This point defines the 3 dB optical bandwidth.

Table 2 shows the results obtained. At 1316 nm the bandwidth of the fibers exceeded the capabilities of the measurement system. Therefore, measurements were taken at 10 MHz and 1200 MHz and fitted to a Gaussian curve, with Table 2 showing these fitted values. The average bandwidth at 1316 nm was found to be 2340 MHz on the 30 km spans. The average bandwidth at 1515 nm was 256 MHz on the 30 km spans and 123 MHz on the 60 km spans. Dispersion data on each individual fiber was not available. Thus, average values, based on sample measurements, of 1.5 psec/nm-km at 1316 nm and 13 psec/nm-km at 1515 nm were used with Equation (1) to obtain calculated values for comparison. The calculated values are 2.6 GHz for the 30 km span at 1316 nm, 206 MHz for the 30 km span at 1515 nm, and 103 MHz for the 60 km span at 1515 nm. Comparing these to the measured values shows good agreement at both wavelengths.

TABLE 2 Single-Mode Field Bandwidth Measurement Data			
Fiber	Length (km)	Bandwidth (MHz)	
		λ=1316nm	λ=1515nm
1	30	2250	254
2	30	2360	263
3	30	2320	262
4	30	2250	250
5	30	2400	254
6	30	2440	254
1+4	60	-	125
2+5	60	-	122
3+6	60	-	123
Bandwidth at 1316 nm extrapolated using Gaussian fit.			

3. CUT-OFF WAVELENGTH

3.1 THEORY

In single-mode fibers a small portion of the higher-order mode, LP_{11} , can propagate to the end of short lengths of fiber (tens of meters), where it can interfere with the fundamental mode and cause modal noise [1]. Short lengths of cable occur in many instances - riser cables, jumper cables, and repair sections. Cut-off wavelength is the media parameter which a transmission engineer must specify to insure that modal noise is reduced to acceptable levels.

The amount of modal noise generated depends on the amplitude of the LP_{11} mode at the end of the short length of fiber. That quantity is proportional to $\exp(-\alpha_{11}L/2)$ where α_{11} is the attenuation of the LP_{11} mode and L is the fiber length. Therefore, to keep modal noise below a certain value requires that $\exp(-\alpha_{11}L/2)$ be less than some constant (which can be determined from experiment). That in turn requires

$$\alpha_{11}L \geq \text{constant} \quad (5)$$

From cut-off wavelength data and from several theoretical treatments [2-4], a relation between the LP_{11} mode attenuation and the effective cut-off wavelength can be found. Therefore, fixing the minimum attenuation allowed also fixes the maximum cut-off wavelength allowed. Using the methods of References 3 and 4, a particularly useful relation between cut-off wavelength measured on 5-meter lengths of fiber and LP_{11} mode attenuation can be derived:

$$\alpha_{11} = 4(z) \frac{\delta\lambda}{10} \quad (\text{dB/m}) \quad (6)$$

In Equation (6), $\delta\lambda$ is the amount (in nm) by which the 5-meter cut-off wavelength, λ_c , exceeds the operating wavelength, λ , that is, $\delta\lambda = \lambda_c - \lambda$. The quantity z , which can be obtained from theory [2,3] or experiment [4], gives the rate at which α_{11} changes with $\delta\lambda$. The value of z is different for different fiber designs. For the moderately-depressed cladding fibers used, $z \approx 1.43$. In general, z will be larger for matched-cladding designs; that is, for such designs the modal noise increases more rapidly as $\delta\lambda$ (the value by which the cut-off wavelength exceeds the operating wavelength) is increased. Note that Equation (6) yields $\alpha_{11} = 4 \text{ dB/m}$ for $\delta\lambda = 0$.

Putting Equations (5) and (6) together yields a design equation relating the cut-off wavelength of the fiber to the minimum length of fiber allowed in the system:

$$65 \log_{10} \left(\frac{L}{5} \right) - \delta\lambda = C \quad (7)$$

Equation (7) is the same result obtained in Reference 4 for the relation between the cut-off wavelength measured and the length of fiber used for the measurement. The constant C in Equation (7) can be obtained from measurements of modal noise in fiber-optic transmission systems. The next section presents results from such measurements.

3.2 MODAL NOISE MEASUREMENTS

A series of measurements were made using the setup shown in Figure 2. The degradation of the system eye margin caused by modal noise was measured as splice loss and distance between splices were varied. Measurements were made with systems transmitting at 90 Mb/sec, 432 Mb/sec, and 1.7 Gb/sec. In each case the cut-off wavelength of the fiber path between the two splices was chosen to be approximately 20 nm above the laser operating wavelength.

As the loss of the two splices was increased, the system eye margin decreased in a faster-than-linear manner. Therefore, if the worst splice-loss case was examined, a linear interpolation to an intermediate value of splice loss would provide a conservative estimate of the degradation expected for that splice loss. Hence, the detailed experiments on the length dependence of the eye margin degradation (modal noise) were done with 3-dB splice losses.

Figure 3 presents the length dependence obtained using a 432 Mb/sec transmitter and 3 dB splices. To use those results to provide a design formula relating $\delta\lambda$ and L , an eye margin degradation of 1% was allowed. The value of L where the line of Figure 3 crossed the 1% level and the value of $\delta\lambda = 21 \text{ nm}$ were then substituted into Equation (7) yielding $C = -15$ for the 432 Mb/sec system. Other measurements yielded $C = -23$ for the 90 Mb/sec system and $C = -6.7$ for the 1.7 Gb/sec system [5]. Therefore, from Equation (7) we calculate that a system transmitting on a fiber with an effective 5-meter cut-off wavelength 52 nm above the laser wavelength will degrade the eye margin by less than 1% for splice separations as short as 25 meters, data rates as high as 1.7 Gb/sec, and splice losses as large as 3 dB. From these results we conclude that systems can operate several tens of nm below the effective cut-off wavelength of the fiber and still have short lengths of fiber produce negligible modal noise.

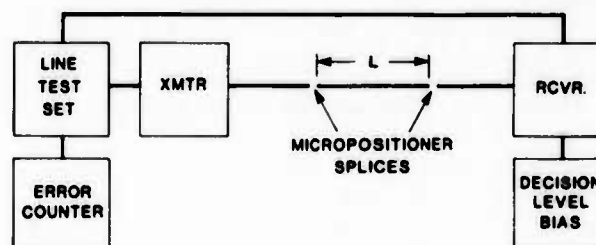


FIGURE 2. MODAL NOISE MEASUREMENT SETUP

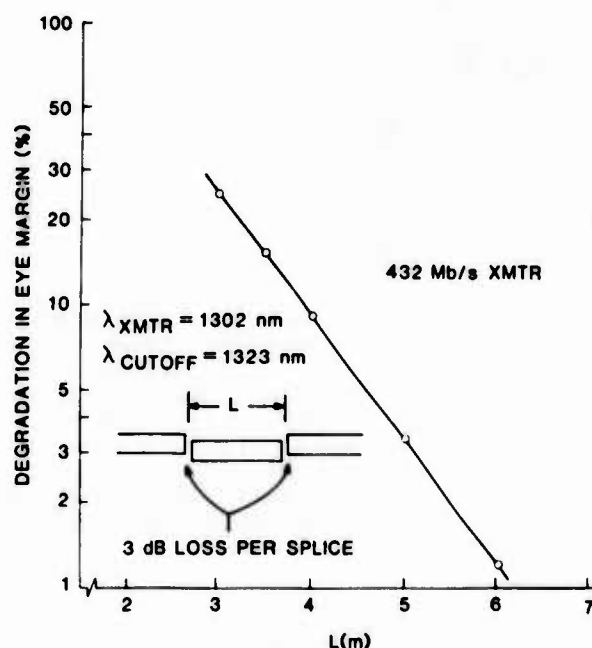


FIGURE 3. THE DEGRADATION OF THE SYSTEM EYE MARGIN (IN %) vs. THE LENGTH OF THE NOISE-GENERATING FIBER.

4. SUMMARY

Measurements on installed single-mode lightguide cables confirm that the system bandwidth of single-mode systems can be accurately predicted when the fiber dispersion, laser spectral width, and span length are known. Concatenation measurements confirm that bandwidth scales inversely with length. Field bandwidth measurements made with commercially available lasers (FWHM ≈ 4 nm) resulted in average bandwidth on a 30 km span of 2.3 GHz at 1316 nm and 256 MHz at 1515 nm.

The degradation of system eye margin due to modal noise was measured on systems operating below the 5-meter cut-off wavelength of the fiber and at data rates as high as 1.7 Gb/sec. These measurements show that modal noise will degrade system eye margin by less than 1% in a 1.7 Gb/sec system transmitting on a fiber with an effective cut-off wavelength 52 nm above the laser wavelength for splice separations as short as 25 meters and splice losses as large as 3 dB.

REFERENCES

1. S. Heckman, *Electr. Lett.* 17, 499 (1981).
2. L. G. Cohen, D. Marcuse, and W. L. Mammel, *IEEE J. Quant. Electr.* 18, 1467 (1982).
3. T. A. Lenahan, *Bell Syst. Tech. J.* 62, 2663 (1983).
4. W. T. Anderson and T. A. Lenahan, *IEEE J. Lightwave Tech.* LT-2, 238 (1984).
5. D. G. Duff, F. T. Stone, and Jingshow Wu, to be published.



Robert W. Tarwater
AT&T Bell Laboratories
2000 Northeast Expressway
Norcross, GA 30071

Robert W. Tarwater received the BSEE degree from the University of Alabama in 1975 and the MSEE degree from the Georgia Institute of Technology in 1977. From 1975 to 1976 he was a design engineer with General Dynamics, Ft. Worth, Texas, working on digital circuit design. In 1977 he joined AT&T Bell Laboratories, Norcross, Georgia, as a Member of the Technical Staff. He is currently a member of the Lightguide Applications and Systems group and is responsible for systems and transmission engineering for single-mode lightguide. He is a member of Tau Beta Pi and Eta Kappa Nu.



Michael J. Maslaney
Tau-Tron, Inc.
3000 Northwoods Parkway
Norcross, GA 30071

Michael J. Maslaney received the B.S. and M.S. degrees in Electrical Engineering from the Georgia Institute of Technology in 1978 and 1979, respectively. From 1979 to 1981 he was a research and development design engineer with the Sources and Analyzer Division of Hewlett Packard, Loveland, Colorado, where he was responsible for high frequency synthesizer design. In 1981 he joined AT&T Bell Laboratories, Norcross, Georgia, as a Member of the Technical Staff. While at Bell Labs, he was responsible for the design of the KS-22839/40 Fiber-Optic Bandwidth Test Set. In 1984 he joined Tau-Tron, Inc., Norcross, Georgia, as Engineering Manager. His current responsibilities include research and new product development in the area of telecommunications test equipment.



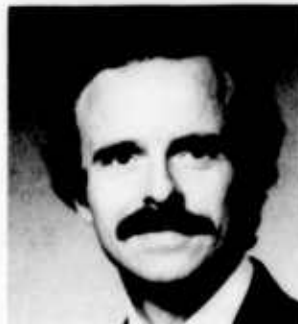
Dan L. Philen
AT&T Bell Laboratories
2000 Northeast Expressway
Norcross, GA 30071

Dan L. Philen received the B.S. degree in Chemistry from Auburn University in 1968 and the Ph.D. degree in Physical Chemistry from Texas A&M University in 1975. From 1976 to 1979 he was a research scientist at Georgia Institute of Technology. Since joining AT&T Bell Laboratories in 1979 he has been engaged in exploratory measurements on optical fiber properties. Dr. Philen is a member of American Chemical Society, Optical Society of America, Sigma Xi, Sigma Pi Sigma, Phi Lambda Upsilon.



Frank T. Stone
AT&T Bell Laboratories
2000 Northeast Expressway
Norcross, GA 30071

Frank T. Stone was born in Brooklyn, NY on August 14, 1938. He received the B.S. degree from Manhattan College, Bronx, NY, in 1960, the M.S. degree from Syracuse University, Syracuse, NY, in 1962, and the Ph.D. degree from the Polytechnic Institute of Brooklyn (now the Polytechnic Institute of New York), Brooklyn, NY, in 1970, all in electrical engineering. From 1960 to 1962 he was a Research Assistant at Syracuse University, working on cryogenic and microwave devices. From 1962 to 1976 he was on the Faculty of the Polytechnic Institute of New York, where his research interests included plasmas, optical communications, and integrated optics. Since joining AT&T Bell Laboratories in 1976 he has been involved in the characterization of fiber optic transmission media. Dr. Stone is a member of the Optical Society of America.



Donald G. Duff
AT&T Bell Laboratories
Crawfords Corner Road
Holmdel, NJ 07733

Donald G. Duff was born in Plainfield, N. J., in 1948. He received the B.S. degree in electrical engineering from the University of Arizona, Tucson in 1970, the M.S. degree in electrical engineering from Stanford University, Palo Alto, in 1971, and D. Engr. degree in electrical engineering from the University of California, Berkeley, in 1977. He joined AT&T Bell Laboratories in Holmdel, N. J., in 1970 and worked on semiconductor device modeling for computer-aided design of integrated circuits. Since 1979 he worked on systems planning and modeling for the FT3C 90 Mb/s wavelength division multiplexed lightwave system. Dr. Duff is a member of Phi Kappa Phi, Tau Beta Pi, and IEEE.

DETERIORATION OF THE SIGNAL QUALITY IN REALISTIC SINGLE-MODE FIBER SYSTEMS

S. Heckmann

Philips Kommunikations Industrie AG
Cologne, West Germany

Summary

In the first part of the paper is shown, in which way the output signal of a generalized system can be calculated for arbitrary analog or digital input signals (multi-path model).

Based on these considerations, the mechanisms, which cause decreasing signal quality in optical systems are discussed. So, for example, linear distortions in a practical single-mode fiber (Intra- and intermodal dispersion) will cause non-linear distortions in the photo current of the receiver.

Then the influence of different disturbance mechanisms is quantitatively analysed, e.g. with respects to signal-to-noise ratio. The theoretically obtained findings have been verified by the results of corresponding experiments.

Introduction

At present, optical communication systems are primarily realized using multimode fibers. The transmission quality of these systems is limited in the main by the spread of the group delay times of the fiber modes. It is for this reason that the single-mode fiber - or rather the fundamental modes fiber - has been considered up until now as the ideal transmission medium.

However, as was demonstrated in 1981, signal distortions caused by interference effects between the various fiber modes must also be expected in systems using single-mode fibers.

If, for instance, a sinusoidal signal is transmitted with an optical system using single-mode fibers, it is possible for the output signal to be distorted in a way shown in the example presented in Fig. 1.

Up to now the causes of disturbance responsible for this and also many other sources of disturbance present in systems of this nature have not, or only partially, been described in literature so that the system engineer in many

cases is not able to identify the causes of disturbance in his particular system and is thus also unable to avoid them.



Fig. 1: Distorted, sinusoidal signal after having been transmitted via a single-mode fiber transmission system.

These sources restrict the measurement accuracy in fiber measurement technology to such a drastic extent under certain circumstances that their identification in this area too is of paramount importance.

It is therefore the aim of this paper to first of all locate by means of highly simplified systems the fundamental causes of signal distortions in systems using single-mode fibers and on this basis to provide an overview of the influence various sources have as well as to indicate the significance of each in practice.

In order to ascertain the fundamental causes of signal distortions in transmission systems using single-mode fibers it is first of all necessary to determine the way in which the system reacts to an arbitrary input signal.

1. Transfer Characteristics of Systems Using Single-Mode Fibers

An optical transmission system is presented schematically in Fig. 2. It is provided with a transmitter on the input side, the optical output $P_T(t)$ of which changes linearly with the signal $V_{In}(t)$ to be transmitted.

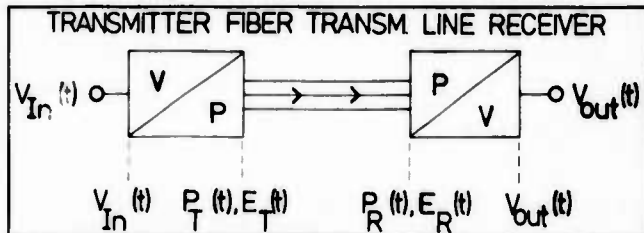


Fig. 2: Schematic representation of a fiber transmission system.

Thus it can be said that:

$$\begin{aligned} P_T(t) &= (A_1 + A_2 \cdot V_{In}(t)) \cdot P_{T0} \\ &= P_T'(t) \cdot P_{T0} \end{aligned} \quad (1)$$

Where $P_T'(t)$ denotes the output power $P_T(t)$ normalized to P_{T0} and is henceforth denoted by the term POWER SIGNAL whereas insignificant constants are signified by A_1, A_2, A_3, \dots

The power-modulated light emitted is coupled into a single-mode fiber line which attenuates the signal by a certain factor C and delays it by group delay time τ .

An optical receiver is situated at the end of the transmission line. This receiver reconverts the incoming optical power $P_R(t)$ linearly into the electrical output signal $V_{out}(t)$.

Therefore:

$$\begin{aligned} V_{out}(t) &= A_3 + A_4 \cdot P_R(t) \\ &= A_3 + A_4 \cdot P_R'(t) \cdot P_{R0} \end{aligned} \quad (2)$$

Whereby $P_R'(t)$ denotes the power signal at the receiver, i.e. the receiver input power $P_R(t)$ related to P_{R0} .

If, at this stage, an explanation is to be given for the non-linear distortions of the signal presented in Fig. 1, it must be ascertained that this is not possible with the described simple linear system.

In order to determine the fundamental causes of signal distortions in systems using single-mode fibers, it is therefore necessary to start with describing the behaviour of the three components comprising transmitter, transmission line and receiver in more detail.

It is assumed here that the electrical parts of the transmitter and of the receiver are ideally suited.

1.1 Transmitter Properties

In order to trace the fundamental causes of signal distortions, the optical source used in the transmitter should be a laser which generates a monochromatic, i.e. sinusoidal carrier of frequency ω_0 .

This carrier is linearly modulated in relation to the power by input signal $V_{In}(t)$ (Eq. 1).

If, at this stage, the transmission behaviour of an optical communication system is to be defined more closely then the actual output quantity of the transmitter, the field intensity impressed into the transmission medium ($E_T(t)$) must be known.

It can be stated in the form of an analytical signal:

$$E_T(t) = r_T(t) \cdot E_{T0} \cdot \exp(j\omega_0 t) \quad (3)$$

Here, the actual signal information is contained in the so-called FIELD INTENSITY SIGNAL $r_T(t)$. E_{T0} represents a complex vector.

As the power is by and large equal to the square of the electrical field intensity, it is true that

$$P_T'(t) = |r_T(t)|^2 \quad (4)$$

so that the field intensity signal is produced by calculating the square root of the power signal.

$$r_T(t) = (P_T'(t))^{1/2} \quad (5)$$

Consequently, even in the event of the power spectrum being band-limited, there exists an infinitely broad field intensity spectrum in general.

If

$$P_T'(t) = 1 - a \cdot \cos(\omega_m t) \quad (6)$$

is selected, then the respective spectrum and thus also the power spectrum consists of three lines at $-\omega_m, 0, +\omega_m$.

$r_T(t)$, which equals the square root of $P_T'(t)$ thus shows, as is presented in Fig. 6, a non-sinusoidal variation.

If the frequency spectrum of $r_T(t)$ is computed,

the respective Fourier series contains an infinite number of terms.

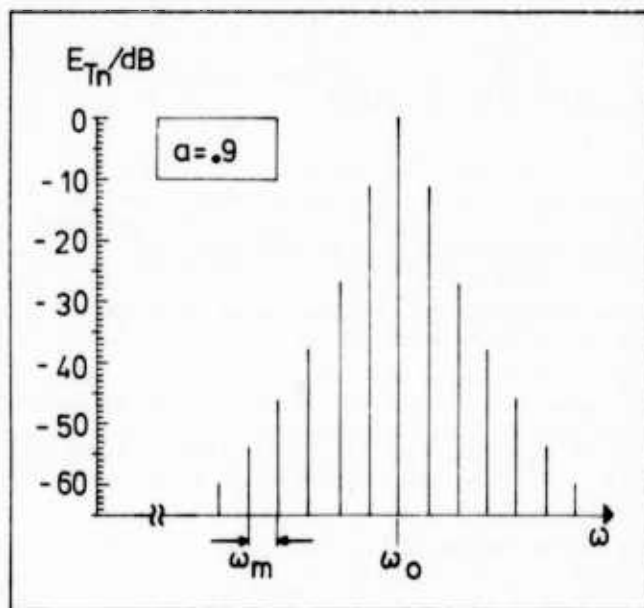


Fig. 3: Magnitude of the amplitude spectrum with sinusoidal power modulation.

Fig. 3 shows the amplitude frequency spectrum of Eq.3 relative to the amplitude of the spectral line at ω_0 which apart from a shift by ω_0 corresponds to the spectrum of $r_T(t)$. In Eq.6, the value selected for a is 0.9.

Besides the wanted power output modulation, unwanted frequency modulation must always also be taken into consideration with a real laser which, amongst other things, is to be ascribed to a temperature modulation of the laser resonator.

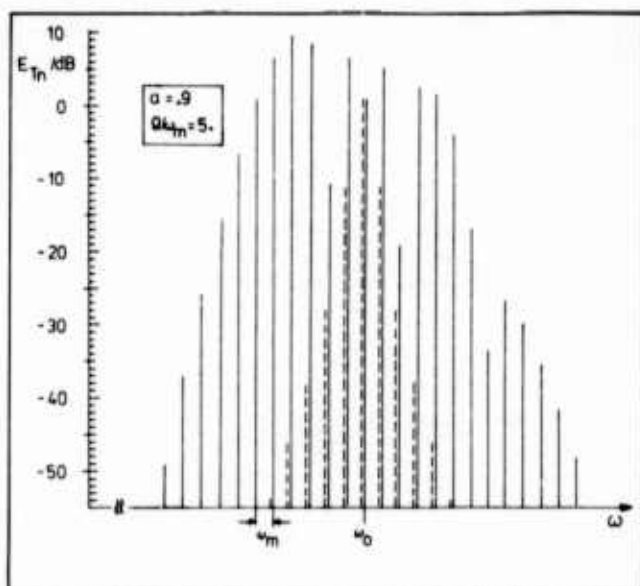


Fig. 4: Magnitude of the amplitude spectrum with sinusoidal power and unwanted frequency modulation

As a result of a signal-correlated unwanted frequency modulation, the spectrum shown in Fig.3 is in general drastically widened.

In Fig.4, the spectrum shown in Fig.3 is represented by dashed lines. The frequency deviation is denoted by Ω . Apart from the signal-correlated unwanted frequency modulation, a frequency modulation dependent of ambient temperature must also be considered. This reduces the signal-to-noise ratio of the system.

The next component to be analysed is the transmission line with regard to its properties.

1.2. Transmission Line

In an ideal transmission line using single-mode fibers only one mode and consequently only one transmission channel should exist which exhibits properties which are independent of frequency, time and level.

In practical systems, however, it must be noted that on the one hand the properties of a channel are of course not ideal (e.g. dependency of the group delay time on frequency) and that, on the other hand, a number of modes propagates, i.e. parallel transmission channels are present.

Basically the independency on time of the properties cannot be assumed too. The geometric length of the transmission line for example, alters with changes in ambient temperature. This dependency on time again also causes a reduction in the signal-to-noise ratio. No further attention, however, is to be given to this in this section.

In order to determine the transfer characteristic of a line using single-mode fibers, the field intensity (Eq.3) impressed by the transmitter is assumed as the input signal. Calculation of the transmission properties can then be performed as follows:

- The first stage is to determine the amplitudes of the fiber modes by calculating the overlap integrals¹ for the laser mode(s) and fiber modes.
- If the frequency spectrum belonging to each mode is multiplied by the relevant propagation factor and the output spectra added, the overall frequency spectrum at the end of the fiber is produced.
- If a second fiber follows, the coupling coefficients between the modes of the first fiber and the modes of the second fiber be ascertained by working out the overlap integrals. With the aid of the relevant propagation factors of the second fiber, it is possible to ascertain the spectrum at the end of the second fiber. The same procedure applies to further transmission media. After the optical output spectrum has undergone inverse Fourier transformation, the time-dependent field distribution is present at the receiver which can be represented in the form of an analytic signal.

Discussion of the transmission behaviour of the transmission line is to be continued using two simple examples.

1.2.1 Line with One Transmission Channel. If a transmission path is assumed which consists of single-wave single-mode fibers, then the receiver field intensity $E_R(t)$ can be described as follows:

$$E_R(t) = r_R(t) \cdot E_{RO} \cdot \exp(j\omega_0 t) \quad (7)$$

In this equation, $r_R(t)$ describes the relevant field intensity signal at the receiver. E_{RO} is a complex vector.

If a constant attenuation C and group delay time τ i.e. ideal properties of the transmission channel, are presupposed, then the field intensity signal $r_R(t)$ is produced from the frequency spectrum of the transmitter field intensity signal to be

$$r_R(t) = r_T(t - \tau) \quad (8)$$

by inverse Fourier transformation.

The receiver field intensity signal therefore represents the transmitter field intensity signal delayed by the group delay time.

In reality, the properties of the transmission channel are, of course, amongst other things, dependent on frequency.

If, for example, the group delay time is dependent on frequency then the individual spectral components of the field intensity signal will be delayed by different amounts.

The field intensity signal is therefore linearly distorted as a result of a dependency on frequency of the channel properties.

1.2.2 Line with Parallel Transmission Channels.

The behaviour of a transmission line with parallel channels is to be discussed using the example of the simplest system belonging to this category.

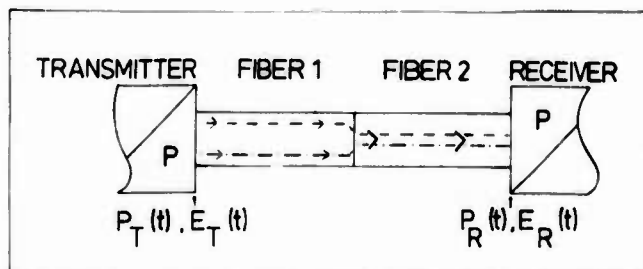


Fig. 5: Schematic representation of a transmission line with two transmission channels.

A transmission line is assumed which contains two parallel transmission channels.

The line represented in Fig. 5 consists of two series-connected single-mode fibers, of which the first fiber conducts two modes, e.g. two orthogonally polarised LP_{01} -modes or, for operation above the cut-off frequency of the LP_{11} -modes, a LP_{01} -mode and a LP_{11} -mode and where, in the second fiber, which for example is coupled via a fiber connector, only one LP_{01} -mode exists.

In this case, there are therefore two transmission channels which in Fig. 5 are represented by a dashed and a dash-and-dot line.

The receiver field intensity is produced accordingly by superposition of the output fields of the individual transmission channels in which the field intensity signals, delayed by different amounts, are contained:

$$E_R(t) = r_{R1}(t) \cdot E_{RO1} \cdot \exp(j\omega_0 t) + r_{R2}(t) \cdot E_{RO2} \cdot \exp(j\omega_0 t) \quad (9)$$

Under the assumption that the properties of the transmission channels are ideal, the receiver field intensity signals $r_{R1}(t)$ and $r_{R2}(t)$ are produced from Eq. 8 whereby τ must be substituted by the relevant group delay time of the channel, i.e. by τ_1 or τ_2 .

The expression resulting from Eq. 9 for $E_R(t)$ comprises two addends since two transmission channels have been assumed.

If the line is composed, for example, of three transmission media, whereby m -modes exist in the first medium, n -modes in the second medium and q -modes in the third medium, then the expression for the receiver field intensity consists accordingly of $m \cdot n \cdot q$ addends which in form correspond to those in Eq. 9.

The receiver field intensity is the input quantity for the third component, for the receiver.

1.3. The Receiver

The receiver should convert the optical power $P_R(t)$ falling onto the receiver's detector linearly into the output signal $V_{out}(t)$ (Eq. 2). Here the Poynting vector $P_R(t)$ on the detector surface is proportional to the square of the field intensity $E_R(t)$ at the receiver input, i.e.

$$P_R(t) = A_5 \cdot |E_R(t)|^2 \quad (10)$$

In Eq. 10, it must be noted that $E_R(t)$ and consequently $P_R(t)$, are not only dependent on time t but also on the location on the detector surface A .

For the sake of clarity, this dependency has not been included in the argument.

The overall power $P_R(t)$ is produced by integration of the Poynting vectors on the detector surface:

$$P_R(t) = \int_A P_R(t) dA \quad (11)$$

As the relationship between the receiver power $P_R(t)$ and the output signal $V_{Out}(t)$ of the system is already known from Eq. 2, the transmission behaviour of systems using single-mode fibers can now be ascertained.

2. Fundamental Causes of Signal Distortions in Transmission Systems Using Single-Mode Fibers

2.1 Single-Channel Transmission

The purpose of this section is to discuss the fundamental causes of signal distortions in systems in which only one transmission channel exists.

If the integration is performed in accordance with Eq.11, the receiver power signal (Eq.2) to

$$P'_R(t) = |r_R(t)|^2 \quad (12)$$

is produced. As already shown, the field intensity signals of the transmitter and receiver correspond apart from a constant delay τ provided ideal channel properties prevail.

Owing to the quadratic relationship between the relevant power- and field intensity signals (Eq.4, Eq.12), the power signals of input and output only differ from one another by the fixed delay time τ .

If the channel properties, however, are dependent on frequency, then the field intensity signal undergoes linear distortions upon transmission.

What significance does this have for the power signal?

As is seen from Fig. 6, the field intensity signal exhibits a non-sinusoidal variation in the case of a sinusoidal power signal and the respective frequency spectrum is infinitely broad (Fig. 3 and Eq. 3).

If the field intensity signal is now distorted, for example, by a dependency on frequency of the group delay time as shown in Fig. 6, then shape-distortions must be expected of the power signal too.

Shape-distortions of a sinusoidal signal can, however, only be explained by non-linear

distortions.

Generally, it can be stated that:

The signal is linearly and non-linearly distorted during single-channel transmission if the channel properties are dependent on frequency.

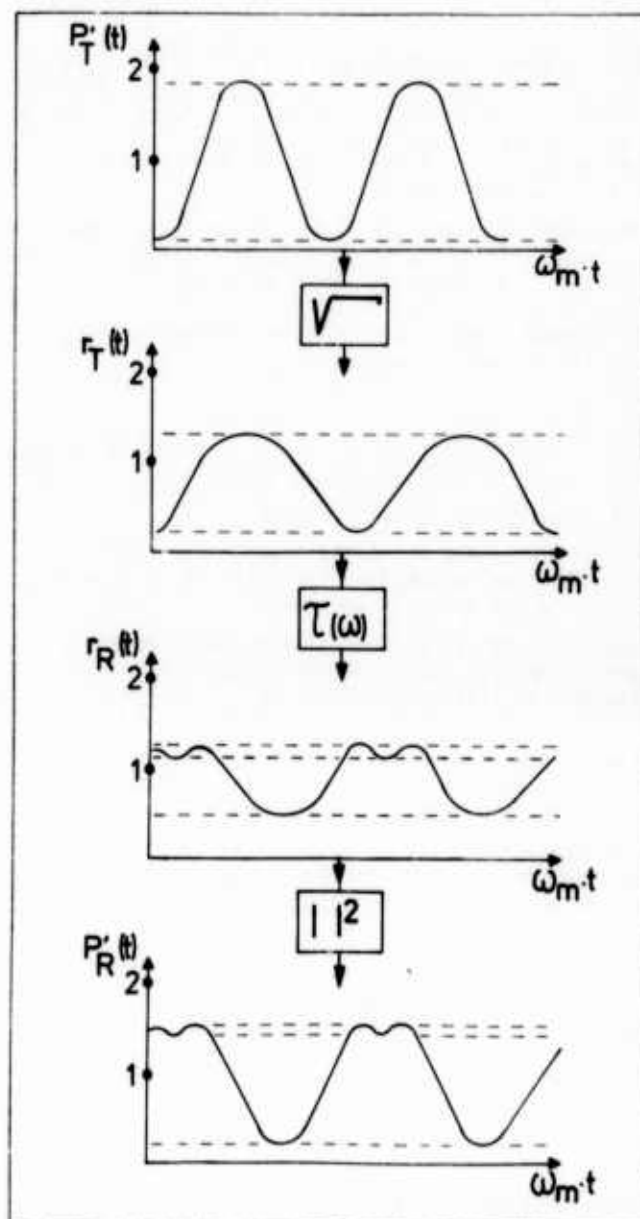


Fig. 6 Distortion of the power signal by a frequency-dependent group delay time in the transmission line.

As appropriate calculations show, the signal-to-noise ratio is not significantly reduced by non-signal-correlated changes in the laser frequency or the transmission line properties occurring in practice.

Generally, it can be said that:

The signal-to-noise ratio is in practice not reduced during single-channel transmission.

2.2 Multi-Channel Transmission

Apart from signal distortions caused by the real properties of the individual transmission channel, further distortions must be expected if the signal is transmitted via parallel channels.

As demonstrated in Section 1.2.2, the receiver field intensity is produced by superposing the fields of the individual channels.

If, once again, the simplest model of a multi-channel transmission line, a line consisting of 2 parallel ideal channels is assumed then the following expression for $P_R(t)$ is produced from Eq. 9 - Eq. 12:

$$P_R(t) = P_{R1}(t) + P_{Rn1}(t) \quad (13)$$

with

$$P_{R1}(t) = P_{R1}'(t) \cdot P_{R01} + P_{R2}'(t) \cdot P_{R02}$$
$$P_{Rn1}(t) = (P_{R1}'(t) \cdot P_{R2}'(t))^{1/2} \cdot P_{R03}$$

After calculation of the absolute value and after integration, three terms are produced which are allocated to the detector powers $P_{R1}(t)$ and $P_{Rn1}(t)$. The $P_{R1}(t)$ element is formed by adding up two differently attenuated and delayed power signals corresponding to the two transmission channels.

This element consequently represents a linearly distorted power signal.

The power element $P_{Rn1}(t)$ contains, amongst other things, the square-root of the product of two power signals delayed by differing amounts and must be ascribed to interference of the output fields of the two transmission channels. It therefore represents an element which corresponds to a non-linearly distorted power signal.

Generally, it can be said that:

The signal is always distorted linearly during multi-channel transmission.

The existence of non-linear distortions and the reduction of the signal-to-noise ratio where non-signal-correlated changes of system parameters take place depends on the field distributions at the receiver input.

If the field distributions are orthogonally arranged then the integrations (cf. Eq. 11) over the interference terms produce the value zero.

In the case for two transmission channels, P_{R03} (Eq. 13) then results in zero.

Generally, it can be said that:

Non-linear distortions and a reduction in the signal-to-noise ratio must be expected if the orthogonality of the output field distributions of the transmission channels is disturbed.

3. Overview of the Signal Distortions in various Single-Mode Fiber Transmission Systems

In this section the influence of various disturbance mechanisms in transmission systems using single-mode fibers is analysed. The aim here is not to describe the properties of the respective systems completely, but primarily to show the type and extent of the distortions in an exemplary fashion.

(i) Thus, the fundamental cause of the distortions is stated in each case.

(ii) The significance of the distortions is indicated. Where necessary, the results of experiments are given and quotes mentioned in which the effects have already been described.

(iii) The distortions are given quantitatively for typical system parameters.

In this connection, the linear distortions (LD) and non-linear distortions (NLD) are characterized with the aid of a sinusoidal input signal $V_{In}(t)$.

If the frequency of the input signal is altered between 0 and the value ω_m , the change in the amplitude of the sinusoidal output signal $V_{Out}(t)$ is regarded as a measure of the LD. This change in amplitude is denoted by B.

The NLD are characterized by the distortion factor K_1 , i.e. by the relationship of the amplitudes of the first harmonic to the fundamental oscillation.

The signal-to-noise ratio (SNR) is characterized with the aid of a DC signal $V_{In} = \text{const.}$

The relationship of the mean value of $P_R(t)$ to the root-mean-square value of the fluctuations superposed on the mean value is denoted as SNR^7 .

3.1 Influence of a Frequency-Dependent Attenuation or Group Delay Time

A single-channel transmission line is assumed.

(i) LD related to the field signal are the fundamental cause (Section 2.1.).

(ii) The LD and the reduction of the SNR can be disregarded. The NLD are only of significance on particular cases where line lengths are long and, in the event of the group delay time being frequency-dependent, where modulation frequencies are high².

(iii) $K_1 = -40$ dB ($\omega_m = 2 \cdot \pi \cdot 1$ KHz, $\Omega = 2 \pi \cdot 30$ GHz, length of the line: 10 Km, operating frequency near OH-peak, hence considerable frequency-dependent attenuation change = .05 dB / (Km · nm))

$K_1 = -50$ dB ($\omega_m = 2 \cdot \pi \cdot 200$ MHz, $\Omega = 2 \pi \cdot 1$ GHz, length of line: 10 Km, frequency dependence of the group delay time: 100 ps/(Km · nm)).

3.2 Influence of Reflections in Connectors or Fibers

A transmission line is assumed which comprises two series-connected single-wave fibers.

(i) A resonator realized by a fiber or a connector behaves as a transmission line with an infinite number of parallel channels with different attenuations and group delay times.

(ii) As the field distributions of the channels are identical, the development of LD is in all cases also accompanied by NLD and a reduction in the SNR. In connectors only the NLD are of significance³. In addition, reflections in fibers also reduce the SNR⁴.

(iii) $K_1 = -46$ dB ($\omega_m = 2 \cdot \pi \cdot 1$ KHz, $\Omega = 2 \pi \cdot 30$ GHz, displacement in the connector: 0.1 mm, 4% reflections)

$K_1 = -34$ dB, SNR = 25 dB ($\omega_m = 2 \cdot \pi \cdot 1$ KHz, $\Omega = 2 \pi \cdot 30$ GHz, length of the fiber: 1 m, 4% reflections)

3.3 Influence of Multimode Lasers or LED's

A single-channel transmission line is assumed.

(i) In the case of the multimode laser, the signal is modulated upon each of the optical carrier frequencies. A corresponding number of parallel transmission channels exists. A system with a LED as the source can be regarded as a system with an infinite number of parallel channels.

(ii) If the mode spectrum generated is constant (no mode-partition noise), neither NLD nor a reduction in SNR is ascertainable. Although the field distributions of the channels are identical

the non-linear power elements (Eq.13) in the frequency are displaced by the amounts of the differential frequencies of the optical carrier frequencies.

Therefore, only LD are of significance⁵.

(iii) $B = -20$ dB ($\omega_m = 2 \cdot \pi \cdot 200$ MHz, $\Omega = 2 \pi \cdot 1$ GHz, length of the line: 10 Km, line width of the optical source (FWHM): 5 nm, frequency-dependency of group delay time: 100 ps/(Km · nm)).

NLD or a reduction in the SNR is noticeable when the generated mode spectrum of the source changes in a way dependent on signal or with time.

If, for example, with a single-mode laser, an erratic change in the carrier frequency occurs when a certain injection current is exceeded (mode hopping), then the line attenuation and/or the group delay time will also change erratically.

This is schematically represented in Fig. 7:

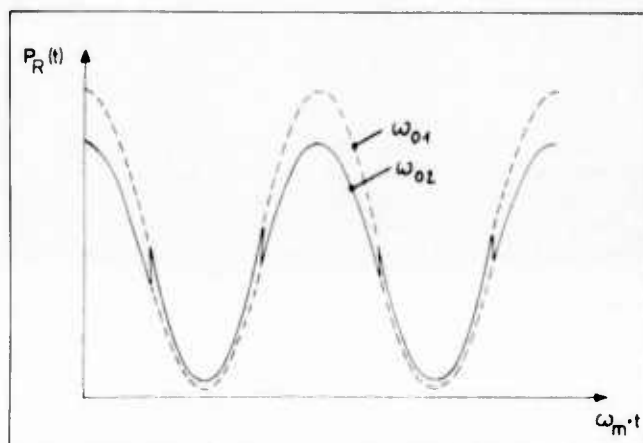


Fig. 7 Schematic representation of a sinusoidal signal distorted by "mode hopping"

In this figure is assumed that the transmitter is coupling a sinusoidal power signal into the line.

The line attenuation for the frequency of ω_{01} should be less than for the frequency of ω_{02} . Once a certain injection current has been reached or, more precisely, a certain temperature, the laser carrier frequency hops from ω_{01} to ω_{02} or vice versa.

An appropriate experiment was conducted using a single-mode laser (HLP 1000 type).

A single-mode fiber of 1.5 m in length, which was operated above the cut-off frequency of the LP_{11} -modes and which behaved like a Fabry-Perot interferometer, was used as the frequency-dependent attenuating transmission medium.

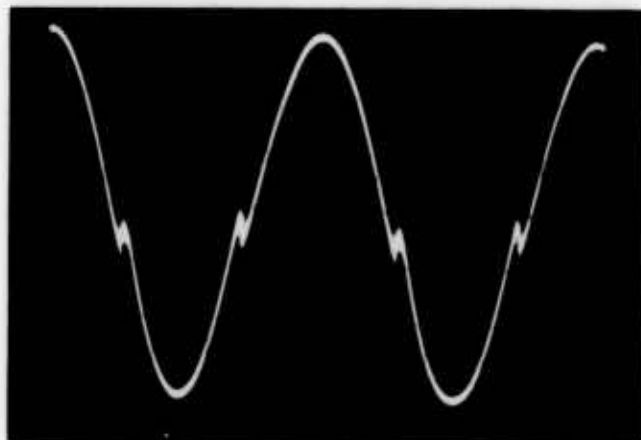


Fig. 8: Experimental demonstration of the influence of "mode hopping" on a sinusoidal signal to be transmitted.

It was possible to observe the respective output signal ($V_{out}(t)$) represented in Fig. 8 when the transmission line was coupled to the laser with low-level reflections. Where reflections back to the laser were high, several mode hops occurred. In the respective oscillogram shown in Fig. 1, the generated carrier frequency therefore hops back and forth between four different values in a way dependent on the injection current.

3.4 Influence of the Difference in Delay Time of the Orthogonally Polarized LP_{01} -modes of the Single-Mode Fiber.

A transmission line is assumed which comprises two series-connected single-mode fibers.

(i) In each fiber, two orthogonally polarized LP_{01} -modes are capable of propagation which differ from each other in their group delay times. Depending on the azimuthal orientation of the first fiber to direction of polarization of the laser light and the azimuthal orientation of the fibers towards each other at the coupling point, 1 to 4 transmission channels exist.

(ii) Depending on the azimuthal orientation of the fibers, LD and/or NLD occur where modulation frequency is high⁶.

(iii) $K_1 = -17\text{dB}$, $B = -2\text{dB}$ ($\omega_m = 2\pi \cdot 200\text{MHz}$, $\Omega = 2\pi \cdot 1\text{GHz}$, length of each fiber: 10 Km, respective group delay time difference: 250 ps, angle between directions of polarization of the laser light and a LP_{01} -mode: 45° , angle between the directions of polarization of a LP_{01} -mode of the first fiber to a LP_{01} -mode of the second fiber: 45°).

3.5 Influence of Polarization-Selective Components

A transmission line is assumed which contains a single-mode fiber and a polarization-selective component connected downstream.

(i) As two LP_{01} -modes are capable of propagation, 2 transmission channels exist. If for example, a polarizer which simulates an integrated optical circuit, is connected downstream of the single-mode fiber, then the orthogonality of the field distributions of the two channels is more or less disturbed depending on the azimuthal orientation of the polarizer.

(ii) In general, a high amount of LD and NLD as well as a drastic reduction in the SNR occur. In a transmission experiment, a single-mode fiber 2 km in length was coupled to a laser (HLP 1000) in such a way that both LP_{01} -modes were excited. A digital signal was used as the transmitter input signal. No distortions were visible when the polarizer set up at the end of the fiber was suitably positioned.

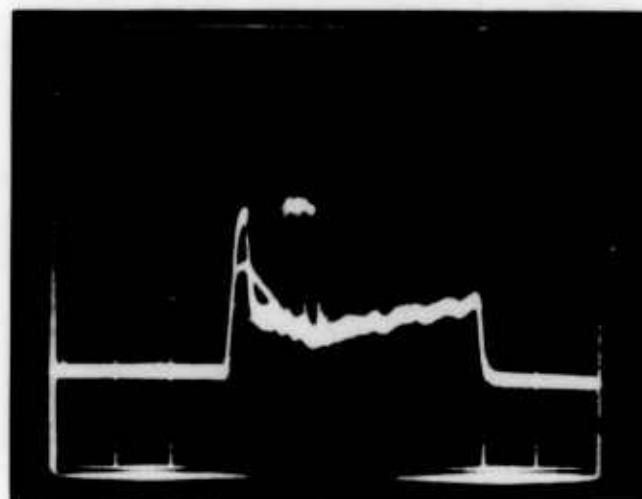


Fig. 9: Distortion of a digital pulse by a polarizer located at the end of a single-mode fiber 2 Km in length.

In Fig. 9, a non-selected polarizer position has been adjusted. Heavy distortions of the digital pulse are recognisable which must be ascribed to the fact that the carrier frequency within the pulse changes due to heating.

The ambiguity of the output signal must be ascribed to "mode hopping".

3.6 Influence of a Single-Mode Fiber Operated Above the "Cut-Off"

A transmission line is assumed which comprises two single-mode fibers connected in series.

(i) In the first fiber, 2 orthogonally polarized LP_{01} -modes and 4 LP_{11} -modes are capable of propagation. In this case, depending on the azimuthal orientation of the fibers and the transversal displacement at the coupling points, 1 to 12 parallel channels exist.

(ii) In general, high LD and NLD as well as a drastic reduction in the SNR occur ⁷. In a transmission experiment, a fiber of 15 m in length operated above the cut-off frequencies of the LP_{11} -modes was coupled to a transmitter with a laser (HLP 1000) in such a way that the LP_{01} -modes as well as the LP_{11} -modes were excited. A subsequent single-mode fiber 5 m in length transmitted the signals to the receiver. The transmission line behaved as a system with 2 parallel channels as only the delay times of the LP_{11} -modes differ considerably from those of the LP_{01} -modes in the first fiber. To begin with, a sinusoidal signal was fed to the transmitter. Upon adjusting a transversal displacement between the fiber axes at the common coupling point, the output signal shown in Fig. 10 was observed.

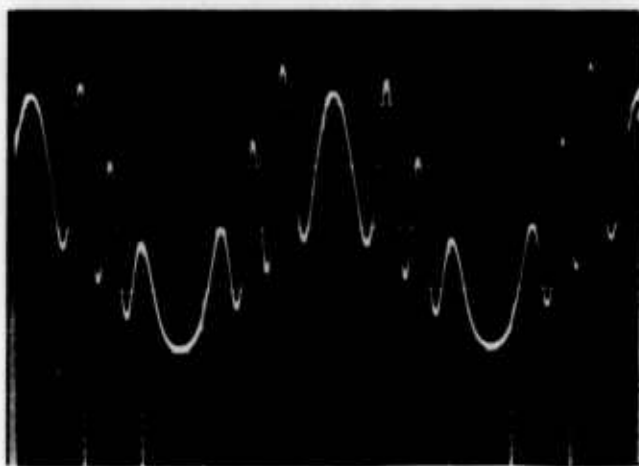


Fig. 10: Distortion of a sinusoidal signal by the LP_{11} -modes of a single-mode fiber 15 m in length.

If the transfer characteristic of the system is calculated theoretically in accordance with the way outlined in Section 1, then an output signal is produced which corresponds well to the one ascertained in the experiment (Fig. 11). The delay time difference between the LP_{11} -modes and the LP_{01} -modes is denoted by Δt . D_0 and D_1 represent the transversal displacement at the beginning and end of the first fiber in relation to the core radius.

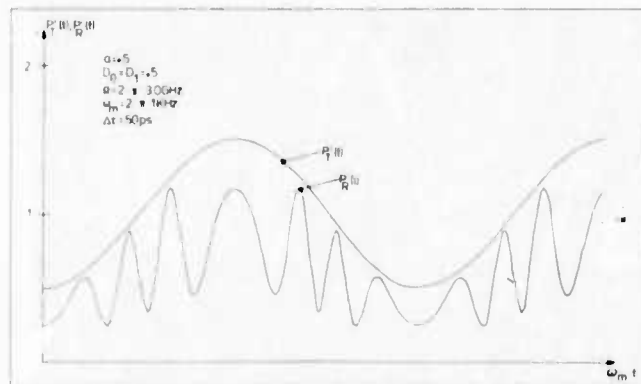


Fig. 11: Calculated influence of the LP_{11} -modes on signal distortion under the conditions belonging to Fig. 10.

If a digital signal is transmitted, a pulse of the output signal looks like that shown in Fig. 12.

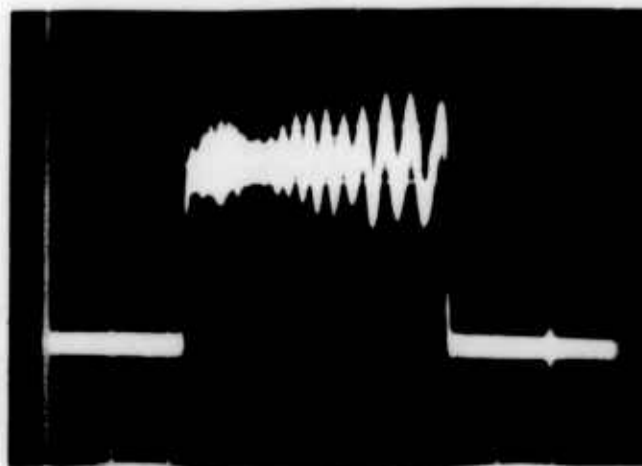


Fig. 12: Distortion of a digital pulse by the LP_{11} -modes of a single-mode fiber 15 m in length.

3.7 Influence of Cladding Modes

(i) If in a transmission line cladding modes are excited in the last single-mode fiber before the receiver and these reach the detector, then a large number of parallel transmission channels exists.

(ii) If the detector surface is of such a size that the entire cladding modes field is completely detected, then only LD occur. If the detector surface is too small, then the orthogonality is disturbed and heavy NLD too and a reduction in the SNR become apparent. In a

transmission experiment, the single-mode laser was coupled via a longitudinal displacement to a single-mode fiber 5 m in length. After a misalignment of the detector the sinusoidal signal transmitted looked distorted as shown in Fig. 13:

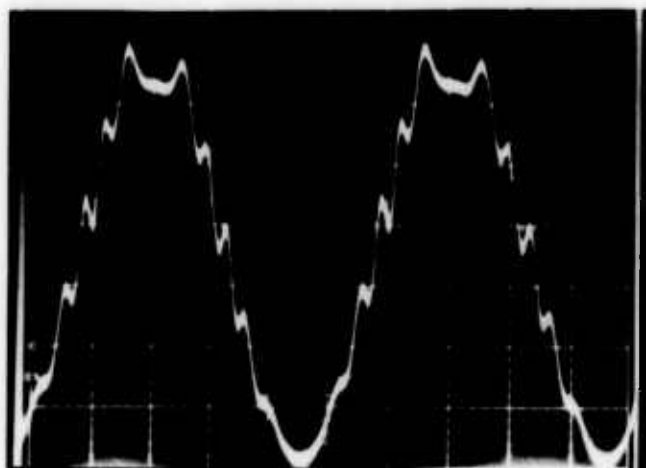


Fig. 13: Distortion of a sinusoidal signal by cladding modes.

Conclusion

The fundamental causes of signal distortions in transmission systems using single-mode fibers were deduced.

As is seen from the overview of the various systems, heavy distortions are chiefly generated by

- Reflections
- Imperfect properties of the optical sources
- Polarizations-selective components
- Single-mode fibers operated above "cut-off"
- and by cladding modes.

Careful consideration must be given to these points when designing transmission systems and measuring equipment.

Acknowledgement

The author would like to thank E.-G. Neumann for many helpful discussions and R.B. Hemmann and E. Meier-Engelen for their support in making this paper possible.

References

- 1 D. Marcuse, "Theory of dielectric optical waveguides", Academic Press, New York 1974
- 2 G.J. Meslener, "Dispersion-induced harmonic distortion in fiber systems using coherent light sources" Proceedings Fifth Topical Meeting on Optical Fiber Communication, THFF 4, Phoenix (Arizona) 1982
- 3 H. Kuwahara, M. Goto, "Generation of harmonic distortion at fibre connectors" Electronic Letters, Vol. 17, No. 18, p. 626 ff, 81
- 4 W. Eickhoff, "Multiple-scattering noise in single-mode fiber systems", Proceedings 7th European Conference on Optical Communications, P4, Copenhagen 1981
- 5 D. Marcuse, "Propagation of pulse fluctuations in single-mode fibers" Applied Optics, Vol. 19, No. 11, p. 1856 ff, 1980
- 6 K. Petermann, "Nonlinear transmission behavior of a single-mode fiber transmission line due to polarization coupling" Journal of Optical Communications, No. 2, p. 59 ff 1981
- 7 S. Heckmann, "Modal noise in single-mode fibers operated slightly above cut-off" Electronics Letters, Vol. 17, No. 14, p. 499 f, 1981

Siegfried Heckmann was born in Wuppertal, Germany in 1951. He studied at the University of Bochum and graduated in 1978 in electrical engineering. 1983 he obtained his doctorate at the University of Wuppertal on the basis of his thesis on a subject taken from the field of communication engineering. Since 1983 he has been active as group leader in the development of P&G Telecommunication Cables and Systems, a member of Philips Kommunikations Industrie AG, where he is responsible for the development of optical measuring equipment.



DESCRIBING DISPERSION IN CONCATENATED SINGLE-MODE FIBER CABLES

Tom C. Olson, Felix P. Kapron, and Tom W. Geyer

ITT Electro-Optical Products Division, Roanoke, VA 24019-0065

SUMMARY

Several empirical data fits are used to describe the chromatic dispersion coefficient of a single-mode fiber in terms of two or three parameters: the zero-dispersion wavelength, the dispersion-slope, and (for one fit) the dispersion-curvature. These fits are then applied to fibers both before and after cabling and to various cable concatenations. Concatenation formulae are given and tested that will enable the system designer to predict end-to-end link dispersion from simple specifications on the constituent cable sections.

INTRODUCTION

It is well known that the total attenuation of a concatenated fiber link can be predicted if the length and attenuation coefficient of each cable section has been measured beforehand. With respect to dispersion or bandwidth, the situation for multimode fiber is considerably less well defined. However, for single-mode fiber, we show that the total chromatic dispersion of a link is predictable from the length and dispersion coefficient of each constituent section. This will assist in system design, and it can reduce any need for link measurements in the field.

First we review how fiber dispersion can be accurately specified in terms of two or three parameters. Then we look for changes in these dispersion parameters as a result of the cabling process. The cable structure is briefly described. Tentative rules for predicting concatenated fiber dispersion are developed. This dispersion is expressed in terms of concatenated dispersion parameters derived from the dispersion parameters of the individual cable lengths. Finally, these rules are

tested by joining fibers within a cable together in several combinations.

METHOD OF MEASUREMENT

The experiment was designed to use single-mode fibers manufactured by both ITT EOPD and another supplier. The fibers were of the dispersion-unshifted (EIA Class IVa) type: optimized for the 1.3 μm wavelength region, although they could be used at 1.55 μm . Numerous group delay versus wavelength measurements were performed on fibers in various combinations described below. We used the common technique of a mode-locked Q-switched Nd: YAG laser pumping a Raman fiber [1] to generate pulses at the multiple wavelengths required. The normalized spectral group delay $\tau(\lambda)$ was in each case fit to three empirical expressions [2] adapted from the literature. The chromatic dispersion coefficient is $D(\lambda) = d\tau/d\lambda$, the wavelength derivative of these expressions.

For dispersion-unshifted fibers, an often used fit to the spectral delay, using λ^2 and λ^{-2} terms, can be written in the form

$$\tau_1(\lambda) = \tau_0 + \frac{S_0}{8} \left(\lambda - \frac{\lambda_0^2}{\lambda} \right)^2 \quad (1a)$$

where τ_0 is the minimum delay (in ps/km) at zero-dispersion wavelength λ_0 (in nm). The chromatic dispersion coefficient (in ps/km-nm) is then

$$D_1(\lambda) = \frac{S_0}{4} \left(\lambda - \frac{\lambda_0^2}{\lambda} \right) \quad (1b)$$

where S_0 (in ps/km-nm²) is the value of the dispersion-slope $S(\lambda) = dD/d\lambda$ at λ_0 . Another expression in which dispersion is proportional to $(\lambda - \lambda_0)/\lambda^2$ is

$$\tau_2(\lambda) = \tau_0 + S_0 \lambda_0^2 \left(\frac{\lambda_0 - \lambda}{\lambda} + \ln \frac{\lambda}{\lambda_0} \right) \quad (2a)$$

$$D_2(\lambda) = S_0 \left(\frac{\lambda_0}{\lambda} \right)^2 (\lambda - \lambda_0) \quad (2b)$$

Finally, a Taylor-expansion may be written

$$\tau_3(\lambda) = \tau_0 + \frac{S_0}{2} (\lambda - \lambda_0)^2 - \frac{C_0}{6} (\lambda - \lambda_0)^3 \quad (3a)$$

$$D_3(\lambda) = S_0 (\lambda - \lambda_0) - \frac{C_0}{2} (\lambda - \lambda_0)^2 \quad (3b)$$

where C_0 (in ps/km-nm³) is the dispersion-curvature $C(\lambda) = -dS/d\lambda$ at λ_0 . The quantities λ_0 , S_0 , and C_0 are called the dispersion parameters for the dispersion coefficient. Near the zero-dispersion wavelength, all forms are reduce to the linear approximation $D(\lambda) \approx S_0 (\lambda - \lambda_0)$.

As an example for one of the uncabled fibers, Figure 1 shows the spectral group delay measured at eight discrete wavelengths. Fit 1 is shown where the best-fit $\tau_1(\lambda)$ of equation (1a) is drawn through the points; the arbitrary value of the minimum delay τ_0 at λ_0 is taken to be zero. Also given is the dispersion coefficient curve $D_1(\lambda)$ of (1b) resulting from the differentiation of the delay.

EFFECTS OF CABLING ON DISPERSION

It is well known that microbend and other effects in cabling can cause attenuation increase in fibers.

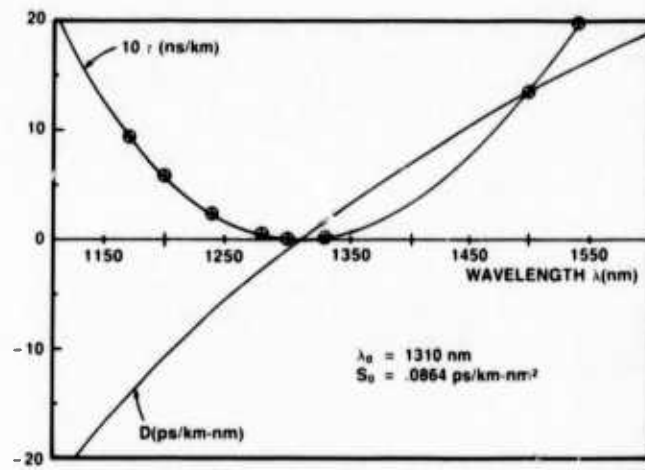


Figure 1.

Moreover, in the case of multimode fibers, the associated mode mixing can alter the dispersion or bandwidth from that measured before cabling. Although no such effect is expected for single-mode fibers, an experiment was designed to test for it.

Figure 2 shows a crosssection of the cable structure [3] that was used. In the open-channel design, a medium density polyethylene (MDPE) six-slotted core is extruded over a metallic or dielectric strength member. Each slot or channel traces an oscillating helical path about the central member, and each spot can accommodate up to nine color-coded optical fibers. A longitudinal polyester tape is applied over the core with an overlap to retain a water-blocking filling compound in each

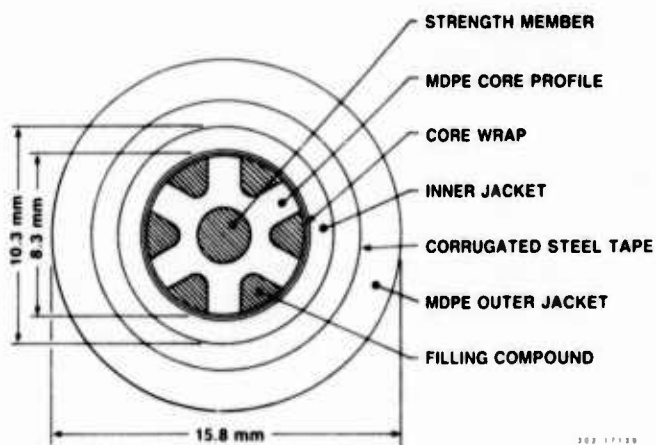


Figure 2.

channel. If rodent protection is necessary, the cable core is covered by an inner polyethylene jacket, over which is applied a plastic-coated steel shield. A black MDPE jacket is extruded over the shield as the shield coating overlaps and fuses to form a watertight barrier.

Nine fibers of 1.03 km length were used: fibers 4 to 9 manufactured by ITT EOPD and fibers 1 to 3 from another manufacturer. The dispersion parameters of Fit 1 obtained both before and after cabling are compared in Table 1:

Table 1.

Fiber	λ_0 (nm)		$S_0 \times 10^3$ (ps/km-nm ²)	
	Before	After	Before	After
1	1308	1305	90.0	86.1
2	1307	1306	85.8	84.6
3	1306	1304	87.2	84.6
4	1306	1316*	84.8	85.7*
5	1315*	1307	89.7*	84.0
6	1309	1312	88.8	88.1
7	1314	1314	84.9	85.8
8	1308	1315*	86.6	88.9*
9	1310	1309	88.6	84.7

An asterisk * denotes a particularly poor fit. A poor fit reduces the reliability of the dispersion parameter values there. Overall, the differences between values before and after cabling are within measurement repeatability for these rather short fiber sections. No systematic change due to the cabling process can be inferred.

DISPERSION FITS TO CABLED FIBERS

To improve measurement repeatability, fibers 4 and 5 were spliced at one cable end to form a longer 2.07 km fiber pair A. Similarly, fibers 6 and 7 formed pair B, while 8 and 9 formed C; fibers 1, 2, 3 were left unchanged. Spectral group delay measurements were performed twice on each sample; values in tables below are the average. Repeatability was about 1 nm on λ_0 , 1 percent on S_0 , and 15 percent on C_0 for measurements on the fiber pairs.

Measurements on the shorter fibers were spread about twice as wide, due to the fact that measurement jitter per unit length increases. Moreover, measurements on the longer pairs were taken from each end. No systematic bidirectional effects were noted, and the values are averaged below.

For each of the cabled fibers, the two dispersion parameters for both Fits 1 and 2 are given in Table 2:

Table 2.

Fiber	λ_0 (nm)		$S_0 \times 10^3$ (ps/km-nm ²)	
	Fit 1	Fit 2	Fit 1	Fit 2
1	1309	1306	89.3	91.3
2	1303	1300	89.3	92.0
3	1305	1302	88.6	90.9
A	1312	1309	91.2	93.1
B	1310	1307	89.2	91.2
C	1313	1310	89.9	91.7

Fiber	σ (ps/km)	
	Fit 1	Fit 2
1	19	27
2	15	23
3	15	22
A	8	11
B	8	13
C	5	14

The quantity σ is the standard deviation of the measured points from the fit curve τ_1 or τ_2 . The dispersion parameters for Fit 3 are given in Table 3:

Table 3.

Fiber	λ_0 (nm)	$S_0 \times 10^3$	$C_0 \times 10^6$
		(ps/km-nm ²)	(ps/km-nm ³)
1	1314	88.2	84.6
2	1309	87.4	82.8
3	1310	87.3	93.2

Table 3 (continued).

Fiber	λ_0 (nm)	$S_0 \times 10^3$	$C_0 \times 10^6$
		(ps/km-nm ²)	(ps/km-nm ³)
A	1312	93.4	21.2
B	1311	91.0	19.5
C	1315	90.7	16.0

Fiber	σ (ps/km)
1	12
2	7
3	7
A	6
B	3
C	3

Note that the dispersion parameter values depend upon the fit used. Over the full range of data points, Fits 3, 1, 2 are preferred in order of smaller deviation [2]. However, Fit 3 has the disadvantage of requiring 3, rather than 2, dispersion parameters. Note also that the fits improve for the longer length fiber pairs for the same reason that repeatability improves.

Only the significant number of digits for each dispersion parameter are shown in Tables 1, 2, and 3. For purposes of computation below, however, another less significant digit is retained to avoid roundoff error.

We now examine how the above fits can be applied when fiber lengths are spliced into a link.

DISPERSION CONCATENATION - THEORY

When two or more single-mode fibers are joined together, the total group delay at any wavelength is assumed to be the sum of the individual fiber delays at that wavelength. This is not the situation in multimode fibers, where mode coupling and equalization effects lead to pulse broadening that increases sublinearly with length, although in a somewhat unpredictable manner. The same would hold in particular bimodal regimes of single-mode fiber, such as just below the cutoff wavelength or with polarization dispersion. Normally, however,

additivity is assumed to hold for the individual fiber delays and for the wavelength derivative chromatic dispersion [4]. We shall test this below.

For any particular fiber 'n', the total dispersion (ps/nm) is the product of the normalized chromatic dispersion D_n (ps/km-nm) and the fiber length L_n (km). Hence the overall total dispersion for a link of 'N' fibers is

$$D \cdot L = \sum_n D_n \cdot L_n \quad (4a)$$

where

$$L = \sum_n L_n \quad (4b)$$

is the total link length. All sums are understood to go from $n = 1$ to $n = N$. Whereas $D \cdot L$ (ps/nm) is the total dispersion, D (ps/km-nm) is the effective normalized chromatic dispersion coefficient for the link. The total dispersion and the source spectrum width (in nm) together determine the link pulse broadening (in ps) or link bandwidth (in GHz) [5].

Each fiber 'n' within the cable link has its dispersion coefficient D_n fit to equations (1), (2), or (3). This gives the zero-dispersion wavelength λ_{0n} , dispersion-slope S_{0n} , and dispersion-curvature C_{0n} (i.e., the dispersion parameters) for each fiber. The dispersion parameters for the overall link can then be obtained as we now show.

For Fit 1, equations (1) and (4) give

$$S_0 = \frac{1}{L} \sum_n S_{0n} \cdot L_n \quad (5a)$$

$$\lambda_0 = \left(\frac{1}{S_0 L} \sum_n \lambda_{0n}^4 \cdot S_{0n} \cdot L_n \right)^{1/4} \quad (5b)$$

For Fit 2, equations (2) and (4) give

$$\lambda_0 = \frac{\sum_n \lambda_{on}^3 \cdot S_{on} \cdot L_n}{\sum_n \lambda_{on}^2 \cdot S_{on} \cdot L_n} \quad (6a)$$

$$S_0 = \frac{1}{\frac{2}{\lambda_0 L}} \sum_n S_{on} \cdot \lambda_{on}^2 \cdot L_n \quad (6b)$$

whereas for Fit 3, (3) and (4) give

$$C_0 = \frac{1}{L} \sum_n C_{on} \cdot L_n \quad (7a)$$

$$\lambda_0 = A - (A^2 - B)^{1/2} \quad (7b)$$

$$S_0 = C_0(A - \lambda_0) \quad (7c)$$

where

$$A = \frac{1}{LC_0} \sum_n (S_{on} + \lambda_{on} \cdot C_{on}) L_n \quad (7d)$$

$$B = \frac{1}{LC_0} \sum_n (2S_{on} + \lambda_{on} \cdot C_{on}) \lambda_{on} \cdot L_n \quad (7e)$$

For each fit, equations (5), (6), or (7) give the expected concatenated link dispersion parameters (and hence the link dispersion coefficient) in terms of the individual section dispersion parameters.

DISPERSION CONCATENATION - EXPERIMENT

To test the rules derived above, several concatenations were tested

Concatenation X - fibers 1 + 2,
length 2.07 km

Concatenation Y - fibers 1 + 2 + 3,
length 3.1 km

Concatenation Z - all fibers (1 + 2
+ 3 + A + B + C),
length 9.3 km

For these concatenations, the measured and calculated dispersion parameters

were compared. The comparison using Fit 1 is given in Table 4:

Table 4.

Concatenation	$\lambda_0(\text{nm})$		$S_0 \times 10^3$ (ps/km-nm ²)	
	Meas	Calc	Meas	Calc
X	1307	1306	88.9	89.3
Y	1307	1306	91.1	89.1
Z	1310	1310	88.7	90.4

Concatenation	$\sigma(\text{ps/km})$
X	11
Y	8
Z	6

As pointed out previously, an additional non-significant digit is used in the computations. We find that agreement between measured and calculated values averages 0.6 nm in λ_0 , and 1.5 percent in S_0 . The comparison using Fit 2 is given in Table 5:

Table 5.

Concatenation	$\lambda_0(\text{nm})$		$S_0 \times 10^3$ (ps/km-nm ²)	
	Meas	Calc	Meas	Calc
X	1305	1303	94.8	91.6
Y	1304	1303	93.4	91.3
Z	1307	1307	90.5	92.3

Concatenation	$\sigma(\text{ps/km})$
X	18
Y	16
Z	15

Agreement averages 1.0 nm in λ_0 , 2.5 percent in S_0 . The comparison using Fit 3 is given in Table 6:

Table 6.

Concatenation	$\lambda_0(\text{nm})$		$S_0 \times 10^3$ (ps/km-nm ²)	
	Meas	Calc	Meas	Calc
X	1311	1320	88.6	87.1

Table 6 (continued).

Concatenation	λ_0 (nm)		$S_0 \times 10^3$ (ps/km-nm ²)	
	Meas	Calc	Meas	Calc
Y	1309	1316	91.2	87.3
Z	1312	1303	88.7	94.9

Concatenation	$C_0 \times 10^6$ (ps/km-nm ³)		σ (ps/km)
	Meas	Calc	
X	124	84	6
Y	143	87	5
Z	138	127	3

Agreement averages 8.5 nm in λ_0 , 4.4 percent in S_0 , 32 percent in C_0 .

Given the dispersion parameters of the individual cabled fibers, the concatenated parameters are best predicted using Fit 1 (equations (1) and (5)), although Fit 2 (equations (2) and (6)) is almost as good. Although Fit 3 (equation (3)) has the best closeness-of-fit to experimental data, its concatenation predictability (equation (7)) is hampered by the fact that the concatenated dispersion coefficient C_0 is the sum of a number of small terms in (7a). Then C_0 appears in the denominator terms of (7d) and (7e) that are used for calculating λ_0 in (7b). This means that an accumulation of small errors in determining C_0 can have a large effect in the determination of the concatenated dispersion parameters.

CONCLUSIONS

The chromatic dispersion coefficients of single-mode fibers have been fitted to three expressions that contain the parameters of zero-dispersion wavelength λ_0 , the dispersion-slope S_0 , and (for one fit) the dispersion-curvature C_0 . Within the repeatability of the measurements, no significant differences were found for fibers before or after cabling, or for signals injected from opposite ends. Moreover, two of the fit expressions were successfully used to accurately predict concatenated dispersion from dispersions of the constituent fibers.

If the fiber or cable manufacturer supplies the two dispersion parameters (within some tolerance) for individual sections, the single-mode systems designer can use these to confidently predict link dispersion. The result will be more accurate than the worst-case value obtained by simply adding wavelength-window dispersion specifications for each section. Moreover, this predictability can reduce the need for end-to-end field dispersion measurement verification.

REFERENCES

- [1] W.F. Love, "Bandwidth Spectral Characterization of GeO₂-P₂O₅-SiO₂ Multimode Optical Waveguides", 6th ECOC, pp 113-116, York (Sept. 1980)
- [2] F.P. Kapron and T.C. Olson, "Accurate Specification of Single-Mode Dispersion Measurements", Symp. Opt. Fiber Measurements, Boulder (Oct. 1984)
- [3] C.K. Kao et al, "Fiber Cable Technology", IEEE LT-2, pp 479-488 (Aug. 1984)
- [4] Chinlon Lin et al, "Optical Pulse Equalization and Low Dispersion Transmission in Single-Mode Fibers in the 1.3-1.7 μ m Spectral Region", 6th ECOC, pp 91-94, York (Sept. 1980)
- [5] F.P. Kapron, "Dispersion-Slope Parameter For Monomode Fiber Bandwidth", OFC 1984, pp 90-92, New Orleans (Feb. 1984)

AUTHORS

All authors are with the ITT Electro-Optical Products Division in Roanoke, VA.



Dr. Tom C. Olson,
Senior Engineer

- Currently involved in a variety of R&D fiber measurements
- 1976 to 1981: preform process engineer at Canada Wire and Cable, Montreal QU, Canada
- 1974 to 1976: postdoctoral fellow in vitreous materials at Catholic University, Washington DC
- 1974: PhD in physics from the University of Massachusetts, Amherst MA
- 6 publications



Dr. Felix P. Kapron,
Senior Technical
Consultant

- Currently involved in optical communications R&D and standards
- 1973 to 1981: fiber-optic research at Bell-Northern Research, Ottawa ON, Canada
- 1967 to 1972: research on the first low-loss fibers at Corning Glass Works, Corning NY
- 1967: PhD in physics from the University of Waterloo, Waterloo ON, Canada
- 56 publications, 12 patents



Mr. Tom W. Geyer
Manager, Fiber
Measurements
Development

- Currently responsible for fiber and cable measurements
- 1977 to 1983: senior product engineer for fiber improvement qualification at Corning Glass Works, Corning NY
- 1977: MSc in mechanical engineering from Brown University, Providence RI
- 2 publications

EFFECT OF SCREW DESIGNS ON QUALITY AND RATE OF FLEXIBLE PVC COMPOUNDS

H. T. Kim

BFGoodrich Company

The selection of a proper screw is the key to getting high quality products at the highest output rate in all extrusion applications including the wire and cable area.

The study of the melting behavior of flexible PVC compounds shows that they follow the melting mechanism described by Tadmor.

Among the various screw designs, barrier screw designs are the most suitable for the wire and cable application because the very principle of the design is to promote this particular melting behavior in an extruder. Comparisons in the performance of different barrier screws and a conventional screw are made using several flexible compounds with varying levels of heat history.

Results show that the level of heat history in a compound has a significant effect on the quality of end product and that barrier screws provide better quality products regardless of the level of heat history in a compound. Among the various barrier screws, the variable pitch barrier screw gives the best result.

The unique positioning of the barrier screw flight to stabilize the solid bed and to maximize the melting capability is the main reason for the success of this screw design.

INTRODUCTION

One of the most important criteria for a good screw design is that it should deliver homogeneous melts at high output rates. In order to achieve this rate goal, numerous exotic screw designs such as mixing screw, wave screw and Maddock screw came into use.

Most of these screws are designed to achieve the high output rate goal by insertion of mixing devices in the flow channel of the screw so as to enhance mixing and homogenization. No consideration was given to the melting behavior of the plastic materials being processed.

These mixing devices, in some cases, create some undesirable effects. High local shear regions around the mixing devices can generate too high

a melt temperature and the stagnation areas around them also are detrimental to heat sensitive materials such as PVC compounds.

In this study, a new approach was taken to design a high performance screw. Rather than inserting more efficient mixing devices, the basic geometry of a screw was altered so as to maximize the plasticating capacity.

The design, a two-channel variable pitch screw, has proven to possess higher melting and pumping capacity and has demonstrated its superior performance over the conventional designs. Furthermore, it has proven to be ideally suited to process heat sensitive materials such as PVC because the absence of stagnation areas in the flow channel eliminates degradation problems and because of a low residence time of materials in the system due to a high pumping capacity of this design.

DISCUSSION

There are two basic functions that a screw has to perform. First, it should have the capability to melt the materials. Secondly, it should have the capability to push those molten materials forward so as to overcome the resistance of the die and to pump the materials through the die.

As shown in Figure 1, the pumping capacity or the output rate of most screws increases linearly with screw speed, whereas the melting capacity increases in a non-linear manner. At a low RPM range, the melting capacity increases sharply and is generally greater than the pumping capacity but as the screw speed increases further it tends to increase at a much slower pace.

At some point, A , the melting capacity becomes less than the pumping capacity, that is, the screw would pump out more than it could melt. In this region, the screw would pump out non-homogeneous material.

On the other hand, if the screw speed is lower than A , extrudates would be homogeneous since the screw would have more capability to melt than it could pump. So, the upper limit on the output rate for this screw is Q_A .

The name of the game in a screw design is to come up with a screw that extrudes homogeneous materials at the highest output rate, that is, a screw that

has a point A at the highest output rate. In other words, a better screw should have the highest melting capacity with its pumping capacity slightly less so that it would extrude homogeneous melts at very high rates.

The pumping capacity of a screw is dependent on the screw geometry, the flow property of the material and the head pressure, and could be controlled based on those variables.⁽¹⁾

The most common way of improving the performance of a given screw is to put mixing devices such as mixing pins in the metering section. What the mixing device does is to retard the pumping and at the same time, to increase the melting as shown in Figure 1. The result is that the melting and the pumping capacities cross each other at an output rate, Q_B which is greater than Q_A , as shown in Figure 1, thus improving the performance.

These mixing devices, although improving the performance of the screw somewhat, also create problems. They create stagnation areas where materials can degrade and cause color changes. So the real question then is "how do you increase the melting capacity of a screw and still make it possible to process flexible PVC?"

In order to answer this question, one has to go back and study the melting behavior of flexible PVC compounds themselves.

Figure 2 shows the freeze experiment samples of Geon 8804, a cable jacket compound in a single screw extruder. It shows that this compound melts in an extruder in the manner described by Tadmor.⁽²⁾ It has also been proven⁽³⁾ that all flexible PVC and some rigid PVC compounds follow the Tadmor model.

One of the problems inherent with flexible PVC compounds in this melting mode is clearly shown in Figure 3. As the melting process proceeds and the solid bed becomes smaller, the solid bed softens, loses its integrity, breaks up and disperses into the melt pool because flexible PVC compounds are softer.

The freeze samples show the solid bed breaks up and disperses into the melts already at the 18th turn. Figure 4 shows a model of this break up phenomenon.

As shown in Figure 3, barrier screws^(4,5,6) are the designs invented to promote the melting of materials that follow the Tadmor melting mechanism. The function of the barrier flight is to physically separate the solid bed from the molten materials and so to ensure that this melting mechanism proceeds without interruption. This type of screw is the only design that has the capability to increase the melting capacity without any mixing device.

The variable pitch barrier screw^(4,7), or so called the Kim screw, is the first screw designed specifically to increase the melting capacity while

meeting the other requirements for processing flexible PVC (Figure 5).

Figure 6 shows the comparison in melting capacities (calculated) between several barrier screws. It shows the variable pitch barrier screw to possess high melting capacity compared to other designs. By controlling the pumping capacity by properly designing the melt channel, this screw design now satisfies both criteria for being an outstanding screw for materials that follow the Tadmor model.⁽²⁾ The principles behind this design have been previously presented, so only the particular features of this design will be discussed.

The main features of this screw are that

- (A) its main solid channel width stays constant and only its depth decreases throughout the melting section in order to maximize the melting rate.
- (B) its melt channel width and depth increase in order to accommodate increases in the amount of melts being generated from the solid channel and to control the pumping capacity.

Maintaining the solid channel width the same as that of the feed section throughout the melting section does more than just increase the melting capacity.

As shown in Figure 7A, as the solid bed moves forward it is forced to push against the barrel surface due to the decreases in the depth of the channel thus making it more efficient for the melting process to take place. It is analogous to a block of butter on a frying pan. The harder the butter is pressed against, the more it melts.

Let's look at the plastiscrew as shown in Figure 7B for contrast. The solid channel is not only getting shallower but also narrower as the solid bed moves forward. The lateral pressure exerted on the solid bed due to the narrowing of the solid channel hinders and slows down the forward movement of the solid bed, thus inducing a surging. If the back pressure is too great, some of the solid might squeeze out and go over into the melt channel. It would reduce the quality of the melt.

The performance of this variable pitch barrier screw has been extensively evaluated and is shown in Table 1. It shows the much greater pumping capacity of the barrier screw compared to either a single stage or to a mixing type screw on Geon 8804, a cable jacketing compound. The higher pumping capacity of this screw can be attributed directly to the unique design of the solid channel.

Table 2 shows the comparison in extrusion rate performance between this screw versus other designs for various flexible PVC compounds.

In all cases, our barrier screw provides homogeneous melts at substantially higher output rates.

CONCLUSIONS

The variable pitch, 2-channel barrier screw is specifically designed to promote a particular melting mechanism characteristic of some plastics materials, including flexible PVC compounds. It is designed to maximize melting and at the same time to have balanced pumping capacity. This screw design substantially improves the quality and output rate of many materials compared with more conventional screw designs.

REFERENCES

1. Squires, P.H., SPE Journal, May 1958.
2. Tadmor, Z., PE&S, 6, 185 (1966).
3. Kim, H.T., Technical Paper at 34th ANTEC, Atlantic City (1976).
4. Kim, H.T., Technical Paper AICHE 70th National Meeting, NY (1977).
5. Barr, R., U.S. Patent #3,698,541.
6. Geyer, P., U.S. Patent #3,375,549.
7. Kim, H.T., U.S. Patent #3,867,079.

TABLE I

PUMPING CAPACITIES OF GEON 8804
BARRIER SCREW VS. OTHER DESIGNS

SCREW SPEED (RPM)	OUTPUT RATE (lb./hr.)		
	30	60	90
Screw Type:			
Single Stage	52	88	127
Mixing Screw	53	89	128
Barrier	53	107	153

TABLE 2

EXTRUSION RESULTS ON VARIOUS FLEXIBLE PVC COMPOUNDS

#	COMPOUND	SCREW TYPE	SCREW DIAMETER (INCHES)	MAXIMUM RATE (L/HR.)	APPLICATION
2	Geon 8730 (Flexible PVC)	Barrier Screw	2 1/2	250	Wire Insulation
		Single Stage	2 1/2	100	
3	Geon 83789 (Flexible PVC)	Barrier Screw	6	3500	Sheet
		Two-Stage	6	1500	
4	Experimental Flexible PVC (30% TiO ₂)	Barrier Screw	3 1/2	600	Profile
		Fluted	3 1/2	930	
5	Geon 80644	Barrier Screw	2 1/2	220	Wire & Cable Insulation
		Mixing	2 1/2	132	

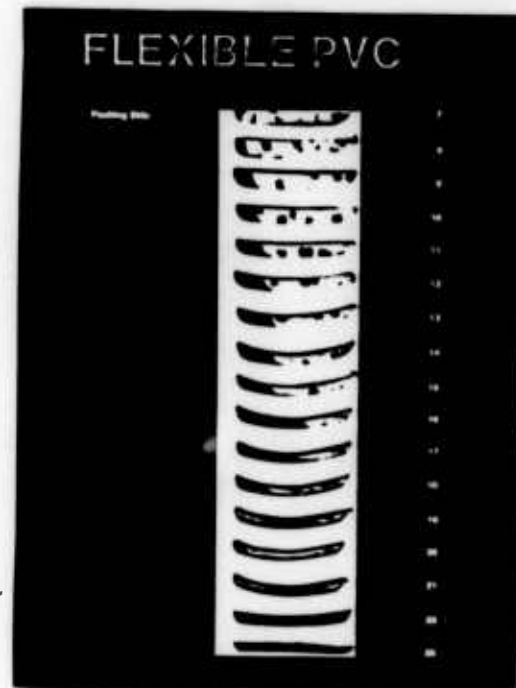
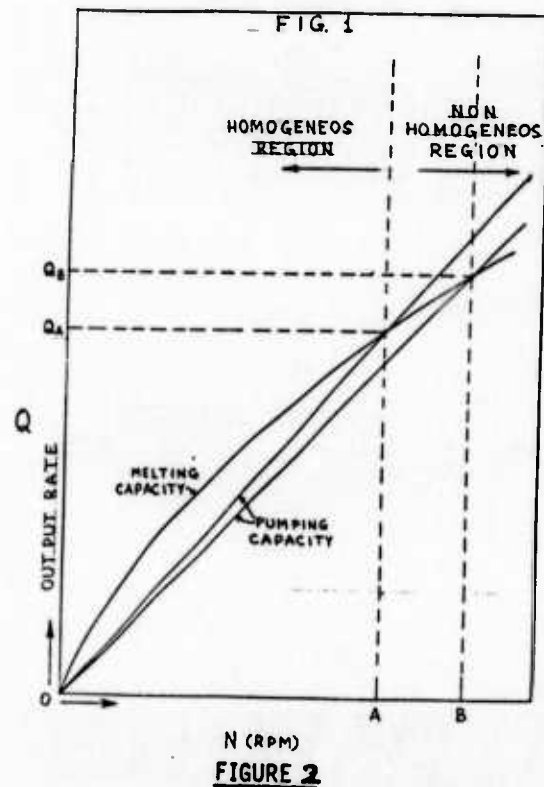
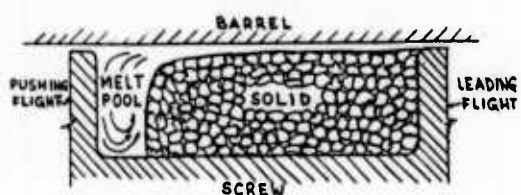


FIG. 3
A STANDARD SCREW



B BARRIER SCREW

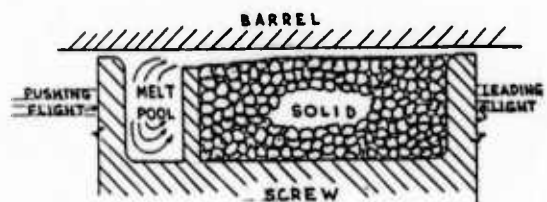
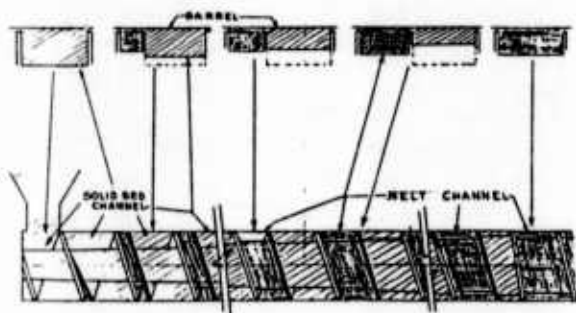


FIG. 4



FIG. 5



COMPARISON OF MELTING CAPACITIES (3 1/2 inch.)

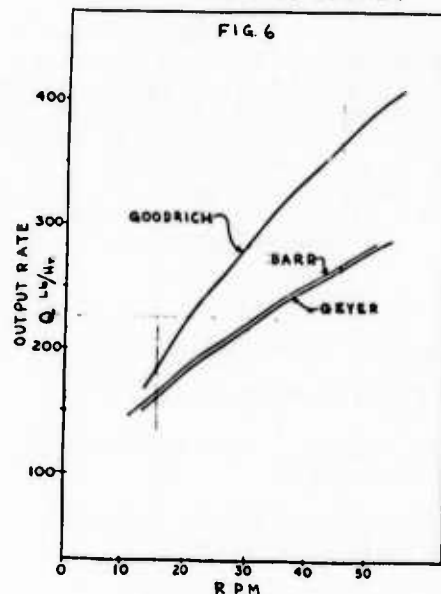
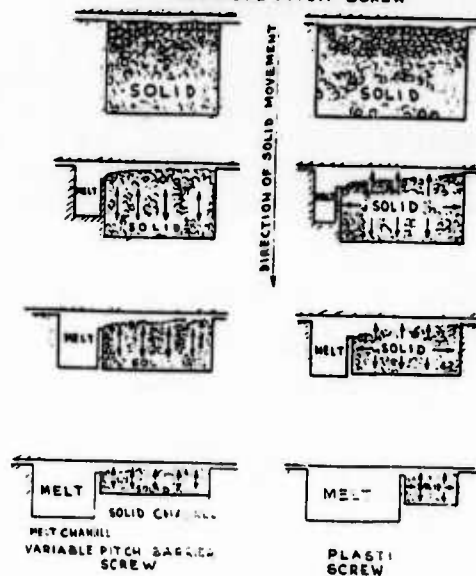


FIG. 7
COMPARISON BETWEEN NORMAL BARRIER SCREWS (PLASTISCREW) AND GOODRICH VARIABLE PITCH SCREW



ULTRA-HIGH SPEED EXTRUSION OF HIGHLY EXPANDED POLYETHYLENE INSULATION FOR COMMUNICATION CABLES

Y. Morita*

T. Takai*

S. Yamaguchi*

K. Nishida**

* Dainichi-Nippon Cable, Ltd.

8 Nishinocho Higashimukaijima
Amagasaki Japan

** Mitsubishi Petrochemical Co., Ltd.

1 Tohocho Yokkaichi Mie Japan

Summary

Ultra-high speed extrusion of highly expanded polyethylene insulation was developed. Major problem in the development was to avoid wire draw down, rough surface of insulation, and extreme elevation of crosshead pressure, in addition to prevention of decrease of mechanical strength and tensile elongation of insulation, deterioration of foam structure and separation of insulation from the conductor, which were usually caused by extruding highly expanded polyethylene for insulation.

As the result, it was found that those problems were closely related to the viscoelastic properties of high density polyethylene and extruding conditions. The optimum design of high density polyethylene was established.

(1) Introduction

Nippon Telegram and Telephone Public Corporation has brought foamed polyethylene insulated local PEC cables into use to meet the growing demand for non-telecommunication services in place of the conventional paper insulated staped cables since 1981. With regards to local PEC cables, improvement in transmission characteristics such as cross talk characteristics and incorporation of cores are demanded by application of foamed plastic insulation technique.

And high density polyethylene, which is excellent in mechanical properties, are used for an insulation material. Cable manufacturers have been asked to achieve above-mentioned requirements.

On the other hand, Western Electric Co., Inc., U.S.A. has been manufacturing foam-skin insulated telecommunication cables with double layer insulation instead of the conventional unexpanded plastic insulated cables since 1973. The foam-skin insulated cables, which were developed to make most of excellent

electrical properties of foamed insulation and to improve mechanical strength and jelly resistance, comprise insulation of highly expanded high density polyethylene, and colored unexpanded skin layer of high density polyethylene there on.

As this structure has come to be adopted in other countries, higher expansion of the foamed polyethylene layer is demanded in accordance with the trend to increase transmission capacity.

The problems arisen from high speed extrusion of highly expanded high density polyethylene insulation are raised in the crosshead pressure, deterioration of surface appearance, and decrease in tensile elongation of the insulation and wire draw down as reported by Rokunohe, Okada, et al.¹⁾

For the remedy, improvement in materials, and manufacturing facilities and conditions has been considered. These problems affect safe and stabilized operation as well as cable quality.

Higher expansion of insulation, in general, degrades foamed structure. It is necessary to decrease open cells for not only prevention of cross talk or flaws but improvement in compression resistance.²⁾

Dainichi-Nippon Cables, Ltd. and Mitsubishi Petrochemical Co., Ltd. jointly researched into the dependency of required properties of the cables such as tensile elongation of the insulation, foamed structure, extruded appearance and crosshead pressure on extrusion process and materials.

As the result of sequential experiments, it was found that these properties depend on melt viscosity and elasticity of high density polyethylene. These two properties of polyethylene are greatly influenced by molecular structure, especially molecular weight distribution (MWD). We succeeded in the development of the cables with balance structure which satisfy all required properties by controlling MWD. Further, application of this technique to the manufacture of foam-skin cable with more highly expanded insulation satisfied

all required properties.

This paper deals with the mechanism by which raise in crosshead pressure, decrease in elongation of insulation and wire draw down, and deterioration of foamed structure and of extruded appearance are caused. Described also is the relation of the mechanism with melt rheology, above all molecular structure.

(2) Experiment

1) Material

The quality of high density polyethylene is influenced by molecular structure, especially MWD. In recent years higher speed extrusion of polyethylene for various products with less thickness has become a requirement along with the maintenance of mechanical strength and long-term reliability of the products. Accordingly MWD has been a point of concern in relation to product quality and a topic of intense research. Extrusion for insulation of communication cables needs such a high shear rate and good foam structure that prepared were samples of insulation materials which were thought to have particular MWD and melt elasticity. Table 1 shows the sample materials used in the various model experiments. They all ethylene-butene-1 copolymer produced with the Ziegler catalyst.

MWD of sample A,B,C are shown in Fig. 1. Sample A with a low MI value of 0.3 dg/min. has extremely asymmetric MWD with a MI_{10}/MI value of 23, showing a large non-Newtonian flow. Its melt strength is 9 g, another remarkable characteristic.

Compared with sample A, sample B has a higher MI value and a nearly symmetric distribution (bi-modal) but has MWD in the lower range, making extrusion possible at 2,000-2,500 m/min. This grade has a melt strength of 4 g, in the middle of the samples considered.

Its density is low at 0.943 g/cm³ and accordingly the residual stress of insulation layer is so low that it gives good tensile elongation.

Sample C was produced, based on the results of samples D - I and the MWD was changed quite drastically. Therefore, it had much lower than A, and B, and also considerably high molecular weight to cover decreased mechanical strength.

Accordingly, its MWD was very wide at $Q=Mw/Mn$ 25.6. However, the distribution symmetry was improved so much that the MI_{10}/MI value lowered down to 17.5. The melt strength was the same as that of sample B at 4 g but foam structure was much better, satisfying crosshead pressure and other requirements.

Azodicarbon-amide was used as the blowing agent. Blowing agent concentration was initially prepared,

Table 1. Characteristics of Materials

SAMPLE	MI	MI_{10}/MI	DENSITY	Mw	Mn	Q	DIE SWELL	VISCOSITY		MELT
	dg/min	-	g/cm ³	X10 ⁴	X10 ⁴	Mw/Mn	r=240	r=8 X10 ⁴ poise	r=2650 X10 ³ poise	STRENGTH g
A	0.3	23.0	0.952	16.7	1.81	9.2	1.70	5.20	1.29	9.0
B	0.6	20.2	0.943	14.3	1.00	14.2	1.53	4.18	1.18	4.0
C	1.0	17.5	0.951	10.2	0.40	25.6	1.50	3.07	0.95	4.0
D	1.1	18.2	0.951	10.6	0.47	22.7	1.93	2.43	0.93	5.2
E	0.4	17.6	0.951	13.3	0.59	22.7	1.95	4.05	1.25	10.3
F	0.6	16.7	0.951	14.4	0.58	25.0	1.58	3.79	1.07	4.8
G	1.8	18.4	0.951	10.8	0.45	24.0	1.57	2.68	0.83	2.6
H	0.3	16.1	0.951	15.8	1.47	10.7	1.45	5.31	1.19	6.7
I	0.4	21.1	0.943	15.3	1.06	14.4	1.56	4.31	1.28	2.6

mixed with polyethylene resin and the led into the extruder. The expansion percentage of the PEC cable was 25-30 % and the azodicarbon-amide concentration was 1 wt.%. Table-2 shows the basic characteristics and test conditions of polyethylene used.

Sample	MI	MI ₁₀ /MI	M _n ×10 ⁴	M _w ×10 ⁴	Q=M _w /M _n
A	0.3	23.0	1.8	16.7	9.2
B	0.6	20.2	1.0	14.3	14.3
C	1.0	17.5	0.4	10.2	25.6

2) Extrusion test

The layout of the extrusion line shown in Fig. 2 consists of a wire drawing machine, preheater, water spray trough and take-up. This line was developed by Dainich-Nippon cables Ltd., and is capable of extruding at a speed of 3,000 m/min. It monitors and controls them accordingly by adjusting the distance between the water spray trough and die.

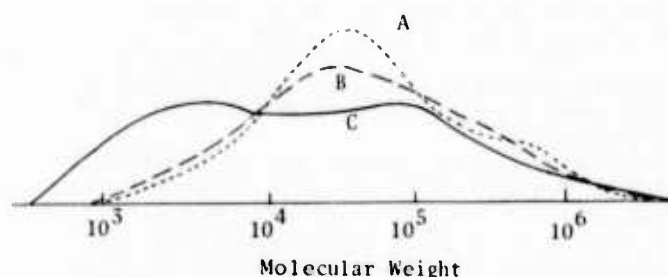
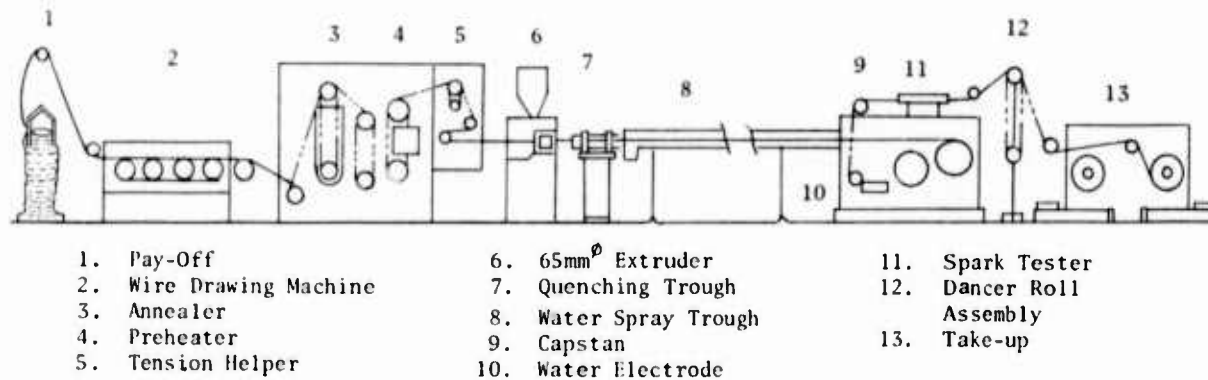


Fig.1 Molecular Weight Distribution of Sample A, B, and C.

Table 2 Test Method and Condition

Item	Instrument	Condition of measurement
Viscosity	Instron Capillary Rheometer	Nozzle L/D=33 90°angle inlet die Temp.=190°C shear rate range
Die Swell	ditto	Measurment of diameter of extrudate from capillary rheometer Die Swell=D(ext)/D(die) Nozzle L/D=3.7 Temp.=190°C
Melt Strength	Melt Tension Tester	Take-Up the strand extrudated from nozzle through strain gauge. Nozzle L/D=3.7 Temp.=190°C
M.W.D (molecular weight distribution)	G.P.C	Solvent:O-DCB(o-dichloro benzene) Column:TOYO SODA's
Surface Roughness	Needle Contact Roughness meter	tolerance 1 μ R max= R heigh- R deep R z = mean of 10 points

Fig.2 Ultra-High Speed Extrusion Line for Foamed HDPE Insulation.



Ultra-high speed extrusion was one of the goals of this experiment, in which PEC cables with 0.4 mm diameter conductors which were considered most difficult to be manufactured are used.

Extruder speed, extruder temperature, and preheat temperature were controlled so that the extruding speed, the insulation diameter, and the expansion percentage would be 1,500 - 3,000 m/min, 0.58mm, and 25 % respectively. In addition, more highly expanded insulation was prepared and tested for examination of foam structure.

Crosshead pressure was measured with a Bourdon's tube fixed onto the extruder crosshead. Conductor diameters, tensile elongation, surface appearance and foam structure were also checked.

(Open cell ratio was calculated by the ratio of connected bubbles to the cross-section of foamed insulation.)

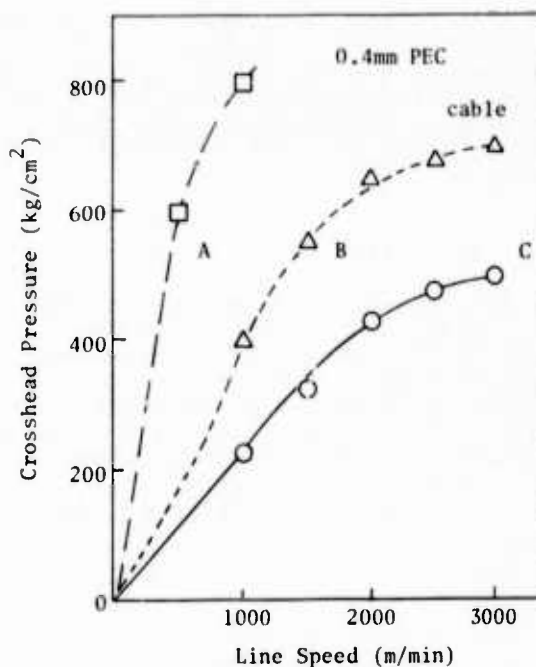


Fig.3 Dependence of crosshead pressure with line speed.

(3) Results and Discussion.

1) Crosshead Pressure

Crosshead pressure heavily depends on extrusion speed. For safe operation, it is important the crosshead pressure be held down. Fig.3 shows the dependency of crosshead pressure on line speed. By raising extrusion speed, the crosshead pressure rises as well. Especially sample A, which easily goes over the safety range of 700 kg/cm², is found unfavourable.

Capillary viscosity and shear rate dependency of samples A and B are shown in Fig.4. A has the higher viscosity in the low shear rate range but at a shear rate of 10³ sec⁻¹ they were close in viscosity due to large non-Newtonian flow. Usually, the shear rate value at the die surface is approximately 5-10x10⁵ sec⁻¹ at an extrusion speed of 2,000 - 3,000 m/min. It can be assumed that the viscosity of these two samples would cross over in this range.

In addition to having a low MI, sample A has a large die swell characteristic. These two facts were noted and their influence on crosshead pressure was checked. According to Fig.5, the following two points are interesting:

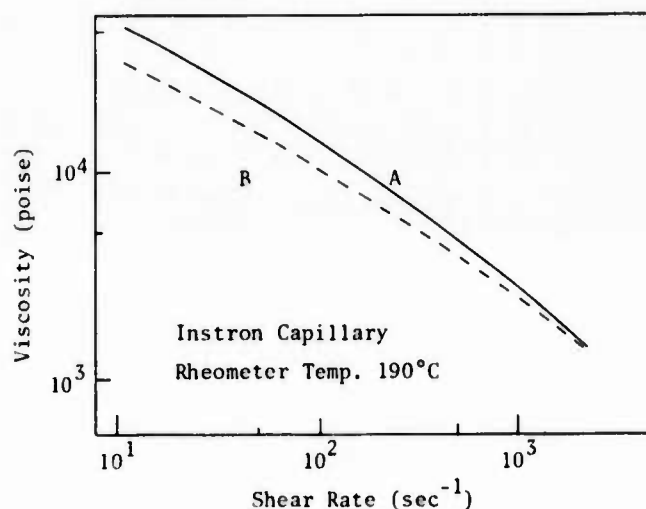


Fig.4 Dependence of viscosity with shear rate of sample A and B.

- Crosshead pressure is low when MI is high
- Even though the MI values are the same, the samples with a larger die swell have higher crosshead pressure
- Sample C and D have similar MI and MI_{10}/MI (therefore similar viscosity vs. shear rate), but it is clear that the die swell influences the crosshead pressure.

It has been pointed out that the difference in bubbling behavior is due to a difference in die swell. As a control experiment unexpanded extrusion was conducted and the results were found similar.

Next, only the extruder was run without operating the line (the Our-put was the same) and the crosshead pressure and viscosity at shear rate of $2,650 \text{ sec}^{-1}$ were plotted in Fig.6.

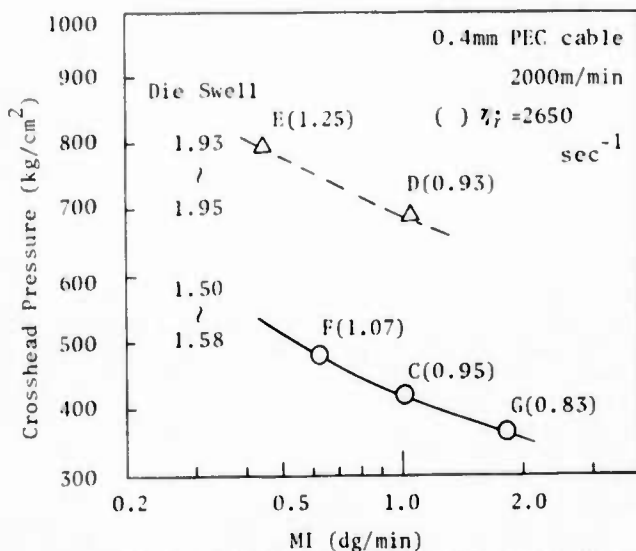


Fig.5 The influence of MI and die swell upon crosshead pressure.

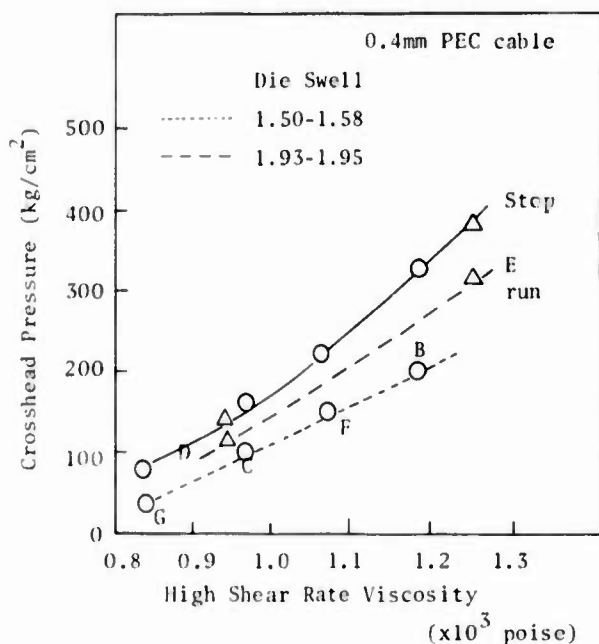


Fig.6 Relation of crosshead pressure to viscosity without running of conductor.

The results show the following:

- d) Crosshead pressure is higher during line-stop extrusion than when the line is in full operation.
- e) Influence of viscosity, not die swell, was a factor during line-stop operation. As the result, it can be said that the relationship between die swell and crosshead pressure was influenced by the drawing flow during operation. (see Fig.7)

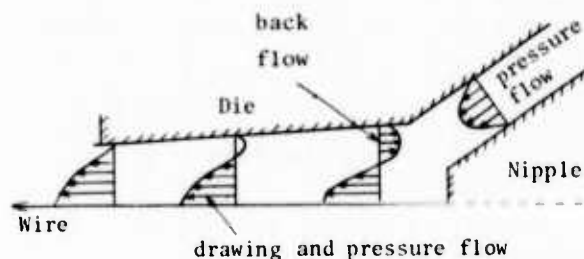


Fig.7 Explanation of back flow proposed by K. Orimo et al.³⁾

The analysis of flow within the die during cable manufacture has been elucidated to a large degree by research with the finite elemental method. According to K. Orimo, the non-Newtonian flow in the nipple area when the line is in operation points to the existence of back flow. In our experiment, however, it can be easily understood that even if the MI and MI_{10}/MI are the same (in other words both having the non-Newtonian flow property) crosshead pressure differs. We think the reason is that width and/or length of the back flow which increases the apparent L/D (Land Length/ Die Exit Diameter) of the melt resin cause the crosshead pressure rise

Therefore, for keeping the crosshead pressure down, it is effective to lower the viscosity and to keep the die swell small so as not to affect the requirements which will be considered below. Sample C was made accordingly. Fig.3 shows that it is of a satisfactory level.

2) Surface Appearance.

Poor surface appearance not only damages cables at the time of twisting but also has a bad effect on capacitance stability. Surface appearance is always

a problem with high speed extrusion. Surface roughness of sample B was measured with a roughness meter and the results are shown in Fig.8. The figure indicates that there was an unevenness every 100 - 150 μ (R_{max} 18 μ). This trend was observed in the case of unexpanded extrusion as well. Therefore this problem can be assumed to lie in the type of material and die with particularly rheological characteristics (MWD). Then samples were prepared with varied MI and MWD and their appearances were compared (see Fig. 9). The solid line represents the sample which had the same low molecular weight as B but a varied high molecular weight value in order to change the MI. Likewise the dotted line represents a sample similar to C with a varied high molecular weight to change the MI. The results show:

- a) The higher the MI becomes, the better the appearance.
- b) The more the molecular weight, especially M_w/M_n lowers, the better the appearance.

Results (a) and (b) coincide with B.H.Bersted⁴⁾, in that the oscillating flow shear rate depends on M_w and MWD during capillary extrusion.

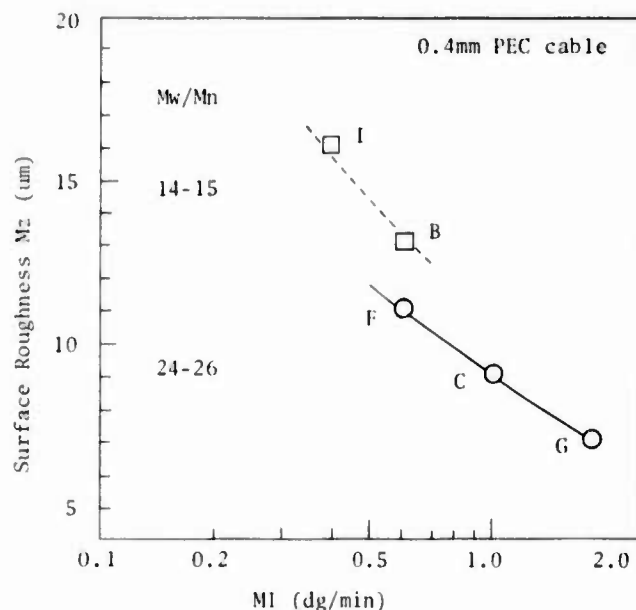


Fig.9 Influence of MI and MWD upon surface roughness.

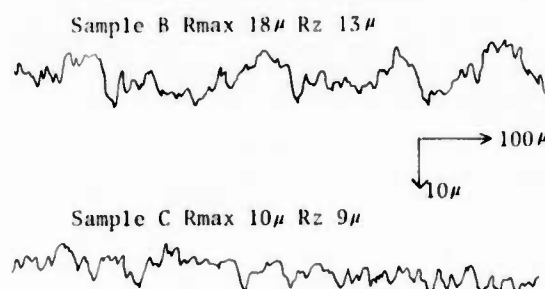


Fig.8 The surface roughness of sample B and C extruded at 2000m/min (0.4mm PEC cable)

3) Foam Structure

Expansion characteristics are made complicated because of the many factors which are at work simultaneously, such as expansion method, extruder, screw, die, extrusion temperature, cooling conditions, cable dimensions, material rheology, type of blowing agent and its concentration, coloring agent, etc. Material characteristics were considered under similar conditions and are reported below. Reduction of the open cell ratio is required to prevent cross talk and to retain compression strength, and property. M.Matsui and Y.Morita who developed chemical expansion²⁾ and C.D.Han who developed physical expansion⁵⁾ both claim that it is necessary to balance the bubble pressure and melt elasticity of the material for the homogeneous and fine foam structure.

Fig. 10 plots the relationship between open cells and melt strength in a 50 % expansion extrusion. It is observed that higher melt strength usually results in good expansion. However, High melt strength does not necessarily prevent poor foam structure. Even though sample A had a high melt strength, it did not expand well. Neither did it have good foam structure. This is because gases were escaped out from the surface or towards the conductor probably by excessive expansion. And the reason for the excessive expansion could be heat generation owing to the high viscosity of the material.

Concluded then is that high speed extrusion (where exothermic generation occurs) should be carried out with material with high melt strength and low viscosity in consideration of high melt strength.

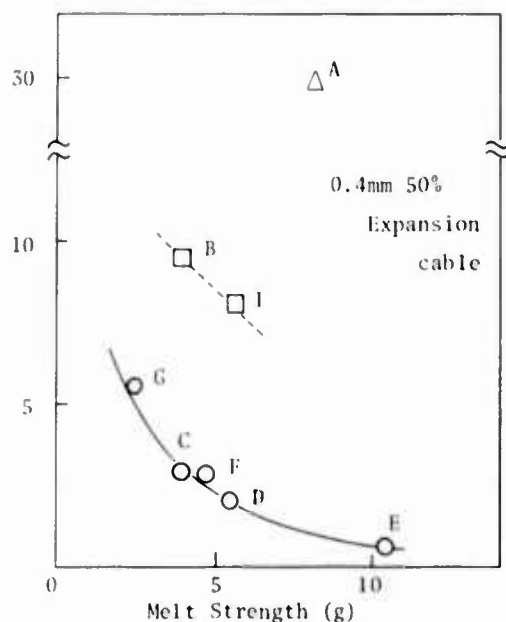


Fig. 10 Relation of open-cell ratio to melt strength.

4) Tensile elongation of insulation.

As is well-known, tensile elongation of the insulation is dependent of the expansion percentage and the preheat temperature of the conductor. Considered was the relationship between tensile elongation and preheat temperature at a particular expansion percentage in order to develop a potentially better material. Fig. 11 shows this relationship.

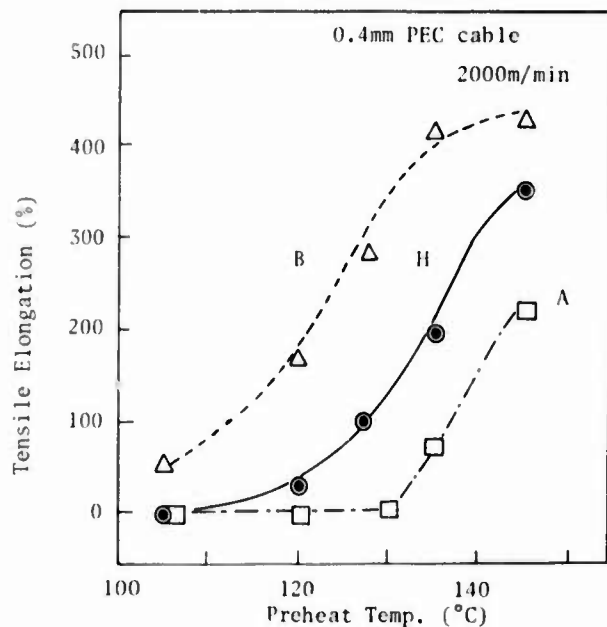


Fig. 11 Relation of elongation of insulation to preheat temperature.

At low temperatures tensile elongation was low but, above a certain temperature, the tensile elongation increased. The tensile elongation of A was 0 % when the preheater temperature was 140 °C ; on the other hand, that of H was 200 % , even though it had similar MI and density with A. The reason for the difference is that H has a much lower molecular weight value than A. Also B had good tensile elongation at low temperatures, and it is thought that this is related to the fact that it has a higher MI and lower density compared to A and H.

At preheat temperatures of 100 - 120 °C , the tensile elongation is low but this temperature range corresponds to the crystallization temperature of high density polyethylene. During the crystallization, the contact surface is thought to be oriented to the extruded direction (i.e. tensional direction) when polyethylene is brought into contact with the cores.

A model test was conducted on samples A and H with tensile elongation of 0 % and 200 % respectively, at preheat temperatures of 125 - 140 °C , to analyze the correspondence between orientation and molecular structure. Natural pellets were placed on a glass plate, melted at 200 °C , and another glass plate was placed over the material. After heating them up to 140 - 190 °C , the plates were moved to be right angle with their original position and then cooled. the birefringence (Δn) was plotted in relation to the hot stage temperature (Fig. 12) .

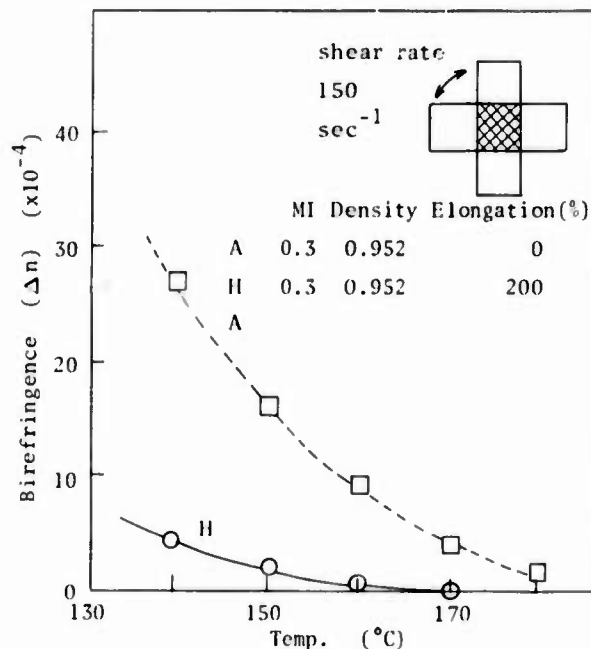


Fig. 12 Relation of birefringence (Δn) to shear temperature.

Results show that materials with high tensile elongation reduce orientation. To reduce orientation, lowering of density and shear viscosity is effective. The former was verified by

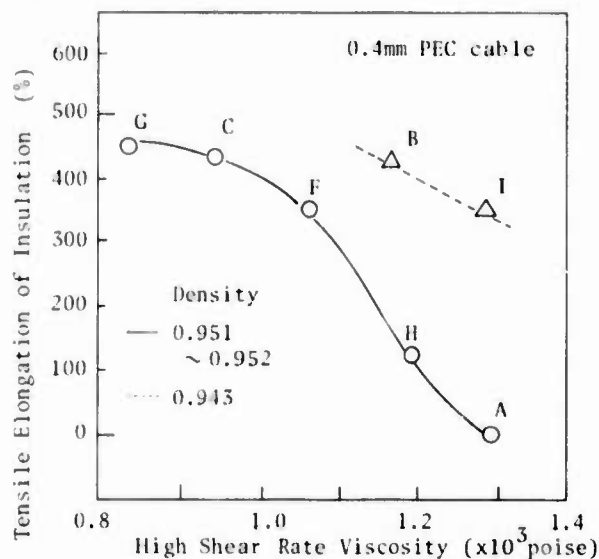


Fig.13 Relation of elongation of insulation to viscosity. (line speed 2000m/min preheat temp. 130°C)

the fact that sample B had good tensile elongation of 0.943 g/cm³, but low density also brings low compression strength of the cable. Then reduction shear viscosity was examined. Fig.13 shows that the relationship between shear viscosity and tensile elongation conform well to this fact.

5) Wire Draw Down

Wire draw down is another problem high-speed extrusion. Materials with low wire draw down are desirable now that the most favorable manufacturing conditions have been established. The raising of the preheat temperature in order to improve tensile elongation of the insulation causes greater wire draw down as shown in Fig. 14. Wire draw down is caused by the die and pressure flow; in other words the difference deriving from the shear stress at the contact surface of the resin.¹⁾ Fig.15 plots the relationship between shear stress of the material (MI and MWD) and conductor diameter. Here again it is proved that a material with high MI and much lower molecular weight prevents wire draw down to a high degree.

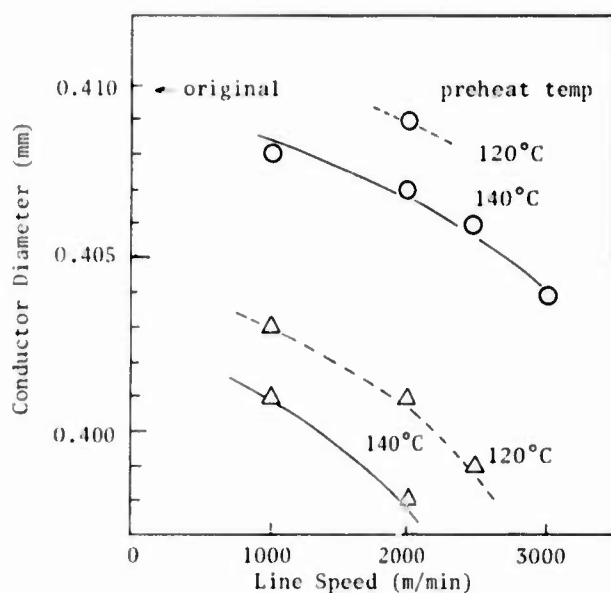


Fig.14 Dependence of conductor diameter upon preheat temp. and line speed. (○; sample C, △; sample B)

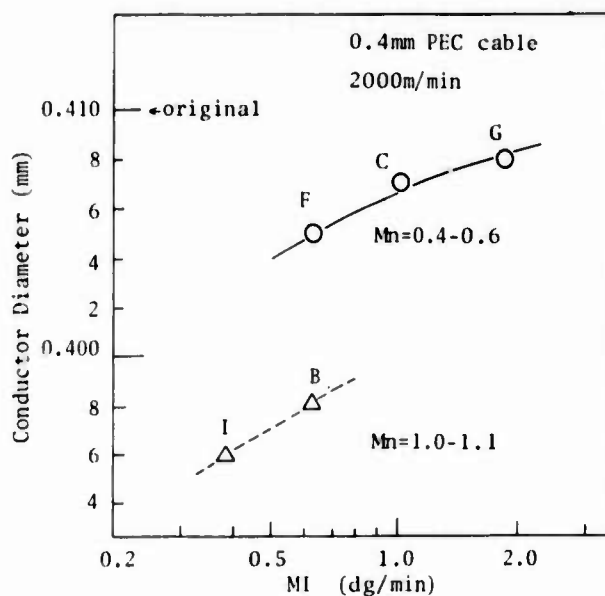


Fig.15 Dependence of conductor diameter upon MI and MWD. (Preheat Temp ; 140°C)

The relationship between the mechanism and material characteristics in crosshead pressure, surface appearance, foam structure, tensile elongation and wire draw down during high-speed extrusion of communication cable production have been discussed above. Table 3 summarizes the results.

The relationship of viscosity and melt elasticity (die swell, melt strength) to molecular structure should be just touched upon. Viscosity lowers as the range of MWD becomes wider. It was found that increase in lower molecular weight is especially effective in lowering

viscosity. As for melt elasticity, M.G.Rogers⁶⁾ reports that the more the high molecular weight increase, the larger the die swell. Our experimentation showed that not only the existence of high molecular weight but also asymmetric molecular distribution itself is a great influence. The relationship between favorable MWD as a model, which was determined by considering the whole balance, and the required properties is schematically illustrated in Fig.16.

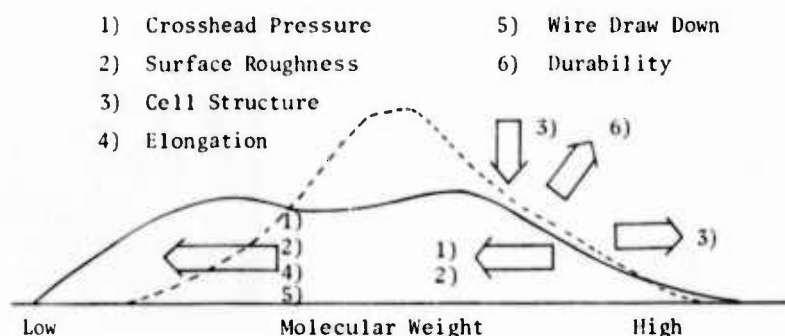


Fig.16 The schematic relation of requirments to MWD.

The dotted line shows original MWD model like sample A. Arrows indicate countermeasures to satisfy each requirments. The real line is MWD of sample C which is obtained with good balance of each arrows.

Table 3 Relation of Requirments to Materil Characteristics

Requirments	Improvement Direction	Viscosity	Die Swell	Melt Strength	Density
Crosshead Pressure	↘	↘	↘		
Surface Roughness	⚡	↘			
Foam(Open-cell ratio)	↘	Optim zoan	↗	Optim zoan	
Elongation of Insulation	↗	↘			↘
Wire Draw Down	↘	↘			
Compression Modular	↗				↗

(4) Cable Characteristics

The above results point to the fact that the resin C is the most appropriate as high density polyethylene to satisfy the required properties discussed above. The application of this resin to PEC and Foam-skin cables was tried.

The characteristics, and SEM picture of a cross-section of PEC insulated cable extruded at a high speed are shown in Table 4 and Fig.17. Good tensile property, surface appearance and foam structure were acquired in all sizes and colors. Furthermore thermal stress cracking resistance was good and no heat shrinkage was observed. The same qualities were verified in the foam-skin insulated cable as well and are shown in Table.5 and Fig.18.

The characteristics of the finished PEC cable are shown in Table 6. They have satisfactorily passed the requirements of Nippon Telegram and Telephone Public Corporation.



Fig.17 SEM micrograph of cross section of PEC insulation.



Fig.18 SEM micrograph of cross section of Foam-skin insulation.

Table.4 Properties of PEC insulation

Conductor Dia. (mm) Properties		Unit	white	0.4 black	brown	0.5 white	0.65 white	0.9 white	Remarks
Line Speed	(m/ min)		3000	3000	3000	3000	1900	1900	Specific Gravity Method
Insulation Diameter	(mm)		0.58	0.58	0.58	0.71	0.9	1.25	
Expansion Percentage	(%)		25	23	24	23	25	27	
Tensile Elongation	(%)		430	430	420	450	480	530	
Tensile Strength	(g)		320	360	350	510	660	1000	
Thermal Stress Cracking Resistance	(hrs)		>1000	>1000	>1000	>1000	>1000	>1000	(1)
Surface Roughness	(μ m)		10	9	10	8	7	6	(2)
Heat Shrinkage	(%)		0	0	0	0	0	0	

(1) 100°C , wrapped around their own diameter.

(2) 100°C , 24 hrs in a talc bath.

Table 5. Properties of Foam-Skin insulation

Conductor Dia. (mm) Properties	Unit	0.4 white	0.65 white	Remarks
Line Speed	(m/ min)	3000	2300	Specific Specific Method
Insulation Diameter	(mm)	0.69	0.84	
Skin Thickness	(mm)	0.03	0.03	
Expansion Percentage	(%)	51	52	
Tensile Elongation	(%)	450	500	
Tensile Strength	(g)	350	390	
Thermal Stress Cracking Resistance	(hrs)	>1000	>1000	(1)
Surface Roughness	(μ m)	10	7	
Heat Shrinkage	(%)	0	0	(2)

(1) 100°C , wrapped around their own diameter.

(2) 100°C , 24 hrs in a talc bath.

Table 6. Electrical characteristic of PEC Cable

Items	Unit	Specification for PEC Cables	0.3-3000prs. PEC Cables
Insulation Resistance	(M Ω -Km)	>2000	518,000
Mutual Capacitance	(nF/Km)	50 \pm 5	50.2
Capacitance Unbalance of pair to pair in the Quad	(pF/500m)	<150	30

(5) Conclusion

A PEC cable using 25 - 30 % expanded insulation extruded at a high speed was manufactured to be replaced with paper insulated cables. The mechanisms were considered to satisfy many required properties. By making most of the results in material design, the most appropriate material was developed. Summary of the results of our experiments are as follows.

- a) Keeping crosshead pressure low requires not only low viscosity but also low die swell.
- b) Die swell influences crosshead pressure only when the line is in full operation.
- c) Foam structure is better when melt strength is high. For high speed extrusion, a material with low viscosity and high melt strength is most suitable.
- d) Good tensile elongation of the insulation is established by the orientation which occurs at the contact surface of the conductor and resin.

- e) Material with low shear stress or low density has low orientation which produces good tensile elongation.
- f) Good appearance and low wire draw down can be achieved by adjusting MI and MWD.
- g) Application of the material which has been produced to satisfy the above six points to not only PEC cables but also foam-skin cables with highly expanded insulation possible.



Yukio Morita

Acknowledgments

The authors wish to thank Mr.J.Hotta and Mr.M.Matsui for their many enlightening discussions and helpful hints. The authors also wish to thank Mr.R.Kitani and Miss.M. Yamagishi for their invaluable assistance in the developmental work.

Material Research laboratory Dainichi-Nippon Cables,Ltd.
Mr.Morita graduated from Osaka University majoring in applied chemistry in 1973. Then he immediately joined Dainichi-Nippon Cables,Ltd. and has been engaged in the research and development of plastic materials for communication cables. Mr.Morita is now sub-chief engineer of Material Reserch Laboratory at Dainichi-Nippon Cables,Ltd.

References

- 1) M.Rokunohe,M.Okada,Y.Oeno,J.Konishi, 24th IWCS Proceedings,pp. 53-62,Nov. 1975
- 2) M.Matsui,Y.Morita, 28th IWCS proceedings,pp.126-136,Nov.1979
- 3) K.Orimo,K.Fuse, J.Soc.Rheology,JPN vol.5 pp.60,1977
- 4) B.H.Bersted,J.Appl.Polym.Sci. vol 28,pp.2777-2791,1983
- 5) C.D.Han,C.Y.Ma,ibd.vol 28,pp.2961-2982,1983
- 6) M.G.Rogers, ibd.,vol 14,pp.1679-1689,1970



Takuma Takai

Production Engineering Department Dainichi-Nippon Cables,Ltd.
Mr.Takai graduated Waseda University majoring in mechanical engineering in 1971. Then he immediately joined Dainichi-Nippon Cables,Ltd. and has been engaged in the production engineering of communication cables. Mr.Takai is now chief engineer of Production Engineering Department at Dainichi-Nippon Cables,Ltd.



Shunichiro Yamaguchi

Electronics and Communication R & Dept.
Dainichi-Nippon Cables.Ltd.
Mr.Yamaguchi graduated Waseda University
majoring in electronics and communication
in 1975.

Then he immediately joined Dainich
-Nippon Cables,Ltd. and has been engaged
in the research and development of commun-
ication cables. Mr.Yamaguchi is now a
member of the Institute Electronics and
Communication Engineers of Japan.



Koji Nishida

Plastic Laboratory ,Product Development
Dept. Mitsubishi Petrochemical Co.,Ltd.
Mr.Nishida graduated master course in
Industrial Chemical Faculty of Fukui
University 1972.

Then he joined Mitsubishi Petrochemical
Co.,Ltd. and has been engaged in the
research and development of
plastics,especially polyolefin.

F. Suzuki, T. Komura and A. Mori

Sumitomo Electric Industries, Ltd.
Tochigi, Japan

Summary

This paper describes the properties and production method of high speed miniature coaxial cables insulated with highly expanded irradiated polyolefin. Advances in computer technology require coaxial cables with a velocity of propagation more than 88% of air and insulation diameters of 1.0mm or less. Until now, the only insulation that could provide these properties was expanded PTFE, but this material is relatively expensive. To address these needs, we have developed an insulation consisting of a small-cell highly foamed polyolefin with a tough polyolefin skin. The cable has a velocity of propagation of 90% of air (3.7nsec./meter) with a diameter of 0.75mm and 1.1mm for the insulation and jacket, respectively. The insulation is irradiated which gives it good thermal stability, mechanical toughness, and resistance to cold flow and solvents.

1. Introduction

Modern computers require coaxial cables with a velocity of propagation equal to 88% of air, insulation diameter of 1.0mm or less and a dielectric constant of 1.3 or less. To meet these properties, the insulation has to have an expansion ratio more than 75% even if fluorocarbons or polyethylene, which have low dielectric constants, are used. According to the ordinary chemical blowing technology for polyethylene, the maximum expansion ratio attainable is about 60% with an insulation diameter less than 3.0mm. Even if the double insulation construction which we have been making from 1978, is used, the maximum expansion ratio is 70%.

Until now, the only insulation that could provide these properties was expanded PTFE. The material is produced as a tape and spirally wrapped around the conductor. However, this material is relatively expensive, the manufacturing process is costly and it provides relatively short cable lengths. To address these needs, we have developed an insulation consisting of a small-cell highly foamed polyolefin with a tough polyolefin skin. The insulation has an expansion ratio of 82% and uses a chemical blowing agent. The insulation is irradiated which gives it good thermal stability, mechanical toughness and resistance to cold flow and solvents. Based on an heat aging tests, we believe the insulation would receive a temperature rating of 105°C in UL specifications.

The insulation has a dielectric constant of 1.20-1.25 and the velocity of propagation is 90% of air (3.7nsec/meter). Cables have been produced with a diameter of 0.75mm and 1.1mm for the insulation and jacket, respectively. This new coaxial cable will be useful for high-speed transmission lines in high density wiring of computers, telecommunications, medical electronics and instrumentation.

2. Extrusion of highly expanded polyolefin

This highly expanded polyolefin can be extruded with an ordinary extruder for expanded polyethylene by modification of several items, as follows:

- (1) Design of the screw to improve homogenization and back pressure
- (2) Die and nipple for double insulation

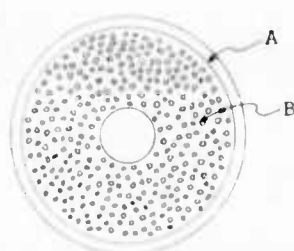
2-1. Selection of material

Selecting a suitable chemical blowing agent and resin for expansion was an important consideration in obtaining highly expanded insulation. It is well known that azodicarbonamide and benzene sulfonyl hydrazide are the preferred chemical blowing agents. In preliminary extrusion tests for the cure of a miniature coaxial cable, the comparison of both chemical blowing agents described above was carried out. As a result of this test, it was shown that azodicarbonamide has a fine cell structure, higher expansion, and a smoother insulation surface. The result of this test suggested that azodicarbonamide should be selected for this purpose.

The insulation compound is a specially formulated polyolefin blend, including antioxidants, lubricants, etc. Several different polyolefins, including high density materials, were blended to obtain a fine cell structure.

2-2. Double layer insulation

An ordinary one layer insulation can achieve a 65% expansion ratio at most. The gas generated by the blowing agent goes off out of the insulation. A double layer insulation was used to obtain higher expansion ratio, and to increase the mechanical strength. Fig.1 shows the construction of the double layer insulation. The inner layer is expanded layer with an expansion ratio of more than 80%, and the outer layer is the solid skin layer.



A: Solid skin
B: Foamed polyolefin

Fig.1. Construction of double layer insulation

2-3. Extruding tools for double layer insulation

Fig.2 shows the tools and the expansion method of double insulation.

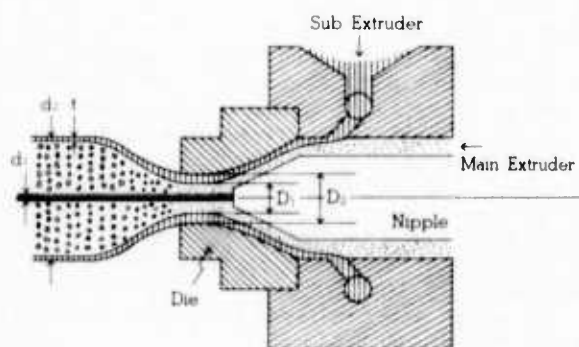


Fig.2. Tools for double insulation and Expansion method

As shown in Fig.2 the resin for the expanded layer from the main extruder and the resin for the skin layer from the sub extruder are extruded as two layers inside of the die. The resin for expansion is expanded after extrusion out of the die, and the resin for the skin layer is spread out by the expanded layer. The gas from the blowing agent is sealed up by the skin layer so as to obtain high expansion.

2-4. Calculation of the inside diameter of the die

Selecting a suitable inside diameter for the die is very important in making a double layer insulation. Because expansion of the expanded layer is started when the resin is extruded out of the die, the inside diameter of die is calculated for when the resins are not expanded. D_1 (diameter of unexpanded resin for expansion) is calculated by the formula (1). As the cross sectional area of the resin for the skin layer is equal between in the die and out of the die, D_2 (inside diameter of die) is calculated by formula (2).

$$D_1^2 - d_1^2 = \left[(d_2 - 2t)^2 - d_1^2 \right] \times \frac{100 - V}{V} \quad V; \text{ expansion ratio (\%)}$$

$$\therefore D_1 = \sqrt{\left[(d_2 - 2t)^2 - d_1^2 \right] \frac{100 - V}{V} + d_1^2} \quad (1)$$

$$D_1^2 - D_2^2 = d_1^2 - (d_2 - 2t)^2$$

$$\therefore D_2 = \sqrt{d_1^2 - \frac{V}{100} \left[(d_2 - 2t)^2 - d_1^2 \right]} \quad (2)$$

2-5. Blowing agent concentration

Fig.3 shows the relationship between the expansion ratio and blowing agent concentration. This was tested by extruding with a diameter of 0.254mm and 1.0mm for the insulation and jacket, respectively. As a result of test, it was decided that the best concentration of azodicarbonamide is 4% for expansion of more than 80%.

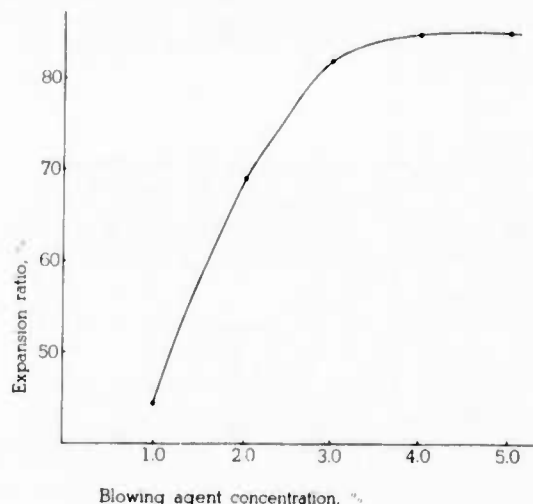


Fig.3. Effect of blowing agent concentration on expansion ratio

2-6. Temperature profile

The melt viscosity of the molten polyolefin affects the expansion ratio and the cell structure. Therefore, the temperature at the front end of the extruder was set lower so as to increase the melt viscosity. Table 1 shows the most preferable temperature profile for producing the maximum expansion ratio.

Table 1. Temperature profile

Feed zone	Compression zone	Metering zone		Cross head	Die
		1	2		
150°C	188°C	195°C	186°C	165°C	165°C

3. Physical properties for the insulation

The highly expanded polyolefin is very weak, even though it has the solid skin layer on the outside. For example, it would be melted immediately if it were touched by a soldering iron. To solve these problems and to improve its reliability as an insulation we irradiated the insulation. Physical properties, described below, are the properties of the new highly expanded irradiated polyolefin.

3-1. Reference rated temperature

Most cables used in computers and other electronic equipment are rated at 80°C by UL. To determine the expected rating temperature for our new cable, we conducted heat aging tests per UL specifications. Aging conditions specified by UL are shown in Table 2.

Table 2. Aging conditions in UL specification
(Subject 758)

Rated temperature (°C)	Aging condition	
	Temperature (°C)	Time (days)
80	113	7
90	121	7
105	136	7

The values for tensile strength and elongation of the aged samples shall be at least 70 percent and 65 percent, respectively, of the values for the unaged samples. Three kinds of samples shown in Table 3, were tested. Test results are shown in Table 4. In the diameter range from 0.65mm to 1.5mm, the insulation met the requirements for a rated temperature of 105°C.

Table 3. Cable samples for aging

Sample No.	A	B	C
Conductor	AWG30(0.254mm) Silver coated copper		
Thickness of expanded layer (mm)	0.14	0.30	0.49
Expansion ratio (%)	82	82	82
Thickness of solid layer (mm)	0.06	0.10	0.13
Diameter of insulation	0.65	1.05	1.50

Table 4. Results of aging test

Rating in UL	Aging condition	Sample		
		A	B	C
80°C	113°C × 7 days	(111)	(101)	(100)
		[106]	[102]	[99]
90°C	121°C × 7 days	(77)	(95)	(101)
		[94]	[91]	[99]
105°C	136°C × 7 days	(75)	(96)	(100)
		[92]	[94]	[100]

() ; Elongation (%)

[] ; Tensile strength (%)

$$\text{Value} = \frac{\text{Value of the aged sample}}{\text{Value of the unaged sample}} \times 100$$

3-2. Soldering

Resistance to damage by solder is very important, for example, when cables are connected to a connector. Samples in Table 3 were tested by the methods of MIL-W-16878, as follows; Specimens of wire, each about 152mm in length, shall be prepared for testing by removing 12.7mm of the insulation at one end. At a point 12.7mm from these ends of the insulation, the specimens shall be given a 90-degree bend over mandrels of their own diameters. These ends shall then be immersed for 5 seconds, to within 3.2mm of the insulation in a pot of molten 60-40 (tin-lead) solder maintained at a temperature of approximately 320°C.

The method and results are shown in Fig.4 and Table 5, respectively.

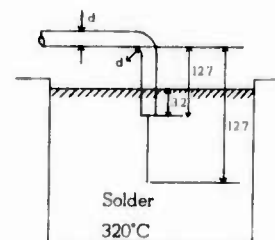


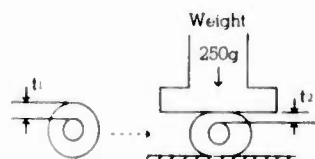
Fig.4. Soldering test

Table 5. Results of soldering test

Item	result
The insulation shall not flare away	Good
The insulation shall not open up over the bend portion	Good
Insulation shrink back (mm)	0.5~1.0

3-3. Deformation

It is important to consider deformation of the insulation during the subsequent manufacturing operations of shielding and jacketing. This is also significant when the cables are placed in compression during termination, clamping, etc. We tested the cables in Table 3 and compared them with expanded PTFE cables having conductor diameters of 0.254mm, and insulation diameters of 1.0mm. Samples were pre-heated for one hour and loaded with 250g weight. Test method and results are shown in Fig.5 and Fig.6.



$$\text{Deformation}(\%) = (1 - \frac{t_2}{t_1}) \times 100$$

Fig.5. Deformation test method

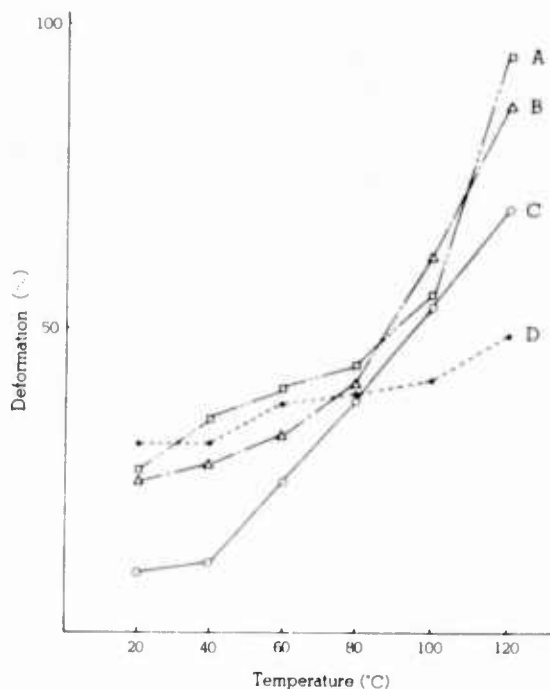


Fig.6. Results of deformation test

Sample A : AWG30×0.65)
 Sample B : AWG30 ×1.05 } ref. Table 3.
 Sample C : AWG30×1.50)
 Sample D : AWG30 ×1.00
 (Expanded PTFE)

As shown in Fig.6, highly expanded irradiated polyolefin insulations are superior to expanded PTFE at room temperature. This means that change in the properties of the cable during the production process for shielding, will be small. At temperature up to 80°C (at which cables are used in equipment), highly expanded irradiated polyolefin is generally equivalent to expanded PTFE.

3-4. Cut-through

Cut-through resistance is another important property. To measure this, we used the method shown in Fig.7. A 0.1mm radius is placed against the insulation, and we measured the weight required to obtain a short between the cutting edge and the conductor. Test samples and results are shown in Table 6. Highly expanded irradiated polyolefin is equivalent to expanded PTFE.

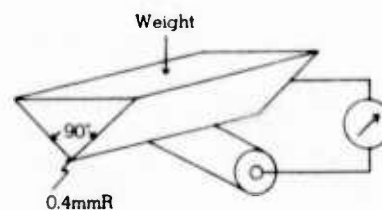


Fig.7. Test method for cut-through

Table 6. Result of cut-through test

Item		Sample-1	Sample-2
Conductor	Material	Tinned copper alloy	
	AWG	30	
	Construction	7/0.1	
Insulation	Material	Expanded PTFE	Highly expanded irradiated polyolefin
	Diameter	0.68mm	0.68mm
Capacitance (PF/m) 1 kHz		75	75
Weight of cut-through (kg)		0.3-1.5	0.5-2.0

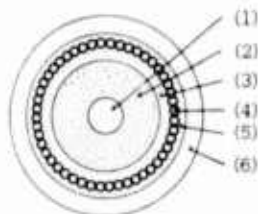
4. Properties of miniature coaxial cables

4-1. Construction

Table 7 and Fig.8 shows the construction and cross section of a high speed miniature coaxial cable with highly expanded irradiated polyolefin.

Table 7. Construction of high speed miniature coaxial cable

Items	Unit	Contents
(1) Conductor	Material	Silver-coated copper alloy
	AWG	32
	Diameter	mm 0.203
(2) Expanded layer	Material	Highly expanded irradiated polyolefin
	Expansion ratio	% 82
	Diameter	mm 0.61
(3) Solid layer	Material	Irradiated polyolefin
	Thickness	mm 0.07
	Diameter	mm 0.75
(4) First shield	Material	Tinned copper
	Construction	40/0.05mm (Spiral wrapped)
	Diameter	mm 0.85
(5) Second shield	Material	Copper coated aluminized polyester
	Construction	0.015mm thick tape wrapping
	Diameter	mm 0.90
(6) Jacket	Material	PVC
	Thickness	mm 0.120
	Diameter	mm 1.14

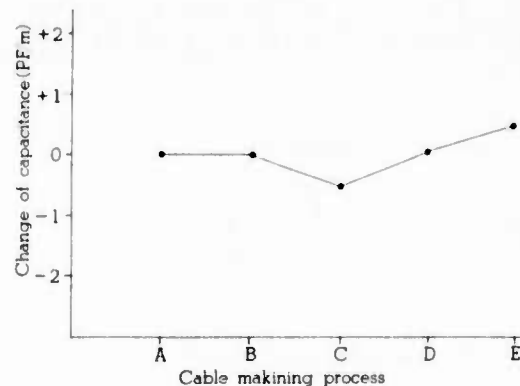


- (1) Conductor 0.203mm silver coated copper alloy
- (2) Expanded layer Highly expanded irradiated polyolefin
- (3) Solid layer Irradiated polyolefin
- (4) First shield 0.05mm tinned copper (Spiral wrapped)
- (5) Second shield 0.015mm copper coated aluminized polyester tape
- (6) Jacket PVC (1.14mm ϕ)

Fig.8. Cross section of high speed miniature coaxial cable

4-2. Change of capacitance

Fig.9 shows the change of capacitance during the cable making process. As mentioned above, the insulation has good mechanical strength and heat resistance due to the solid layer and irradiation. As shown in Fig.9, the change of capacitance is small, and process control can be done easily.



- A : Extrusion of insulation
- B : Irradiation
- C : First shielding
- D : Second shielding
- E : Jacketing

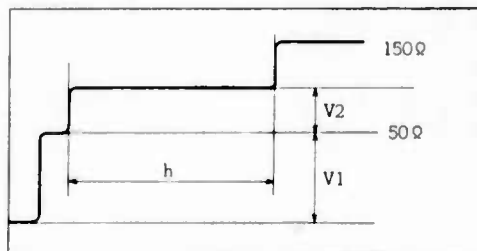
Fig.9. Change of capacitance during cable manufacture

4-3. Electrical properties

Table 8 shows electrical properties of the high speed miniature coaxial cable. Propagation delay time of 3.7nsec/m means the velocity of propagation is 90% of air. Fig.10 shows the test method for characteristic impedance (Z_0) and propagation delay time (T_d) with a TDR.

Table 8. Electrical properties of high speed miniature coaxial cable

Items	Result
Characteristic Impedance (Ω)	74.3
Propagation delay time (nsec/m)	3.70
Attenuation (dB/km)	
@ 5MHz	98.8
@ 10MHz	137.3
@ 20MHz	190.4
@ 40MHz	266.7
@ 80MHz	372.5
@ 100MHz	417.7
Capacitance (PF/m)	
@ 1KHz	55.9
Conductor resistance @ 20°C (Ω /km)	639.2
Insulation resistance (M Ω /km)	>1,000



Sample length (ℓ) : 2m

$$Z_0 = \frac{V_1 + V_2}{V_1 - V_2} \times 50$$

$$T_d = \frac{(h) \times (\text{nsec/div.})}{\ell \times 2}$$

Fig.10 Test method of Z_0 and T_d with TDR

4-4. Physical properties

Several physical properties were tested.

(a) Heat aging

Completed cables were placed for 7 days in an air oven maintained continuously at $98 \pm 2^\circ\text{C}$. After cooling for about one hour at room temperature, the cables were wound and unwound ten consecutive times, within a period of 5 minutes, on a mandrel whose diameter is about 11mm. Dielectric strength and cracking of the insulation or jacket were checked.

(b) Cold bending test

Cables and a mandrel having a diameter of 11mm were conditioned at $-40 \pm 2^\circ\text{C}$ for one hour. Cables were then removed from the cold chamber and immediately bent 3 turns around the mandrel within a period of 12 seconds. Dielectric strength and cracking of the insulation and jacket were checked.

(c) Flammability

Completed cables were tested according to VW-1 in UL specification.

(d) Shrinkage after heat cycle test

Cables were subjected to a heat test. The temperature was programmed from 60°C to -20°C over a 6 hour/cycle. After the exposure for 10 cycles, shrinkage of the insulation from the end of the outer conductor was measured. Sample length was 50cm.

(e) Pull-out strength

Pull-out strength between the inner conductor and the insulation was measured. We also measured the pull-out strength between the first shield and the second shield and jacket (which are bonded together during extrusion). Strength was tested using a tension tester and the maximum strength was recorded. Fig.11 shows the test method for pull-out strength. Test results are listed in Table 9.

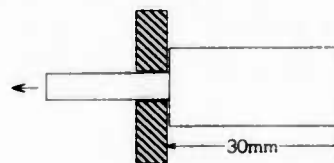


Fig.11 Test method for pull out strength

Table 9. Physical properties of high speed miniature coaxial cable

Items		Result
Heat aging ($98^\circ\text{C} \times 168\text{Hrs}$)	Cracking	Good
	Dielectric strength	Passed ($1000\text{Vrms} \times 1\text{min}$)
Cold bending ($-40^\circ\text{C} \times 168\text{Hrs}$)	Cracking	Good
	Dielectric strength	Passed ($1000\text{Vrms} \times 1\text{min}$)
Flammability (VW-1)		Passed
Shrinkage of insulation ($60^\circ\text{C} / -20^\circ\text{C} \times 10\text{cycles}$)		0.35~0.45mm
Pull out Strength	Inner conductor	0.2~0.5kg/30mm
	Jacket	0.5~0.8kg/30mm

5. Application of the new material to other cables

The new highly expanded irradiated polyolefin insulation is applicable to various types of cables because of its features of high transmission speed, low capacitance and small diameter, etc. Table 10 shows examples of other highly expanded irradiated polyolefin insulated cables. Though these three cables are used mainly for internal wiring of computers and measuring equipment, this new material can be used for multi-conductor cables for external wiring between equipment. For example, small diameter multi-conductor cables with 20-80 shielded insulated conductors can be used for external interconnection between a main system console and a hand held probe for ultrasonic diagnostic system.

6. Conclusion

The new highly expanded irradiated polyolefin and its extrusion technique were developed for supplying miniature coaxial cables with stable quality and lower price to a market that requires even faster transmission speed and smaller cables in the future. The new cable insulated with a highly expanded irradiated polyolefin with about 82% expansion has excellent properties when compared to conventional cables. The new material makes it possible to produce various types of miniature coaxial cables and multi conductor cables.

7. Reference

1. Y.Toda and T.Nakahara, et al., "A Highly expanded Polyethylene Insulated CATV Coaxial Cable" 22nd International Wire and Cable Symposium, 1973.
2. M.Yuto and T.Nakahara, et al., "Novel Extrusion Process For Robust Highly Expanded Polyethylene Insulated Coaxial Cables" 25th International Wire and Cable Symposium, 1976.
3. F.Suzuki and A.Mori, et al., "Microcoaxial Cables Insulated With Highly Expanded Polyethylene By Chemical Blowing Method" 27th International Wire and Cable Symposium, 1978.



Fumio Suzuki

Sumitomo Electric Industries, Ltd.
1, Taya-cho,
Totsuka-ku,
Yokohama,
Japan

Fumio Suzuki finished the chemical Engineering Course of Arai High School in Niigata Prefecture in 1958.

He joined the Research Division of Sumitomo Electric Industries, Ltd. in 1958, and worked on application research of high polymers especially polyvinyl chloride for wire and cables. Mr. Suzuki is now Senior Engineer of Communications R & D Department and a member of the Society of Polymer Science of Japan.



Akinori Mori

Sumitomo Electric Industries, Ltd.
3-3, Satsuki-cho,
Kanuma-city,
Tochigi-prefecture
Japan

Akinori Mori received his B.S. degree in mechanical engineering from Kyusyu University in 1970. He then joined Sumitomo Electric Industries, Ltd., and engaged in development and design of plastic cables. Mr. Mori is now Assistant to Manager, Industrial Electronics Wire Section, Electronics Wire Division.



Toshiro Komura

Sumitomo Electric Industries, Ltd.
3-3. Satsuki-cho,
Kanuma-city,
Tochigi-prefecture
Japan

Toshiro Komura received his B.S. degree in applied chemical engineering from Kyushu University in 1981. He then joined Sumitomo Electric Industries, Ltd., and engaged in manufacturing of plastic cables. Mr. Komura is now a member of Electronics Wire Division.

Table 10. Constructions and properties of highly expanded irradiated polyolefin insulated cables

Items \ Type		AWG30-SXSLAV (50)	AWG30-SXBV (100)	AWG32x2SXLAV
Conductor	Material	Tinned copper alloy	Silver-coated copper	Silver-coated copper alloy
	Strand	7/0.1	1	1
	Diameter (mm)	0.3	0.254	0.203
Inner Insulation	Material	Highly Expanded Polyolefin (Expansion Ratio 82%)	Highly Expanded Polyolefin (Expansion Ratio 82%)	Highly Expanded Polyolefin (Expansion Ratio 82%)
	Diameter (mm)	0.56	1.35	0.80
Outer Insulation	Material	Polyolefin	Polyolefin	Polyolefin
	Thickness (mm)	0.07	0.10	0.10
	Diameter (mm)	0.70	1.55	1.0
Irradiation of Insulation		Irradiate	Irradiate	Irradiate
Twist		-	-	2 Conductors
First Shield	Material	Tinned copper (Spiral wrapped)	Tinned copper (Braided)	Aluminized Polyester Tape (Spiral wrapped)
	Diameter (mm)	0.80	2.05	1.10
Second Shield	Material	Copper coated Aluminized polyester Tape (Spiral wrapped)	-	-
Jacket	Material	PVC	PVC	PVC
	Thickness (mm)	0.18	0.2	0.38
	Diameter (mm)	1.20	2.45	3.06x2.86
Conductor resistance (Ω /Km)		340	337	670
Dielectric strength 1.0KVrmsx1min.		Pass	Pass	Pass
Insulation resistance (M Ω -Km)		1000	1000	1000
Capacitance @1KHz (PF/m)	Conductor-Conductor	-	-	18
	Conductor-Shield	80	37.3	36
Characteristic Impedance TDR (%)	Conductor-Conductor	-	-	160
	Conductor-Shield	51	102	102
Propagation delay time	(nsec/m)	3.70	3.70	3.75

COMPUTER PREDICTION OF COAXIAL CABLE STRUCTURAL RETURN LOSS DURING CORE EXTRUSION

Leonard Visser

Belden
Geneva, Illinois

SUMMARY

Most periodic defects in coax are introduced during the core extrusion process. These defects can ultimately lead to structural return loss (SRL) spikes of sufficient amplitude to make the finished cable worthless. A method has been evaluated which predicts the SRL performance of coax based on real time measurements of the core during extrusion. Thus defects can be detected early in the manufacturing process before most of the cost is added. The accuracy of this method has been tested with encouraging results despite the many assumptions and simplifications which were made. The computer program developed to make these predictions can be supplied with artificial data. You can then study the effect of periodic defect waveshape on the structural return loss. This has been done for several interesting cases. The good correlation between predictions and test results of finished cable advocate implementing this method as a production control tool.

INTRODUCTION

Structural return loss is important when even relatively small reflections of transmitted RF energy cannot be tolerated. CATV installations are a common application of coaxial cable where small reflections affect performance. Video signals which undergo reflections in the transmission line result in ghosting or noise when viewed on the TV. Every non-ideal transmission line will reflect some of the incident wave of a transmitted signal. Structural return loss is the signal strength relationship of the reflected wave to the incident wave.

Part of the incident wave is reflected each time the cable impedance changes in value. Each of these reflections contribute to the SRL of the entire cable. The impedance a signal sees as it travels down the cable can vary in the following ways:

- 1) Abrupt and localized changes which may cause large reflections affecting many frequencies.
- 2) Randomly distributed changes of small and random amplitude. The resulting reflections do not add in phase.

- 3) Periodic changes which continue throughout the cable length. The reflections add in phase at certain frequencies causing SRL spikes.

We will be considering the third type of variation in the following discussion. Our experience has been that most SRL testing failures have been caused by these periodic impedance fluctuations. Further, most of these fluctuations are created during extrusion of the dielectric material to form the coax core. Our objective has been to determine if SRL can be predicted based on measurements of core diameter and dielectric constant. Also, the predictions should be made relatively quickly while the core is being extruded. This will result in two benefits. Detection of flawed product will occur as soon as possible. Second, feedback to the extruder operator will be almost instantaneous as attempts are made to correct a detected problem.

The approach we have taken to make these predicted SRL measurements is similar to that presented by R.

Mathiew, Y. Peltier and A.J. Ghazi.¹ The main differences are the result of increasing the data sampling frequency by at least an order of magnitude. This is necessary to monitor core extrusions running at 1000 ft/min and for predictions extending to 1 GHz in frequency. Linear capacitance could not be measured at these speeds over a short section of cable, so core diameter is the only measured parameter. Use of the discreet fourier transform of sampled data to detect periodicities is the key to this method.

FUNDAMENTAL CONSIDERATIONS

The cable impedance is a function of three basic cable parameters. They are the inner conductor diameter, d , the outer conductor's inner diameter, D , and the dielectric constant, ϵ . The relation is:

$$Z = \frac{60}{\sqrt{\epsilon}} \ln \left(\frac{D}{d} \right) \quad 1$$

Assuming a tight fit between the shield and the coax core, D is equal to the core O.D. The dielectric constant can be easily calculated from the linear capacitance. Thus, if you measure d , D , and capacitance at every point along a coax core, the impedance will be known as a function of cable length. From this impedance function, the reflection coefficient, ρ , could be determined

exactly for the cable or any section thereof. The return loss would then be known by the relation:

$$SRL = 20 \log \left(\frac{1}{1 - P} \right) \quad 2$$

Unfortunately, complete knowledge of these parameters could not be obtained in real time during extrusion, nor could the numbers be analyzed by a digital computer with sufficient speed. To speed things up the following assumptions are made.

- 1) Only the core diameter needs to be measured to determine impedance fluctuations in the finished cable.
- 2) Random diameter fluctuations will be sufficiently small that they can be treated as periodic.
- 3) Periodic fluctuations continue throughout the cable length.
- 4) A few hundred measurements of core diameter will be sufficient to characterize the section of core examined.

The first assumption seems to be the most dangerous. It implies that the other two parameters, d and ϵ , need not be measured. Also that no periodic defects are introduced during the application of the shield and jacket. Yet it is usually a valid assumption as will be seen.

PREDICTION METHOD

The method for predicting SRL consists of three major steps. First, the core diameter is monitored to obtain a block of data. Second, the data is processed in a computer to calculate the SRL. Third, the results are displayed on a graph similar to the charts obtained in sweep testing of finished cable. The process can be shown in block diagram form.



Analog Measurement

The core diameter is measured with a laser micrometer. The output is an analog signal which is updated every 20 milliseconds. The range of the signal was typically set at ± 5 mils deviation full scale.

Filtering

Since the data is sampled at discrete time intervals, a filter is required to eliminate all frequencies above two times the sampling frequency. This prevents aliasing of these higher frequencies which could cause low frequency spikes in the SRL prediction. The filter cutoff frequency is a function of sampling frequency which varies with linespeed. We used a switched capacitor, low pass filter whose cutoff frequency is programmable via a clock frequency.

A/D Conversion

The filtered analog data is converted to digital values at a predetermined sampling rate. The converter has 12 bit resolution. This digital data is fed into a computer.

FFT, SRL Calculation

A computer is used to process the diameter data. To detect periodic fluctuations, a fast fourier transform is used to transform the data from the time to the frequency domain. The FFT is best done on a number of samples which is a power of 2. A choice of 256 or 512 samples results in sufficient frequency resolution in the SRL prediction. The upper frequency limit is often determined by the application for which the coax is intended. Typical values are 500 and 1000 MHz.

The first step is to calculate the sampling interval required and to capture the raw data. The interval is calculated from:

$$\text{Sampling Interval} = \frac{V_p}{4 F_{\max}} \cdot \frac{1}{\text{Line speed}} \quad 3$$

Where V_p = velocity of propagation and F_{\max} is upper frequency limit of the prediction. The samples are then taken at this interval and stored in an array $F(\Delta D)$.

The actual diameter as a function of $F(\Delta D)$ is then calculated based on a scaling factor and the nominal core size. This is called $F(D)$.

Next the impedance is calculated from the stored diameter values using

$$Z = .63 V_p \ln \left(\frac{D}{d} \right) \quad 4$$

Then the array containing the impedance is passed to an FFT routine which returns the magnitude of the impedance fluctuations as a function of frequency, $F(\Delta Z)$.

The attenuation, α , of the cable is calculated using:

$$\alpha = \sqrt{f} \frac{K}{Z_0} \left(\frac{1}{D} + \frac{1}{d} \right) \quad 5$$

Where K is a constant that depends on the units used. This is done at each frequency, f , which corresponds to the elements in the array $F(\Delta Z)$. Z_0 is the cable characteristic impedance, D and d are the nominal core O.D. and the wire O.D. respectively.

Finally, the SRL is calculated from the ΔZ values using:

$$SRL = -20 \log \left(\frac{Z_0 \alpha}{.91 \Delta Z} \frac{N S}{I} \frac{1}{1 - e^{(-2\alpha L)}} \right) \quad 6$$

Where $S = V_p/4 F_{\max}$, N is the number of samples taken, I is the array subscript which ranges from 1

to $N/2$, and L is the length of cable for which the prediction is being made. The SRL values are negative which aids in plotting the results.

Plot Results

Once the diameter measurements are processed, the SRL prediction can be plotted. The convention is to plot SRL with values increasing in the negative X direction. An X, Y plot is made of the SRL vs. frequency. We were able to direct the plot to either a graphics CRT or a pen plotter.

CORRELATION: PREDICTED VS. MEASURED

Many samples of coax core were monitored to predict the SRL. The cable types included RG-59/U, 6/U and 11/U. The dielectric materials included both solid and foam polyethylene and solid polypropylene. The predicted curves look similar to the charts made during the sweep test of finished cable. To determine if the predicted spikes match those measured in finished cable, great care had to be taken to match the monitored length of core to the finished piece of cable used for testing.

An example of the results obtained appear in Figures 1 and 2. Here Figure 1 is the computer prediction and Figure 2 is the finished cable test results. One prominent spike is seen at 260 MHz. The predicted amplitude and the measured amplitude match almost exactly at 25 dB. The grass levels do not form such a good match. This was expected since the grass level or noise level is a function of random impedance fluctuations which cause reflections whose phases do not match. The program treats random fluctuations as periodic. We have observed cases where the core had large random diameter fluctuations. The computer prediction then shows the grass too high (small SRL values) and true periodic induced spikes were masked (hidden in the grass).

Inducing Controlled Spikes

Often there would be no outstanding features to base a comparison on. To obtain data from a known and controllable source, a device was added to the extrusion line to generate SRL spikes. This is the same type device used by W.L. Roberts and F.N.

Wilkenloh² in their studies. It is simply a sheave that has been fitted with adjustable unbalancing weights. The conductor is wrapped once around this before entering the extruder crosshead. As the wire moves, the weights produce a sinusoidal tension variation. This results in core diameter fluctuations whose period is related to sheave diameter.

We used 8 inch and 16 inch diameter sheaves which were unbalanced with 1 or 2 pound weights. The sheaves produced spikes at the frequencies given by:

$$F_{\text{spike}} = \frac{V_p}{2C} \quad 7$$

Where C is the circumference of the sheave or defect period. For our sheaves, spikes were produced at 78 and 155 MHz for solid dielectrics and 92 and 183 MHz for foam dielectrics.

Spikes were induced in both foam and solid cores. The core was monitored to give 15 predictions. This core was then braided and jacketed prior to SRL sweep testing. Once testing was completed, the predicted spike amplitudes were compared to the measure values. The amplitudes ranged from 22 to 37 dB. The mean deviation of the predictions from the measured values was -0.1 dB. The standard deviation of the differences was 2.9 dB. The maximum difference was a 33 dB prediction for a 27 dB spike. This correlation and that obtained from additional trials has proved to be acceptable.

PREDICTIONS USING ARTIFICIAL DATA

Various diameter or impedance waveshapes can be fed into the analysis portion of the program to see the effect on SRL. Figure 3 shows the envelope of peaks resulting from sinusoidal core diameter fluctuations of 0.1, 0.2, and 0.5 mil amplitude. The dimensions used are for an RG-59/U coax, 1000 ft. long. As you can see, the fluctuations produce smaller reflections (larger SRL values) at low frequencies. This is because the cable attenuation and length allow fewer cycles of the defect to be 'seen' by the RF signal. At high frequencies, many cycles are seen and each reflection adds in phase to produce a large SRL spike.

The effect of cable length on SRL is shown in Figure 4. In general, a shorter length of cable will result in smaller SRL. This is because fewer cycles of the defect are present. At high frequencies the length has less effect because attenuation has eliminated most of the reflected signal originating at the far end of the cable.

If the defect or impedance periodicity is sinusoidal, then only one frequency will be affected. This is shown in Figure 5. When the waveform of the impedance fluctuation is not perfectly sinusoidal, harmonics will be seen along with the fundamental frequency. Figure 6 shows the SRL curve resulting from a nearly perfect square wave fluctuation. The fundamental frequency is the same as the sine wave of figure 5. In some cases, the harmonics can have larger amplitudes than the fundamental spikes. Confusion can result when attempting to identify the cause of such spikes in a cable sample.

Discreet or isolated impedance changes do sometimes occur. An improperly terminated or pigtailed cable is a possible source of such a change. An exaggeration of this type defect consists of a length of 50 ohm cable connected to a 75 ohm line. The computer analysis of this situation is shown in Figure 7. A 46 inch piece of 50 ohm coax attached to a 1000 foot length of 75 ohm coax was modeled. You can see that almost all frequencies are affected. The spacing of the humps in the curve is indicative of the defect size.

Cable with SRL sweeps that look similar to Figure 7 have been seen during quality control testing. The cause can usually be identified and cut out of the cable, sometimes leaving a salvageable length. Figure 8 is the result of testing the cable modeled for Figure 7. The resemblance is obvious. The

prediction curve is about 5 dB off at the low frequency end. This is because the program treats all cable defects as periodic. The 200 feet of cable 'examined,' when 512 samples are used with a F_{max} of 500 MHz, are essentially repeated enough times to make up the cable length, L . Given the attenuation for our RG-59/U coax model, at low frequencies the false repeating impedance step can be seen for several cycles.

CONCLUSIONS

This method for predicting SRL during core extrusion has proven successful. Attempts to correlate the predicted spike amplitude to the measured amplitude for finished cable have shown good agreement. The grass levels or noise levels in the SRL curve are not always accurately predicted, however. The method is designed to correctly handle periodic cable defects only. To reduce the levels predicted resulting from random core diameter fluctuations, averaging may be used. This was tried with good results. The predictions can be made at 1 minute intervals using an HP-9816 desk top computer, programmed in BASIC. Most of this time is consumed in sampling the data and performing the FFT calculations. The program can be used to analyze various types of cable defects to see the effect on SRL. Use of the method allows real time detection of periodic defects at the core extrusion stage of cable manufacture. Thus an excellent quality control and diagnostic tool is available.

REFERENCES

- 1) R. Matheiu, Y. Peltier and A.J. Ghazi, "Structural Return Loss Performance Evaluation of Materials and Elements for High Quality Coaxial Cables", Proc. International Wire & Cable Symposium, 1976.
- 2) W.L. Roberts and F.N. Wilkenloh, "Effects of Nonuniform Coaxial Cable on CATV Signal Quality", Comm/Scope Corporation.
- 3) J.A. Olszewski and H. Lubars, "Structural Return Loss Phenomenon in Coaxial Cable", Proc. of the IEEE, Vol. 58, No. 7, July 1970, pp. 1036 - 1050.
- 4) IEEE Digital Signal Processing Committee, "Programs for Digital Signal Processing", 1969, IEEE Press.
- 5) E. Oran Brigham, "The Fast Fourier Transform", 1974, Prentice-Hall, Inc.



Leonard J. Visser
Belden
2000 S. Batavia Ave.
Geneva, IL 60134

Mr. Visser received a B.S. in Physics from the University of Northern Iowa in 1980. He joined Belden in 1980 as a Research Engineer at the Technical Research Center in Geneva, Illinois. As an Electronic Product Development Engineer, Visser is now responsible for computerizing cable test procedures, new product development and technical services.

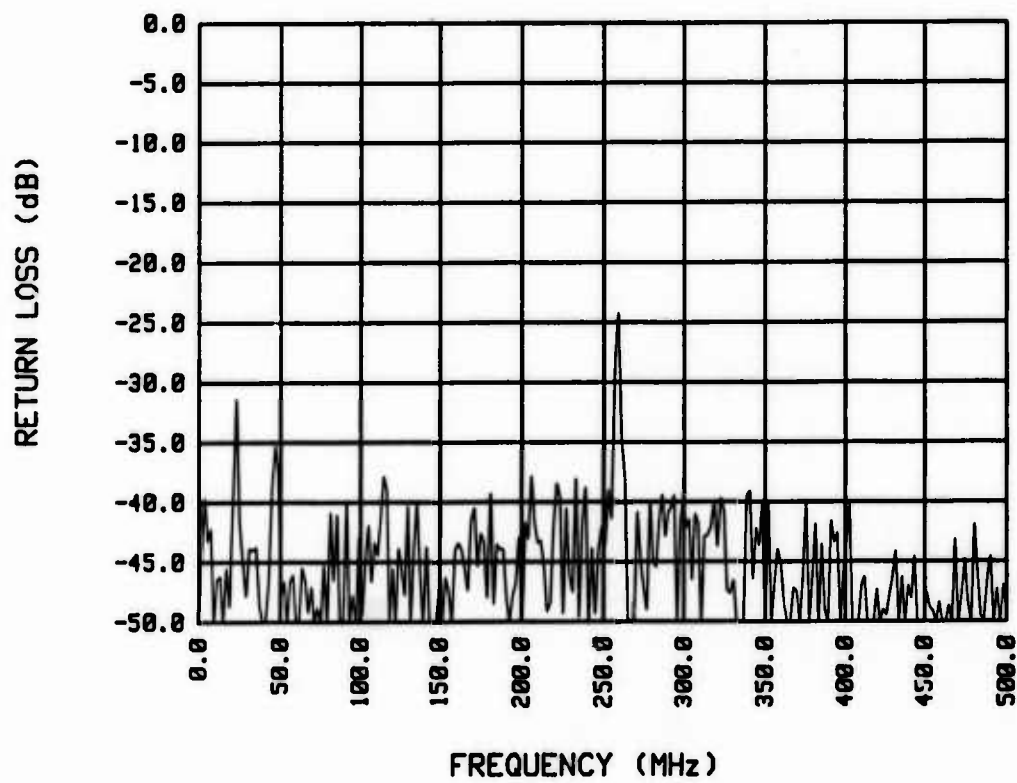


Figure 1. Typical computer prediction of return loss.

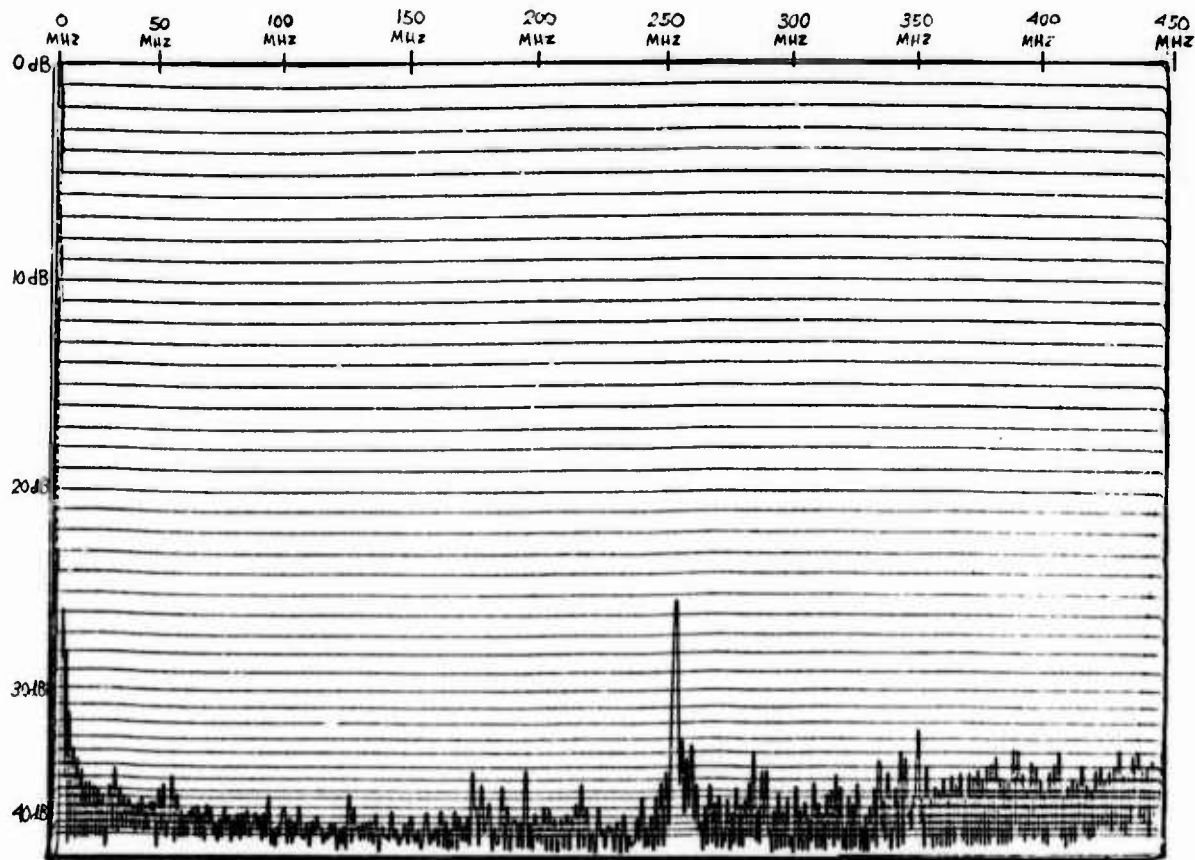


Figure 2. Return loss measured on finished cable.

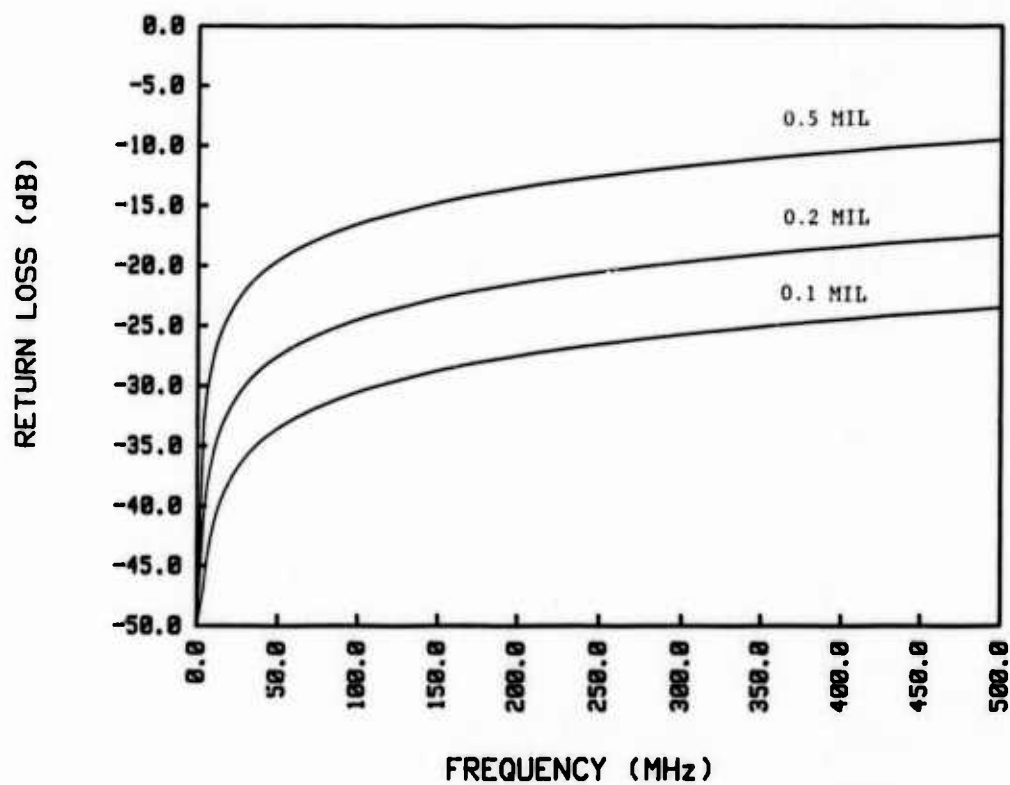


Figure 3. Envelope of peaks resulting from sinusoidal core diameter fluctuations of 0.1, 0.2, 0.5 mil amplitude. Assumes RG 59/U 1000 ft. long.

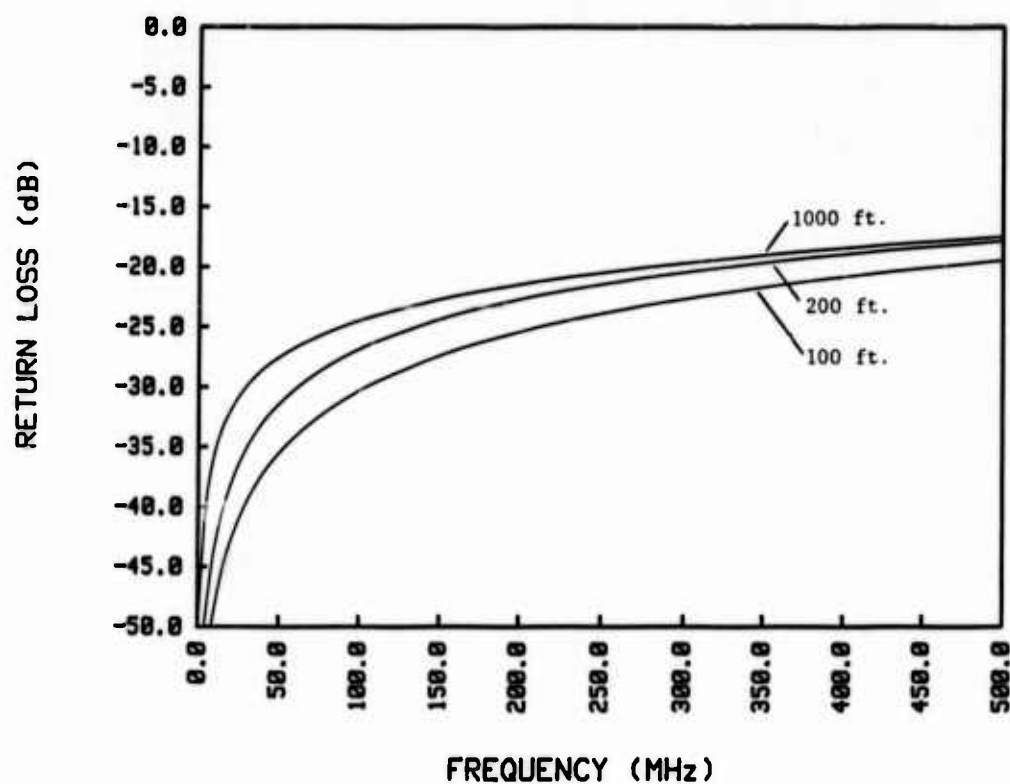


Figure 4. Envelope of peaks resulting from 0.2 mil amplitude fluctuations for 1000, 200 and 100 ft. lengths of RG 59/U.

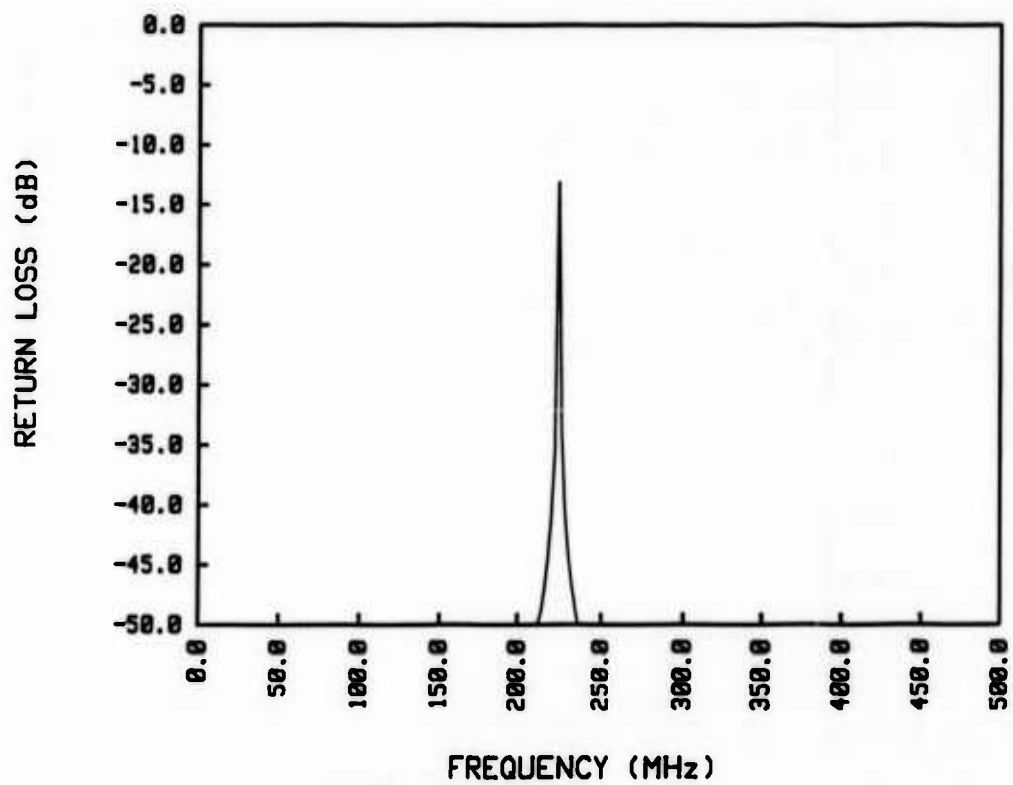


Figure 5. Sinusoidal impedance variation at single frequency.

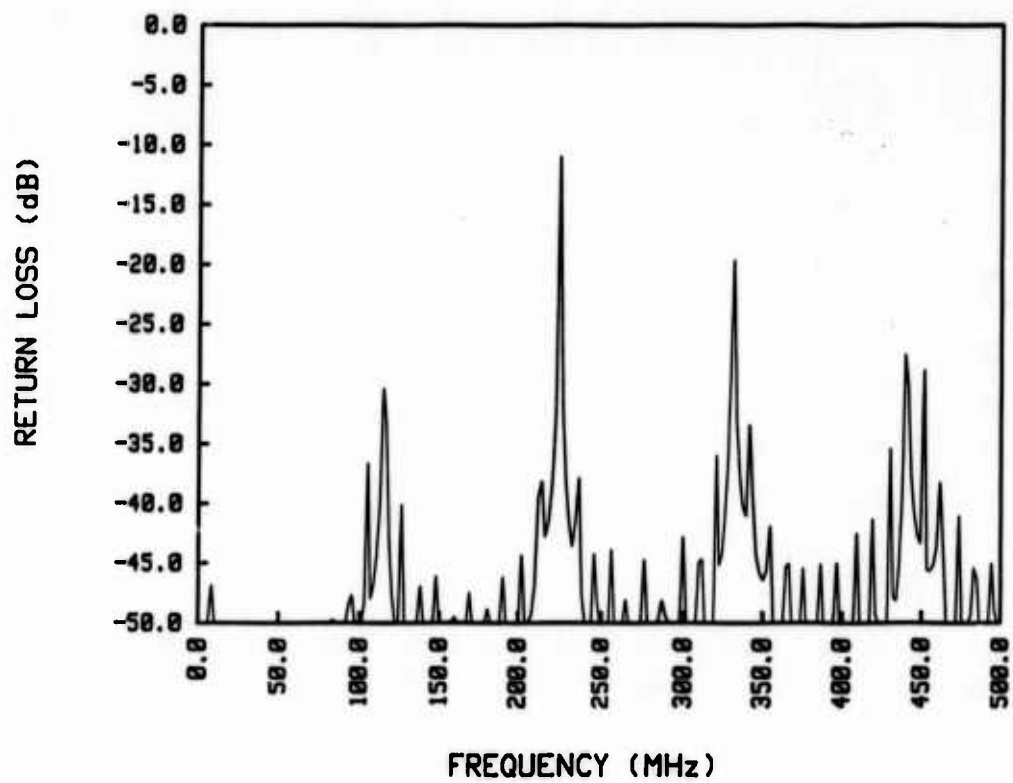


Figure 6. Square wave impedance variation at single frequency.

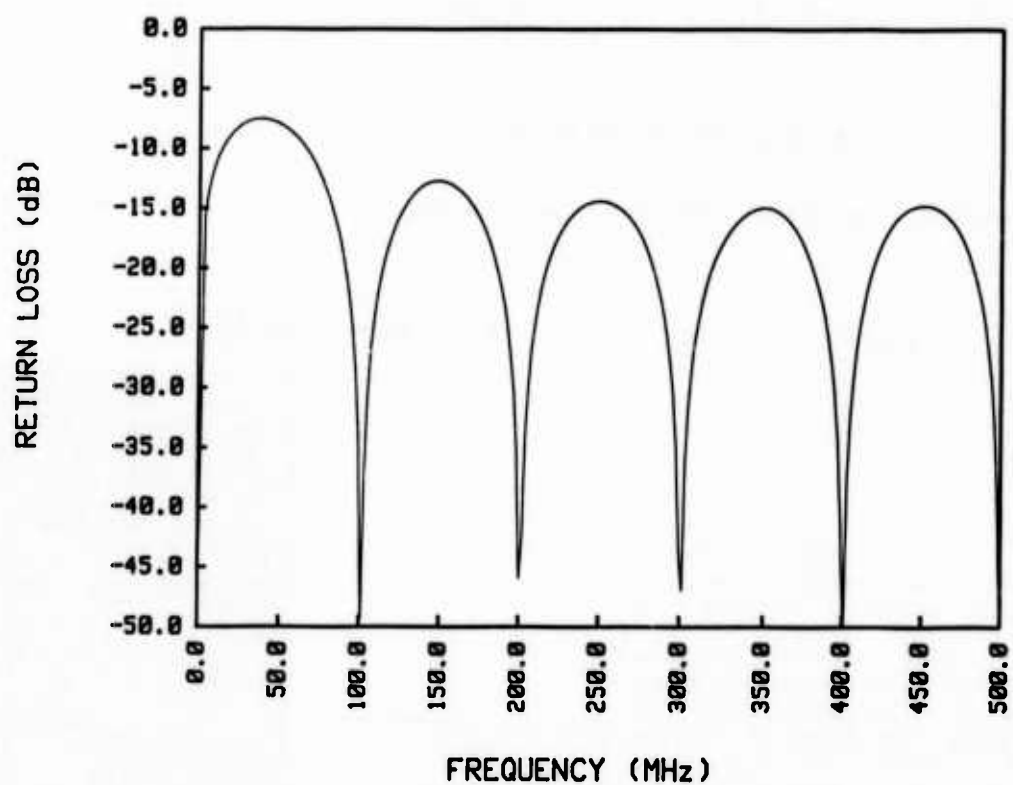


Figure 7. Predicted SRL for 46 inch piece of 50 ohm coax followed by 1000 feet of 75 ohm coax.

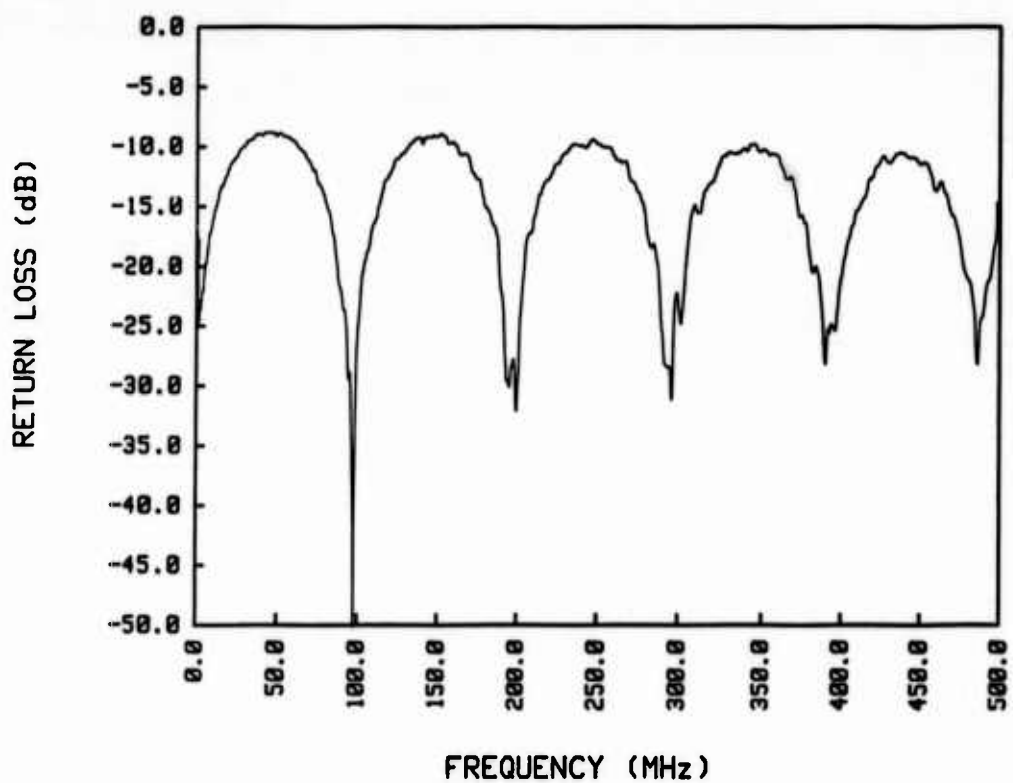


Figure 8. Measured SRL for 46 inch piece of 50 ohm coax followed by 1000 feet of 75 ohm coax.

MULTIPULLING AND CABLING IN LINE : A NEW PROCESS

GOURONNEC Alain, LE NOANE Georges, GROSSO Philippe, VALETTE Philippe, GUEGAN Yvon, BENOIST André

CNET/LANNION B - LAB/ROC/FCO - Route de Trégastel - 22301 LANNION

ABSTRACT

The feasibility of the Multipulling and Cabling in Line (MCL) has been investigated for the development of the optical fiber mass production needed for the cabling of broadband networks. This new method can be considered as the first experiment in the world. So the multipulling and the cabling in line process will be a future cable technology permitting the mass production of optical cables for local broadband networks. The integration of these two technologies now permits a real decrease in the costs and an increase in the reliability of the transmission systems.

INTRODUCTION

The use of optical fibers for broadband multiservice network is now planned on a large scale. Thus the economical aspect of low cost optical cables production is the most important problems to be solved. Recent cables costs evaluations show that it is necessary to study and to develop a fully mass production of optical cables. Some studies tend to improve the preform manufacturing process by increasing the preform size, others aim to decreasing the cost of the pulling by increasing the pulling speed. Now and other procedure is possible to cope with the necessary mass production of optical fibers :

"The Multipulling and Cabling in Line" (fig. 1)

Based on the V-groove or the U-groove cable, that integration of two independent technologies enables to obtain a low cost manufacturing optical cables for the local multiservice network.

The MCL process (fig. 2) consists in :

- a multipulling apparatus
- a cabling equipment

Figure 1

The MCL process
(Multipulling
apparatus)



TECHNICAL DESCRIPTION OF THE MCL PROCESS [1, 3]

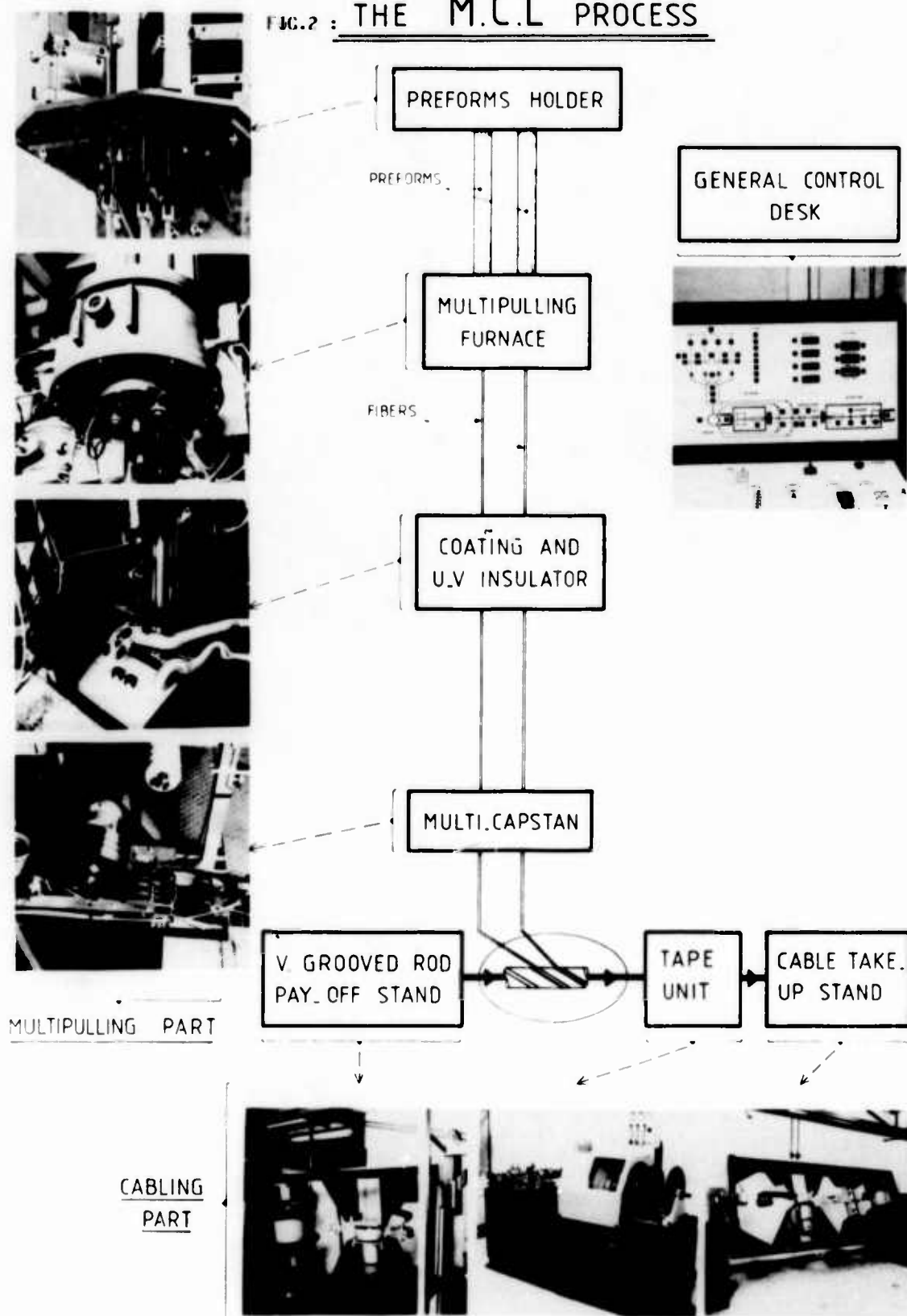
The multimulling apparatus

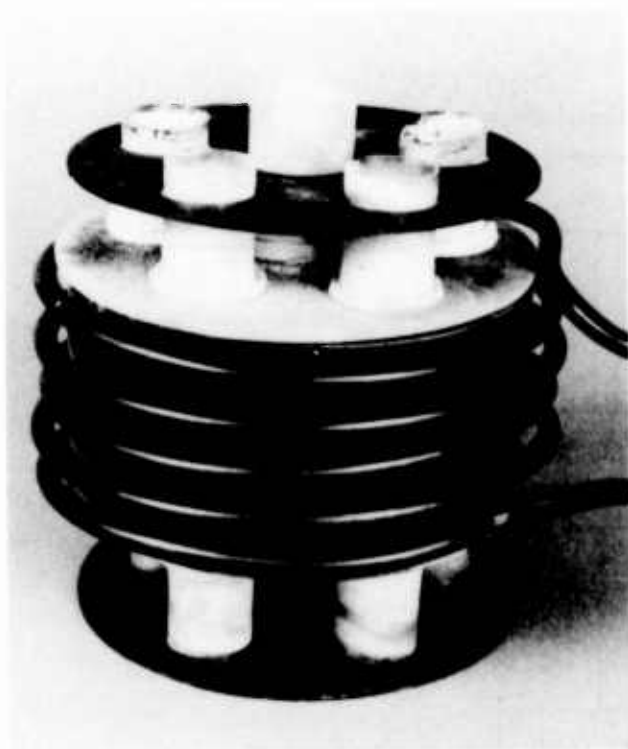
The multipulling furnace and the coating technique :

The multipulling apparatus permit the simultaneous drawing of several preforms (1 to 10). The furnace consists in a cylindrical graphite susceptor having 160 mm in diameter, 70 mm in high with as many laboratories as preforms to be pulled (fig. 3). These laboratories are drilled where the maximum efficiency of the induction field is obtained (fig. 4).

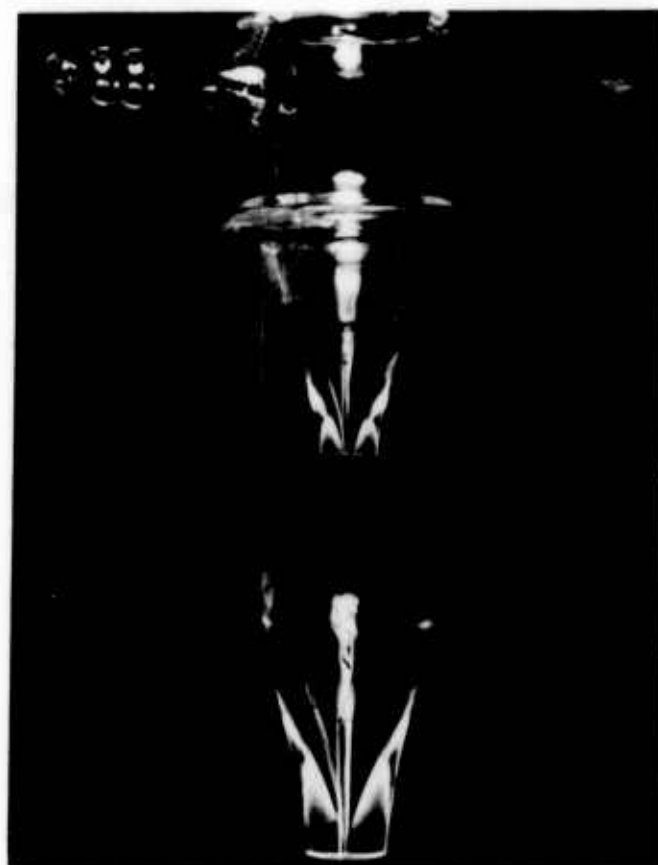
Thus a very good thermal distribution (35 mm of hot zone size and 20 mm of inside diameter) associated with a good temperature stability ($\pm 2^\circ\text{C}$ to 1960°C) is obtained. Several multicavities furnaces were developed corresponding to the different unit cables. The results presented in this paper have been obtained in a four cavities furnace.

FIG.2 : THE M.C.L PROCESS

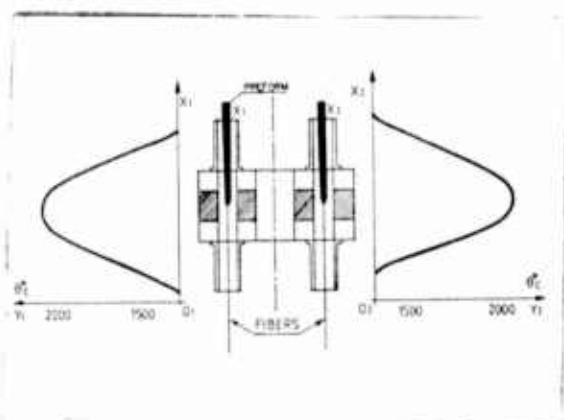




- Figure 3 -
The multipulling furnace



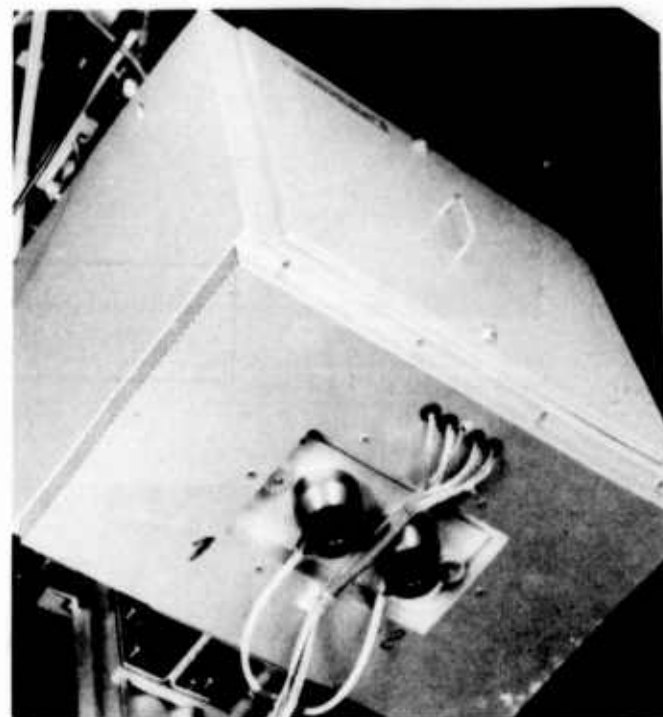
- Figure 5 -
A self pressured double glass die



- Figure 4 -
Thermal distribution of the furnace

The coating system consists in as many self pressured glass dies (fig.5) as pulled fibers. The diameter of the dies is $250\text{ }\mu\text{m}$ giving an overall fiber diameter of $220\text{ }\mu\text{m} \pm 2\text{ }\mu\text{m}$. An U.V. cured epoxy acrylate resin is used as coated material.

A new U.V. insulator has been developed for the simultaneous curing of the fibers coatings (fig.6).



- Figure 6 -
Two fibers U.V. insulator

The multipulling system :

On the pulling machine the capstan speed is kept constant to avoid any intermediate equipment between the capstan and the cabling machine (fig.7).



- Figure 7 -
The multipulling capstan

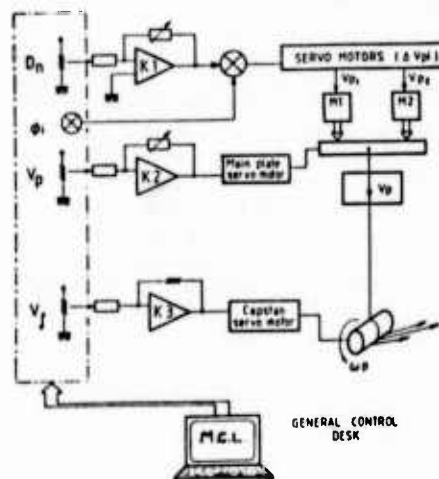
The fibers diameters are kept constant with an especially designed preform holder which permits the introducing of the preforms in the furnace at different speeds. This preform holder is made of two systems: (fig.8).

- A main plate driven by a closed loop control direct current servo-motor monitored by the in line diameter measurement of one of the fiber.

- As many secondary preforms holders as preforms to be pulled, each of them driven by an auxiliary direct current servo motor monitored by a recorded signal depending of each preform. So the equations of the pulling conditions, giving the relationships between preforms and fibers volumes are the followings :

The speed of the main plate gives for all the preforms the equation (1).

$$U_p (D_N)^2 = C^{te} = V_{fN} \quad (1)$$



- Fig.8 -
The MCL Servo-system

where $\left\{ \begin{array}{l} V_p = \text{main plate preform holder speed.} \\ D_N = \text{diameter mean value of the preforms} \\ \text{multipulled (or nominal diameter} \\ \text{of one of the preforms)} \\ V_{fN} = \text{MCL speed} \\ D_{fN} = 125 \mu\text{m in the experiment} \end{array} \right.$

The secondary preform holder gives for each particular preform the equation (2)

$$D_{pi} = D_N = p_i \quad (2)$$

where $\left\{ \begin{array}{l} D_{pi} = \text{Recorded diameter profile for} \\ \text{preform } i \\ \Delta p_i = \text{Differential diameter profile} \\ \text{recorded signal} \end{array} \right.$

The general equation for the MCL servo system is given by the equations (3) and (4)

$$V_p (D_N)^2 + \sum_{i=1}^N V_{pi} (\Delta p_i)^2 = V_{fN} (D_{fN})^2 \quad (3)$$

$$V_p (D_N)^2 + \sum_{i=1}^N V_{pi} (\Delta p_i)^2 = V_{fN} (D_{fN})^2 \quad (4)$$

THE CABLING MACHINE

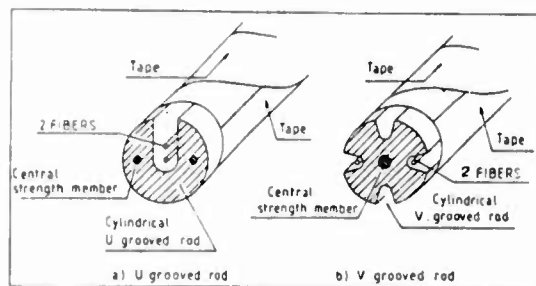
In France and more and more in others countries there is a particular interest for loose cable structures where the fibers are simultaneously layed free of tension in their protections supports [2] (fig.9). V-grooved cables has been designed for this purpose and are very well adapted to be manufactured in line with the multipulling. These V-grooved cables are based on reinforced plastic tensile strength with peripheral helicoidal grooves where the fibers are laid. To permit the in line integration of the multipulled and the cabling techniques the following procedure has been developed :

- The plastic unit, with it V-grooves must be manufactured previously to the cabling with an adapted extruder.

- The reel of the plastic V-grooved rod is placed on the pay off stand of the cabling machine. The central rod is pulled with a constant tension (typically 5 to 50 daN) during the M.C.L. procedure.

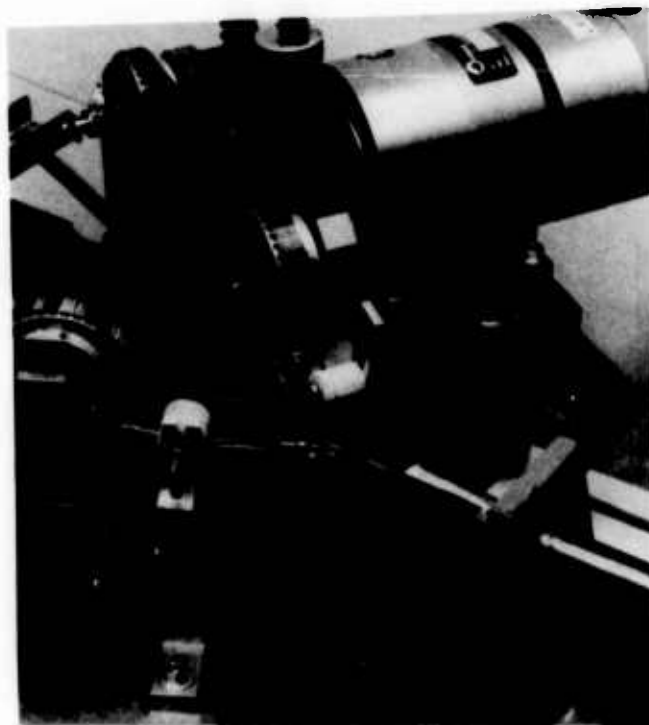
- The V-grooves pitch are controlled by a rotating cursor which monitored the rotation speeds of the pay off stand and the take up stand of the machine. Then the fibers directly during the pulling process, are placed in the grooves by an automatic fiber injector (fig.10). A servo system permits the control of the difference of linear speeds between the V-grooved central rod and the multipulled fibers. The fibers over length needed in this cable design to insure a good cable construction, free of microbendings, is fixed by a signal order defined as a sliding coefficient k . (fig.11). After laying the fibers in the grooves, a plastic tape is applied to maintain the fibers in their grooves.

The MCL process is performed by a programmed automaton ordered from the general control desk (fig.12).



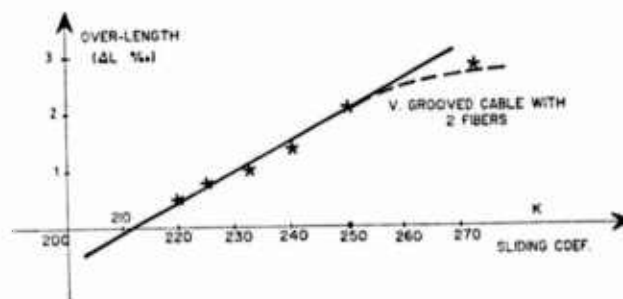
- Fig.9 -

Cables broadband network



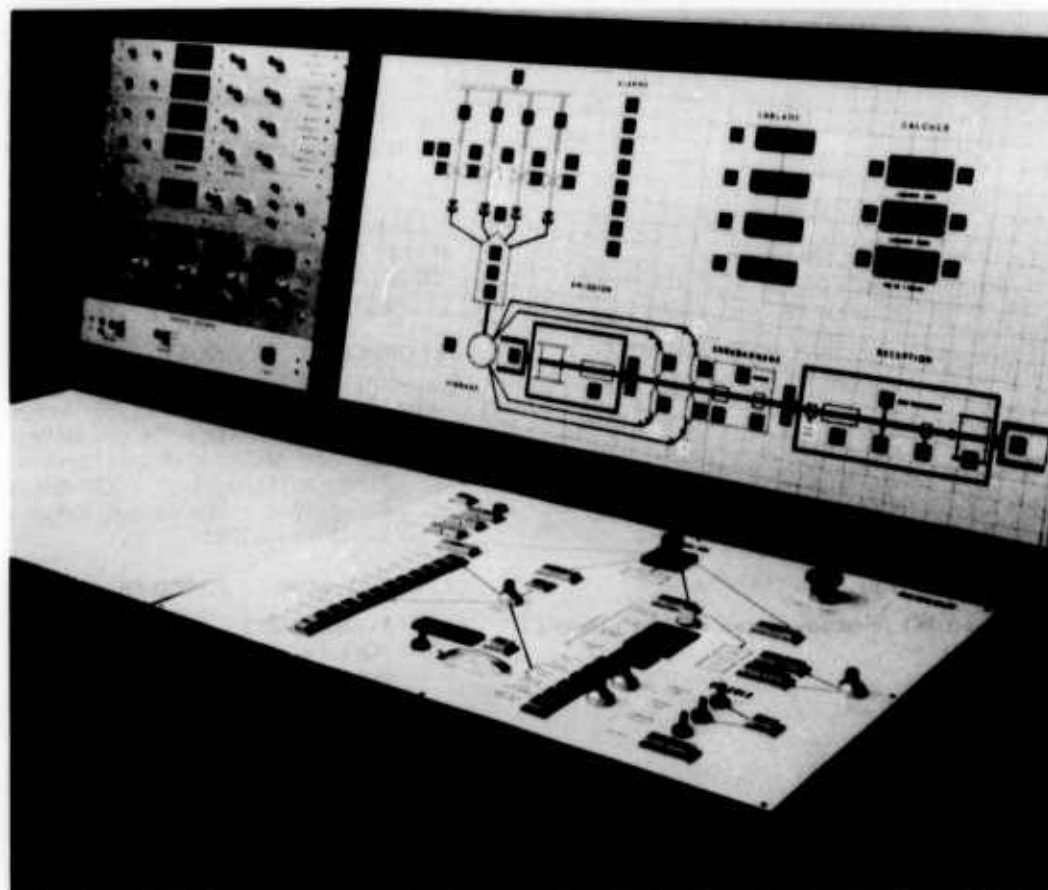
- Fig.10 -

Automatic fibers injector



- Fig.11 -

Fiber over length as a function of the sliding coefficient



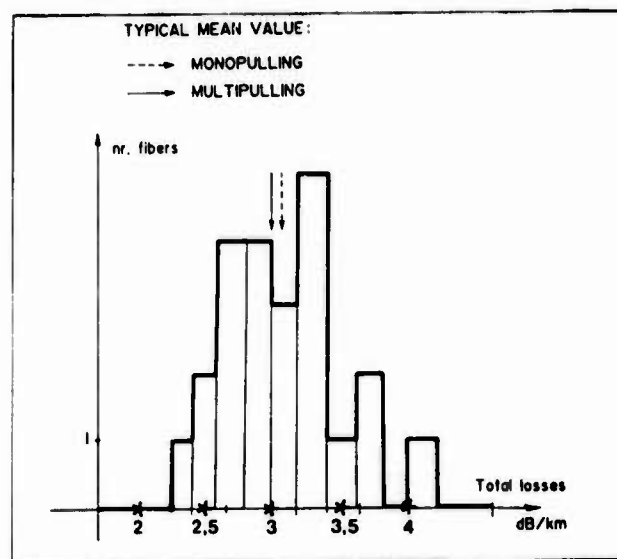
- Fig.12 -

The general control desk

RESULTS

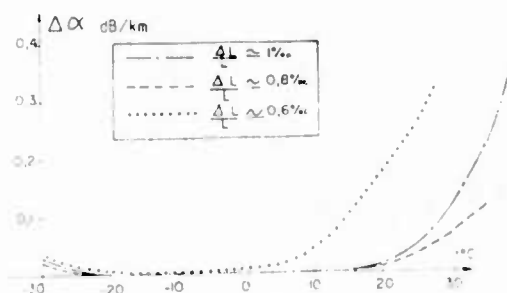
Several cables have been manufactured using this M.C.L. process.

The multipulled fibers have an outer diameter of $125 \mu\text{m} \pm 1,5 \mu\text{m}$. The tensile strength evaluation of the coated fibers is similar to that of the usual pulling ($> 2 \text{ daN}$ for 1 m long samples). The total losses of the fibers are at a mean value of $3,1 \text{ dB/km}$ at $0,85 \mu\text{m}$ (fig.13). The coupling of the multipulling and the cabling is realized at an initial speed of 10 meters per minute. The MCL speed reached 30 meters per minute during the experiment. The technical realisation permits a maximum speed of 50 m/mn for the MCL process while the multipulling itself can pull the fibers at 100 m/mn . Using optical coders makes it possible to obtain the needed precision of linear speeds approaching 10^{-4} . So we realise some optical cables units with different over-lengths. These cables elements are submitted to thermal tests in order to optimize the thermal qualities of the unit cable manufactured (fig.14).



- Fig.13 -

Total losses evaluation of the multipulling process



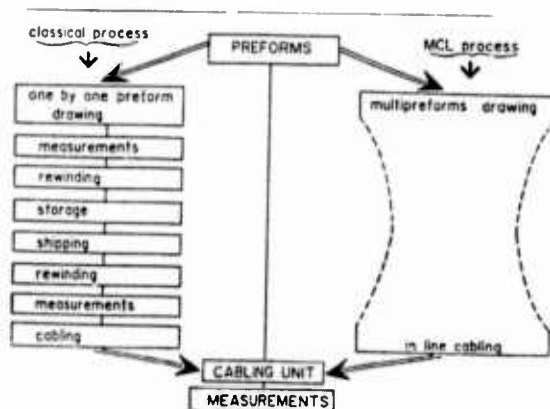
- Fig.14 -

Thermal test on MCL V-grooved two fibers element cable

CONCLUSION

We have demonstrated that the multipulling and cabling in line process could be one of the future cable manufacturing technique permitting the needed optical cables mass production for subscriber broadband networks.

Moreover this technique is able to reduce the optical cable cost because many intermediates productions steps such as measurements, rewinding and shipping of fibers are avoided (fig.15). Thus the industrial development of the M.C.L. technique is now on the way in France.



-Fig.15 -

Process manufacturing comparison

ACKNOWLEDGEMENTS

The authors want to thanks Dr.Bouillie for its helpfull discussion and support during the MCL development.

They want also thanks many of their colleagues for their participation to the development of the MCL, particularly MM. MELLINA S. LE MEUR A., LECEAI A., BERNABLE A., BOBLIN and MAREC.

REFERENCES

1. - GOURONNEC Alain - "a graphite induction furnace desing and application to optical fiber multipulling" - 6th European Conference on optical fibre communication, York, 16-19 Sept.1980
2. - G.LE NOANE - D.BOSCHER - B.NONCLERCQ - A.ZACANIARIS
"Optical fiber cables using V-grooved cylindrical units : high performance cables". Fiber and integrated optics, Volume 4, Number 1, p.67..... p.94, 01.1982
3. - GOURONNEC Alain - LE NOANE Georges
Fibres et câbles optiques
Verres et réfractaires- Vol.38, n° 2, Mars-Avril 1984.

Alain GOURONNEC



Graduated from the "Conservatoire National des Arts et métiers" in 1978. He is in charge of the drawing and cabling studies for optical fibers at the optical fibers and cables department at the C.N.E.T.

Georges LE NOANE



Graduated from the "Ecole Nationale Supérieure des Arts et métiers" in 1970. Since 1979 he is the head manager of the optical fibers and cables Department (F.C.O) at C.N.E.T.



Philippe GROSSO

Graduated from the "Conservatoire National des arts et métiers" in 1979. He joined the French Post Office in 1983 where he is in charge of the MCL development.



Michel VALETTE

He joined the French Post Office in 1969. He is in charge of the mechanical realisations for the FCO department.



Yvon GUEGAN

He joined the French Post Office in 1976. He is in charge of the multipulling development for the FCO department.



André BENOIST

He joined the French Post Office in 1963. He worked at the pulling studies development and he is presently in charge of the MCL servo-system studies.

DEVELOPMENTS OF UNDERCARPET DATA TRANSMISSION CABLES

T. Yamamoto, N. Hirasaka, H. Yokosuka, K. Seto

Fujikura Ltd.
1-5-1 Kiba, Koto-ku, Tokyo 135, Japan

ABSTRACT

Wiring system of an office buildings has become much complex and use of cables in a room for electricity, telephone and especially data transmission has been increasing rapidly, because that computers and other business machines are used very much in the office for rationalization of the office work. The problem is how to install the cables in the office. The undercarpet wiring system (UCWS) has solved the above mentioned problem. We have developed various undercarpet cables especially for the data transmission system such as multi-conductor type cable, coaxial type cable and optical fiber type cable. We have evaluated them and have obtained good results of tests. These cables have been applied for practical use of various data transmission system solving the problem of cable installation.

1. INTRODUCTION

The undercarpet data transmission cables (UCDC) are very thin flat cables and are installed under carpet squares. Therefore, they should satisfy various requirements in addition to characteristics of the conventional round cables. We have manufactured three types of UCDC, multi-conductor type, coaxial type and optical fiber type cable and have evaluated them about following characteristics.

- (1) Electrical characteristics
- (2) Mechanical characteristics
- (3) Environmental characteristics

They have shown good test results and have proved actually their excellent characteristics by installation to the practical use. The evaluation and the practical use of them are presented.

2. REQUIREMENTS OF UCDC

The UCDC has to meet following requirements in addition to electrical characteristics based on use of conventional round type cable in order to be installed between carpet square and floor.

- (1) Thinner
- (2) Easy to be bent
- (3) Withstand for mechanical damage
- (4) Flammability
- (5) Proof against environmental condition
- (6) Easy to connect or link

3. CONSTRUCTION OF UCDC

Considerable points and the countermeasures to decide the construction of the cables are shown in Table 1. In Figure 1, 2, 3, the constructions of each cable are shown after consideration.

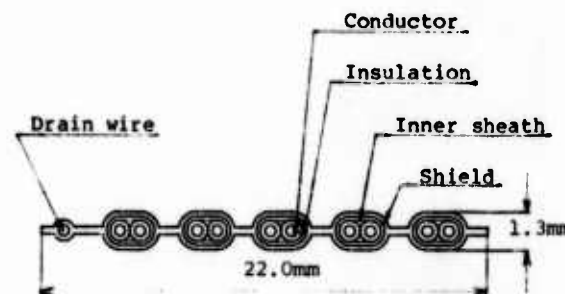


Figure 1 Multi-conductor type cable

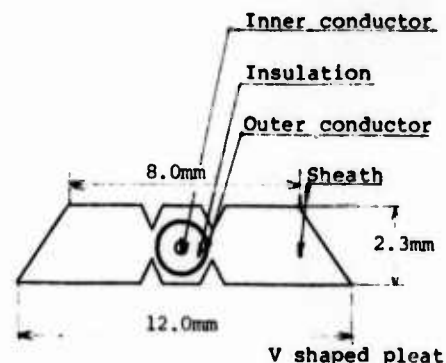


Figure 2 Coaxial type cable

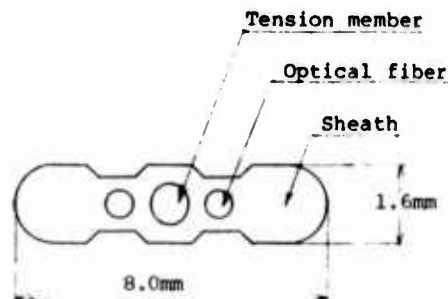


Figure 3 Optical fiber type

Table 1 Consideration of cable construction

Cosiderable point	Countermeasures		
	Multi-conductor type	Coaxial type	Optical fiber type
To reduce cross-talk	To select type of shield construction. (To make pair shield.)	—	—
To reduce attenuation	To adopt polyethylene insulation.	To adopt foamed polyethylene insulation	To adopt low loss fiber.
Variation for system	Easy selection of number of conductors and their sizes.	Easy selection of Characteristic Impedance. (50, 75, 93 ohms)	Easy selection of fiber types.
Strength against compression	To select insulation material and to adopt inner sheath.	To select shape of sheath with pleats.	Tension member setting in cable core.
Easy connectting to equipment	Easy strippable sheath.	Easy strippable sheath. To apply V shaped pleat to sheath.	Easy strippable sheath.
To make cable thin	To design shape of sheath.	To design shape of sheath.	To design shape of sheath.
Water proof and flammability	To select materials.	To select materials.	To select materials.
Ease of bending for a flat way	Flexible construction.	Flexible construction.	Flexible construction. Tension member setting in cable core. It brakes the over abundant.
To reduce bending strain	—	—	Optical fiber setting near the tension member in cable core.

4. TEST ITEMS AND METHODS

(2) MECHANICAL TEST

(1) Electrical test

Table 2 Electrical test methods

ITEM	METHOD	SPECIMEN
Conductor resistance	*JIS C 3005	Multi-conductor and coaxial type
Insulation resistance	JIS C 3005	Multi-conductor and coaxial type
Dielectric Strength	JIS C 3005	Multi-conductor and coaxial type
Capacitance	JIS C 3005	Multi-conductor and coaxial type
Characteritic impedance	JIS C 3501	Multi-conductor and coaxial type
Attenuation	JIS C 3501	Multi-conductor and coaxial type
Cross-talk (NXT,FXT)	---	Multi-conductor type

*JIS: Japanese Industrial Standard

Table 3 Mechanical test methods

ITEM	METHOD	SPECIMEN
Compression test	2-1	all types
Impact test	2-2	all types
Bending test	2-3	optical fiber type
Repeated compression test	2-4	optical fiber type

2-1 Compression test

This test was proved with compression weight on both flat and bended parts of cable as shown in Fig. 4, 5, using a plane of the fixed outerdiameters of bar. Then numerical value of weight, which cause a short, were measured. For optical fiber type, the relativity of attenuation and compression weight was figured out.

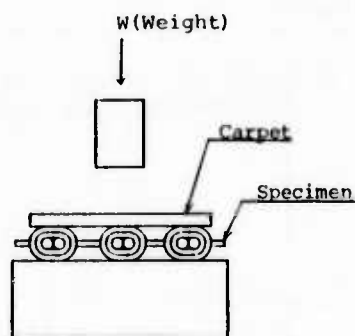


Figure 4 Compression test

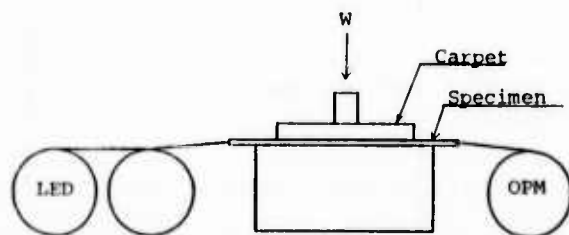


Figure 5 Compression test for optical fiber type

2-2 Impact test

To investigate whether there is a wire snap's or withstand the dielectric strength test in water and external appearance, a metallic weight was dump. Each test condition is shown in Fig. 6, 7. For optical fiber type the relativity of attenuation and bombarid altitude.

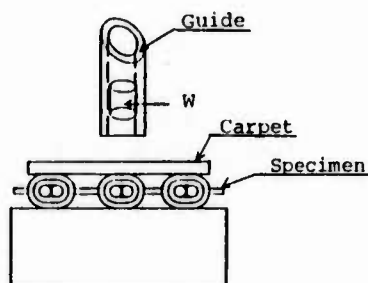


Figure 6 Impact test

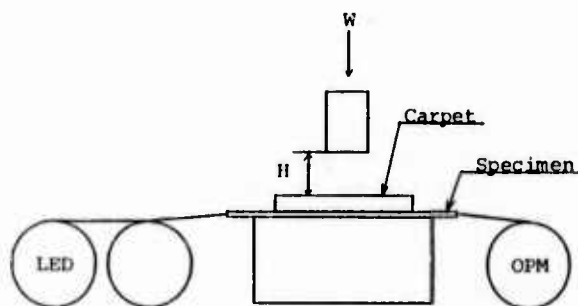


Figure 7 Impact test for optical fiber type

2-3 Bending test

It is the test that the relativity of attenuation and bend radius using a measuring line in Fig. 8.

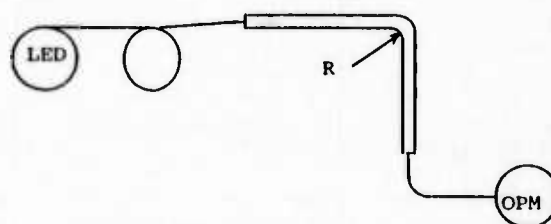


Figure 8 Bending test for optical fiber type

2-4 Repeated compression test

It is the test that the relativity of attenuation and repeated compression, using a measuring line in Fig. 9.

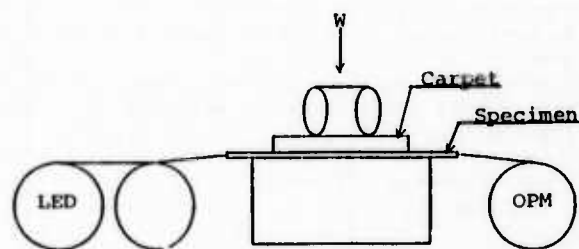


Figure 9 Repeated compression test for optical fiber type

(3) Environmental test

Table 4 Environmental test methods

ITEM	METHOD OR CONDITION	SPECIMEN
Heat cycle test	MIL STD 202D	All types
Water proof test	100°C x 5 Min. In methanol for 1 hour	All types
Aging test	113°C x 168 hours	All types
Humidity test	MIL STD 202D	All types
Flammability	UL Subject 758	All types

5. TEST RESULTS

The follows are examples of the cable characteristics observed. For them there must be no perceptible problem for practical use.

(1) Electrical test

Table 5 Results of electrical test

ITEM	UNIT	RESULT	
		Multi-conductor type	Coaxial type
Conductor resistance	Ω/Km 20°C	Less than 147.5	—
Insulation resistance	$\text{M}\Omega\text{-Km}$ 20°C	More than 5000	More than 1000
Dielectric Strength	V/1min.	AC 350 or DC 500	AC 1000
Capacitance	nF/Km	Less than 100	69 ± 4
Characteristic Impedance	Ω	See Fig. 10	See Fig. 12
Attenuation	dB/Km	See Fig. 10	See Fig. 12
Cross-talk (NXT, FXT)	dB/100m	See Fig. 11	—

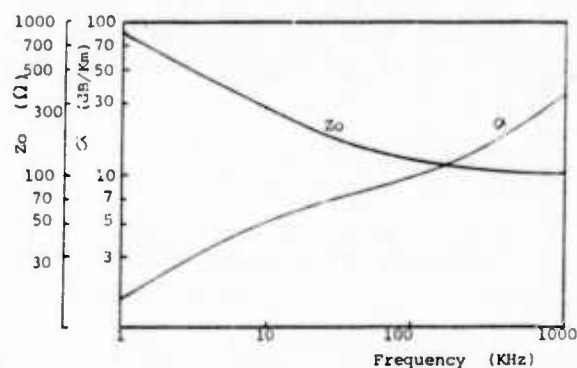


Figure 10 Characteristic impedance (Z_o) and attenuation (α) of multi-conductor type

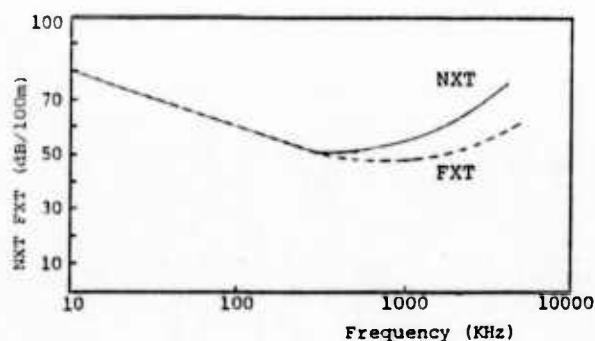


Figure 11 Cross-talk of multi-conductor type

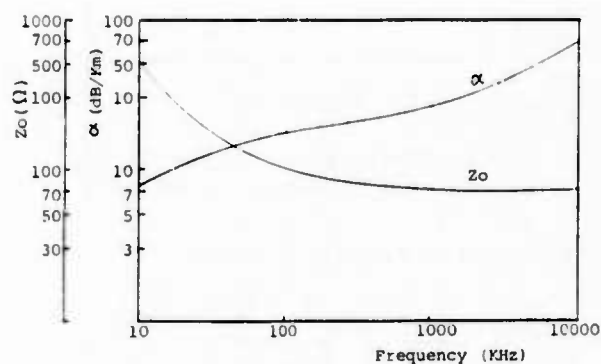


Figure 12 Characteristic impedance (Z_o) and attenuation (α) of coaxial type

(2) Mechanical test

Table 6 Results of mechanical test

ITEM	TEST CONDITION & UNIT	RESULT		
		Multi-conductor type	Coaxial type	Optical Fiber type
Compression test	Flat way (kg/cm^2)	More than 1760 (Breaks)	More than 710 (Breaks)	See Fig. 13
	90°C Bending (Kg/cm^2)	More than 1170 (Breaks)	More than 700 (Breaks)	See Fig. 13
Impact test	5 pound x 5ft	Good	Good	Good and See Fig. 14
Bending test	—	—	—	See Fig. 15
Repeated Compression* test	(times) W= 50Kg	40000	40000	40000

* The number of times was taken in the occasion the carpet square was torn.

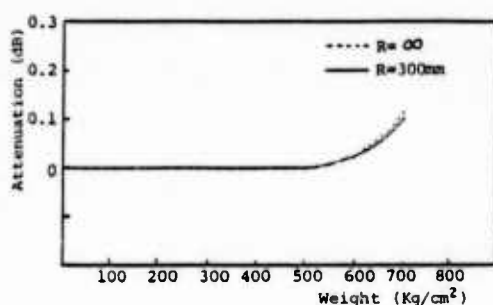


Figure 13 Compression test of optical fiber type

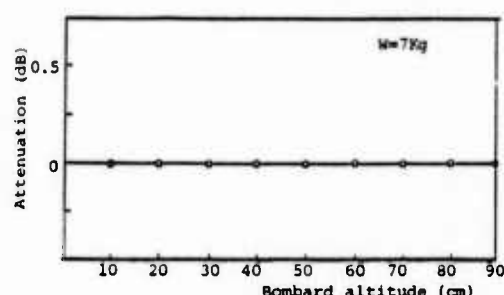


Figure 14 Impact test of optical fiber type

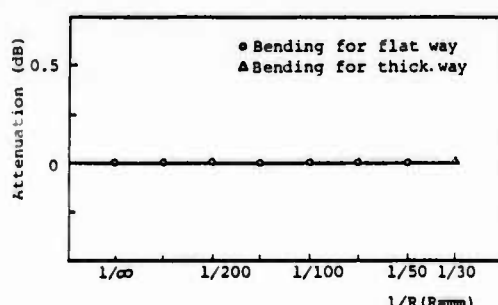


Figure 15 Bending test of optical fiber type

(3) Environmental test

Table 7 Results of environmental test

ITEM	RESULT
Heat cycle test	Good
Water proof test	Good
Aging test	Good
Humidity test	Good
Flammability test	Good

6. EXAMPLES OF PRACTICAL USE

The Undercarpet data transmission system (UCDS) we newly developed has been applied to offices in various systems such as Computer data transmission system, Banking system, Local Area Network and so on. Following figures show two cases of practical use for computer system of our company and for the Automatic Tellers Machine (ATM) system in the bank, one of our customer.

(1) Systematic use of coaxial and fiber optic type UCDC in computer system

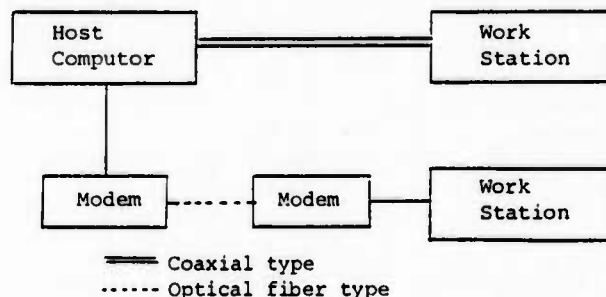


Figure 16 Blockdiagram of computer system

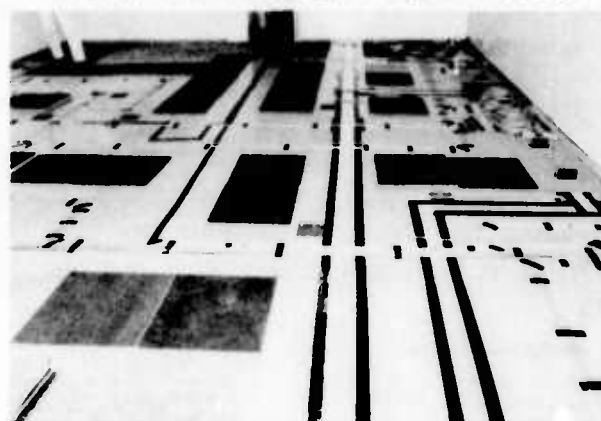


Photo 1 Under installation of computer system



Photo 2 Computer room after installation

(2) Systematic use of multi-conductor type UCDC in banking system

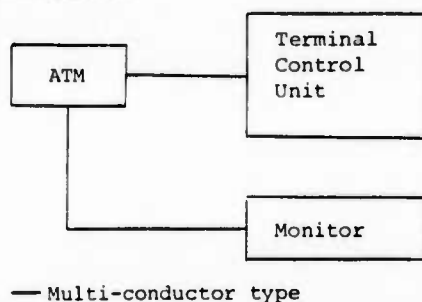


Figure 19 Blockdiagram of banking system

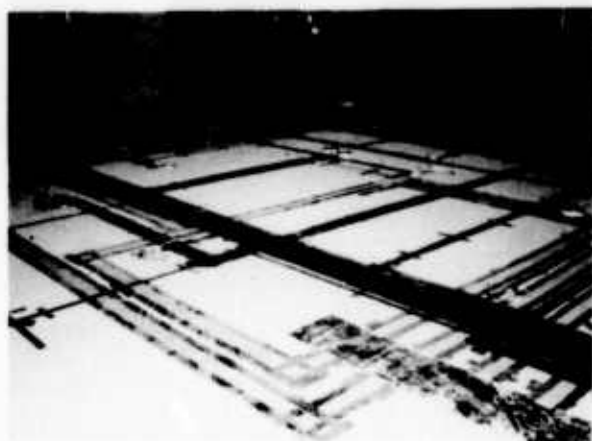


Photo 3 Under installation of banking system



Photo 4 Bank after installation

7. CONCLUSION

We were able to obtain satisfactory results of electrical, mechanical and environmental characteristics test after hard experiments, besides to introduce examples of practical use to the public. It is the urgent tasks for us to expand and standarize the practical use of UCDS. Moreover, we strongly believe that this system must be established its status as a revolutionary one being appreciated to be a capable system as well as the already developed under carpet power and telephone systems.

8. ACKNOELEDGEMENT

The authors would like to thank many colleagues of FUJIKURA Ltd. for the helpful manufacturing and development of UCDS for this study.

9. REFERENCE

- (1) M. Shimizu et al FUJIKURA technical review No.66, 91, 1983
- (2) MIL STD 202 "Test methods Electronic & Electrical component parts"
- (3) JIS C 3005 "Testing methods for plastic insulated wires and cables"
- (4) JIS C 3501 "Radio-Frequency coaxial cable"
- (5) UL subject 758 "Standard for insulated single-conductor AWM"



Tomohiro Yamamoto

FUJIKURA Ltd.
1440 Mutsuzaki,
Sakura-shi
Chiba-ken 285, Japan

Mr. Yamamoto, a member of the Institute of Electrical Engineers of Japan, recieved B.E. degree in electrical engineering from Kyushu University in 1967. He joined Fujikura Ltd. has been engaged in engineering and manufacturing of electronic wires and cables. He is now a Manager of Electronic wire manufacturing section.



Noriyasu Hirasaka

FUJIKURA Ltd.
1-5-1 Kiba, Koto-ku,
Tokyo 135, Japan

Mr. Hirasaka, a member of the Institute of Electronics and communication Engineers of Japan, recieved B.E. degree in electronic engineering from Saitama University in 1976. He joined Fujikura Ltd. has been engaged in enginnering of electronic wires and cables. He is now an Engineer of Electronic Components Division.



Hiroshi Yokosuka

FUJIKURA Ltd.
1440 Mutsuzaki,
Sakura-shi
Chiba-ken, Japan

Mr. Yokosuka graduated in mechanical engineering course from Tokyo metropolitan Technical junior College in 1967. He joined Fujikura Ltd. has been engaged in engineering of telecommunication cable Research & Development. He is now a assistant chief of Telecommunication cable Section.



Katsuyuki Seto

FUJIKURA Ltd.
1440 Mutsuzaki,
Sakura-shi
Chiba-ken, Japan

Mr. Seto, a member of the Institute of Electronics and communication Engineers of Japan, recieved B.E. degree in electronic engineering from Yokohama National University in 1980. He joined Fujikura Ltd. has been engaged in enginnering of telecommunication cable Research & development. He is now an Engineer of Telecommunication cable Section.

A HYBRID LOCAL AREA NETWORK CSMA/CD METHOD BY USING OPTICAL FIBER AND COAXIAL CABLES

Y. ENOMOTO J. KIKUCHI T. TAKAHASHI K. NEGISHI T. KATO S. ISHIKAWA

The Furukawa Electric Co. Ltd., Tokyo, Japan

ABSTRACT

This paper describes hybrid local area network that uses both coaxial cable and optical fiber cable.

Ethernet, which uses coaxial cable, is one of the best local area networks in operation, providing flexibility and extendibility. However, coaxial cable is not suitable for high-noise-level environments and long-range transmission. This paper describes the most suitable system for such conditions. Our system combines optical fiber transmission with coaxial transmission.

The paper explains the method and structure of the whole system, and the components (optical fiber, optical transceiver, optical star coupler, optical repeater, coaxial cable, coaxial transceiver, tap for coaxial cable) used. Lastly, we discuss data obtained from tests of a development system.

1. Introduction

The expansion of distributed processing brought about by sophisticated computer utilization and microprocessor advances has created a demand for sharing of system resources, including hardware, software, and data bases, and for intersystem communication. Local area networks organically couple resources and enable communication.

Local area networks can be divided into a variety of types, depending on the operating mode and control method. Roughly speaking, they include star, ring, and bus types. The CSMA/CD (Carrier Sense Multiple Access with Collision Detect) method with a bus mode as represented by the Ethernet proposed by Xerox and other companies, is the most advanced office automation network system in commercial use.

International standards based on Ethernet are being established for the CSMA/CD method. Ethernet is expected to become an IS (International Standard) of the ISO (International Organization for Standardization) sometime in 1984.

We have developed a local area network system called INFONET, which is a hybrid system incorporating the superior characteristics of optical fiber cable in high-noise environments while retaining the flexibility and expandibility of the coaxial cable Ethernet.

2. Configuration of hybrid system

Figure 1 shows the configuration of our hybrid system for the CSMA/CD method, using optical fiber and coaxial cables. As shown in the diagram, the system consists of a coaxial cable (up to 500 m/segment), coaxial transceiver, transceiver cable (up to 50 m), repeater, optical transceiver, optical star coupler, optical fiber cable, and other components.

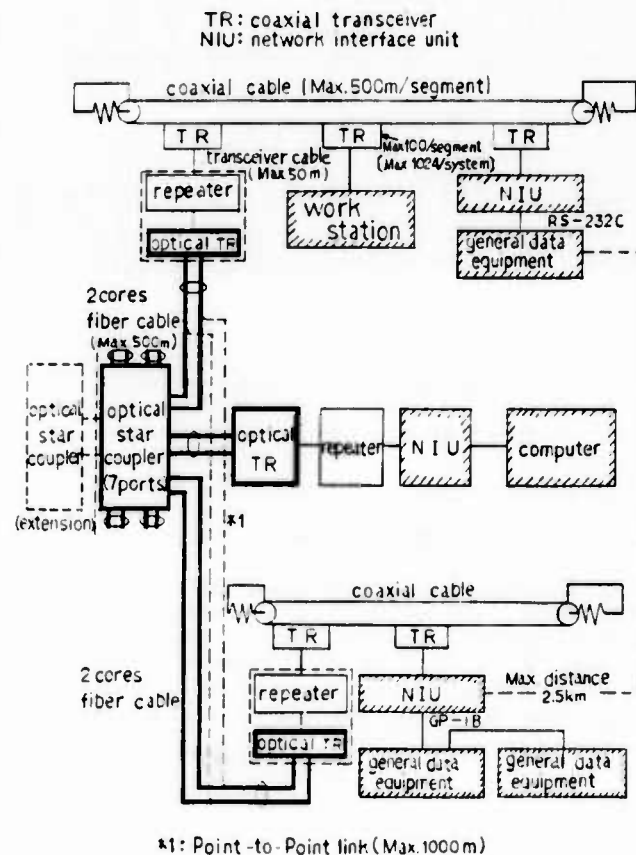


Figure 1 Hybrid system configuration

Figure 2 shows the configuration of the Ethernet system, which is well known as a CSMA/CD system. As the diagram shows, the system consists of a coaxial cable, coaxial transceiver, transceiver cable, repeater, remote repeater, and other components. The difference between these systems is that the Ethernet repeater and remote repeater section (figure 2) are replaced with an optical transmission system in the hybrid system (figure 1).

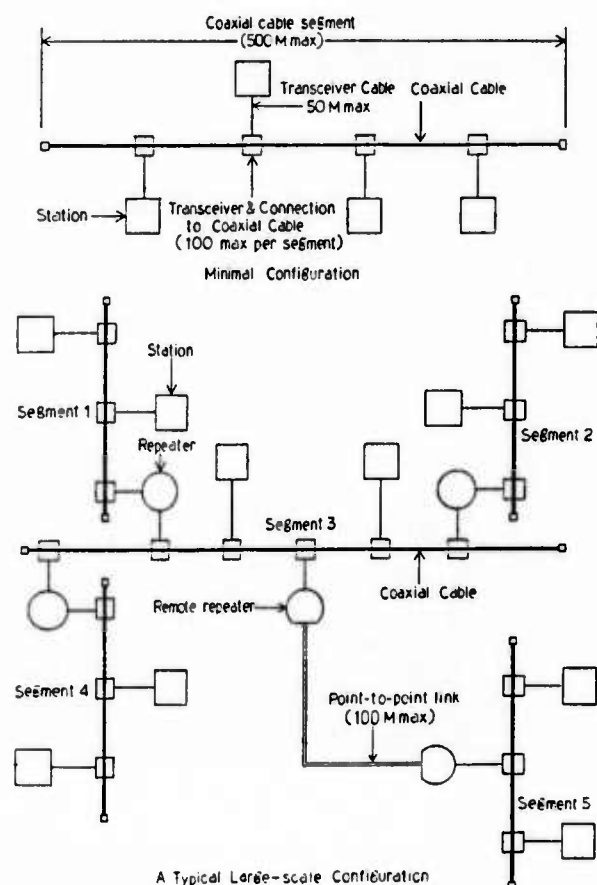


Figure 2 Ethernet system configuration

3. System components

3.1 Coaxial cable and transceiver cable

Specifications for the coaxial cable used in this hybrid system are slightly different from those for the Ethernet system. The difference is that the center conductor of the coaxial cable is stranded wire for more secure connection at taps (couplers to connect coaxial transceivers and coaxial cable). Table 1 shows the specifications of the coaxial cable.

Item	Specification
Center conductor	Tin coated stranded copper wire
Insulation	Formed polyethylene
Insulation diameter	6.2 mm
Shield	Foil laminated tapes and tin coated copper braids
Sheath	Vinyl (orange color)
Cable diameter	10.3 ± 0.25 mm

Table 1 Specification of coaxial cable

3.2 Tap

We chose stranded wire as the center conductor of the coaxial cable, inserting the gap center conductor in the stranded wire to ensure complete contact of the tap center conductor. Figure 3 shows the construction of the tap.

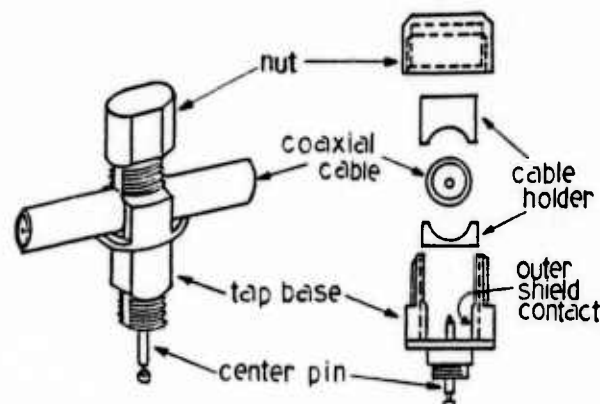


Figure 3 Tap construction

3.3 Coaxial transceiver

Figure 4 is a block diagram of the coaxial transceiver. Photo 1 shows the coaxial transceiver, including the tap. Specifications for this coaxial transceiver conform to the Ethernet specifications.

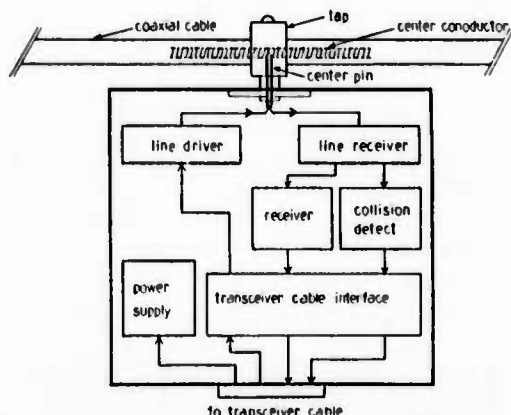


Figure 4 Coaxial transceiver block diagram

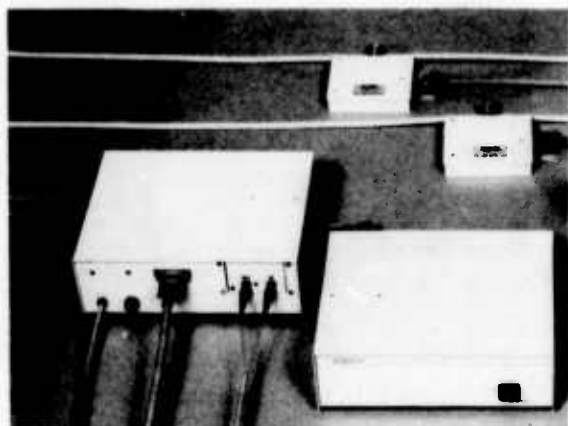


Photo 1 Coaxial transceiver, repeater, optical transceiver

3.4 Optical transceiver, optical star coupler, and repeater

The hybrid system uses an optical repeater system comprising an optical transceiver, optical star coupler, repeater, and two cores optical fiber cable, as shown in figure 5.

The repeaters in the hybrid system are exactly the same as those for coaxial systems. The electrical interface of the optical transceiver is the same as that of a coaxial transceiver. The optical transceiver mounts in the repeater housing. If no optical repeater system is connected, the coaxial transceiver for another coaxial cable segment is connected by transceiver cable instead of mounting an optical transceiver to function as a coaxial repeater.

The repeater controls the data flow from both segments ($Rx1 \rightarrow Tx2$, $Rx2 \rightarrow Tx1$), as well as collision signal flow when a collision takes place; removes data distortion in the regenerating circuit; and regenerates timing signals. Figure 6 shows the repeater block configuration.

The optical star coupler we developed is a seven-branch type. This is an active coupler connecting inputs and outputs of seven systems to O/E and E/O converters through seven bundled optical fibers. The coupler has an expansion terminal on an electrical signal level, permitting installation of additional optical star couplers.

The optical star coupler detects a collision on the optical transmission line by monitoring the mean level of the electrical signal in the initial stage of the O/E converter. This level doubles (compared with normal state) when a collision takes place. The detected collision signal is transmitted to the optical transceiver as an 8-MHz signal (normal data signals contain 5- and 10-MHz components only) and is redetected in the optical transceiver. It is output through a collision detection wire as a 10-MHz collision signal in accordance with the coaxial transceiver specification.

Some data fragments may be produced in return to the own receiving side of signal sent to the optical transceiver, due to the optical star coupler construction, and the propagation delay time of the optical fiber. We use the fact that the Ethernet system has frame intervals of $9.6 \mu s$ to mask return signals received inside the repeater during this short time, preventing output to other segment.

This hybrid system can function as a remote repeater under Ethernet specifications by directly coupling two optical transceivers, with no optical star coupler.

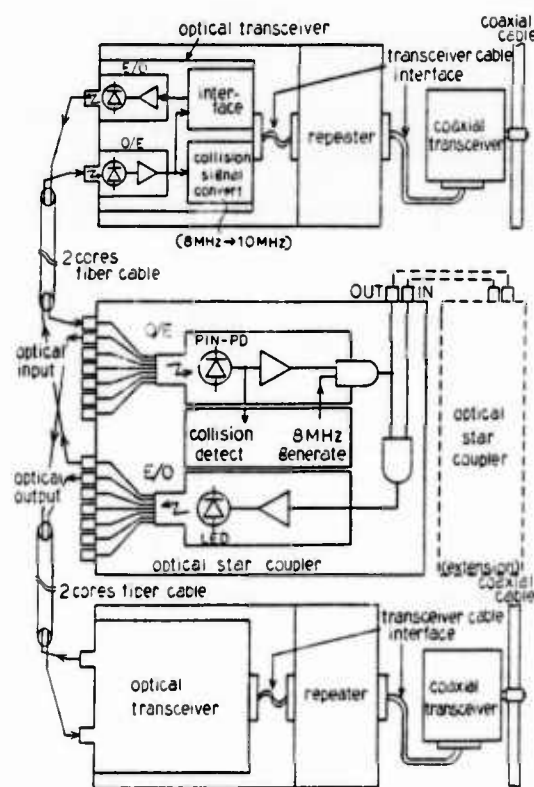


Figure 5 Optical repeater system configuration

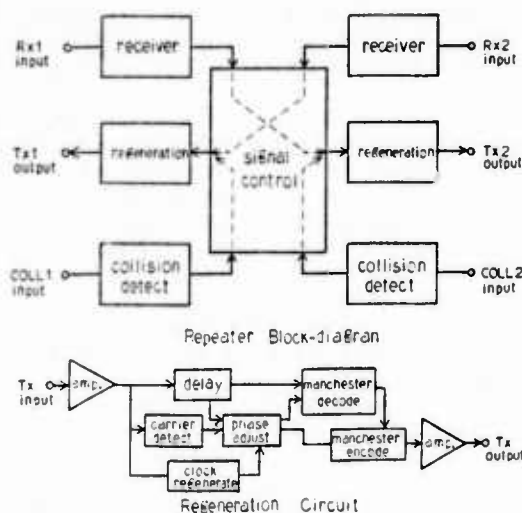


Figure 6 Repeater block configuration

Tables 2 and 3 show the main optical repeater system specifications and optical fiber cable specifications. Photo 2 shows the optical star coupler.

Item	Specification
Optical transmission	
optical output level	-17~-25dBm(Adjustable)
optical input level	-20~-27dBm
optical fiber	80/125 um step index fiber
optical connector	FC type
transmission signal	10Mbps(manchester coding)
Optical star coupler	
input/output number	7/7
optical output level	-17~-20dBm(Adjustable)
optical input level	-25± 0.5dBm
optical fiber	80/125 um step index fiber
optical connector	FC type
transmission signal	10Mbps(manchester coding)
electric interface (for extension)	ECL
electric interface connector	BNC type
optical collision signal	8MHz
Repeater	
interface	transceiver cable interface
tolerance of regenerating pulse width distortion	20ns

Table 2 Optical star repeater system main specification

Item	Specification
Optical fiber	Step index silica glass fiber
Core diameter	80± 4 um
Fiber diameter	125± 3 um
N.A.	0.24
Fiber cord jacket	PVC (orange color)
Fiber cord diameter	2.8± 0.3 mm
Fiber cable	2 cores
Fiber cable sheath	PVC (orange color)
Fiber cable outer diameter	aproximate 11 mm

Table 3 Optical fiber cable specifications

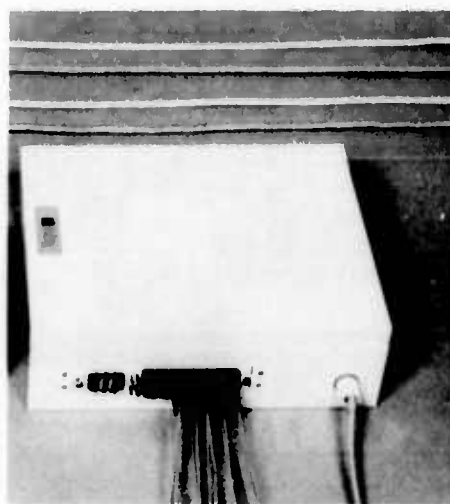


Photo 2 Optical star coupler

Photo 3 shows the polished edges of the bundle of seven optical fibers used in the optical star coupler. The bundled fiber diameter is 400 μm and a core size is 82.5/125 μm.

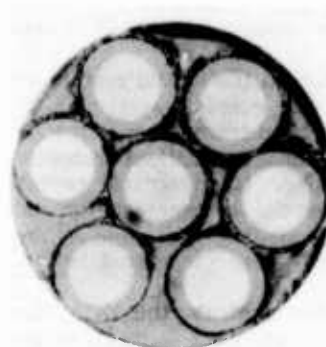


Photo 3 Edges of seven-core optical fiber bundle

4. Test results

4.1 Temperature characteristics of optical transceiver optical

Figure 7 shows the temperature characteristics of the optical output level of the optical transceiver, an important factor in the collision detection function of the optical star coupler. The diagram shows the temperature characteristics for ambient temperatures between -10 and +50°C. The variation width is 0.5 dB or less.

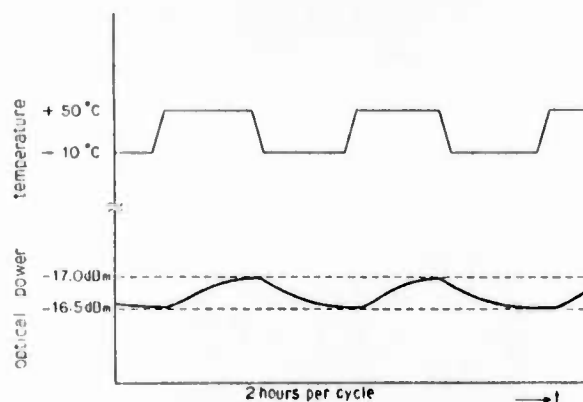


Figure 7 Temperature characteristics of optical transceiver optical output level

4.2 Repeater data reproduction ability

The repeater is required to output data after reshaping, regenerating, and retiming serial data that has been distorted in the coaxial cable and relay transmission lines. Photo 4 shows the regeneration capacity. This satisfies Specification tolerance of regenerating pulse width distortion, ± 20 ns.

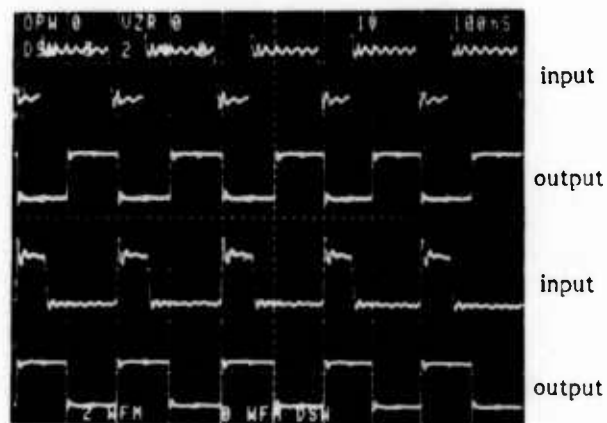


Photo 4 Repeater data regenerative capacity

4.3 Tap reliability test

To demonstrate the reliability of the tap connection, contact resistance was measured before and after test under the following test conditions:

a. Vibration test

Amplitude +1 mm (total amplitude 2 mm)
Vibration frequency 20 Hz
Vibration cycles One million cycles

b. Heat cycle test

Temperature range -20 to +60°C
Number of cycles 100 cycles (two cycles/day)

Figure 8 and table 4 shows the contact resistance measurement method and the test results. The contact resistance value includes the resistance of the center pin, approximately 2 milliohms.

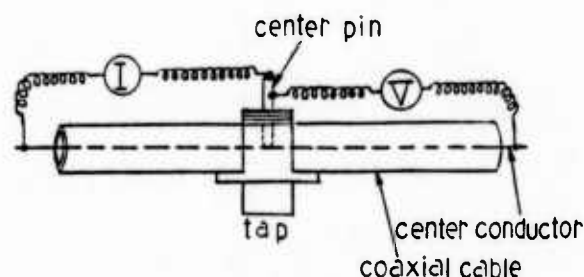


Figure 8 Contact resistance measuring system

Sample No.	(milliohm)					
	Vibration test			Heat cycle test		
	before	after	fluctuation	before	after	fluctuation
1	2.14	2.32	0.18	2.08	2.58	0.50
2	2.06	2.10	0.04	2.07	2.61	0.54
3	2.03	2.03	0.00	2.07	2.69	0.62
4	2.06	2.13	0.07	2.15	2.80	0.65
5	2.14	2.08	-0.06	2.03	2.88	0.85
\bar{x}	2.086	2.132	0.046	2.08	2.712	0.632

Table 4 Tap reliability test data

5. Example of test operation

The hybrid system was also tested and operated in a building. Figure 9 shows the route in the building. In this example, a coaxial repeater was installed halfway, and the system had coaxial cable only. In the near future, however, we plan test with an optical repeater instead of the coaxial repeater. There are 107 coaxial transceivers in the entire system. Photo 5 shows a coaxial transceiver mounted near the ceiling, photo 6 shows the coaxial transceiver with its cover mounted for good appearance. Figure 10 shows an example of the reflection characteristics of the coaxial cable after mounting transceivers. The reflection level is -25 dB or less, that is, less than 0.32%, at 5 and 10 MHz. This fully satisfies the required standard of 7% or less.

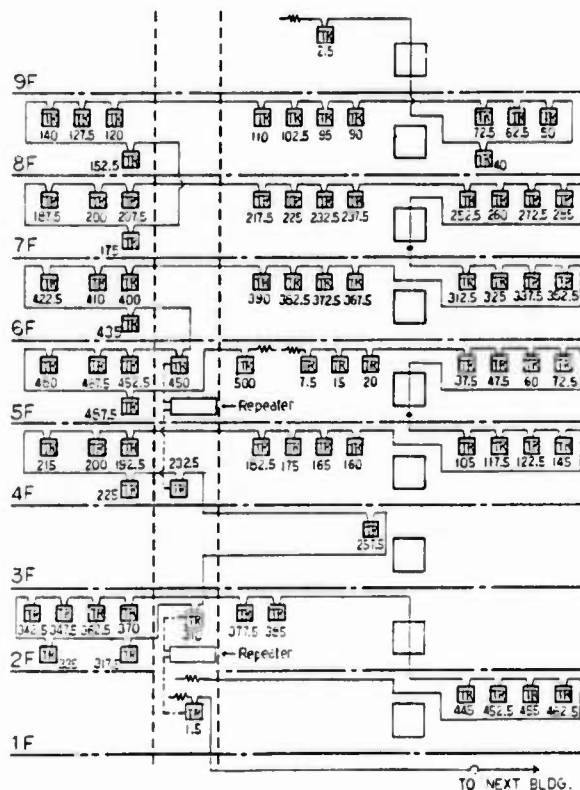


Figure 9 Example of installation route in building

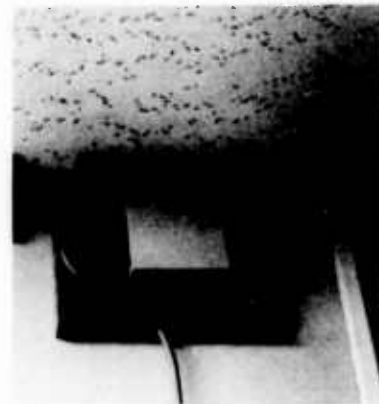


Photo 5 Coaxial transceiver mounted on coaxial cable



Photo 6 Coaxial transceiver with protection cover

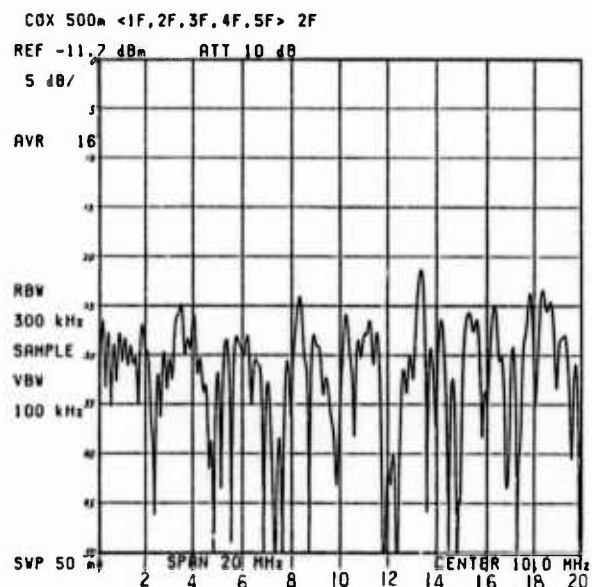


Figure 10 Reflection characteristics of coaxial cable after mounting coaxial transceiver

6. Conclusions

Development of this hybrid system expands installation freedom; the system can now be installed in locations where the noise environment is poor, such as in power cable ducts, improving the flexibility and expandability as a local area network. After incorporation of minor changes, this hybrid system will meet the international standard now being formulated.

In conclusion, the authors hope that this system will contribute to further development of local area network systems.

7. Reference

Xerox, etc. [The Ethernet A Local Area Network Data Link Layer and Physical Layer Specifications Version 1.0]



YOSHIO ENOMOTO

The Furukawa Electric Co.,Ltd.
6-1 Marunouchi 2-chome
Chiyoda-ku Tokyo,Japan

Mr.Enomoto,Assistant Manager, System & Equipment Department of Telecommunication Division
He received his B.SC in electric engineering from Yokohama National Univ. in 1972.



JUNICHI KIKUCHI

The Furukawa Electric Co.,Ltd.
6-1 Marunouchi 2-chome
Chiyoda-ku Tokyo,Japan

Mr.Kikuchi,Staff Engineer, System & Equipment Department of Telecommunication Division.
He graduated from Tokai Junior Univ. in electric engineering,1968.



TOMOKI TAKAHASHI

The Furukawa Electric Co.,Ltd.
6-1 Marunouchi 2-chome
Chiyoda-ku Tokyo,Japan

Mr.Takahashi,Assistant Manager, System & Equipment Department of Telecommunication Division.
He received his B.SC in mechanical engineering from Chiba Univ. in 1971.



KUNIO NEGISHI

The Furukawa Electric Co.,Ltd.
6-1 Marunouchi 2-chome
Chiyoda-ku Tokyo,Japan

Mr.Negishi,Assistant Manager Engineering section of Electronic Appliance wire & Products Division.
He received his B.SC in electric and electronic engineering from Sophia Univ. in 1972.



TATSUZO KATO

The Furukawa Electric Co.,Ltd.
6-1 Marunouchi 2-chome
Chiyoda-ku Tokyo,Japan

Mr.Kato,Assistant Manager, Engineering section of Electronic Appliance wire & Products Division.
He received his B.SC in Telecommunication engineering from The Univ. of Electro-communications in 1972.



SATOSHI ISHIKAWA

The Furukawa Electric Co.,Ltd.
6-1 Marunouchi 2-chome
Chiyoda-ku Tokyo,Japan

Mr.Ishikawa,Staff Manager, Fiber optics & System Department Telecommunication Division.
He received his M.SC in electronic engineering from Niigata Univ. in 1970.

PLENUM, SMALL-DIAMETER OPTICAL FIBER CABLE

Osamu Ichikawa, Yasunori Saito, Tetsuji Ono, Shigeru Tanaka, Akinori Mori

Sumitomo Electric Industries, Ltd.
1, Taya-cho, Totsuka-ku, Yokohama, Japan

Abstract

In optical fiber cables for Local Area Networks (LANs), there are various indoor uses such as in offices and plenums. At present special performances such as safety against fire, and manageability in accordance with their individual environmental usage have been required. For this reason, the development of the optical fiber cables with versatile usability characteristics have been expected. Realizing this goal, the newly developed cable is of a make where optical fibers are housed in spiral grooved spacer of small diameter, and the cable material is mainly composed of low smoke fluoropolymer. Having conducted various evaluational tests on this cable, it was confirmed that this cable had better thermal and mechanical characteristics, and sufficient inflammability, which qualified this cable to be used both in offices and plenum chambers.

1. Introduction

At present, the optical fiber cables for indoor use have been used in a wide range, for example LAN, data link, telephone and computer networks. Considering only LAN use for instance, various optical fiber cables have been developed in accordance with their use in environments and places, but, there are problems involved such as the cables having poor versatility in uses and their handling such as jointing being complicated. Places for the cable are largely classified into two categories, office and plenum area. The plenum area means where ventilation is effected, and includes spaces over ceiling and below floor and inside walls. For these areas, it is very important for the safety against fire, for which the dispersion of smoke was in many cases avoided by setting cables in metal conduit or by sealing cables by metal sheath. However, because these methods require more time and cost for the installations, it developed a tendency for the composite materials of the cable themselves to be changed to those of inflammable and low smoke natures such as fluoropolymer. However, the fluoropolymer has poor workability and large contraction in low temperature, and the problem is to control these adversities. When the optical fiber cable is used within office, the manageabilities

such as flexibility and small diameter are important factors. Although small cable diameter is required in plenums in most cases with narrow spaces, making smaller diameter has its limit in respect to protection against external mechanical forces such as impact and compression, and it has been the important point for how much this smaller diameter could be achieved. This time we have developed the indoor optical fiber cable for LAN with versatile utilities in whole indoor areas. In this paper, the design and characteristics of the newly developed optical fiber cable are described.

2. Cable Design

Cable structure and fiber's planning particulars are given below:

2.1 Fiber Structure

Structural elements of 2 types of fiber are indicated in Table 1. The type I is the structure used for this cable and the type II is the one in standard use in Japan for the public communications. In respect of the optical fiber for LAN, it should be beneficial to have larger refractive index difference in order to minimize losses in bending, coupling, splicing and connecting. Larger core diameter is also preferable from the view point of coupling and connecting. In addition to above, in consideration of transmission capacity and fiber cost, the structural parameter of the type I was largely set as core diameter 62.5 μ m and Numerical Aperture (NA) 0.29 and refractive index profile was made of graded type. In consideration of smaller diameter cable and manageability of fiber splicing, coating of the fibers was made by a tight buffer structure with buffer layer of 0.4mm outer diameter silicone resin and outer jacket of 0.7mm outer diameter. For purpose of low smoke, the outer jacket was made of ETFE (ethylene-tetrafluoroethylene).

2.2 Cable Structure

For designing indoor optical fiber cable, consideration shall be paid to the following points, namely, (a) manageability, (b) reliability,

(c) versatility, and (d) safety against fire. In particular for selection of its structure, considerations must be paid to smaller diameter, flexibility, protection against lateral external force and thermal property. Table 2 indicates results of comparative evaluations of various smaller diameter cables. The core configurations of cord type, twisted core type and spacer type⁽¹⁾ are based on high strength fiber with high Young's modulus (Kevlar for instance), rod (FRP or steel wire) and grooved spacer including the rod, respectively. Cord type and twisted core type are suitable for making the cable diameter smaller, however, no efficient for protection against lateral external forces, which by increment of protective layer, lose smallness of diameter. On the other hand, the spacer type has better performances than other types on the whole. By the reason as stated above, spacer structure was used for this cable. Further, the problems of workability and thermal property accompanied with use of fluoropolymer are solved by spacer structure and smaller diameter. Strength member at the core was made of twisted steel wires in consideration of the flexibility of the cable. In Fig. 1, structures of the optical fiber cable (type A) developed this time and of the optical fiber cable for non-plenum (type B) using materials similar to conventional indoor optical fiber cable for comparison of characteristics are indicated. For the type A, 2 optical fibers coated with ETFE are housed in each groove of FEP (fluorinated ethylene-propylene) spacer which is capable of housing up to 4 fibers, and its outer circumference is wound by polyimide tape and outer sheath of 0.5mm thick FEP is given with an outer diameter of 4mm. For the type B, 2 fibers of nylon coating are housed in spacer of HDPE with its outer circumference wound by PET (polyester) tape and outer sheath of 0.75mm thick PVC (polyvinyl-chloride) is given with 4.5mm outer diameter. Photograph 1 indicates appearance of the type A.

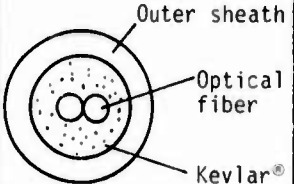
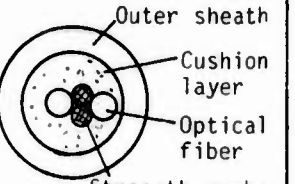
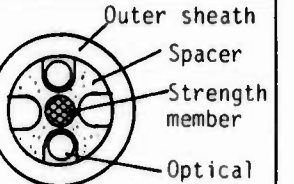
Table 1 Fiber Structure

Type		I	II
Glass fiber	Core dia. (μm)	2.5	50
	Outer dia. (μm)	125	125
	NA	0.29	0.20
Buffer coating		Silicone resin 0.4mm O.D.	
Outer coating		ETFE 0.7mm O.D.	Nylon 0.9mm O.D.



Photo 1 Outside view of plenum small diameter optical fiber cable

Table 2 Comparison of cable structure with small diameter

Item \ Type	Cord type	Stranded core type	Grooved spacer type
Cross section			
Small-diameter	A	A	B
Flexibility	A	B	A
Anti-kink	C	A	A
Anti-lateral force	B	B	A
Thermal property	C	A	A
Total quality	B	B	A

A: Excellent B: Good C: Poor

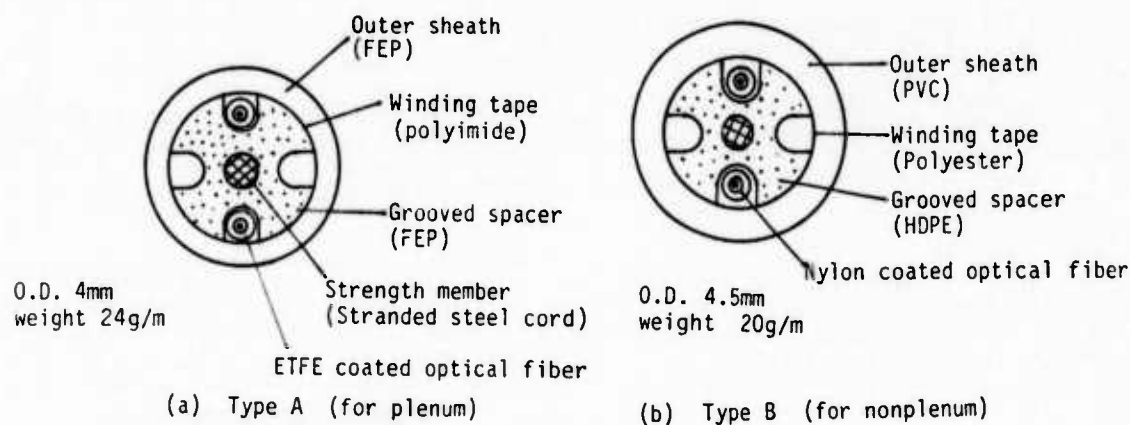
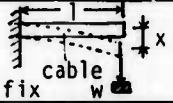


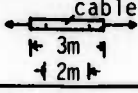
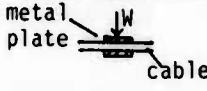
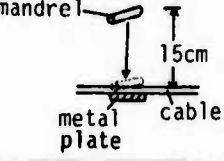



Fig. 1 Cable structure

Table 3 Test method and objective property

Item	Test method		Objective
Mechanical Test	Flexibility	sample length : 30cm, 20cm, 10cm weight : 0 → (10gf step) hold time at each weight: 1 minutes 	displacement of free end $x > 10\text{cm}/100\text{gf}$ at 30cm-long sample
	Flexure	mandrel dia. : 20mm bending number : 10,000 times (30cycle/min) weight : 5kgf 	no breaking at 1000 times of bending
	Bending	mandrel dia. : 80, 40, 30, 20, 10mm bending angle : 360 x 5 degrees 	no loss increase at the bending diameter of 80mm
	Tensile strength	sample length : 3m measuring length : 2m hold time at each load : 1 min. 	breaking load > 40kgf
	Compression	plate length : 100mm compressive load : 0 → 1,000kgf (50kgf step) 	no breaking
	Impact	mandrel dia. : 25mmφ impact energy : 15cm x 1.5kgf interval length of drop point : 1cm (50drop times) 	no breaking
Thermal Test	Temperature	cable condition : wound on aluminum reel (winding dia. 250mm) fiber length : 1m temperature range : 150°C ~ -50°C	loss increase $\Delta\alpha < 0.1\text{dB/km}$ at -40°C ~ +80°C
	Heat	cable condition : hunged and bundled in coiled condition fiber length : 500m temperature : 200°C x 170 hrs 	$\Delta\alpha < 0.1\text{dB/km}$ after 1 hour
Flame Test	(VW-1)	temperature of the tip of flame : 836°C or higher combustion time : 15 seconds x 5 times	to pass the spec. of VW-1
	(IEEE-383)	temperature : 816°C or higher (75mm apart from the burner) combustion time : 20 minutes	to pass the spec. of IEEE-383

3. Characteristics

Table 3 indicates testing methods for various tests for mechanical characteristics, heat and fire, and their target values. Measurement of transmission loss was made with LED light source of 0.85 μ m wavelength.

3.1 Mechanical Characteristics

(1) Flexibility

Fig. 2 indicates flexibility of this cable (type A). Displacement of each load from initial position on the free end of the cable is the value obtained when the cable is set horizontally with its free end weighted and kept for 1 minute. For small sample of 10cm, it has displacement of 6cm for 100 gf load, which proves that it has sufficient flexibility.

(2) Bending

Fig. 3 indicates transmission loss increase when the cable is wound around a mandrel for 5 turns. Bending diameters when the transmission loss increases 0.1dB were found to be as small as 20mm and 10mm for type A and type B respectively. The reason for the type A's characteristics being to some extent different from the type B is that the groove for the type A is narrower than the type B, where for the type B, depth and width of the groove is 0.9mm, while for the type A, it is 0.8mm, and the movability of fibers are restricted by the grooves.

(3) Flexure

Fig. 4 indicates fluctuation characteristics of transmission loss as the result of repeated bending tests. It shows that significant loss fluctuation is almost nil for both type A and type B, and that there was no breakage of fiber observed after bendings for 10,000 times.

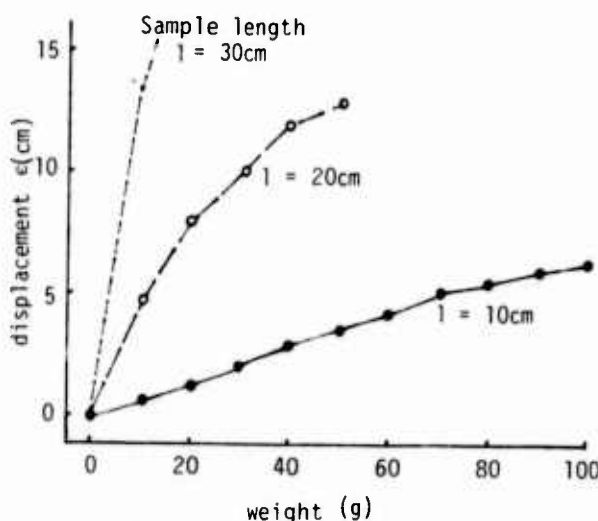


Fig. 2 Flexibility property

(4) Tensile Strength

Fig. 5 indicates elongation as the result of tensile strength test. Loads for 0.5% elongation and breakage were same for the type A and the type B, which were 40Kgf and 80Kgf respectively. Fluctuation in transmission loss was almost not observed up till just before the breakage.

(5) Compression

Fig. 6 shows transmission loss fluctuation at pressure test using pressure board of 100mm length. The indicated value was less than 0.2dB under 1000Kgf load for both type A and type B and residual transmission loss was not observed after the load was removed.

(6) Impact

Fig. 7 indicates transmission loss fluctuation at impact test to side of metal column of 25mm diameter, where the value indicated was less than 0.05dB for both type A and type B with impacts of 50 times. The reason why the type B is to some extent stabler than the type A is the larger effect of cushioning against impact as the results of thicker outer sheath and larger groove.

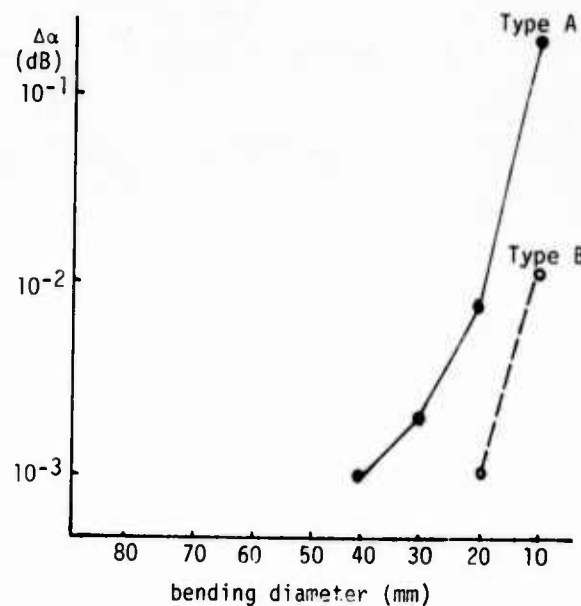


Fig. 3 Bending property

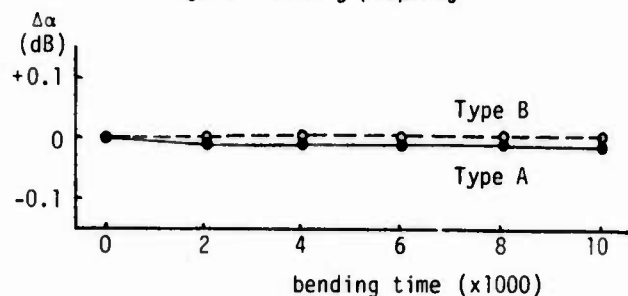


Fig. 4 Flexure property

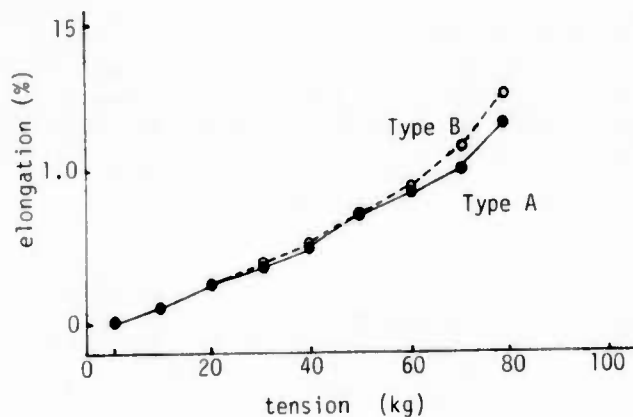


Fig. 5 Tensile strength property

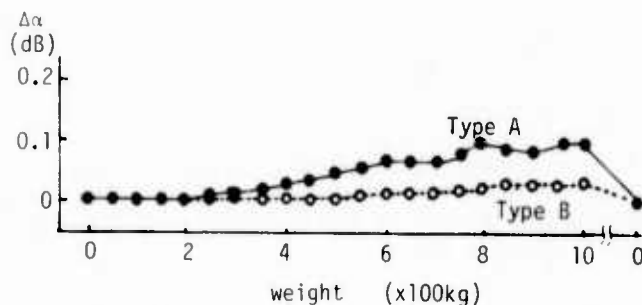


Fig. 6 Compression property

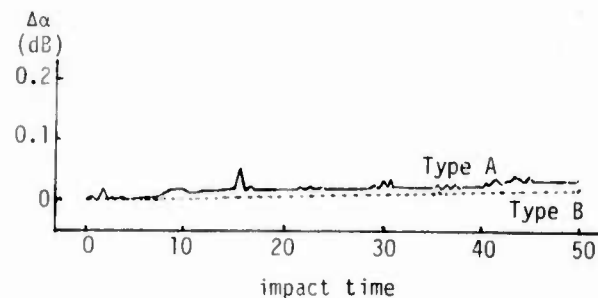


Fig. 7 Impact property

3.2 Thermal Characteristics

(1) Temperature

Fig. 8 indicates transmission loss fluctuation for the optical fiber cable (type A) at $-50^{\circ}\text{C} \sim +150^{\circ}\text{C}$ temperature where the loss increase was about 0.1dB/km at $-50^{\circ}\text{C} \sim +150^{\circ}\text{C}$ range. For $-50^{\circ}\text{C} \sim +100^{\circ}\text{C}$, it was quite stable. The temperature at using environment is in $-40^{\circ}\text{C} \sim +80^{\circ}\text{C}$, which poses no problem.

(2) Heat

Fig. 9 shows the changes in transmission loss wavelength characteristics when this cable (type A) is left for 170 hours at 200°C temperature. No significant transmission loss increase was observed while and after the test was conducted.

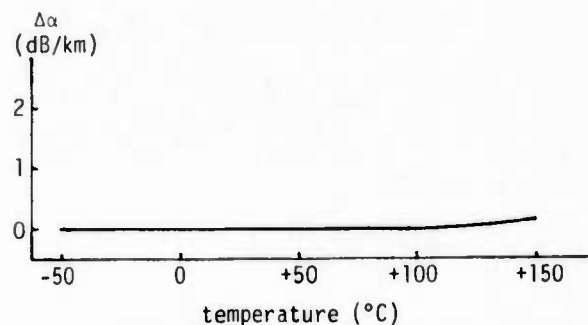


Fig. 8 Temperature-transmission loss property

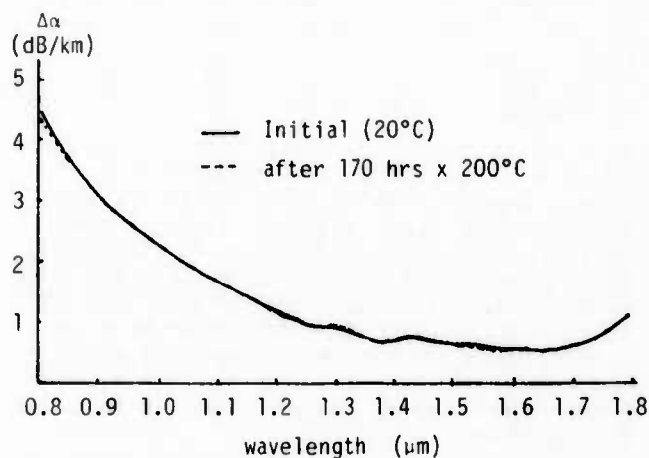


Fig. 9 Loss spectra of cable measured under initial conditions (20°C) and 170 hours later ($+200^{\circ}\text{C}$)

3.3 Inflammability

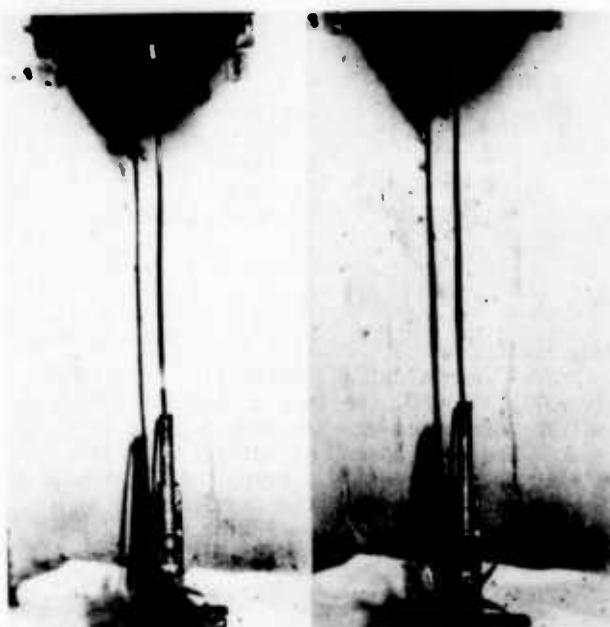
The following studies were conducted on inflammability when the cable is on fire;

(1) VW-1 (Vertical Wire) Flame Test

Photograph 2 indicates burnt conditions of the cable just after VW-1 test is commenced for type A and after the test is over. Combustion was conducted 5 times for 15 seconds, however, the fire was self-extinguished within 1 second for each time.

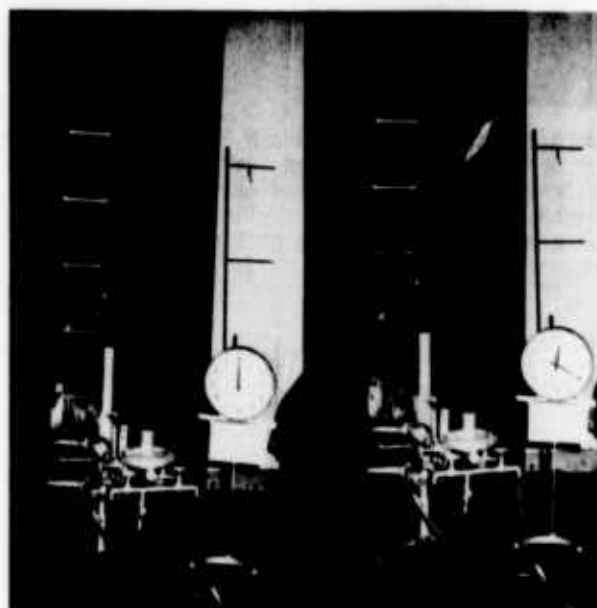
(2) IEEE 383 (Vertical Tray) Flame Test

Photograph 3 indicates how vertical tray test is conducted on type A based on standard of IEEE 383, and Fig. 10 shows temperature changes with time at each place. At a place 30cm distant, the temperature was around 150°C . While on fire for 20 minutes, and no effect of the combustion was observed. The damaged cable length was 300mm and lingering flame time was 0 second.



(a) at the start (b) after five combustions

Photo 2 View of the VW-1 flame test before and after five 15-second combustions



(a) at the start (b) after 20-minutes combustions

Photo 3 View of the flame test based on the standard of IEEE-383 before and after 20 minutes combustions

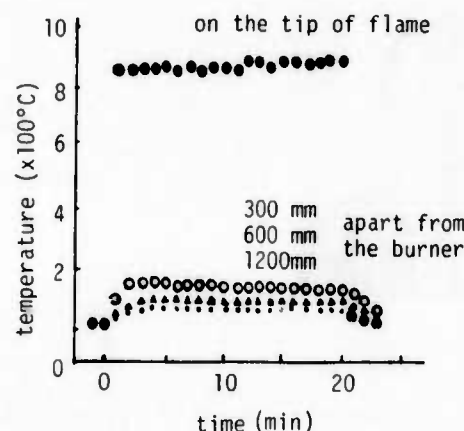


Fig. 10 Temperature property of cable under the test of IEEE-383

3.4 Less Smoke

This cable (type A) is composed of materials emitting less smoke and with flameretardancy, and being the cable with smaller diameter, few problem exist in respect of smoke to be emitted from the cable.

As aforesaid, this cable is considered to have sufficient characteristics necessary in practical uses without having problems in respect of mechanical, thermal and inflammable properties.

4. Conclusion

We have designed and produced the optical fiber cable with a purpose of developing indoor optical fiber cable with versatility for LAN, and confirmed by the various evaluation tests that it had sufficient performances necessary in its partical uses. We expect that this kind of cable can contribute to improve workability in installation and handling of the indoor optical fiber cable for LAN, both in plenum areas of severe using environment and within offices where importance is attached to managebility of the cable.

References

- (1) O. Ichikawa, et al., "Development of Nonmetallic, Loose-groove Spacer-type Optical Fiber Cable", 31st I.W.C.S., Nov., 1982



Yasunori Saito
Sumitomo Electric
Research Triangle, Inc.
P.O. Box 13445
Research Triangle Park,
N.C. 27709,
U. S. A.

Yasunori Saito received his B.S. degree in Electrical Communication Engineering from Tohoku Univ. in 1969. He then joined Sumitomo Electric Industries and has been engaged in research and development of high frequency transmission lines including fiber optics. Mr. Saito is a manager engineering of Sumitomo Electric Research Triangle Inc., and a member of the Institute of Electronics & Communication Engineers of Japan.



Osamu Ichikawa
Sumitomo Electric
Industries, Ltd.
1, Taya-cho,
Totsuka-ku,
Yokohama, Japan

Osamu Ichikawa received his B.S. degree in Electrical Communication Engineering from Tohoku University in 1980. He then joined Sumitomo Electric Industries and has been engaged in research and development of optical fiber and cables. Mr. Ichikawa is a member of Yokohama R & D Group, and a member of the Institute of Electronics & Communication Engineers of Japan.



Tetsuji Ono
Sumitomo Electric
Industries, Ltd.
1, Taya-cho,
Totsuka-ku,
Yokohama, Japan

Tetsuji Ono received his M.S. degree in Synthetic Chemistry from Nagoya Institute of Technology in 1975. He then joined Sumitomo Electric Industries and has been engaged in research and development of optical fiber and cables. Mr. Ono is a senior engineer of Yokohama Research and Development Department, and is a member of the Institute of Electronics & Communication Engineers of Japan.



Shigeru Tanaka
Sumitomo Electric
Industries, Ltd.
1, Taya-cho,
Totsuka-ku,
Yokohama, Japan

Shigeru Tanaka was received a M.S. in 1976 from Tokyo University. He joined Sumitomo Electric Industries, Ltd. in 1976, and has been engaged in research and development of optical fiber cable. He is a member of Institute of Electronics & Communication Engineers of Japan.



Akinori Mori
Sumitomo Electric
Industries, Ltd.
3-3, Satsuki-cho,
Kanuma-city,
Tochigi-prefecture
Japan

Akinori Mori received his B.S. degree in mechanical engineering from Kyusyu University in 1970. He then joined Sumitomo Electric Industries, Ltd. and engaged in development and design of plastic cables. Mr. Mori is now Assistant to Manager, Industrial Electronics Wire Section, Electronics Wire Division.

Optical Fiber Under-Carpet Cable System

K. Omae F. Takahashi A. Otake M. Nomura T. Mishima

The Furukawa Electric Co., Ltd.
Tokyo, Japan

Abstract

This paper describes a compact and flexible optical fiber under-carpet cable system. The under-carpet cable contains two fibers which are individually protected in Nylon pipe with filling compound. A pair of steel wires with larger diameter than coated fiber are also in bedded loosely in Nylon extruded pipes and placed at the both sides of the fibers. Since all the fibers and steel wires are free in pipes, this cable can be easily bent in any directions with minimized stress on fiber without loss increase. It can be installed and bent under floor tile or carpet with minimum bending radius of 50 mm. It also allows the lateral pressure of 10000 N/cm², and impact of 5 pounds - 5 feet load. The transmission is stable enough against temperature change, and transmission loss variation is less than 0.1 dB/km in the temperature range of -20°C ~ +60°C.

Both ends of this cable are terminated by connectors that allows the movement of strength member for easy handling and reasonable level of pulling force. Connection loss of less than 0.45 dB is achieved. Connectors are protected by the protector with thickness very close to that of regular office carpets.

1. Introduction

In the office, cable with smaller size and larger information capacity is now required for office automation. Optical fiber cable system satisfies these requirements with its superior characteristics. But the optical fiber has several demerits, on the other hand. One is the weakness for lateral force. In the case that the lateral force is imposed on the optical fiber, it causes loss increase and breakage of optical fiber finally. The other is the difficulty of connection with each fiber. Conventional optical fiber cable and its connector are too large size to be introduced into office. We developed the new type of the optical fiber cable system to overcome these problems.

2. Constitution of the optical fiber under-carpet cable system

The optical fiber under-carpet cable system consists of the connectorized under-carpet cable, protector of connector and connectorized termination cable as shown in Fig. 1. One example of optical fiber under-carpet system configuration is shown in Fig. 2. If cable route is to be

extended in the future, additional optical fiber under-carpet cable will be connected with this flat connector, so that route expansion is easily achieved.

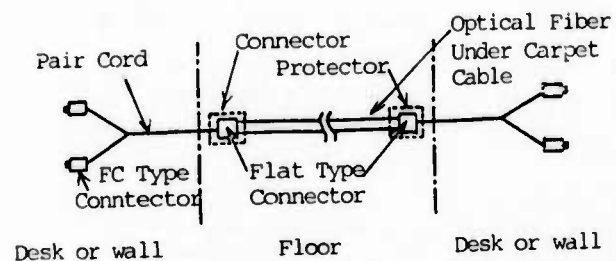


Fig. 1 Constitution of Optical Fiber Under-carpet Cable System

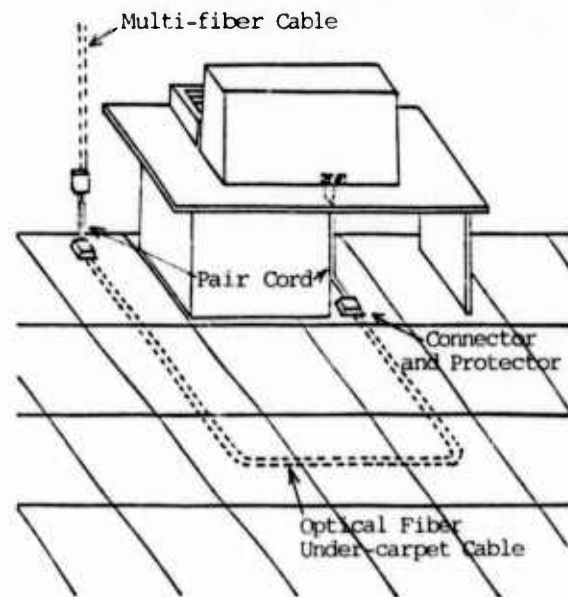


Fig. 2 Example of Optical Fiber Under-carpet Cable System

3. Optical fiber under-carpet cable

Cable structure is shown in Fig. 3. At the center of this cable, two optical fibers are contained in Nylon pipes which are filled with oil. This pipe protects the optical fiber from a sudden bend and elongation. The dimension of the optical fiber is shown in Table -1.

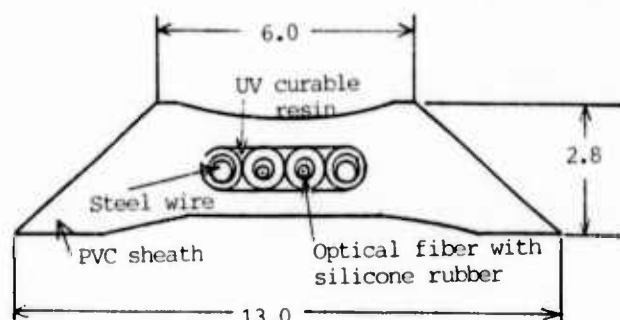


Fig. 3 Structure of Optical Fiber Under-carpet Cable

	Diameter
Outer Diameter	125 μm
Core Diameter	50 μm
Coat Diameter	400 μm
Index Difference	1 %

Table-1 Diameter of GI Fiber

At both sides of the optical fibers, two steel wires are placed. And these steel wires are contained in Nylon pipes. It is very easy to bend this cable in horizontal direction. These four pipes are combined by UV curable resin.

This unit is covered with PVC sheath. There is a dent at the center of this cable. Both sides of this cable are thinner than the center. Therefore, the center of this cable is harder to break by lateral force than the sides.

Characteristics of cable

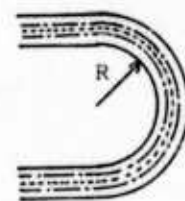
The characteristics of optical fiber under-carpet cable are as follows.

(i) Bend Test

A loss and distortion are measured. The test results are shown in Fig. 4(a), Fig. 4(b).

The plus distortion means elongation and minus distortion means compression.

In the case of horizontal bend, actual fiber distortion is much smaller than calculated value. Calculated value is derived from following assumption. This assumption is that optical fiber is fixed at the center of Nylon pipe and unmovable.



Horizontal Bend

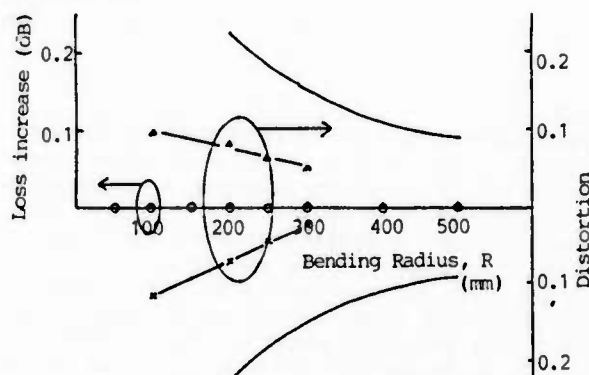
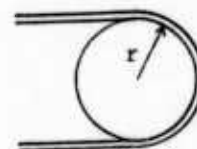


Fig. 4(a) Relation Among Loss Increase, Horizontal Bending Radius, R and Distortion



Vertical Bend

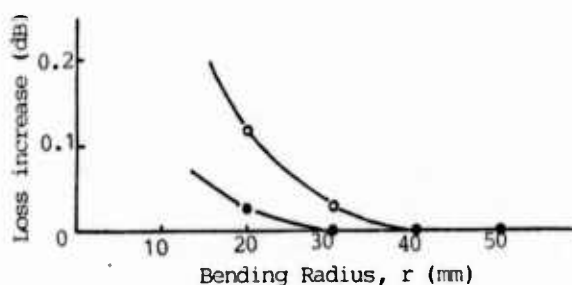


Fig. 4(b) Distortion Between Loss Increase and Vertical Bending Radius, r.

This low distortion is achieved by loose structure of Nylon pipe.

If there is a sudden bend or distortion at a local place, the distortion may be distributed longitudinally. Measured distortion is much smaller than calculated value. This difference is caused by this relation.

In the case of vertical bend, fiber distortion is caused at the surface. At the outer surface, distortion is elongation

and at the inner surface distortion is compression. So total fiber distortion is not detected. Actual installation conditions are as follows.

Horizontal bend Not less than $RH = 250$ mm
Vertical bend Not less than $RV = 50$ mm

Horizontal bend condition corresponds to the half size of tile carpet. And vertical bend condition corresponds to the condition that fiber surface distortion is below 0.15 %. At both conditions, this cable has no loss increase and there is very small distortion which is below 0.2 %.

(ii) Impact Test

Impact test was done by two conditions. Each condition is shown as follows.

Condition A : Load 1 pound, 3 pound, 5 pound
Times 3 times for each
Impact Place 1 cable
Height 5 feet

Condition B : Load 1 pound, 3 pound, 5 pound
Times 3 times for each
Impact Place 2 crossed cables
Height 5 feet

At the Condition A, this cable endures the impact load. There is a small damage at 5lb x 5ft and 1 time but no loss increase. In the case that cable is covered with carpet, there is no damage and no loss increase by 5lb x 5 ft x 3 times.

At the Condition B, cable sheath is damaged by 5lb x 5ft x 3 times. And loss increase occurs. A steel sheet which is 0.5 mmT x 10mmW x 20 mmL is used between 2 cables. In this case, Condition B is regarded as Condition A. We get the same results as Fig. 5(a) in the Condition B. In the case that cable crossing point is covered with carpet, there is no loss increase and no damage on cable.

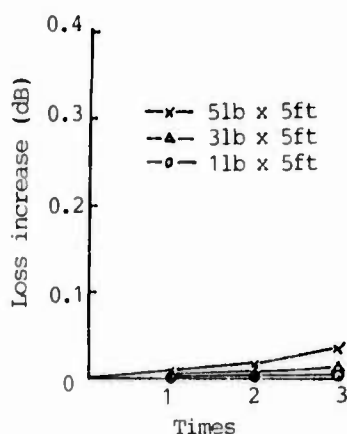


Fig. 5(a) Impact Test on Cable

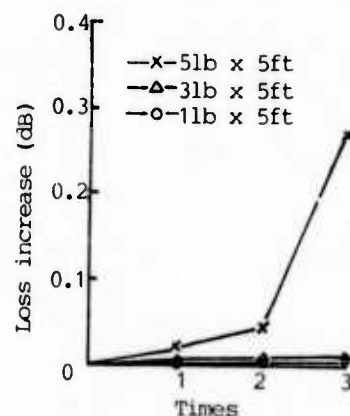


Fig. 5(b) Impact Test on Cable Crossing Point

(iii) Compression Test

According to 2 following conditions, compression test is done by these conditions.

Condition A : Compression force on a Cable
Condition B : Compression force on two crossed cables
Crossing Point

At the condition A, there is no loss increase until 1000kg/cm² force. But at the Condition B, there occurs loss increase from 200 kg/cm² force. Then we introduce the steel sheet which was used in impact test. We get good improvement of compression test, of which result is similar to Fig. 6(a). If we don't use this steel sheet, the compression force is concentrated to steel wire. The steel wire has very small size, 0.6 mmφ, and crossing point of steel wires is very small. So at the condition B, steel wires are deformed at the crossing point and optical fiber is bent by steel wires. In the case of usage of steel sheet, we can prevent the concentration of compression force. So we can get the improvement of compression test result at Condition B.

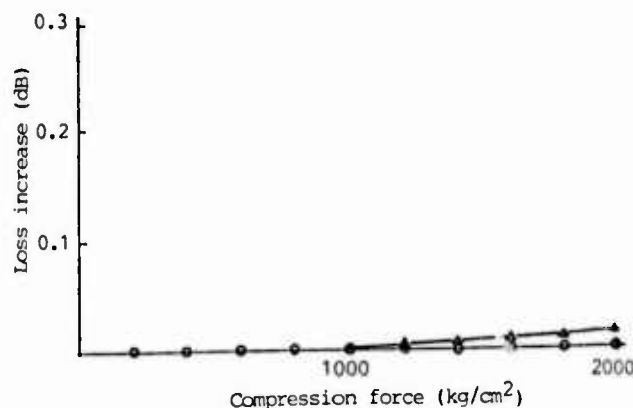


Fig. 6(a) Compression Test on Cable

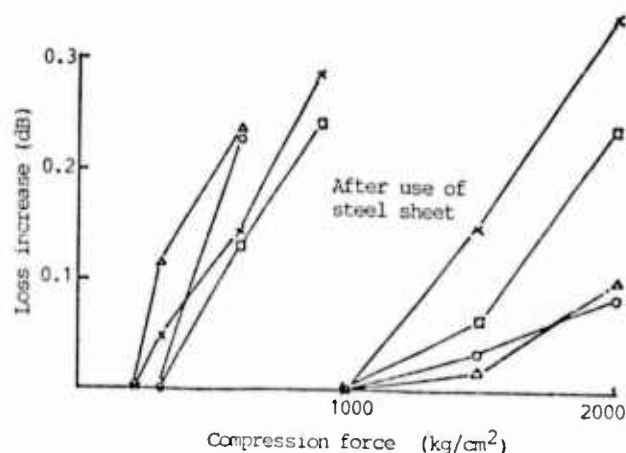


Fig. 6(b) Compression Test on Cable Crossing Point

(iv) Temperature Test

The result of temperature test is shown in Fig. 7. Temperature region is from -20°C to 60°C . Time chart is shown. There is no loss increase within this temperature region. Sample length is 250 m. And this heat cycle is continued to 5 cycles, but no loss increase occurs.

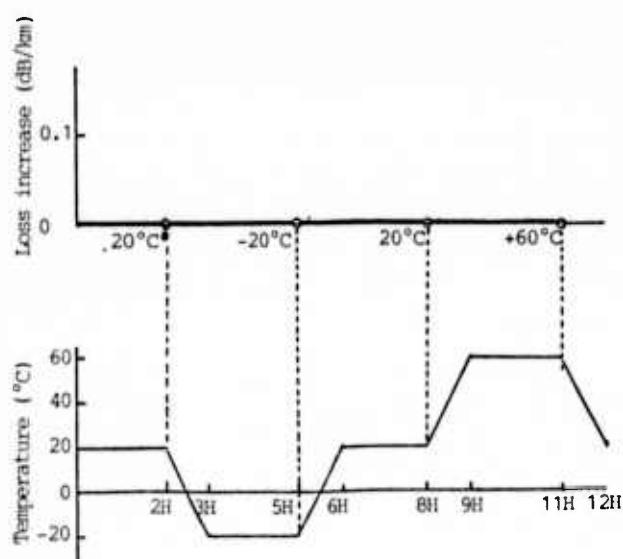


Fig. 7 Temperature Test

4. Connector & Protector

In this cable system, no splicing joint is necessary. But in future, this cable system may extend longer. We think in

this system small connector is necessary.

For future extension, this cable route will be extended by connector joint. Constitution of this flat connector and protector is shown in Fig. 8(a) and Fig. 8(b). Protector is made of plastics.

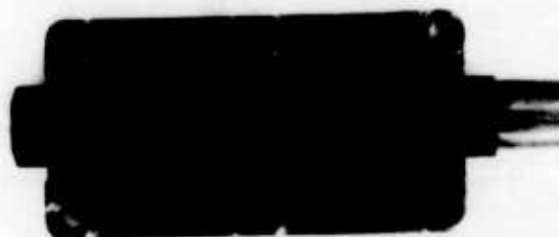


Fig. 8(a) Photograph of Flat Connector



Fig. 8(b) Photograph of Covered Flat Connector with Protector

In Fig. 9, the loss distribution of this connector is shown. Average loss is 0.45 dB. The structure of this connector is shown in Fig. 10.

This connector is mated by guide rods. The optical fibers only are fixed here, so silicone oil which is filled in Nylon pipe, doesn't flow out. Two fibers are connected by this connector simultaneously. Connector size is 20 mmW x 35 mmL x 6 mmT. Steel wires of under-carpet cable are not fixed in this connector. Because when this cable is bent to horizontal direction, the steel wires move. Inner wire juts out and outer wire is absorbed. In this connector the end of steel wire is stored in steel pipe loosely in consideration of this phenomena. And this cable is easy to bend to horizontal direction.

The size of protector is 65 mmW x 100mmL x 11 mmT.

The protector is weaker than the other parts, because it is made of plastics. When 1 pound x 5 feet load is imposed on it, it is broken. So this protector shall install below the desk and so on.

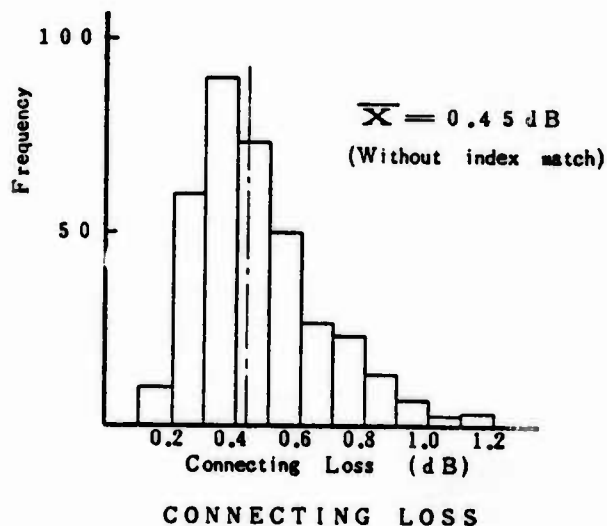


Fig. 9 Loss Distribution of Connector

5. Optical fiber pair cord with connector

The termination cable is more flexible than the under-carpet cable. This cable consists of 2 optical fiber cords. Each size of cord is 3 mm. And 2 cords are extruded simultaneously. One side of this cable is terminated by FC type connector¹, and the other side is terminated by flat connector.

6. Conclusion

In consideration of a new office automation, we developed the optical fiber under-carpet cable system. We conclude that this under-carpet cable system can clear the following test conditions.

Bend Test

Horizontal direction	Not less than R=250mm
Vertical direction	Not less than R=50mm

The size of the tile carpet is 500mm x 500mm. Therefore, the bend condition of horizontal direction is not less than R=250mm. The bending radius of the vertical direction is decided in consideration of convenience.

Impact Test : 3lb x feet

When a lady steps on this cable by high heeled shoes, it is said that the impact is 1.5lb x feet. For safety, we decide this value as the twice of 1.5lb x feet.

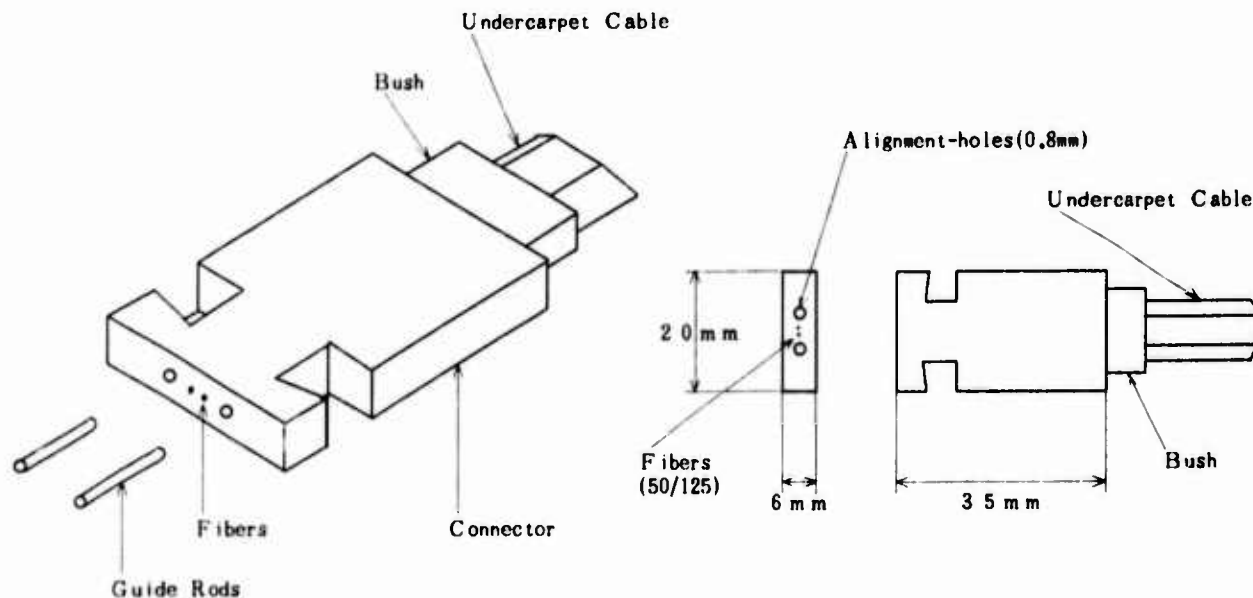


Fig. 10 Construction of Multi-Connector for Under-Carpet Cable

Compression Test : 120 kg/cm²

When a lady steps on this cable by high heeled shoes, it is said that the compression force is 60 kg/cm². For safety, we decide this value as the twice of 60 kg/cm². This condition is severest, we think.

Temperature Test : 0°C ~ + 50°C

Reference

1. IEC SG-46E DOCUMENT
FC TYPE CONNECTOR



Kazuya OMAE

The Furukawa Electric Co., Ltd.
6 Yawata-Kaigan-Dori
Ichihara,
Chiba, Japan

Mr. OMAE graduated from Kyoto Univ. 1974, and joined The Furukawa Electric Co., Ltd. in 1974 and has been engaged in development of the measurement of optical fiber, E/O and O/E, and now development of optical fiber cable.

Mr. OMAE is now an assistant manager of Optical Fiber Cable Development Group, Research & Development Department, Telecommunication Division at The Furukawa Electric Co., Ltd. and a member of the Institute of Electronics and Communication Engineers of Japan.



Fumio TAKAHASHI

The Furukawa Electric Co., Ltd.
6 Yawata-Kaigan-Dori
Ichihara,
Chiba, Japan

Mr. Takahashi graduated from Tokyo Institute of Technology 1981, and joined The Furukawa Electric Co., Ltd. in 1981, and has been engaged in development of optical fiber cable.

Mr. Takahashi is now an engineer of Optical Fiber Cable Development Group, Research & Development Department Telecommunication Division at The Furukawa Electric Co., Ltd. and a member of the Institute of Electronics and Communication Engineers of Japan.



Akihiro OTAKE

The Furukawa Electric Co., Ltd.
6 Yawata-Kaigan-Dori
Ichihara,
Chiba, Japan

Mr. Otake graduated from Tohoku Univ. 1974, and joined The Furukawa Electric Co., Ltd. in 1974 and has been engaged in development of coaxial cables, optical fiber cables, and now development of accessories of optical fiber cables.

Mr. Otake is now an assistant manager of Fiber Optics Apparatus Group, Research & Development Department, Telecommunication Division at The Furukawa Electric Co., Ltd. and a member of the Institute of Electronics and Communication Engineers of Japan.



Michihiko NOMURA

The Furukawa Electric Co., Ltd.
6-1 Marunouchi 2-chome,
Chiyoda-ku, Tokyo, Japan

Mr. Nomura graduated from Waseda Univ. 1971 and joined The Furukawa Electric Co., Ltd. in 1971, and has been engaged in development of telecommunication cable.

Mr. Nomura is an assistant manager of Telecommunication Cable Section, Telecommunication Division at the Furukawa Electric Co., Ltd.



Takashi MISHIMA

The Furukawa Electric Co., Ltd.
6 Yawata-Kaigan-Dori
Ichihara,
Chiba, Japan

Mr. Mishima graduated from Koshu-Tokai Univ. 1980 and joined The Furukawa Electric Co., Ltd. in 1980, and has been engaged in development of telecommunication cable. Mr. Mishima is an engineer of Research & Development Department, Telecommunication Division at The Furukawa Electric Co., Ltd.

OPTIMIZING SHORT DISTANCE FIBER OPTIC LINKS A REAL WORLD APPROACH

David R. Maack and John J. Magera

EOtec Corporation
West Haven, CT

I. SUMMARY

A study was done evaluating the "real world" performance of short distance fiber optic data links coupling an LED directly to a detector. Detector current was used as a fundamental criteria for measuring the effectiveness of a particular system consisting of an LED, a connector system, a fiber-cable, and a detector. The results indicate that the most cost effective method to increase received power is to increase fiber core size.

This study was performed by experimentally measuring the detector current in a fiber optic data link as multiple samples of different types of each component were interchanged. The results were analyzed by statistical methods in order to evaluate the effectiveness of each of the component types.

II. INTRODUCTION

The use of fiber optics in short distance data links is increasing rapidly as designers and users alike become more familiar with this new technology. Currently, the industry offers these customers a multitude of fibers, cables, connectors, sources, and detectors. Unfortunately, the available design data and component specifications are not always easily applied to short distance data link design especially when manufacturing tolerances and performance variations must be considered. In addition, most of this data is based on long length or steady state assumptions not all of which are valid for a short distance link.

In the "real world" the optimization of a data link must be based on the performance of the system as a whole with the basic criteria being the ability of the receiving end to recognize the information. A fundamental measurement of this ability is detector current because, all else being equal, an

increase in detector current means an increase in the safety margin for a system.

This study was undertaken to examine the actual performance of a short distance, source to detector data link with detector current as the measure of system performance. An experimental methodology was used comprised of multiple samples of different types of each component. Various combinations were assembled and detector current was measured.

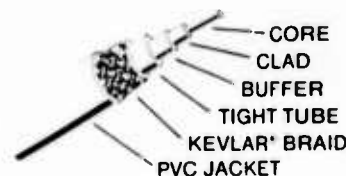


Figure 1. Cable Construction

III. SAMPLE PREPARATION

The sample matrix of components used in this study is shown in Table 1. The various types of each component were selected to be representative of those products that are generally promoted for short distance data links. The total number of available products, however, is several orders of magnitude greater. Also, not all possible combinations of this matrix were fabricated or tested.

A total of seven fiber types were fabricated into cable and then terminated using three different connector systems. The same cable construction was used for all fiber types because cable construction is an environmental design criteria, not an optical criteria. The specific construction used is shown in Figure 1

Table 1. SAMPLE MATRIX

<u>Component</u>	<u>Designation</u>	<u>Specification/Description</u>	<u>Manufacture</u>	<u>Cost</u>
Fiber	50 x 125 CSB	3.0db/km;NA = 0.21	Corning Glass	\$ 0.23/meter
	100 x 140 CSB	5.0db/km;NA = 0.28	Corning Glass	0.55/meter
	100 x 140 type F	5.0db/km;NA = 0.29	Spectran Corp.	0.50/meter
	200 micron PCS	6.0db/km;NA = 0.40	EOtec Corp.	0.35/meter
	200 micron HCS	8.5db/km;NA = 0.35	E.B. Industries	0.50/meter
	400 micron PCS	6.0db/km;NA = 0.40	EOtec Corp.	1.50/meter
	.060 Crofon	> 1000db/km;NA = 0.53	Dupont, Inc.	N.A.
Cable	Tight tube	3mm O.D.;Kevlar braid	EOtec Corp.	N.A.
Connector	Resilient plastic	Optimate SFR;1.0db	AMP, Inc.	\$ 1.50-4.00
	SMA-906	Stainless Steel Nose;1.0db	Amphenol N.A.	16.00
	SMA-SA	Aluminum Insert Nose;1.0db	OFTI, Inc.	7.00
LED	MFOE-1200	900uw @ 820nm	Motorola	11.00
	OP-133W	6mw @ 940nm	Optron, Inc.	1.40
	CFQ 24	400uw @ 830nm	Amperex	9.80
Detector	OP-802W	NA @ 820nm	Optron, Inc.	1.60
	UDT 2DP-1	0.45A/W @ 850nm	UDI, Inc.	2.25
	BPF 24	0.40A/W @ 750nm	Amperex	7.65

and is an accepted design for the office and most process control environments.

All terminated assemblies were 1 meter long with the same connectors on each end. Assembly techniques were in accordance with the manufacturer's recommendations and ground and polished to a 1 micron finish. Multiple samples of each LED and detector were purchased.

IV. TEST PROCEDURES

All measurements were made using the test set-up shown in Figure 2, consisting of a Keithly Model 225 current source, and Optronic Model 730A Radiometer and two special mounting fixtures. These fixtures were designed so that individual LED's and detectors could be inserted into various bulkheads which matched the sample's connector system. All leads were soldered to insure good electrical contact.

The procedure for all measurements was as follows:

1. Insert LED in proper bulkhead and solder leads.
2. Adjust current source for 100 milliamps.
3. Insert detector in proper bulkhead and solder leads.

4. Connect sample assembly and read radiometer in microamps.

5. Remove assembly and reverse ends.

6. Reconnect and remeasure.

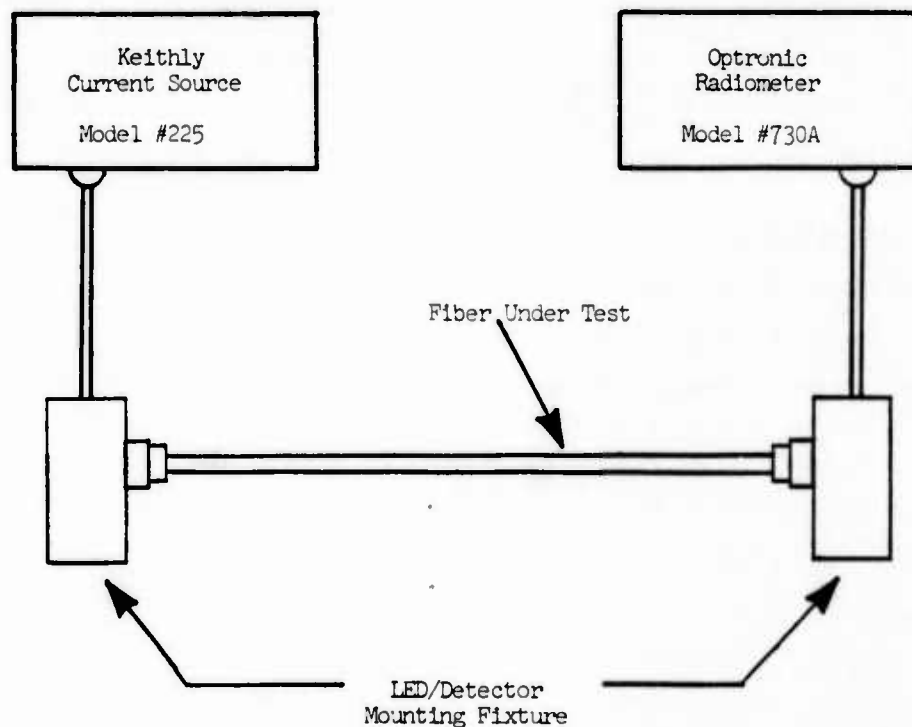
Cable assemblies measured earlier were periodically remeasured to verify test method stability and repeatability.

V. RESULTS AND DISCUSSION

The results of the testing were arranged much that six separate variables were identified and analyzed. Multiple samples of each component allowed standard deviations to be calculated which are representative of "real world" performance. Each of these six studies are presented in the following tables and discussions. Fixed components are those that the same sample was used for all testing in that study.

Table 2. Connector Material Study I.

The goal of this study was to determine the difference between an SMA connector with an all stainless steel nose and an SMA connector with an aluminum insert in the nose. The other components of this link were chosen to magnify any differences, i.e., small core



fiber and a low powered LED. The results clearly show that the all stainless component produced greater average detector current by 0.6 db, however, its cost is considerably higher. This difference was attributed to the better mechanical and dimensional stability of stainless steel over aluminum. As other parameters of the system are changed such that this stability becomes less important, the optical difference these two connector constructions should decrease. Previous work performed with 100 x 140 fibers confirm this.

Table 2. Connector Material Study I.

Connector Type	Material	Detector Current Microamps	
		Average	Variance
SMA-906	All Stainless	0.084	.001
SMA-SA	Aluminum Nose	0.073	.002

Fixed Components

LED: OP133W
 Detector: UDT 2DP-1
 Fiber: 50/125 CSB

Table 3. Connector Material Study II.

Fiber Type	Detector Current-Microamps			
	Resilient Plastic		Aluminum Nose	
	Average	Variance	Average	Variance
100x140 type F	6.12	.08	3.23	0.76
200 micron PCS	5.30	.23	7.22	1.64
400 micron PCS	8.85	.45	28.67	5.61

Fixed Components

LED: MFOE-1200
 Detector: UDT 2DP-1

Table 3. CONNECTOR MATERIAL STUDY II.

In this study, the aluminum nose SMA and resilient plastic connector were examined. In order to cover probable real world combinations, three fiber types with a high power LED were measured and compared. The results suggest that with the 100 x 140 fiber the plastic connectors are superior while for PCS fibers, the SMA's are superior. Further analysis of the three fiber types in the SMA connector is reasonably consistent with theory in that delivered power is proportional to the square of the core diameter ratio. This is not true of the

resilant plastic connectors where all three fiber types produce similar values. This inconsistency along with the high current for the 100 x 140 fiber is probably due to an unrecognized variable. Variances are reasonably low, less than 1 db, and most likely due to a combination of connector tolerances and LED tolerances.

Table 4. Assembly Study

Fiber type	Detector Current-Microamps			
	High Power LED		Low Power LED	
	Average	Variance	Average	Variance
50x125-CSB	1.11	.01	.07	.002
100x140-CSB	2.51	.14	.36	.040
100x140-Type F	3.23	.76	.46	.060
200 micron PCS	7.22	1.64	.49	.110
200 micron HCS	8.19	.77	1.18	.120
400 micron PCS	28.67	5.61	2.57	.810

Fixed Components

High Power LED: MFOE-1200
Low Power LED: OP133W
Detector: UDI 2DP-1
Connectors: 906-SA

Table 4a.

Fiber type	Power Gain -db	
	High Power LED	Low Power LED
50x125 CSB	-3.5	-7.0
100x140 CSB	0	0
100x140 Type F	1.1	1.1
200 micron PCS	4.6	1.3
200 micron HCS	5.1	5.1
400 micron PCS	10.6	8.5

Table 4. ASSEMBLY STUDY

In this study, the effect of fiber types was examined for both a high power and a low power LED. The results are quite consistent with expectation, i.e., a larger core delivers greater power. The high power LED averages about 8 db more current, however, it is 8 times more expensive. Variances are about 1 db indicating small performance differences between multiple assemblies of the same configuration.

Table 5. LED STUDY

The purpose of this study was to examine the variance in detector current for different samples of a specific LED. Both high power and low power devices were analyzed with four different fiber

types. Variance is definitely higher for the high power LED's. The relationship of the various fiber types supports the data analyzed from Table 4.

Table 5. LED Study

Fiber type	Detector Current-Microamps			
	MFOE-1200		OP-133W	
	High Power LED		Low Power LED	
	Average Variance		Average Variance	
100x140 CSB	3.30	.90	0.33	.02
100x140 Type F	2.61	.55	0.44	.03
200 micron PCS	6.32	2.18	0.86	.12
400 micron PCS	27.61	7.66	2.28	.07

Fixed Components

Detector: UDI 2DP-1
Connector: 906-SA
All Assemblies

Table 5a.

Fiber type	Variance-db	
	High Power	Low Power
100x140 CSB	1.1	0.2
100x140 Type F	0.8	0.2
200 micron PCS	1.3	0.5
400 micron PCS	1.1	0.2

Table 6. DETECTOR STUDY

The purpose of this study was to examine the variance in detector current for different samples of a specific detector. Again, both high power and low power LED's and five fiber types were analyzed. Variance is significantly lower than in any of the previous studies suggesting a very high uniformity among samples of this detector. This is not surprising considering the ratio of a detector's active area to fiber core area. Again, the relative current for the various fiber types supports the data from Table 4.

Table 7. DEVICE STUDY

This study was done to analyze the performance of various matched LED-detector combinations with different fiber types. All components of these links were fixed, i.e., a single sample and measurement; consequently standard deviation values were unavailable. Initial analysis further confirms the results of Table 4. Detector current is

Table 6. Detector Study

Fiber type	Detector Current-Microamps			
	Detector UDT 2DP-1		High Power LED	
	High Power LED		Low Power LED	
	Average	Variance	Average	Variance
100x140 CSB	1.83	.07	0.28	.02
100x140 Type F	2.43	.03	0.36	.03
200 micron PCS	4.79	.26	0.57	.18
200 micron HCS	5.28	.17	0.76	.05
400 micron PCS	23.34	.63	1.90	.11

Fixed Components

Connector: 906 SA
High Power LED: MFOE-1200
Low Power LED: OP-133W
All Assemblies

Table 6a.

Fiber type	Variance-db	
	High Power	Low Power
100x140 CSB	0.1	0.2
100x140 Type F	0.1	0.3
200 micron PCS	0.2	1.1
200 micron HCS	0.1	0.2
400 micron PCS	0.1	0.2

approximately proportional to the square of the fiber core diameter ratio.

Further analysis shows that detector current is significantly influenced by LED-detector combination. The following comments apply.

1. The high power LED produces a higher detector current.

2. Different detectors have very measurable differences in sensitivity.

3. The gain produced by a high power LED vs. a low power LED is dependent on the detector type.

One of the more important conclusion of the data from Table 7. is the role of the detector. As expected, a more expensive detector gives better performance. Unexpected, is that this performance gain is dependant on LED power. A better detector helps a low powered LED system better than a high powered LED system.

VI. CONCLUSIONS

The results of this study clearly suggest that optimization of short data links for LAN's, process control, and sensor applications requires a system approach with an understanding of the "real world" contribution of each component. This understanding must include not only the performance variations, but the relative importance or weighted value of each component. Some have a much greater cost effectiveness than others.

The purpose of this work was to examine the performance of each component in a fiber optic link consisting of an LED, a detector, a fiber, and a connector system. The following general guidelines and conclusions apply.

1. **Fiber:** Fiber core diameter is the most cost effective way to increase detector current. In systems requiring high bandwidth a graded index fiber is necessary. The results of this study clearly show that 100 x 140 fiber gives substantially better optical performance than the 50 x 125 fiber at about twice the cost. System optimization will depend on the maximum link length and the total quantity of fiber required.

Table 7. Device Study

Fiber Type	Detector Current - Microamps				
	LED Detector	MFOE-1200 UDT 2DP-1	MFOE-1200 OP-802W	OP-133W OP-802W	OP-133W UDT 2DP-1 CQF24 BPF24
50/125 CSB		1.15	0.23	0.009	0.08 .003
100/140 CSB		2.68	0.76	0.054	0.38 0.12
200 micron PCS		8.90	2.74	0.068	0.59 0.37
400 micron PCS		36.60	11.97	0.46	3.55 .70
.60 Crofon*		8.37	36.40	2.21	4.84 .15

Connector: 906 SA (* Resilient Plastic)

Fixed Components: All

In systems operating at lower bandwidths, the 200 micron core step-index PCS fiber offers improved optical performance at a substantial cost reduction especially since termination problems have been resolved.^① An additional advantage of the larger core fibers is their improved performance when using the lower cost LED's and connectors.

2. Detector: The sensitivity of the detector is a very crucial consideration. A small increase in cost can substantially increase detector current and the performance of the system. System optimization will usually favor a reasonably high quality detector.

3. LED: As the power output of the LED is increased, both the detector current and the system cost increase. In general, high power LED's are 8 to 10 times the performance, but also are 8 to 10 times the cost of low power devices. System optimization will usually favor the lowest cost LED that will give an adequate safety margin.

4. Connectors: The termination system has a secondary effect on detector current as compared to the other components. Although better and more expensive connectors resulted in increased performance, their cost is hard to justify. The optical selection should be based on mechanical and environmental needs.

The design of a specific fiber optic link requires a lot of considerations which include mechanical, environmental, and electronic parameters in addition to the optical. Cost effective optimization is best accomplished through a systems approach based on the "real world" performance and interaction of each part.

1. D. R. Maack, J. J. Magera, "A Real World Approach to Plastic Clad Silica Fiber Termination", SPIE Proceedings Volume 479, Arlington, Virginia (1984).

2. D.R. Maack, J. J. Magera, "Termination of Plastic Clad Silica", 30th International Wire and Cable Symposium, Cherry Hill, NJ (Nov. 1981).

3. R. Cooper, "Fiber Optic Connector Splice Loss Measurements: The Laboratory vs. The Real World", FOC West, San Francisco, CA (Sept. 1981).

4. A. Z. Moss, J. H. Aumiller, J. Uradnisheck, "In-The-Field Connections With Fiber Optic Cables", 28th International Wire and Cable Symposium, Cherry Hill, NJ (Nov. 1979).

5. R. L. Warkentine, "Termination Technique for Plastic-Clad Fused Silica Fiber Optic Cables", First Fiber Optics and Communications Exposition, Chicago, IL (Sept. 1978).

6. J. F. Dalglish, "A Review of Optical Fiber Connection Technology", 25th International Wire and Cable Symposium, Cherry Hill, NJ (Nov. 1976).

7. Military Standard, "Fiber Optic Test Methods and Instrumentation", DOD-STD-1678, Method 6010, Method 8040.

Mr. Magera is Quality Assurance Manager at EOTec Corporation. He received his B.S. degree in Electrical Engineering from Bridgeport Engineering Institute in 1979. He is also a graduate of the U.S. Naval "Class A" School in Electronics. He has extensive experience in mechanical strength testing, optical fiber characterization, and physical properties measurement techniques. Prior to joining EOTec, Mr. Magera was with Exxon Enterprises.

Mr. Maack is Director of Engineering at EOTec Corporation. He received concurrently a B.S. degree in Nuclear Science and a B.S. degree in Physics from Lowell Technological Institute in 1969, and a Masters in Business Administration from the University of New Haven in 1982. At present, he is pursuing his doctorate. His fiber optic experience began at Times Wire and Cable and continued at Galileo Electro Optics in 1977 through 1980 when he joined EOTec.

DESIGN OF CUSTOMER PREMISES FIBER OPTIC CABLES

J. T. Loadholt
T. M. Williamson

AT&T Bell Laboratories
Norcross, Georgia 30071

ABSTRACT

The growth of fiber optic communications networks on customer premises is stimulating the development of cables and associated hardware which are optimized for the intrabuilding environment. The unique physical characteristics of this environment strongly influence the selection of optical fiber, materials, and mechanical performance criteria for the cables.

Considerable mechanical analysis is required to design fiber optic building cables which will perform in a cost-effective manner. This paper reviews the physical characteristics of the customer premises environment which are pertinent to cable design. Extension of fiber static fatigue analysis to a vertically hanging cable is presented as an example of the need for thorough evaluation of cable performance in buildings. Finally, several cable design guidelines are presented.

INTRODUCTION

Many proposals for fiber optic local area networks and wideband customer-premises systems are being advertised and described in the literature. These early entry systems are being assembled with hardware which is not necessarily optimized for building applications. The indoor environment is in some ways (e.g., temperature variations) less severe than the outside plant. However, the cable distribution facilities in commercial buildings demand cable designs that are mechanically robust but at the same time easy to install and terminate.

The unique characteristics of the building environment directly influence the selection of fiber, materials, and mechanical performance criteria for the cables. Considerable mechanical analysis is required to design fiber optic building cables to withstand the installation and service conditions common to customer premises. This paper

will review the physical characteristics of the building environment which are pertinent to cable performance. Static fatigue analyses for a variety of cable loading situations will serve as examples of the overall evaluation necessary for building cables. The paper concludes with a discussion of cable design guidelines which result from these considerations.

ENVIRONMENT

The building cable environment is the traditional customer premises where an extensive family of metallic cables now exists. The customer premises ranges from small businesses occupying a few floors to large businesses in multi-floor buildings. The campus environment, in which the customer has several buildings separated by distances up to several kilometers, is also an expected application. Each application will have its own specific cabling needs which are a direct function of the size of the system and the available cable distribution facilities. In short, the lightguide cable must go into conduits, ducts, and plenums as would any other communications cable. This environment sets many of the physical requirements for the cables.

A first step in building cable design is to quantify specific requirements dictated by the environment and relate those to the properties of cabled fiber. Pulling loads and bend radii are particularly important and are derived from the physical characteristics of the building. There are three distinct categories of cable routing facilities to consider: underfloor, ceiling, and riser. Table I lists the types of facilities that commonly occur in each category. Large buildings may have hybrid facilities involving several of these systems. Table I includes apparatus closets as a category. Though not a routing system, these closets are an important consideration in cable handling since they provide

TABLE I
BUILDING ENVIRONMENT

- UNDERFLOOR
 - Cellular
 - Conduit
 - Duct
 - Raised
- CEILING
 - Conduit
 - Plenum
- RISER
 - Conduit
 - Open
- APPARATUS CLOSETS
 - Underfloor Access
 - Ceiling Access

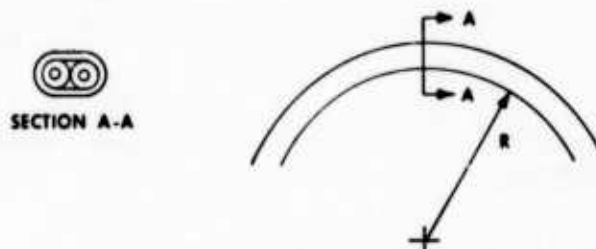
access to the cable distribution system. Here, cable design must be compatible with interconnection apparatus designs.

Conduit is a very controlled environment for cable and is commonly used in floors and ceilings. Most conduit for communications purposes is either 2" or 4" in diameter. The standard bend radius for 90° turns in 2" conduit is a very comfortable 9". Even if 1" conduit is considered, 90° elbows have a generous 5.75" radius. The risk of failure at a bend can be determined as a function of bend radius, fiber characteristics, and cable structure. For example, the duplex cable structure of Figure 1 is commonly used in optical datalinks in building systems and may be pulled through conduit. When the cable is bent, its oval shape insures that the fibers will assume the most favorable orientation (least-stressed), meaning the minimum allowable bend radius for the cable is that for an individual fiber. The maximum bending stress σ_b in the fiber resulting from a bend radius R is defined by

$$\sigma_b = \frac{E r_f}{R} \quad (1)$$

where E is Young's modulus for glass (10^7 psi) and r_f is the fiber radius. For a 125 micron diameter fiber proof-tested at 50 kpsi, the bending radius at which the maximum fiber stress equals the proof test level is 0.5 in. Thus, a short-term minimum bend radius of one-half inch is a conservative but reasonable recommendation for the

duplex cable. A real concern in cable design is that for some of the other systems, there is no mechanism for radius control in the access area or at turns. Cables must withstand applied point loads at access points in addition to the pulling loads.



DUPLEX CABLE IN BENDING

FIGURE 1

FIBER STRENGTH AND STATIC FATIGUE

Fiber strength strongly influences the cable design needed to meet installation requirements. As a guarantee for minimum strength, fibers are proof-tested prior to cabling. The proof-test level is selected based on expected loads during cable manufacturing, installation, and service and on the cable structure to be used.

Static fatigue is time-dependent failure induced by subcritical* residual stresses on the fibers. The time-to-failure is very much affected by the residual stress level, initial surface flaw size distribution, proof-test level, and environmental conditions, i.e., moisture (1) and temperature (2). Residual loading on the cable usually exists after installation. In conduit, for example, the cable remains in tension as shown in Figure 2 after an ideal straight run. The stress is maximum at the center and decreases linearly to the end of the conduit. Residual stress is present in bends even in the absence of tensile loading, and the stress level is affected by the bend radius. Practical installations will vary greatly, with several bends at arbitrary spacings and possibly with other cables present. The presence of bends can significantly influence the cable pulling loads. After installation in conduit or ducts, the cable will be subjected to a superposition of tensile and bending stresses. Static

*A stress below the fracture strength of the fiber.

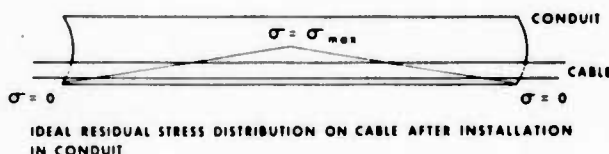


FIGURE 2

fatigue analysis of coated fused silica fibers subjected to uniform uniaxial tension and localized bending is well documented. (3-6) However, building applications are requiring that analysis be extended to include different loading combinations as seen in conduit.

Another loading condition of particular interest in customer premises is a cable hanging vertically in a riser shaft. In this case the long term loading is due to the weight of the cable. In less than ideal cases, such as pulling a cable into a crowded riser shaft, additional tensile loading may also occur. The following discussion summarizes results obtained for uniform uniaxial tension and localized bending. Results of static fatigue analyses for hanging loads are then introduced and compared to those of the other stress distributions.

Uniform Uniaxial Tension

A Weibull model is commonly used to characterize the distribution of tensile strength for fiber of a defined gauge length. A typical Weibull plot and strength histogram for 10m. long fibers is shown in Figure 3. (5) When applied, the stress field σ_{It} is constant over the entire volume as depicted in Figure 4. Hence, the largest surface flaw would result in fracture. The risk of failure I_t for this case is

$$I_t = \left(\frac{\sigma_{It}}{\sigma_0} \right)^m V \quad (2)$$

where m and σ_0 are Weibull shape and scale parameters and are strong functions of gauge length L . (7) The stressed volume is represented by $V = \pi r_f^2 L$. The risk has a positive nonzero value if the stress field lies within the tensile strength range of the fiber. The corresponding probability of failure F_t is given by

$$\ln \ln (1 - F_t)^{-1} = m \ln \sigma_{It} + k \quad (3)$$

where $k = \ln (\sigma_0^{-m} V)$. The values for m and k from Figure 3 are 1.86 and -14.0, respectively. From the models of crack

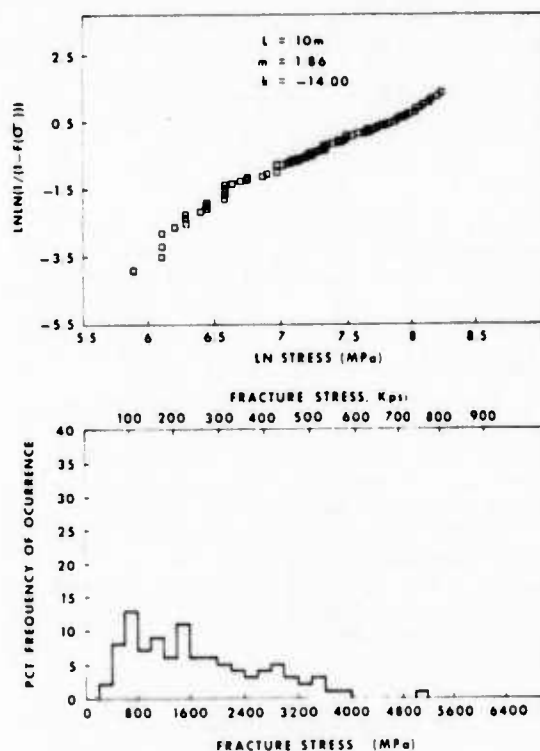


FIGURE 3
A TYPICAL WEIBULL PLOT AND STRENGTH HISTOGRAM FOR 10-m LONG LIGHTGUIDES

(REFERENCE 5)

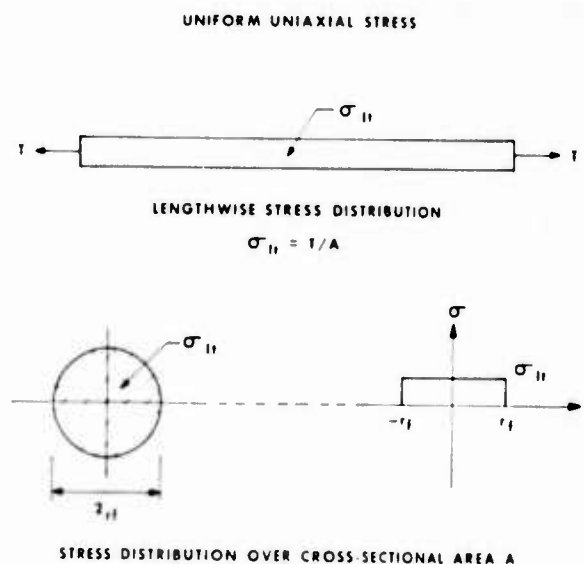


FIGURE 4

growth, the probability of failure at time t_f due to a subcritical uniform stress σ_t is given by

$$\ln \ln (1 - F_t)^{-1} = \frac{mn}{n-2} \ln \sigma_t + \frac{m}{n-2} [\ln t_f - \ln B] + k \quad (4)$$

where B is a constant that is a function of moisture level, geometric profile of the flaw, and critical stress intensity.

Bending Stress

When a fiber is bent, a tensile stress distribution σ_{Ib} is introduced on the outer surface as depicted in Figure 5. The surface stress is nonuniform around the periphery and is linear with radius. Thus, the largest surface flaw does not necessarily limit the strength. The risk of failure I_b and corresponding probability of failure F_b for one 180° bend can be expressed by (5)

$$I_b = p_1 \left(\frac{\sigma_{Ib}}{\sigma_o} \right)^m v \quad (5)$$

$$\ln \ln (1 - F_b)^{-1} = m \ln \sigma_{Ib} + k + \ln p_1 \quad (6)$$

where p_1 is a stressed volume reduction factor accounting for the fact that the lower half of the fiber cross-section is in compression and, thus, does not contribute to flaw growth. (5)(6) Assuming in the worst case that the subcritical bending stress σ_b from Eqn. 1 is constant over the periphery, the static fatigue failure F_b at time t_f due to σ_b is

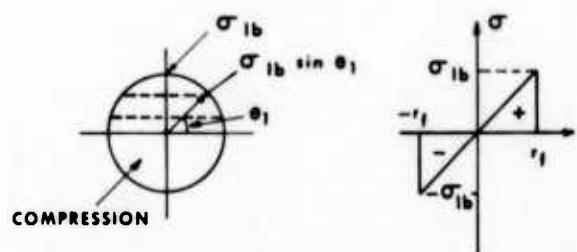
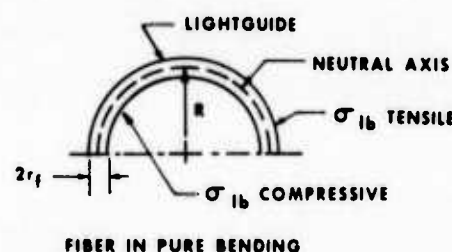
$$\ln \ln (1 - F_b)^{-1} = \frac{mn}{n-2} \ln \sigma_b + \frac{m}{n-2} [\ln t_f - \ln B] + \ln p_1 + k \quad (7)$$

For the example of duplex cable in bending discussed previously, the results of reference 5 indicate that a long-term minimum bend radius of 1.5 inches will provide a failure probability of less than 1 in 10,000 in 40 years.

Hanging Stress

Riser installation produces a third stress distribution common to customer premises. When a fiber hangs vertically with no twists or bends, the stress field (weight/cross-sectional area) is linearly distributed along the length with the maximum stress occurring at the upper support as shown in Figure 6 (notice the similarity to the

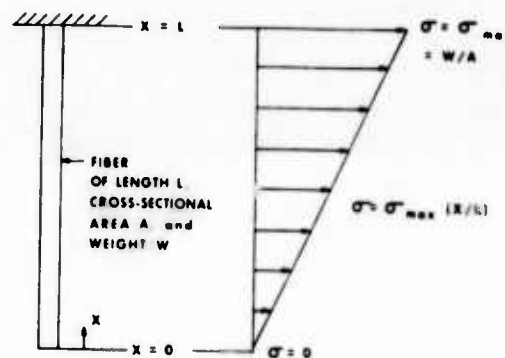
BENDING STRESS



STRESS DISTRIBUTION OVER CROSS-SECTIONAL AREA

FIGURE 5

HANGING STRESS



LENGTHWISE STRESS DISTRIBUTION

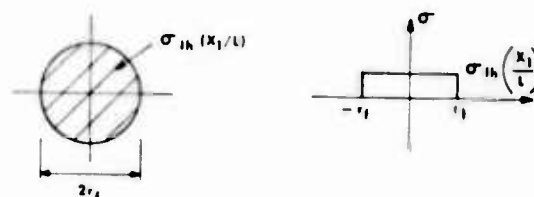


FIGURE 6

situation of Figure 2). The fiber cross-section is stressed uniformly at any point x ($0 < x < L$), but the surface stress is not constant along the fiber length. Thus, once again, the critical surface flaw is not necessarily the largest flaw. By preliminary analyses (8), the risk of failure I_h for a hanging fiber is

$$I_h = \frac{1}{m+1} \left(\frac{\sigma_{Ih}}{\sigma_o} \right)^m v \quad (8)$$

The corresponding expression for failure probability F_h is given by

$$\ln \ln(1-F_h)^{-1} = m \ln \sigma_{Ih} + k - \ln(m+1) \quad (9)$$

For static fatigue concerns, a worst case assumption that the applied stress is uniform along the length can be made. The resulting static fatigue failure probability F_h at time t_f for a hanging fiber subjected to σ_h can be expressed as

$$\ln \ln(1-F_h)^{-1} = \frac{mn}{n-2} \ln \sigma_h + \frac{m}{n-2} [\ln t_f - \ln B] - \ln(m+1) + k \quad (10)$$

Granted, this analysis is based on the weight of bare fiber, which, in a practical sense, would not be that significant. However, problems can occur if other cable components were coupled to the fibers, thereby introducing additional stresses.

COMPARISON OF STRENGTH DISTRIBUTIONS

As a measure for determining the most serious loading condition, the nonuniform fiber strengths σ_{Ib} and σ_{Ih} can be compared directly with the standard uniform tensile strength σ_{It} using the expressions for risk of failure. For equal probability of failure in bending and uniform tension ($I_b = I_t$), a strength ratio can be defined by (5)

$$\frac{\sigma_{Ib}}{\sigma_{It}} = p_1^{-1/m} \quad (11)$$

Likewise, comparing hanging and uniform tensile strengths ($I_h = I_t$), the strength ratio becomes

$$\frac{\sigma_{Ih}}{\sigma_{It}} = \left(\frac{1}{m+1} \right)^{-1/m} \quad (12)$$

The parameter m is typically greater than one, so a three-way comparison for equal failure probability yields that uniform tension is the worst case, followed by hanging and bending, respectively. Figure 7 illustrates the failure versus load distributions for all three loading conditions. Long term failure probabilities can also be compared using the static fatigue analyses; Figure 8 illustrates such comparisons for a 40 year lifetime.

FIGURE 7
FRACTURE STRENGTH DISTRIBUTION FOR 10m COATED FIBER
FROM FIGURE 3 $m = 1.86$, $k = -14$

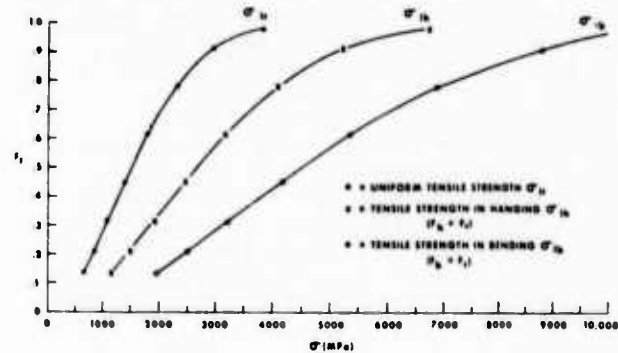


FIGURE 7

FIGURE 8
STATIC FATIGUE - STRESS DISTRIBUTION FOR $t_f = 40$ yrs
 $m = 1.86$, $k = -14$ AMBIENT (45% RH, 22°C)

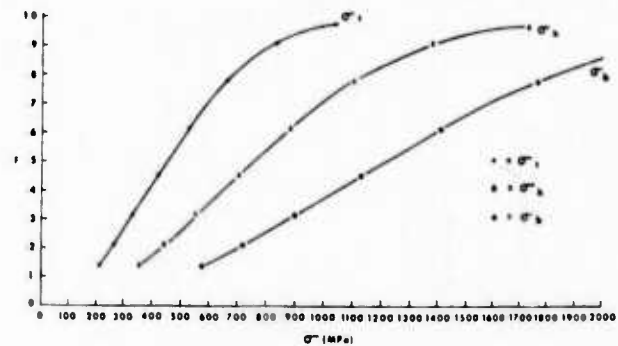
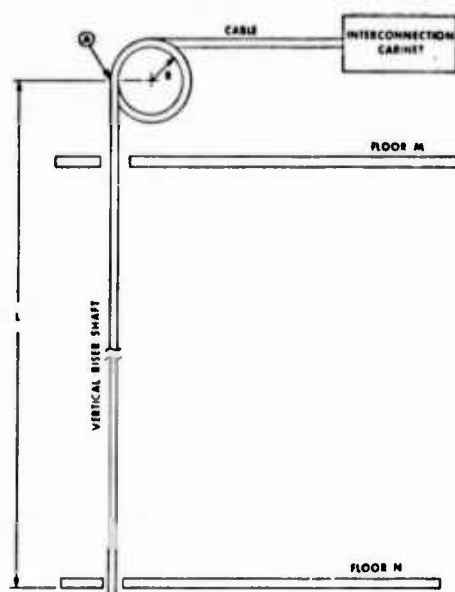


FIGURE 8

Using these analyses, both cable design and cable performance requirements can be derived. Three types of loads can be defined which account for acceptable static fatigue criteria for cable installation and service. First, rated tensile load (RTL) produces the fiber proof strain on the cable when it is loaded in uniform tension. The RTL can be viewed as the maximum instantaneous load that can be applied to the cable with zero probability of fiber failure and is not to be confused with cable breaking strength. Second, the installation load is defined as the maximum load that can be sustained for the duration of the installation pull with acceptable risk of failure. A typical time might be 30 minutes. Third, residual load is defined as the load which can be sustained for the duration of service life, 10 years or longer, again with acceptable risk of failure. With the analyses above, the special conditions encountered in a building can be dealt with as extensions of these basic definitions, keeping risk of failure constant.

An illustrative example of the use of these analyses is shown in Figure 9. In this situation a cable exits from an interconnection cabinet in an apparatus closet on floor M, is formed into a slack/restraining loop of radius R , and then drops a distance L (unsupported) vertically down the riser shaft. (An alternative scenario omits the cable loop and simply secures and guides the cable around a 90° bend of radius R). The loading situation in the unsupported length of cable corresponds to that of Figure 6. At point A the vertical loading is superimposed on the



TYPICAL BUILDING CONFIGURATION
FIGURE 9

bending load due to the radius R . As the cable traverses the loop, the axial cable load due to the hanging weight of the unsupported length L decays exponentially (due to the "capstan" effect) so that the horizontal section of cable is essentially unloaded. Clearly, the highest stress situation is at point A.

Several practical questions now arise. For example, what should the minimum loop radius R be? How long an unsupported length L is allowable? Obviously, the two parameters R and L are dependent upon one another. The answers to the above questions are functions of cable weight per unit length, cable construction, design lifetime, temperature/humidity conditions, and allowable risk of failure. With this information and the analyses presented, one can determine which, if either, loading condition is dominant and make suitable tradeoffs between R and L .

BUILDING CABLE DESIGN AND REQUIREMENTS

As indicated above, the cable design must preserve the optical performance of the fiber in a variety of physical situations. Several design guidelines can be identified as a result of the preceding discussions. The following sections present these guidelines in a manner to illustrate the cable design process.

Fiber Selection

The choice of fiber for use in customer premises applications is, of course, dependent on many system considerations. The characteristics of the fiber have a substantial impact on cable design. Hence, the fiber selection process must consider mechanical as well as optical parameters. Reference (9) describes a fiber optimization study for telephone loop applications which arrived at a recommendation for 62.5/125 micron (core/cladding diameters) fiber for operation with 1300 nm wavelength LED sources. The study considered a number of parameters including intrinsic and extrinsic losses, bandwidth, microbending sensitivity, and coupling efficiency to LED sources. The latter two considerations are very important for intrabuilding networks, thus making the 62.5/125 micron fiber attractive as a standard offering for these applications. Since this fiber has suitable performance over many kilometers, its use is also advantageous for campus systems. Fiber microbending sensitivity is significant as a key determinant of both system performance and cable design.

Material Selection

Material selection similarly requires special considerations. All building cables should be fire retardant; cables used in certain applications must meet specific flame tests. For example, cables going into risers must meet flame spread criteria; in addition, cables in plenums must have very limited smoke production. Such considerations must be factored into the physical design of the cable and will limit the candidate materials for buffering and jacketing. PVC is the most common fire retardant insulation and jacket material used in copper building cables, while fluoropolymers are used as jackets for plenum cables.

Besides the fire retardancy limitations on material selection, there are constraints on mechanical properties as well. The combinations of moduli and

expansion coefficients of the cable materials influence the stresses seen by the fiber during physical handling and thermal fluctuations. Such effects are amplified by microbending-sensitive fiber designs. Thus, cabled fiber, with appropriate fire retardant materials, must be characterized by both strength analyses and environmental evaluations to guarantee performance.

Cable Structure

While a number of cable design approaches have been successful for outside plant applications, the building environment presents a unique set of criteria. There are fundamental questions to consider in choosing a suitable structure. For example, customer access to fibers may be frequent, thus dictating the need for individual fiber protection and identification. Stranded structures, with individually buffered fibers in tight layers, enhance the capability of achieving flexibility and small size for small fiber count (<12) cables. A fiber color code scheme could also be easily implemented in this design. Ribbon structures, on the other hand, might be suitable in buildings where a large number of fibers may interconnect a few points with little probability of rearrangement.

The stranding lay length of the fibers and strength member is important for both optical and mechanical purposes. Stranded fibers are permanently bent, affecting loss and residual bending strain. Moreover, when a uniform tensile load is applied, a twisting moment is generated, and there is diametric contraction of the core. (10) The lay length of the strength member would also determine the degree of contraction. In terms of overall cable bending properties, a short fiber lay length would provide more flexibility but at the risk of higher longitudinal strains. (11) Also, a short lay implies higher losses due to excessive bending and additional strains. Thus, there is a definite tradeoff between mechanical and optical properties in the selection of stranding lay lengths.

Microbending loss results from longitudinal strain, thermal buckling, and lateral perturbations and can emerge during cable manufacturing, installation, and service. This mechanism can be controlled by careful selection of materials and their dimensions in addition to the manner in which they are processed. Component placement in the cable structure is critical to obtain a desirable stress distribution over the

cross-section of the cable, i.e., to limit stress exerted on the fibers. The fibers should be placed as close to the neutral axis of the cable as possible to allow a larger degree of freedom for bending. For hanging applications, the cable weight-to-strength ratio should be minimized. The weight of the cable will also influence the load required to pull the structure through conduit. Moreover, flexibility is necessary to ease pulls around conduit bends.

Fiber optic building cables should be all-dielectric to avoid any potential grounding problems that may arise when they are installed with electrical media in existing raceways. This fact, in conjunction with the desire for light weight and flexibility, requires some thought for the selection of a suitable strength member and its placement in the cable structure. Coupling to the strength member is important to minimize fiber loading both during installation and service life. The amount of coupling between the component layers controls the distribution of applied load. External strength offers an advantage over central strength in that it also protects against lateral forces, i.e., impact and compression, which are commonly seen in building applications.

SUMMARY

Cable design for customer premises applications requires that analyses be tailored to the application. The user and the environment present many requirements to the cable designer, who is constrained by such diverse factors as system loss and bandwidth, building codes, and the physical characteristics of the cable distribution facilities.

Cable and system designs must be coordinated to insure adequate optical performance after installation. The cable designs must be compatible with available routing facilities and interconnecting hardware. Application requirements and standards for cables will undoubtedly contain many functional criteria, with cable strength and bending properties among the more important. The extension of static fatigue analysis to the vertically hanging situation is one example of the need to characterize cable performance in applications which are unique to the building environment. Future analyses must further examine the complexity of such installations, especially the superposition of uniaxial, bending and hanging loads.

REFERENCES

1. D. Kalish, B. K. Tariyal, and H. C. Chandan, "Effect of Moisture on the Strength of Optical Fibers," Proc. 27th IWCS, pp. 331-341, November 1978.
2. H. C. Chandan and D. Kalish, "Temperature Dependence of Static Fatigue of Optical Fibers Coated with a UV-Curable Polyurethane Acrylate," J. Am. Cer. Soc., Vol. 65, No. 3, pp. 171-173, March 1982.
3. W. Weibull, "A Statistical Theory of the Strength of Materials," Proc. Royal Swedish Institute for Engineering Research, No. 151, pp. 5-45, 1939.
4. D. Kalish and B. K. Tariyal, "Probability of Static Fatigue Failure in Optical Fibers," Appl. Phys. Lett., Vol. 28, No. 12, pp. 37-44, November 1981.
5. P. D. Patel, H. C. Chandan and D. Kalish, "Failure Probability of Optical Fibers in Bending," Proc. 31st IWCS, Cherry Hill, New Jersey, pp. 37-44, November 1981.
6. M. Fox, "Theoretical Fatigue Life of Helically Stranded Optical Fibers," Opt. and Quant. Elec., Vol. 15, pp. 253-260, 1983.
7. D. Kalish, B. K. Tariyal, and R. O. Pickwick, "Strength Distributions and Gage Length Extrapolations in Optical Fibers," Amer. Cer. Soc. Bull., Vol. 56, No. 5, pp. 491-503, 1977.
8. T. M. Williamson, to be published.
9. M. J. Buckler, "Fiber Design for the Subscriber Network," Proc. 10th ECOC, Stuttgart, Germany, September 1984.
10. T. C. Cannon and M. R. Santana, "Mechanical Characterization of Cables Containing Helically Wrapped Reinforcing Elements," Proc. 24th IWCS, pp. 143-149, November 1975.
11. B. R. Eichenbaum and M. R. Santana, "Analysis of Longitudinal Stress Imparted to Fibers in Twisting an Optical Communication Cable Unit," BSTJ, Vol. 56, No. 8, pp. 1503-1512, October 1977.



Theresa M. Williamson is a member of Technical Staff at AT&T Bell Laboratories, Norcross, Ga. She received the B.E.E. and M.S.E.E. degrees from Georgia Institute of Technology in 1981 and 1982, respectively. She joined Bell Laboratories in 1981 and is a member of the Building Cable Group.



J. T. Loadholt is a Member of Technical Staff at AT&T Bell Laboratories, Norcross, Georgia. He received a B. E. E. degree from Georgia Institute of Technology in 1970 and an M. S. in Electrical Engineering from the University of Illinois in 1971. He joined Bell Laboratories in 1970 and is a member of the Building Cable Group.

THE CLARIFICATION OF MOVEMENT OF NON-METALLIC SELF-SUPPORTING OPTICAL CABLE
CAUSED BY WIND AND THE DESIGN OF ITS INSTALLATION AT STEEL PYLONS

E. HAYASAKA*, Y. ISHIHATA*, H. HORIMA**

S. HISANO**, T. SHISHIDO*** and T. OMORI***

* TOHOKU ELECTRIC POWER CO., INC.
** SUMITOMO ELECTRIC INDUSTRIES, LTD.
*** KITANIHON ELECTRIC WIRE CO., LTD.

3-7-1, ICHIBAN-CHO, SENDAI 980, JAPAN
1, TAYA, TOTSUKA-KU, YOKOHAMA 244, JAPAN
1-2-1, KORIYAMA, SENDAI 982, JAPAN

Abstract

The non-metallic self-supporting optical cable to be used for overhead optical transmission lines installed across steel pylons was developed with a prehanger construction. It is of vital concern to clarify the cable movement caused by wind in order to put the non-metallic optical cable into practical use. For that purpose wind loading of the cable was evaluated in the wind tunnel and then the cable movement and aeolian vibration by wind were measured in the field test. In result it was proved that the field data of cable tension increase and horizontal swing vs. wind velocity well coincided with the theoretical calculation and it was also found that the occurrence of aeolian vibration could be considered difficult in the newly developed non-metallic optical cable. The design of installation of the non-metallic optical cable at steel pylons has become to be feasible from these results.

1. Introduction(1)(2)(3)

Report was made previously to the effect that the extremely high nature of practical use of the non-metallic optical cable for jointly installing on steel pylons developed for long distance optical transmission using the overhead transmission line was clarified by various fundamental experiments. The fundamental construction of this cable is shown in Fig. 1.

Plastic connection piece Suspension wire

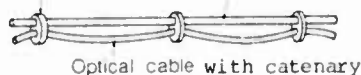


Fig. 1 Appearance of prehanger type non-metallic optical cable for long span use

To find the construction for setting the appropriate fitting location of the non-metallic optical cable to the steel pylons for the practical use in full scale, the demonstration test was conducted with regard to the following items and thereby effective data were obtained.

- ① In the wind tunnel experiment, the measurement of the drag and lift coefficients of the non-metallic optical cable at the respective wind velocities.

- ② Using the regulated tension loader, the measurement of creep characteristics of the non-metallic optical cable at 20 % U.T.S.(Ultimate Tensile Strength).

- ③ Under the actual meteorological condition at the field site, the measurement of aeolian vibration and horizontal swing amount of the non-metallic optical cable.

Also although the continual variation measurement of tension and transmission loss of this optical cable has been conducted ever since December 1982 by stringing it on Nagaoka Test Line of Tohoku Electric Power Co., Inc., as of July 1984, the transition with a very stable situation has taken place.

Report is given herein based on these results because this non-metallic self-supporting type optical cable was confirmed to provide the reliability fully being possible to use in practise.

2. Construction and features of cable

The non-metallic optical cable shown in Fig. 1 (called as prehanger type hereunder) has the suspension wire constituted of FRP (Fiber Glass Reinforced Plastic) rod and the round non-metallic optical cable arranged in parallel. These suspension wire and round optical cable are fixed at each constant interval by the plastic connection piece being the so-called cable of prehanger construction. The optical cable itself is constituted as catenary which is made longer by about 0.5 % compared to the suspension wire.

At the elongation of suspension wire less than 0.5 %, the optical cable is of the construction that does not sense its elongation. In the range of small elongation of less than 1 %, the construction is so arranged to increase the equivalent Young's Modulus of FRP suspension wire.

As the varied configuration of prehanger type, the SZ twisted type cable was designed and manufactured as shown in Fig. 2. Against the round optical cable which has the plastic connection piece set at the interval of P, the optical cable is twisted at the location of 1/2P. And this location is fixed by the plastic connection piece.

The SZ twisted type optical cable used in the experiment this time has the reversing twist of SZ applied alternately at the location of 1/2P.

At such twisted condition, the round optical cable is made to have the presence of 0.5 % slack compared to the suspension wire. This construction was manufactured to simulate the self-supporting stranding (SSS) construction which is known generally as the self-supporting construction that enables the reduction of wind loading.

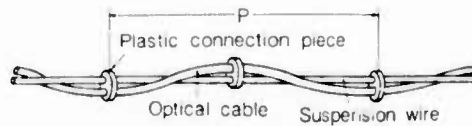


Fig. 2 SZ twisted type

Compared with the prehanger type, beside the problem that the manufacturing process of SZ twisted type is complicated, it is as previously reported that the external force concentrates at the location where the FRP suspension wire crosses with the round optical cable during the long length squeezing test thus being liable to sustain the impairment of optical fiber.

The construction and features of the prehanger type and the cable similar to SSS construction are summarized in Table 1.

Table 1 Construction and features of non-metallic optical cable of prehanger type and SZ twisted type

No.	Cable type	Manufacture length	Cross sectional construction of cable	Side face construction of cable	Features of cable
1	Tape-spacer type 4-fiber cable (Prehanger type)	800	 Dimensions: 27.8, 10, 15.5	 500mm Suspension wire and cable itself are jointly installed.	Manufacture of cable itself is very easy. Attachment of cable slackness is easy. Mechanical strength of cable itself is large. Loss temperature characteristics is stable.
2	Tape-spacer type 4-fiber cable (SZ twisted type)	300	 Dimensions: 27.8, 10, 15.5	 1000mm Cable itself is twisted 180° in left and right alternately for every fixed interval.	Manufacture of cable itself is easy. Twisting of cable is rather difficult. Crossing point of cable and suspension wire is likely to sustain mechanical damage. Loss temperature characteristics is stable.

3. Result of measurement

3.1 Wind loading characteristics

Wind loading of the prehanger type non-metallic optical cable and the SZ twisted type non-metallic optical cable set in the wind tunnel was measured for the respective velocities. And by the following equations of relationship, the drag coefficient C_d and the lift coefficient C_l were obtained.

$$P_d = \frac{1}{2} \rho C_d D V^2 \quad \text{-----} \quad \textcircled{1}$$

$$P_l = \frac{1}{2} \rho C_l D V^2 \quad \text{-----} \quad \textcircled{2}$$

whereas,

P_d : Wind loading due to drag force (kg/m)

P_l : Wind loading due to lift force (kg/m)

ρ : Air density (=0.12)

C_d : Drag coefficient

C_l : Lift coefficient

D : Effective outer diameter of cable

V : Wind velocity (m/s)

Fig. 3 and Fig. 4 show the measured result respectively of the drag coefficient C_d and the lift coefficient C_l .

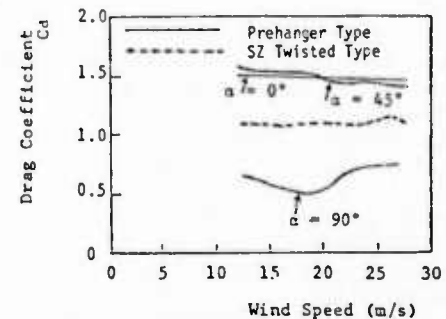


Fig. 3 Measured results of drag coefficient C_d of non-metallic optical cable

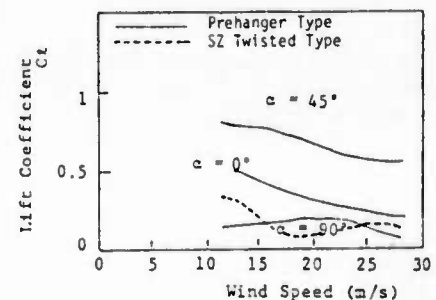
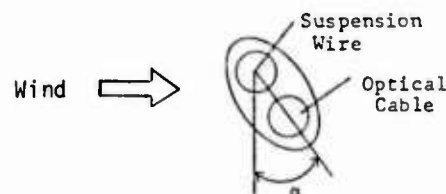


Fig. 4 Measured results of lift coefficient C_l of non-metallic optical cable

[Note] In the above drawings, α is set as described below.



Since it can be fully anticipated that the prehanger type cable will turn to the lee side centering the suspension wire by wind loading, the measurement was conducted for 3 points viz. $\alpha=0^\circ$, $\alpha=45^\circ$ and $\alpha=90^\circ$. It was indicated that as for the prehanger type optical cable, the rotation due to wind loading has the impact on lift force.

As for SZ twisted type cable, the drag coefficient C_d and the lift coefficient C_l both indicated the trend close to those of round type cable being averaged in the longitudinal direction of cable.

3.2 Creep characteristics

Fitting the prehanger type optical cable to the creep testing machine, tension of 1,000 kg (about 20 % UTS) is applied as the load by the constant tension device. And by measuring the gage length 2500 mm using dial gauge against the lapse of time, creep value was obtained. The outline of creep testing machine is shown in Fig. 5 and the result of measurement is shown in Fig. 6.

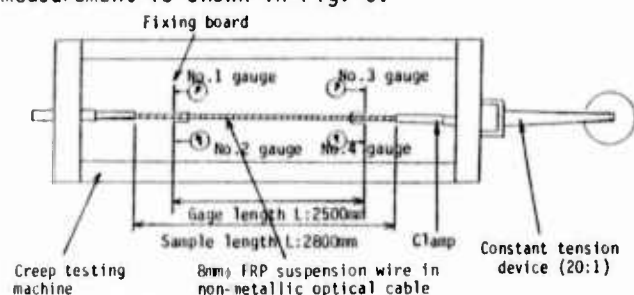


Fig. 5 Outline of creep testing machine

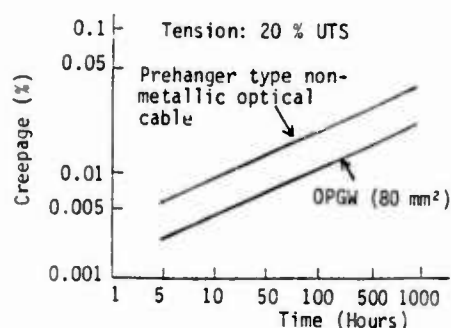


Fig. 6 Creep characteristics of non-metallic optical cable

The creep of prehanger type cable is 0.04 % after the lapse of 1,000 hours. Although this value indicated about 2 times larger than 0.017 %, viz. the creep value after lapse of 1,000 hours against 20 % UTS of OPGW (80 mm²) set forth as comparison in the drawing, this value can be fully taken into consideration from the viewpoint of design for stringing.

3.3 Field test situation

3.3.1 Demonstration test at Kasatoriyama Test Line of Sumitomo Electric Industries, Ltd.

Over the period of about 2 months from July 1983, the prehanger type cable and the SZ type cable were respectively installed for 153 m with the tension of 370 kg at very windy region in Mie Prefecture, Japan.

Thereby the behaviour of non-metallic optical cable against wind was investigated preponderately. Fig. 7 shows the schematic diagram of test and Photo 1 shows the test view. The wind velocity and wind direction of meteorological condition were measured

by the propeller type wind velocity and wind direction meter (primary wind sensor) located at the middle part of span, the tension variation due to wind was measured by tension meters T_1 and T_2 , aeolian vibration was measured by accelerometer G_1 and G_3 and the horizontal swing value was measured by accelerometer G_2 and G_4 .

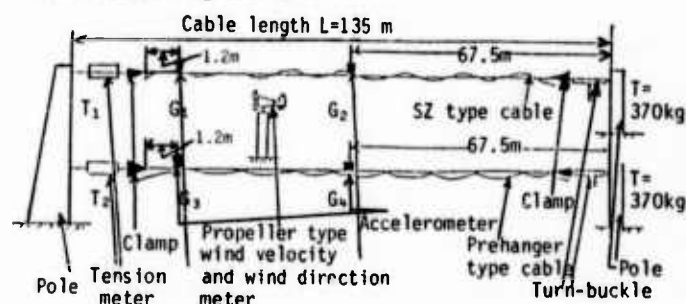


Fig. 7 Schematic diagram of field test



Photo 1 View of field test

Although Fig. 8 shows the frequency distribution of wind velocity, the value close to 40 m/s was recorded at the time of typhoon. Although Fig. 9 shows the wind direction, the wind hits almost all the cables perpendicularly.

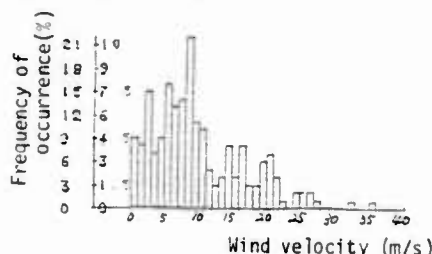


Fig. 8 Frequency distribution of wind velocity during field test

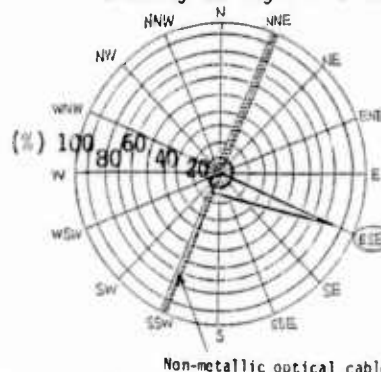


Fig. 9 Wind direction during field test

Fig. 10 shows the result of measuring the tension increase of cable against the wind velocity. The measured result well agrees with the calculated result using the drag coefficient of $C_d=0.88$ for prehanger type cable and $C_d=1.3$ for SSS simulated SZ type cable. Tension increase T_2-T_1 can be calculated from the following equation.

$$\frac{(q_2 W_c)^2 S^2 E}{24 T_2^2} - \frac{T_2}{A} = \frac{(q_1 W_c)^2 S^2 E}{24 T_1^2} - \frac{T_1}{A} + \alpha(t_2 - t_1)E \quad (3)$$

whereas,

W_c : Cable weight ($=0.19$ kg/m)

S : Spacing of span ($=135$ m)

A : Cross sectional area of suspension wire
($=50.2$ mm²)

T_2 : Tension at q_2 (kg)

E : Young's modulus of FRP ($=4800$ kg/mm²)

$$q_2 = \frac{\sqrt{P_2^2 + W_c^2}}{W_c^2}, \quad P_2 = \frac{1}{2} \rho C_d D V_2^2$$

$C_d = 0.88$ (Prehanger type cable)

$= 1.3$ (SZ type cable)

D_e : Effective outer diameter of cable
($=21.5$ mm $\times 1/\sqrt{2} = 15.2$ mm)

V_2 : Wind velocity at q_2 (m/s)

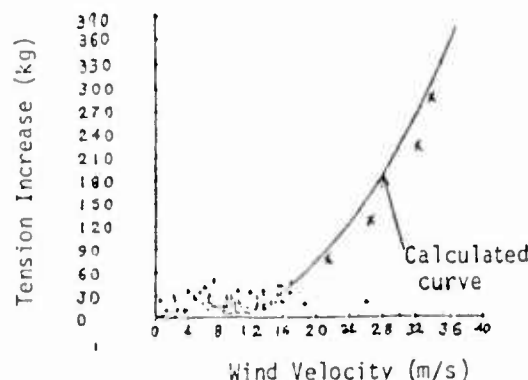
ρ : Air density ($=0.12$)

T_1 : Tension at q_1 ($q_1=1$)

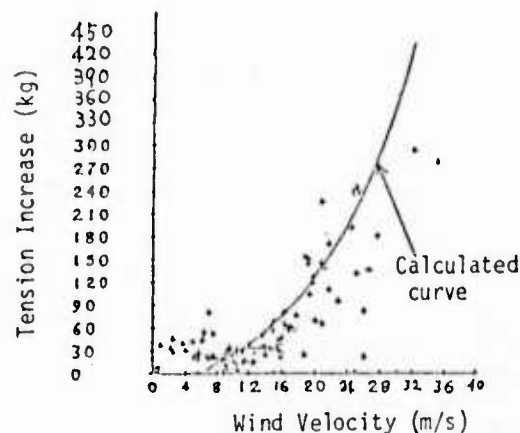
α : Coefficient of linear expansion of cable
($=7.67 \times 10^{-6}$ 1/ $^{\circ}$ C)

t_1, t_2 : Temperature at q_1 and q_2 ($^{\circ}$ C)

The vertical deviation of the cable installed and the wind blowing angle were ignored in the calculation.



(a) Result for prehanger type cable



(b) Result for SZ twisted cable

Fig. 10 Measured result of cable tension increase vs. wind velocity

The measurement result of horizontal swing of the cables is respectively shown in Fig. 11. Likewise the measured values agree well with the calculated values. The horizontal swing value y can be expressed by the following equation.

$$y = d_2 \sin \theta_2$$

whereas,

$$d_2 = \frac{W S^2}{8 T_2}$$

θ_2 = Rotation angle (degree)

$$W = \sqrt{P_2^2 + W_c^2}$$

W = Resultant load (kg/m)

$$\theta_2 = \tan^{-1} \frac{P_2}{W}$$

S = span length ($=135$ m)

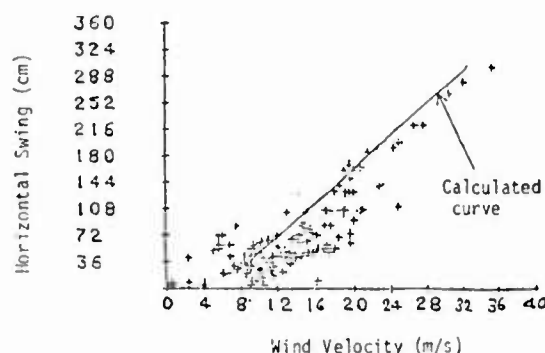
$$P_2 = \frac{1}{2} \rho C_d D V_2^2$$

T_2 = Tension of cable (kg)

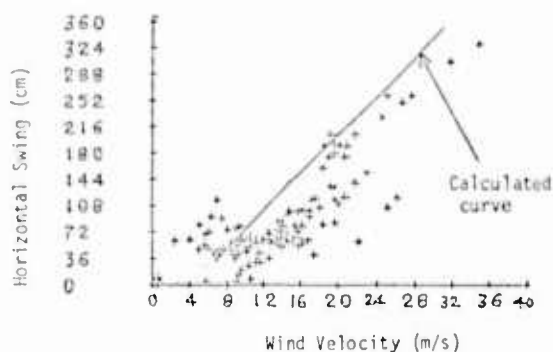
P_2 = Wind loading due to drag force (kg/m)

Wind loading due to lift force was ignored.

As regards aeolian vibration, the measurement result of the relationship between total vibration amplitude (p-p) and wind velocity is shown respectively in Fig. 12. In the wind velocity range that creates aeolian vibration, the vibration amplitude is less than 0.05 mm for both prehanger type cable and SZ type cable. Thus, conclusion can be made that there is no problem in the aeolian vibration with respect to actual stringing.

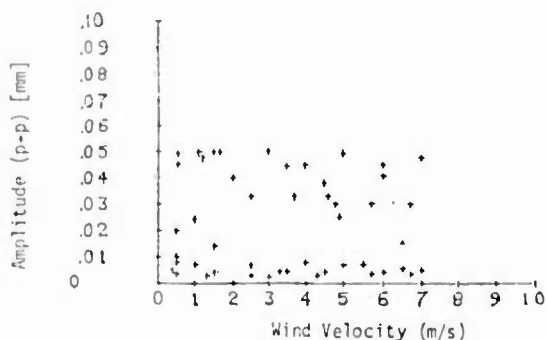


(a) Result for prehanger type cable

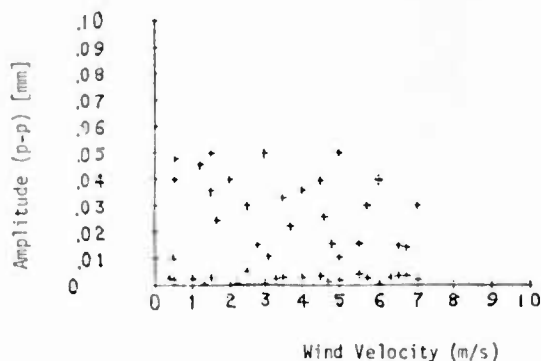


(b) Result for SZ twisted cable

Fig. 11 Measured result of cable horizontal swing vs wind velocity



(a) Result for prehanger type cable



(b) Result for SZ twisted cable

Fig. 12 Measurement result of relationship between total vibration amplitude and wind velocity as regards aeolian vibration

3.3.2 The situation of field test at Nagaoka Test Line of Tohoku Electric Power Co., Inc.

In December 1982 prehanger type optical cable was installed respectively for 2 spans (span spacing of 313 m and 300 m, sag 5.0 m/300 m, tension 420 kg) and 1 span (span spacing 300 m, sag 2.5 m/300 m tension 850 kg). From the time of completing the installation, snow accretion of optical cable was observed, variation of temperation and tension as

well as transmission loss were continually monitored and recorded. As of July 1984, transmission characteristic was extremely stable against wind, snow and temperature variation with no observation of creep.

4. Installation of non-metallic optical cable on steel pylon

Based on the data of the drag coefficient and others obtained so far, the conditions for the case of actually stringing non-metallic optical cable of prehanger type shown in Fig. 1 on steel pylon were studied. About 10-20 % tension of UTS (Every Day Stress) is thought to be appropriate, taking the creep characteristics of FRP suspension wire into consideration. The installation parameters, calculated in this range are shown in Table 2. Next let us study the installation location of non-metallic optical cable to steel pylon.

Since non-metallic optical cable is an insulated construction, despite its contact to the power transmission line and earth, the possibility of leading to serious failure is little. However, it is desirable to fully secure the clearance between those mentioned above. Based on the calculated result of Table 2 and on the calculated result of horizontal swing due to wind turbulence, the result of studying the installation location of optical cable to steel pylon for 154 KV power transmission is shown in Fig. 13.

To secure the clearance, it can be considered to be most advantageous to install the optical cable at the center part of steel pylon. Also if the free degree of clearance is large such as that the distance above ground can be fully taken, FRP suspension wire of small diameter is permitted to be used. On the contrary, if the tolerance of steel pylon strength is large, FRP suspension wire of large diameter is permitted to be used. As such, the optimum design of optical cable matching with the condition of installation can be considered.

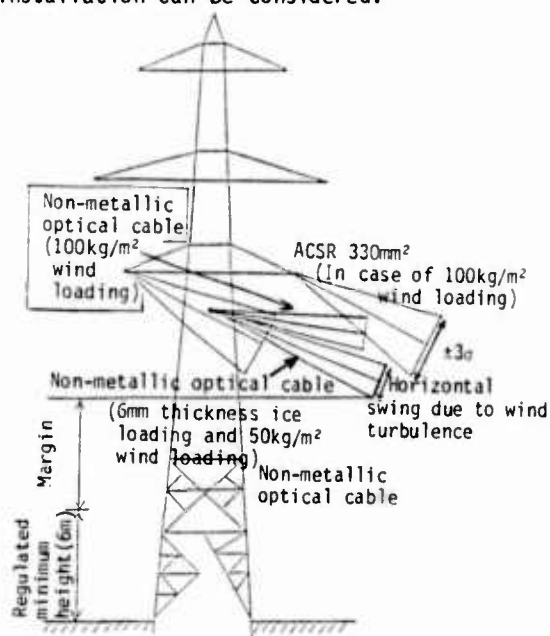


Fig. 13 Installation location of non-metallic optical cable to steel pylon

Table 2 Installation parameters of non-metallic optical cable

Span (m)			300						400						500					
Sag rate of optical cable itself (%)			0.5																	
FRP suspension wire size (mm ϕ)			6			8			8			10			10			12		
Design of EDS (%)			10	15	20	10	15	20	10	15	20	10	15	20	10	15	20	10	15	20
Worst condition (100 kg/m ² wind loading)	+10 $^{\circ}$ C	Dip (m)	14.1	12.9	12.0	11.4	10.2	9.27	17.6	15.9	14.6	15.1	13.3	12.0	21.1	18.8	17.1	18.7	16.3	14.6
		Tension (kg)	977	1065	1146	1333	1487	1642	1541	1706	1856	1986	2241	2494	2209	2482	2730	2728	3120	3497
		Rotation angle (°)	83.2	83.2	83.2	81.5	81.5	81.5	81.5	81.5	81.5	79.6	79.6	79.6	79.6	79.6	79.6	77.6	77.6	77.6
		Safety factor	3.1	2.8	2.6	4.0	3.6	3.2	3.4	3.1	2.9	4.2	3.7	3.3	3.8	3.3	3.0	4.4	3.8	3.4
At times without the load of wind and snow accretion	-20 $^{\circ}$ C	Dip (m)	5.14	3.45	2.61	3.96	2.66	2.02	7.13	4.76	3.60	6.12	4.11	3.11	9.66	6.44	4.87	8.66	5.79	4.38
		Tension (kg)	317	473	626	569	845	1113	561	841	1110	883	1315	1737	873	1310	1734	1263	1890	2499
	0 $^{\circ}$ C	Dip (m)	5.36	3.58	2.69	4.15	2.77	2.09	7.41	4.93	3.71	6.38	4.26	3.21	10.0	6.67	5.01	8.99	6.00	4.51
		Tension (kg)	305	456	606	543	812	1077	540	811	1077	846	1267	1684	843	1265	1683	1217	1824	2425
	+20 $^{\circ}$ C	Dip (m)	5.57	3.72	2.78	4.35	2.89	2.16	7.69	5.12	3.83	6.65	4.43	3.31	10.4	6.91	5.17	9.33	6.22	4.65
		Tension (kg)	293	438	586	518	780	1043	520	781	1043	812	1219	1632	815	1221	1633	1172	1759	2351
	+40 $^{\circ}$ C	Dip (m)	5.80	3.87	2.88	4.55	3.01	2.23	7.98	5.32	3.96	6.93	4.61	3.42	10.7	7.16	5.33	9.68	6.45	4.80
		Tension (kg)	287	421	567	494	748	1008	501	753	1010	779	1173	1580	788	1179	1583	1130	1695	2279
	+60 $^{\circ}$ C	Dip (m)	6.03	4.03	2.98	4.77	3.14	2.31	8.27	5.52	4.09	7.22	4.79	3.53	11.1	7.42	5.50	10.0	6.70	4.96
		Tension (kg)	271	405	548	471	717	973	484	725	978	748	1127	1528	763	1137	1534	1090	1633	2207

5. Conclusion

As the result of conducting the study and demonstration of the clarification of the range of cable movement due to wind and the design of the location of installing the cable on steel pylon for power transmission line which were the subjects this time set towards the full scale practical use of non-metallic self-supporting type optical cable, a satisfactory result was possible to be obtained. The application of the non-metallic optical cable for long span use to the practical line is intended to be implemented hereafter.



Eiji Hayasaka
Tohoku Electric Power
Co., Inc.
7-1, 3-chome,
Ichibancho,
Sendai, Japan

References

- (1) E. Hayasaka, M. Maeda, H. Horima, T. Nakatani, T. Kumakura and N. Abe, "Non-Metallic Optical Fiber Cable Incorporating Fiber Reinforced Plastic Catenary for Aerial Application", IOOC '83, Tokyo, June 1983.
- (2) E. Hayasaka, F. Ohtsuka, M. Monma, S. Ohira, H. Horima, K. Yamashita, M. Dazai and N. Abe, "Non-Metallic Optical Cable with Optical Fiber Catenary for Long Span Aerial Application", IWCS, 1983.
- (3) E. Hayasaka, S. Ohira, F. Otsuka, H. Horima, M. Nakaseko, K. Yamashita, T. Shishido and T. Omori, "Development of Non-Metallic Optical Fiber Cable for Long Span Aerial Use (Part II)", IECE, Japan, CS83-173, February 1984.

Eiji Hayasaka was born in 1950 and received the M.S. degree from Tohoku University in 1974. He then joined Tohoku Electric Power Co., Inc. and has been engaged in the section of communication and electronics engineering. He is now a senior staff member of Integrated Communication Network Development Office and a member of the Institute of Electronics and Communication Engineers of Japan and the Institute of Electrical Engineers of Japan.



Yoshinori Ishihata
Tohoku Electric Power
Co., Inc.
7-1, 3-chome,
Ichibancho,
Sendai, Japan

Yoshinori Ishihata was born in 1954 and received the M.S. degree from Tohoku University in 1979. He then joined Tohoku Electric Power Co., Inc. and has been engaged in the section of telecommunications and electronics engineering. He is now an engineer of Integrated Communication Network Development Office and a member of the Institute of Electronics and Communication Engineers of Japan.



Takeo Shishido
Kitanihon Electric
Wire Co., Ltd.
1-2-1, Koriyama
Sendai 982
Japan

Takeo Shishido was born in 1939. He joined the Kitanihon Electric Wire Co., Ltd. and has been engaged in development and design of communication cables and accessories. He is now a Manager of Communication Division.



Hiroaki Horima
Sumitomo Electric
Industries, Ltd.
1, Taya-cho,
Totsuka-ku, Yokohama
Japan

Hiroaki Horima was born in 1947. He received the M.S. degree for engineering from Osaka University in 1972.

He joined Sumitomo Electric Industries Ltd. and worked on the development of CATV coaxial cables, multi-pair PEF-insulated junction cables and low loss unbalanced type cables.

Thereafter he concentrated on the development of optical fiber cables. He is now Senior Engineer of Fiber Optics Division in Sumitomo Electric Industries Ltd. He is a member of the Institute of Electronics and Communication Engineers of Japan.



Toshiyuki Omori
Kitanihon Electric
Wire Co., Ltd.
1-2-1, Koriyama
Sendai 982
Japan

Toshiyuki Omori was born in 1943 and received the B.E. degree from Tohoku Gakuin University in 1966. He joined Kitanihon Electric Wire Co., Ltd. and engaged in research and development of communication cables, power cables and accessories for these cables. He is now a Section Manager of Engineering Division.



Satoshi Hisano
Sumitomo Electric
Industries, Ltd.
1, Taya-cho,
Totsuka-ku, Yokohama
Japan

Satoshi Hisano was born in 1960 and received the B.E. degree from Sizuoka University in 1983. He joined Sumitomo Electric Industries, Ltd. in 1983, and has been engaged in development and design of optical fiber cables. He is a member of the Institute of Electronics and Communication Engineers of Japan.

COMPUTERISED METHOD OF PREDICTING CABLE PULLING-IN TENSIONS

John Macaulay

British Telecommunications plc
Wembley, England

SUMMARY

The strength-to-weight ratio is considered to be an important mechanical parameter when designing an optical fibre cable. To gain a realistic value for this parameter such that long lengths of cable can be installed requires much laborious calculation and testing. This paper describes how the problem was approached using a computer to do the tension calculations and comparisons of the practical results. It covers the equipment used in the computing system, the equipment used in the practical measurements and discusses the results.

BACKGROUND

The designers of the Proprietary Optical Line System (POLS) Cable (1) chose different design philosophies to package the fibres and constructed the cable around the method of packaging. The result was cables with different dimensions and different mass. Little was known of the forces required to install long lengths of optical cable but it was recognised that the cable lengths to be led would be about 1km for multimode cables and 2km for singlemode cables. A further requirement was that there should be very little or no residual strain in the fibre after installation since this could lead to a stress corrosion situation causing premature failure of the fibre.

The force required to pull a cable into a duct network is a function of the mass of the cable and therefore the strength-to-weight ratio was a suitable parameter to call up for the optical fibre cable. This allows the cable designer the freedom to choose a method of cable construction which will suit his production techniques. A further stipulation was applied in that the strain level in the fibre should not exceed 0.25% when the cable was loaded to its maximum load. This maximum load would be the strength-to-weight ratio times the weight of 1km of cable.

What value of the strength-to-weight ratio should be applied to ensure that long lengths of cable could be installed given that there is a multitude of duct configurations and duct conditions to be satisfied?. Some experience had been gained on installing 500m lengths of 60MHz 18 tube co-axial cable by using a manual method of calculating the cable tensions. However this was mainly for a dedicated newly constructed duct route. Optical fibre cable would be required to be installed in any duct available. The task of doing manual calculations for optical fibre routes and then measuring the tensions to install the cable would take years if a representative sample was to be taken. A quicker method would have to be found.

It was decided to employ a computer to speed up the calculations and to use new, more accurate, techniques for measuring the actual loads experienced by the cable which would prove the theory used by the algorithm. This work would help in specifying the optical fibre cable but there is also a spin off in that it could be used as a powerful planning tool.

PHILOSOPHY

All BT external plant is recorded on large scale Ordnance Survey maps. The routes taken by the duct network is accurately located on these maps and these are used to measure the duct deviation when doing the manual calculations. The collection of primary data from these maps is a laborious operation, so this would have to be computerised to make it quicker. Manual calculation involves taking approximations rather than apply the equations involved. The computer would easily apply the already digitised data from the map to the equations. The computer could produce the results in any format. The computer could be used to compare results from the practical trials provided the results were recorded in digital form. A philosophy employing these ideas, with as much

flexibility as could be envisaged, was developed and put into practice.

THE COMPUTER HARDWARE

The system described here was chosen for compatibility with the existing desk top computer; there are many variations which could usefully be employed to perform the same task. Diagram 1 shows a schematic of the system which comprises of a computer, a graphics tablet, a file manager, an interactive plotter, a data logger and a printer and, because all the equipment is connected by the General Purpose Interface Bus (GPIB), a bus analyser with an associated printer. Photographs 1 & 2 shows the Working Set Up. The computer acts as the system controller and this system uses a 64k desktop computer which had been used for transmission measurements on optical fibre and hence the large memory. The graphics tablet was chosen for the size of its active area which must be large enough to take double 1:2500 (25 inches to the mile) Ordnance Survey map as well as the logging menu which will be described later.

A triple drive file manager was chosen because this allowed three types of disc to be allocated. The allocation of these discs are a program disc which holds all the software for the system operation and calculation, the primary data disc which stores all the data which is logged from the Ordnance Survey maps and the secondary data disc which stores the calculated data and also allows for the copying of primary data.

The interactive digital plotter is used to provide diagrams for use in the field exercises and give a plot of the route under consideration with the calculated tensions printed next to the salient points on the route.

The printer is used to provide tables of calculated results. The data logger really forms part of the practical measuring system but is required in the computing system to bring the practical results into the system for comparison with the theoretical results.

The bus analyser is a useful instrument to have in the system to assist with debugging and to discover when corruption of the bus occurs. The instrument used here monitors the bus continuously by cycling the traffic through its memory. If a corruption occurs then its memory can be dumped on to the associated printer and hence the reason for the corruption discovered.

THE COMPUTER PROGRAM

The software for the system is called CABTEN which stands for cable tensions. It consists of several small sub programs which allows for a flexibility of requirement as one progresses through the routine. The main menu for CABTEN has the following options:

- Log Data
- Data Listing
- Correct Data
- Force Calculation
- Plot Data
- Copy Data Disc in Drive 1

Log Data

Prior to obtaining the graphics tablet the only method of obtaining data from the Ordnance Survey maps was through the interactive digital plotter. It was found that this was unsuitable because of the sensitivity of the joystick control and the need to enter auxiliary data through the keyboard of the computer.

The graphics tablet has a programmed menu imaged on to an area of its surface when the program is booted up. This allows the program to be controlled from the tablet by a single button cursor. The layout of the menu is shown in Diagram 2. The menu allows for the twenty data values for each data point to be logged quickly. Some of the data values are used for reconstructing the geography of the route and the rest are used for calculating the cumulative tension as the tension algorithm progresses through the data that has been logged.

Some of the features of this program are that if the menu is skew when imaged then a correction will be applied when calling the menu items. Similarly when the Ordnance Survey map is placed on the tablet, the skewness is taken into account when the data points are logged. When logging takes place the values are displayed on the computer screen and at this stage any data value can be altered before the block is stored for that data point. Normally a cable route will be covered by 40 maps and these could be to a scale of 1:2500 or 1:1250. The program can cope with these various sizes of maps in any order and in fact will cope with non standard scales as long as the National Grid is accurately located on the map or diagram.

Sequential logging of the salient data points of the route is necessary.

Data Listing

It is an essential task to take a data listing of the data points that have been logged. The reason for this is that the data point with its block of data values is now stored in a file which has been named to incorporate the map reference of the data point. It is necessary to call that file name when using that point for the start or end of an operation. This method of naming the data point makes that point unique within a 10km square. This could, of course, be increased to a 100km square or a 1000km square when using 6 figure grid reference and incorporating more digits in the file name.

Correct Data

It was stated under data logging that the data points must be logged sequentially. Mistakes can be made since there can be more than one duct route along the side of the road and these routes may or may not enter every manhole or jointbox along the route. This program allows for the deletion or insertion of a data point. Further it allows the examination of the data values within a data point and the opportunity to change or correct a data value.

When secondary data discs have been created from primary data it is possible to change the new cable mass, new cable diameter and existing cable diameter data points between specific data points.

Force Calculation

Two options are allowed in this program. One can either specify the force that may be applied to the cable and let the program find the distance that it may be pulled into that part of the duct network or one can specify the length to be pulled in and find the force required to pull it that distance. The first option is more useful to the planning engineer since he will have the limiting value of force that may be applied to the cable and therefore maximise the length that he may install in the duct network. The second option is of use to the development engineer in specifying the strength-to-weight ratio for the cable. He will know the factory lengths that may be manufactured and requires to know what strength the cable must have such that the cable may be installed in these lengths. This sub program allows the development engineer to gather the data easily. The program can be made to start at the beginning of the route and

calculate the tension for a given length, say 1km, and then return to the next sequential jointing point after the first specified and calculate the tension for the given length. This can also be carried out working backwards through the route so that every situation for that given length may have a force value. This force value can be stored on the third disc for further statistical analysis. It can be seen that by using the correction program a different cable design may be observed in the same duct situation or in an occupied duct with various levels of occupancy.

In using data generated by such means one must be sure that the data is valid and so it must be tested. This can be done by testing a few of the possible lengths in the route by measuring the actual force to install the cable in these lengths.

Plot Data

This program allows the data to be plotted geographically with the tension information printed against the salient points. This is useful when carrying out the practical cabling exercises. It is also a feature that could be used by the planning engineer when issuing instructions for a cable installation.

Copying

This small program allows for the generation of further data without effecting the original data associated with the geography of the route thereby allowing flexibility to the development engineer in changing the specification of the cable under consideration or in changing the duct occupancy or duct conditions.

PRACTICAL MEASURING SYSTEM

As explained earlier, theoretical data must be tested to make sure that it is valid and this has been done with the following system shown in Diagram 3. The measuring system comprises of a data logger which has a limited intelligence, an active cabling rope, a tachometer and a phase delay equipment.

The Active Cabling Rope

Previous to this development tensions were measured using a three wheeled device in front of the winch. The problem with this method was that a correction had to be made for the cabling rope and the correction was a function of the duct route that was being cabled. In some instances it was found that the

cabling rope completely masked the installation of the optical fibre cable. It was decided that a method of measuring the actual tension experienced at the head end of the cable must be found. The active cabling rope fulfilled this requirement.

The rope is of a woven kevlar with two copper conductors in its core. The rope can withstand a force of some 20kN but is normally operated at 10kN. Attached to the head end is the load measuring head shown in Diagram 4, Photograph 3 and is made up from a load stud connected to a 4-2 wire transmitter / amplifier working a 10/50mA current loop. The loop is supplied a voltage by the power source and is completed by a card in the data logger.

The Data Logger

This instrument is used to log the force required during the pulling-in operation. Photograph 4 shows it in use on a practical measurement exercise. It completes the 10/50mA current loop of the active cabling rope. It is an intelligent instrument that can be programmed to log at different rates for different thresholds of load value. This is useful for data suppression. When low loads are being logged then the logging rate is slow but when high loads or peak loads are encountered then the logging rate is fast allowing peaks to be caught and recorded.

The Tachometer

This device, Photograph 5, is used as a distance meter. Rather than log the speed of installation it is used to count the revolutions against the time base of the data logger. Hence with force measured against the same time base we can process the results to give a force against distance into the duct which is what we want to know.

Phase Delay Equipment

The phase delay equipment (2) is used to monitor the strain in the fibre during the cable installation and can be recorded on the time base of the data logger. Hence a cable load to fibre strain plot can be obtained for the installation. By using pulse delay measurements for before and after installation we can test for any residual strain in fibre.

RESULTS

Diagram 5 shows a geographical plot of a cable installation which was logged

using the graphics tablet and then outputted on the plotter. Ancillary information has been suppressed because of the size limitation of this paper. Diagram 6 shows a practical measurement of this route taken by the active cabling rope and shows the surging that takes place when a cable is pulled into the duct. Diagram 7 shows three curves which are the theoretical tension predicted by the computer, the average tension of the actual pull and the increase of the peaks of the surging from the actual pull.

The first feature that shows up is that the estimated back tension at the start of the pull was too low. This still leaves the estimated tension lower than the true tension encountered in the pull. The coefficient of friction for the calculation was taken as 0.3 which is the laboratory measured value for lubricated duct. The duct was silted and a better estimate would have been around 0.35-0.4 which of course would have given a higher tension.

The highest tension that the cable experiences is the peak surge tension and if we consider what causes the surging then perhaps we can predict the true tension that the cable experiences. The surging is caused by a longitudinal vibration set up in the cable because of the stretch in the cabling rope and the difference in the static and dynamic coefficient of friction. Therefore it would seem plausible to use the static coefficient of friction when calculating the tensions.

Further work is being done on occupied duct situations and on particularly arduous routes where advice on cabling has been sought.

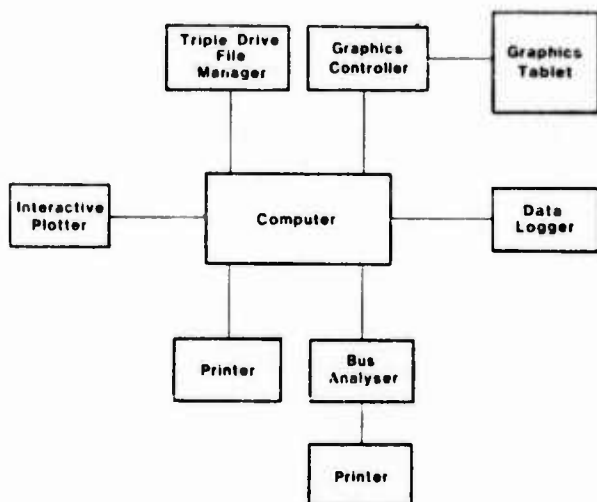
REFERENCES

- (1) C J LILLY AND D R BISSELL

"Some Initial Results and Experience of Operational Optical Fibre Systems in the UK" 7th European Conference on Optical Communication, Copenhagen 1981.

- (2) M H REEVE, R KASHYAP, S HORNUNG, S A CASSIDY

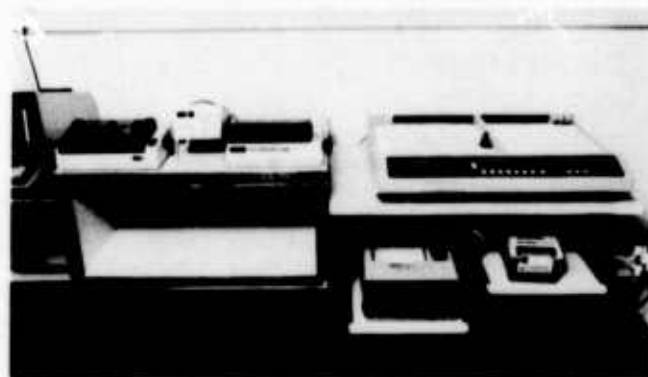
"Continuous Optical Fibre Strain Measurement During Optical Cable Installation" 30 IWCS Fort Monmouth 1981



THE SYSTEM
Diagram 1



Photograph 1



Photograph 2

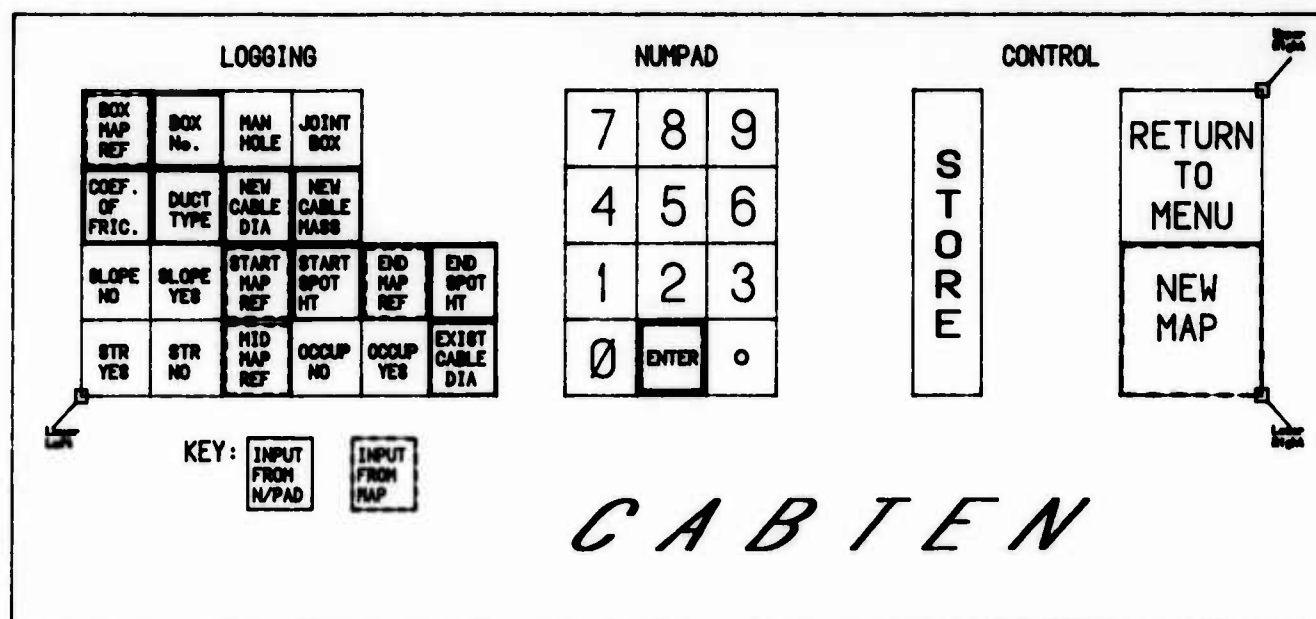
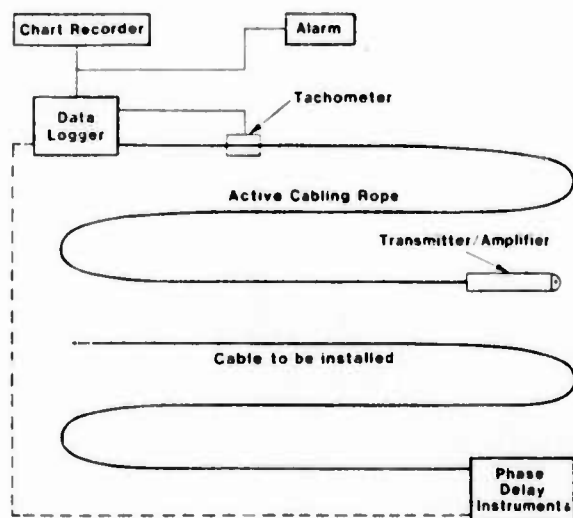
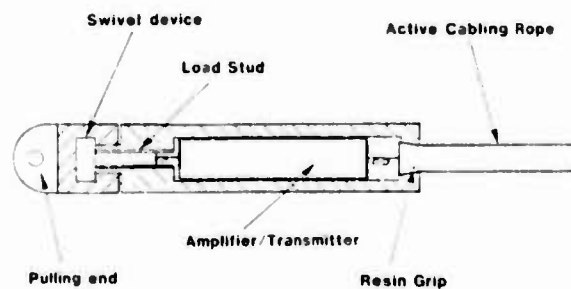


Diagram 2



FIELD MEASURING SYSTEM

Diagram 3



LOAD MEASURING SWIVEL FOR ACTIVE CABLING ROPE

Diagram 4

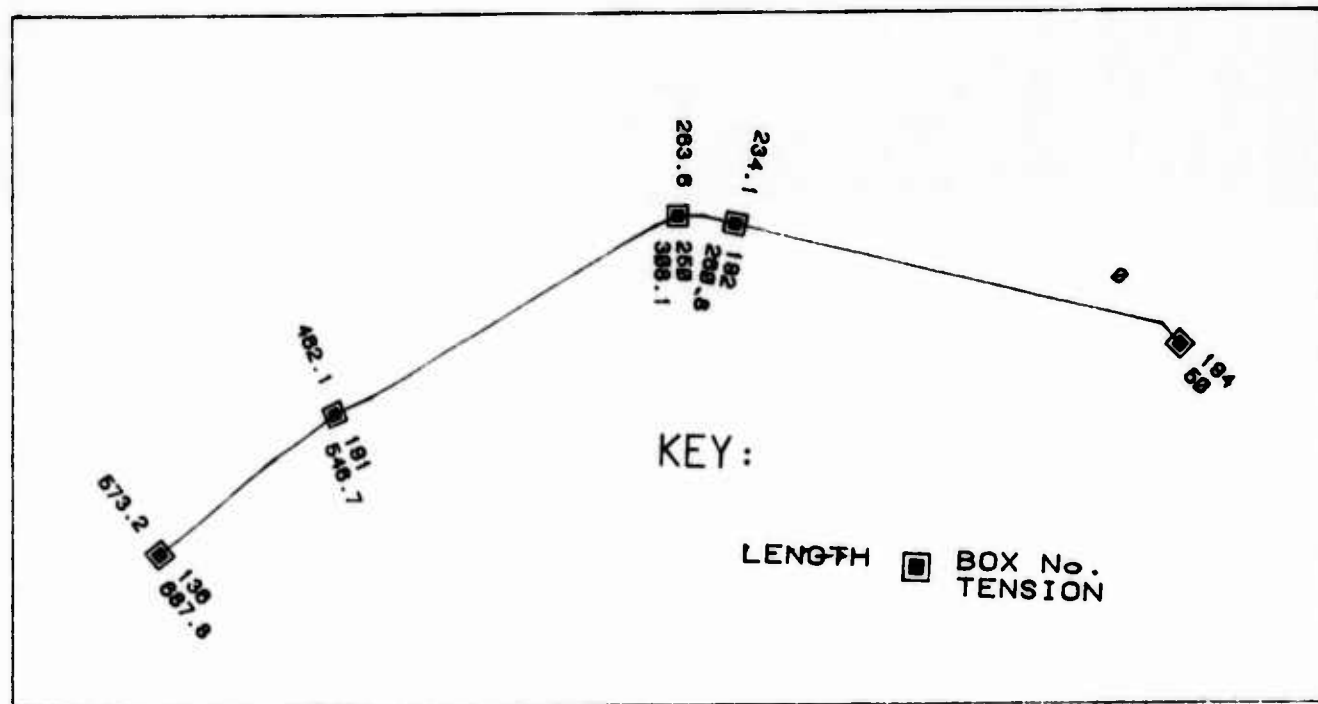


Diagram 5

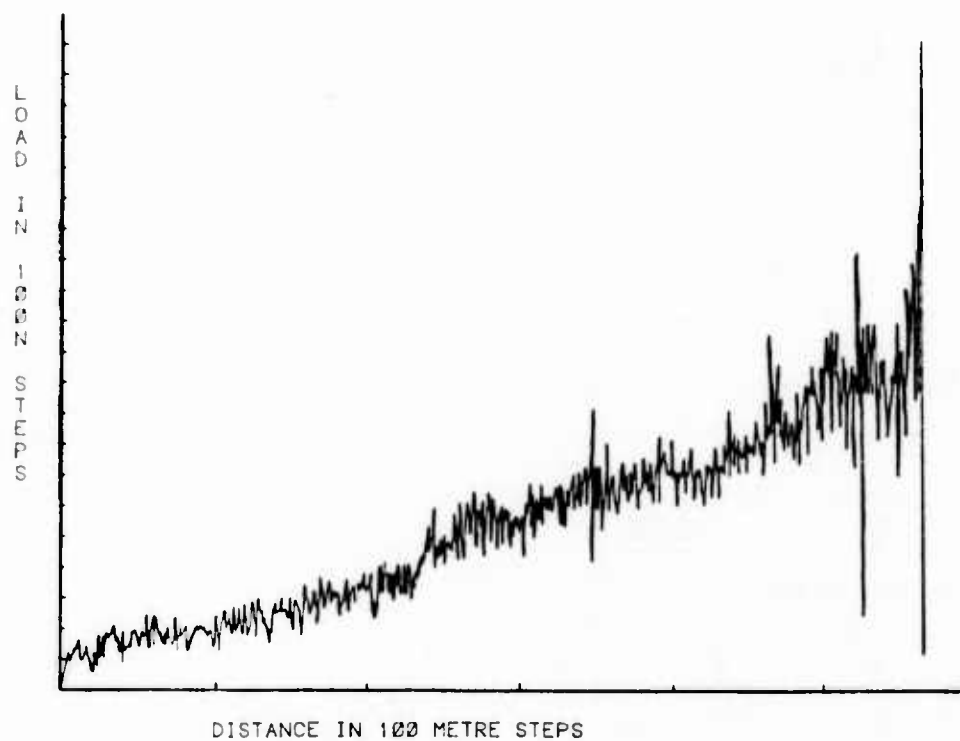


Diagram 6

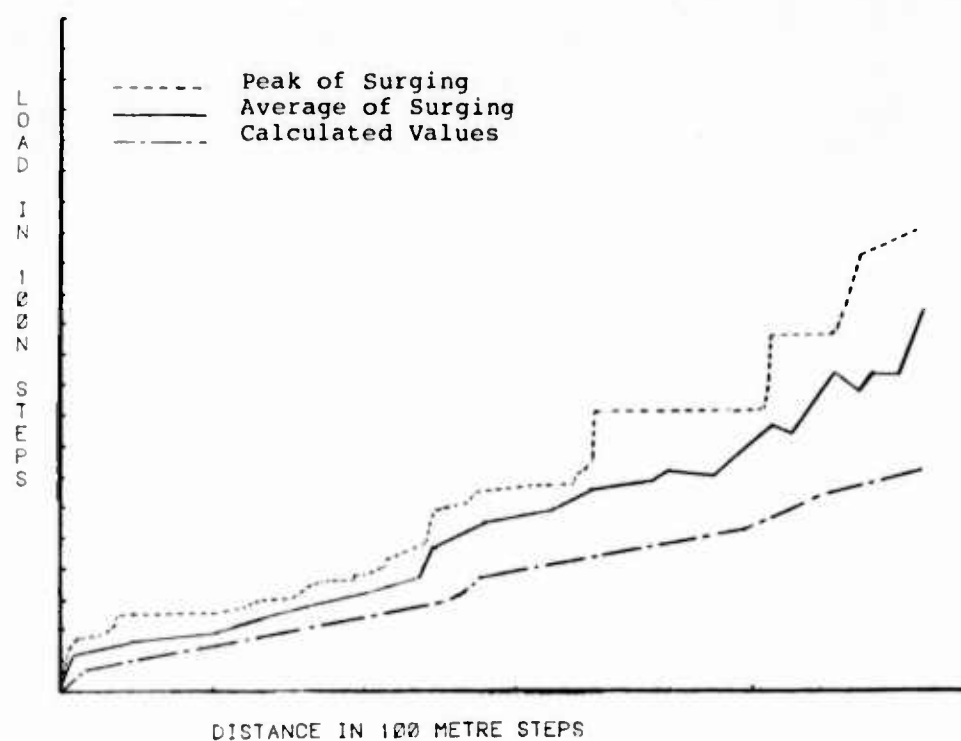


Diagram 7



Photograph 3



Photograph 5



Photograph 4



Mr Macaulay is responsible for the design approval of all Trunk and Junction optical fibre cables for the British Telecom Network. He obtained an Honours B.Sc. in Mechanical Engineering from the Heriot-Watt University in 1974 and has since worked for the External Plant Development Division of British Telecom on the mechanical aspects of cable design.

DIGITAL TRANSMISSION SYSTEM BY OPTICAL FIBERS
LASHED TO THE GROUND WIRE OF HIGH TENSION LINES

C.G. CORTINES

F.J. SAEZ DE LA MAZA

F. GOMEZ MARTIN

STANDARD ELECTRICA, S.A.
SANTANDER - SPAIN

ABSTRACT

The paper shows the feasibility of the optical fiber application as a transmission medium in the telecommunication networks of Electrical Power Transportation and Distribution Companies, taking advantage of the mechanical support of high tension lines for the optical cable laying. A 220 Kv. electric line is used as a support for the communication optical cable, installed in an area with extreme environmental temperatures around -20°C and $+40^{\circ}\text{C}$. Lengths between towers (span lengths) go from 200 to 430 m.

At the present time, both the cable and equipments manufactured by STANDARD ELECTRICA, are installed and satisfactorily working. From May 1983 and throughout 1984 the system is being subject to a test program, the result of which will be the essential part of the applied research project. Different solutions have been studied and tested in the cable laying and its installation, and a wide testing program has been carried out in order to evaluate the mentioned solutions.

INTRODUCTION

Due to the glass properties as a light propagation medium, the optical fiber transmission systems are suitable for transmitting information in the production, transformation and electric power distribution installations. As a matter of fact, the insulating properties of the glass forming the fiber and the lack of electrical current in the transmission make the fiber a highly safe medium in high tension environments, due to its immunity to all types of electrical or electromagnetic disturbances and its transmission quality even in cases of high electrical discharges, great earth potential differences and noises induced by different causes.

The project describes tries to demonstrate the feasibility of using this transmission medium in the private telecommunication net

works of the electric industry, but with a new solution for the cable installation: lashing the optical fiber cable to the ground wire of high tension lines. We know of some experiences of this kind which have been carried out in Europe, although with substantial differences from the system used by us.

The mentioned project has been carried out under an applied research program jointly with IBERDUERO, S.A., a Spanish electric power company, and STANDARD ELECTRICA, S.A., and in general terms, the project stages can be summarized as follows: Development, design, manufacturing and equipment field tests; establishing the types of laying, evaluation of the phenomena produced in the system by the environmental conditions, and the main objective of our project, already achieved, was to communicate two electrical energy Substation by means of a 2 Mbit/s Optical System through the corresponding cable lashed to the ground wire of the high tension line.

SYSTEM'S CONFIGURATION AND

OPTICAL CHARACTERISTICS OF THE CONNECTION

Figure 1 shows a block diagram of the full system which is basically formed by two PCM equipments of 30 channels, two optical terminals, the optical cable lashed to the ground wire and a measuring system. The system thus formed permits a double performance: traffic transmission and the carrying out of an extended test program.

The PCM system has 30 channels. The tram series is received by the optical terminals and once properly codified, the electrical impulses are converted into light impulses. This inversion is basically done by a laser diode ($\lambda = 850 \text{ nm}$), controlled by its excitation circuit. The light information is coupled to the fiber for its transmission. As far as reception is concerned, a weak light signal is transformed into an electri

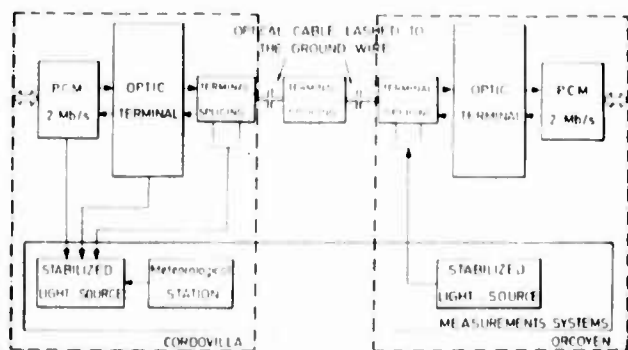


FIG 1 BLOCK DRAGAM OF THE GENERAL SYSTEM

cal signal by means of an avalanche photo-detector ($\lambda = 850 \text{ nm}$). This electronically processed electric signal is regenerated, recovering the reception tram series and its synchronisms. The regenerated signal is properly codified for its transmission to the PCM reception part.

The losses permitted in the carrier for a $\leq 10^{-9}$ error rate with the APD/laser option used in the system are 60 dB.

ELECTION OF THE CABLE LAYING

The use of optical fiber cables by transportation and electrical energy distribution companies is increasing due to the advantages of this transmission medium in front of the traditional radio or metallic conductor systems.

The cable types which have so far been used are basically the following:

- Steel or aluminium alloy ground wire incoorporating inside the optical fibers^{2,3}.

This solution may be interesting for new lines although we consider that this means a high percentage on the total cost per km of energy transportation line conventionally equipped. In already working lines with a conventional ground wire, its replacement by the new wire is uneconomic.

- Self-supported Optical Fiber, Cable independent of the ground wire^{4,5}.

The already commercialized cables of this type showed span length limitations (up to 500 m). There are⁶ at the present time valuable experiences⁶ which have solved this problem, reaching 1,000 m span lengths. This is therefore an interesting cable.

- Optical Fiber Cable lashed to the Ground Wire.

This cable has the advantage of using a quite conventional optical fiber cable which is therefore much cheaper than the previous solutions. Its versatility is its main attraction, as it can be used for installation of energy transportation.

on lines. It also can be used both on working or new lines independently of the span length.

This was the solution adopted.

LINE'S GENERAL CHARACTERISTICS - GROUND WIRE

In order to check the feasibility of the optical cable lashing to the ground wire, the firm IBERDUERO chose among its transportation routes one offering a particular characteristic. Thus, a high tension line joining two conveniently apart substation near Navarra, a Northern Spanish city, was selected. The weather conditions are extreme in this zone. In summer, temperatures higher than 40°C are reached, and in winter they can drop down to -20°C . The distance between the substations known as Cordovilla and Orcoyen 1 is 7,302 m. The 220 KV existing line in single circuit was used as the electric line supporting the communication cable. The towers were equipped in their upper part with just one ground wire of 53 mm^2 section.

Figure 2 shows a diagram with towers, distance between spans and where the cable joints are found.

In the follow table are the ground wire characteristics:

CHARACTERISTICS OF THE GROUND-WIRE	
Material	Galvanized steel
Type	12 wires of 2.37 mm ϕ
Total diameter	9.5 mm
Breaking load	6,670 kg
Weight	0.45 kg/m
Termal expansion coef.	12×10^{-6}

This wire is laid in such a way that at the most frequent temperature along the year, i.e. 15°C , it has a load of 820 kg, reaching 2,050 kg in most unfavorable conditions such as -15°C and $180 \sqrt{d}$ ice overload ("d" being the outer diameter for 310 m average span).

THE OPTICAL CABLE

All the materials forming the cable are dielectric. The cable is formed by a central strength member around which and totally covering it, 6 optical fibers and 3 polypropylene filled filaments are stranded in just one layer. This core, formed by a central cord and nine elements around it, is covered by two tapes applied on closed helix and overlapped. Afterwards, the cable sheath formed by a first layer of extruded

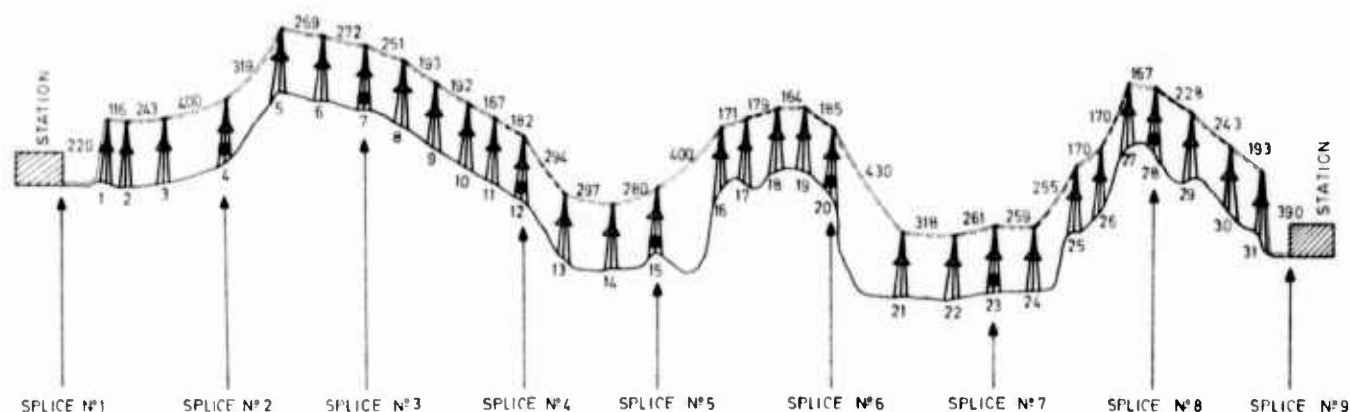


FIG. 2 DIAGRAM OF THE ROUTE

plastic material is applied. Over this sheath, Kevlar threads are longitudinally applied and a new layer of extruded plastic material is applied on these threads.

Characteristics of the materials forming the cable

a) Central Strength Cord

Material: Kevlar 49.
Diameter: 2 mm
Breaking load: 400 kg
Elongation at break: 2%
Weight per meter: 3.6 g

b) Filament Fillings

Material: Polypropylene.
Diameter: 1.2 mm (no tension)
Breaking load: 13.5 kg
Weight per meter: 0.5 kg

c) Wrapping Tapes

No. of tapes: 2
Material: Each tape is formed by two polyester layers and one foam layer in the center.
Width: 10 mm
Thickness: 0.2 mm

d) Resistant Threads

No. of threads: 24
Material: Kevlar 49
Breaking load: 22 kg
Elongation at break: 2%
Weight per meter: 0.16 g

e) Cable Sheath

Material: 0.3 Black Polyethylene
Thickness of the inner plastic layer: 0.5 mm
Thickness of the outer plastic layer: 1.0 mm
Resistant Kevlar threads are placed between both layers.

f) Optical Fibers

Type: Multimode, graded index
Core and cladding material: Doped silica as per MCVD.
Core diameter: 50 ± 3 microns
Cladding diam.: 125 ± 6 "
First coating material: Silicone
First coating diameter: 220 microns
Secondary coating material: Nylon
Secondary coating diameter: 0.95 ± 0.03 mm

Final Cable's Characteristics

a) Mechanical and Dimensional

Radial thickness of sheaths plus resistant threads: 2 mm
Cable's outer diameter: 9 mm
Weight: 50 kg/km
Maximum tensile strength (short term): 200 kgf
Tensile strength (long term): 100 kgf
Minimum admissible bending radius: 15 cm
Temperature range:
- During installation: From 0 to 60°C
- At work: From -20 to +70°C
Weight of wooden reel: 15 kg

b) Transmission of Fibers

Attenuation at 850 nm: 3.5 dB/km
Dispersion at 850 nm: 2 ns/km
Bandwidth: 300 Mhz . km at 850 nm
Numerical aperture: 0.21

Figure 3 shows a transversal section of the cable.

DESIGN OF THE AUXILIARY OVERHEAD TROLLEY FOR CABLE LAYING

Among the possible solutions, it was decided to use the auxiliary overhead trolley for the optical fiber cable laying. This trolley would roll on the ground wire, with an operator joining both cables together and placing fastening coils at regular intervals.

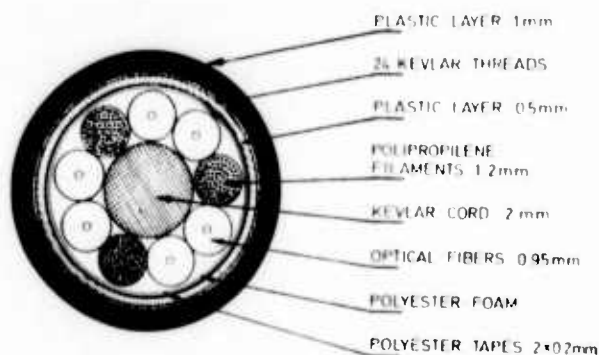


FIG 3 CABLE TRANSVERSAL SECTION

The trolley was designed with 17 cm diameter wheels, and with the back wheel which should always move forward on a fastening coil having a steering wheel fixed to one of the wheels which is driven by the operator riding the trolley. Likewise, the trolley has a brake and a simple system allowing it to pass from one side of the tower to the other without letting down the reel to the ground. The reel goes installed on a loose axis in the trolley, and the trolley together with the reel, operator and accessories weighs around 180 and 194 kg, depending on the optical fiber cable lengths.

The overhead trolley is shown in Figure 4.



FIGURE 4: AUXILIARY OVERHEAD TROLLEY

FASTENING COILS

The fastening coils should meet the following conditions: on one side, fastening the cable not too tight, and on the other, allowing an easy rolling of the trolley. Several types were tested: A plastic fastening coil with an elliptical inner section formed by a 7 mm diam. rod, which was rejected during the tests because the trolley was difficult due to the rod thickness and coil movement as the wheel passed over. Another coil, formed by an Aluminium Alloy with 3.5 mm thick wire, 17 mm diam. and 9 cm lay was rejected due to the material deformation. Finally, several coils of galvanized steel 2.54 mm thick, diameters around 15.5 and 18 mm and helix lays 7 x 14 cm were tested. One of these last coils with 16.75 mm inner diameter, 7 cm helix lay and 70 cm long was finally adopted.

Separation between coils was 35 cm and in order to prevent wind vibrations, right and left alternate coils were placed as there is a variation in the aerodynamic profile of the ground wire when placing the optical fibers. All this was carried out as a consequence of the results of tests which were performed prior to installation and which will be described farther on.

Figure 5 shows a view of the fastening coils.



FIGURE 5: FASTENING COILS

JOINTINGS AND SPLICINGS

The optical fiber cable pieces have lengths from 950 the shortest to 1,235 m the longest. For this reason, 7 splices were foreseen in the line, located in the towers at their first stage, i.e., approx. 10 m from the ground.

The fiber jointings were performed using two machines, one of them working with microflame fusion⁷ and the other by electrical arch fusion. With it, we tried to analyze both types of splices under every standpoint, i.e. feasibility, quality and life.

Once the fibers were spliced, the splicing was reinforced with thermo-retractile sleeves, and all of it was inserted in flat jointing houses of an Aluminium Alloy fully watertight and fixed to the tower structure.

TESTS PRIOR TO CABLE INSTALLATION

A series of tests were performed prior to the cable's final installation in order to solve all possible problems of the cable laying.

According to the results obtained, the auxiliary laying trolley as well as the fastening coils and separation described, were designed. The following studies will be specifically described.

a) Study of the cable with point load

From the study of a cable balance with a load centered in a given point of the span, we reached the conclusion that a 175 kg approx. load, the ground wire reached the maximum tension foreseen by the regulations in force. For checking the validity of the theoretical calculations an experimental test was carried out in Jan. 1983. Between towers 1 and 3 of the 380 KV Vitoria-Ixaso line, near Vitoria Substation, a steel cable was laid approx. 1 meter from the ground. This cable was identical and in the same tension conditions as that in the Cordovilla-Orcoven 1 line. These two spans have lengths of 239 and 440 m and are almost equal to the average and maximum spans of Pamplona line.

The test consisted of a theoretical calculation of the heights to be produced after hanging a 340 kg weight, and its practical checking. A 5.31% maximum error was detected in the 230 m span, and a 3.55% error in the 440 m span, the difference decreasing from the center to the towers. It was also noted that the error was always found in the same direction, arising from the cable settlement. This indicates that the theoretically calculated tensions were higher than the real ones obtained in the fields. The results were accepted.

b) Strength Attenuation Variations

An important subject that we wanted to study was the relation existing between the mechanical tension supported by the ground wire and the attenuation produced in the optical fiber cable.

For this, a steel cable identical to the one being handled was installed at the Vitoria Substation with a (tensing & untensing system) and electric dynamometer continuously indicating the steel cable strength. Two tests were performed: In the first, the optical fiber cable was lashed to a 2,000 kg strength from the ground cable. The strength was decreased to 600 kg and again increased until reaching 3,000 kg, and finally decreased to 2,000 kg. In the second test, the optical fiber cable was lashed to 800 kg strength in the ground wire. It was increased up to 3,000 kg and decreased to

1,900 kg, keeping this strength all night long.

The optical fiber cable lashed was 85 m long, and the fibers were spliced at the ir ends forming a loop, in order to obtain a continuous wire of 500 m. The attenuation values were measured at regular intervals: of 100 kg in the first place and afterwards 250 kg mechanical strength variation in the steel cable. The results were highly satisfactory as it was noted that the mechanical stress increase in the ground wire does not vary the O.F. cable attenuation.

c) Vibrations

The vibration tests were carried out with a vibrator LING DINAMIC SISTEM 710L model, with an oscillator-amplifier TPO-1K.

A 35 m optical cable length was prepared and lashed to the corresponding ground wire, with the already described fastening coils placed at different distances. The optical fibers had been spliced forming a loop for the continuous control of the possible attenuation variation or fiber cracking by means of a reflectometer.

The test started with a sweeping of frequencies from 3 Hz to 100 Hz and with variations of the energy applied by the oscillator-amplifier. This sweeping was repeated tensing 1,700, 1,300 and 900 kg the ground wire with the optical cable lashed. Considering its behavior and the span possibilities, 3 (resonance frequencies) were selected: 60, 27 and 9 Hz, and the following test conditions were decided:

Stress: 900 kg

No. of cycles: 10×10^6 (in each of the three frequencies)

Approx. (free wave) amplitude in the ground cable:

2 to 6 mm at 60 Hz

4 to 10 mm at 27 Hz

10 to 18 mm at 9 Hz

Once the tests were concluded in the established conditions, no variation was noted in the fibers attenuation which was continuously recorded by the reflectometer and no sheath failures were detected due to the lashing.

d) Cable Qualification before Installation

The values obtained in the cable before installation are shown in the following

table. The fibers attenuation was measured in the field with a reflectometer. The remaining tests were performed in the laboratory.

Piece	Length m	Fiber No.	Attenuation at 850 nm dB/km	Dispersion ns/km	Core diam. microns	Cladding diam. microns	Numerical aperture
1	1,048	1	2.70	1.7	50	125	0.21
		2	3.70	2.2	50	125	0.21
		3	3.80	1.2	50	125	0.20
		4	3.70	1.7	49	125	0.21
		5	3.98	2.3	50	124	0.21
		6	3.19	1.2	50	125	0.21
2	952	1	4.97	1.2	50	125	0.21
		2	3.35	0.9	49	125	0.21
		3	2.94	1.5	49	125	0.20
		4	2.94	1.3	50	125	0.21
		5	3.30	1.5	50	125	0.22
		6	3.45	1.2	51	125	0.21
3	1,235	1	2.97	2.2	50	126	0.21
		2	2.74	1.2	50	125	0.20
		3	2.91	1.7	48	125	0.21
		4	2.76	0.9	50	125	0.21
		5	2.82	1.7	50	125	0.21
		6	2.74	1.7	50	124	0.20
4	950	1	3.25	1.7	51	125	0.21
		2	2.80	1.2	50	125	0.21
		3	3.15	1.7	51	124	0.22
		4	2.80	1.2	50	125	0.21
		5	2.85	0.9	49	126	0.21
		6	2.74	2.2	50	125	0.21
5	1,186	1	3.39	2.3	51	126	0.20
		2	3.27	1.7	50	125	0.21
		3	3.19	1.2	49	125	0.21
		4	3.07	1.7	51	125	0.21
		5	3.39	2.2	49	125	0.22
		6	3.27	1.2	50	125	0.21
6	1,094	1	3.34	2.3	50	124	0.21
		2	3.08	2.2	50	125	0.21
		3	2.95	0.9	49	125	0.21
		4	2.77	1.7	50	125	0.22
		5	2.95	1.7	49	125	0.21
		6	2.64	2.2	49	124	0.22
7	1,098	1	3.08	1.7	50	125	0.21
		2	4.84	0.9	50	125	0.21
		3	3.00	1.2	51	125	0.22
		4	2.77	2.3	50	125	0.21
		5	2.81	2.2	49	124	0.21
		6	2.90	2.2	50	125	0.21
8	1,151	1	2.55	2.3	50	125	0.21
		2	3.06	1.2	50	125	0.21
		3	2.72	1.2	51	125	0.21
		4	3.06	0.9	51	125	0.21
		5	2.72	1.7	49	124	0.20
		6	2.98	1.7	50	125	0.21

Likewise, the following tests were carried out in the cable's polyethylene sheath with the following results:

TEST	PIECE No.							
	1	2	3	4	5	6	7	8
Tensile Strength, kg/cm ²	147	132	150	160	160	137	160	140
Elongation at break, %	550	550	500	550	500	450	450	550
Cracking	COMPLIED	C	C	C	C	C	C	C
Shrinkage	1.31	1.32	1.54	1.47	1.42	1.52	1.84	1.33
Impact Resistance -40°C	COMPLIED	C	C	C	C	C	C	C

The test methods used were as per ASTM⁸ norms.

INSTALLATION AND LONG-TERM RESULTS

A view of the installation works is shown in Figure 6.



FIGURE 6: INSTALLATION WORKS

Once the line's installation and splicing was concluded, end to end measurements were performed in each of the fibers. Concerning the attenuation variations with respect to the attenuation values obtained before reel installation, we can say:

- 1) Attenuation decreased except in 3 fibers, in which it increased 0.1 dB.
- 2) The decrease is around 0.2 and 0.7 dB/km, the most frequent being 0.5 dB/km, which was noted in 12 fibers.

The following table shows the attenuation decrease distribution:

DECREASE	0	.1	.2	.3	.4	.5	.6	.7	.8	.9
No. OF FIBERS	1	2	6	4	6	12	5	5	2	2

Regarding the splicings, these were qualified one by one as we were trying to test the two splicing techniques: with microflame and electric arch machine.

The attenuation values obtained per splicing are given in the following table:

Reel	Situation	Splicing No.	Splicing Attenuation, dB						Type of Machine
			Wire 1	Wire 2	Wire 3	Wire 4	Wire 5	Wire 6	
1/2	Tower 4	1	0.2	0.3	0.1	0.1	0.4	0.1	Electric Arch
2/3	Tower 7	2	0.5	0.3	0.4	0.1	0.1	0.3	" "
3/4	Tower 12	3	0.1	0.1	0.1	0.1	0.1	0.5	" "
4/5	Tower 15	4	0.2	0.1	0.1	0.1	0.1	0.4	" "
5/6	Tower 20	5	0.1	0.2	0.3	0.5	0.2	0.4	Microflame
6/7	Tower 23	6	0.4	0.2	0.5	0.3	0.3	0.5	" "
7/8	Tower 28	7	0.3	0.2	0.2	0.1	0.2	0.2	" "

As it can be seen, splicings Nos. 1, 2 and 3 were performed with the electric arch machine, and the microflame machine was used in splicings 5, 6 and 7. The summary of the values obtained with both machines is:

ATTENUATION, dB		0.1	0.2	0.3	0.4	0.5
SPlicing PERCENTAGE	Arch	59	8	12.5	12.5	8
	Microflame	11	39	22	11	17

From these values we concluded that the arch machine obtains notably better results than the microflame machine.

According to the above, end to end measurements were performed in the line with the following results:

Fiber	Total Attenuation (dB/8,346 m)	Attenuation dB/km
1	25.35	3.04
2	26.72	3.20
3	26.82	3.21
4	25.93	3.11
5	27.91	3.34
6	25.69	3.08

The attenuation decrease noticed in the total line with respect to the initial value in each cable piece is due in the first place to the cable unrolling, since the attenuation decreases in the fibers as these are changed to a most suitable position. This had already been noticed in previous experiences. In the second place, the splicings were performed according to a previous splicing chart in order to optimize the line's attenuation. However, this procedure would not have been necessary due to the equipments margin.

At the present time, the system has been working for one year with a 2 Mbit/s system with satisfactory results. The line has been subject to an exhaustive test program throughout its working life, as the measurements of the system and its components are

an essential part of the applied research project, and a higher experience in the use of this type of installation could be obtained according to the test program in the different stages of the project.

The test program will continue until the end of 1984 and it is carried out by means of a measuring system installed in the same line. This consists of a data procuring equipment continuously recording all the interesting parameters. These parameters come from photometers in the optical terminal which measure the optical cable attenuation and the light emission power, and from a meteorological station installed in the roof of the building. This system records the wind speed and direction, inside and outside temperatures, optical fiber attenuation and the light power of the optical terminal as well as any other interesting parameter.

CONCLUSIONS AND FUTURE ASPECTS

Considering the measures obtained at the laboratory and during installation, as well as those throughout the test period, the conclusion was reached that the mechanical support of high tension lines can be used for the optical cable laying, as well as the feasibility of the optical fibers as a transmission medium in the private telecommunication networks of the electrical power transportation and distribution industry.

The method of lashing the optical fiber cable to the ground wire is therefore very simple, and does not require the use of especially designed optical cables. Without rejecting at all the already existing methods, the mentioned procedure opens a great way for the installation in the existing high tension lines with a ground wire, or for future lines where the economical, quality and easiness factors be more important than any other type of factors.

ACKNOWLEDGEMENTS

The authors publicly thank the firm IBERDUE RO, S.A., especially Messrs. A. López Suero and J.M. Madrazo for their active collaboration in this project, which would not have been possible without their cooperation, experience and help.

REFERENCES

- 1 - A new optical waveguide transmission system for the Telecommunication networks of Electric Power Supply Companies
By K. Fischer, W. Möller, W. Rüger and A. Tannhäuser.
- 2 - Field trial of composite fiber-optic overhead ground wire.
By S. Kubota, I. Matsubara and other.
IWCS Proceedings 1983.

- 3 - Furukawa O.P.G.W. system (Optical fiber composite overhead ground wire).
The Furukawa Electric Co., Ltd.- Tokio
No. EDP - 2001. Feb. 1984.
- 4 - Self-supporting metal free optical fiber cable for large span length.
By W. Schmidt, K. Kimnich, S. Metz.
Standard Electric Lorenz AG. Germany.
- 5 - Optical cables for aerial application.
By O.R. Bresser, N.K.F. Philips Teleco
mmunication Review, July 1982.
- 6 - Non-metallic long span aerial cable with optical fibers for the use at 1.3 μ m.
By H.G. Haag and P.E. Zambow. AEG Telefunken. IWCS Proceedings 1983.
- 7 - Optical and mechanical characteristics of microflame fusion splicing of optical fiber.
By B.F. Rondan and A.A. Morales. Standard Eléctrica. IWCS Proceedings 1982.
- 8 - ASTM's D-638, D-1693, D-1248, D-746.



FRANCISCO J. SAEZ DE LA MAZA was born in 1947. He graduated in 1967 from the Escuela Técnica de Ingenieros of Santander as an Industrial Technician. He worked at STANDARD ELECTRICA's Development Laboratory and from 1983 he is the responsible for the Optical Fiber Laboratory of the Cable Division.



FIDEL GOMEZ MARTIN was born in 1937. He graduated in 1963 from the Escuela Técnica Superior de Ingenieros de Telecomunicación of Madrid with a degree in Telecommunications. He now is the Chief Engineer at Standard Eléctrica's Cables Division, responsible for the Line's Research and Development Dept., including the Optical Fiber Group.



CARLOS G. CORTINES was born in 1944. In 1968 he graduated from the University of Valladolid with a degree in Physics. He joined STANDARD ELECTRICA, and was responsible for the Transmission Measurements Laboratory. From 1982 he is the head of the Optical Fiber Group of Standard Eléctrica's Cables Division.

TACTICAL FIBER OPTIC SYSTEM REQUIREMENTS

By

Vasilios E. Kalomiris

U.S. Army Communications-Electronics Command
Fort Monmouth, New Jersey 07703-5202

ABSTRACT

This paper will outline the unique features of a militarized fiber optic system. The stringent requirements that make tactical systems a challenge to the fiber optic industry are summarized. The requirements are broken down to the component level. These demands on components are necessary to assure successful system operation. The compilation of specifications is presented in tabular form to serve as a reference for those interested in satisfying a host of ground system needs.

INTRODUCTION

The advantages offered by fiber optic technology have surpassed the expectations of even the most optimistic scientists and continue to unfold. Within about fifteen years the progress on the silica doped fiber designs, including step index and graded index multimode and step index single mode, has led to extending the system operating wavelength from 0.85 μm to 1.3 μm and beyond with a significant reduction in attenuation with levels approaching 0.25 dB/km. Additional experimental work on other exotic fiber compositions is in progress with anticipate reduction in attenuation to levels of 10^{-3} dB/km.

The Army, recognizing the advantages of fiber optic technology, has been involved in the development of fiber optic components and systems with the main objective of replacing the twin metallic coaxial cable. The introduction of fiber optics in a tactical environment can be a success only if the components comprising the system can satisfy the unique requirements of the military environment and also can be shown to have service life not less than comparable equipments used in the commercial fixed plant communication systems.

The Army, as soon as the fundamental exploratory development work on the fiber optic system AN/GAC-1 was completed, embarked vigorously on an engineering development program with the objective of replacing the currently used twin metallic coaxial cable, associated transmitters, receivers, repeaters, and ancillary equipment with fiber optics.

It is demanded by the user community that the new technology, in order to be accepted, provide greater technical advantages and cost benefits over the present technology, as well as, meet all the present system requirements. The successful fielding of the new technology is highly dependent on the timely and coordinated integration of the particular components. The individual components, before they qualify for the subject system, must undergo a very comprehensive sequence of testing which verifies technical performance, human factors evaluation, cost effectiveness, and design to unit production cost.

Since the main application is the replacement of twin coaxial cable which is the "work-horse" of the Army's communication network for ground tactical communication trunking links, only this ground tactical applications will be considered. The system operation in the tactical field requires that the fiber optic cable be ruggedized and designed to withstand the repeated deployment and retrieval offered by a rough terrain and its adverse conditions. It is also understood that the same fiber optic system operate in any climate for cost effectiveness and simplification. Thus, the environmental performance must include temperatures from -46°C to $+71^{\circ}\text{C}$ as a minimum requirement.

This paper will address the environmental and mechanical characteristics that a tactical fiber optic system and its components have to meet before qualification for fielding; comparison to a fixed plant fiber optic communication system will be emphasized.

SYSTEM

The on-going work for the Fiber Optic Transmission System (Long Haul), FOTS(LH)¹, was undertaken with the consideration that the fiber optics should be introduced into the tactical field with minimum changes to related electronics, multiplexers, etc., already available in shelters. In addition, the fiber optic system was constrained to interface with external digital multiplexed traffic rates 4.736 Mb/s and 18.816 Mb/s over the optical fiber. The need was recognized for system

operation in link lengths of one to eight kilometers without a repeater and up to sixty-four kilometers with seven repeaters. The fiber optic system requirements², are listed in Table 1.

TABLE 1

TACTICAL FIBER OPTIC SYSTEM REQUIREMENTS

Repeater Spacing	8 km
BER	10^{-9} for max link length 64 km
Transmission Rate	4.736 and 18.816 Mb/s
Maintenance Orderwire	Analog and Digital
Maintenance Orderwire	35 dB
Channel SNR	
Heat Dissipation	No Circulation Fans Within Equipment
System MTBF	500 hrs for 20 km/24 hr mission Configuration/ Duration
Fault Locations	Identification of Last Operating Repeater within ± 2 meters in one km cable
Temperature Extremes	Per MIL-STD-810
1. Storage and Transit	-46°C to +71°C
2. Starting	-46°C
3. Continuous Operating	-46°C to +52°C + Solar Radiation of 360 BTU/SQ. FT./HR.
Environmental Conditions	Per AR-70-38, MIL-STD-454, MIL-STD-810
Transportability	Withstand the effects of handling during transport
EMC/EMI	MIL-STD-461A
Built-In Test/ Maintenance	Detect Greater than 98% of Faults
Diagnostics	With less than 1% False indication

CABLE ASSEMBLY

The fiber optic cable assembly consists of one kilometer of two fiber, optical cable terminated with hermaphroditic lens connectors.

CABLE

The fiber optic cable which is the basic element of the system is all dielectric and contains two tightly buffered optical fibers, see Table 2. The cross-section of the cable is shown in Figure 1 and its characteristics in Table 3. The main requirements imposed on the fiber optic cable are survival in the tactical field which requires that the cable be ruggedized; in addition the cable must meet the constraints of weight and reel capacity that the link length will allow. A diameter of 5.6 mm was selected meeting the above constraints. This cable diameter allows for packaging 1 km cable on existing DR-15 and RC-453 cable reels

and maintaining the weight of a full reel at a nominal 100 lbs.

TABLE 2

OPTICAL FIBER REQUIREMENTS

Fiber	Dual Wavelength 0.85 and 1.3 μ m Graded Index Multimode, 50/125
Numerical Aperture	0.22
Bandwidth	400 MHz-km
Construction	Tightly Buffered
Diameter	1 mm OD
Proof Test Level	100 kpsi
Temperature	-46°C to +71°C
Performance	
Radiation Hard	

CABLE DESIGN

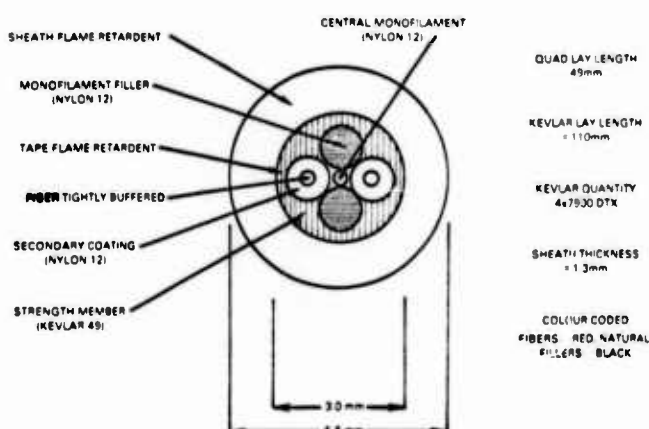


Figure 1. TACTICAL CABLE DESIGN

TABLE 3

TACTICAL FIBER OPTIC CABLE REQUIREMENTS

		METHOD
Cable Construction	All dielectric	
Outer Diameter max	6 mm	
Tensile Strength	1780 Newtons (400 lbs)	
Temperature Cycling	-46°C to +71°C	4020
Storage	MIL-STD-810D	
Altitude Cycling	MIL-STD-810D	520
Freezing Water Immersion		
Ice Crush	DoD-STD-1678	4050

TABLE 3 (Cont)

Cyclic Flexing	DoD-STD-1678	2010
Cold Bend	DoD-STD-1678	2020
Impact Damage		
1. Room Temperature	DoD-STD-1678	2030
2. -46°C	DoD-STD-1678	2030
3. +71°C	DoD-STD-1678	2030
Radial Compressive Strength	DoD-STD-1678	2040
Cable Twist-Bend	DoD-STD-1678	2060
Tensile Loading	DoD-STD-1678	3010
Flammability	DoD-STD-1678	5010
Fungus	MIL-STD-810D	508.3
Reasonably Priced		

TABLE 4

TACTICAL FIBER OPTIC CONNECTOR REQUIREMENTS

Hermaphroditic	Two Fiber Connector
Insertion Loss	< 2 dB Lens, < 1 dB Butt Joint
Mating Durability	2,500 cycles
Ease of Interconnection	Minimum force, positive locking
Connector Tensile Strength	DoD-STD-1678, Method 3010, Procedure II
Adequacy of Dust Cap	MIL-STD-810D, Procedure I, Method 512.1
Field Cleanability	No special kits allowed
Impact	MIL-STD-1344, Method 2015
Vibration	MIL-STD-1344, Method 2005.1
Salt Fog	MIL-STD-1344, Method 1001.1
Fungus	MIL-STD-810D, Method 508.3
Leakage (Immersion)	MIL-STD-810D, Method 512.2
Sand and Dust	MIL-STD-810D, Method 510.2
Temperature Cycling	MIL-STD-1344, Method 1003.1
Temperature Storage	DoD-STD-1678, Method 4010
Altitude Cycling	MIL-STD-810D, Method 520
Freezing Water Immersion	DoD-STD-1678, Method 4050
Humidity	MIL-STD-810D, Method 507.2
Shock	MIL-STD-810D, Method 516.3
Weight	0.91 kg Plug/ 0.4 kg Receptacle
Flammability	MIL-STD-1344, Method 1012
Reasonably Priced	

TRANSMITTER/RECEIVERS

The fiber optic transmitters and receivers operate at 1.3 μ m wavelength and are comprised of a LED transmitter and a PIN-FET receiver

which are designed to electrically interface with the existing equipment in the Shelter Modified Group Modem (MD-1026) and optically interface with the fiber optic transmission medium.

The optical transmitters which have been currently selected for use in tactical communications systems are LED based since they are more reliable and simpler than laser sources. In addition, LEDs offer fewer safety hazards to the user. The LED is qualified to the JAN-TXV level of MIL-S-19500, including radiographic inspection.

The physical characteristics of an LED transmitter for a tactical communications system are listed in Table 5.

TABLE 5

LED PHYSICAL CHARACTERISTICS

Packaging	14 Pin Dual Inline Package
Fiber Retention	10 N (2.3 lbs)
Fiber Optic Pigtail	1 m (39.3 inches) (Fiber identical with the one used in cable)
Heat Transfer	Provided by the area between pins
Fully Hermetic	No epoxies internal to seal

The optical transmitters are designed to meet the environmental requirements listed in Table 6.

TABLE 6

LED ENVIRONMENTAL REQUIREMENTS

Operating Temperature	-55°C to +85°C
Storage Temperature	-55°C to +125°C (Humidity performed when exposed to 95% RH for continuous and intermittent periods.)
Barometric Pressure	
1. Storage and Transit	Sea level to 12200 m
2. Operating	sea level to 3050 m
Vibration and Shock	Induced during transportation
Radiation Hardness	
Safety	

The characteristics of the optical transmitter are listed in Table 7.

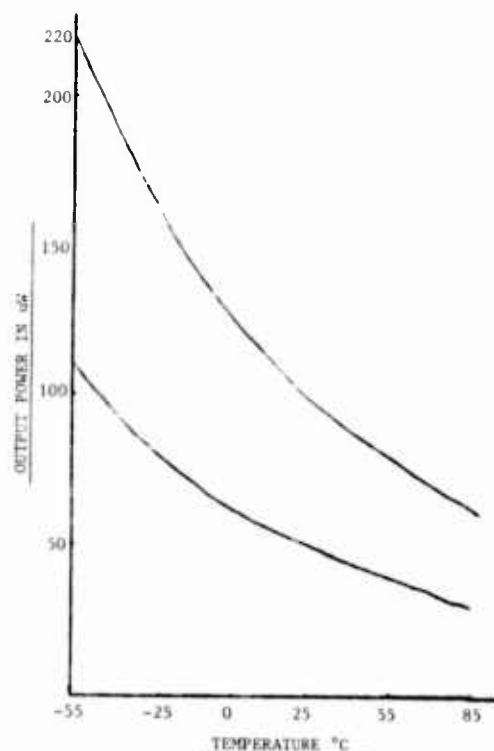
TABLE 7

LED OPTICAL CHARACTERISTICS

Peak Output Power @ 150 mA	See Figure 2 (Function of heat sink temperature)
Emission Spectra	
Drive Current	150 milliamperes
Absmax Drive Current	200 milliamperes

TABLE 7 (Cont)

Nominal Forward Voltage	1.8 volts @ 150 mA
Drop (Less than)	
Bias Conditions	
(No performance degradation IV rev bias dir after subjection to)	
Center Wavelength @ 25°C	1250 \pm 15 nm
Temperature Dependence	0.700 nm/°C
(Over entire operating temperature range)	
Linewidth @ FWHM	< 100 nm
(Over entire operating range)	
Optical Rise/Fall Time	< 8 nanoseconds
(10% to 90%)	
and Drive Current Change From	
25% to 100% of	150 milliamperes
Linearity Sufficient To Maintain	< 15% of AC.P
(Total harmonic distortion)	
Contrast Ratio for	< 1.5% of output P
4 Milliamperes	Defined at
Drive Current	150 milliamperes

Figure 2. LED P_{out} in mW v temperature in °C

The transmitters in order to qualify have to meet the requirements listed in Table 8. The screening tests are performed in accordance with MIL-STD-750.

TABLE 8

LED SCREENING TESTS

	MIL-STD-750, Method
Fiber Retention	10 N
Internal Visual	2073
Stabilization Bake	1032
(At max temp)	
Temperature Cycling	1051 Test Cond. B
Constant Acceleration	2006
(Y, orientation 10,000 G min)	
Seal	1071
1. Fine Leak	Test Cond. H
2. Gross Leak	Test Cond. C
Radiography	2076
Burn-in (168 hrs)	1038 Test Cond. B
External Visual	2071
Mechanical Shock	MIL-STD-750, Method 213
(Half-size pulse @ 100 G's)	

PIN/FET transimpedance optical receivers have been selected for use in the first tactical communications system. They are qualified to hybrid level of MIL-M-38510, including radiographic inspection.

The physical characteristics of PIN/FET receiver modules are listed in Table 9.

TABLE 9

PIN/FET PHYSICAL CHARACTERISTICS

Packaging	14 Pin Dual Inline Package
Lead Material	Type A or B per MIL-M-38510
Finish	Type C
Heat Transfer	Provided by the area between the pins
Fiber Optic Pigtail	Fiber identical to fiber in cable
Fully Hermetic	No epoxies internal to seal

The PIN/FET receivers are designed to meet the environmental requirements listed in Table 10.

TABLE 10

PIN/FET RECEIVER ENVIRONMENTAL CHARACTERISTICS

Operating Temperature	-46°C to +85°C
Storage Temperature	-55°C to +125°C
Humidity (Hermetically Sealed)	95% RH
Barometric Pressure	
1. Storage & Transit	Sea level upto 12200 m
2. Operating	Sea level upto 3050 m
Vibration and Shock	Transportation, rough handling
Radiation Hardness	With the exception of exception of
	1. Module Responsivity
	2. Frequency Response
	3. Output Noise Voltage
Post Radiation Exposure Responsivity	94%
Post Radiation Frequency Response (From DC to 15 MHz)	94%
Post Noise Voltage (RMS)	
	285 to 420 mv for (-46 + 80°C)
	or -46 to 22°C 285 mv
	23 to 35°C 317 mv
	36 to 80°C 420 mv

The characteristics of an optical receiver for a tactical communication system are listed in Table 11.

TABLE 11

PIN/FET RECEIVER OPTICAL CHARACTERISTICS

Spectral Sensitivity	1100 - 1400 nm
Optical Damage - Withstanding	5 mwatts
Input Optical Power Level (pp) for 5×10^{-11} BER	-44.5 dBm to -4.5 dBm 35.5 uw to 355 uw
Responsivity (No AGC) (Full AGC)	5.3×10^4 to 5.9×10^4 $\frac{v}{w}$ 5.3×10^3 to 5.9×10^3 $\frac{v}{w}$
Frequency Response	100 Hz to 20 MHz min
Group Delay	4 nansecs for 4 KHz to 15 MHz
Linearity	1 dB compression/decompression max
Output Noise Voltage (Temperature Dependent)	180-265 microvolts max

Receiver sensitivity versus temperature is shown in Figure 3.

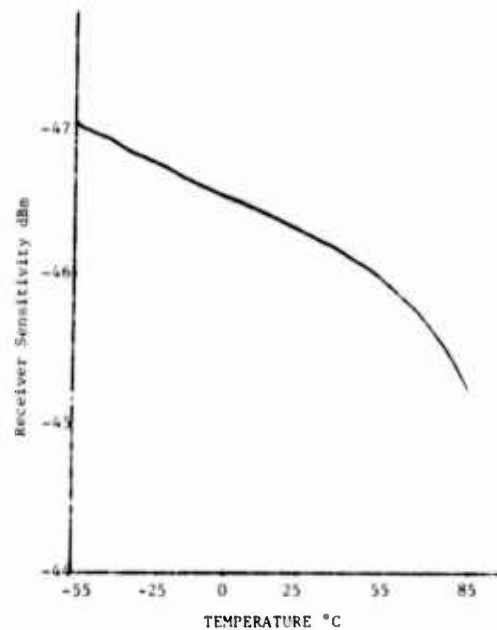


Figure 3. Receiver Sensitivity v Temperature

The receivers are evaluated in accordance with MIL-STD-883 for qualification. The screening tests are listed in Table 12.

TABLE 12

PIN/FET RECEIVER SCREENING TESTS

		Per MIL-STD-883 Method
Fiber Retention	10 N min	
Internal Visual		2017
Stabilization Bake	24 hrs min	1008 Cond B
Temperature Cycling		1010 Cond A
Constant Acceleration		2011 Cond B
in Y_1 orientation		
Visual Inspection	Defective parts	
Interim (Pre-burn-in)	Electrical parameters	
Burn-In-Test	160 hrs @ 100°C	1015
	160 hrs @ 125°C	
Seal		1014
	1. Fine	
	2. Gross	
Radiography Inspection		2012
Resistance to Solvents		2015
Bond Strength		2011
Moisture Analysis	6000 ppm max at 100°C and 1 atm Pressure	1018

The stringent requirements³ that a tactical fiber optic system must meet to qualify for fielding are listed and compared with the requirements of a fixed plant communications system, see Table 13.

TABLE 13

FIXED PLANT VERSUS TACTICAL FIBER OPTIC COMMUNICATIONS SYSTEM

<u>ITEM</u>	<u>FIXED PLANT</u>	<u>TACTICAL SYSTEM</u>
Mobility	Permanent and Protected	Rapid Mobility 50% of Systems in Place for < 10 hrs
Installation	Underground or Aerial	On Ground, Underground or Aerial
Climate	Stable Environment Equipment Easily Qualifies	Severe Climatic Conditions Materials and Equipment Specifically Designed
Radiation Hardness	Metallic Strength Members Commonly Used	Severe Problems, All Dielectric Cables Required, Terminals and Equipment EMP/EMI Resistive
Cable Length	No Significant Constraints	Significant Constraints, No Splices, Use of Connectors and Existing Deploying & Retrieving Equipment
Durability	No Significant Problems	Handling and Environmental Factors Necessitate Highly Durable Cable
Flexibility	One Time Installation	Handling and Low Temperature Performance Require Highly Flexible Cable
Weight/Bulkiness	No Significant Problems	Need to Reduce Installation Time, Logistical Requirements and Improve Cost Effectiveness
Repeaters	Repeaters Might Not Be Required. Repeaters May Be Remotely Powered	Repeaters Required Must Be Fully Mil-Qualified and Uses Battery Power
Ancillary Equipment	Industrial Grade	Most of Equipments Used for Repair or Monitoring Must Be Mil-Qualified
Installation Machinery	Continuously Improving Upgraded Techniques	Same Equipment as the One Used for Twin-Coax Cable Same Techniques

CONCLUSION

When the physical, environmental and optical characteristics of a tactical fiber optic system are examined, it becomes apparent that significant differences between fixed plant telecommunications systems and tactical communications systems exist. The components and system, as a whole, for a fixed plant installation will not meet the requirements of a tactical environment. These differences in requirements necessitate additional research and development work to obtain acceptable components. This is a direct cause for delays in fielding and increases in cost of the militarized fiber optic system.

Although the differences between the fixed plant and tactical field communications systems are significant, the Army has made significant progress and advancement so that by the middle of next year, the first fiber optic tactical

system complete with its primary and ancillary equipment will undergo Developmental and Operational Testing. Full production is expected for 1987.

REFERENCES

1. A.G. Mondrick, C. Chiu Chan, V. Mordowitz and M. Weinberg, "FOTS(LH): The Army's Long Haul Fiber Optic Transmission System," Signal Magazine, November 1983.
2. USA CECOM, Development Specification, "Fiber Optic Transmission System Long Haul, 27 May 1981.
3. H. Wichansky, L.U. Dworkin, S. DiVita and A. Mondrick, "Survivability of Army Fiber Optic Systems" SPIE, August 1981.

BIOGRAPHY



Vasilios E. Kalomiris, a project leader with the Center for Communications Systems of the U.S. Army Communications and Electronics Command, is responsible for fiber optic component and system development. He is a member of the Tri-Service Group, Chairman of the Working Group on Fibers, Cables, and Connectors. He is also a member of The Technical Cooperative Program JTP-12 on Fiber Optics and a member of the P6.7 Committee on Fiber Optic Standards. Previously, he worked for ITT-EOPD as a project engineer where he designed an air-layable fiber optic cable. Prior to joining ITT-EOPD, Vasilios was associated with General Cable Corp. R&D as a research engineer. Projects included electronic equipment calibration, communications cable design and evaluation, material evaluation and work on the first flexible superconductive power cable for Brookhaven National Laboratory. A graduate of New York University (B.A., B.S.E.E. and M.S.E.E.) he is a member of I.E.E.E. and The Technical Chamber of Greece (Society of Professional Engineers).

OPTICAL SUBMARINE CABLE WITH STRESS FREE FIBERS
EVEN AT EXTREME LEVELS OF CABLE ELONGATION

H. Damsgaard, A. Baungaard Sørensen, Ax. Andersen,
N. Enggaard, L. Grüner-Nielsen and H. Rosendal

NKT Elektronik,
95, Brøndbyvestervej, DK-2600 Glostrup, Denmark

Abstract

A stranded optical submarine cable construction has been optimized for application in moderately deep waters, where anchors and fishing equipment occasionally may be expected to interact strongly with the cable. The fibers have been observed to be stress free up to the extreme level of 1.9% of cable elongation.

A test cable was broken by pulling it at a right angle with an anchor. At breakage the force applied to the anchor was 39 tons. The maximum tension experienced by the cable close to the anchor area was determined to be less than 30 tons corresponding to less than 0.6% of cable elongation. All fibers broke within 0.5 m from the anchor.

By the introduction of a large stress free interval of the fibers, excellent mechanical properties and a most satisfactory degree of safety have been achieved. Consequently, long term stable operation and low repairing costs are to be expected.

Introduction

The fiber optic cable constitutes a vital part of optical communication systems. Therefore, it is necessary to ensure long term optical and mechanical stability of the cables operating under different and severe conditions and this is in particular the case for optical submarine cables due to their high repairing costs.

The main requirements are that no excess loss be observed and stress corrosion be avoided. The latter means that the fibers must be protected against static fatigue.

One solution to both of these requirements is to keep the fibers stress free during installation and operation as well as during and after having exposed the cable to strong external forces. Therefore (persistent) cable elongation, caused for example by cable rupture, should be properly accounted for in the design of the cable.

In cooperation with the Danish Posts & Telegraphs and the Danish Industrial Research & Development Fund, NKT has initiated a project with the purpose of developing an optical submarine cable optimized for application in moderately deep waters densely trafficked by all types of ships and heavily exploited by fishing activities.

The stipulated tensile force applicable to the cable without imposing stress to the fibers is 40 tons. In case of breakage, fiber fracture and fiber strength degradation is not to occur at a distance of more than 25 m away from the point of breakage. At a depth of 60 m, the tolerance for water penetration is set at a distance of max 10 m from the point of breakage during 24 hours.

A series of experiments has been successfully carried out resulting in a cable simultaneously meeting said requirements.

The basic objective has been to keep the fibers stress free even at extensive cable elongations. Cable elongation caused for example by fishing equipment, by anchors, or during installation is then totally absorbed by the cable construction without imposing stress to the fibers.

A most efficient way to achieve the non restricted movement of the fibers has proven to be a loose plastic (1, 2, 3) tube extruded around the fibers in such a way that the fiber excess length within the tube is as large as obtainable considering the actual geometrical parameters in the stranded cable structure. The fiber excess length is fully controllable by the extrusion process and it is measured by a light pulse delay technique (4).

First, the cable design is described. Next, some of the results from our experimental investigations, such as cable elongation - fiber stress characteristics, spectral attenuation curve, diagnosis of cable rupture, and other properties are presented and discussed.

Cable Design

The cross section of the cable is shown in Fig. 1. The loose tube secondary coated optical fibers are stranded around a central tension member. The tubes are filled with a high viscosity silicone oil characterized by a small temperature dependence of viscosity. To achieve a high level of cable elongation before stressing the fibers, the dimension of the tubes is quite large and additionally, the tubes are extruded around the fibers in such a way that 0.9% of fiber excess length is obtained with the implication that the fibers are positioned in the outside region of the tube in the final cable as indicated by Fig. 1. Thereby the resulting cable elongation necessary to cause fiber stress becomes 2%. The actual design parameters are given in Table 1 and Fig. 1.

Table 1 Design Parameters of Optical Submarine Cable.

Fiber, outer dia	0.125 mm
Primary coating, outer dia	0.280 mm
Radius of curvature of fibers	70 mm
Fiber excess length within the loose tube secondary coating	0.9%
Tube diameters	1.6/2.6 mm
Cable elongation with stress free fibers	2%

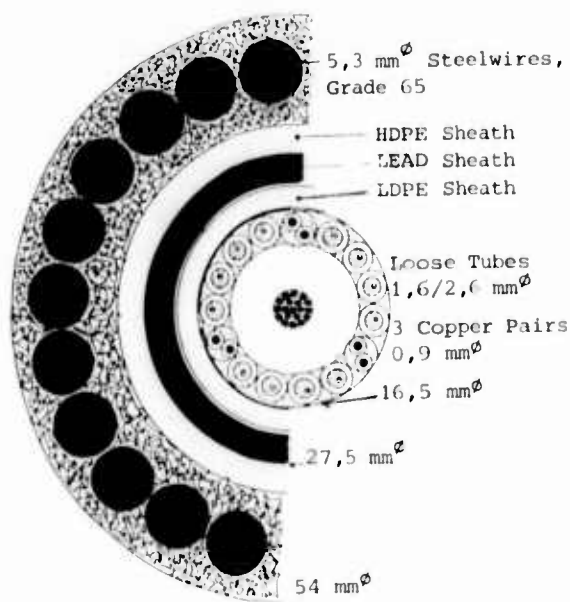


Fig. 1

Cross section of optical submarine cable optimized for application in moderately deep water areas.

Measurements, Results, and Discussion

A typical spectral attenuation curve for a MCVD single mode fiber applied in a 5 km long test cable is shown in Fig. 2. The loss is observed as 0.47 dB/km and as 0.34 dB/km at 1.3 μ m and 1.55 μ m, respectively.

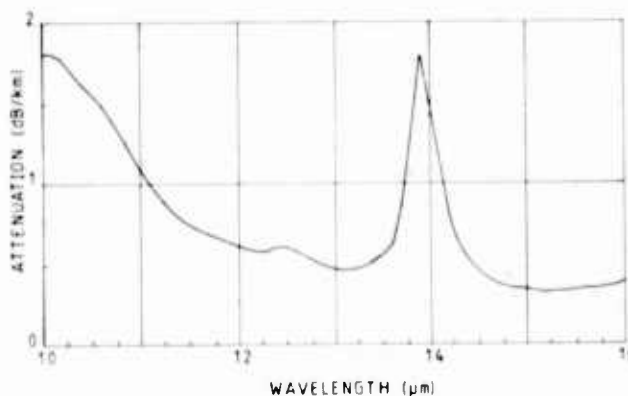


Fig. 2

Typical spectral attenuation curve for a single mode fiber applied in a 5 km long optical submarine test cable. No excess loss was observed during the cabling processes.

The fiber excess loss at 1.3 μ m as well as at 1.55 μ m introduced by the cabling processes was zero within measuring uncertainty, 0.03 dB/km.

Prior to the stranding long wavelength excess loss is observed because of fiber buckling due to the large amount of fiber excess in the plastic tube. However, in all cases this additional contribution to the loss at long wavelengths disappears after stranding.

The fiber excess length within the loose, filled plastic tube has been achieved by proper extrusion conditions and it has been measured by a light pulse delay technique described previously (4). Fig. 3 shows a typical measured tube elongation - fiber elongation curve and the excess length is observed to be 0.9%.

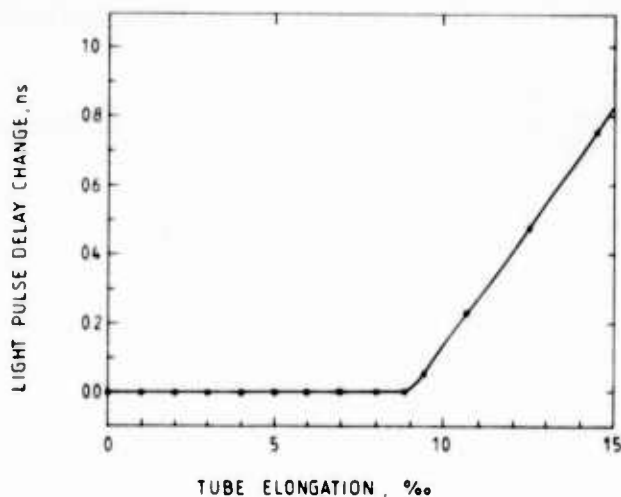


Fig. 3

Tube elongation - pulse delay change curve for a secondary coated fiber at 20°C. The fiber excess length is observed to be 0.9%.

This very important parameter is well controlled over a wide range by changing manufacturing conditions. Filled secondary loose tube coated fibers characterized by different values of fiber excess lengths have been fabricated and used in a test cable.

In Fig. 4 the measured cable elongation - fiber elongation characteristics for 37 m of this cable is shown. The three curves belong to different values of fiber excess length in the tubes prior to stranding: A: -0.15%, B: 0.5% and C: 0.9%. The difference between these values is observed to be consistently preserved during the cabling processes. The cable elongation necessary to cause fiber stress is 1.85% i.e. about 1.5 promille less than predicted by our theoretical calculations taking into account the geometry of the cable structure, only. This small deviation between theory and experiment, about 7%, is assumed to be caused by the tension applied to the tubes during the stranding, and quantitative agreement has therefore been concluded.

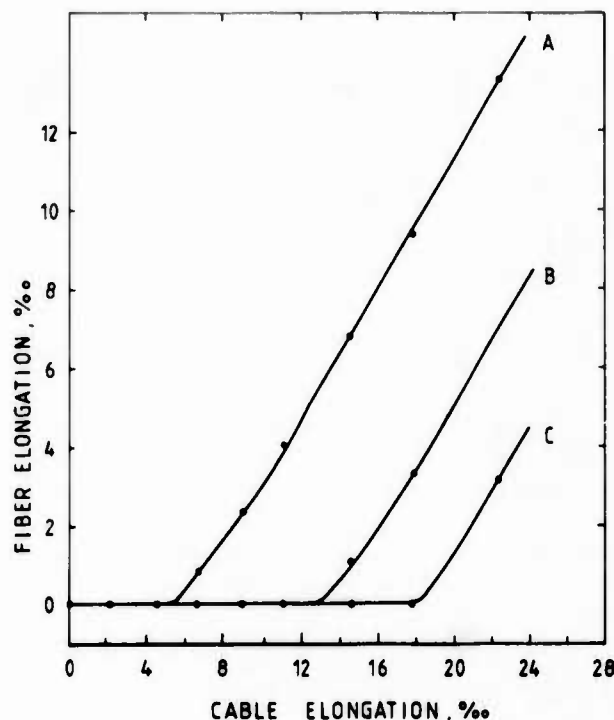


Fig. 4

Cable elongation - fiber elongation characteristics for a 37 m long test cable. The three curves belong to different values of fiber excess in the secondary coating prior to stranding: A: -0.15%, B: 0.5%, C: 0.9%. The difference between these values has been consistently maintained during the cabling processes. Also the observed fiber stress free cable elongation for the three fibers agrees very well with theory.

Fig. 5 shows the actual measured cable strain - force curve for our cable structure. It should be noted that 25 tons of cable tension causes less than 0.5% of cable strain, and 40 tons, which is the very limit of our test equipment, causes less than 1.5% of elongation. These values should be compared to the fiber stress free elongation of 1.9% and to the tensile force requirements of the cable i.e. 40 tons without imposing stress to the fibers. So even in the most extreme situations the fibers are stress free.

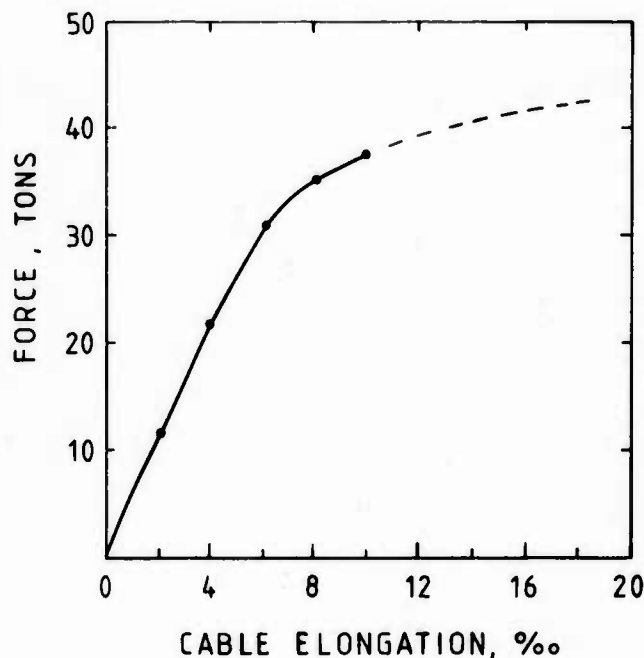


Fig. 5

Measured applied force versus cable elongation for an optical submarine cable of the design shown in fig. 1. When reading this curve it should be noted that the fiber stress free range has been measured to be approximately 1.9%.

In addition to the main requirements discussed in the previous sections, the cable construction has proved to meet other strong requirements very convincing as well.

By backscatter measurements, simultaneous bending around a 3 m diameter wheel and a pulling tension of 10 tons representing an (extreme) field installation situation have been investigated. No change was observed in the backscatter signal neither during nor after the experiment.

In case of multiple bendings back and forth on a 1 m diameter wheel none of the constituting cable layers were damaged at all.

By a practical coiling experiment 300 m of cable was coiled in a 2.5 m loop.

Finally 6 atmospheres of water pressure have been exposed to a cable end for 24 hours. No water at all was observed more than 7,5 m away from the cable end.

To investigate the cable breakage properties a cable tearing experiment was carried out. About 350 m of armoured submarine cable was buried to a depth of 0.75 m in sandy soil. An anchor was

hooked to the middle of the cable and the anchor was torn at a right angle to the longitudinal axis of the cable by using heavy military vehicles. The cable was fixed in both ends using heavy vehicles as well.

During the experiment the load cells at the cable ends read 23 tons at maximum load. The load cell connected to the anchor read 39 tons at break. After cable breakage the force needed to pull the torn cable ends (175 m) longitudinally out of the soil was approximately 4 tons. The longitudinal force experienced by the cable a short distance from the anchor is therefore $(4 + 23)$ tons, corresponding to only 0.6% of cable strain.

Consistently our diagnosis of the torn cable showed that all of the fibers were broken within 0.5 m from the anchor.

However, the force experienced by the cable at a short distance away from the anchor-area at breakage, presumably depends strongly upon the actual conditions such as type/ size of anchor and on speed of breakage. This is the reason for the large safety margin of fiber stress free cable elongation included in our cable construction.

Further, it is emphasized that even if the cable is persistently elongated in a neighbourhood of the position of breakage, the fibers are still completely stress free. Consequently, in cases of breakage of installed submarine cables of this type, it is only necessary to replace short lengths of cable, simultaneously guaranteeing long term stability due to the non stressed fibers.

Conclusion

A newly developed, armoured stranded type optical submarine cable construction has become unique with regard to application in moderately deep, heavily trafficked water areas by increasing the fiber stress free cable elongation to 1.9%.

More than 35 tons of cable tension are required to induce 1% of elongation and 1.9% is necessary to cause fiber elongation.

By pulling in the cable with an anchor to cause a cable breakage, the tension applied to the anchor at breakage was 39 tons. The maximum tension experienced by the cable at a short distance away from the anchor area was determined to be less than 30 tons corresponding to less than 0.6% of cable strain. This had

less than 0.6% of cable strain. This had the important implication that all the fibers were broken within 0.5 m away from the anchor, and this is an extremely satisfactory result.

Theoretically as well as experimentally the construction has proven to meet very strong requirements, specifically with a view to avoiding fiber stress even during and after having exposed extreme external forces, to the cable.

Finally, the developed submarine cable performs most satisfactory with regard to optical and mechanical properties and a large safety margin is included in the construction to assure stable operation for a very long time.

Acknowledgements

The authors are most grateful to the staff of the Danish Posts and Telegraphs for many helpfull and inspiring discussions during this work. We also wish to thank the Danish Industrial Research & Development Fund for their financial support to the project. Finally we wish to thank the Royal Danish Army Combats for their assistance rendered during the cable tearing experiments.

References

1. G. Le Noane and M. Lenoir
Submarine Optical Fiber Cable
Development in France.
Proc. IEEE, 7D.4 (1982)
2. P. R. Bark, U. Oestreich, and
G. Zeidler
Stress-Strain Behaviour of
Optical Fiber Cables
Proc. IWCS, 385 (1979)
3. H. Yamamoto, Y. Namihiro and
Y. Niino
Optical Fiber Unit for Optical
Submarine Cable,
Electr. Lett. 19, 125 (1983)
4. H. Damsgaard
Thermal Properties of Loose
Tube Secondary Coated Optical
Fibers Experimentally Discussed
by a Relative Light Pulse Delay
Technique.
Proc. IWCS, 429 (1983)



Axel Andersen, was born in Køge, Denmark in 1920. He received his M. Sc. degree in Mechanical Engineering in 1946 from The Technical University of Denmark. Since 1948 he has been with NKT working in different research areas such as cable machinery and during the last years development of optical fiber cables.



Lars Grüner-Nielsen
NKT Elektronik
95, Brøndbyvestervej
DK-2600 Glostrup
Denmark

Lars Grüner-Nielsen, was born in Copenhagen, Denmark, in 1959. He received his M. Sc. degree in 1983 in Electrical Engineering from The Technical University of Denmark. In 1983 he joined the R & D department for optical fibers and cables of NKT Elektronik.



Niels Enggaard
NKT Elektronik
95, Brøndbyvestervej
DK-2600 Glostrup
Denmark

Niels Enggaard, was born in Copenhagen, Denmark in 1952. In 1975 he became a Master Electrician and from 1977 to 1983 he was a supervisor for Electrical Installations in different Danish major companies. Since 1983 he has been working as a Technical Specialist in the fiber optic R & D department of NKT Elektronik.



Asger Baungaard
Sørensen
NKT Elektronik
95, Brøndbyvestervej
DK-2600 Glostrup
Denmark

Asger Baungaard Sørensen was born in Urlev, East Jutland, Denmark in 1926. He received his M. Sc. degree in Electrical Engineering in 1952. Since 1953 he has been with NKT working in different research areas such as HV-cables, Electronics, Telecommunication and during the last years optical communication, primarily development of optical fiber cables.



Hans Rosendal
NKT Elektronik
95, Brøndbyvestervej
DK-2600 Glostrup
Denmark

Hans Rosendal was born in Glostrup, Denmark in 1940. In 1968 he received his M.Sc. degree in Electrical Engineering from the Technical University of Denmark and joined NKT working with cable development and design, from 1982 specifically design of optical fibre cables. In 1984 he joined the cable design department of NKT Telecom Cables.



Hans Damsgaard
NKT Elektronik
95, Brøndbyvestervej
DK-2600 Glostrup
Denmark

Hans Damsgaard, né 1956, is a graduate of the University of Aarhus in Physics. Upon graduation he got a PhD-degree from the Technical University of Denmark and NKT, the thesis dealing with the performance of robust optical fibers. Since then he has been working in the optical fibers Research and Development department of NKT Elektronik.

HYDROGEN EVOLVING TENDENCIES OF CABLE FILLERS AND OPTICAL FIBER COATINGS

William E. Dennis, David A. Sierawski, Donald N. Ingebrigtsen

Dow Corning Corporation
Midland, Michigan

ABSTRACT

The attenuation of signal in optical fibers caused by the diffusion of molecular hydrogen into the core of the fiber is well documented. The tendency of thermally curing silicones to initially produce large amounts of hydrogen is also well documented. We have tested a variety of silicones: thermal and UV curing coatings and grease-like cable fillers as well as some non-silicone materials and found that the tendency to generate significant amounts of hydrogen is limited to the class of thermal curing silicones.

This tendency to form hydrogen in thermal curing silicones is due to the residual silicon hydride species which remain after the coating is cured. This silicon hydride reacts with water and other protic compounds to form molecular hydrogen. When this residual silicon hydride has been depleted the formation of hydrogen virtually ceases.

In contrast, the hydrogen generating tendencies of the UV curing silicone coating and silicone cable fillers were no greater than that of carbon based materials.

I. Introduction

The attenuation of signal in optical fibers caused by the diffusion of hydrogen into the core is well documented (1-7) and although the amount of attenuation which occurs can be minimized by the materials used in the cable and the design of the fiber the consensus of opinion is that all sources of hydrogen in optical fiber cables should be eliminated or reduced to a minimum. Consequently the hydrogen generating tendencies of the materials used in the manufacture of optical fiber cables have been investigated. (2,7)

One of the materials which has been examined is the silicone coating used by some manufacturers to provide the primary and microbending protection for optical fibers. The results of these investigations show that thermally cured silicones which have been used as coatings for optical fibers generate significantly higher amounts of hydrogen when exposed to humidity and elevated temperatures than any of the other coatings tested. This has led some investigators to conclude that silicones as a generic family of polymers should not be used in optical fiber cables.

The purpose of this paper is to provide experimental data and chemical evidence to change this conclusion and demonstrate that silicone materials provide significant value to the optical fiber cable when they are properly selected and used. This paper reports measurements of the amount of hydrogen generated by a number of silicone materials in various environments of heat and humidity. The generation of large amounts of hydrogen occurs with platinum catalyzed thermally curing elastomers and not with silicones in general.

II. Discussion

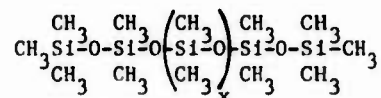
Background

Silicone is a term commonly used by people outside of the silicone industry to describe a family of polymers, usually elastomers, which have good temperature characteristics and environmental stability. In reality the term, silicone, encompasses a broad class of materials which ranges from low viscosity fluids through high modulus elastomers to hard brittle resins.

The silicone materials of greatest interest to the wire and cable industry are: elastomers, which can be used as coatings for optical fibers and, compounds, which can be used as lubricants and water blocking agents.

Chemistry

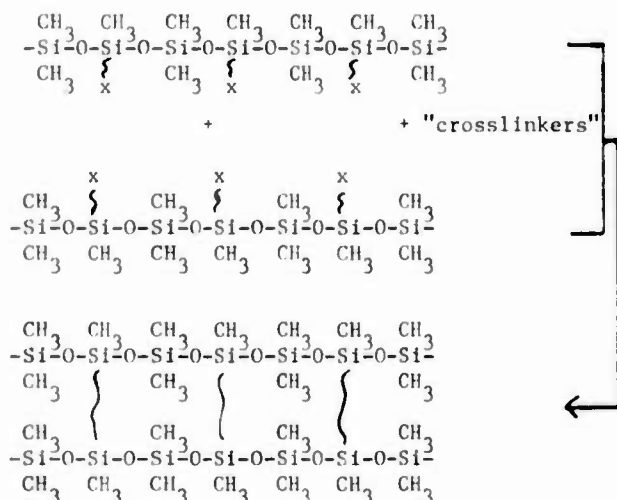
The most common types of silicone materials available commercially are based on polydimethylsiloxane. This is because the chemistry and processing of this polymeric structure are well understood and it is produced from readily available starting materials. Most polydimethylsiloxane polymers are linear and are liquid except at very high molecular weights.



This liquid can be transformed into an elastomer by introducing reactive sites on the chain which can be used to link it to other polymer chains through reactive ingredients called crosslinkers. The modulus of an elastomer is controlled by the number of crosslinks per unit volume and their location in the polymer. This process of converting a liquid silicone mixture

into an elastomer is referred to as "cure".

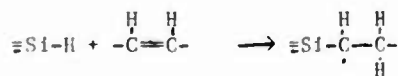
~ x = Reactive Group



The very large number of commercially available silicone elastomers stems from this basic concept of linking polymer chains together. The variety of elastomers comes from the numerous ways of forming this crosslink, and the large number and combinations of fillers, additives, and stabilizers which are used.

The degree of substitution of the methyl groups on silicon by other substituents, the nature of these substituents, molecular weight of the polymer chain and the tertiary structure of the polymer can all be varied. All of these parameters affect the processing, curing, handling, stability and final properties of the elastomer.

One method of curing an elastomer which is widely used in the silicone industry is the addition of a silicon-hydride bond to an olefin or carbon-carbon double bond using platinum as a catalyst. This is referred to as addition cure and it is one example of many ways of curing an elastomer by an addition mechanism.



This method of curing a silicone elastomer has many attributes which makes it useful in a large number of applications:

- 1) There are no low molecular weight by-products formed.
- 2) The volume of the cured elastomer is similar to the uncured volume and there is low shrinkage.
- 3) The cure rate can be accelerated by increasing the temperature.

All of these attributes are important in the coating of optical fibers and consequently this type of silicone elastomer has been used in the coating of optical fibers.

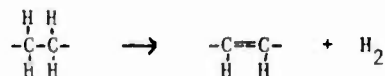
Most, if not all, of the commercially available silicone elastomers which use the addition of a silicon-hydride to an olefin for cure are formulated with an excess of the silicon-hydride above the stoichiometric ratio of olefin. This practice allows the formulator to achieve adequate rates of cure and control of the physical properties. In most applications this small excess of unreacted silicon-hydride is innocuous. Although hydrogen was probably generated in some of these applications no problems were reported until its use in fiber optics. When this type of elastomer is used as a coating for optical fibers this slight excess leads to the formation of a damaging amount of hydrogen in the presence of water.

This formation of hydrogen is due to the hydridic nature of the hydrogen atom attached to silicon. In the presence of compounds containing protons this hydridic hydrogen combines with the proton to form molecular hydrogen. The most common protic compound in the environment is water.



This reaction with protic materials is catalyzed by acids, bases and the platinum catalysts incorporated in the formulation to cure the elastomer. The rate of hydrogen evolution from freshly cured elastomers of this type is quite high, but, when all of the excess silicon-hydride has been reacted the hydrogen evolved from such formulations virtually ceases.

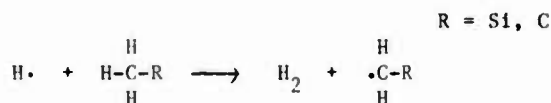
In fact, the hydrogen content of silicone polymers is much lower than that of organic polymers and the number of mechanistic routes possible to the formation of hydrogen are fewer. For example, there are few if any carbon-carbon bonds which contain vicinal hydrogen atoms. These hydrogens in organic polymers can be eliminated in a dehydrogenation reaction to form an olefin and hydrogen.



The hydrogen generation in silicones reported to date has been related to the use of platinum catalyzed, thermally curing elastomers which contain silicon-hydride crosslinkers. It is not a general problem for silicone based materials. Another class of silicones which have been evaluated recently as optical fiber coatings are UV curing silicones. These materials do not depend on the presence of silicon-hydrides for cure and, consequently, would not be expected to form significant amounts of hydrogen. This is also true for many of the room temperature vulcanizing (RTV) elastomers which cure through a condensation mechanism.

Cable fillers should also show low hydrogen generating tendencies since they are non-curing materials and utilize no crosslinkers.

Another source of hydrogen could be from the free radical attack of a hydrogen radical on a hydrogen atom attached to carbon. This reaction mechanism is possible for both silicone and carbon based polymers.



High temperatures are required for this reaction to take place at any appreciable rate and this mechanism does not appear to be significant in most optical fiber applications.

One of the concerns of optical fiber cable manufacturers is the formation of hydrogen from the interaction of moisture with the metallic components of the cable. One route for the transport of water vapor to the metal interface is through the water blocking compound itself. This transport is a function of the solubility of the water in the water blocking compound and the diffusivity of the compound. Water vapor is less soluble in silicone compounds than it is in most organic compounds. Therefore, the concentration of water at the surface of the metal is less and the rate of hydrogen formation from the interaction of water with the metal should be lower.

III. Methodology and Results

The hydrogen generating tendencies of silicone materials were measured in a series of experiments.

Silicon-Hydride Addition Curing Elastomers

In one series, four elastomers which cure by silicon-hydride addition to an olefin were maintained at a variety of temperature and humidity conditions in sealed containers:

- 1) 50% Relative Humidity at Room Temperature
- 2) 75% Relative Humidity at Room Temperature
- 3) 50% Relative Humidity at 70°C
- 4) 95% Relative Humidity at 70°C

The amount of hydrogen which formed after 1 day and 7 days exposure was measured. (See Table I) In all cases except two the amount of hydrogen formed was significant and above the detection limits. Two samples at 50% RH and room temperature did not form significant amounts of hydrogen in one day but had formed hydrogen by the seventh day. The reason for this induction period has not been determined but could be related to the amount of excess silicon-hydride in the formulation, the amount of catalyst and/or the extent of cure.

In many cases, particularly those in which large amounts of hydrogen were generated, the amount of hydrogen measured after 7 days was lower than that measured after 1 day. This is probably due to loss of hydrogen through the septum because of its high diffusivity.

Comparison of Various Silicone Cure Systems

In another series of experiments the amount of hydrogen generated by elastomers which cure by silicon-hydride addition to an olefin, by a condensation mechanism and by UV cure were compared. In this series the samples were maintained at 95% RH for either 24 hrs, 48 hrs or 72 hrs. In this series only the sample which contained silicone-hydride formed a measurable amount of hydrogen. (See Table II)

Rate of Hydrogen Formation from Silicon-Hydride Cure System

In another experiment the rate of hydrogen formation from an elastomer containing silicon-hydride was measured. The elastomer was cured at 140°C for 10 minutes, allowed to cool to room temperature and sealed. The amount of hydrogen generated was measured 24 hrs later and the bottle left open at ambient conditions. Twenty-four hours before each subsequent measurement the bottle was resealed and then left open after the measurement. The initial value was very high and even after 27 days at ambient conditions the amount of hydrogen generated within a 24 hr period was substantial. (See Figure)

Autoclaving of Silicon-Hydride Curing Elastomer

The effect of completely reacting the excess silicon-hydride was determined in a separate experiment. A silicon-hydride curing elastomer was prepared and held at 95% RH for 24 hrs and 96 hrs. The amount of hydrogen which formed was significant and consistent with previous results. This sample was then autoclaved for 1 hr at 175°C and then the amount of hydrogen which it generated was measured after 24 hrs and 96 hrs at 95% RH. The amount of hydrogen decreased but was still above the detection limits. This same sample was autoclaved an additional 4 hrs at 175°C and remeasured under the same conditions. At this time the hydrogen level was below our detection limits. A small amount, 0.5 gm, of a silicon-hydride containing polymer was then added to this sample and it was sealed under the same conditions for 48 hrs. A very large amount of hydrogen was generated. This demonstrates that the system was still capable of forming hydrogen and that the decrease in the amount of hydrogen which was seen after autoclaving was due to depletion of silicon-hydride and not inactivation of the catalyst. (See Table III)

In a similar experiment, a dimethylsiloxane fluid containing platinum catalyst and another containing both platinum catalyst and a silicon-hydride polymer were maintained at ambient conditions in sealed containers for 48 hrs and then analyzed for hydrogen. Hydrogen was not detectable in the fluid without the silicon-hydride polymer but the sample with it contained >19 µgm of hydrogen/gm of sample.

Comparison of Silicone and Organic Water Blocking Compounds

In another series of experiments silicone compounds and organic water blocking agents were exposed to:

- 1) 50% Relative Humidity at Room Temperature
- 2) 75% Relative Humidity at Room Temperature
- 3) 95% Relative Humidity at Room Temperature
- 4) Ambient Conditions at 70°C

A total of 6 cable filling materials were used, 3 silicone compounds and 3 organic compounds. None of the materials generated a measurable amount of hydrogen under any of the conditions after 1 day and 7 days exposure.

IV. Conclusions

Silicone materials which do not contain silicon-hydride bonds do not form large amounts of hydrogen when exposed to high humidity. Silicone elastomers which do contain silicon-hydride bonds form large amounts of hydrogen under the same conditions. The excess silicon-hydride which remains after cure is the source of this hydrogen and when this species is removed by reacting it completely the generation of hydrogen ceases.

Silicone elastomers which cure by mechanisms other than silicon-hydride addition to olefins are more appropriate for applications like the coating of optical fibers which are very sensitive to hydrogen. The best candidate is a silicone elastomer which cures rapidly by exposure to UV radiation. The standard RTV elastomers cure too slowly. Another approach would be to completely remove any residual silicon-hydride species from the thermally curing silicones after cure or formulate such elastomers so that they do not contain an excess of silicon-hydride. However, the safest approach is to avoid the problem completely by using silicone elastomers which do not contain silicone-hydride.

V. Experimental

Sample Preparation and Handling

All elastomers were cured using the recommended ratio of curing agent to base polymer and the recommended cure conditions.

All of the investigations with elastomeric materials used 50 ml. serum bottles as the container both for curing the elastomer and monitoring the hydrogen generation except for the UV curing silicone elastomer which was cured as a thin coating and then scraped into the serum bottles. In all other cases the serum bottles were left open during the curing reactions. The samples were maintained under various exposure conditions and then the bottles were sealed with a Teflon backed silicone disc using an aluminum crimp cap during the monitoring of the hydrogen generation. The samples of materials weighed between 4 and 12 grams.

The gases in the head space were analyzed by withdrawing a 0.2 to 2.0 cc sample using a gas syringe. These gases were analyzed by gas

chromatography using a gas chromatograph equipped with a thermal conductivity detector and a 1/8" x 8' stainless steel column containing 5 Å 60/80 mesh molecular sieves. Nitrogen was used as the carrier gas. The peak heights of the elutants were measured and compared with known standards.

The viscous compounds and cable filling materials were added to 1 oz. vials and sealed with rubber septums. Sampling of the gases in the head space were performed in the same manner as the elastomers.

Calibration

External calibration was used to determine the response factor of hydrogen in each series of samples.

A well characterized silicone polymer containing approximately 2 micrograms (μgm) of hydrogen per gram was used as the standard. This standard was weighed into a 00 size gelatin capsule, then placed inside a 000 size capsule. The double jacketed capsule was placed in a 50 ml serum bottle containing 15 mls of aqueous alcoholic potassium hydroxide and immediately sealed. Four to five mls of the headspace gas was removed with a syringe to allow for expansion of the hydrogen gas. The bottle was inverted to prevent hydrogen from diffusing through the rubber septum. After the capsule dissolved the bottle was placed in an oven at 60°C for 30 minutes. When the bottle had cooled to room temperature, nitrogen was bled into bottle until it was at atmospheric pressure. The gas in the headspace was removed and measured as described above. A response factor was calculated based on the volume of the headspace, the amount of silicon-hydride present and the height of the hydrogen peak in the gas chromatogram.

References

- 1) Beales, K. J., Cooper, D. M. and Rush, J. D., Electron. Lett. 1983, 19, pp. 917-919.
- 2) Uchida, N., Uesugi, N., Murakami, Y., Nakahara, M., Tanifuji, T. and Inagaki, N., Post Deadline Paper 9th European Conference on Optical Communication, Geneva, Switzerland, October, 1983.
- 3) Noguchi, K., Murakami, Y., and Ishihara, K., Electron. Lett., 1983, 19, pp. 1045-1046.
- 4) Murakami, K., Noguchi, K., Ishihara, K., and Negishi, YI, Electron. Lett., 1984, 20, pp. 227-228.
- 5) Kimura, T. and Sakaguchi, S., Electron. Lett., 1984, 20, pp. 315-317.
- 6) Ogai, M., Orimo, K., Kamiya, T., Takashina, N., and Azuma, M., Post Deadline Paper, W12, Optical Fiber Conference, January, 1984, New Orleans, Louisiana.

- 7) Mies, E. W., Philen, D. L., Reents, W. D., and Meade, D. A., Post Deadline Paper, W13, Optical Fiber Conference, January, 1984, New Orleans, Louisiana.

Table I

Hydrogen Generation of Silicone-Hydride Addition Cure Elastomers

Elastomer	Micrograms of Hydrogen Evolved per Gram of Sample			
	50% RH Room Temp.	75% RH Room Temp.	50% RH 70°C	95% RH 70°C
A				
1 Day	<0.008	0.084	0.66	0.72
7 Days	0.060	0.084	1.26	1.40
B				
1 Day	0.058	0.28	0.56	0.82
7 Days	0.072	0.062	1.04	0.70
C				
1 Day	<0.010	0.14	0.52	0.62
7 Days	0.090	0.068	0.78	1.02
D				
1 Day	2.24	2.64	9.52	12.58
7 Days	1.18	2.10	5.84	10.44

Table II

Hydrogen Generation of Different Elastomers Exposed to 95% RH

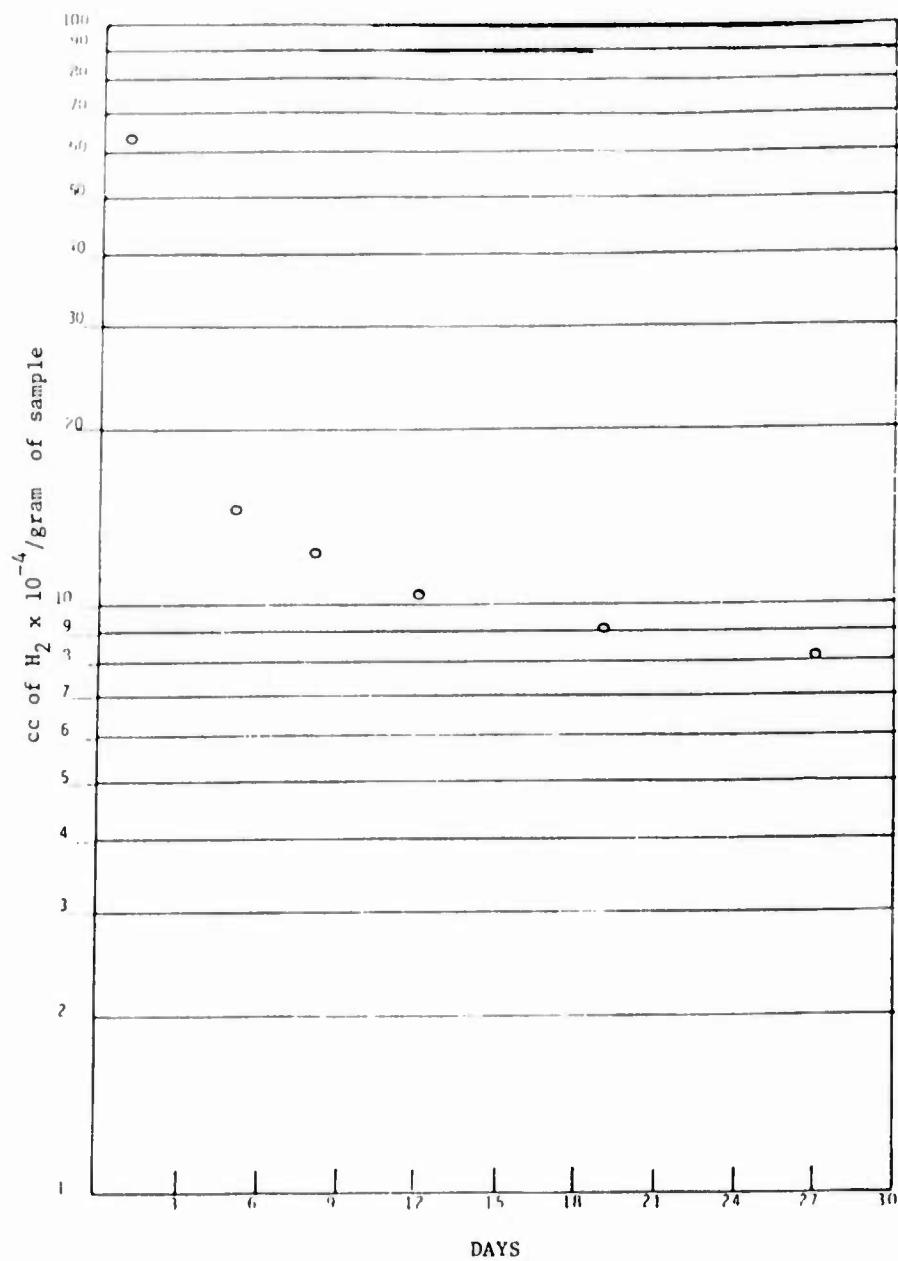
Elastomer Type	Micrograms of Hydrogen Evolved per Gram of Sample		
	24 hrs.	48 hrs.	72 hrs.
C - Thermal Cure (Si-H Addition)	0.114	-	0.036
E - 1 Part RTV (Condensation)	<0.004	-	-
F - 2 Part RTV (Condensation)	<0.004	-	-
G - UV Cure	-	-	<0.006

Table III

Hydrogen Generation of an Si-H Elastomer After Autoclaving

Condition	Micrograms of Hydrogen Evolved per Gram of Sample	
	24 hrs at 95% RH	96 hrs at 95% RH
As Cured	0.054	0.172
After 1 hr Autoclave 175°C	0.030	0.048
After 5 hrs Autoclave	<0.0046	<0.005
*After Si-H Addition	6.28	-

RATE OF HYDROGEN FORMATION
VS. TIME FOR AN ELASTOMER
CONTAINING SILICON-HYDRIDE





William E. Dennis received a B.S. degree in Chemistry from Alma College in 1962 and a Ph.D. in Synthetic Organic Chemistry from Wayne State University in 1966. He has worked for Dow Corning since 1966 in various research and development laboratories. He is currently a Specialist working with silicone materials designed for the optical fiber and cable industry. He is a member of The American Chemical Society, Sigma Xi, and The Optical Society of America.



Donald N. Ingebrigtsen received his B.S. degree from Valparaiso University in 1951 and an M.S. degree in Analytical Chemistry from the University of Iowa in 1953. He has been with Dow Corning for over 31 years starting in 1953 as an Analytical Chemist in the methods development group. He has supervised several different groups during this time including quality assurance, process stream development, spectroscopy and chromatography sections. At the present time he is an Associate Scientist in Analytical Research where he is involved with special projects and problem solving.



David Alan Sierawski received his B.S. in 1971 and M.S. in 1973 from the University of Missouri-Rolla in 1973. He joined Dow Corning upon graduation in their Consumer Products group at Greensboro, North Carolina. In 1975, he transferred to Electrical/Electronics Technical Service and Development in Midland, Michigan, where he is presently working. His major product developments have been for silicone caulks, fire resistant foams, protective coatings for semiconductor devices and fiber optics.

QUALIFICATION TESTING OF FIBER OPTIC CABLES

Ronald Ohlhaber, Purita Angeles
and Ted Ulijasz

Belden
Technical Research Center
2000 S. Batavia Ave.
Geneva, IL 60134

SUMMARY

This paper discusses tests required to assure both operation and survival of fiber optic cable in various environments. It covers various qualification testing associated with the fibers and cable structures. These tests include temperature cycling, tensile loading, flexing, flammability and impact resistance for optical fiber and cable. The results of these tests are presented in some detail. Also discussed is the nature of the test procedures. The data show that extensive testing of various properties is essential to assure satisfactory operation.

INTRODUCTION

Fiber optic cables must survive a variety of adverse conditions and continue to transmit a certain level optical signal. A series of environmental, mechanical and optical tests for qualification, are typically employed to assure the cable meets operating requirements. Currently there exist over 50 different tests that can be specified for cable qualification. However, for most cables the real world conditions before and after installation never approach the test levels required during the qualification.

One exception is temperature exposure where what may appear as satisfactory qualification testing can be misleading since cables can experience more severe environments. For example, cables designed for indoor applications may be transported by unpressurized cargo aircraft where the temperature drops to -55°C or they may be stored in desert warehouses with temperatures of over 60°C (140°F). Such unforeseen temperature conditions are a common occurrence.

Qualification testing, in addition to assuring that the cable meets suitable operating requirements, is often used as the criterion for cable selection. Consequently, the results of such testing can be critical to cable marketability.

This paper describes temperature testing for both the fiber and cable. The results indicate that certain fiber and cable require exten-

sive testing to assure that irreversible adverse effects do not affect their operation. Flammability is also described with suggested methods for screening cables before performing extensive flame tests. Basic mechanical tests are also discussed with emphasis on variations resulting from the test methods employed.

FIBER QUALIFICATION

At present there exist over 30 specific tests for optical fibers. Probably the most critical test is optical transmission over a required temperature range, because of the physical effect elevated temperatures can have on plastic material dimensions.

Today the most stable and widely used fibers are of graded glass core and glass cladding construction. The glass portion of these fibers has an extremely large temperature range. However, the fiber must have a protective outer plastic coating. This results in limiting the operating temperature range.

While all glass fibers are protected by their outer coating, it is still typical to have less than 0.3 dB/km attenuation change over the -60° to 85°C range. Testing for such performance involves placing the fiber in a chamber where the temperature can be suitably controlled. As part of this test it is necessary to assure that the fiber will remain free from mechanical stress and will not be affected by sharp bends, frost or other temperature-induced external factors.

Plastic clad silica fibers (PCS) are more susceptible to temperature since the refractive index of plastic which is used to contain and guide the optical radiation changes with temperature. For cladding materials such as common silicones, the refractive index increases with lower temperatures, thereby causing the fiber to lose its optical transmission properties at some point below freezing. Heat can also affect the plastic refractive index or darken the plastic by producing absorption centers.

Due to such conditions it becomes extremely important to exten-

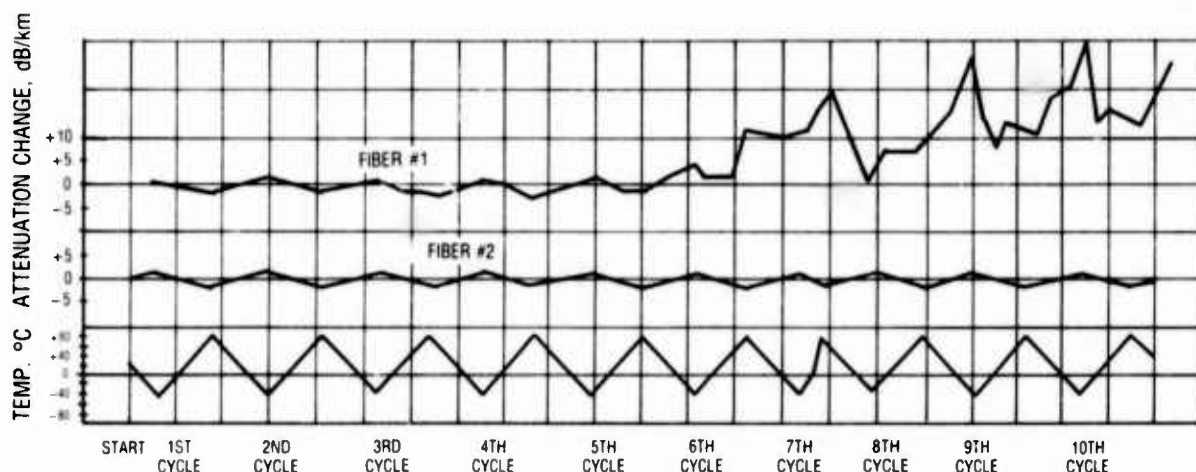


Figure 1. Temperature cycling test for two optical fibers from different production lots.

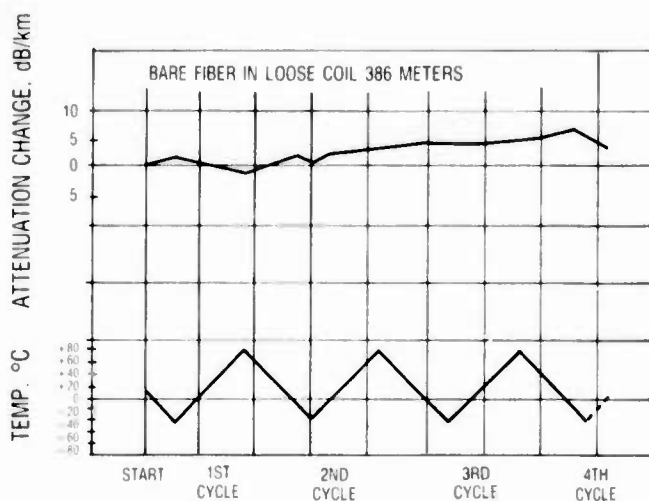


Figure 2. Temperature cycling of a 386m fiber sample.

sively test these fibers. Figure 1 shows a typical -40 to +80°C cycling test and the associated transmission for two optical fibers of the same construction, but from different manufacturing lots. After the sixth cycle Fiber No. 1 starts to exhibit an increased attenuation; this increases to above 10 dB/km for all temperatures thereafter.

Delayed responses like the foregoing are common when resulting from changes in the plastic cladding. Figure 2 shows a similar result for another fiber where only two cycles were required to obtain a marked change in transmission. Usually this indicates that heat aging is affecting the fiber. This can be more readily identified by directly heat aging the fiber as in the test results presented in Figure 3. Here two fibers were held at 80°C and 100°C while being compared to a reference fiber at room temperature. The test showed the aging period results in decreased transmission when returned to room temperature.

Such variations have been found with all types of fibers due to various coating defects or incomplete curing of the coating materials. Most important to the resulting cable is that the testing must expose the fibers to conditions that will simulate worst case lifetime conditions. For this reason, both temperature cycling and long term temperature testing is necessary.

CABLE TEMPERATURE TESTING

Successful temperature qualification of the fiber does not guarantee its performance in a cable structure. Cables can exert forces on fibers that result in fiber bending or elongation which increases the optical attenuation. The mechanism generating these forces at various temperatures depends on the specific cable.

Loose buffer tube or slotted core cables are generally affected by extremely low temperatures where an excess of fiber results in microbending. Tight buffer cables can have an equivalent effect when the fiber is contained by materials which become more rigid as the temperature decreases.

Other effects such as high temperature shrinkage of the plastics can also change the cable's length with respect to the optical fibers. Because of these factors both temperature cycling and extended storage temperature tests are required. In addition, temperature shock tests should also be employed to assure that no structural slippage effects are possible.

Temperature cycling tests are a critical indicator of cable performance. Any shifting of the fiber attenuation values from cycle to cycle indicates some physical change. Figure 4 presents the testing for a cable where there is a continual degradation in performance over the first four cycles. For this cable it appears that each cycle to +80°C results in shrinkage that causes the optical attenuation at cold temperatures to increase. For such a cable, a storage temperature test at 80°C for 240 hours should effectively indicate any problems.

In addition to simple monitoring of the optical attenuation it is also possible to determine if localized regions are responsible for any increases. This can be caused by regions in loose buffer tube cables where the amount of excess fiber varies. A similar condition exists

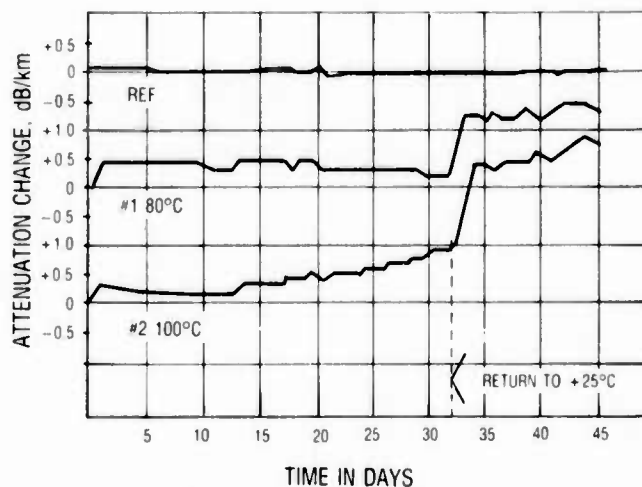


Figure 3. Heat aging effect on the optical transmission of a fiber sample held at three temperatures.

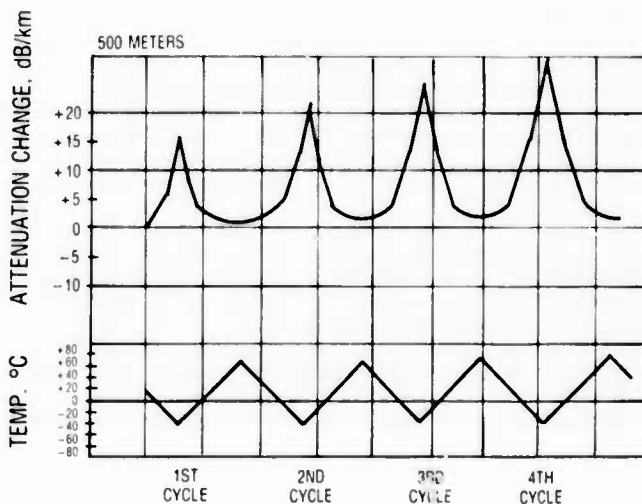


Figure 4. Optical cable temperature testing while monitoring fiber transmission.

in tight buffer constructions if the fiber letoff tensions vary during cabling. For both cable types the effect is evident when exposing the cable to a low temperature near the point where increased attenuation is exhibited.

The method of observation is to employ an optical time domain reflectometer (OTDR) for attenuation measurements. Photographs of the OTDR traces from two experimental cables, one with uniform and the other with nonuniform excess fiber distribution, are shown in Figure 5. The upper scope photo is for the normal uniform fiber, indicating a less than 3 dB/km attenuation for the 2.1 km fiber length at -45°C. The lower photo is for a fiber which has regions of excess length causing an increased slope and correspondingly higher attenuation. In this case, the 2.1 km fiber has a total attenuation on the order of 12 dB, but regions with the original 3 dB/km attenuation also exist.

Uniform fiber distribution is critical since the amount of fiber excess can quickly affect the attenuation. This results from the nonlinear increase in attenuation with the percent of fiber excess as indicated in Table 1 for a loose buffer tube construction. While the values given are for 1 km fiber length, the change in fiber excess from 0.2 to 0.3% results in almost four times increase in attenuation. Consequently,

localized regions where higher excess values exist can cause major changes in performance.

Table 1. Optical Attenuation Variation with Fiber Excess

Percent Effect Fiber Excess	Increase in Optical Attenuation
0.0	0.0 dB/km
0.1	0.3
0.2	4.0
0.3	15.0

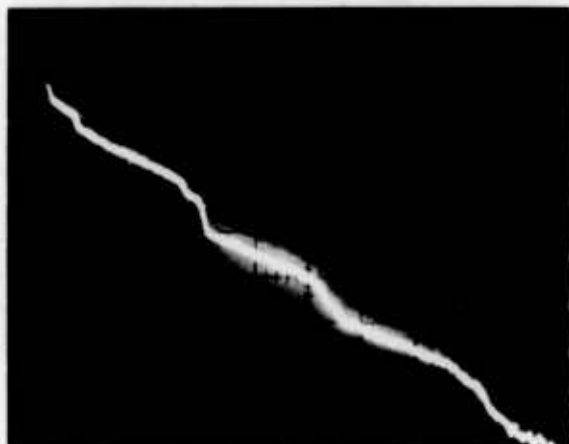
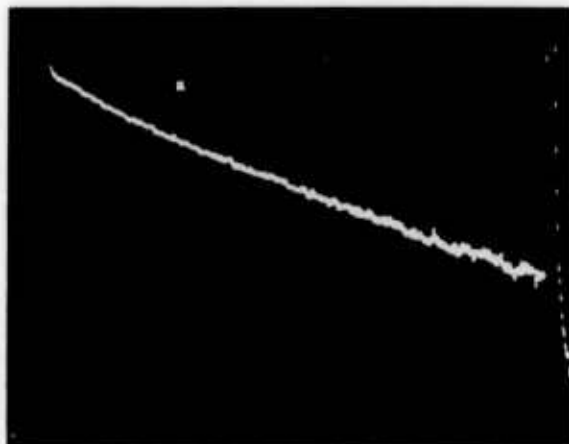


Figure 5. Photographs of OTDR measurements for a uniform fiber (top) and a fiber with regions of excess length (bottom) at -45°C.

TENSILE STRENGTH

Cable tensile strength can usually be predicted with a high degree of accuracy by calculating the elongation force for the strength members needed to produce a predetermined maximum elongation of the optical fibers. While tensile loading may not alter transmission it must be considered for installation and potential long term effects.

When employing strength members such as braided Kevlar*, the braid structure can result in different elongation performance. Figure 6 shows a 40% elongation variation when using different Kevlar strand lay angles (picks per inch, PPI). Such variations in design must be considered for suitable cable properties.

*Registered Trademark of E.I. DuPont

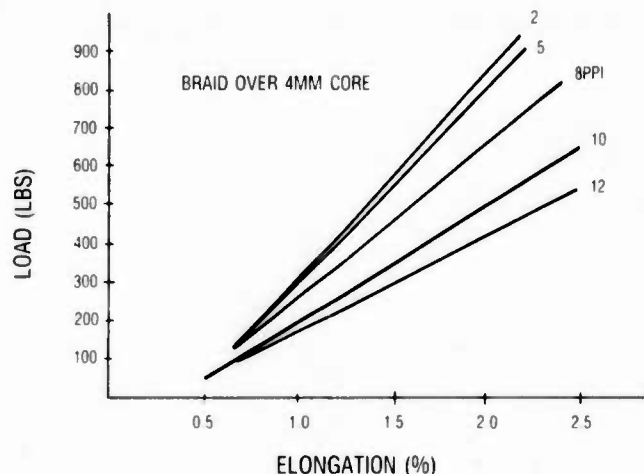


Figure 6. Cable elongation due to tensile loading for different braid angles (PPI).

Tensile testing is possible using short lengths with an Instron unit. The unit shown in Figure 7 has the cable wound around mandrels for clamping. This test generally provides accurate results for cables under 4mm O.D., but for larger cables the breaks appear at the mandrels. The reason for such breakage is that the tension is not uniformly distributed across all the strength members at the curve on the mandrel.

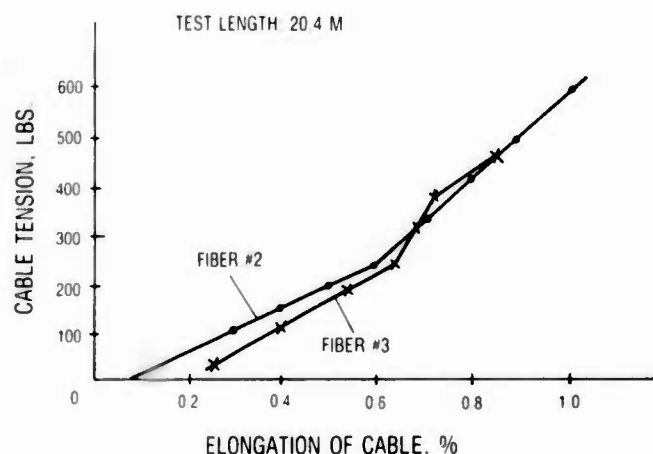


Figure 7. Tensile testing of cables using a short gage length.

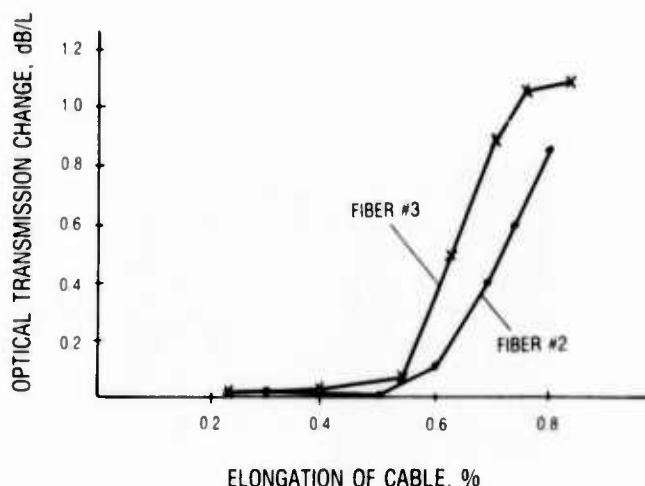
Large diameter cable tension testing is better done on equipment where longer distances and large sheaves are employed. Here the cables may be pulled by Kellems grips. Tests on this equipment have yielded results which confirm the loading expected by Kevlar strength members.

In addition to monitoring the fiber transmission it is also possible to measure the actual fiber elongation. This assures that the attenuation increase is due to the cable elongation and not from crushing at the regions being gripped. The monitoring system consists of modulating an optical emitter at a frequency such as 57 MHz and detecting the fiber output with an electro-optic interfaced vector phase voltmeter. An electrical reference signal is supplied by the emitter unit.

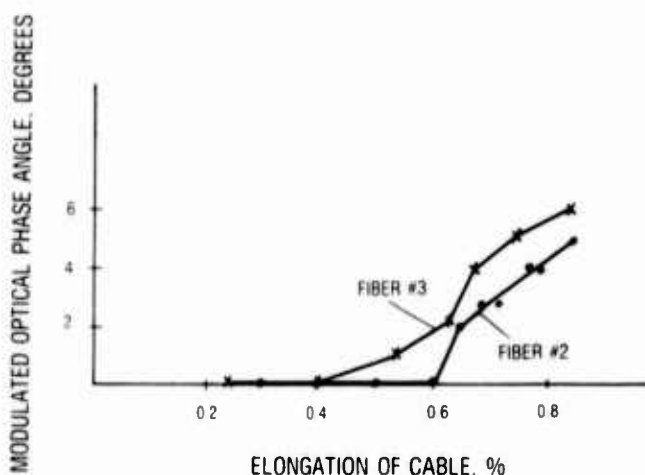
Figure 8. Tensile testing with a 20.4 meter sample length of loose buffer tube cable.



a. Cable tension and resulting elongation.



b. Change in optical transmission with cable elongation.



c. Shift in phase angle due to cable elongation.

to the voltmeter and any shift in phase can be related to a change in the fiber propagation length. The propagation length in the fiber increases as the fiber is stretched due to tensile loading inside the cable.

Figure 8 presents test results for a multifiber loose buffer tube cable construction where a 20.4m length was placed under load. Initially the cable elongation was plotted with respect to the pulling tension showing the expected linear relationship. During this test, both fibers' optical attenuation increases after approximately 0.5% elongation as shown in Figure 8b. Confirmation of this elongation is demonstrated by a corresponding change in the modulated signal phase angle seen in the data on Figure 8c. This confirms that after an initial elongation of 0.5% the fibers begin to experience tensile loading and extend in length. Such testing is extremely valuable in assuring adequate cable strength and performance.

FLAMMABILITY

Cables for indoor applications are currently designed to pass various flammability requirements such as UL VW-1, IEEE-383 70,000 BTU/hr. and UL-910 (Steiner Tunnel Test). The ability of a cable to pass a given test depends on its construction and materials.

The VW-1 or vertical flame test is the easiest to perform since the samples are typically mounted in a laboratory hood while exposed to repeated applications of a burner. Criteria for passage are failure to burn upward to a flag and no dripping of burning material.

When performing this test the outer jacket generally plays a major role in causing the flame to extinguish and in the prevention of burning droplets. For this reason, it is necessary to assure that samples with the minimum and maximum jacket wall thickness are tested.

The 70,000 BTU/hr flame test is more complex in that sufficient cable must be employed to cover an 8 foot long, 12 inch wide ladder. A 10 inch wide burner and a large enclosure are required. During the test considerable cable is generally consumed by the burner flame.

Due to the cost associated with this test, it is possible to prescreen cable samples by burning a group of 18 inch long samples in a vertical position. Table 2 presents the results for 5 cables of 3mm O.D. with similar core materials and different jackets. By measuring the flame heights, jacket damage and flame propagation time during application of the burner, it is possible to evaluate these cables for the possibility of passing IEEE-383.

Table 2
Screening for 70,000 BTU/hr Flame Test

Sample	Flame Height (in)	Jacket Damage (in)	Flame Propagation Time (Min.)
A	10	7	1.5
	11	7	2.0
B	12	7.5	1.5
	12.5	8.0	1.5
C	14	10	2
	14	10	2.5
D	15	12.5	3.5
E	20	15	2.5

This screening test was then followed by an actual 70,000 BTU/hr test in which samples A and B passed, while C, D and E failed. Use of the screening technique permits a rapid and considerably less costly evaluation of cable designs.

The UL-910, Steiner Tunnel Test requires still more extensive facilities. Here a special duct-type tunnel structure is required with approximately 250 meters of cable per test. Passage of the test requires both low flame propagation and low smoke.

At present there is no simple screening method for the UL 910 Test. Table 3, however, indicates the variation between a cable composed of PVC inner members with an outer fluorocarbon jacket and a totally fluorocarbon cable. Based on these data and tests with a radiant heat chamber described by C.J. Arroyo, which measures smoke emission

and thermal flux in the sample, there is some potential to provide initial screening methods.¹

Table 3
Steiner Tunnel Test Results on a
Two-Fiber Optic Cable

Sample	Jacket Material	Flame Spread	Peak Optical Density	Average Optical Density
A	PVC inner and fluorocarbon outer	19.5	1.34	0.30
B	Fluorocarbon inner and outer	1.5	0.02	0.01

As was previously mentioned, the ability of a particular cable style to successfully pass any of these tests is a function of the construction and amount of materials employed. Consequently, it is critical that the quantity of material and dimensional tolerances are considered so that samples with the same volumes of plastics are tested.

MECHANICAL TESTING

Tests for a cable's survival under mechanical forces are critical to its lifetime and operation. The ability to pass crush, impact and bend tests depends on the cable's physical ruggedness. These tests also must be carefully performed to assure accurate results.

Crush tests on multifiber cables can often be misleading when a short length plate is employed. Figures 9 and 10 show the range of forces possible to induce the various levels of attenuation.

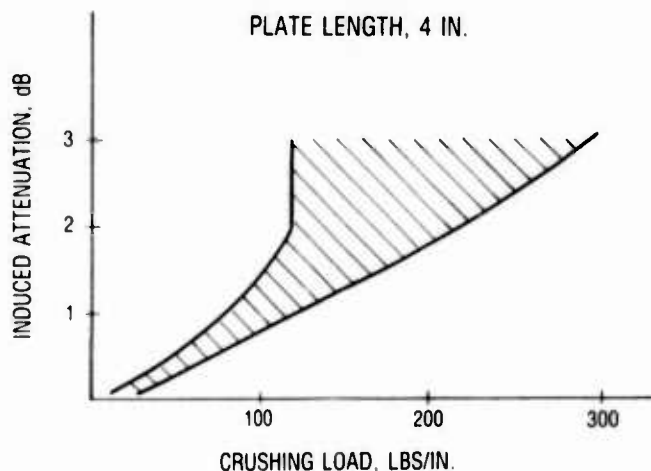


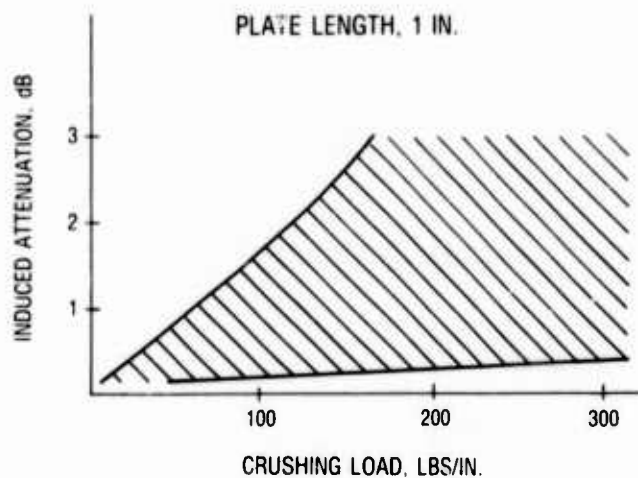
Figure 9. Crush testing a six fiber cable with a 4 inch long plate.

By extending the plate length to 4 in., the crush load variation range is considerably reduced since the fiber under test is more likely to experience a portion of the loading. Thus the range for a 3 dB induced attenuation has changed from 150 to 10,000 lb/in. with the 1 in. plate to only 125 to 300 lb/in. with a 4 in. long plate. However, in both cases the minimum load is in the 125 lb/in. range. This means that careful testing of cables with a 1 inch plate is usually satisfactory providing the cable is suitably orientated.

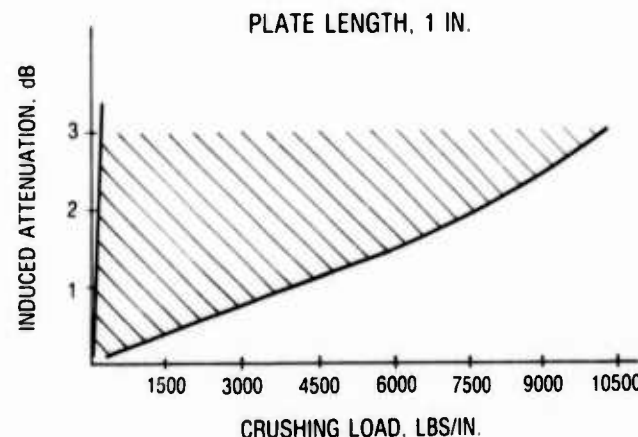
An alternative to this test is to monitor transmission of all fibers and thereby establish the worst case condition. This means a far more complex experimental apparatus.

Impact testing is similar to crush testing when dealing with multifiber cables; for the results will vary with the fiber being monitored. Once again a number of tests with different cable rotational orientations is required to arrive at realistic results.

Although cable flex and twist bend tests produce results which depend on the fiber monitored, other effects can vary the results. Here it is important to assure that no cable slippage occurs. One method



a. Lower load level results.



b. Complete region of test results.

Figure 10. Crush testing a 6 fiber cable with a 1 inch long plate.

to prevent this is to mark the cable jacket. The jacket should also be examined to assure that there is no internal bunching; this is a sign that fiber damage may result.

After bending and flexing, the cable jacket can be removed to establish inner damage or movement of the various members. A cable which had major shifting of the Kevlar braid is shown in Figure 11. Its braid had an initial excessive lay length that caused movement of the strands. This situation can be corrected by increasing the number of picks per inch during the braiding operation.

CONCLUSION

Complete evaluation of fiber optic cables requires not only testing a wide variety of parameters but also depends on the methods and number of tests employed. To assure consistent performance over the operating range and after storage at various temperatures it is necessary to perform a number of test cycles across these ranges. Flammability and mechanical tests require a representative sample and monitoring of the correct fiber. While a limited number of typical qualification tests have been discussed in this paper, the principles set forth apply to many other similar measurements when dealing with cable constructions.

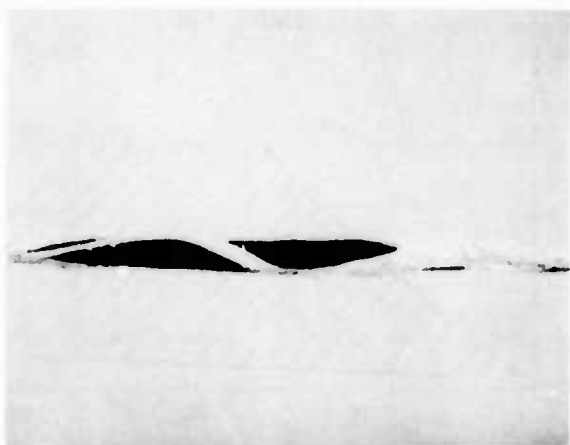


Figure 11. Cable with displaced Kevlar braid after flex testing.

Reference:

1. C.J. Arroyo, N.J. Cogelia, R.J. Darsey, "Thermal Behavior of Experimental Plenum Cable Sheaths Determined in a Radiant Heat Chamber," International Wire & Cable Symposium Proceedings, 1981.



Ted Ulijasz received a B.S. Degree in Physics (1969) and M.S. Degree in Electronics Engineering Technology (1974) from Northern Illinois University. Ulijasz is a Belden Product Development Engineer with responsibilities for fiber optic cables and associated components. These comprise optical links for communications, control, and data transfer. Prior to joining Belden, Mr. Ulijasz worked in Engineering for The Fermi National Accelerator Laboratory in Batavia, Illinois.



Purita Angeles received a B.S. in Chemical Engineering from the University of the Philippines. She joined Belden in 1980. She is now a Product Development Engineer for Fiber Optics at the Belden Technical Research Center in Geneva, Illinois.



Ronald Ohlhaber received a B.S. Degree in Physics from Loyola University and a M.S. Degree, also in Physics, from DePaul University in 1965. He is presently the Product Development Manager for Fiber Optics located at Belden's Technical Research Center in Geneva, Illinois. Prior to joining Belden, he was engaged in fiber optic and electro-optic research as a staff member at the IIT Research Institute. He has worked in similar areas for government and industry.

Prevention of Hydrogen Gas Induced Loss in Optical
Fibers by Proper Lightguide Cable Design

D. L. Philen and C. H. Gartside, III
AT&T Bell Laboratories
2000 Northeast Expressway
Norcross, Ga. 30071

ABSTRACT

Hydrogen gas generated by aging or corrosion of lightguide cable materials may enter the optical fibers causing an increase in attenuation. The mechanism for this loss increase is explained, and it is shown that the key to avoiding this problem is the proper selection of materials and construction techniques in the cable design.

INTRODUCTION

It is now widely recognized that molecules such as hydrogen can diffuse into optical fibers [1-3]. An optical fiber that has been saturated in an atmosphere of hydrogen will show a broad loss increase of about 6 dB/km at 1.24 microns, and 0.2 dB/km at 1.31 microns due to absorption by molecular hydrogen [4,5]. This loss increase is reversed when the hydrogen atmosphere is removed and the absorbed hydrogen outdiffuses. However, hydrogen gas that has diffused into the fiber may also chemically react with constituents of the fiber. This can result in a permanent loss increase at 1.38 microns (Si-OH), 1.41 microns (Ge-OH), and 1.6 microns (P-OH). The sensitivity of fibers to these loss increases has also been linked to high levels of phosphorus in the fibers [6]. Fibers that contain abnormally high levels of phosphorus (8%) tend to react with hydrogen at elevated temperatures to produce permanent loss increases. The 1.41 and 1.6 micron absorption bands overlap in the long wavelength region to cause unacceptable loss increases at 1.55 microns [7,8]. Both temporary and permanent loss increases can be prevented through careful cable design resulting in negligible hydrogen gas generation.

CABLE DESIGN

For both multimode and single mode fibers, AT&T Technologies manufactures lightguide cables based on two design concepts - ribbon and stranded fiber type cables. As illustrated in Figure 1, lightguide ribbon cables are based on packaging 12 fibers between two adhesive backed polyester tapes [9].

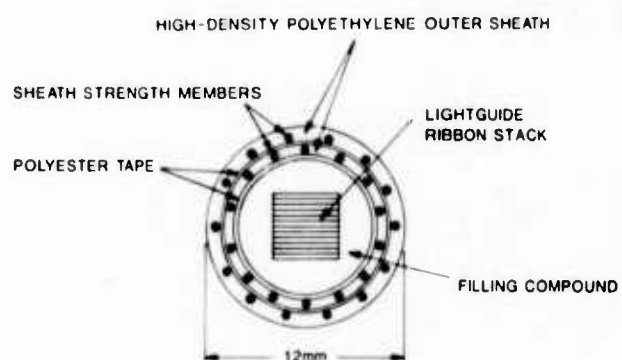


FIGURE 1. LIGHTGUIDE RIBBON CABLE

Up to 12 ribbons may be stacked into a rectangular array for fiber counts as high as 144 per cable. After twisting the ribbons, a loose plastic tube is extruded over the core. Finally, a steel reinforced high density polyethylene sheath is applied over the core tube. The steel wires are applied helically in a cross-ply construction, yielding a torque balanced cable. Metal layers in a polyethylene oversheath may be used to provide protection against rodent and lightning damage (RL sheath). The cable is available with factory installed array connectors allowing for rapid mass splicing for both multimode and single mode fibers [10]. Individual fiber splicing is also possible. Multimode systems are available with operating wavelengths of 820nm and 1300nm. The single mode systems are available with an operating wavelength of 1310nm with upgrade capability at 1550nm.

The stranded cable designs are based on a stranded-fiber unit type construction [11,12]. The unit consists of fibers helically stranded around a fiberglass strength member contained within a plastic tube. The tube is filled with a soft filling compound, providing a water-blocked design and fiber buffering from microbending. Cables are manufactured with units containing between 4 and 16 fibers and one, three, and six units per cable core to give fiber counts ranging from 4 to 96 per cable. A variety of sheath designs are available to meet various field conditions. These include: low friction steel reinforced sheaths for duct installations, non-metallic reinforced sheaths and sheaths incorporating corrugated copper and stainless steel layers, providing lightning and rodent protection.

Figure 2 shows a single unit cable accommodating up to 16 fibers. The polyethylene sheath is reinforced with two layers of steel wires and also contains a bonded flat copper or aluminum layer for lightning protection. While the standard production of this design uses copper, acceptable performance using aluminum has also been demonstrated, as shown in this paper.

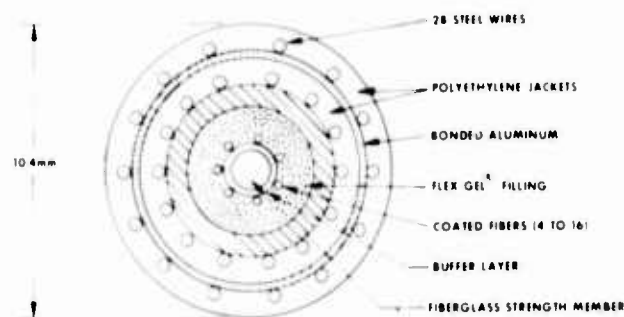


FIGURE 2 SINGLE UNIT CABLE - CROSSPLY SHEATH WITH ALUMINUM SHIELD

In figure 3, a three unit construction containing between 18 to 48 fibers is illustrated. This cable contains corrugated copper and stainless steel layers.

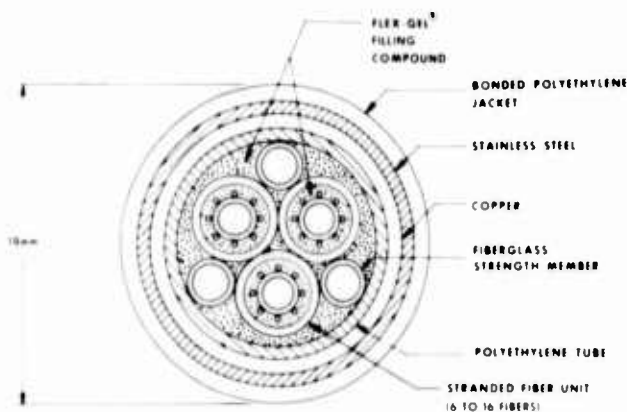


FIGURE 3 THREE UNIT CABLE - RL SHEATH

In evaluating the potential for hydrogen induced loss, the materials used in these designs field testing over a period of three years was carried out on ribbon cable.

MATERIAL TESTING

One possible source of hydrogen production is the decomposition of materials during cable aging. Since the effects of material decomposition are not usually apparent until after many years have elapsed, there is an obvious need for proper accelerated aging tests. Accelerated aging can be accomplished by monitoring the hydrogen evolved from cable materials at high temperatures. Testing should also be performed on the complete cable samples since synergistic effects may produce hydrogen even though the individual materials do not. The temperature level of testing must also be chosen carefully since reactions that proceed at high temperatures such as 200 degrees Celsius, are often times insignificant under normal operating temperatures. Based on such high temperature tests, many desirable and acceptable materials could be needlessly excluded. Instead, the complete cable structure should be examined at several temperatures in the region of 75 to 200 degrees Celsius. By use of an Arrhenius plot (log of rate vs. $1/\text{Temp}$), a rate of hydrogen production at the expected operating temperature may be obtained. One may then calculate a hydrogen pressure expected at the end of the cable life.

The materials used in AT&T Technologies cables as well as possible alternate materials have been tested and the equilibrium partial pressure (in atm of hydrogen) at 40 degrees C after 20 years has been estimated. The estimates are listed in Table 1. These estimates are based on an Arrhenius plot and the conservative assumption that no hydrogen diffuses out of the cable. That is, a worst case, totally sealed system. Based on the results of Table 1, the partial pressure of hydrogen in the cable caused by material decomposition is negligible. However, the data clearly shows that silicone should not be used as a fiber coating since in these tests, it produced several orders of magnitude more hydrogen than any other material. For the cables shown in Figures 2 and 3, despite detectable amounts of hydrogen being evolved at 200 degrees Celsius, hydrogen generation at typical service temperatures such as 40 degrees, would produce a negligible accumulated hydrogen pressure - less than 0.0001 atmospheres after 20 years. (Even though local temperatures may reach 75 degrees under some conditions, the time weighted average of such exposure is 40 degrees Celsius.)

TABLE 1

MATERIALS	PRESS. HYDROGEN (atm) at 40 degrees and 20 years
Fiber Coating	
Silicone*	5.5
Nylon*	6 X10-4
Urethane Acrylate	2.6 X10-9
Desolite**	<1.3 X10-9
Strength Member	
Glass/Epoxy	<3.6 X10-8
Steel	N/A
Strength Member Buffer	
SEBS	<1.8 X10-8
Hytrel	5.6 X10-3
Tube and Sheath Materials	
PVC	<5.2 X10-6
HDPE	<3.8 X10-7
LDPE	<1.7 X10-7
Filling Compound	
Flex-gel [13]	<1.2 X10-7
Complete RL Cable	5.6 X10-5

* Materials NOT used in AT&T Technologies Cables.

** Desolite: Trade name of Desoto, Inc.

LABORATORY CABLE TESTING

In addition to material decomposition, hydrogen gas may also be produced by electrochemical corrosion of metals comprising the cable structure. For the stranded fiber cable designs illustrated in Figures 2 and 3, the effect of corrosion was investigated through testing at an elevated temperature. In the three unit cable, the area between the copper and steel was flooded with slightly acid sea water as a corrosive medium. The cable was maintained at a constant temperature of 40 degrees C. and the loss was monitored as a function of wavelength for the characteristic hydrogen signature at 1.24 microns. An identical cable with aluminum substituted for copper was similarly tested. Within ten days, the aluminum-steel cable showed a significant hydrogen peak at 1.24 microns. This peak continued to increase for about 40 days when it reached 6 dB/km. The peak did not increase any further, indicating that the cable was saturated with one atmosphere of hydrogen. The copper-steel cable, however, has shown no loss increase whatsoever after six months of testing under identical conditions. These results agree with predictions based on the electrochemical potential differences of the two metals involved. Once the source of hydrogen is removed, the increased loss returns to normal. The time constant for the return depends on the diffusion rate of the hydrogen out of the cable.

This experiment shows that cables containing aluminum and steel can potentially generate hydrogen due to corrosion. Whether they do or not, however, is dependent on cable design. For example, the single-unit cable shown in Figure 2 contains aluminum and steel. However, the aluminum in this cable is flat and bonded on both sides to polyethylene. The aluminum is also coated with a protective polymer layer to prevent bare metal from contacting the steel, but the design must also allow for possible defects or failure of the polymer coating. Thus, even though steel wires are in contact with the aluminum, water cannot migrate easily into the interface since the aluminum is bonded to the polyethylene. With a water pressure of 90 psi, one week was required to force water 50 meters through the cable. However, the water traveled along the inner steel wires that are not in contact with the aluminum. After six months of testing, this cable structure has shown no signs of hydrogen production. Therefore, while steel and aluminum result in hydrogen generation in the first case, this cable has acceptable performance because its inherent design characteristics prevent the water from bridging the steel and aluminum, and subsequent corrosion.

FIELD TESTING

A ribbon based cable was installed under actual field conditions in Chester, New Jersey, in the Fall of 1980. In one section of the experimental route, the cable was buried directly in a swamp, immersing the cable in water. The experimental multimode fibers in this cable contained high levels of phosphorus (9%) and theoretically should have exhibited an increased sensitivity to hydrogen induced loss effects. (Standard production multimode fibers contain only 1% phosphorus.) However, the cable sheath was of the steel reinforced cross-ply design without an aluminum layer and should not have been a source of hydrogen production. Figure 4 shows that the loss of the fibers is the same as the initial loss, when measured three years later. The apparent increase at 1.05 microns is due to a different spectral filter being used in the later tests. There is absolutely no indication of any increase at the hydrogen peak of 1.24 microns. This confirms the hypothesis that the only practical solution to hydrogen induced loss problems is a cable design that is not susceptible to hydrogen production, and that with such a design the inclusion of phosphorus in the fiber is not deleterious.

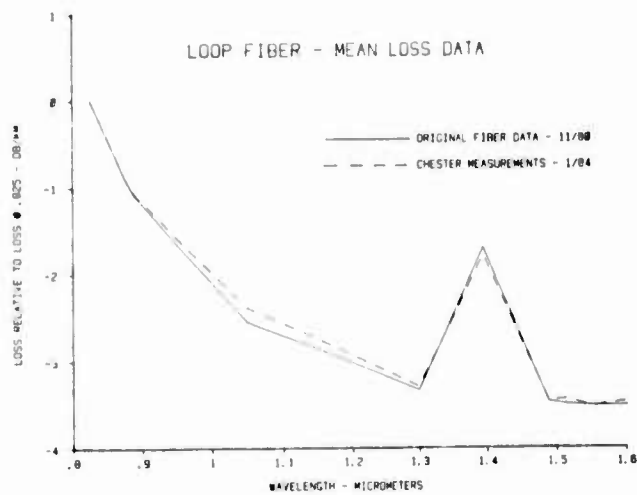


FIGURE 4

CONCLUSIONS

Since hydrogen gas may cause both permanent and temporary loss increases in various spectral regions, the only solution to both problems is to avoid the possibility of hydrogen production within the cable. Hydrogen production from both corrosion and thermal decomposition sources must be minimized through careful material selection and cable construction. For both mechanisms, cables can be designed that will produce negligible quantities of hydrogen, and will therefore be free of any hydrogen induced loss increases.

REFERENCES

1. Stone, et al., Opt. Lett., 7, 297 (1982).
2. Uesugi, et al., Electron. Lett., 19, 762 (1983).
3. Mochizuki, et al., Electron. Lett., 19, 745 (1983).
4. Beales, et al., Electron. Lett., 19, 917 (1983).
5. Mies, et al., OFC 84, New Orleans, paper W13-3.
6. Uesugi, et al., Appl. Phys. Lett., 43, 327 (1983).
7. Nakahara, et al., Electron. Lett., 19, 1004 (1983).
8. Tanaka, et al., Electron. Lett., 20, 284 (1984).
9. Gagen, et al., 28th IWCS, Cherry Hill, N.J., (1979).
10. Miller, BSTJ, Vol. 57, No. 1, (Jan. 1978).
11. Gartside, et. al., ICC'84, Amsterdam (1984).
12. Gartside, et. al., ECOC '83, Geneva (1983).
13. Sabia, et. al., IWCS, Cherry Hill, New Jersey (1982).



Dan L. Philen received the B.S. degree in Chemistry from Auburn University in 1968 and the Ph.D. degree in Physical Chemistry from Texas A&M University in 1975. From 1976 to 1979 he was a Research Scientist at Georgia Institute of Technology. Since joining AT&T Bell Laboratories in 1979 he has been engaged in exploratory measurements on optical fiber properties. Dr. Philen is a member of the American Chemical Society, Optical Society of America, Sigma Xi, Sigma Pi Sigma, and Phi Lambda Upsilon.



Charles Gartside is a Lightguide Cable Designer with AT&T Bell Laboratories. Prior to joining Bell Labs in 1980, he has held engineering positions with Argonne National Laboratories and Westinghouse Electric Corporation. He received his undergraduate education at Widener College and holds a Ph.D. in Mechanical Engineering from Carnegie-Mellon University. Dr. Gartside is a member of the American Society of Mechanical Engineers, Sigma Xi, and Sigma Pi Sigma; and is a Registered Professional Engineer.

A PRODUCT ASSURANCE PROGRAM FOR FIBER OPTICS

R. E. Depp, B. P. McNicholl, J. F. Raye

Defense Electronics Supply Center
Dayton, Ohio 45444

Abstract

As a basis for qualification to military fiber optics specifications, manufacturers will be required to establish, implement and maintain a Product Assurance Program. This program must demonstrate and assure the design, materials, production, inspection and testing of fiber optic devices are adequately controlled to sustain operation in a military environment. Discussion of the program requirements will be in the following areas:

- *Management Responsibility for Quality
- *Product Assurance Program
- *Organization
- *Design, Processing, Manufacturing, Testing and Calibration Procedures
- *Records to be Maintained
- *Self Audits
- *Process Control

Introduction

In the past two years, the emergence of fiber optics from the laboratory into military usage has been accelerating. This is evidenced by the scheduled release of the following military fiber optic specifications requiring qualifications, by early 1985:

- *DoD-D-24620 - Detector, Fiber Optic
- *DoD-C-24621 - Couplers, Fiber Optic
- *DoD-S-24622 - Sources, Fiber Optic
- *DoD-S-24623 - Splices, Fiber Optic
- *DoD-D-KKKKK - Connector, Hermaphroditic Fiber Optic
- *DoD-C-83522 - Connector, FSMA, Fiber Optic
- *DoD-C-85045/2 - /5 Cable, Fiber Optic (dated 1980).

The military fiber optics industry is relatively new. Now is an opportune time to incorporate operating procedures which will insure usage of effective process control techniques. Our experience has shown that these techniques are necessary to insure system performance resulting in the production of reliable, high quality fiber optic components for use in military systems.

The Defense Electronics Supply Center (DESC) is now using a Standard Operating Procedure (SOP) for Fiber Optic Product Assurance during its qualification process. The military services are also currently working on a new military standard for a Product Assurance Plan that incorporates this SOP. Fiber Optic communication systems are by their very nature a series of components which span relatively long distances. These systems will be deployed in hostile environments which are subject to many extremes that will damage components not specifically designed and carefully manufactured to ensure they meet all applicable design and system performance criteria.

Basic reliability theory illustrates that any system (Fiber Optic) which has a single series of components is highly susceptible to any "ONE" of the components failing. For example, if one compares the reliability (i.e., probabilities of performance for a specified time) of several systems that contain components with varied component probabilities for 10,000 hours he would find the results as shown in Table I. This table assumes only 10 components in series which is a conservative number of components.

Table I

Probability of each serial component lasting 10,000 hrs.	Resulting 10 component system probability of operating 10,000 hrs.
.95	.598
.96	.665
.97	.737
.98	.820
.99	.904
.999	.990
.9999	.999

This table dramatically illustrates the positive impact on system reliability that can result from increasing the average component life probability by only a few percent. When the cost of making field repairs and mission down time are considered, the quality approach detailed in this paper is essential for military systems.

Management Responsibility for Quality

Before any quality program can succeed, the total commitment of top management is a necessity. For too long, the quality departments of many manufacturers have been in conflict with the production and sales departments over whether products passed quality requirements. Even worse there have been conflicts in the company over whether the products should be submitted to all of the needed testing.

Experience has shown that companies with an absolute commitment to quality will consistently produce the better products. That commitment always translates into a quality policy that dictates products will not be shipped without the specific knowledge that all quality requirements have been met.

In a quality oriented company one will find a dedication to:

- *100% Conformance to military specification requirements
- *Determination of performance and reliability

A company quality policy must evolve that recognizes that remaining competitive will require continual vigilance for quality and improvement in products. This product improvement can take the form of building a better mousetrap or it can be from corrective actions. Corrective actions will be addressed later in this paper. In order to succeed, top management must make all employees aware of his or her contribution to quality.

THE REAL TEST OF QUALITY POLICY IS ITS APPLICATION DURING EVERYDAY PRODUCTION PRESSURES.

Product Assurance Program

Our qualification procedures require a manufacturer to develop a Product Assurance Program. This program must be documented and approved by our qualification personnel. The product assurance document may be part of manufacturer's quality manual or it may be a separate document.

In either case the document used for a military fiber optics product must describe how a company implements and maintains a Product Assurance Program.

The following list contains examples of categories that must be included and approved by the Qualifying Authority:

- *Process control
- *Material inspection and Control
- *Product traceability
- *Self-audit requirements
- *Organization structure and lines of authority
- *Calibration of equipment

- *Test facilities
- *Identity and performance requirements for distributors
- *Procurement and production control documentation
- *Training
- *Failure analysis and corrective action plan
- *Failure reporting and records
- *Handling and packaging procedures

The Product Assurance Document is the day-to-day operating document used to describe the procedures that in total will insure that the company does it right the first time. Having a written Product Assurance Plan implemented by the Quality Department and considered mandatory for training of employees will insure an operating standard that employees will follow. This is provided management commitment is transmitted to the line operator.

Organization

A formal organizational structure clearly delineating the lines of authority is essential to insure communication and authority for actions taken in everyday operations. This is usually accomplished by having procedures posted at each position on the line.

For the Product Assurance Program, it will be required that a company document the lines of authority for the quality and production organizations. These organizations must have separate, direct and equal lines of authority originating from the Plant Manager or Higher Authority.

Design, Processing, Production Test and Calibration Procedures

In order to establish a quality conformance plan much preplanning is necessary. The procedures necessary for insuring that the quality goals are being met interlocks the items in this section.

Design:

Some of the questions which must be answered in order to develop and construct a high quality Fiber Optics system are:

- *In what environments must the fiber optic component operate? How long?
- *What is the expected life? Corollary: what is the expected failure rate?
- *What materials are necessary? Are materials easily obtained in volume?
- *Capital equipment costs?
- *Safety requirements?
- *Is the design producible with an acceptable yield?

All of these items and many more must be addressed by the company using their

engineering expertise to design the components and by testing of the materials of the final design to prove its potential. The successful interface of their design and the firm control of materials utilized are paramount to development of a reliable design.

The Quality Department must document how raw materials are inspected and how the quality is specified and insured through incoming inspection control procedures. Items such as segregation of discrepant materials, sampling, analysis of problems in materials disposition and any subsequent necessary notification to quality, production and vendors must be documented and available to Government Qualification personnel.

Processing:

Prior to processing a controlling system must have at least: in-process specifications, production travelers, engineering change control, traceability of materials, formal instructions for operators, scheduling department, and preventative maintenance procedures. A proper Product Assurance Plan will address these and other items that the manufacturer believes are essential for control. The Quality Department must insure procedures are documented and followed.

Production:

The actual production personnel must mesh what must sometimes seem like endless detailed instructions into a product with a high yield, high quality-and of course with no mistakes! This might be accomplished by the proper mix of good supervision, quality control down to line operators, training and feedback through statistical quality control methods. In-process inspection (tollgate) by quality personnel is usually found in use by quality manufacturers because of the obvious quick response to any process deviations that are developing.

IF QUALITY IS EMPHASIZED
QUANTITY WILL FOLLOW...

Test and Calibration Procedures

The two items are obviously linked together. Testing products to military specifications or contracts must be done with precisely calibrated equipment. Fiber optics specifications require that conventional equipment must be periodically calibrated to MIL-STD-45662.

MIL-STD-45662 requires traceability to the National Bureau of Standards for primary calibration standards. Optical testing equipment is more difficult because known standards for some measurements are not easily obtainable or have not been formally established. The testing of fiber optic

components may take many forms and until somewhat uniform testing is implemented across the industry it may be somewhat difficult to control. This makes it essential that a manufacturer obtain suitability for the equivalence of tests.

The materials utilized should be tested before production to insure that at the earliest possible moment defects can be rejected. During production, various 100 percent screens may take place to stress components and identify defective parts. Examples of this would be processing of fiber optic cable for Dielectric Withstanding Voltage (DWV) during reel takeup or 100 percent burn-in for fiber optic detectors and sources. Many types of environmental tests are also utilized to stress fiber optic components to identify and weed out early failures of weak components.

A manufacturer should insure that the quality department is checking all testing being performed by the production department via a roving inspector and tollgate quality control personnel for points where critical tests are conducted.

Records to be Maintained

The use of correct up-to-date records signed by a responsible company official should be emphasized by the program plan and taught by the company in their training classes. It is essential that a responsible company official sign off on all lots released for shipment. This is a mandatory requirement. A company will find it very difficult to convince our auditors that they performed required operations and testing if the records are deficient.

Examples of the Records that we will require:

- *Failure analysis (both in house and field failures)
- *Certificates of compliance for raw materials.
- *Corrective actions for failures showing first lot affected.
- *Production travellers must show inspection tollgates & material traceability.
- *Marketing agreement with authorized distributors.
- *Calibration
 - Standards certificates of traceability to NBS.
 - Recall records
 - Maintenance records
 - Out-of-tolerance equipment record
- *ALL MILITARY TESTING (electrical, optical, environmental, Group A, B, C etc.)
- *Training
- *Process changes
- *Process control (e.g., statistical methods such as \bar{X} and R charts)
- *Inspection stamp assignment (If used)

Self-Audit

Assuring that these practices are being carried out requires a periodic check. We believe the self-audit to be a viable plan for accomplishing this task. The Product Assurance Program should include all areas where failure to self-audit could allow faulty products to escape and be shipped.

The self-audit requirement will be mandatory for all manufacturers qualifying to the fiber optics program. The audit must be accomplished by trained quality personnel appointed by the quality director.

Independence of the auditor from production constraints must be a primary consideration. In order to facilitate a complete self-audit a checklist system compatible to our audit requirements should be utilized for the self-audit areas. At least the following areas shall be audited and any others considered necessary by the manufacturer to insure quality:

- Calibration
- Training Effectiveness
- Assembly Operation
- Failure Analysis
- Electrical & Optical testing
- Document Control
- Test Methods for Military Items
- Design Change Control
- Environmental Control
- Incoming Inspection
- Corrective Actions Effectiveness
- Inventory Control and Product Traceability
- Final Test

Any deficiencies found must be documented and corrective actions agreed to by the quality director or material review board prior to implementation. All audit reports must be filed, monitored by the Quality Department, and available to subsequent audits by our auditors. The frequency of self-audits shall be no longer than one year and records of such maintained for three years.

Process Control

The control of a process will take many forms. Whatever form it takes it must at least ensure that a company must control "critical" production processes.

Process control must start with new material inspection with traceability to the production lot. This would be interfaced with a combination of statistical quality control sampling procedures along with control techniques such as \bar{x} and R charts and 100% inspection. Utilizing 100% inspection should only be done at critical steps for a specified time. It should be done where a factor could affect safety or when a new process or change

is incorporated.

Today the diversity of techniques available for statistical quality control make it possible for trained quality personnel to tailor a program to meet any process situation. Most techniques have process control charts utilized which will determine if:

*Variations are "random" or chance.

*Variations are "assignable" e.g., operator error, dies wearing, material defective, etc. Whatever the techniques used a company must have quality improvement goals that the entire quality assurance program will realize. Just inspection to separate good from bad parts is only half the job. A company must be serious about finding and eliminating all types of defects.

Without good control techniques to eliminate error, manufacturers will find it more difficult in the future to meet customers' use of newer methods of lot acceptance sampling. Lot acceptance sampling techniques of companies' products are getting tighter every year. The industry standards are now generally in parts per million (PPM).

Semiconductor manufacturers are now advertising quality levels of 99.75% or better average outgoing quality.¹ This translates to 2500 parts defective in a million! They have found process control is essential since each manufacturing step may produce an "irreversible change"² which could produce a scrapped lot if control isn't maintained. The goals of a company should be to try and continually reduce their outgoing defect rate.

National Semiconductor Corporation began in 1978 to decrease their outgoing electrical defect rate from 10,000 parts per million. National has reduced their average outgoing failure rate to 150 PPM and their corporate goal is 100 PPM in 1985.³

The ultimate corporate quality goal should be to have a quality system so well respected they can have their products shipped directly to stock without incoming inspection for electrical parameters.

Conclusion

In determining the effect of a Product Assurance Plan on quality a company must determine what it can live with for an outgoing quality level in terms of costs and personnel. Then the requirements of a military specification or other customer documents must be studied to determine if that company does conform to all requirements of quality and reliability.

One idea we have tried to emphasize is that quality is everyone's business in a company but the motivation, leadership and support must come from the top. Without this support, quality will be sporadic at best and declining at worse.

Finally, I leave you with some words written by Philip B. Crosby⁴: "In 1961, I created the concept of Zero Defects. It said we had to lay out a clear statement of what we wanted people to do. We didn't want grade level like in schools and we didn't want "quality levels" like in statistics. What we wanted was to do the job right the first time!"

References:

¹ Larry C. Giunipero, "Statistical Quality Control: It Worked In Japan," Electronic Buyers News, 12 Dec. 1983, p. 27.

² Nancy A. Karabatos, "Quality in Semiconductor Manufacturing," Quality Magazine, Aug. 84, p. 91.

³ Ibid., p. 21.

⁴ Philip B. Crosby, "Quality Without Tears-The Art of Hassle-free Management," Quality Magazine, June 1984, p. 76.



Brian McNicholl is Chief of the Passive Devices Branch in the Qualifications Division of the Engineering Directorate at the Defense Electronics Supply Center. He received his Bachelor of Electrical Engineering degree from Michigan Technological University in 1970. Mr. McNicholl is studying for a master's degree in Logistics Management from Central Michigan University.



Robert E. Depp, a native of Selma, Ohio, received his bachelor's degree in physics from Central State University in 1969, and was awarded the Master of Science degree in Logistics Management, in 1973 from the School of Systems and Logistics, Air Force Institute of Technology. He is currently employed at the Defense Electronics Supply Center in Dayton, Ohio. He has served as a project engineer for electron tubes and as the Chief of Parts Control Branch B and as Chief of the Assignee Activity in the Standardization Division. He is currently Chief of the Qualifications Division. He is a member of SOLE #5395, and also belongs to the Institute of Electrical and Electronic Engineers (IEEE).



John Raye graduated from Miami University in 1972 with a Bachelor Science in Industrial Technology. Mr. Raye worked at Belden Wire and Cable before joining the Defense Electronics Supply Center in 1974. Mr. Raye is presently working at DESC as an Electronics Engineer Group Leader for Qualification of Fiber Optic Devices in the Directorate of Engineering.

CABLE DESIGN TO MINIMIZE HYDROGEN-INDUCED ATTENUATION INCREASES IN OPTICAL FIBER

K. Abe, R. Lowe and E. Thomson

Northern Telecom Optical Systems Division
Kanata, Ontario, Canada

ABSTRACT

Extensive investigations of H_2 -induced fiber attenuation increases have been performed for several single mode fiber material designs under a variety of environmental conditions. The observations made in this study indicate that the H_2 -induced attenuation increase can appear in most of the currently available fibers regardless of the material composition and that the effect is enhanced when the fiber is stressed. Based upon these conclusions, the emphasis of our efforts has been placed on cable design modifications which minimize the H_2 effect. Firstly, the loose cable structure was designed to minimize the stress in the cabled fiber under any foreseeable installation conditions. Secondly, the H_2 concentration in the cable was suppressed to below 0.005% by eliminating cable components which could generate H_2 at elevated temperatures and/or under humid conditions. An activation energy analysis based on the saturation levels of the H_2 -induced attenuation increases predicts that with a cable of this design, the expected maximum attenuation increase would be less than 0.01 dB/km at 80°C at 1550nm.

INTRODUCTION

Recently, numerous reports have been published regarding the effects of environmental hydrogen on the transmission properties of optical fibers. These effects have been shown to be due to a combination of the presence of interstitial hydrogen [1] which is a reversible phenomenon, the permanent conversion of hydrogen to hydroxyl in the glass [2], and a wavelength dependent loss increase also associated with the diffusion of hydrogen into the fiber [3]. Most of these results have concentrated on effects relating to multimode rather than single mode fibers. The purpose of this paper is firstly, to report on the temperature dependence of the transmission loss for single mode fibers containing different core dopant materials in order to estimate the long term losses for these fibers under realistic conditions of temperature and hydrogen gas concentration. Secondly, this work describes cable design modifications that minimize the H_2 effect on cabled fiber.

I. ACCELERATED FIBER TESTING IN H_2 ENVIRONMENT

Experimental

Most of the single mode fibers used in these experiments were of a depressed-index cladding design fabricated by the MCVD technique and coated with a silicone resin. The cladding consisted of a phosphorus and fluorine doped silica. The fiber cores contained silica co-doped with either P(0.3 atm.)/Ge(1.2%) or F(0.2%)/Ge(2.5%). To evaluate the performance of the fibers in a hydrogen environment, the samples were placed in an air-tight chamber and heated to temperatures in the range of 80°C to 200°C under a pressure of 1 atm in 100% hydrogen. The spectral attenuation of each sample was recorded periodically between 1000 and 1600nm during the tests which lasted from 400 to 1000 hours. The loss evolution of a P/Ge doped-core fiber heated at 175°C in 1 atm. hydrogen is shown in Fig. 1. There are several important points to note. First, there is no evidence of loss contributions due to interstitial hydrogen, the effects of which would be apparent from the growth of the peak at 1240nm. This can be explained by noting that the chamber is purged with N_2 prior to each measurement. At this temperature the H_2 can then very quickly diffuse out of the fiber. Second, the formation of SiOH, GeOH and POH centers are clearly indicated by the growth of peaks at 1385, 1420 and approximately 1600nm, respectively. Third, a previously reported [3] wavelength-dependent loss contributes substantially to the overall attenuation of this fiber type. Finally, the loss increase saturates after some 300-400 hours of treatment. In contrast to this, Fig. 2 shows the results for a F/Ge doped core fiber (no phosphorus) heat-treated in hydrogen at the same temperature. Notice that by far, the dominant loss component in this fiber is a much larger wavelength dependent loss. Tests conducted on fibers of similar composition in the absence of H_2 fail to show this loss phenomenon. Also, as expected, this fiber does not exhibit the effects attributable to the POH. Similar observations were made at 150° and 200°C. At 80° and 120°C, residual contributions from molecular hydrogen can be seen.

Discussion

For P/Ge doped fiber, the loss increases at 1300nm were plotted as a function of time and the results are shown in Fig. 3 for 125°, 150°, 175° and 200°C. The saturation of the incremental loss described above is clearly evident for those fibers exposed to temperatures above 125°C. The saturation levels measured at various temperatures were fit to the following equation,

$$(\Delta\alpha)_{\max} = (\Delta\alpha)_0 e^{-E_a/RT}$$

The activation energy (E_a) determined in this method was 5.6 kcal/Mol. which is substantially lower than previously reported values of approximately 15 kcal/Mol. [2] which were determined from the loss increases prior to the saturation. Similar analysis for F/Ge doped fiber resulted in the activation energy of 7.7 kcal/Mol.

During the course of the investigations including fiber samples with other types of material design, strong evidences were discovered indicating that the H_2 induced loss increase is associated with Ge in the core and also stress induced in the core either externally or internally due to differential thermal expansion properties of the core/cladding material.

Fig. 4 shows spectral attenuations before and after the heat treatment in H_2 when a fiber, which consists of silica cladding and Ge doped core, was stressed by applying winding tension.

Conclusion

(1) Assuming that the H_2 induced loss increase is proportional to the square root of the H_2 concentration [2,4], the maximum attenuation increase expected at 80°C at 1550nm is approximately 0.01 dB/km when the H_2 concentration in the cable is 0.005%. This estimate is based upon the activation energy analysis described above for P/Ge doped fiber. Furthermore, only the irreversible loss increases are incorporated in this estimate.

(2) Reversible loss increases associated with interstitial H_2 were not investigated extensively in this study. However, existing reports indicate that the effect does not depend upon material compositions of fiber and is not a concern as long as the H_2 concentration is below 10% because the maximum H_2 solubility in silica is proportional to the H_2 concentration in the environment, and the typical loss increase at 1300nm due to interstitial H_2 is reported to be approximately 0.2 dB/km at 100% H_2 , 1 atm. pressure [3].

(3) Fibers are more susceptible to H_2 under stress and with the higher Ge concentration. The depressed-index cladding design allows us to use less Ge as compared with matched-index design.

(4) High P concentration in the core causes substantial attenuation increases at 1550nm region. However, the activation energy analysis monitoring the attenuation increases at 1550nm indicates that the effect is not worse than P free fiber as long as the P concentration is below approximately 0.3 atm. %. This conclusion is consistent with the previous report [5].

II. CABLE DESIGN TO MINIMIZE EFFECTS OF H_2

Based upon the conclusions of the accelerated fiber testing in H_2 environment, it is evident that the following cable design criteria are essential to achieve a long term reliability for installed cable: (i) Minimize H_2 concentration in the cable; (ii) Minimize the permanent stress in cabled fiber. A loose structure cable such as the example shown in Fig. 5 together with installation methods to minimize fiber stress under any field condition readily satisfy the criterion (ii). In order to meet the criterion (i), all the cable components for the cable structure shown in Fig. 5 are separately tested in terms of their H_2 emission. Sample material was placed in a glass container, heating the sample at 75°C over 24 hours. The H_2 concentration of the atmosphere within the container was measured using gas chromatography. Sensitivity of the detection method was 0.001%. The test results are summarized in Table 1. Note that the measured H_2 concentration was normalized to a unit cable length. The test results indicate that major sources of H_2 are silicone coating for fiber, galvanized steel strength-member and aluminum sheath. Actual cable samples of this material design were tested in terms of H_2 concentration in the cable and the spectral attenuation was measured while the sample cables were heated at 75°C over 4 days. Approximately 5% of H_2 was detected from gas extracted from the inside of the cable. Fig. 6 indicates a slight increase of the attenuation peak at 1240nm indicating existence of interstitial H_2 molecules. However, there was no permanent increase in the attenuation over the test period. This interpretation was confirmed by the recovery of the 1240nm peak to the original level, which is attributable to SiOH instead of H_2 , after the cable was purged with He over 3 days at 75°C.

Based upon these observations, the silicone coating, the strength member, and aluminum sheath were replaced with UV acrylate coating, stainless-steel strength member and steel sheath. A combination of the new materials was placed in a glass container simulating the modified cable material design and H_2 emission was measured after heat treatment at 75°C over 25 hours. The H_2 level was below the detection limit of 0.001%. Based upon this test result, an actual cable sample was made and the tests on the cable were repeated at 75°C. After approximately 1 month of the heat treatment, no H_2 or attenuation increase were detected.

It should be further noted that field-installed cables with a material design not incorporating the modifications discussed in this paper were investigated in terms of their attenuation changes at 1300nm. The original cable attenuations measured in the factory were compared with the field measurement which took place approximately one half year later (after one summer). The results shown in Table 2 do not show any indication of changes.

Conclusion

Even though the mechanism of the H_2 effect on fiber is still not well enough understood to allow reliable prediction of fiber life time, it is evident that the following precautions in cable design are essential to ensure longevity of cabled fiber: (1) Minimize stress in cabled fiber. A loose structure cable design together with appropriate installation methods will ensure a negligible level of residual stress; (2) Knowing that the interstitial H_2 effect is not related with material composition of fiber, it is essential to minimize H_2 concentration cable regardless of the type of fiber. For the particular type of cable discussed in this paper, it was demonstrated that the H_2 concentration in the cable can be suppressed to below 0.001% by simply replacing a few H_2 generating cable components with alternative materials. Currently, consistency of H_2 generating characteristics of new materials has not been fully investigated. Furthermore, the H_2 generation depends to some degree upon the preparation method of the sample such as the way the metal component was cut simulating sheath damage, etc. Considering these uncertainties, a maximum H_2 concentration of 0.005% was used for lifetime estimation.

REFERENCES

- [1] Beales, K.J., Cooper, D.M. and Rush, J.D.: "Increased attenuation in optical fibers caused by diffusion of molecular hydrogen at room temperature". *Elect. Lett.*, 1983, 19, pp. 917-919.
- [2] Tanaka, S., Kyoto, M., Watanabe, M. and Yokota, H.: "Hydroxyl group formation caused by hydrogen diffusion into optical glass fiber", *Elect. Lett.*, 1984, 10, pp. 283-284.
- [3] Pitt, N.J. and Marshall, A.: "Long term stability of single-mode optical fibers exposed to hydrogen", *Elect. Lett.*, 1984, 20, pp.512-514.
- [4] Plessner, K.W. and Stannard-Powell, S.J.: "Attenuation/time relation for OH formation in optical fibers exposed to H_2 ", *Elect. Lett.*, 1984, 20, pp. 250-253.
- [5] Ogai, M., Orimo, K., Kokura, K., Kamiya, T., Takashina, M., and Azuma, M.: "Infrared Loss Increase of Silica Fiber", Conference on Optical Fiber Communication, Jan. 23-25, 1984.

Table 1. H_2 From Cable Components

	%*
Al-PE (in air)	0.1
Al-PE (wet)	9.5
Galvanized St. strand	0.5
Silicone coated fiber	0.3-0.9
Acrylate coated fiber	0.002-0.01
St.-St. strand Dry and Wet	<0.001
RPS (Ni/plastic coated St.)	0.02
PE Core + PE sheath	<0.02
Powder Dry, Wet	<0.002
PIC pair	<0.001
Al-peth/RPS lubricant	<0.001
Binder and mylar wrap	<0.001
Ink	<0.002
Combination of materials simulation stealpeth Dryfil cable with acrylate coated fibers and St.-St. strength member	<0.001

* H_2 concentration was measured after heating the sample at 75°C over 25 hrs. The measured concentration was normalized to the volume of a 6 slot cable with 50 fibers.

Table 2. 1.3 μ m Attenuation of Field - Installed Cables

Cable #1 (Aerial, Al + Steel-sheaths, 2.9 km)

Fiber #	Field Measurement*, (dB/km)	Factory Measurement*, (dB/km)	Difference (dB/km)
1	0.42	0.47	-0.05
10	0.48	0.46	0.02
20	0.46	0.46	0.00
28	0.47	0.49	-0.02
37	0.51	0.47	0.04
44	0.43	0.40	0.03
			Av. 0.00

Cable #2 (Aerial, Al + Steel-sheaths, 2.8 km)

Average difference for 5 fibers: 0.02

Cable #3 (Duct, Al-sheath, 2.5 km)

Average difference for 6 fibers: -0.02

* The field measurements were performed approximately one-half year (one summer) after the field installation. The attenuations were compared with the factory measurements which were performed just before shipping of the cables.

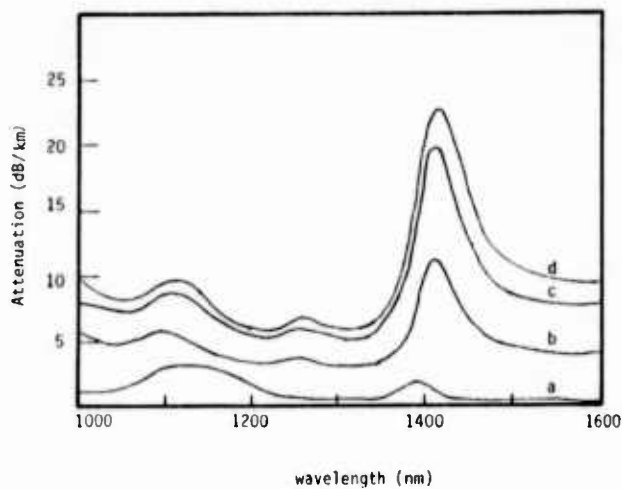


Fig. 1 Loss evolution for a P/Ge doped core fiber exposed to 1 atm. of hydrogen at 175°C: a; 0 hrs; b; 82 hrs., c; 223 hrs., d; 460 hrs.

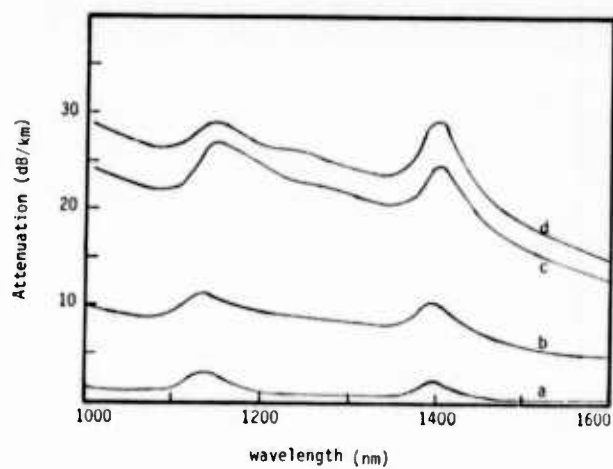


Fig. 2 Loss evolution for a F/Ge doped core fiber exposed to 1 atm. of hydrogen at 175°C: 0 hrs., b; 65 hrs., c; 221 hrs., d; 671 hrs.

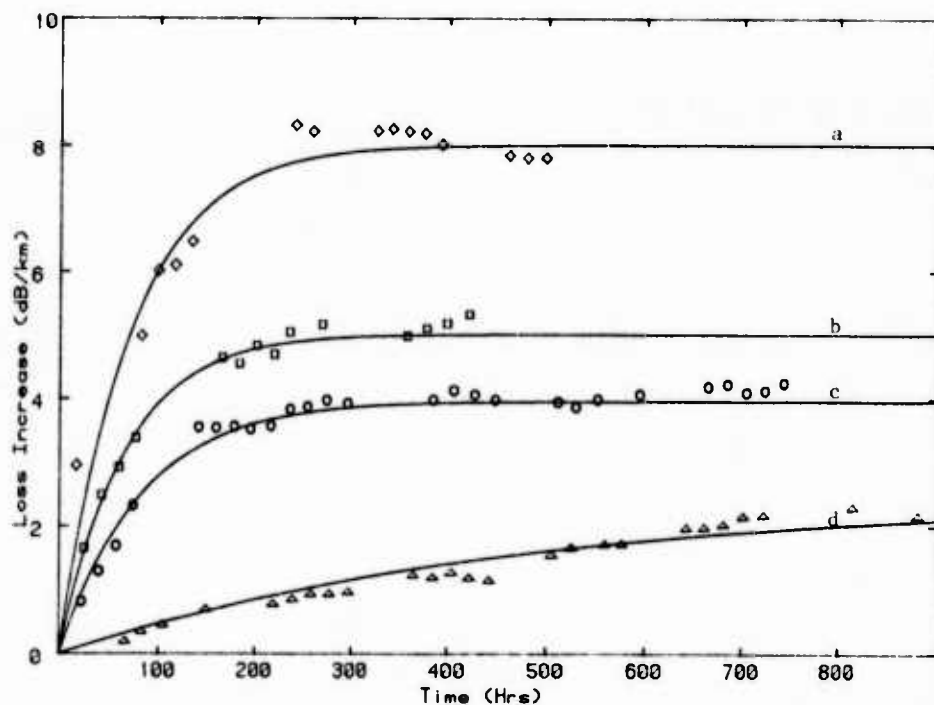


Fig. 3 Incremental loss at 1300 nm as a function of time for a P/Ge doped core fiber in hydrogen: a; 200°C, b; 175°C, c; 150°C, d; 125°C.



Fig. 5 Cable structure

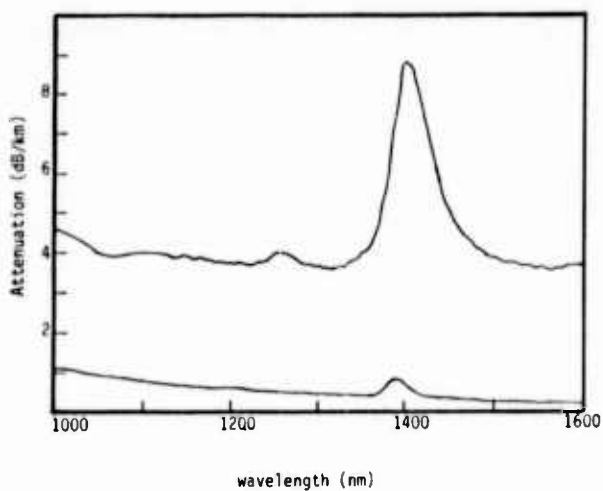


Fig. 4 Spectral attenuation for a Ge doped core fiber under stress: before and after exposure to hydrogen at 200°C over 262 hrs.

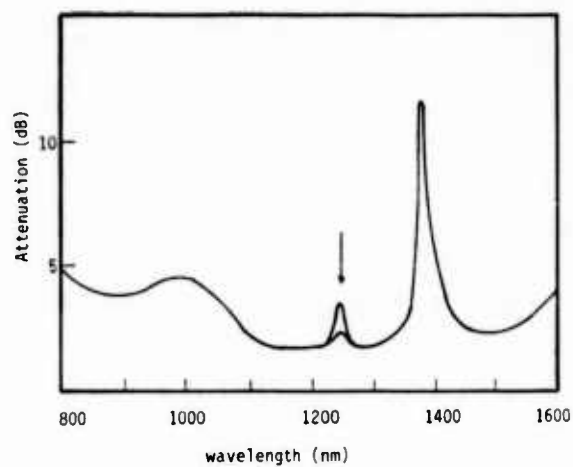


Fig. 6 Spectral attenuation of a fiber in a cable without the material design modification, before and after heating at 75°C, 4 days.



Koichi Abe received a Ph.D. in chemistry from the University of Tokyo in 1970. He joined Bell-Northern Research in 1973, where he was involved in optical fiber fabrication process development. In 1983, he was transferred to Northern Telecom as a Manager of fiber R&D/pilot plant of Optical Systems Division.



Richard Lowe received a Ph.D. in Physical Chemistry from Queen's University, Kingston, in 1976. He joined Bell-Northern Research, Ottawa, in 1980 as a member of the scientific staff and was involved in the development of low loss optical waveguides and fiber characterization techniques. In 1983, he was transferred to the newly founded R&D lab. of Northern Telecom Optical Systems Division. Currently, he manages the fiber research department of the organization.



J.E. Thomson has a B.Sc. (1969) in Electrical Engineering from the University of Alberta, an M.Sc. (1970) in the Science of Materials from Imperial College, London and D.Phil. (1973) physics from Oxford University. Since joining Northern Telecom's Optical Systems Division in 1981 he has been involved with optical fiber manufacturing and testing methods and optical cable materials design and testing.

Authors Index

Abe, K.	424	Hulin, J. P.	174
Allsworth, T.	123	Hunn, R. A.	166
Andersen, A.	395	Hyder, J. C.	220
Anderson, G.	258	Ichikawa, O.	338
Andrews, P. V.	58	Ijiri, Y.	160
Angeles, P.	409	Ilardo, C. S.	14
Arioka, R.	50	Indyke, D. M.	1
Baba, A.	258	Ingebrigtsen, D. N.	401
Bark, P. R.	98	Ishihata, Y.	82, 365
Baungaard Sørensen, A.	395	Ishikawa, M.	118
Benoist, A.	316	Ishikawa, S.	331
Books, J. T.	1	Iwamoto, Y.	67
Chalk, D.	141	Johnson, D.	228
Clarke, F. B.	40	Joubert, J. T.	166
Cobb, G. S.	197	Kakii, T.	184
Collins, R. P.	207	Kalomiris, V. E.	388
Copp, R. L.	146	Kaneko, T.	160
Cornelison, K.	130	Kapron, F. P.	276
Cortines, C. G.	380	Kato, T.	331
Damsgaard, H.	395	Kaufman, S.	5
Dazai, M.	244	Kawabata, S.	118
deBlok, C. M.	193	Keiser, G. E.	190
Dennis, W. E.	401	Khan, M. M.	19
Depp, R. E.	419	Kikuchi, J.	331
de Vecchis, M.	174	Kim, H. T.	283
DiNenno, P. J.	40	Kinard, M. D.	207
Dudek, S. P.	123	Kincaid, J. W., Jr.	228
Duff, D. G.	261	Kish, P. P.	213
Duffy, J. J.	14	Kitayama, Y.	118
Enggaard, N.	395	Kojima, T.	251
Enomoto, Y.	331	Komura, T.	300
Eoll, C. K.	152	Koshika, S.	82
Fleck, M.	130	Kumazawa, Y.	251
Fujise, M.	67	Lawrence, D. O.	98
Gartside, C. H., III	415	LeNoane, G.	316
Geyer, T. W.	276	Loadholt, J. T.	220, 357
Goldring, T.	76	Lowe, R.	424
Gomez Martin, F.	380	Maack, D. R.	123, 351
Gouronnec, A.	316	Macaulay, J.	372
Grigsby, R.	58	Maeda, T.	160
Grosso, P.	316	Magera, J. J.	351
Grune, G. L.	108	Malluck, J. F.	197
Grüner-Nielsen, L.	395	Maslaney, M. J.	261
Guegan, Y.	316	Massey, J. R.	197
Guida, T. J.	5	Matthijsse, P.	193
Haibara, T.	50	Mayr, E.	98
Hakamata, N.	184	McAlarney, J.	258
Hale, A. L.	237	McBride, L. E.	141
Hasegawa, S.	82	McDonough, M. T.	58
Hayasaka, E.	82, 365	McGettigan, P. A.	213
Hayashi, Y.	160	McNicholl, B. P.	419
Hazelden, R. J.	58	Mio, K.	160
Heckmann, S.	266	Mishima, T.	345
Hilliard, L. A.	108	Mitchell, D. M.	207
Hirasaka, N.	324	Mori, A.	300, 338
Hisano, S.	365	Morita, Y.	287
Horima, H.	245, 365	Muenchinger, W. O.	1
Hughes, H.	166	Nakane, F.	251

Nakasuji, M.	244	Suzuki, F.	300
Negishi, K.	331	Suzuki, S.	184
Nishida, K.	287	Tabata, Y.	82
Nomura, M.	345	Tachikura, M.	50
Oestreich, U.	98	Takahashi, F.	345
Ohashi, S.	251	Takahashi, T.	331
Ohlhaber, R.	409	Takai, T.	287
Ohtsuka, F.	82	Tanaka, H.	160
Olson, T. C.	276	Tanaka, S.	338
Omae, K.	345	Tarwater, R. W.	261
Omori, T.	365	Tewarson, A.	19
Ono, T.	338	Thomson, E.	424
Otake, A.	345	Touchais, T.	174
Philen, D. L.	261, 415	Ulijasz, T.	409
Przybyla, L. J.	5	Usui, Y.	184
Raye, J. F.	419	Valette, P.	316
Reginato, L. L.	146	Visser, L.	308
Rice, D. H.	190	Vokey, D. E.	76
Rosendal, H.	395	Warren, P. C.	34
Saez De La Maza, F. J.	380	Watanabe, M.	244
Saha, S.	58	Weiss, W. C.	146
Saito, Y.	118, 338	West, D. E.	207
Schmidt, J. A.	146	Williams, J. L.	5
Seto, K.	324	Williamson, A. H., Jr.	197
Share, S.	258	Williamson, T. M.	357
Shibuya, K.	251	Yamaguchi, S.	160, 287
Shishido, T.	365	Yamamoto, T.	324
Sierawski, D. A.	401	Yokosuka, H.	324
Smith, J. C.	258	Yokota, H.	244
Spencer, H. J. C.	92	Yonechi, S.	102
Stone, F. T.	261		



IWCS

International Wire & Cable Symposium

**SPONSORED BY U.S. ARMY COMMUNICATIONS-ELECTRONICS COMMAND
(CECOM)**

FORT MONMOUTH, NEW JERSEY

12, 13, 14 November 1985

HYATT CHERRY HILL, CHERRY HILL, NEW JERSEY

Please provide in the space below a 100-500 word abstract (20 copies) of proposed technical paper on such subjects as design, application, materials, and manufacturing of Communications and Electronics Wire and Cable of interest to the commercial and military electronics industries. Such offers should be submitted no later than 12 April 1985 to the Headquarters, US Army Communications-Electronics Command, ATTN: DRSEL-COM-D-4, Fort Monmouth, New Jersey 07703-5202.

TITLE: _____

AUTHORS: _____

COMPANY: _____

ADDRESS: _____

Staple

Fold here

Stamp

Commander
US Army Communications-Electronics Command
ATTN: AMSEL-COM-D-4
Fort Monmouth, NJ 07703-5202

Fold here